

UNCLASSIFIED

AD NUMBER
AD881795
NEW LIMITATION CHANGE
TO Approved for public release, distribution unlimited
FROM Distribution authorized to U.S. Gov't. agencies and their contractors; Critical technology; Jan 1971. Other requests shall be referred to Air Force Rocket Propulsion Laboratory, Attn: DOG/STINFO, Edwards AFB, CA, 93523.
AUTHORITY
AFRPL ltr, 29 Sep 1971

THIS PAGE IS UNCLASSIFIED

AIR FORCE REUSABLE ROCKET ENGINE PROGRAM

XLR129-P-1

FINAL REPORT

AFRPL-TR-71-1 VOL II

JANUARY 1971

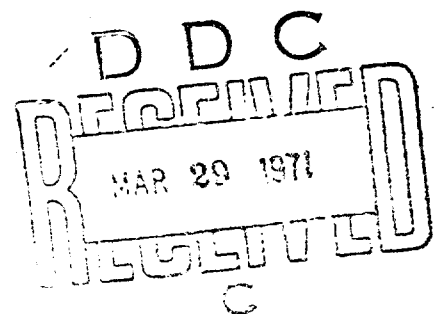
STATEMENT #2 UNCLASSIFIED

This document is subject to special export controls and each transmittal to foreign government or foreign nationals may be made only with prior approval of *Air Force Rocket Propulsion*

*Laboratory, Attn: DOG/STINFO
Edwards AFB Calif 93523*

Prepared Under
Contract F04611-68-C-0002 for
Air Force Rocket Propulsion Laboratory
Edwards Air Force Base, California 93523

Reproduced From
Best Available Copy



FOREWORD

This final report describes the Air Force XLR129-P-1 Reusable Rocket Engine Program conducted during the period 6 November 1967 to 15 August 1970, ✓ and is submitted in accordance with the requirement of Contract F04611-68-C-0002.

This effort was the second phase of the Air Force Cryogenic Rocket Engine Advanced Development Program, Project 2 of the Program Element 63408R.

This publication was prepared by the Pratt & Whitney Aircraft Florida Research and Development Center as report PWA FR-3832.

This Technical Report has been reviewed and is approved.

Robert E. Probst
Captain, USAF
Program Manager
Air Force Rocket Propulsion Laboratory

SECTION V COMPONENT DEVELOPMENT

A. PREFURNER INJECTOR AND IGNITION SYSTEM

1. Introduction

The preburner is an oxygen-hydrogen combustor that provides hot gases to drive the oxidizer and fuel pump turbines. Liquid oxygen and gaseous hydrogen are pumped to the preburner injector in varying mixture ratios and flowrates depending on the engine operating point. These propellants are ignited by a spark augmented torch igniter and burned in the transition case duct. Hot gases resulting from this combustion are divided and flow through the oxidizer and fuel pump turbines before being discharged through the fuel side of the main burner injector into the main burner chamber. Because hot preburner gases are used to drive the fuel and oxidizer pump turbines, the design temperature profile is 150°R peak-to-average to permit operating the turbines at the maximum allowable average temperature.

The preburner ignition system is composed of a hydrogen cooled, continuous burning, oxygen-hydrogen torch. Double spark plug igniters are provided for the torch, and each has a separate exciter box for system redundancy. The spark plugs ignite the torch, which ignites the preburner propellant mixture.

Fuel and oxidizer flow to the torch from tapoffs in the supply line downstream of the preburner fuel and oxidizer valves. Before ignition, the propellants entering the chamber are gaseous. After ignition and turbopump startup, the propellants entering the chamber are liquid. Two orifices in series on the oxidizer side of the igniter decreases the steady-state mixture ratio. The effect of resistance in a double orifice is additive in the liquid phase and is nonadditive in the gaseous phase. This reduces the liquid phase oxidizer flowrate.

2. Summary, Conclusions, and Recommendations

A fixed fuel, dual tangential oxidizer preburner injector was designed and detailed and two preburner injectors were fabricated during the program. A detailed description of the design task is presented in the Demonstrator Engine Design Report AFRPL-TR-70-6.

Fourteen firings were made with the first preburner injector. The initial six tests displayed unacceptable temperature profiles and suffered damage to the uncooled combustion liner. Tests seven through fourteen demonstrated acceptable temperature profiles and only minor erosion and heat discoloration of the combustion liner was evident.

Eight firings were made with the second preburner injector. The second injector performed satisfactorily and no modifications were necessary.

As a result of hot firing on the first injector, the following modifications were made to both injectors:

1. A positive seal, replacing a sliding sheet metal seal, was installed between the injector faceplate and housing.

2. Thermal relief slots were provided on the downstream injector housing inboard of the bolt circle.
3. Outer element oxygen flow was directed inward toward the combustion chamber axis to reduce the combustion liner heat load.
4. Procedures were developed to ensure that no oxidizer injection element primary hole blockage was present either in fabrication or calibration.
5. A compartmented transpiration-cooled, inner combustion liner section was incorporated in the upper 2 in. of the original uncooled liner.

The general conclusions that can be made from the preburner rig tests are:

1. The temperature profile is acceptable for driving the fuel pump turbine.
2. A transpiration-cooled liner is necessary in the high energy release zone of the preburner chamber.
3. The addition of the transpiration cooled section of the preburner liner will allow operation of the preburner at any cycle condition above 20% thrust. The preburner liner temperatures show a decrease in operating level as thrust is increased even at high average combustion temperatures. The preburner can be operated at 20% thrust, mixture ratio of 5 with no distress to the liner. It is expected that increasing the cooling flow will allow satisfactory operation at 20% thrust, mixture ratio of 6 and 20% thrust, mixture ratio of 7 conditions.

Because the temperature profile was satisfactory and the preburner liner was adequate above 20% thrust it was decided to run the preburner injector in the hot gas system test rig.

A torch igniter for the preburner was designed and detailed, and two preburner igniters were fabricated.

The first torch igniter was bench fired 23 times for a hot time totaling 688.9 sec. The igniter bench firing qualified the igniter for use in the hot gas system rig and hot turbine fuel pump rig. The first igniter performed satisfactorily in both of these rigs.

The second torch igniter was bench fired five times for 161.4 sec of hot time. The bench tests qualified the second igniter for use in the hot firing rigs. As a result of the preburner testing it is recommended that a method of supporting the injector faceplate, other than tangs integral in the Rigimesh, be studied. This is in an effort to eliminate the slight face erosion that occurs adjacent to the tangs. In addition, the faceplate porosity could be increased to

provide margin against face erosion. It is also recommended that the outer row of the hexagonal pattern of injection elements be revised to eliminate the six corner patterns near the wall that appears to cause local liner wall distress.

3. Hardware Description

a. General

Figure 251 is a location drawing of the preburner injector and ignition system. Figure 352 is a cross section of the fixed fuel dispersion area preburner injector and is keyed to the following description of the preburner injector.

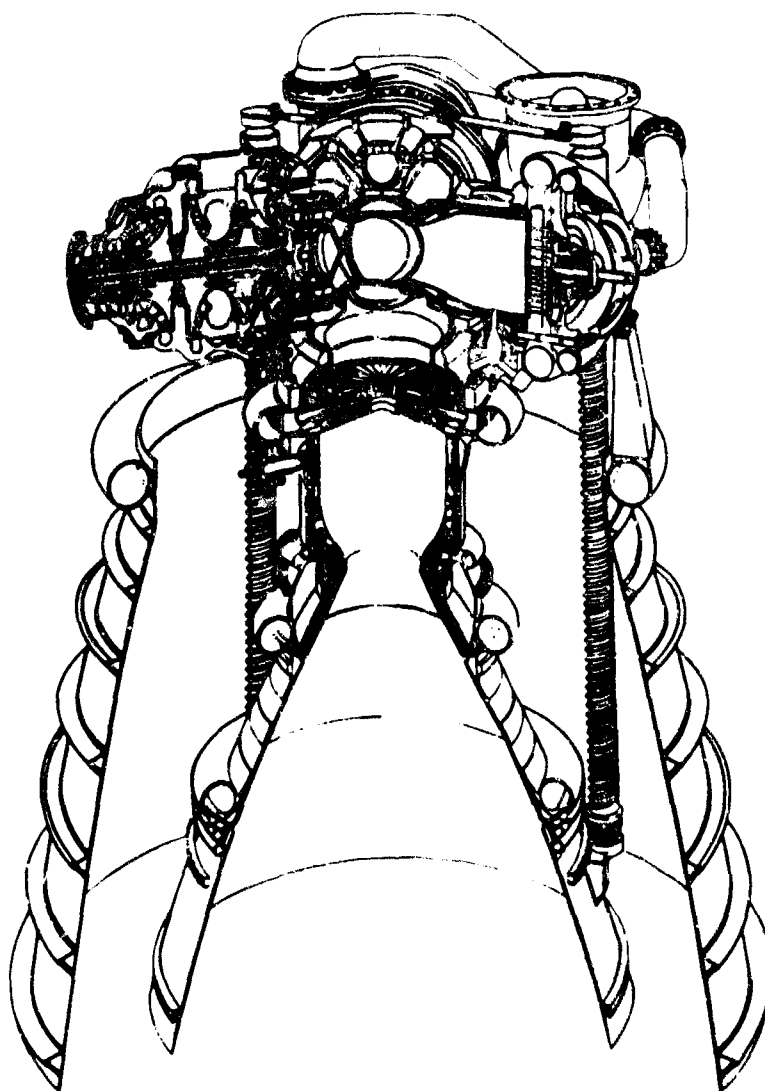


Figure 351. 29 Reusable Rocket Engine,
Preburner Injector and Igniter
Location

FD 31414A

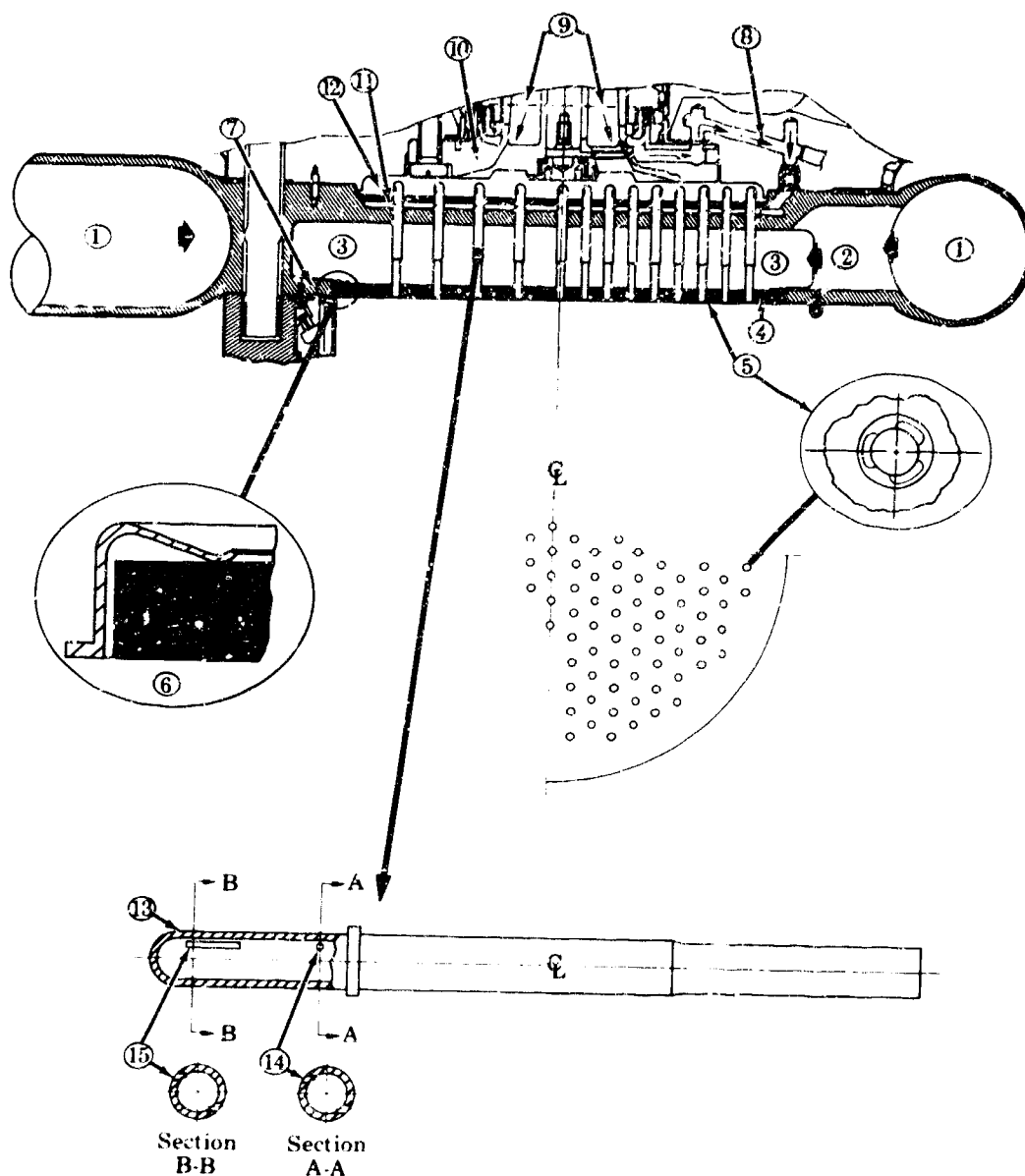


Figure 352. Demonstrator Engine Preburner Injector FD 25976A

Fuel is supplied to the circular fuel manifold (1) by the fuel system. The fuel then flows through the feed holes (2) into the manifold (3) behind the faceplate Rigimesh (4) and is metered into the combustion chamber through annuli (5) around each oxidizer element of which there are 253. A spring seal (6) is used between the faceplate and the preburner injector housing (7) to minimize fuel flow between the loose fitting faceplate and the housing. The oxidizer is supplied from the preburner oxidizer valve, which controls and meters the total oxidizer flow to primary (8) and secondary (9) flow passages in the oxidizer valve housing (10). Two oxidizer flows, primary and secondary, are used to maintain a difference of at least 6% above chamber pressure at all engine cycle points for stable combustion. The series of flow passages (8 and 9) deliver oxidizer to

the primary (11) and secondary (12) supply manifolds. Oxidizer is transferred to the combustion chamber through individual oxidizer elements (13). Each element has flow entries machined tangentially to the tube ID; circular holes for the primary flow (14) and rectangular slots for the secondary flow (15). Because element length is governed by the heights of the fuel cavity (3), primary oxidizer (11) and secondary oxidizer (12) manifolds, these heights are kept to a minimum, consistent with low distribution losses.

b. Injector Housing

The preburner injector housing is fabricated of Inconel 718 (AMS 5663). This housing has 28 equally spaced slots on a 6.03 in. radius, to allow gaseous hydrogen to flow from the fuel manifold to the fuel manifold behind the faceplate. Primary oxidizer flow enters the primary oxidizer manifold through six equally spaced ports in the preburner injector housing. Two additional ports have been provided to house a Kistler probe for measuring primary oxidizer dynamic pressure, and a static pressure probe. The primary oxidizer volume is 7.74 in.³ Secondary oxidizer flow enters the secondary oxidizer manifold directly from the preburner oxidizer valve. The secondary oxidizer volume, which includes all the volume downstream of the preburner oxidizer valve shutoff and upstream of the orifices on the oxidizer elements, is 27.11 in.³ There are twenty-eight 0.1-in. diameter holes provided in the injector housing to supply fuel as coolant to the transition case preburner duct inner flow liner.

c. Oxidizer Elements

The preburner injector incorporates 253 oxidizer elements arranged in a hexagonal pattern as shown in figure 353. The oxidizer elements have a 0.124-in. ID and have flow entries machined tangential to the tube ID. The primary entry is a 0.015-in. diameter hole and the secondary entry is a rectangular slot 0.167 by 0.020 inch. Counterclockwise rotation, as viewed from upstream, is induced by tangential entry elements. The element has an A_s/A_o ratio of 0.555 and an L/D ratio of 17.3. Each element is fabricated of AISI 347 stainless steel (AMS 5571) and has an integral collar resting against the injector main housing for axial positioning prior to brazing the elements to the oxidizer plate and the injector housing with gold-nickel braze.

d. Faceplate

The porous preburner injector faceplate is fabricated from woven and sintered wire mesh. The porosity will allow airflow at a volume of 40 scfm/ft² at a pressure differential of 2 psi discharging to atmospheric pressure. The Rigimesh faceplate contains the fixed area fuel annuli, which are centered circumferential to each oxidizer element by three tangs. Fuel annuli provide a fuel injection area of 4.53 in.² that creates a 200-psid fuel pressure drop at an engine mixture ratio of 7 at 100% thrust. The faceplate is held in place by copper brazing the positioning tangs to the oxidizer elements. The tangs are 0.040 in. wide and are recessed 0.155 to 0.165 in. to prevent fuel flow separation occurring around the tangs continuing past the faceplate.

A spring seal is provided at the outer circumference of the injector faceplate to prevent fuel leakage. The seal is fabricated from Inconel 718 (AMS 5596) and absorbs a 0.003-in. deflection caused by axial shrinkage of the oxidizer nozzle element relative to the main housing when cryogenic oxidizer flow is

initiated. The seal also allows a maximum radial shrinkage of 0.011 in. caused by liquid hydrogen fuel cooling of the porous faceplate.

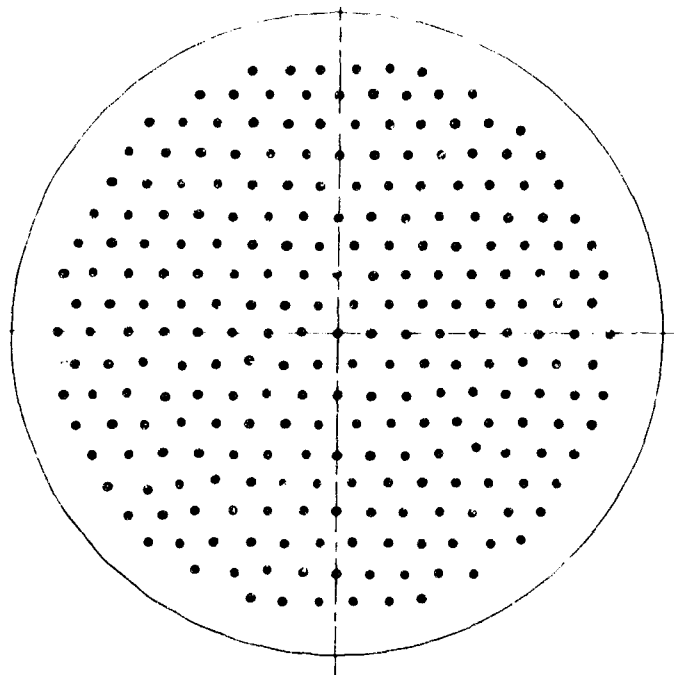


Figure 353. Preburner Injector Face Pattern

FD 25387A

Fuel enters a plenum in the cover through the fuel inlet fitting, located on the side of the cover. Fuel is injected into the chamber through an orifice concentrically formed around the oxidizer element. The oxidizer is injected into the chamber through the oxidizer element fitting, located concentric to the axial centerline of the cover assembly.

e. Preburner Torch

The preburner torch assembly consists of a cover, chamber, sleeve and other detail parts shown in figure 354.

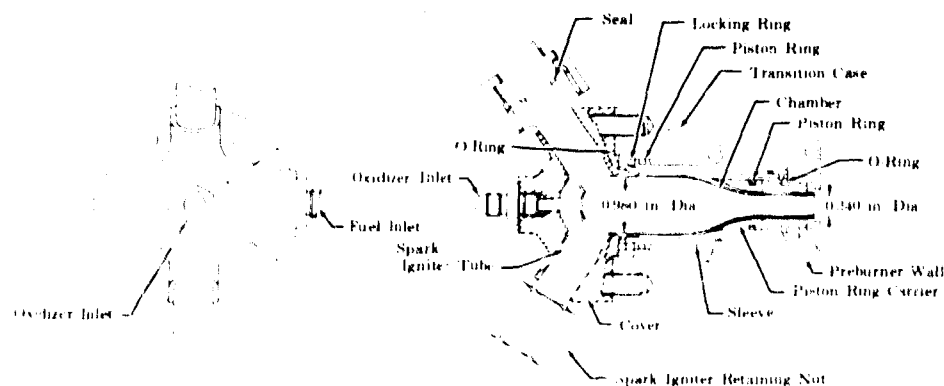


Figure 354. Preburner Torch Assembly

FD 31814

The cover, with the attached chamber, bolts to a spherical branch of the transition case that aligns the discharging combustion products across the center of the preburner chamber. The cover is fabricated from Inconel 718 (AMS 5662) and contains two spark igniter tubes, an oxidizer element, and a fuel inlet fitting. A removable orifice plug is installed in the oxidizer fitting. Each spark igniter tube houses a spark plug igniter attached to the cover by a lockwired nut.

The cylindrical chamber section is fabricated from copper (AMS 4500), and is brazed to a hemispherical cap welded to the base of the spark igniter tubes shown in figure 355. The spark igniter tubes are brazed to the inside of the cover assembly. A copper (AMS 4500) piston ring carrier fabricated of Inconel X-750 (AMS 5667) is brazed to the chamber at the nozzle end to ensure a piston ring seal fabricated of Inconel X-750 (AMS 5667). The piston ring bears circumferentially on the internal wall of the igniter sleeve to permit axial and transverse thermal growth of the chamber.

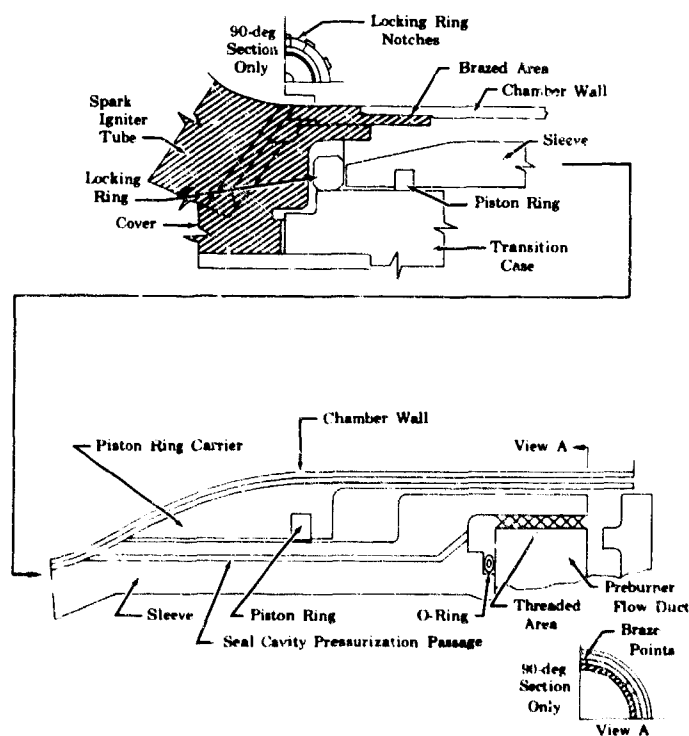


Figure 355. Preburner Torch Assembly Mounting and Sealing

FD 31815

The igniter sleeve is fabricated from Inconel 718 (AMS 5663) and forms the outer structural liner for the chamber. It also provides an annular passage for coolant flow. The sleeve is threaded into the preburner flow duct. It is torqued to 350 lb-in. plus any slight additional rotation required to align the locking ring slot with a locking ring notch in the transition case. The locking ring prevents loosening of the sleeve. The threaded end of the sleeve houses a seal that is loaded by the applied torque on the threads. The cavity formed between the seal and threads is pressurized through a passage from the liner coolant supply. Pressurization of the cavity causes leakage of coolant into the

combustion chamber thus keeping combustion products from leaking outward through the threads. A forward piston ring seal, fabricated from Inconel X-750 (AMS 5667), bearing circumferentially against the transition case flange, permits axial and transverse thermal growth of the sleeve.

Fuel enters a plenum in the cover through the fuel inlet fitting, located on the side of the cover. Fuel is injected into the chamber through an orifice concentrically formed around the oxidizer element. Oxidizer is injected into the chamber through the oxidizer element fitting, which is located concentrically to the axial centerline of the cover assembly.

Fuel coolant also flows through a series of orifices that reduce fuel pressure on the outside of the chamber wall to the approximate internal pressure of the chamber. These orifices are located circumferentially at the rear of the chamber. The orifices redistribute the fuel flow evenly over the outside diameter of the chamber, and fuel exits at the preburner flow duct. A seal cavity pressurization passage in the sleeve wall transfers pressure to the vicinity of the inside diameter of the O-ring at the base of the threads. This pressure ensures that leakage past the threads will be fuel rather than combustion products.

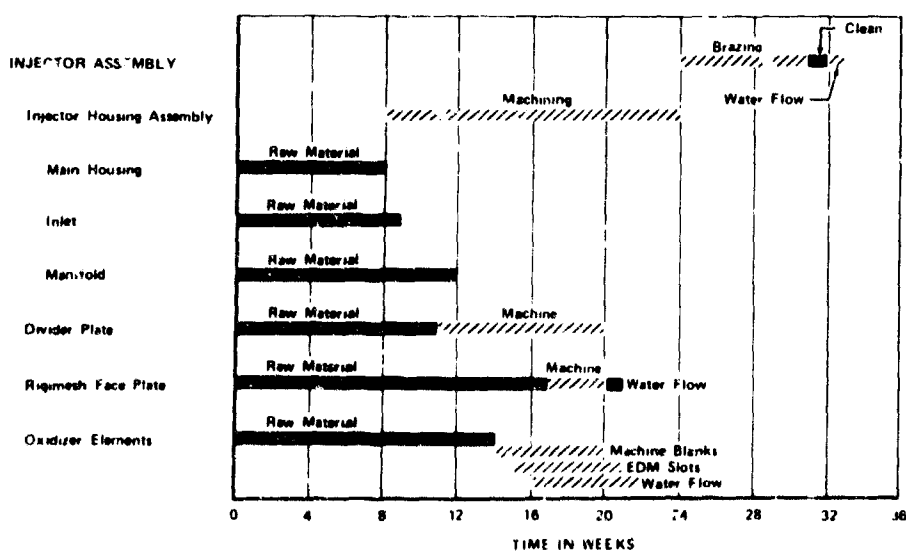
f. Electrical

Refer to Section VI Controls System for discussion of the electrical ignition system.

4. Fabrication

Table XXXI portrays the materials purchase timetable.

Table XXXI. Preburner Injector Materials Purchase Timetable



a. Injector Housing

Two preburner injector housings were fabricated by a vendor. The major parts of the housing are the wraparound manifold outer halves, inlet horn, inlet transition, and the housing body, shown assembled in figure 356. Each of these subassemblies was machined from Inconel 718 forgings in solution condition and welded.



Figure 356. Injector Housing Fabricated by Vendor FE 86397

The integrity of the welds was assured by X-ray after the root weld pass. On the first injector housing two small areas of weld porosity were found by X-ray of the root pass. These spots were routed out, welded, and re-X-rayed. The second X-ray revealed the welds to be good. The housing vendor also fabricated the divider plate and fuel faceplate to ensure alignment of each hole and avoid any problem in assembly around the element.

Both injectors were finish machined after welding and solution heat treated. The overboard seal grooves, between the injector housing and preburner oxidizer valve, were machined to accept Parker 8814 V-seals.

b. Oxidizer Elements

Two vendors fabricated the oxidizer elements in two steps. The first step consisted of fabricating the element blank, including everything but the tangential slots, from seamless AISI 347 stainless steel tubing drawn to the correct inside diameter. The AISI 347 tubing was cut into lengths sufficient for one element. Then, the top of the element was rolled closed. The outside features were machined and the hole remaining in the end of the element was

sealed with copper braze, thus forming the element blank. A typical element blank is shown in figure 357. The element blanks were shipped for P&WA's inspection where dimensional checks are made. Approximately 10% of the element blanks were rejected because of dimensional deviations. The blanks were X-rayed to check wall thickness and the condition of the braze thickness at the upstream end, and approximately 12% of the remaining blanks were then rejected. Figure 358 shows a typical X-ray of the element blank.

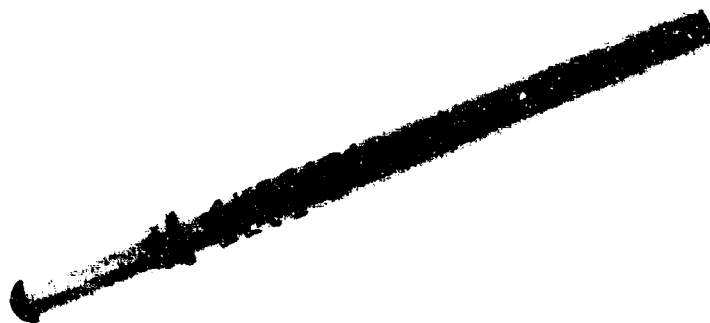
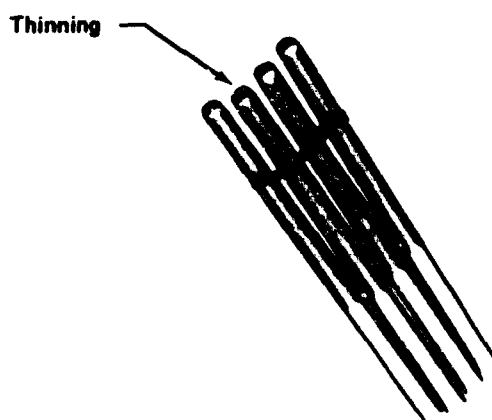


Figure 357. Element Blank

FE 96149



Blanks X-Ray Inspected for Wall Thinning and Excessive Braze Metal

Figure 358. Blanks X-ray Inspected For
Wall Thinning

FD 38363

To obtain 1353 finished elements required to make the individual oxidizer-to-fuel match discussed later in this section, it was necessary to manufacture 1718 element blanks.

The element blanks were taken by another vendor who machined the primary and secondary tangential entries by the electric discharge machining process (EDM). As the EDM vendor turned out finished elements, they were individually water flowed at P&WA to determine if the element effective area was satisfactory. Figure 359 shows the results of the water flow after approximately 450 elements had been accumulated. The elements, labeled original on the chart, had a secondary element population average falling 12 to 13% above target. All elements to this point had physical dimensions shown in figure 360.

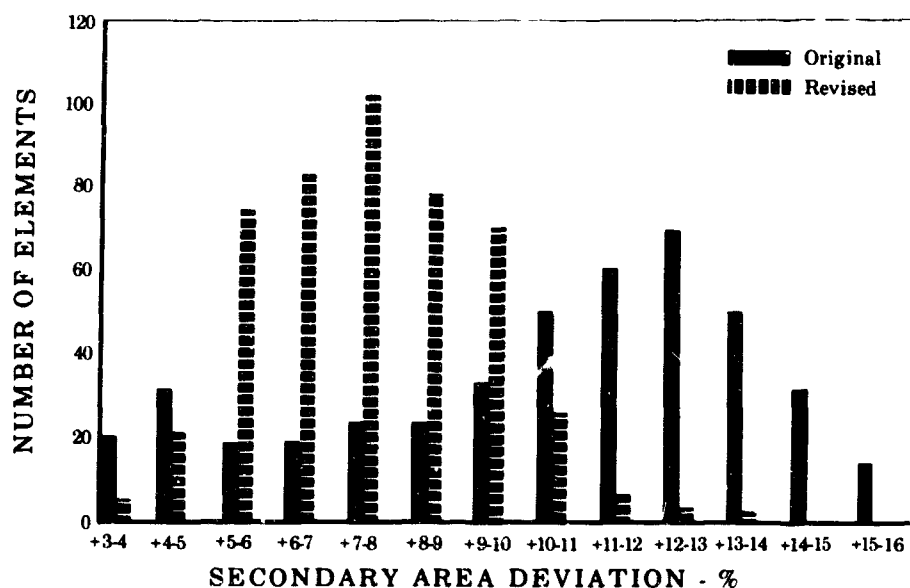


Figure 359. Preburner Injector Element
Secondary Flow Area Deviations

FD 29189

To bring the secondary element effective area closer to that desired, the physical dimensions of the secondary slot were reduced to those shown in figure 361.

Water flow of the oxidizer elements that incorporated the primary and secondary slot size change show the primary A_{pd} is on target and the secondary A_{cd} is 7% high. No further correction was made to the secondary slot sizes.

Figure 362 shows the flowrate of the elements after all finished elements had been received and flowed. The flowrate shown is dual flow, that is, both primary and secondary. The flow split for the dual flow is set at 13% indicating primary flow is 13% of total flow. The flow split of 13% is approximately equivalent to the flow split at 100% thrust and a mixture ratio of 7, where the average combustion temperature is the highest.

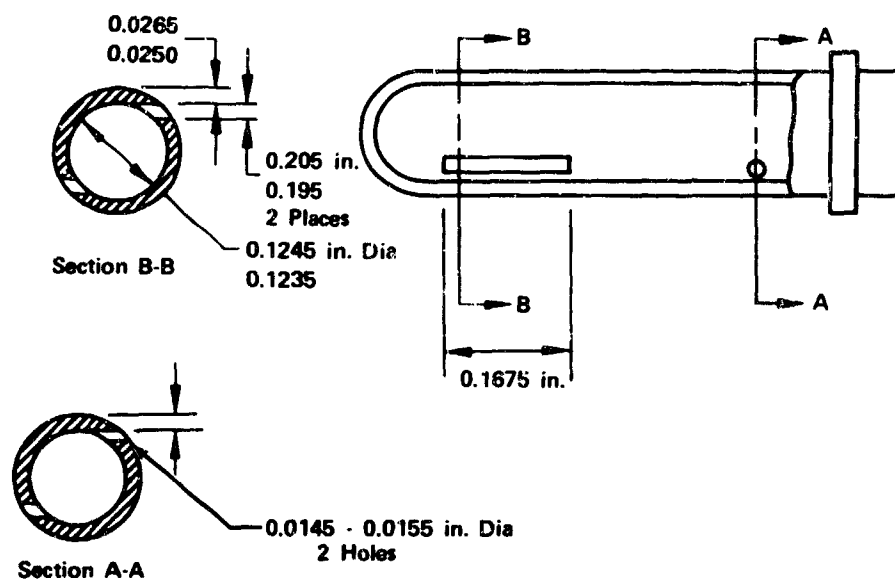


Figure 360. Physical Dimensions of Elements

FD 38365A

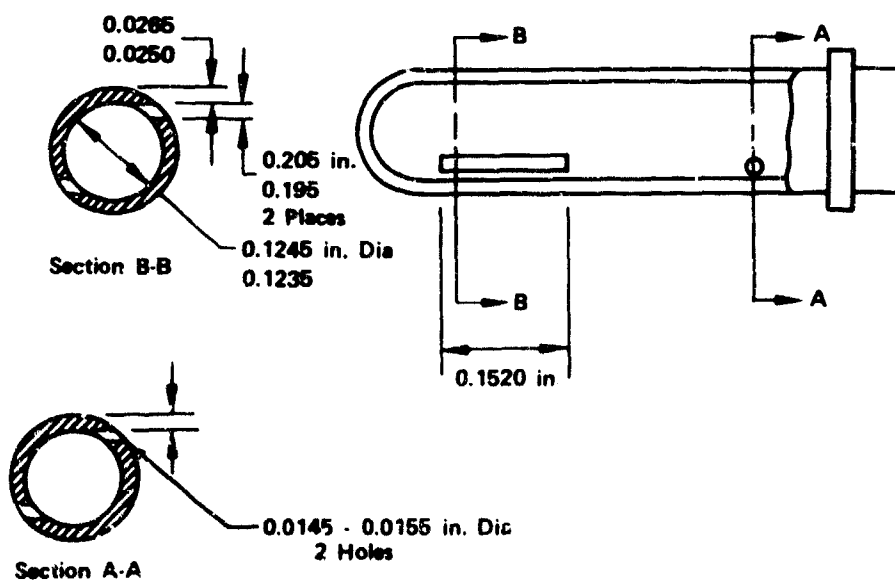


Figure 361. Physical Dimensions of Secondary Slot

FD 38365

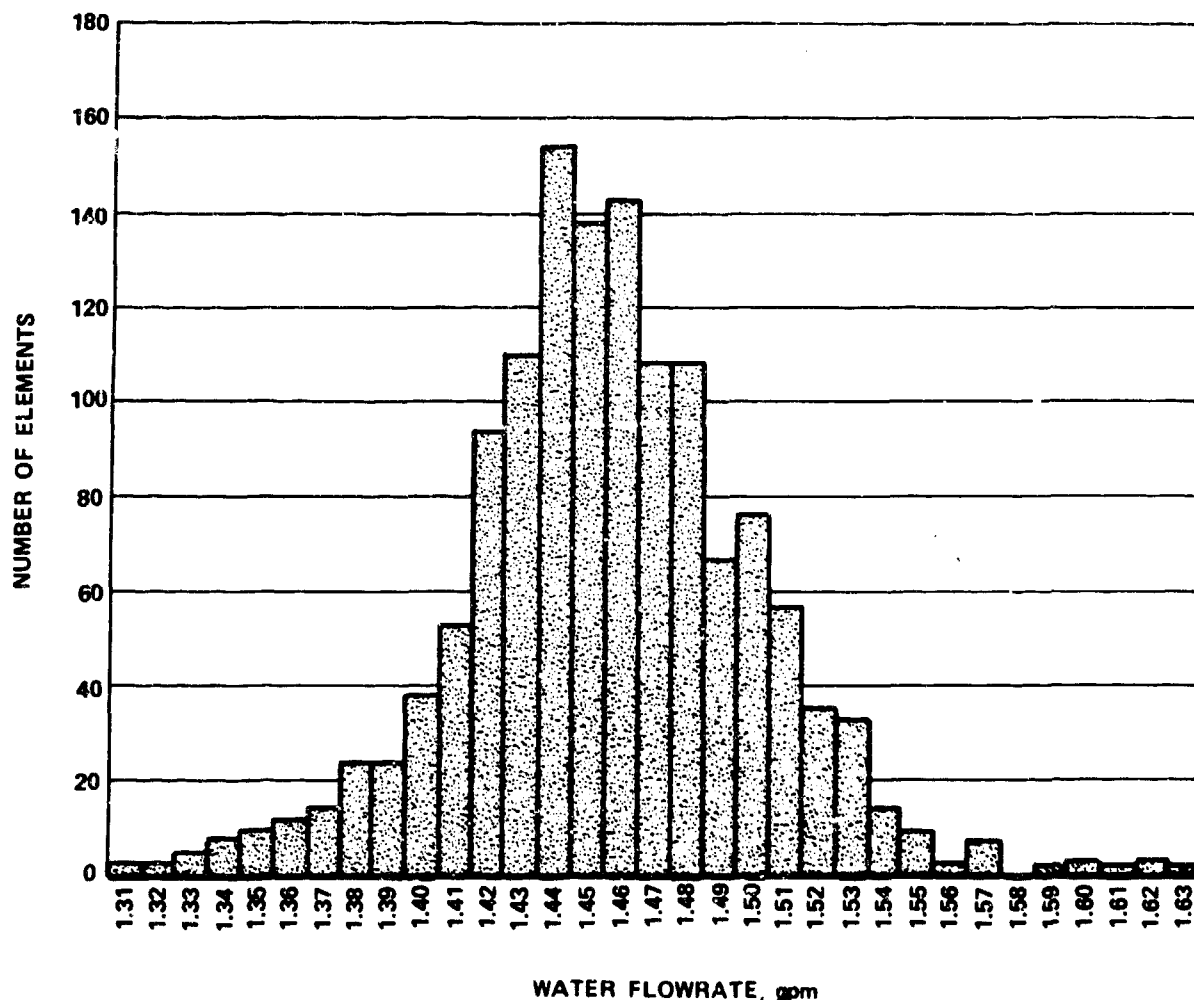


Figure 362. Element Flowrate Distribution

FD 38366A

c. Faceplate

Two fuel faceplates were made from 12 x 64 weave N-155 Rigimesh. Porosity was 34.9 versus 40 scfm/ft² as design target. The material was delivered in sheets to blueprint thickness to the primary machine vendor where it was machined into a disk before orifices were drilled and counterbored by the tape controlled machine. The tangs were then electric discharge machined referencing the previously positioned holes. Figure 363 illustrates the first plate.

Upon delivery, the plates were dimensionally inspected and then water flowed to determine the individual fuel hole A_{cd} distribution for matching with the oxidizer elements. Both plates had a normal distribution curve of effective area with a narrow range (8.9%) total band, see figure 364, but the total A_{cd} from summation of individual fuel hole A_{cd} 's was 18.5% lower than the target of 3.69 in.²

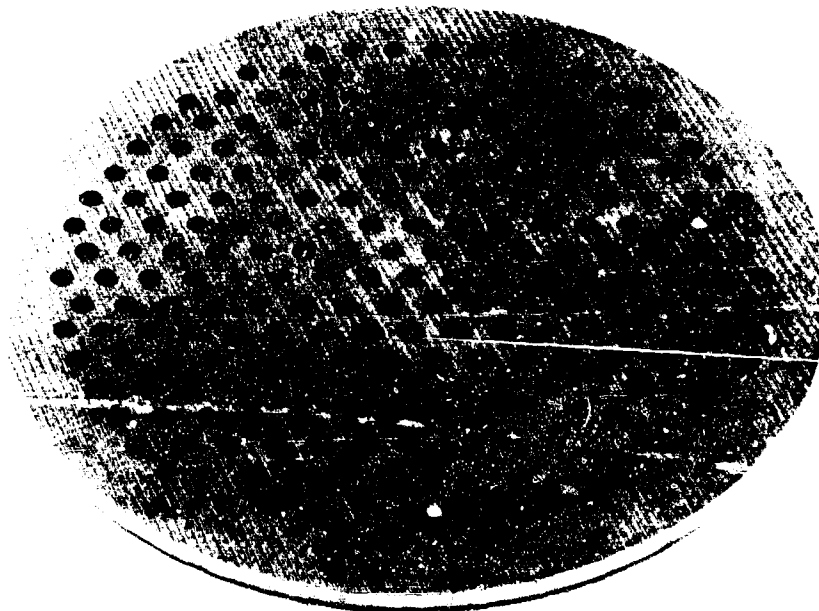


Figure 363. Faceplate Initial Build

FE 86395

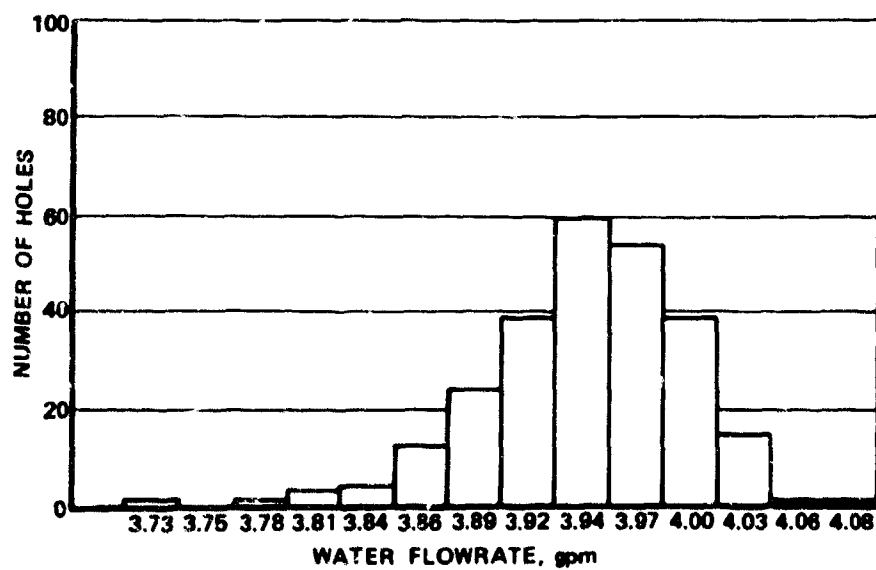


Figure 364. Normal Distribution Curve of Effective Area With A Narrow Range (8.9%) Total Band

FD 38367

Because the fuel hole size was dimensionally correct and thus could not explain why the summation of individual hole A_{cd} 's was low, it was decided to calibrate the fuel faceplates on GN_2 . The effective area obtained from GN_2 flows was 25% higher than water flow A_{cd} for both plates. From the above information it was concluded:

1. GN_2 A_{cd} more closely approximates GH_2 A_{cd} than H_2O A_{cd}
2. The difference between A_{cd} from GN_2 vs A_{cd} from water for the new plate is accountable to sharp leading edges on both plates
3. The A_{cd} for both plates will be very near design target.

Therefore, no modifications were made to either plate.

d. Injector Assembly

Before assembly of the injectors was begun, an element selection for both assemblies was made on the basis of a mixture ratio computed from water flows of the oxidizer elements and the faceplate orifices. Individual fuel locations were matched with an oxidizer element to within 0.69% of constant mixture ratio as limited by the lowest measurable flow increment. Proper braze fits for each joint at each location were verified from inspection records. The originally planned fabrication sequence is shown in table XXXII. Figure 365 shows the four braze joints of the injector assembly numbered in the order of the braze cycle. Fabrication of the second injector was postponed pending successful brazing on the first assembly. The element-to-housing braze of the first injector was run in hydrogen at 2385-2395°R for 10 minutes. Sixty of the 253 joints were void of braze because the braze material crept up the tube and plugged the primary slots. Fortunately, these tubes were removable by hand. It was thought that lack of contact between the braze wire and housing counter-bore promoted preferential wetting of the element. For the rebraze, new constant mixture ratio elements were selected and fitted into the housing through the double loop braze wires that were firmly snapped in the housing counterbores. As an added precaution, heat shields were placed over the elements to prevent a radiation temperature gradient between the elements and the housing during the braze cycle. No change was made to the cycle. Inspection of the rebraze revealed four braze voids similar to those in the first braze cycle. A second rebraze using the same corrective action was made and resulted in all good joints.

Table XXXII. First Preburner Injector

Braze Joint Location	Braze Alloy	Alloy Melt Temperatures, °R		Heat Cycle Temperatures, °R
		Solidus	Liquidus	
Element to Housing	PWA-698 Gold-nickel	2195	2210	2385-2395
Element to Divider Plate	PWA-698 Gold-nickel	2195	2210	2260-2270

Table XXXII. First Preburner Injector (Continued)

Element to Housing Seal	PWA-698 Gold-nickel	2195	1750	2240-2250
Element to Rigimesh	PWA-707 Silver	1880	2100	2180-2190
Precipitation Heat Treat				1785 for 8 Hours 1610 for 8 Hours

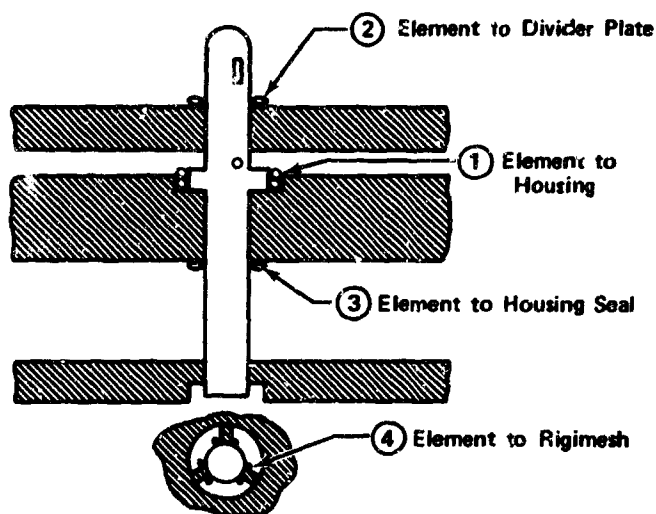


Figure 365. Four Braze Joints of the Injector Assembly

FD 31519A

The divider plate was then installed over the elements with a press tool that contacted the plate at various points to equally distribute the load. Measurements were taken to ensure the plate was fully seated. Braze rings were loosely fitted around each element and a 1/16 in. diameter braze wire was tack welded to the plate-housing interface for the braze made at 2260 to 2270° R for 10 minutes in GH₂. All braze joints were good after one cycle.

The third braze was for the element-to-housing joint on the fuel cavity side. This joint, designed to guarantee an oxidizer-to-fuel seal, was accomplished using braze wires loosely fitting around each element and run in GH₂ at 2240 to 2250° R for ten minutes.

Post-braze inspection revealed 20 of the fillets were incomplete and many appeared porous. It was concluded that gas, trapped by the first element-to-housing braze, was created causing the porous condition.

A helium leak check of the element-to-housing joint, which the first and third braze operations formed, showed no leak at 50 psig. Because the leak check was successful and adequate fillets on the oxidizer side of this joint had been formed, no attempt was made to correct the low quality fillets on the fuel side of the joint. A helium leak check of the element-to-divider plate joint revealed helium leaks in five locations. These leaks were believed to originate

under the plastic cap that sealed the secondary slot during the leak check and not from the braze joint itself. However, if the leak was from the braze joint, it would leak from primary to secondary, and would not be of sufficient quantity to affect the flow split.

A check of the grain structure of the first injector prior to the Rigimesh face braze revealed varying amounts of eta phase in the Inconel 718 structure. The injector was returned through a 2210°R heat treatment for two hours in an effort to place the eta phase back into solution. The maximum heat treat temperature was limited to 2210°R because the gold-nickel brazed material used to braze the elements in place has an initial liquidus temperature of approximately 2210°R. It would be undesirable to hold the part for two hours at a temperature above the initial melting temperature of the braze material. The cooldown from the heat treat temperature of 2210°R was modified to accomplish a 40° F/minute or greater. Rapid heating and cooling rates in the 1960° to 2160°R range, where eta phase is expected to form, were achieved by hot loading into a hot oven and extra cooling fans, and hydrogen purge.

A check of the injector grain structure as seen in figure 366 after the 2210°R heat treatment showed no change in the condition of the eta phase present before heat treat. Because of the limitation on maximum heat treat temperature imposed by the braze joint, no further solution heat treating to eliminate the eta phase was performed.

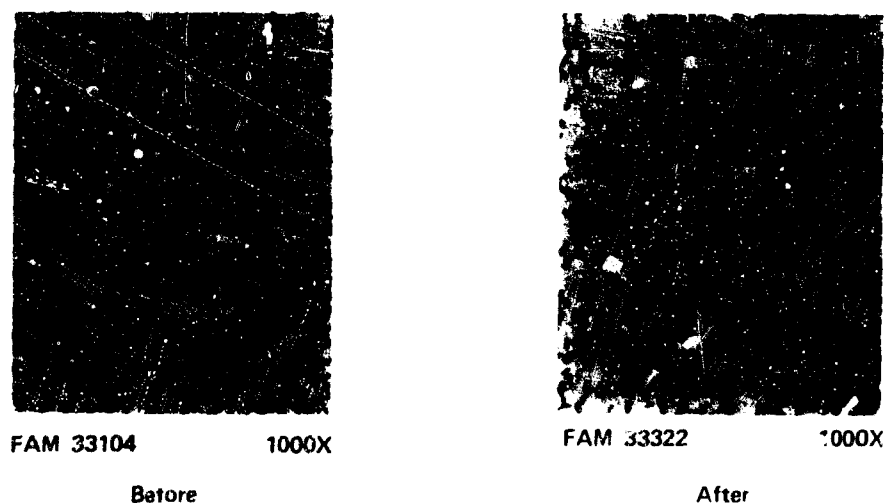
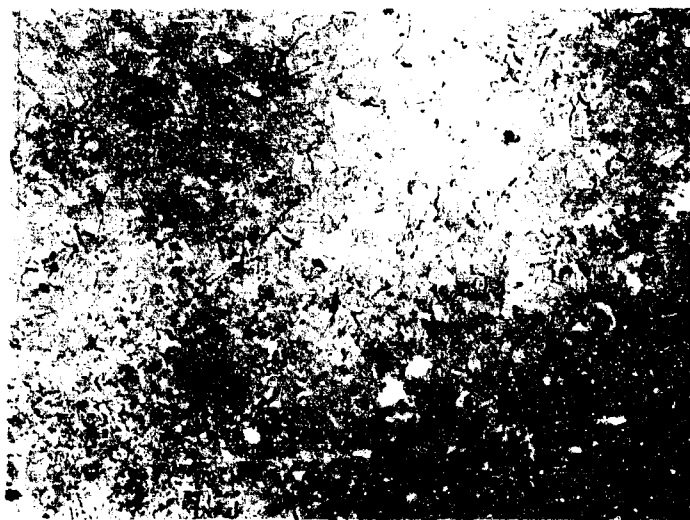


Figure 366. (Injector Grain Structure) Microstructure FD 38372
of Injector Housing Before and After
Solution Heat Treatment

In preparation for the faceplate braze, the silver plated fuel seal was tack welded to the housing to the depth for adequate seal preload before the faceplate was pressed over the tubes. Braze material for the tang-to-element joints was applied as horseshoe shaped wires over the tangs. The braze cycle (2185°R for 10 minutes) was combined with the precipitation heat treat cycle to reduce setup time. Post-braze inspection showed 67 voids, which was considered acceptable.

An inspection of the injector grain structure by the Materials Laboratory revealed a satisfactory precipitation of the strengthening gamma prime phase as seen in figure 367. The amount of eta phase had increased a small amount in one of the three forgings that form the injector assembly.



1000X

FAM 33524

Figure 367. Microstructure of Injector Housing After Faceplate Braze and Precipitation Heat Treatment

The first injector had the elements cut to the proper length using the elox process. This completed all the machining required for the injector. Proof pressure tests were then conducted on the injector at an ambient temperature to 1.2 times the maximum operating pressure reduced by ratio of yield strength at ambient temperature to yield strength at operating temperature.

The injector was then water flowed to check the effective flow area. The water flow of the oxidizer side of the injector showed the overall secondary A_{cd} to be 3.8% above target and the primary A_{cd} to be 10.7% below target. Both were considered acceptable.

The overall fuel A_{cd} was 17% lower than expected on water flow. The A_{cd} (3.05 in²) across the faceplate was 15.9% lower than was expected from the individual fuel hole water flows. The fuel side of the injector was also flowed on gaseous nitrogen for correlation with water flow data. As had been expected, the combination inlet, manifold, and cross-over hole A_{cd} was 6% higher and the fuel faceplate A_{cd} was 18.5% higher with gaseous nitrogen than with water. The gaseous nitrogen flow verified the low fuel plate A_{cd} obtained with the water flows.

A closer inspection of fuel flow area revealed an accumulation of braze material in the fuel slot as shown in figure 368. This braze accumulation was expected to be the cause of the low fuel plate A_{cd} . A hand held broach type tool was used on the injector fuel slots to remove the excess braze material without removing any material from the fuel slot itself. Burrs created by the removal of braze material were removed in an acid solution.

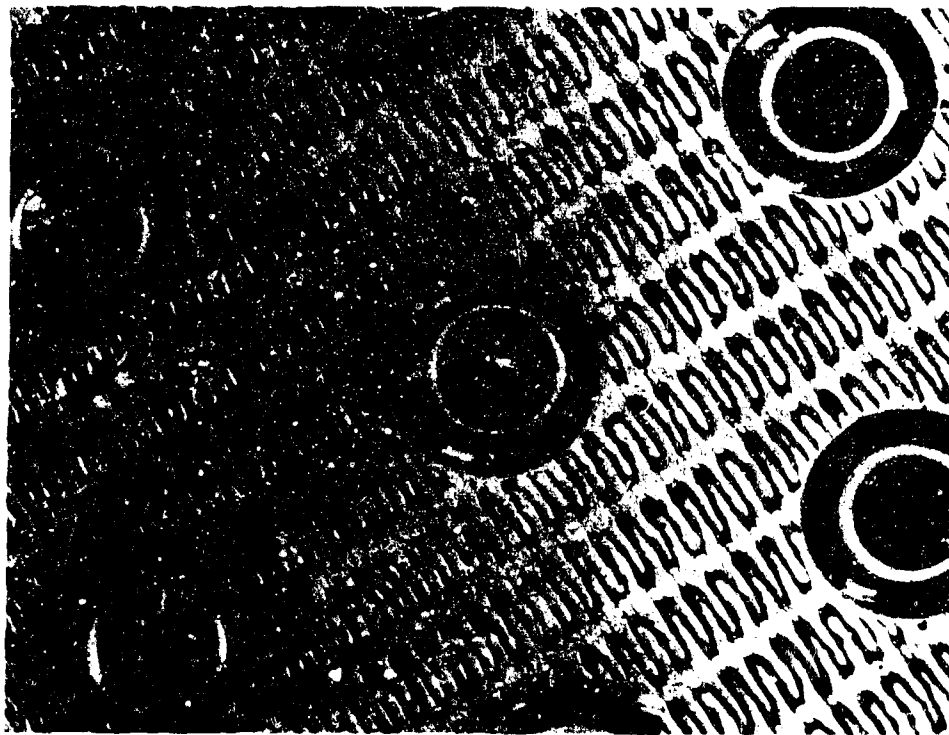


Figure 368. Braze Material in Fuel Slots

FE 87393

A visual inspection of the first injector was made after the braze material had been removed with a hand held broach tool and chemical deburr. The inspection revealed that some braze blockage in the fuel flow area still existed. The fuel side of the injector was water flowed to determine the effectiveness of the mechanical braze removal process. The fuel A_{cd} was only 6% higher than before, which was unacceptable.

To remedy the braze blockage, the braze was completely etched away in a nitric acid bath. The faceplate was removed and visual inspection of the parts did not reveal any braze remaining in the fuel flow area.

The faceplate was returned to the injector and mechanically held in place by a tool supporting the face at the outer edge. A water flow of the injector showed a fuel A_{cd} (2.95 in²) only 2.7% lower than the summation of the individual fuel hole calibration and was considered to be the more accurate baseline flow for water. A gaseous nitrogen calibration of the first injector with the face held on by the tool showed the face A_{cd} to be 15% higher than the same test using water as a calibration fluid.

Conclusions obtained from injector flow tests were:

1. Gaseous nitrogen produced an A_{cd} 25% higher than the A_{cd} obtained with water when the fuel holes were individually flowed

2. Gaseous nitrogen produced an A_{cd} 15% higher than the A_{cd} obtained with water when the injector assembly was flowed with the face clamped on
3. The water A_{cd} 's of the fuel face, when individually flowed, agree with the injector assembly water A_{cd} when the face is clamped on
4. The water CD on the present injector was much lower than the observed hot firing CD from the Supporting Data and Analysis (SDA) injector testing.
5. The water and hot firing CD's on the Supporting Data and Analysis (SDA) injector were relatively high (above 0.8).

Table XXXIII lists the various A_{cd} combinations that could develop and their effect on fuel pressure drop. Because it was expected that hydrogen would act more like nitrogen, combination 3 was judged to be most probable. It was decided to rebraze the faceplate without any area changes and to modify fabrication procedures to eliminate braze blockage. Because of this question, it was decided to further postpone fabrication of the second injector until the first injector was hot fired and the true face A_{cd} determined.

In preparation for the braze cycle, the injector was solution heat treated at 2210°R for one hour. A microanalysis of the housing after the solution cycle, as seen in figure 369, showed the housings to be in the best solution condition since microanalysis began. The percentage of eta phase, over-aging and lack of recrystallization was reduced significantly.

Two actions were taken to eliminate the braze blockage. First, during the next faceplate braze cycle, the braze "horseshoes" were chemically etched from 0.020 in. diameter to 0.010 in. diameter, reducing the braze material by a factor of four. Ceramic spacers were made to position the horseshoes at the tang-to-tube joint. The injector was brazed at 2185°R for 10 min and precipitation heat treated by the same combination cycle previously used. Inspection of the faceplate showed the completed braze to be unacceptable. Approximately 13% of the braze joints were void, or partially void of braze material. Approximately 43% of the fuel holes had visually discernible braze material blockage. The braze material had not satisfactorily wet the mating hardware, and in some cases, the braze appeared not to have properly melted.

This situation led to melt and alloy testing of the PWA 707 braze wire used for the brazes. It was shown there was no difference in chemical composition for the 0.010 in. diameter and 0.020 in. diameter wires and that the material had significantly better wetting characteristics at temperatures above 2210°R. It was then decided to combine the solution heat treat for one hour at 2210°R with the braze at 2245°R for 10 min in an attempt to melt and properly run the braze material. The injector was furnace brazed again with the combined cycle. Visual inspection of the braze joints after braze cycle showed the braze joint to be good. There was no discernible braze blockage in the fuel flow area and only three braze voids existed.

The injector was flow calibrated on water. The fuel faceplate A_{cd} and overall fuel A_{cd} was the same as the A_{cd} 's obtained when the faceplate was clamped on with no braze at faceplate joint. The oxidizer primary and secondary A_{cd} 's were the same as when originally calibrated.

Table XXXIII. Preburner Fuel Area Calibration

Combination Number	$\frac{A_{cd}}{A_{cd}} \frac{\text{Manifold}}{\text{Face}}$	Calculated Overall A_{cd}	Percent Over- all A_{cd} From Target	Percent Overall ΔP From Target	Remarks
1	$\frac{7.07}{2.95}$	2.72	-21.8	+60.5	1. Manifold A_{cd} from average water flow data. 2. Face A_{cd} from water flow with face clamped on.
2	$\frac{7.43}{3.10}$	2.86	-17.8	+46.6	1. Manifold A_{cd} of 7.07 increased by 5% based on SDA tests. 2. Face A_{cd} of 2.95 increased by 5% based on SDA tests.
3	$\frac{7.43}{3.40}$	3.09	-11.2	+25.9	1. Manifold A_{cd} of 7.07 increased by 5% based on SDA tests. 2. Face A_{cd} from GN_2 flow with face clamped on.
4	$\frac{7.43}{3.80}$	3.38	-2.8	+5.2	1. Manifold A_{cd} of 7.07 increased by 5% based on SDA tests. 2. Face A_{cd} from summation of individual GN_2 flows.
5	--	Measured 2.65	-23.8	+72.5	Overall A_{cd} from water flow with face clamped on.

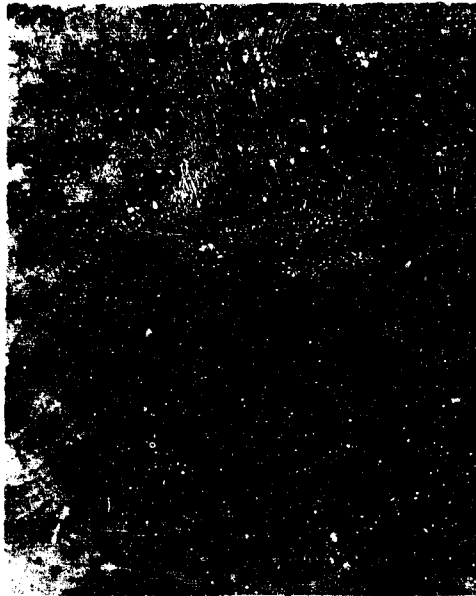


Figure 369. Microstructure of Injector Housing After FD 38374
Final Solution Heat Treatment Before
Rebrazed of Faceplate

The injector was precipitation heat treated and a microanalysis was made. The microstructure remained acceptable and the injector was then ready for rig testing.

After six hot firings on the No. 1 injector as described in the test section, it was decided to start the assembly of the second injector, taking additional steps to ensure that no braze blockage of the primary holes occurred. In preparation for continuing the injector assembly, injector housing was solution heat treated at 2360°R for one hour. Heating and cooldown rates of 40°F/minute or greater were used for this solution cycle.

All process changes developed during fabrication of the first assembly were incorporated, plus two new changes 1) using chromium chloride stop-off material around the primary slots and 2) electron-beam welding of the divider plate to the housing. Both of these changes were incorporated to prevent braze blockage of the primary slots. Table XXXIV summarizes processes originally planned for fabrication of the second injector. The first three gold-nickel braze joints, element-to-housing, element-to-divider plate, and element-to-housing seal were made without problem according to the original schedule. Gas flows of the individual primary slots showed that none had become plugged with braze material and during the braze cycles, and helium leak checks of element-to-housing joints showed all to be leak free.

Before the fuel faceplate was assembled for brazing, two modifications were made to the housing. The thermal relief slots as put in the first injector were incorporated and the housing was machined to accept a positive-type faceplate seal designed to withstand greater manifold injection pressures than the seal used in the first injector. Figure 370 shows a cross section of the new seal configuration.

Table XXXIV. Original Fabrication Sequence

Braze Joint Location	Braze Alloy	Alloy Melt Temperature, °F		Heat Cycle Temperature, °R
		Solidus	Liquidus	
Element to Housing	PWA 698 Gold-nickel	2195	2210	2285 - 2245
Element to Divider Plate	PWA 698 Gold-nickel	2195	2210	2260 - 2270
Element to Housing Seal	PWA 698 Gold-nickel	2195	2210	2340 - 2350
Solution Heat Treat	- -	- -	- -	2210 for 1 hr
Element to Rigimesh	PWA 707 Silver	1880	2100	2240 - 2250
Precipitation Heat Treat	- -	- -	- -	1785 for 8 hr 1610 for 8 hr

The faceplate braze was done as the last successful cycle of the first injector, i.e., 0.010 in. diameter braze wires, ceramic holders, solution-heat treated at 2210°R for one hour, brazed at 2245°R for 10 min, and then precipitation heat treated. Inspection revealed accumulation of braze material at many locations, 165 voids or non-brazed joints, and traces of contamination on the face. It was later determined that grinding fluid that had seaked into the ceramic holders caused the contamination which was probably responsible for many of the braze voids.

It was then decided to clean the injector by using GH₂ at 2245°R for one hour. Inspection showed only 75 voids remaining, but most of the blockage and all of the contamination had been cleaned away.

Because 75 voids would jeopardize the strength of the plate, it was decided to rebraze the injector just as the first cycle, including precipitation, except that verified clean ceramic holders would be used. Post-braze inspection revealed there were still 42 voids, none of which were newly created.

Because of such limited success with these brazes, further investigations were made to check the wettability of the silver braze material to N-155 Rigimesh. During the time required to prepare these braze samples, the injector was taken to an outside vendor for electron-beam welding of the divider plate and fuel plate seal to the housing and Rigimesh. The vendor also ran samples to investigate electron-beam welding of the braze voids which proved unsatisfactory because the joint could not be uniformly heated.

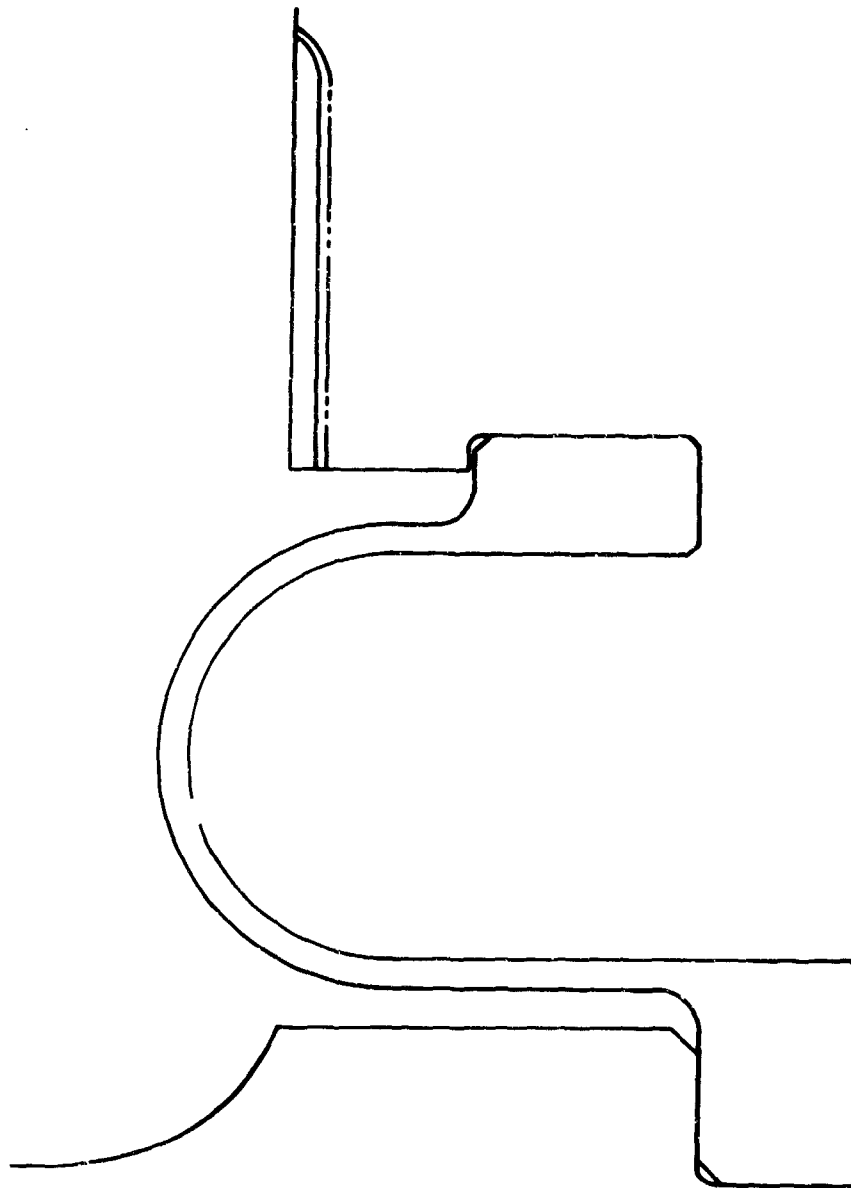


Figure 370. Cross Section of the New Seal Configuration FD 40252

Evaluation of the braze samples and further study of the braze technique led to the following conclusions and recommendations:

1. A diameter of 0.020 in. does not wet as completely as 0.010 in. diameter wire
2. Wetting of the 0.010 in. diameter wire was good except for slight film of contamination
3. High temperature silver flux would remove contamination already present at the braze voids

4. Abrasive cleaning of the 0.010 in. wire would remove any surface film and contamination
5. Use of ceramics was not advisable because of the possibility of contamination.

The injector was then successfully rebrazed at 2245°R for one hour using abrasively cleaned 0.010 in. diameter wires that were secured without ceramic holders, at the end of this braze cycle no braze voids existed, and the fuel flow area was free of braze blockage. After braze acceptability was determined, the injector was precipitation heat treated.

At this time evaluation of hot run data indicated a need to reduce the heat flux on the chamber wall. Another FRDC combustion rig program (NASA) showed that scarfed oxidizer elements would reduce the heat flux to the chamber walls by 50%.

The scarfed injector face pattern was concentric ring design, and the outer row, which composed 42% of the elements, was scarfed at a 45 deg angle. The second row which contained 28% of the elements was scarfed at a 22-1/2 deg angle.

A scarfed element is made by cutting the element exit at an angle to the element axis. The scarfed element does two things that contribute to reducing heat flux on the chamber wall:

1. Shifts the injected cone axis away from the chamber wall.
2. Changes the mass distribution from the element so that less mass is injected adjacent to the chamber wall.

It was therefore decided to scarf the elements of the second preburner injector through the three outer rows. The third row of injector was chosen as the stopping point because the hot firing data indicated a fall-off in combustion temperature in line with the third row of elements. Thus scarfing the outer three rows of elements should shift oxidizer mass into the low temperature region.

The outer three rows of elements contain 50% of the total elements in the second injector. The outer row was scarfed at a 45 deg angle, the second row at 33-3/4 deg and the third row at 22-1/2 deg as shown in figure 371.

The injector flange and O-ring grooves were then remachined to correct warpage experienced during the several heat cycles.

The final operation was a proof pressure test planned to 5450 psi or 1.2 times maximum operating pressure ratioed by strength differences from temperature. A proof factor of only 1.035 was achieved because outer fiber stresses in the inlet horn had locally reached 183,000 psi, the proportional limit, and local yielding was not felt advisable at this time. The injector was then through fabrication and ready for inspection and rig use.

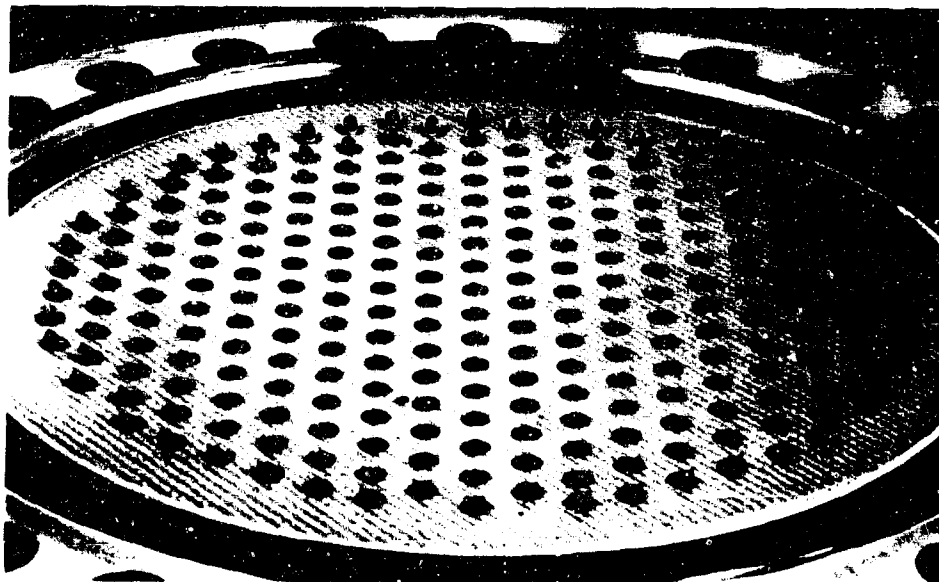


Figure 371. Outer Three Rows of Oxidizer Elements FDC 37431
Elements Scarfed on Second Injector

e. Preburner Torch Igniter

The cover, piston ring, and sleeve were machined from Inconel 718. The chamber was made from a copper alloy AMS 9550. The chamber and spark exciter were all brazed to the housing.

5. Testing

a. Test Set-Up

Figure 372 shows a cross section of the preburner injector test rig consisting of the Bill-of-Material preburner oxidizer control valve and injector, and adapted Phase I combustion chamber assembly.

Major components of the preburner injector test rig are fastened by high strength studs and bolts. Previously, studs were loaded by hydraulic rams while strain was monitored by strain gages. Because this method was expensive and time consuming, it was decided to develop a simpler method.

Tests were conducted to determine the accuracy of angle-of-turn, torque, and bolt elongation measurement methods. The first series of tests was made on a 250K Phase I dome, preburner injector, and combustion chamber fastened by 18 1-in. diameter PWA 1010 studs that were all strain gaged. The second test series was made on a 250K Phase I combustion chamber and backpressure simulator joined by forty-eight 5/8 in. diameter studs, 24 of which were strain gaged. The accuracy of each loading method was determined from maximum to minimum load deviations among the strain gaged studs.

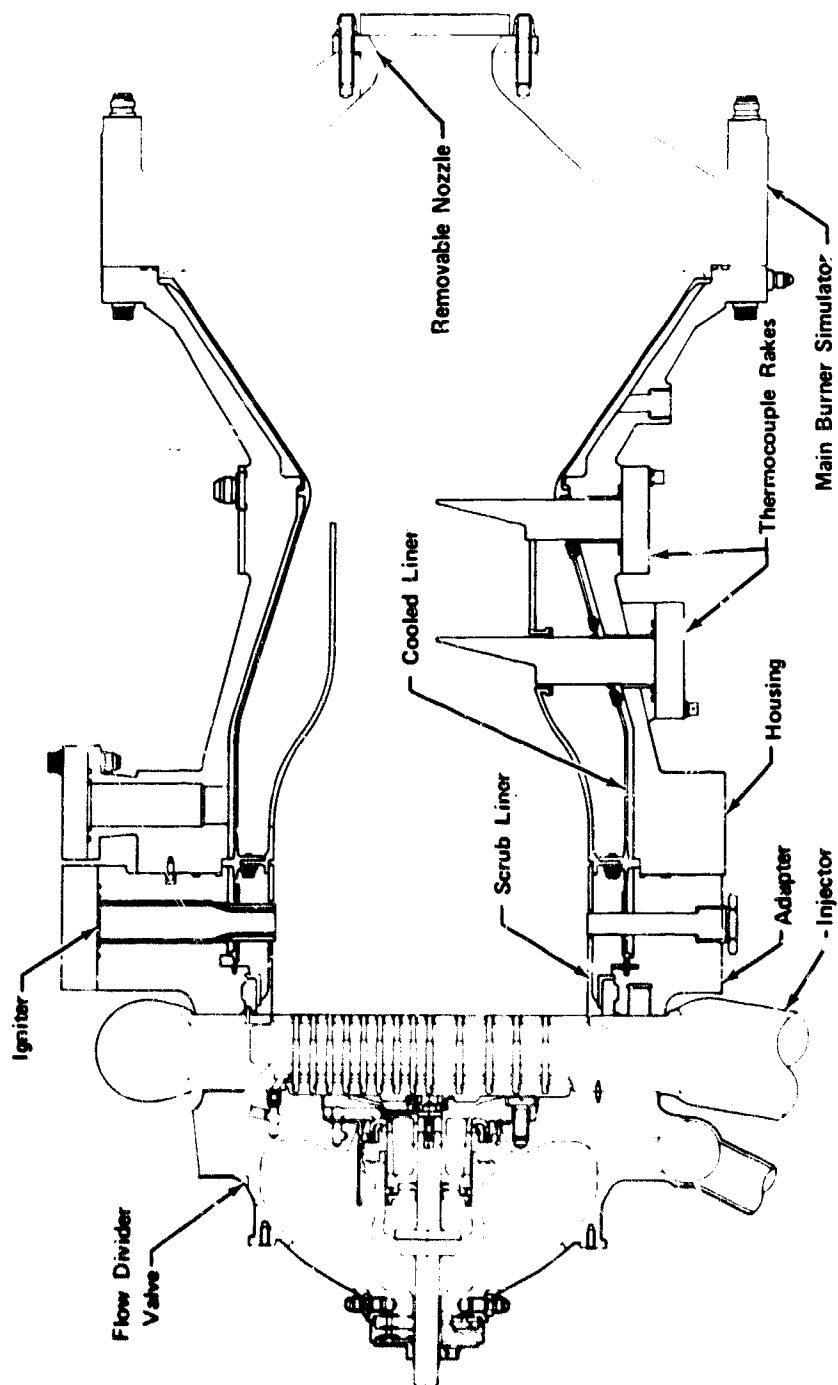


Figure 372. Preburner Test Rig

FD 31511A

The tests were accomplished by first torquing the nuts until the seal was just compressed and when any additional turning would result in bolt strain. From this point, the nuts were loaded through incremental angles of turn. The angle-of-turn was measured by a pointer attached to the loading wrench that moved across a protractor positioned around the stud. At each angle-of-turn level, nut torque, bolt deflection, and stud strain were recorded.

Figure 373 shows the total load deviation obtained by angle-of-turn is 20% in the range of interest. Figure 374 shows that elongation deviation at all average stress levels is greater than actual load deviations shown in figure 373. Finally, figure 375 shows large torque deviations, as high as 90%, at all stress levels.

It was concluded that (1) torque loading was too inaccurate, (2) elongation measurement was not as accurate as angle-of-turn measurement and (3) angle-of-turn loading was sufficient where total load deviations within 20% were acceptable.

As a result of the trial angle-of-turn tests, it was decided to use the angle-of-turn method to load all bolts holding major components on the preburner rig. Initial calibrations with strain gages were used to determine the angle-of-turn required for the various bolts used in the rig. Table XXXV lists the angle-of-turn required to load the bolts for the preburner rig.

The preburner oxidizer control valve, a redesigned, lightweight version of the Phase I test item, is bolted to the injector by Bill-of-Material studs which are loaded by angle-of-turn methods. High strength Inconel adapters between the Bill-of-Material flanges and mild steel facility propellant lines are required to keep bending loads within limits.

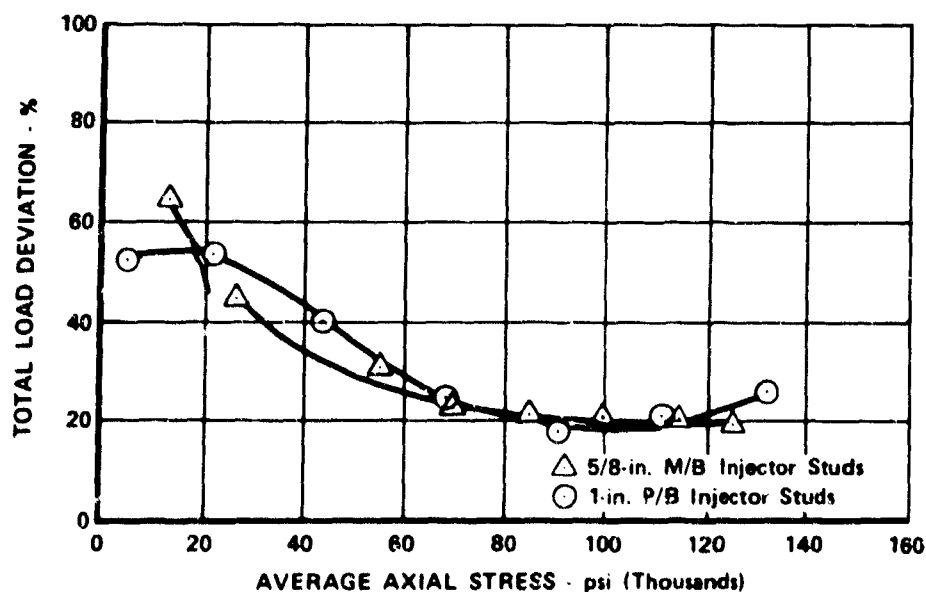


Figure 373. Angle-of-turn Load Deviation vs Axial Stress

FD 45906

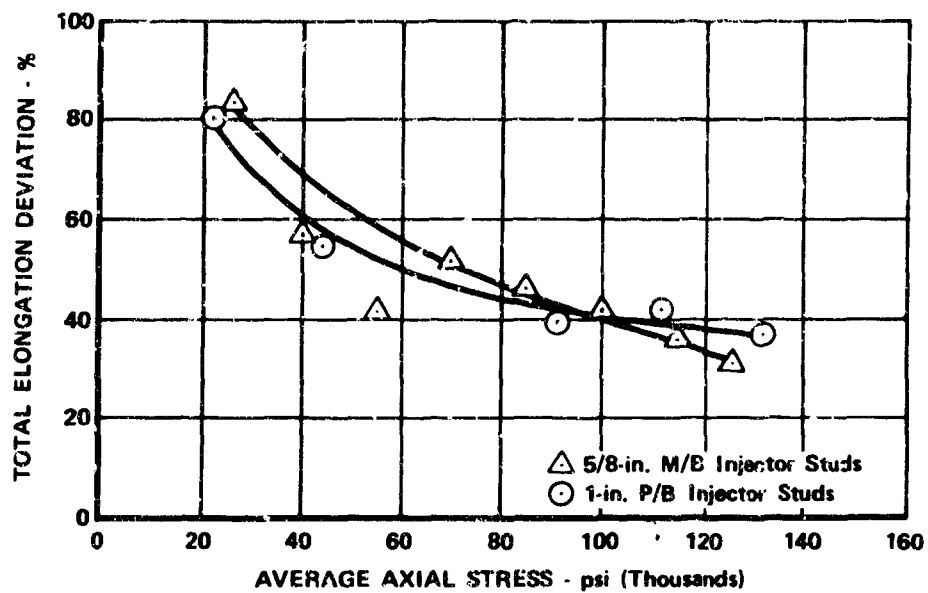


Figure 374. Bolt Elongation-Deviation vs Axial Stress

FD 45907

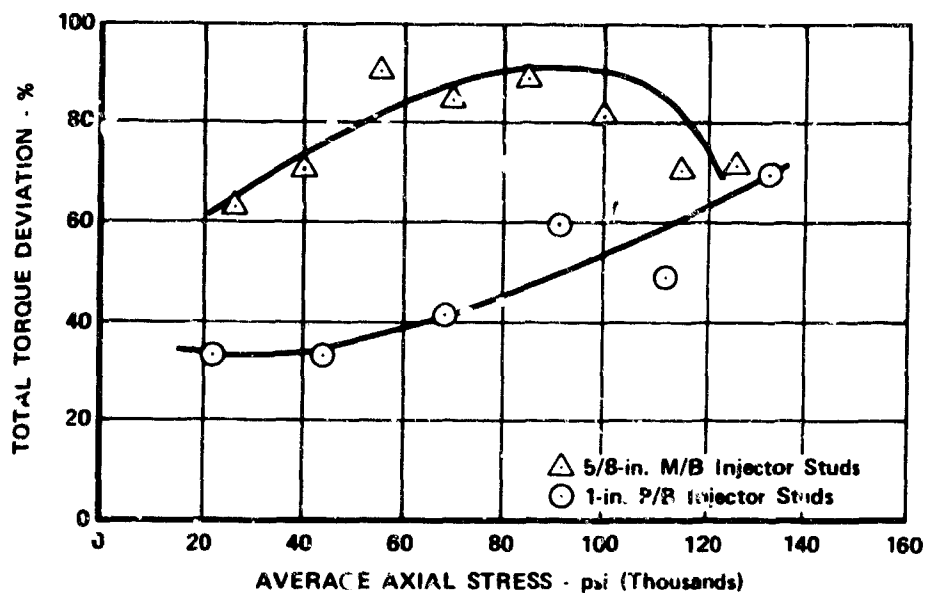


Figure 375. Bolt Torque Deviation vs Axial Stress

FD 45908

Table XXXV. Bolt Loading Requirements for Preburner Rig

Location	Desired Bolt Load (lb _f)	Torque (lb _f)	Angle-of-Turn (deg)
Injector-Oxidizer Valve-Adapter	32,000	500	180
4 in. Adapter-Combustion Chamber	69,000	500	95
Combustion Chamber-Backpressure Simulator	29,600	500	250
Injector-Fuel Inlet Adapter	14,350	500	75

Another Inconel adapter was required for the fuel inlet flange of the injector. The studs attaching the preburner oxidizer valve and injector are threaded into the 4 in. Inconel spacer adapting the injector to the existing Phase I combustion chamber.

Principal components of the combustion chamber assembly are (1) the 4 in. spacer previously mentioned, (2) the chamber shell, (3) the exhaust back pressure simulator, (4) chamber shell coolant liner, (5) uncooled combustion liner simulating those in the Bill-of-Material preburner duct, and (6) temperature rakes in the 11 in. and 15 in. planes from the injector face. Combustion instrumentation is located in the spacer section, duplicating positions used for Phase I and SDA testing.

b. Instrumentation

Table XXXVI lists typical instrumentation for both the test rig and facility. Locations of rig instrumentation including rake thermocouples are shown in figure 376.

For rig protection, several parameters are monitored for critical operational levels by advance or abort comparator circuits. Excessive combustion temperature is monitored by advance and abort circuits on characteristically hot rake thermocouples and skin thermocouples on both combustion liners. Low combustion temperature advance circuits are similarly linked to the rakes and igniter temperature probe. Purge protection to the oxidizer secondary during primary only operation is assured by an advance level for minimum helium venturi upstream pressure. Structural integrity for the valve and injector is maintained by advance circuits for excessive differential pressure between the dome and the injector secondary cavity and for excessive differential pressure between the injector fuel manifold cavity and the combustion chamber.

High response Kistler transducers, to monitor injection and combustion stability, are used in the oxidizer dome, secondary, and primary cavities, in the fuel manifold, and in the combustion chamber.

c. Test Plan

Objectives of the original preburner injector test program were to conduct tests and perform the analyses of these tests to evaluate temperature profile, combustion stability, combustion efficiency, engine start evaluation, and durability. Seven tests were planned to achieve the above objectives and are outlined in table XXXVII.

Table XXXVI. Preburner Instrumentation

I.	Pressure				
	Description	Number of Trans- ducers	Digital Computer Channels	Strip Charts	Oscillo- graphs
A.	Oxidizer				
	Preburner Flowmeter Upstream	1	1	1	1
	Pump Simulator Upstream	1	1		
	Pump Simulator Downstream	1	1	1	
	Dome Cooldown Vent Orifice Upstream	1	1	1	
	Dome Vent Orifice Differential	1	1	1	
	Preburner Filter Differential	1	1		
	Dome Inlet Pressure	1	1		
	Dome-Chamber Differential	1	1		
	Injector Primary	1	1	1	1
	Injector Primary Differential	2	2		1
	Injector Secondary	1	1	1	1
	Injector Secondary Differential	2	2		
B.	Fuel				
	Gas Bottle Discharge	1	1		
	Preburner Liquid Flowmeter Upstream	1	1		
	Preburner Gas Flowmeter Upstream	1	1		
	Pump Simulator Upstream	1	1		
	Premixer Liquid Inlet	1	1		
	Premixer Gas Inlet	1	1		
	6-in. Mixer Liquid Inlet	2	2		
	6-in. Mixer Gas Inlet	1	1		
	6-in. Mixer Discharge	1	1		
	Pump Simulator Upstream	1	1		
	Mixer Vent Upstream	1	1	1	
	Mixer Vent Differential	1	1		
	Filter Upstream	1	1		
	Filter Differential	1	1		
	Injector Manifold	2	2	1	1
	Injector Differential	1	1	1	1
C.	Combustion				
	Combustion Chamber	6	6	1	1
	Torch Igniter Chamber	1	1		

Table XXXVI. Preburner Instrumentation (Continued)

		Number of Trans- ducers	Digital Computer Channels	Strip Charts	Oscillo- graphs
I.	Pressure				
	Description				
D.	Miscellaneous				
	Igniter Fuel Supply	1	1	1	
	Downstream Cooling Liner Orifice Differential	1	1		
	Downstream Cooling Liner Supply	1	1	1	
	Igniter Oxidizer Supply	1	1	1	
	Pressure Channels:				
	43 Power Supplies				
	43 Digital				
	10 Strip Chart				
	8 Oscillographs				
II.	Temperature				
	Description				
A.	Oxidizer				
	Run Tank Discharge	1	1		
	Preburner Flowmeter Upstream	1	1		
	Pump Simulator Upstream	1	1	1	
	Preburner Filter Inlet	2	2		
	Pump Simulator Vent Upstream	1	1		
	Dome Vent Upstream	1	1	1	
B.	Fuel				
	Liquid Tank Discharge	1	1		
	Preburner Liquid Flowmeter Upstream	1	1		
	Preburner Gas Flowmeter Downstream	1	1		
	Pump Simulator Upstream	1	1	1	
	6-in. Mixer Liquid Upstream	1	1		
	6-in. Mixer Gas Inlet	1	1		
	Mixture Discharge	1	1	1	
	Mixture Vent Orifice Upstream	1	1		
	Fuel Inlet Temperature	1	1		
C.	Combustion				
	Combustion Temperature Rakes	26	26	4	2
	Igniter Combustion Probe	1	1	1	1
D.	Internal				
	Combustion Chamber Cooling Liners	10	10	2	
	Igniter Liner	2	2	1	

Table XXXVI. Preburner Instrumentation (Continued)

II. Temperature		Points of Measure- ment	Digital Computer Channels	Strip Charts	Oscillo- graphs
Description					
E.	Nitrogen Jacket				
	Oxidizer Lines	2	2		
	Fuel Lines	1	1		
F.	Miscellaneous				
	Oxidizer Sampling System	1	1		
	Temperature Channels:	60			
	RSMT Channels:	14			
	CC Channels:	45			
	Strip Charts:	12			
	Oscillographs:	3			

III. Miscellaneous		Points of Measure- ment	Digital Computer Channels	Strip Charts	Oscillo- graphs
A.	Flows				
	Oxidizer Volumetric, Coil No. 1	1	1		1
	Oxidizer Volumetric, Coil No. 2	1	1		
	Oxidizer Volumetric Flow Counter	1	1		
	Liquid Hydrogen Volumetric, Coil No. 1	1	1		
	Liquid Hydrogen Volumetric, Coil No. 2	1	1		
	Liquid Hydrogen Volumetric Flow Counter	1	1		
	Gaseous Hydrogen Volumetric, Coil No. 1	1	1		
	Gaseous Hydrogen Volumetric, Coil No. 2	1	1		
	Gaseous Hydrogen Volumetric Flow Counter	1	1		
B.	Thrust				
	Load Cell No. 1	3	3		
	Load Cell No. 2	3	3		
	Load Cell No. 3	3	3		
	Master Load Cell	3	3		
C.	Position Indication				
	Rig Valves	2	2	1	2
	Stand Valves	14	14		14
D.	Voltages				
	Igniter Spark Indication	1			1
	Igniter Spark Voltage	1	1		1
	Start Signal	1	1		1
	Advance to Shutdown Signal	1	1		1

Table XXXVI. Preburner Instrumentation (Continued)

III. Miscellaneous		Points of Measure- ment	Digital Computer Channels	Strip Charts	Oscillo- graphs
E. Combustion Stability					
Chamber Pressure Frequency		3			3
Measurement Channels:		44			
Digital Channels:		40			
Strip Charts		1			
Oscillograph Channels:		24			

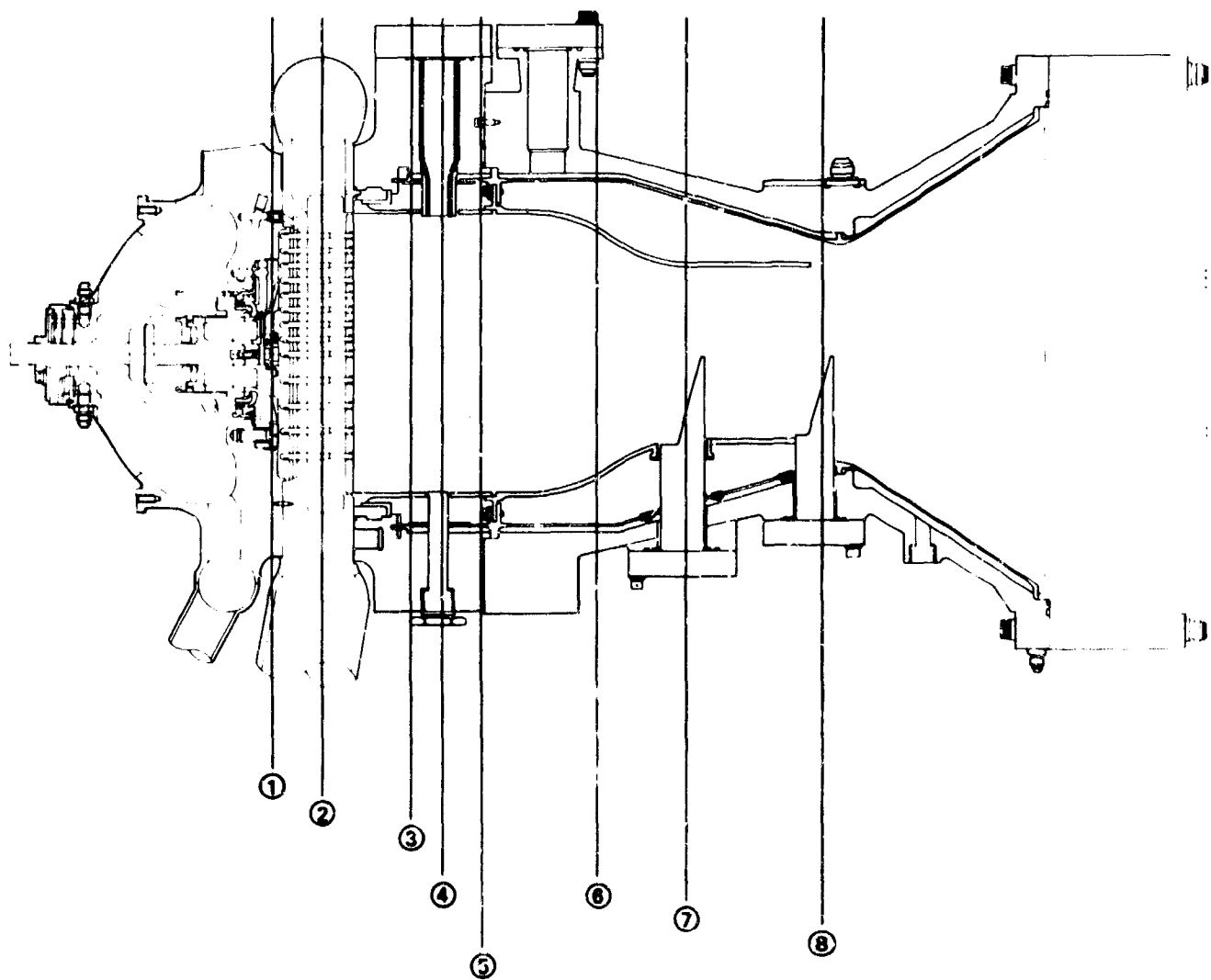
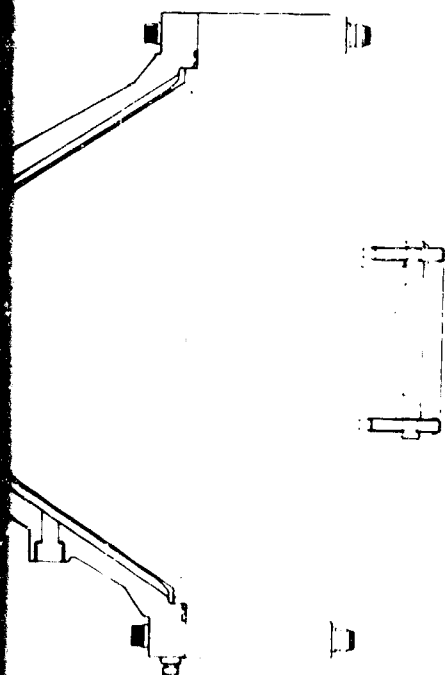


Figure 376. Preburner Rig Instrumentation



- ① Secondary Static Pressure
Primary Static Pressure
Dome Static Pressure
Secondary Kistler (2)
Primary Kistler
Secondary Temperature (4)
Secondary ΔP High
Primary ΔP High
- ② Fuel Manifold Pressure
Fuel Injector ΔP High
Fuel Kistler
Fuel Manifold Temperature
- ③ Scrub Liner Temperature (3)
- ④ Chamber Kistler (2)
Chamber Pressure (3)
Pulse Guns (4)
- ⑤ Igniter Combustion Temperature
Igniter Barrel Temperature
- ⑥ Cooled Liner Temperature
- ⑦ Combustion Temperature (24)
- ⑧ Combustion Temperature (40)
Chamber Pressure
Chamber Kistler

FD 38370

381 / 382

Table XXXVII. XLR129 Preburner Injector

Pretest Matrix

Test No.	Injector No.	Purpose	No. of Data Points	Engine Percent Thrust	Preburner Chamber Pressure (psia)	Preburner Combustion Temperature (°R)	Engine Preburner Mix. Ratio	Propellant Inlet Temperatures (°R) Oxidizer	Fuel	Remarks
1	1	Temperature Profile, Combustion Stability, η_c , Throttling, Mixture Ratio, Propellant Temperatures and Durability	9	20	732	1393	5 .716	200	125	Pulse
				20	719	1795	6 .950	200	147	1,3,4
				20	710	2181	7 1.185	200	166	Pulse
				35	1320	1355	5 .700	204	132	3,4
				55	1300	1740	6 .910	204	155	3,4
				35	1280	2180	7 1.170	204	177	3,4
2	1	Temperature Profile, Combustion Stability, η_c , Throttling, Mixture Ratio, Propellant Temperatures and Durability	5	50	2010	1488	5 .763	208	142	Pulse
				30	1958	1827	6 .962	207	163	3,4
				50	1915	2157	7 1.158	207	183	Pulse
				75	3280	1713	5 .89	220	159	Pulse
				75	3097	1934	6 1.021	213	172	3,4
				75	3006	2235	7 1.205	211	180	Pulse
3	1	Temperature Profile, Combustion Stability, η_c , Throttling, Mixture Ratio, Propellant Temperatures and Durability	2	100	4367	2086	8 1.112	220	183	Pulse
				100	4174	2325	7 1.261	215	197	Pulse
				10	330	1405	5 .740	180	115	3,4
4	1	Ignition, Durability	1	100	4822	2015	5 1.067	226	183	Pulse
				100	4822	2015	5 1.067	226	183	Pulse
5	1	Start Transient, Engine Shutdown and Durability	2	100	4822	2015	5 1.067	226	183	Pulse
				100	4822	2015	5 1.067	226	183	Pulse
6	2	Temperature Profile, Combustion Stability, η_c , Throttling, Mixture Ratio, Propellant Temperatures, Engine Shutdown and Durability	9	20	732	1393	5 .716	200	125	Pulse
				20	719	1795	6 .950	200	147	1,3,4
				20	710	2181	7 1.185	200	166	Pulse
				35	1320	1355	5 .700	204	132	3,4
				55	1300	1740	6 .910	204	155	3,4
				35	1280	2180	7 1.170	204	177	3,4
7	2	Temperature Profile, Combustion Stability, η_c , Throttling, Mixture Ratio, Propellant Temperatures, Engine Shutdown and Durability	5	50	2010	1488	5 .763	208	142	Pulse
				30	1958	1827	6 .962	207	163	3,4
				50	1915	2157	7 1.158	207	183	Pulse
				75	3280	1713	5 .891	220	159	Pulse
				75	3097	1934	6 1.021	213	172	3,4
				75	3006	2235	7 1.205	211	180	Pulse
8	2	Temperature Profile, Combustion Stability, η_c , Throttling, Mixture Ratio, Propellant Temperatures, Engine Shutdown and Durability	5	100	4367	2086	8 1.112	220	183	Pulse
				100	4174	2325	7 1.261	215	197	Pulse

The listed pre-burner rig conditions are taken from Design Table No. 6

* Tests 6 and 7 will be made with the No. 2 Injector to qualify its use with the transition case.

The first three preburner tests were planned to investigate the performance and temperature profile across the throttling range. These tests would incorporate procedures developed during Phase I testing and during SDA Task to achieve ignition and controlled transients to 20%, and throttling transients from 20 to 100% thrust. The test rig start sequence was to ignite and ramp to 20% thrust at conditions equivalent to engine operation at a mixture ratio of 5 and then to subsequent levels using a schedule shown in figure 377.

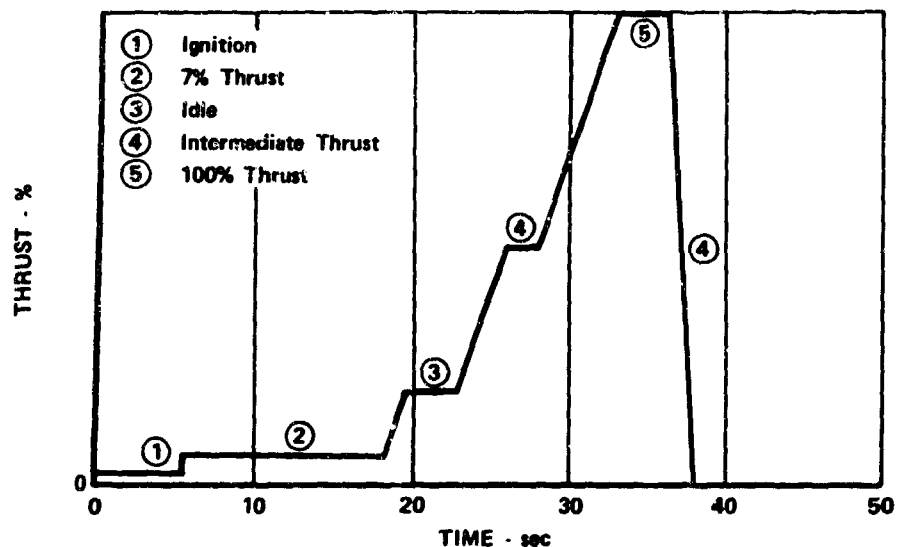


Figure 377. Test Sequence for Preburner Testing

FD 21276D

The fourth test would be a demonstration of the ability to ignite the rig with the predicted engine propellant flowrates.

The fifth test was to ignite with the propellant supply pressures at a level that will allow a pressure rise during a transient to idle that simulates the engine start transient pressure rise. The fifth test would also shut down during oxidizer purge flowrates that were planned for use in the engine.

The sixth and seventh test would be used to qualify the second preburner injector for use with the transition case by demonstrating its temperature profile and combustion stability.

d. Hot Firings

Twenty-two hot fire tests were made on five builds of preburner test rig 35131 and 36133 between 13 August 1969 and 14 February 1970. A test summary is shown in table XXXVIII. Because of problems associated with chamber wall burning and a poor temperature profile during the first six rig tests, the actual tests deviated considerably from the original test plan. A description of the objectives, results, and recommendations of each test is presented in the following section.

Table XXXVIII. Preburner Test Results

Build	Run	Preburner Chamber Pressure (psia)	Percent Thrust (%)	Engine Mixture Ratio	Average Combustion Temperature (°R)	Maximum Temperature Minus Average Temperature (°R)	Comments
Rig 35131 Using No. 1 Injector							
1	1.01	669	20	5	1306	72	Burned through uncooled scrub liner uncooled
		672	20	6	1722	98	
		673	20	7	2115	114	
		1247	35	5	1263	121	
2	2.01	693	20	5	1302	215	Uncooled scrub liner blued in same area as build 1
		691	20	6	1639	190	
2	3.01	691	20	5	1303	159	Uncooled liner blued area burned through
		700	20	6	1702	234	
		704	20	7	2090	263	
3	4.01						LOX flowmeter Error caused advance at +1.4 sec
3.	5.01						Liner thermo- couple error caused advance at +6.7 sec
3	6.01	726	20	5	1430	539	Added transpira- tion-cooled liner and two new temper- ature rakes in burned area. Burned through transpiration-cooled liner in same area as builds 1 and 2.
		741	20	6	1827	621	
		739	20	7	2297	611	
4	7.01	701	20	5	1349	216	Full duration run of 52.9 sec
		2020	50	5	1402	190	
4	8.02						Advanced at +1.4 sec due to high outer com- bustion liner tempera- ture
4	9.01						Advanced at +1.4 sec due to high outer com- bustion liner tempera- ture
4	10.02	694	20	5	1349	196	Fuel injector ΔP error caused advance at +29.1 sec
4	11.01	2032	50	5	1415	119	Full duration run of 35.0 sec
		1985	50	6	1769	155	
		1964	50	7	2106	173	
4	12.01						Outer liner temperature error caused advance at +16.4 sec
4	13.01	3283	75	5	1692	150	Outer liner temperature error caused advance at +25.0 sec
		2982	75	7	2268	244	
4	14.01	2967	75	7	2254	252	Overboard fuel leak caused advance at 30.5 sec
		4276	100	6	2050	200	

Table XXXVIII. Preburner Test Results (Continued)

Build	Run	Preburner Chamber Pressure (psia)	Percent Thrust (%)	Engine Mixture Ratio	Average Combustion Temperature (°R)	Maximum Temperature Minus Average Temperature (°R)	Comments
Rig 35133 Using No. 2 Injector							
	1.01	724.4 2071	20 50	5 5	1344 1427	280 155	Full duration run of 28.36 sec. Liners are in good condition.
	2.01						False low FHe purge pressure advance at 17.53 sec which is prior to reaching 20%/5, due to sequencer patching error.
	3.01						False high scrub liner temperature advance at 6.8 sec, which is prior to reaching 20%/5 due to incorrect voltage level setting on the comparator circuit.
	4.01						Low igniter combustion temperature at 3.1 sec prior to SSV up caused by foreign material in igniter GOX metering orifice.
	5.01	707.2 708.4 708.4 2042 1998 1964	20 20 20 50 50 50	5 6 7 5 6 7	1368 1765 2145 1429 1797 2138	207 258 275 203 217 267	Full duration run of 44 sec. Liners in good condition. Small dime sized eroded area in zone one of the transpiration liner.
	6.01						False high combustion temperature advance at 23.72 sec, which is prior to reaching the first data point caused by bad patch pin connect in the controls board. Liner still in good condition.
	7.01	2957	75	7	2190	252	False low combustion temperature advance at 26.4 sec, which is near the end of the 75% 7 data point caused by burned instrumentation cable. Liner is still in good condition.
	8.01	2964	75	7	2203	258	Manual advance at 28.2 sec, which is just prior to reaching 100% data point, because of stand fire.

Run 1.01 of the preburner test rig was programed as run 1 of the original test matrix. Test purposes were to evaluate temperature profile, combustion stability, propellant temperature effects, and hardware durability at engine mixture ratios of 5, 6, 7, and thrust levels of 20, 35, and 50%, respectively. Pulse guns were scheduled to fire at mixture ratios of 5 and 7 at 20 and 50% thrust.

The run was automatically advanced at 33.75 sec during set point at a mixture ratio of 5 at 35% thrust.

There was no chugging during the run as experienced during supporting SDA task preburner testing. An 80 grain pulse charge was fired into the combustion chamber at 20%, mixture ratio of 5. The pulse gun, programed at 20% mixture ratio of 7, failed to fire.

Three programed data points were taken at 20% thrust. After the rig was ramped to 35%, mixture ratio of 5, an external fire burned through an instrumentation lead to an automatic advance circuit and shut down the rig.

A visual inspection of the rig after shutdown revealed burn damage to the inner uncooled liner and the outer cooled liner. There was damage to the 4 in.-spacer and chamber shell and could be externally observed. The injector face was in good condition as shown in figure 378. The injector face had local discolored spots, but no metal erosion occurred. The rig was removed from the test stand for further examination of the burned liners.

In this report, only the 15-in. plane temperature distribution plots will be shown because 15 in. is more representative of the distance to the turbine first rotor from the faceplate which is approximately 19.4 in. from the injector face.

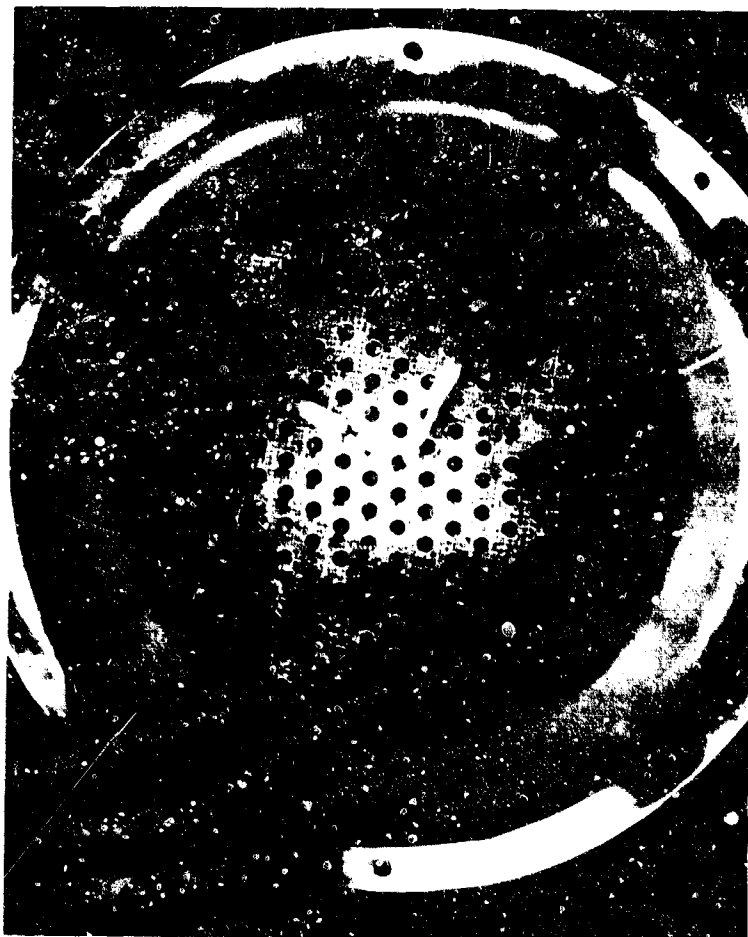


Figure 378. Injector Face With Local Discolored Spots

FF 88463

Table XXXIX shows the radial distance from the chamber centerline to each thermocouple by thermocouple position numbers.

Table XXXIX. Radial Distance of All Rake Thermocouples to Chamber Centerline

Thermocouple Position	Radial Distance From Chamber Centerline	
	Rakes No. 3, 4, 6	Rake No. 5
1	0.618	0.573
2	0.844	0.799
3	1.070	1.025
4	1.296	1.251
5	1.522	1.477
6	1.748	1.703
7	1.974	1.929
8	2.200	2.155
9	2.426	2.381
10	2.652	2.607

Note: Chamber radius is 2.821 in. at the plane of the thermocouples.

The conditions that were predicted and attained are shown in tables XL, XLI, XLII, and XLIII. The maximum-to-average temperature of 97.7°R at 2111°R average temperature at the 15 in. plane is acceptable. It should be pointed out that the majority of the liner damage, as will be discussed later, is in a quadrant of the combustor near the 5 o'clock position as viewed through the nozzle not covered by the two thermocouple rakes. The angular position of the two thermocouple rakes, viewed upstream through the nozzle, is shown in figure 379. The temperature distribution is satisfactory and is shown in figures 380 and 381.

Table XL. Predicted vs Actual Performance for 20% Thrust, Engine Mixture Ratio of 5, Rig 35131-1 Run 1.01

	Predicted	Test Results
Chamber pressure - psia	733.4	669.0
Total oxidizer flow - lb/sec	9.59	9.26
Oxidizer primary flow - lb/sec	5.367	6.57
Oxidizer secondary flow - lb/sec	4.22	2.68

Table XL. Predicted vs Actual Performance for 20% Thrust,
Engine Mixture Ratio of 5, Rig 35131-1 Run 1.01
(Continued)

	Predicted	Test Results
Total fuel flow - lb/sec	13.76	13.52
Injector Fuel Flow - lb/sec	13.38	13.30
Upper coolant liner flow - lb/sec	0.2506	0.11
Lower coolant liner flow - lb/sec	0.1832	0.12
Injector mixture ratio	0.716	0.696
Overall mixture ratio	0.697	0.684
Combustion temperature - °R	1394	1333
Flow divider valve position - %	25.8	25.4
Oxidizer injector primary ΔP	310.5	NAV
Oxidizer injector secondary ΔP	4.7	NAV
Fuel injector ΔP		
Oxidizer injector temperature - °R	200	190
Fuel injector temperature - °R	125.4	138.3
Temperature profile (11 in.) - °R	0	136
Temperature profile (15 in.) - °R	0	72
Average temperature (11 in.) - °R	1394	1353
Average temperature (15 in.) - °R	1394	1306
Oxidizer primary/total flow split	0.5596	0.60
Oxidizer primary injector $A_{cd} - \text{in}^2$	0.0550	NAV
Oxidizer secondary injector $A_{cd} - \text{in}^2$	0.3509	NAV
Fuel injector A_{cd} (Overall) in^2	3.47	NAV
η_c^* (Based on P_c , wt) - %	100	96.8

Table XL. Predicted vs Actual Performance for 20% Thrust,
Engine Mixture Ratio of 5, Rig 35131 Run 1.01
(Continued)

	Predicted	Test Results
η_c * (Based on average temperature at 11 in.) - %	100	99.1
η_c * (Based on average temperature at 15 in.) - %	100	98.0

Table XLI. Predicted vs Actual Performance for 20% Thrust,
Engine Mixture Ratio of 6, Rig 35131-1 Run 1.01

	Predicted	Test Results
Chamber pressure - psia	719.2	672
Total oxidizer flow - lb/sec	10.42	10.36
Oxidizer primary flow - lb/sec	5.674	7.38
Oxidizer secondary flow - lb/sec	4.75	2.98
Total fuel flow - lb/sec	11.30	11.23
Injector fuel flow - lb/sec	10.97	11.03
Upper coolant liner flow - lb/sec	0.2058	0.09
Lower coolant liner flow - lb/sec	0.1486	0.10
Injector mixture ratio	0.950	0.94
Overall mixture ratio	0.922	0.92
Combustion temperature - °R	1796	1741
Flow divider valve position - %	25.8	25.3
Oxidizer injector primary ΔP	346.6	NAV
Oxidizer injector secondary ΔP	5.42	NAV
Fuel injector ΔP		NAV
Oxidizer injector temperature - °R	200	191

Table XLI. Predicted vs Actual Performance for 20% Thrust,
Engine Mixture Ratio of 6, Rig 35131-1 Run 1.01
(Continued)

	Predicted	Test Results
Fuel injector temperature - °R	147.5	160
Temperature profile (11 in.) - °R	0	171
Temperature profile (15 in.) - °R	0	98
Average temperature (11 in.) - °R	1796	1741
Average temperature (15 in.) - °R	1796	1722
Oxidizer primary/total flow split	0.5445	0.598
Oxidizer primary injector A_{cd} - in. ²	0.0550	NAV
Oxidizer secondary injector A_{cd} - in. ²	0.3681	NAV
Fuel injector A_{cd} (Overall) - in. ²	3.47	NAV
η_c^* (Based on P_c , wt) - %	100	95.0
η_c^* (Based on average temperature at 11 in.) - %	100	98.5
η_c^* (Based on average temperature at 15 in.) - %	100	97.8

Table XLII. Predicted vs Actual Performance for 20% Thrust,
Engine Mixture Ratio of 7, Rig 35131-1 Run 1.01

	Predicted	Test Results
Chamber pressure - psia	710.1	673
Total oxidizer flow - lb/sec	11.08	11.1
Oxidizer primary flow - lb/sec	5.863	7.89
Oxidizer secondary flow - lb/sec	5.22	3.16
Total fuel flow - lb/sec	9.64	9.49
Injector fuel flow - lb/sec	9.35	9.33

Table XLII. Predicted vs Actual Performance for 20% Thrust,
Engine Mixture Ratio of 7, Rig 35131-1 Run 1.01
(Continued)

	Predicted	Test Results
Upper coolant liner flow - lb/sec	0.1756	0.07
Lower coolant liner flow - lb/sec	0.1253	0.09
Injector mixture ratio	1.185	1.18
Overall mixture ratio	1.149	1.16
Combustion temperature - °R	2181	2142
Flow divider valve position - %	25.8	25.2
Oxidizer injector primary ΔP	369.9	NAV
Oxidizer injector secondary ΔP	5.97	NAV
Fuel injector ΔP		NAV
Oxidizer injector temperature - °R	200	191
Fuel injector temperature - °R	166.5	176
Temperature profile (11 in.) - °R	0	206
Temperature profile (15 in.) - °R	0	114
Average temperature (11 in.) - °R	2181	2141
Average temperature (15 in.) - °R	2181	2115
Oxidizer primary/total flow split	0.5291	0.608
Oxidizer primary injector A_{cd} - in ²	0.0550	NAV
Oxidizer secondary injector A_{cd} - in ²	0.3855	NAV
Fuel Injector A_{cd} (Overall) - in ²	3.47	NAV
η_c^* (Based on P_c , wt) - %	100	95.1
η_c^* (Based on average temperature at 11 in.) - %	100	98.4
η_c^* (Based on average temperature at 15 in.) - %	100	97.7

Table XLIII. Predicted vs Actual Performance for 35% Thrust,
Engine Mixture Ratio of 5, Rig 35131-1 Run 1.01

	Predicted	Test Results
Chamber pressure - psia	1348.7	1247
Total oxidizer flow - lb/sec	18.28	17.5
Oxidizer primary flow - lb/sec	6.267	7.17
Oxidizer secondary flow - lb/sec	11.23	10.29
Total fuel flow - lb/sec	25.91	25.2
Injector fuel flow - lb/sec	25.10	24.8
Upper coolant liner flow - lb/sec	0.465	0.21
Lower coolant liner flow - lb/sec	0.343	0.22
Injector Mixture ratio	0.729	0.70
Overall mixture ratio		
Combustion temperature - °R	1423.9	1262
Flow divider valve position - %	38.2	36.3
Oxidizer injector primary ΔP	418.2	NAV
Oxidizer injector secondary ΔP	13.3	NAV
Fuel Injector ΔP		NAV
Oxidizer injector temperature - °R	204.0	194
Fuel injector temperature - °R	135.4	139
Temperature profile (11 in.) - °R	0	158
Temperature profile (15 in.) - °R	0	121
Average temperature (11 in.) - °R	1423.9	1262
Average temperature (15 in.) - °R	1423.9	1263
Oxidizer primary/total flow split	0.3581	0.384
Oxidizer primary injector A_{cd} - in. ²	0.0550	NAV

Table XLIII. Predicted vs Actual Performance for 35% Thrust,
Engine Mixture Ratio of 5, Rig 35131-1 Run 1.01
(Continued)

	Predicted	Test Results
Oxidizer secondary injector A_{cd} - in^2	0.5531	NAV
Fuel injector A_{cd} (Overall) - in^2	3.47	NAV
η_c^* (Based on P_c , wt) - %	100	96.3
η_c^* (Based on average temperature at 11 in.) - %	100	96.2
η_c^* (Based on average temperature at 15 in.) - %	100	96.0

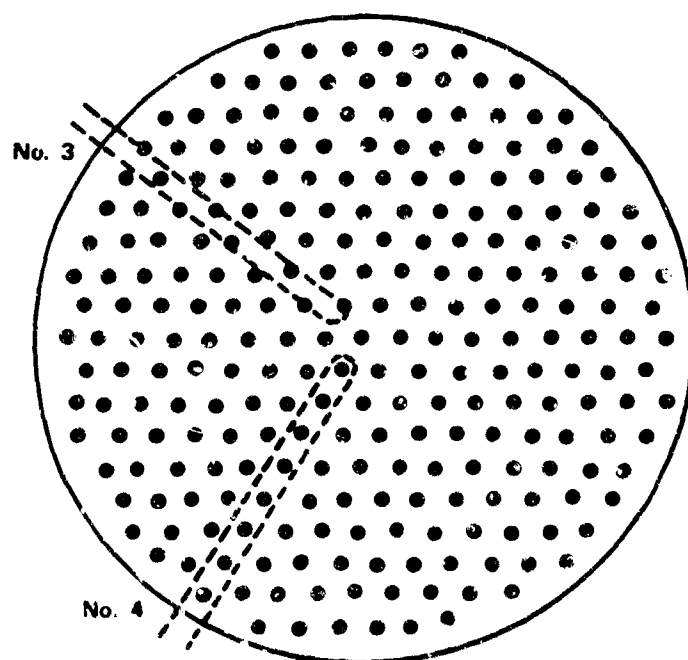


Figure 379. Two Thermocouple Rakes, Viewed Up-
stream Through the Nozzle, Test 5.01

ID 38375

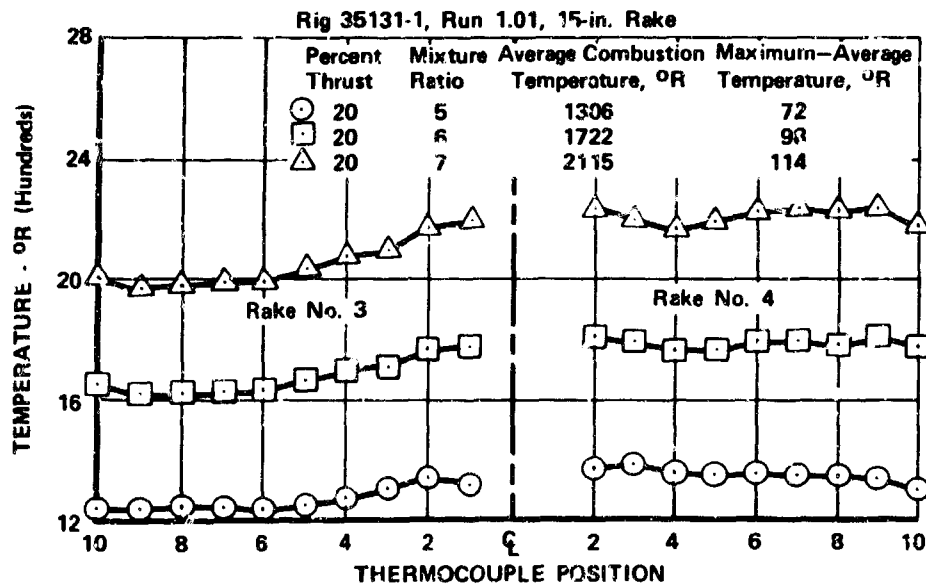


Figure 380. Temperature Distribution, 20% Thrust FD 44041

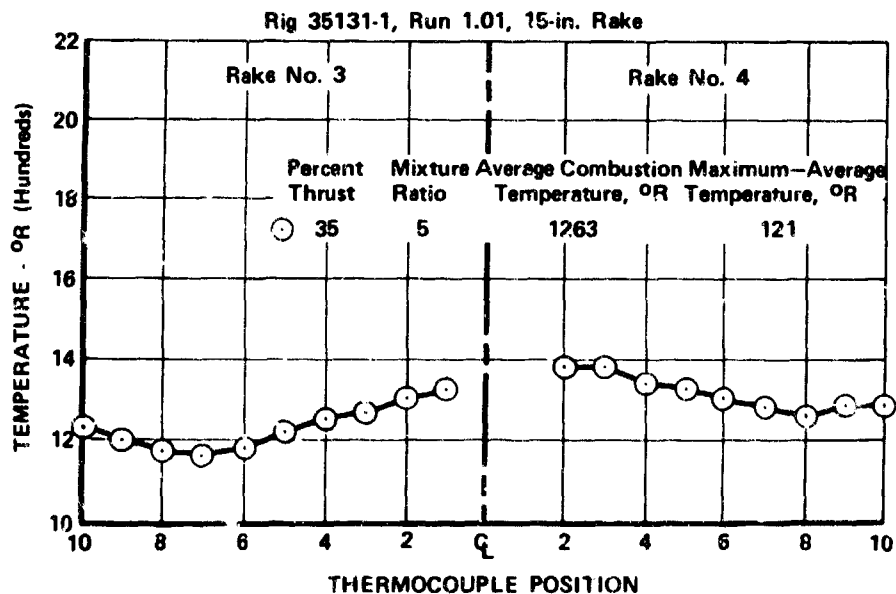


Figure 381. Temperature Distribution, 35% Thrust FD 44043

It was determined from the outer combustion liner temperatures that liner damage was sustained just after the oxidizer flow was introduced into the secondary cavity of the injector. Figure 382 indicates that until oxidizer flow reached the secondary cavity, the cooling liner temperature was lower than average combustion temperature, but after secondary flow was started, cooling liner temperature rapidly climbed above the average combustion temperature to approximately the melt temperature.

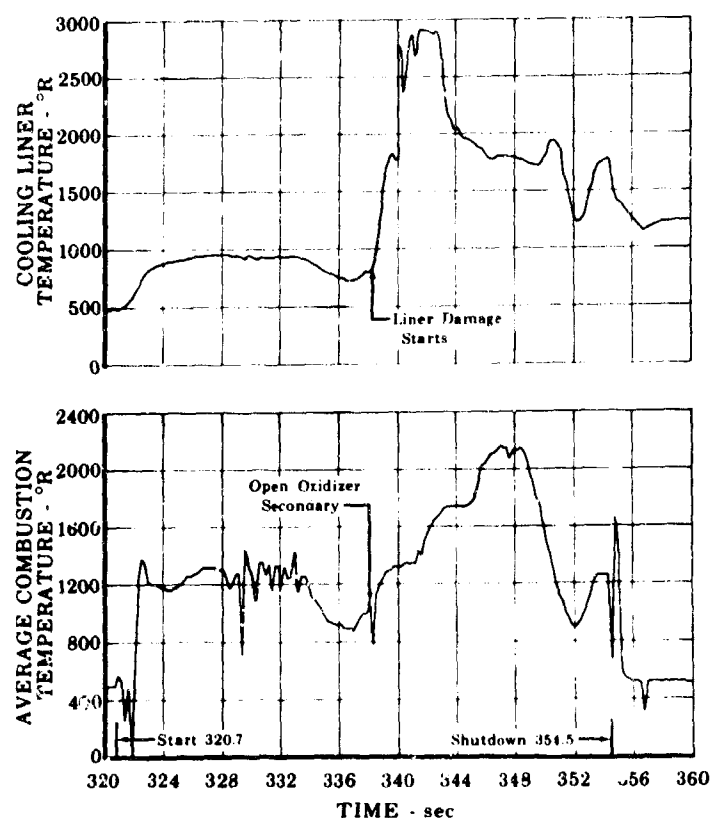


Figure 382. Oxidizer Flow Reached Secondary Cavity of the Injector FD 33181

Figure 383 shows that combustion noise was 4 psi peak-to-peak at 20% thrust and $r = 5$ before and after the 80 grain charge was fired through a 20,000 psi burst disk into the combustion chamber. The pulse charge created an 86 psi and 60 psi overpressure at axial planes 2.7 in. and 18 in. from the injector. Chamber pressure decreased to its normal noise level in 3 msec. Also observed from the chamber pressure trace in figure 383, low frequency instability was not encountered during the run.

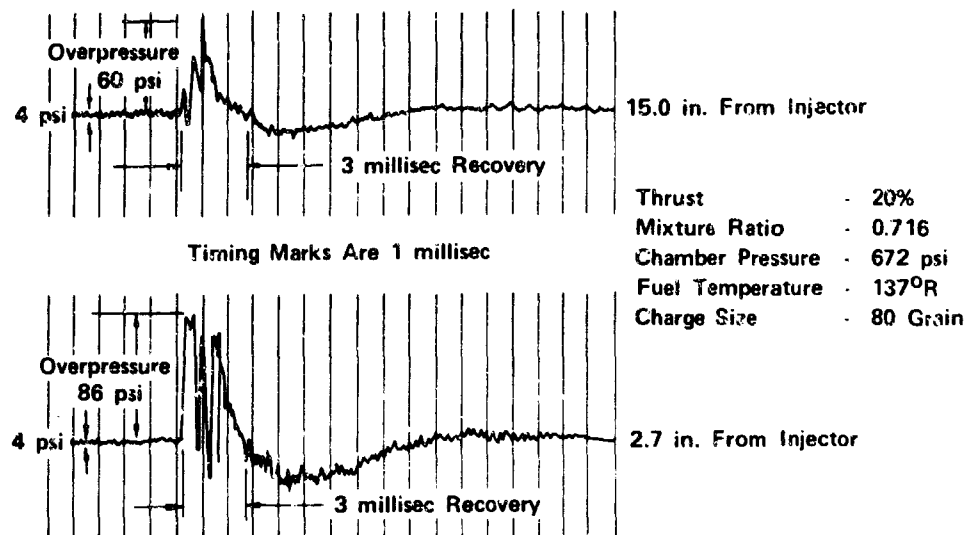


Figure 383. Preburner Chamber Pressure During Pulsing, Test 1.01 FD 31515A

Disassembly of the rig revealed that burning propellants from the outer injection elements had impinged the inner uncooled liner. This action melted a hole in the inner liner and molten metal was thrown against the outer cooled liner. The holes provided a flowpath for burning propellants between the outer cooled liner and chamber shell. Because of the shape of the liners, the flowpath had a static pressure differential of approximately 15 psid between the upstream entrance and downstream discharge. Therefore, burning propellants continuously were drawn through the holes in the liner. The seal at the parting face, between the 4 in. spacer and chamber shell, became hot and leaked burning propellants overboard, damaging an instrumentation cable, and causing rig shutdown. Figure 384 shows the damage to the inner liner viewed from the injector face cooling downstream. Note the damage occurred in a quadrant away from the thermocouple rakes, which are visible.

Closer examination of the injector revealed small holes in the top of eleven oxidizer elements where the tubes are rolled and sealed with copper braze. It was believed this condition existed during run 1.01 and could have contributed to liner damage by injecting unatomized liquid oxygen that reached the chamberwall. It was believed that during the 50% nitric acid etch, which removed the face plate from the first injector assembly to cure the low fuel A_{cd} caused by excessive braze material, some form of acid, either fumes or liquid, reached the braze at the end of the element and etched away the copper braze seal, thus forming the holes that were discovered.

After review of the hot firing data, which indicate no combustion abnormality, it was concluded that liner damage was caused by burning propellants striking the liner walls. Therefore, oxygen from the outer elements would be directed inward by bending the tips of the elements, and the liner walls would be further protected by adding liner film cooling.

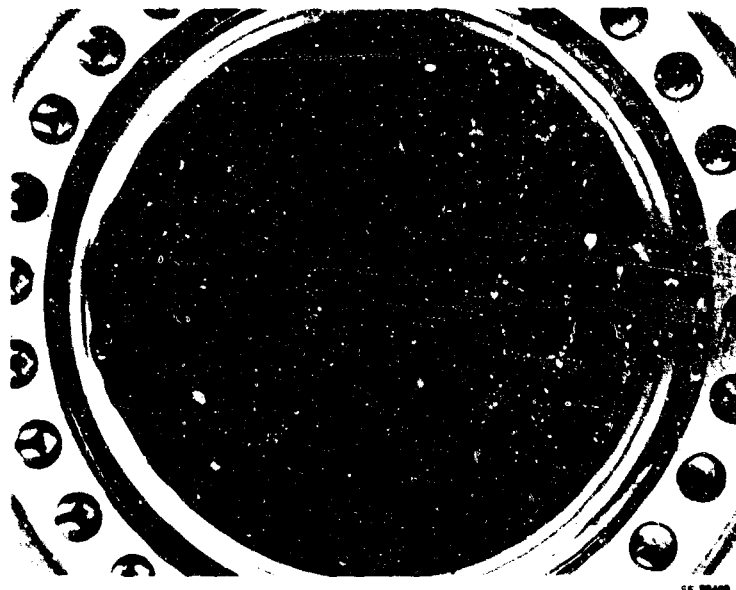


Figure 384. Preburner Scrub Liner After
Test 1.01

FD 33182A

Teardown inspection also revealed a surface crack on the injector housing. The crack was approximately 0.015 to 0.030 in. deep and 1.5 in. long. The crack is on the 0.300 in. thick section of the injector housing where the injector face spring seal is attached. During the braze operation, the crack originated in the tack weld that holds the injector faceplate seal in place, and propagated outward into the parent material of the Inconel 718 housing.

After evaluation of performance data and the rig teardown results, the following changes were made to the injector and the test rig:

(1) Injector

The crack in the injector housing was routed out and inspected by zygo and a microscope to assure the old weld and braze were completely removed. Cracks and holes in 72 element tops were sealed by a gold-nickel heliarc torch braze and 108 equally spaced 0.018 in. diameter holes were electrical discharge machined around the outer diameter of the Rigimesh fuel faceplate to provide film coolant to the scrub liner. To give additional protection to the liner, the ends of the outer row oxidizer elements were bent 10 to 15 deg towards the injector center line to redirect LO_2 away from the scrub liner. These modifications are shown in figure 385.

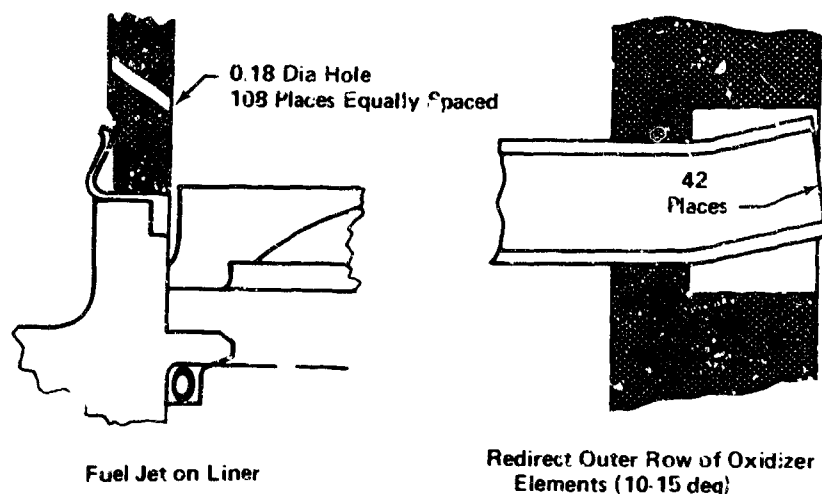


Figure 385. Preburner Injector Fixed to
Prevent Uncooled Liner Damage

FD 33178B

The injector was tested with water flowing on the fuel and oxidizer sides to observe the pattern created by the rework. The 108, 0.018 in. diameter holes flowed water in small solid streams and the flow was relatively uniform from hole to hole. It was noted that the face spring seal between the fuel faceplate and the oxidizer housing leaked a significant amount in some circumferential locations during water flow. Water flowing at 35 psid, the maximum pressure where visual observations were made, revealed the seal was still leaking. Flow emanating from the tilted oxidizer elements was observed to be undisturbed, except that the cone axis was shifted by the amount the element was tilted, as observed in individual element water flow samples.

(2) Combustion Chamber Assembly

The 4 in. spacer had been eroded in one area by leaking hot gas during the run. This area was routed out, rewelded, X-rayed, and machined to the original configuration. The burned area in the adapter was routed out, rewelded, X-rayed, and then remachined to blueprint configuration. The combustion chamber shell was replaced by another remaining from Phase I tests.

To eliminate the negative differential pressure existing between the combustion chamber and the chamber shell to coolant liner annulus, a pressure dam for the first 2 in. of the annulus was made by welding a spacer ring to the coolant liner. The pressurized area was vented by 40 equally spaced 0.067 in. diameter holes in the spacer ring. Figure 385 also details this configuration.

For additional protection from liner damage, skin thermocouples were attached to the replacement scrub liner. These skin temperatures were to be monitored during subsequent hot firings.

The preburner rig was rebuilt with the modifications previously described and mounted in E-8 test stand for further hot firings.

Run 2.01, the preburner rig was programed for mixture ratios of 5 and 6 at 20% thrust with a pulse gun to fire at the end of the mixture ratio of 5 data

points to demonstrate the temperature profile, combustion stability, durability of the scrub liner. The run was manually advanced after 22.12 sec constituting a full duration run.

A visual inspection of the rig after shutdown showed no damage to the uncooled liner. There was some bluing of the liner in the area around pulse gun No. 2, but burning did not occur. The injector face appeared unchanged. Maximum liner temperature recorded during the second run was 940°R. During run 1.01, the liner temperature at 20% thrust and a mixture ratio of 6 was over 2000°R. Because visual damage and liner temperature was acceptable, it was decided to proceed with the next run.

Run 3.01, similar to run 2.01, was designed to demonstrate temperature profile, combustion stability, and hardware durability at mixture ratios of 5, 6, and 7 at the 20, 35, and 50% thrust levels. The run was automatically advanced at 27.73 sec, just after the 20% thrust and mixture ratio of 7 point, by a high scrub liner temperature. An 80 grain pulse charge was fired at 20% thrust and mixture ratio of 5. Another pulse charge was programmed to fire at 20% thrust and mixture ratio of 7, but the pulse did not fire when the signal was given. The pulse charge did fire just after the advance signal was triggered. No instability was encountered before or after the pulse charges were fired.

Postrun visual inspection of the rig revealed damage to the scrub liner. The scrub liner was burned through upstream of the No. 2 pulse gun creating a hole approximately 0.5 in. diameter. Metal erosion of approximately 0.5 in. existed upstream of the hole. Another hole was burned through at 150 deg, viewed upstream. There were two other areas of metal erosion approximately 0.5 in.², one located at 90 deg and the other about 135 deg. There was no damage to other parts, except the scrub liner. The injector face remained in good condition with no metal erosion occurring as shown in figure 386. The local discolored spots appeared more distinct and more numerous. The rig was removed from the test stand for further investigation of liner damage.

Figure 387 shows the temperature distribution exhibited during run 3.01. The profile is acceptable in both the 11 and 15 in. plane as it was in run 1.01. The predicted and attained conditions are the same as those previously shown in tables XL, XLI, and XLII. At this point, the data still does not indicate the cause of liner damage. The results of the pulse gun firing were similar to that described for run 1.01.



Figure 386. Injector Face Showing Good Condition Without Metal Erosion

FE 89765

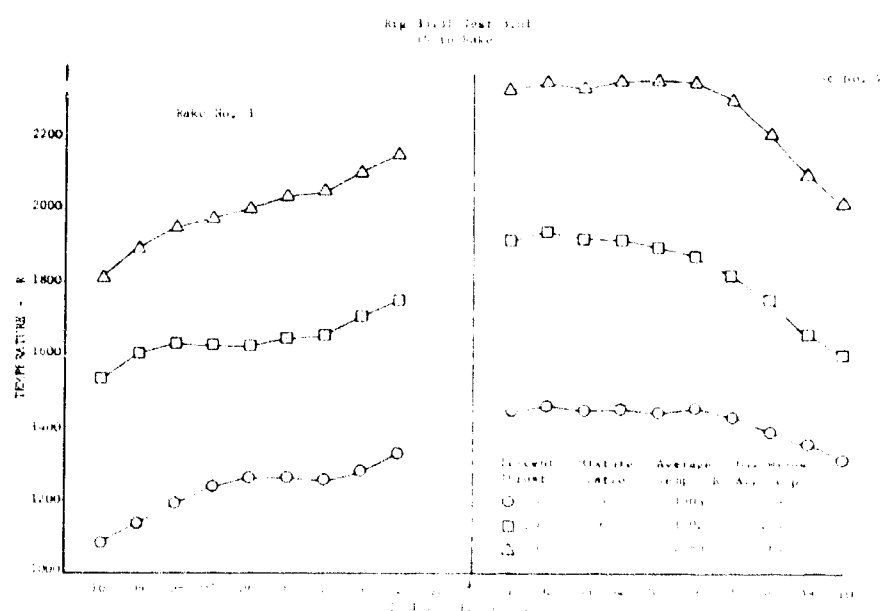


Figure 387. Fixed Area Preburner Temperature Profile

DF 79852

Inspection during rig disassembly revealed extreme erosion of the scrub liner, bluing of the lower convergent scrub liner, reappearance of the crack in the injector housing, but no other rig damage.

In general, the patterns of burning seen on builds 1 and 2 scrub liners were similar, as seen in figures 388, 389, 390, and 391. These photographs were taken with the build 1 scrub liner setting on top of the build 2 liner for comparison purposes. Fixes made to the injector after build 1 did decrease and delay the wall burning experienced in the first run since wall burning did not occur until 20% thrust and a mixture ratio of 7. Because the wall burning pattern was similar in builds 1 and 2, an asymmetrical flow pattern from the injector was suspected.

The injector was water flowed to observe the flow patterns of the fuel and oxidizer. Water flow on the fuel side of the injector showed large amounts of seal leakage between the injector face and the injector housing at the face spring seal. In general, no seal leakage was found in the areas where the liner was burned or discolored. Areas where the seal leaked are shown in figure 392. There is a weak correlation between the lack of seal leakage in the 5 o'clock area and the fact that liners of runs 1.01 and 1.03 were badly burned in this area.

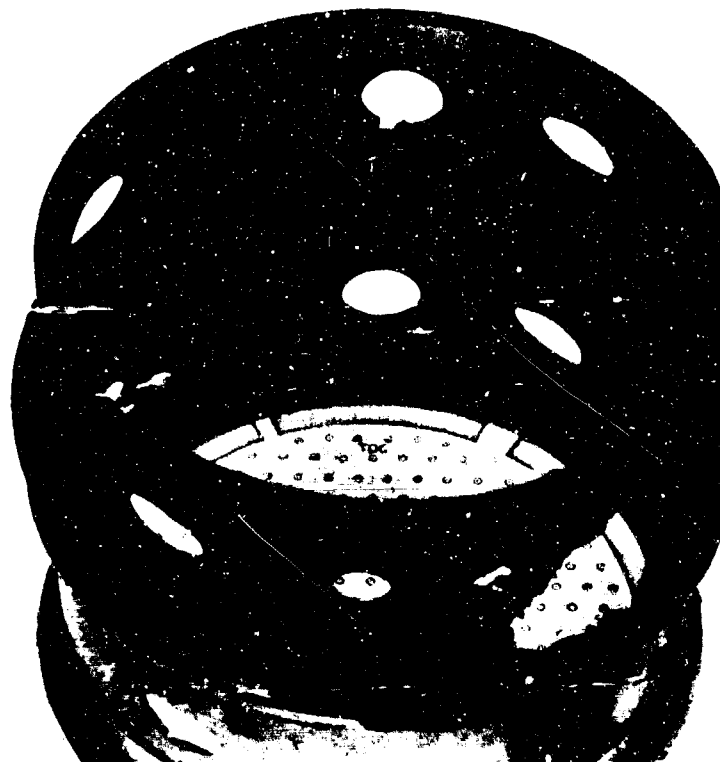


Figure 388. Scrub Liner Burning Pattern, Top Dead Center View KE 90242



Figure 389. Scrub Liner Burning Pattern, 90 deg View

KE 90105



Figure 390. Scrub Liner Burning Pattern, 180 deg View

FE 90106

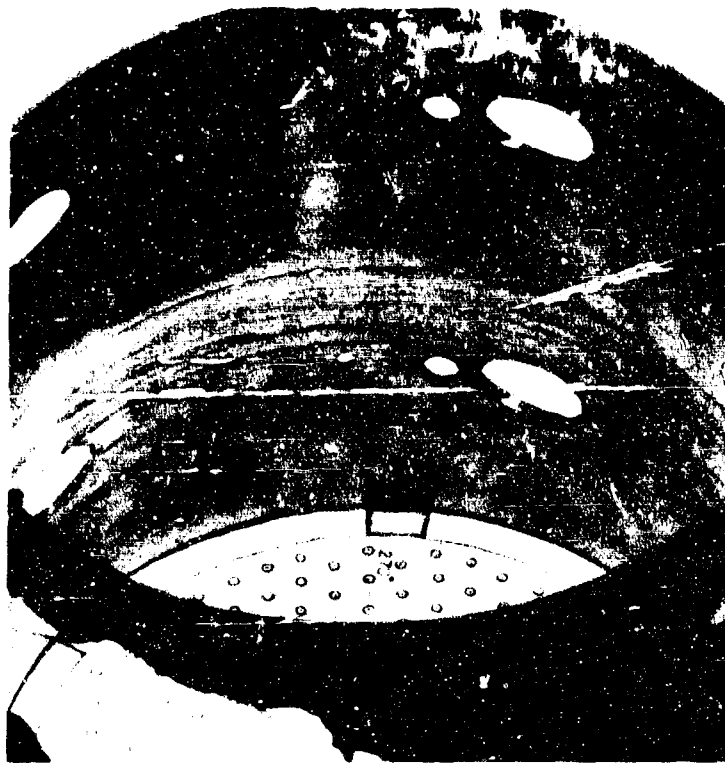


Figure 391. Scrub Liner Burning Pattern,
270 deg View

KE 90107

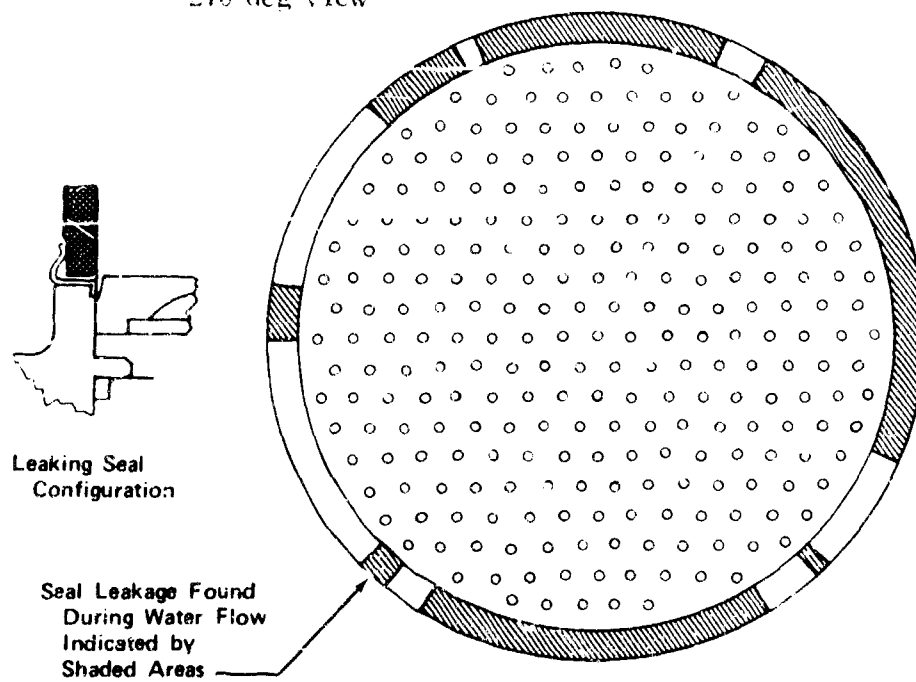


Figure 392. Areas of Spring Seal Leakage After
Build 2 Testing

FD 37333B

Water flow on the oxidizer side of the injector showed a tendency for the spray to travel towards the scrub liner wall more at the ends of the hexagonal pattern. Two of the six corners had a stronger tendency to flow toward the chamber wall than to the other corners. These two corners aligned with the burned through hole and the metal eroded area on the scrub liner wall. Twelve elements displayed the tendency to spray towards the wall. The left side of figure 393 shows how the oxidizer elements are redirected.

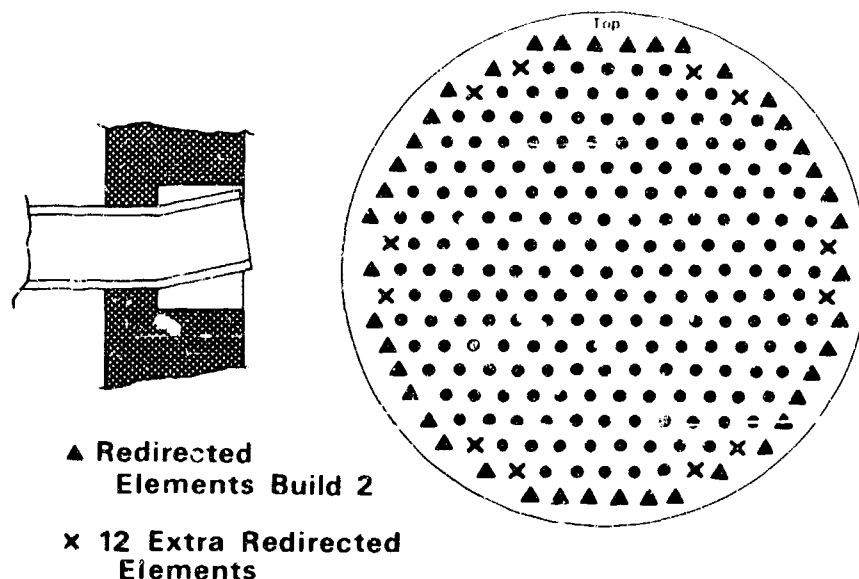


Figure 393. Injector Element Pattern Showing 12 Redirected Elements

FD 34766A

Since the data did not indicate any problems with profile, it was concluded that liner burning was caused by injected liquid oxygen impingement on the chamber wall and this created heat flux magnitudes beyond the capability of the film cooling incorporated in build 2. The water flow of the injector indicated the oxidizer source could be the twelve elements on the ends of the hexagonal face pattern.

The following test rig repairs and modifications were made after study of performance data, water flow tests, and rig inspection results:

a. Injector

Four thermal relief slots to prevent additional cracking were machined in the injector housing fuel seal land. One of these slots was positioned to eliminate the existing crack. Section A-A of figure 394 shows the injector after machining the thermal relief slots. During rig running, just after start when cold fuel is being introduced into the injector, the thin portion of the injector housing where the crack, that originally started at a tack weld, exists, cools off more rapidly than the heavy section of the injector housing at the bolt circle. This creates high hoop stress in the thin section which propagated the crack. The addition of four thermal relief slots broke the hoop of the thin section, thus relieving the stress.

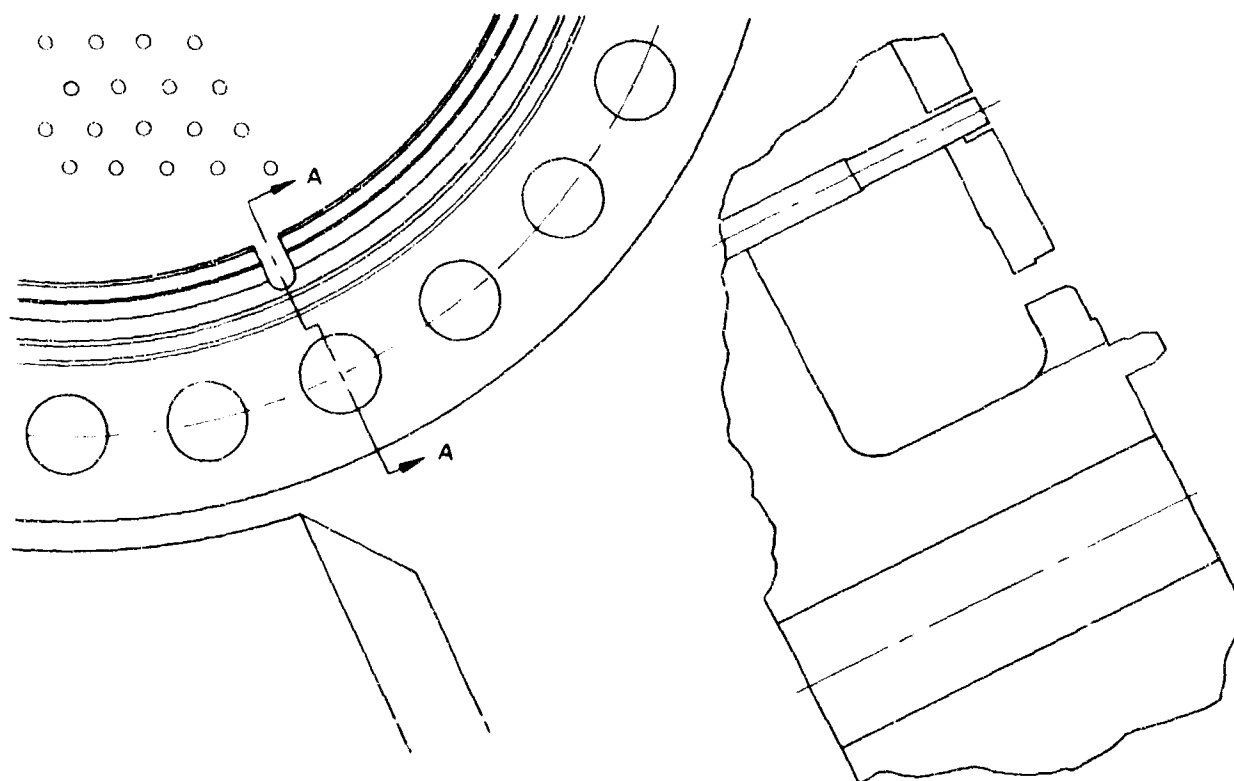


Figure 394. Injector Thermal Relief Slots

Section A-A

The fuel faceplate spring seal was removed and replaced by a positive seal. The positive seal is flexible sheet metal that is welded on one side to the injector housing and on the other to the fuel faceplate. The flexibility of the seal allows for both axial and radial thermal expansion of the faceplate relative to the injector housing.

To correct the tendency of the oxidizer spray toward the wall, the 12 element tips were tilted 12 to 15 deg toward the chamber centerline, similar to that done to the outer row elements after build 1. The 103 film coolant holes were welded shut in favor of the new transpiration-cooled scrub liner. Figure 395 shows these injector and liner modifications.

b. Combustion Chamber Assembly

A transpiration-cooled scrub liner, also shown in figure 395, was incorporated in build 3 of the test rig. The transpiration system was fed by a line tapped in the injector fuel inlet line. An orifice in the supply line was used for flow measurement. A passage in the 4 in. spacer supplied the flow to the three liner zones. Consistent with build 2, skin thermocouples were attached to the scrub and coolant liners.

Two additional 10-point rakes were added at the 15 in. station making a total of four rakes each spaced 90 deg to this plane. The rakes, located as shown in figure 396 were added to obtain temperature profile data on the side of the rig experiencing most of the wall burn damage.

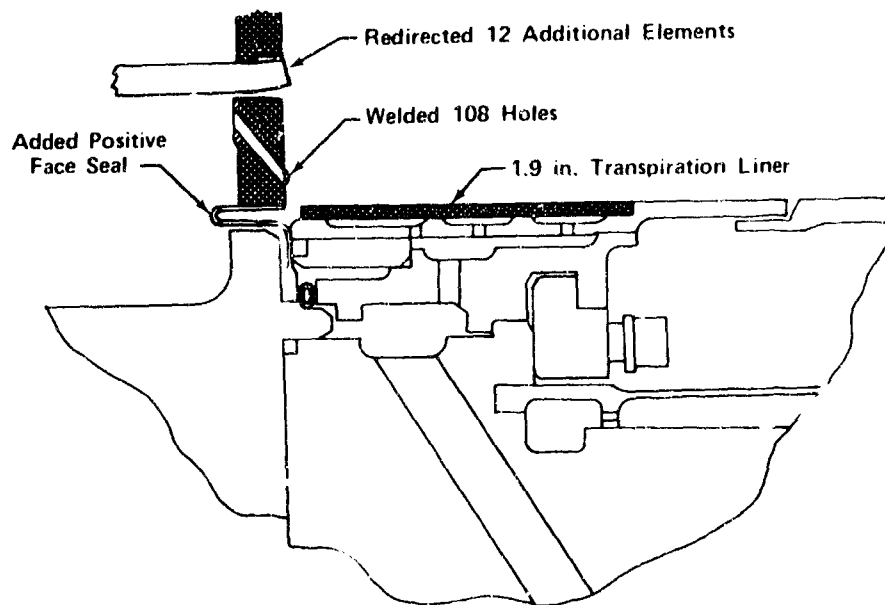


Figure 395. Modification Made to Preburner For Build 3 FD 38327

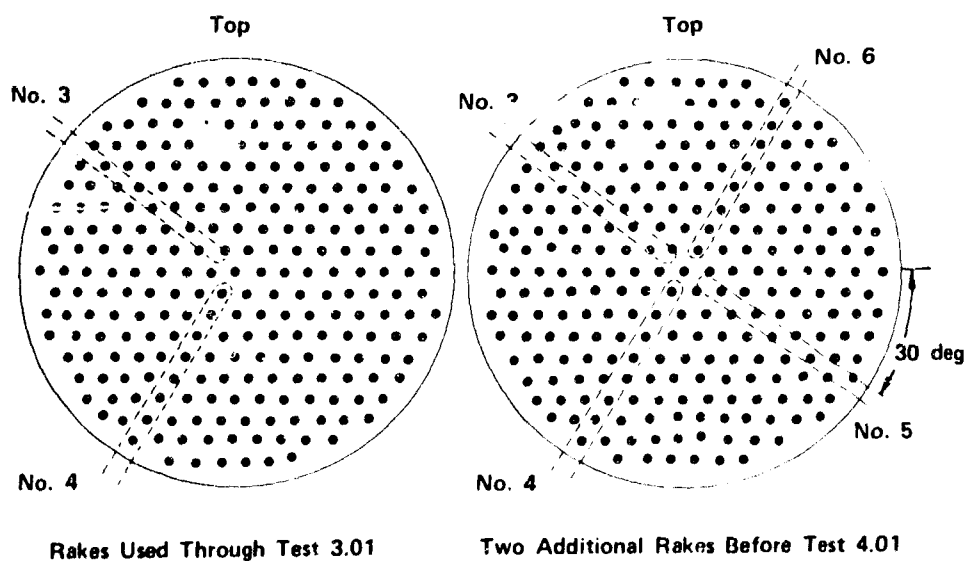


Figure 396. Rakes Added to Obtain Temperature Profile Data FD 37392B

The preburner rig was assembled with the modifications described, and the rig was mounted in E-8 test stand for continued hot testing.

The objectives of the fourth preburner run, 4.01, were to demonstrate durability of the new transpiration liner as well as temperature profile, combustion stability, and propellant temperature effects at engine mixture ratios of 5, 6, and 7 at the 20% thrust level. The programed run duration was 32.4 sec.

The test was automatically advanced after 1.4 sec because of a high combustion temperature. This high temperature was caused by an oxidizer flowrate approximately three times higher than the required level, although the flowmeter signal controlling the oxidizer flow indicated the required flowrate was being delivered to the rig. The rig hardware remained in good condition after test 4.01.

The flowmeter was removed and disassembled for inspection. No mechanical problem was found with the flowmeter parts, but the meter was rebuilt with new bearings. No electrical deficiency was found, but all meter coils were replaced. It was concluded that the meter had iced internally causing a faulty flow signal.

The 5.01 test program was a repeat of the 4.01 program. The run was advanced after 6.7 sec because of a faulty indication of a high outer-cooled liner temperature. A post-run investigation revealed the thermocouple that triggered the advance was intermittently open. The faulty thermocouple was deleted from the automatic advance for the next run. The rig hardware remained in good condition after test 5.01. The injector face after run 5.01 appeared the same as before, as shown in figure 397.

The 6.01 test program was a repeat of the 4.01 program. The run was advanced after 32.2 sec by a faulty high fuel injector differential pressure. The advance occurred only 200 msec before the programed manual shutdown, and the run was essentially complete. The faulty fuel injector differential pressure was caused by a lagging chamber pressure signal to the low side of the measuring transducer.

Inspection of rig hardware after test 6.01 revealed damage to the transpiration-cooled Rigimesh liner in the same general area damaged after tests 1.01 and 3.01. The rig was removed from the test stand for investigation of liner damage. Inspection after disassembly of the rig showed damage was confined to the transpiration-cooled liner section and the liner extension as shown in figure 398. The remainder of the rig was in good condition. A post-run 6.01 injector photograph is shown in figure 399.

The predicted and attained rig conditions were basically the same as previously shown in tables XLI, XLII, and XLIII for run 1.01, except the temperature profile was worse because of high temperatures exhibited on new rake No. 5. Temperature distribution at the 15 in. plane is shown in figures 400, and 401. Note that rake No. 5 indicates temperatures near the chamber wall are near the melting temperature of the wall material even at the 15 in. plane. These data indicate that chamber wall damage is caused by poor distribution of injected mixture causing high mixture ratios in the damaged area and not caused by injected oxygen impingement on the wall as had previously been suspected.



Figure 397. Injector Face Condition After Run 5.01 KFE 92453

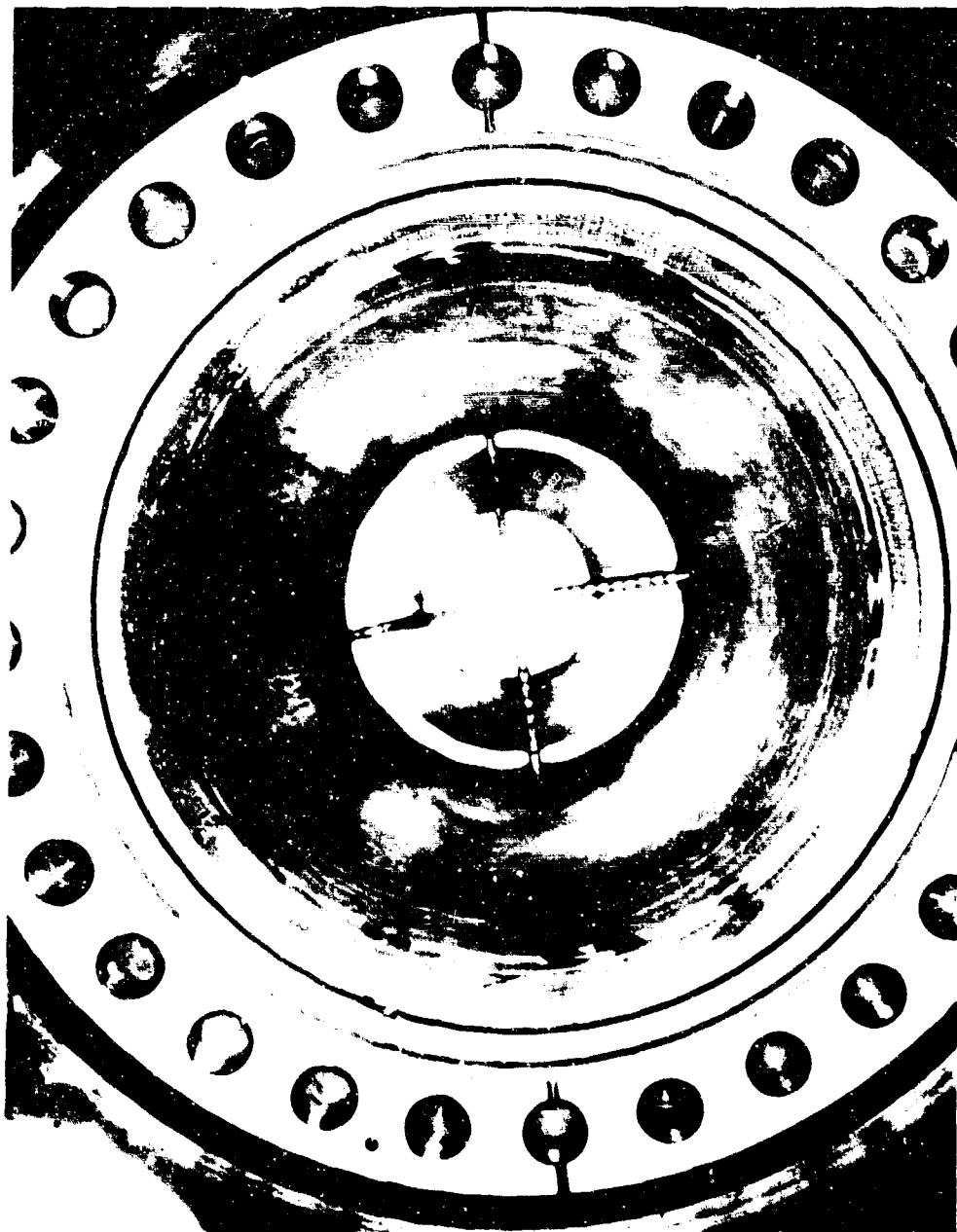


Figure 398. Liner Damage Sustained During Test 6.01 FD 34763



Figure 399. Injector Shown After Run 6.01

FE 92467

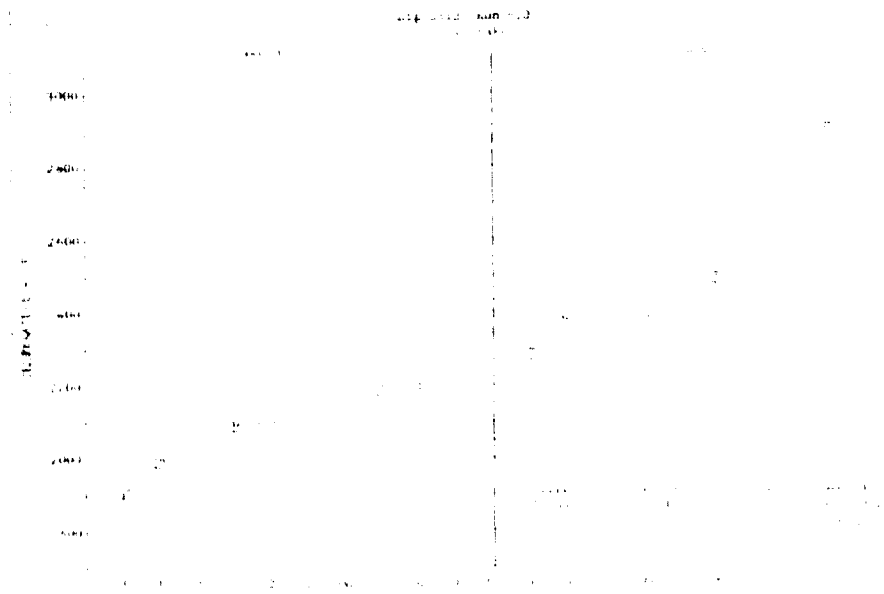


Figure 400. Fixed Area Preburner Temperature Profile, Run 6.01 DF 78953

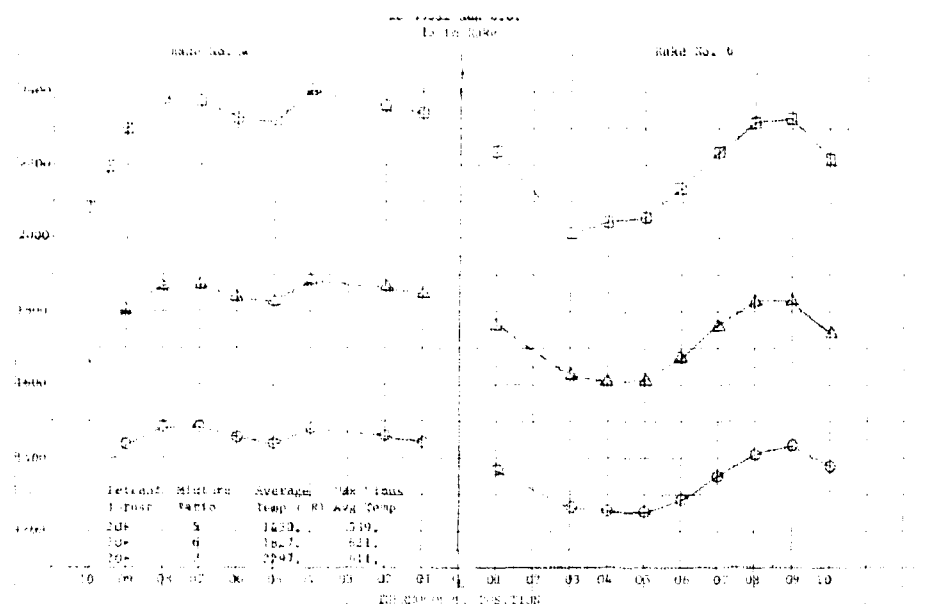


Figure 401. Fixed Area Preburner Temperature Profile, Run 6.01 DF 78954

Since the damage to the cooled liner caused by a high mixture ratio in run 6.01 was generally the area damaged during runs 1.01 and 3.01, it is suspected that the high mixture ratio is caused by maldistributed propellants from the injector. There are many possible causes for maldistributed propellants from the injector, but the more obvious possibilities are considered:

1. Maldistribution originating inside the injector because of primary, secondary, or fuel manifolding
2. Maldistribution of the secondary flow originating inside the preburner oxidizer valve
3. Variation of individual secondary A_{cd} caused by primary and secondary interaction
4. Variations in individual primary, secondary or fuel A_{cd} caused by assembly processes.

At this point, an injector and oxidizer control valve cold flow program was initiated. A total of 21 flow tests were made, but because of errors in flow tooling, only seven tests proved significant. Table XLIV lists each of these tests.

The first test was a nitrogen backflow test of the primaries to determine if any were blocked. The gas flowed into the element through a hypotube with a rubber gasket to seal at the tube entrance. Flow through secondary slots was prevented by plastic shrunk over each tube end. Gas is supplied from storage bottles and then passes through a pressure regulator and flowrater before entering the flow tool. Figure 402 illustrates the test setup.

Table XLIV. Injector Flow Test Tabulation For Profile Correlation

Test	Conditions	Results
Oxidizer primary GN ₂ flow	Backflowed primaries with secondaries capped	Many primary holes blocked
Dual water flow	Primary manifold tooling supplied primary cavity. Separate tool supplied individual secondaries.	Low primary-secondary interaction as predicted
Dual water flow	Preburner Oxidizer Valve (PBOV) installed and flow collected from individual elements	PBOV has no significant effect on flow distribution
Dual water flow	OCV installed with spacer to increase secondary cavity volume	Increased volume has no effect on flow distribution
Fuel GN ₂ flow	Injector flowed with GN ₂ simulating fuel velocity while mounted on test stand plumbing	High fuel flow in quadrant of thermocouple rake No. 5 caused by test stand plumbing
Fuel GN ₂ flow	Same as previous test except fuel filter close coupled to injector fuel inlet	Relocating filter flattened fuel flow distribution
Oxidizer primary GN ₂ flow	Back flowed primaries with secondaries capped after final cleaning	Six elements with primary holes blocked. A _{cd} of others acceptable

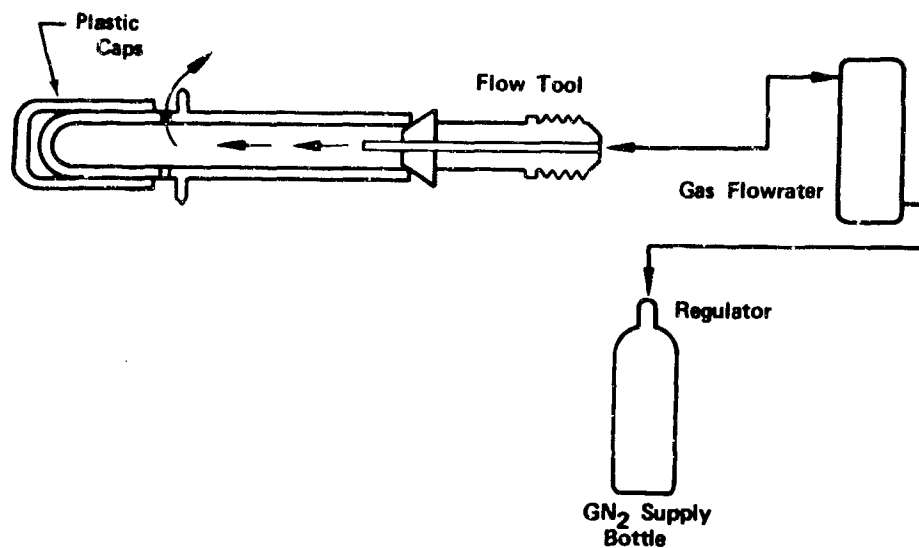


Figure 402. Element Test Set Up

FD 38371

Results of the test showed that six elements had totally blocked primaries and 83 were significantly blocked. Figure 403 shows the results of the mathematical technique used to determine primary blockage. The number adjacent to each location is the ratio of the normalized gas flows obtained during test No. 1 to the normalized water flows of individual elements before injector assembly. Normalization is simply a comparison of an individual flow to the average of all similar individual flows or $W_p \times N/W_p$. A ratio below 1.0 means the element primary A_{cd} is a lower percentage of the total injector primary A_{cd} for gas flows as compared to preassembly water flows, thereby indicating blockage. Elements with ratios below 0.92 were considered blocked and are shaded on figure 403 with boundary lines drawn around the shaded elements. No conclusive correlation between plugged or partially plugged primary holes and liner wall burning could be drawn.

Injector X-rays later showed four small heavy areas of braze material around the outer row of elements. Two of these areas are adjacent to plugged elements while the other two were near the partially plugged elements. Bore-scope inspection of the element ID confirmed braze blockage in the primary holes of the six plugged elements.

The second test was a joint water flow of the primary and secondary. The objective of the test was to determine if a significant reduction of primary A_{cd} , and therefore a lower tube internal pressure, would permit excessive secondary flow. The entire primary circuit was continuously flowed, while each secondary was separately flowed. A manifold to route water to the primary supply ports was made, so there was access to the secondary manifold cavity. All secondaries except the one being flowed were sealed with plastic caps. For each test, total primary flowrate and individual element secondary ΔP were set at simulated 20% thrust simulation points, and the flowrate recorded for each secondary. Figure 404 shows the test setup.

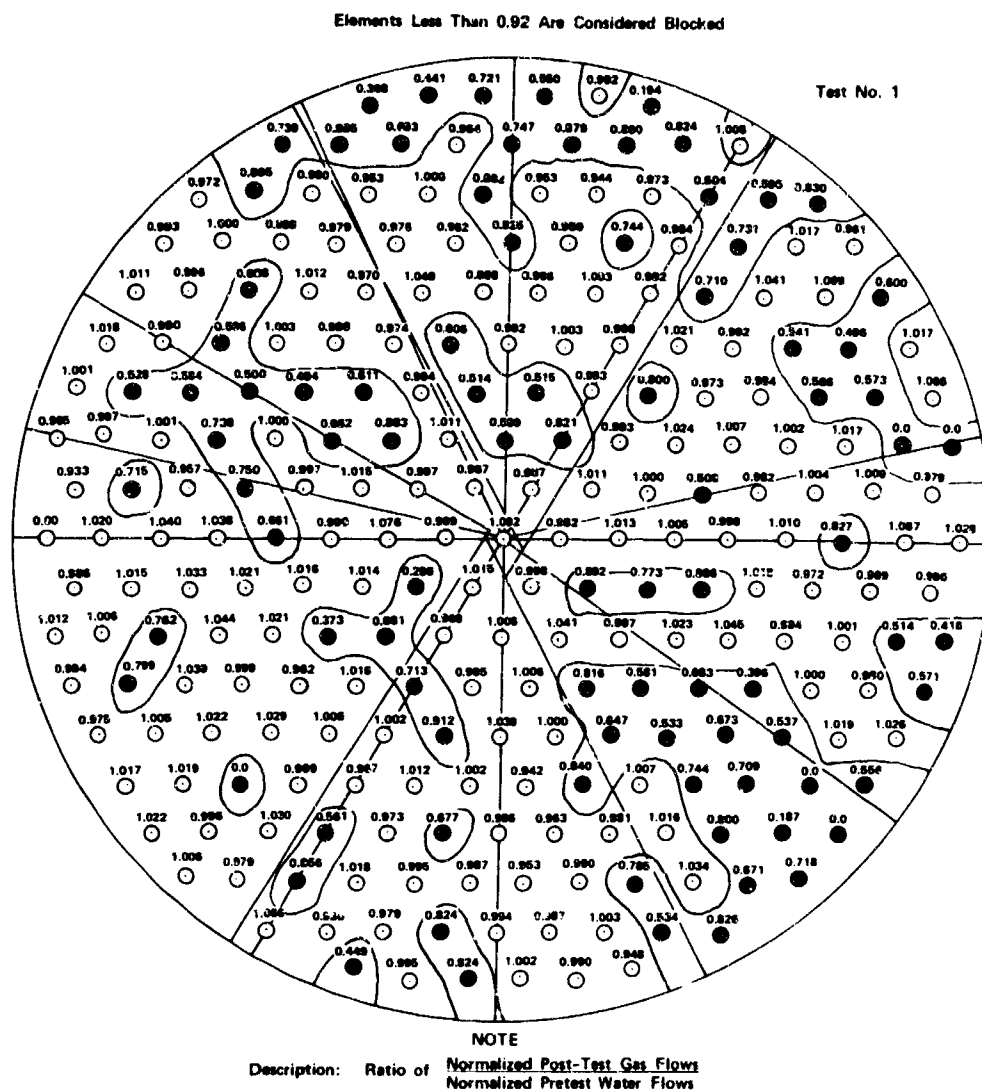


Figure 403. Elements Considered Blocked Having Ratios Below 0.92

FD 38224

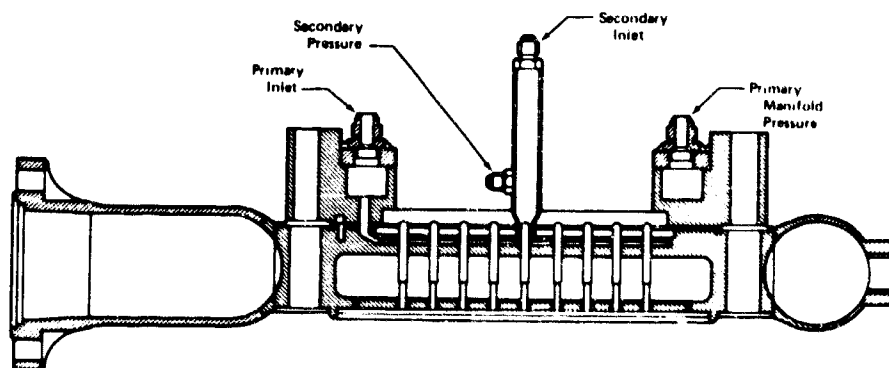


Figure 404. Dual Water Flow Test Set Up

FD 38259

Figure 405 shows a comparison of the temperature profile computed from the above dual flows to the actual profile seen during hot runs at the 1 thrust level. The dual flow combustion temperature for each rake thermocouple is computed from the aggregate mixture ratio of all the locations falling within a 0.5 in. radius of the projection of the thermocouple on the injector face. The mixture ratio is determined from the element oxidizer water flows in test 2 and the fuel orifice preassembly water flows. The element oxidizer flow is the sum of the measured secondary flow and the primary flow computer as a percentage of the total primary flow. Because there was only a weak correlation for rake No. 4, plugged primaries via primary-to-secondary interaction effects apparently did not cause propellant maldistribution.

The third test was a water flow of the oxidizer control valve and injector to determine what effect the valve has on flow distribution. Flows were collected from each element by tooling that was fitted over the tube ends as shown in figure 406. Flow conditions were set by adjusting the total water flow into the injector and the proper stroke of the control valve. For this test, the 20% thrust flows and valve positions were set to investigate the level where wall burning and poor profile had been experienced. Test 3 was performed for the sector of the No. 5 temperature rake, the area of poor profile and most severe wall burning. Flow results were used to predict a temperature profile for rake No. 5 using analytical techniques discussed in test 2. The flat profile seen in figure 407 indicated the valve did not cause maldistribution of LO_2 and therefore was not responsible for the actual profile or wall burning.

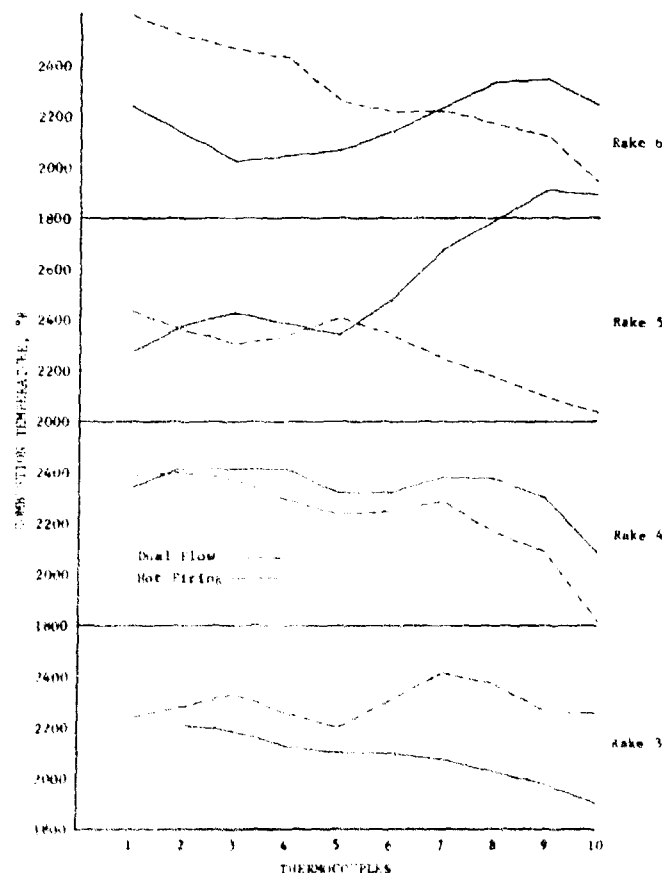


Figure 405. Temperature Based On Dual Flows

DF 78969

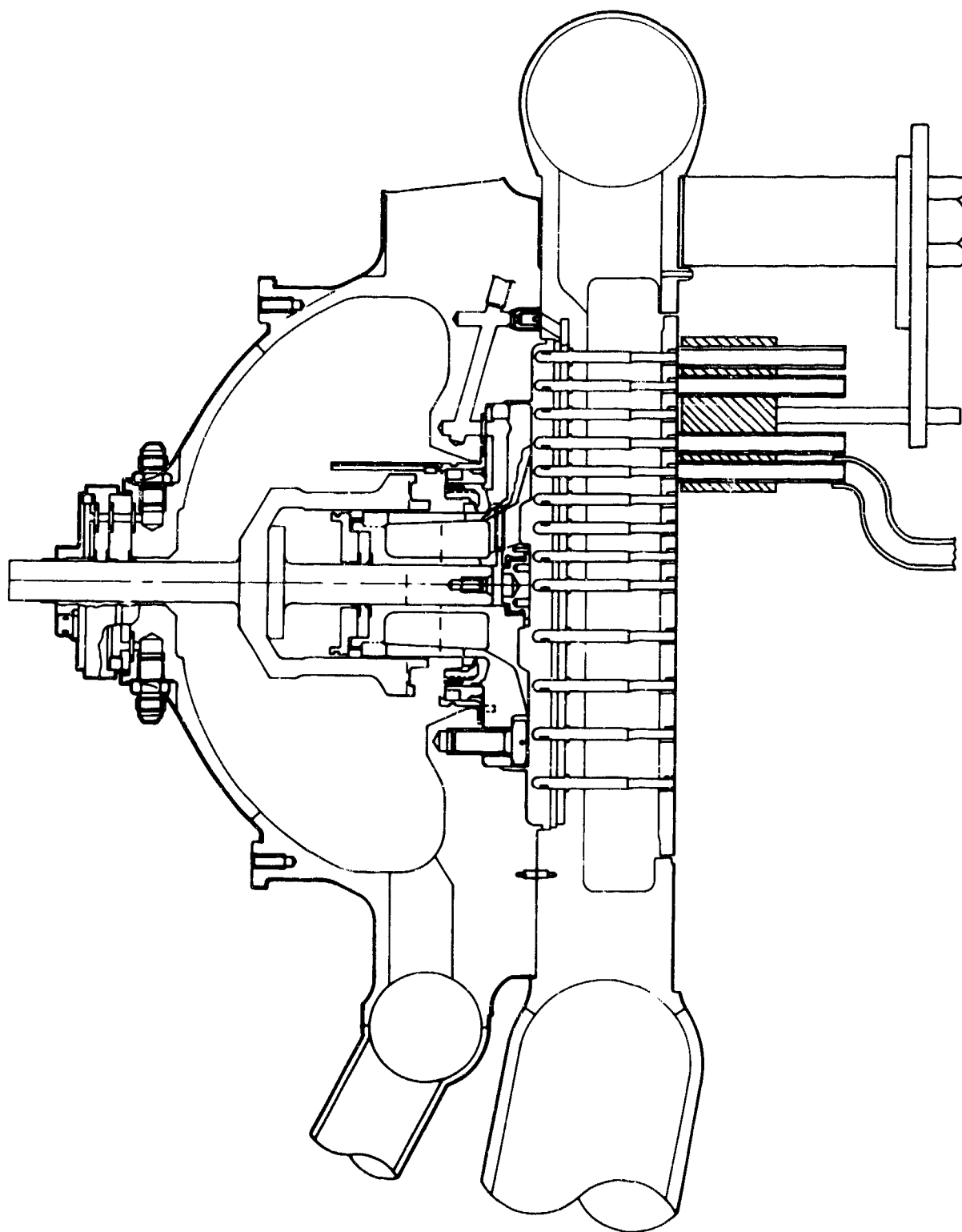


Figure 406. Cross Section of Injector With Flow Collectors

FD 31504C

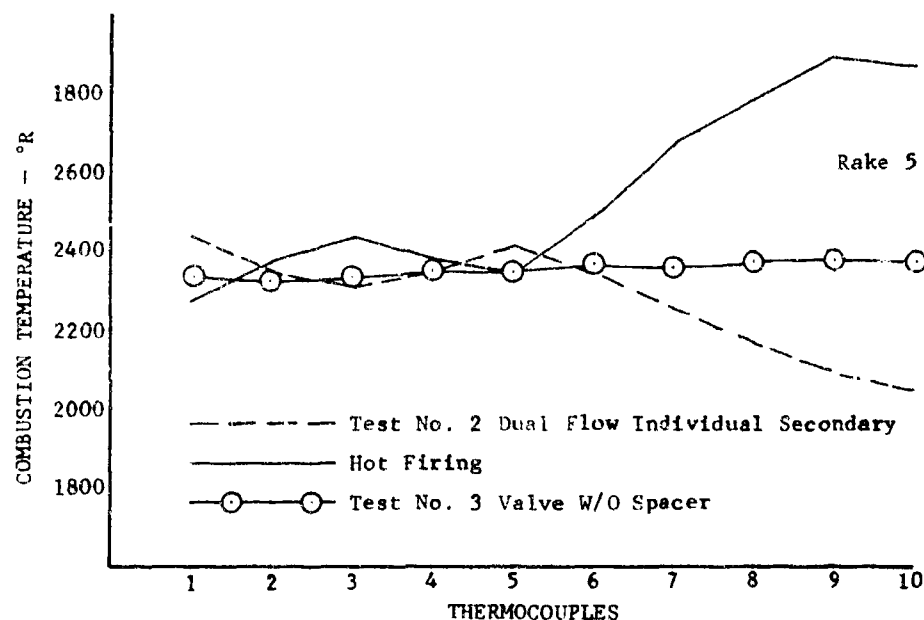


Figure 407. Combustion Temperature

DF 78971

The fourth test was a repeat of the third except that a 0.250 in. spacer was installed between the injector and control valve as shown in figure 408. This was done to investigate the effect of increased secondary cavity volume, minimized in the B/M configuration. Again, the results were used to predict a temperature profile for rake No. 5. Figure 409 shows this plot compared with similar results from tests 2 and 3. It was concluded the spacer would not have value in improving secondary distribution and was evidenced by the slightly deteriorated temperature profile.

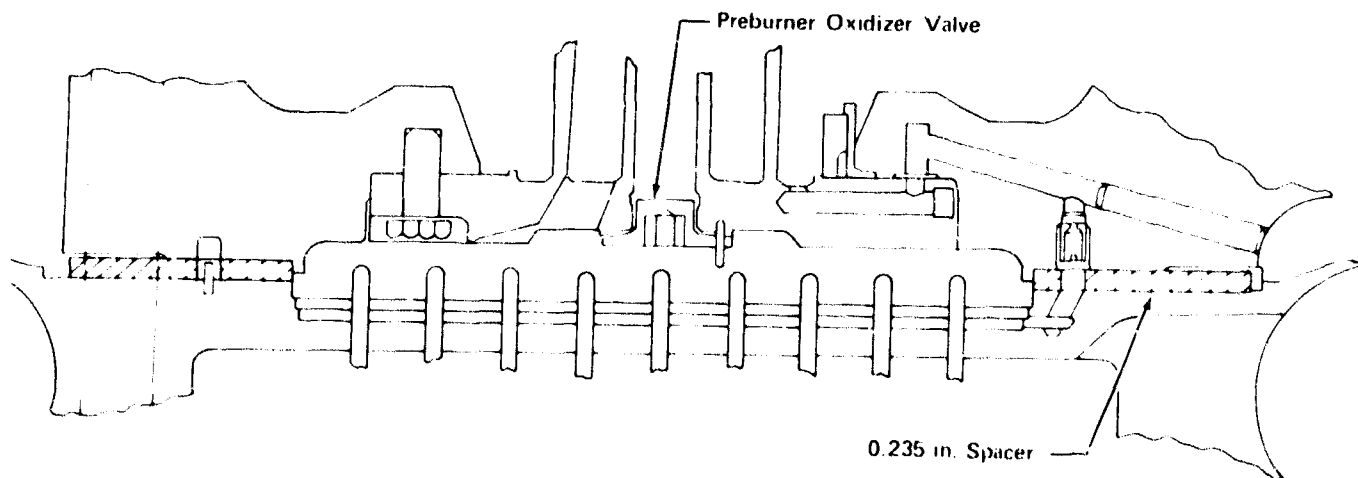


Figure 408. Preburner Injector and Oxidizer Control Valve With Spacer

FD 38260

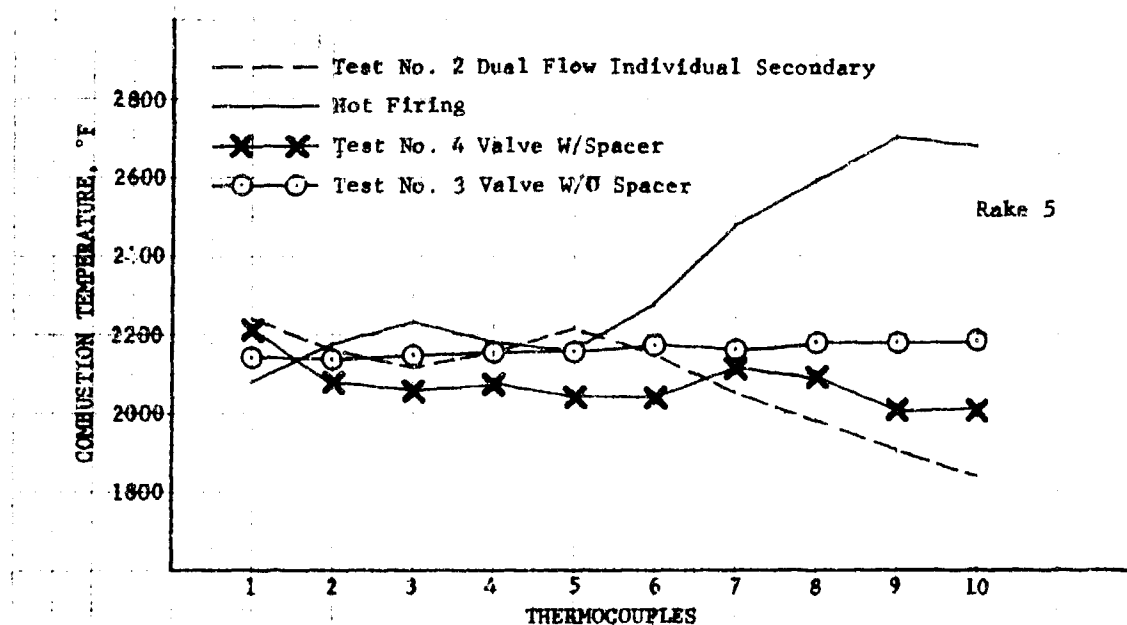


Figure 409. Combustion Temperature

DF 78972

The fifth test was a nitrogen flow test of the fuel injector and the E-8 fuel inlet supply line for the effect that plumbing had on fuel distribution. The injector was positioned in the test stand exactly as it was when mounted in the test rig. Nitrogen flowed through the entire fuel inlet line at simulated GH_2 velocities, thereby entering the injector at simulated run conditions.

A hand tool, positioned over the fuel orifice discharge, was used to measure static pressure at each location, thereby relating the flow distribution across the face. Figure 410 shows the injector in the stand and the static pressure tool.

Pressures and flows at each location were compared to an average computed from summation of all flows. With perfect distribution, the ratio for each location would be 1.0. The ratio for each location is shown in figure 411. It can be seen that ratios for sectors 1, 3, 4, 5, and 6 are generally less than 1.0, and greater than one (2.8%) in sector 2. This shows that there would be excessive fuel flow in this sector, contrary to the expected, when associated with poor profile and wall burning. The elbow in the stand plumbing upstream of the inlet horn caused packing of the fuel flow on one side of the injector.

The fuel filter was close coupled to the fuel inlet horn for the sixth test and is shown in figure 412. The fifth test was repeated and results shown in figure 413 indicate distribution had flattened. A ratio average near 1.0 was obtained for each sector. Fuel filter pressure loss redistributed the fuel before reaching the inlet, thereby improving distribution throughout the manifold.

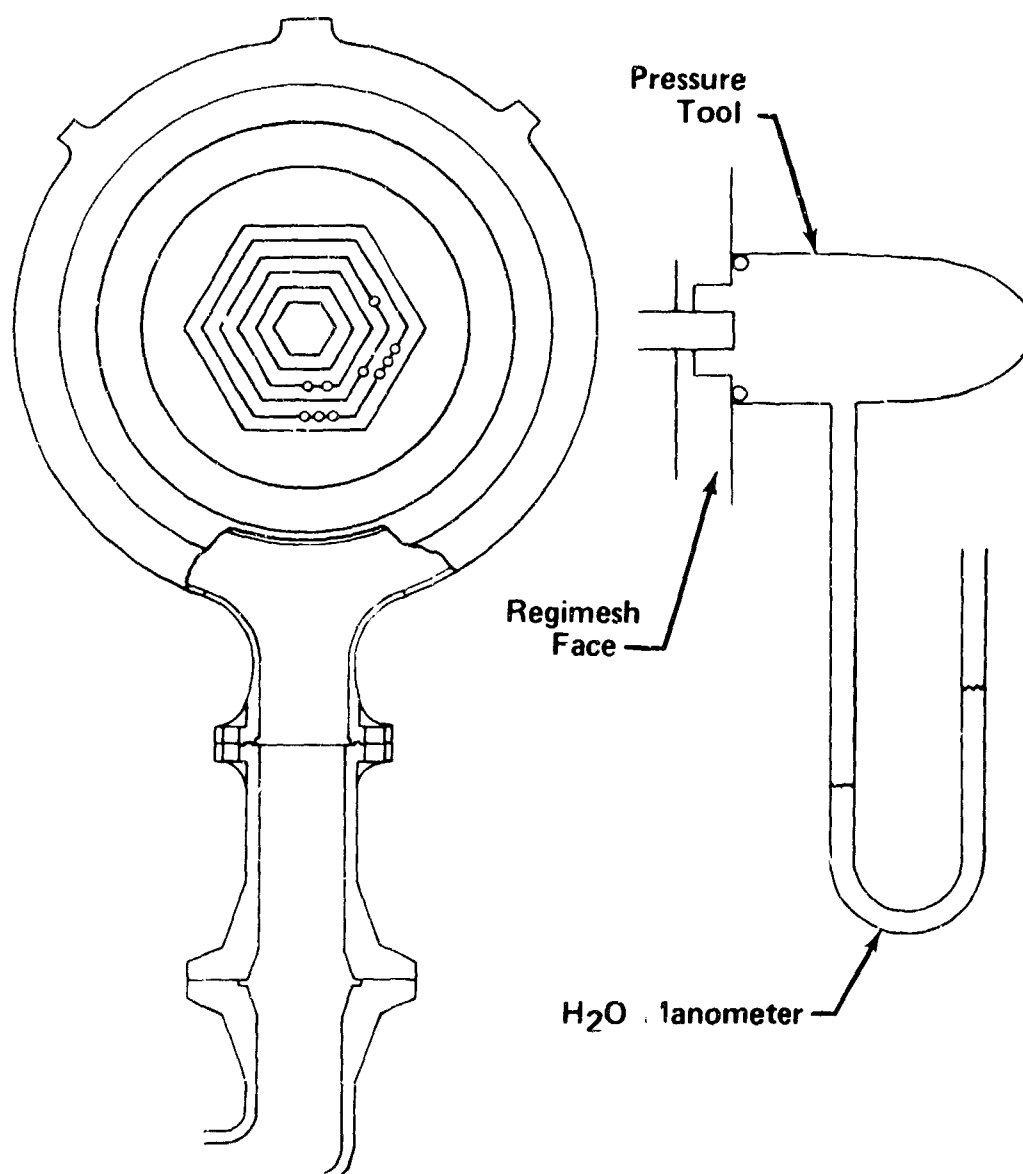


Figure 410. Injector in Stand With Static Pressure Tool

FD 37332E

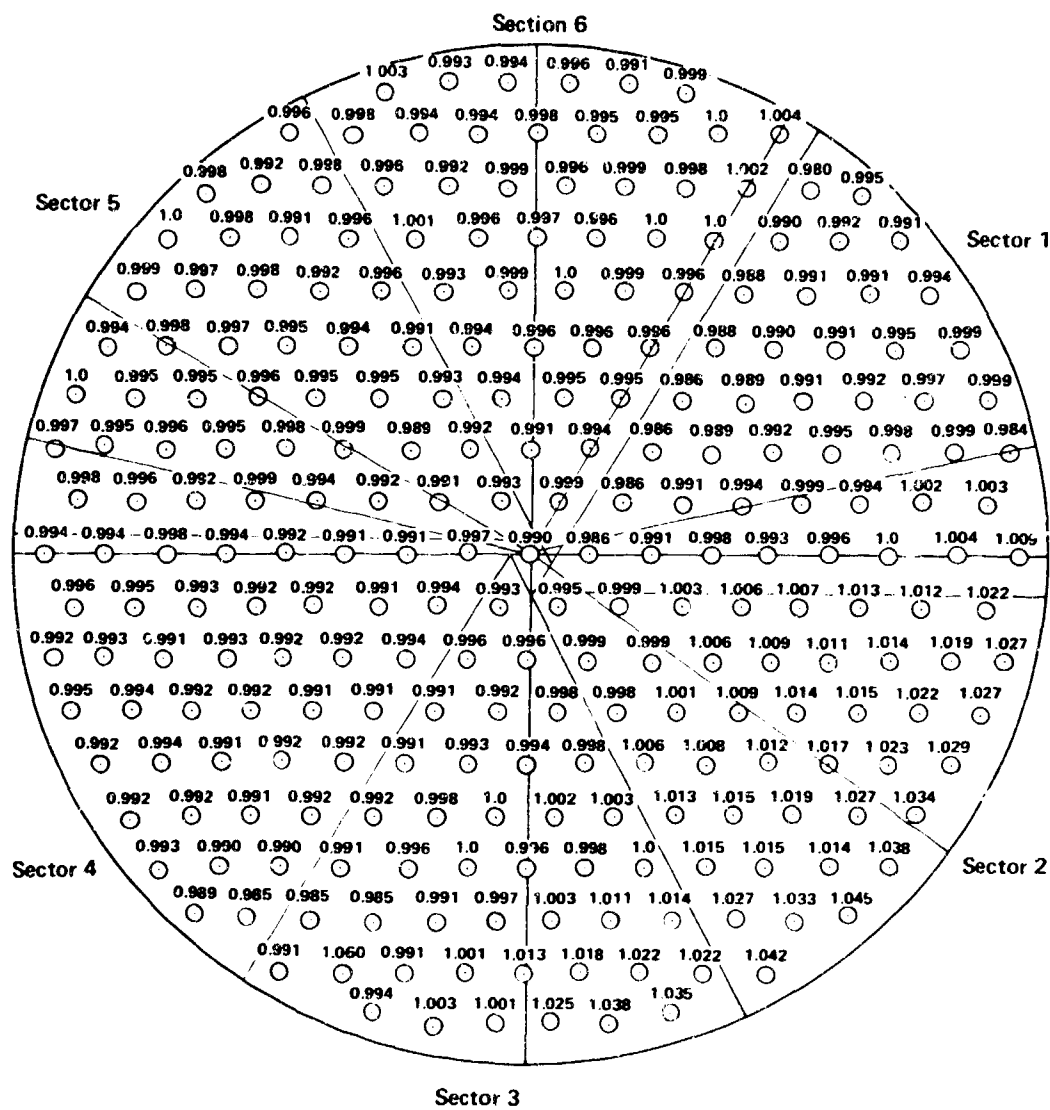


Figure 411. Ratio of Individual Pressure To Average Pressure For Fuel Side GN₂ Flow Without Close Mounted Filter

FD 38261

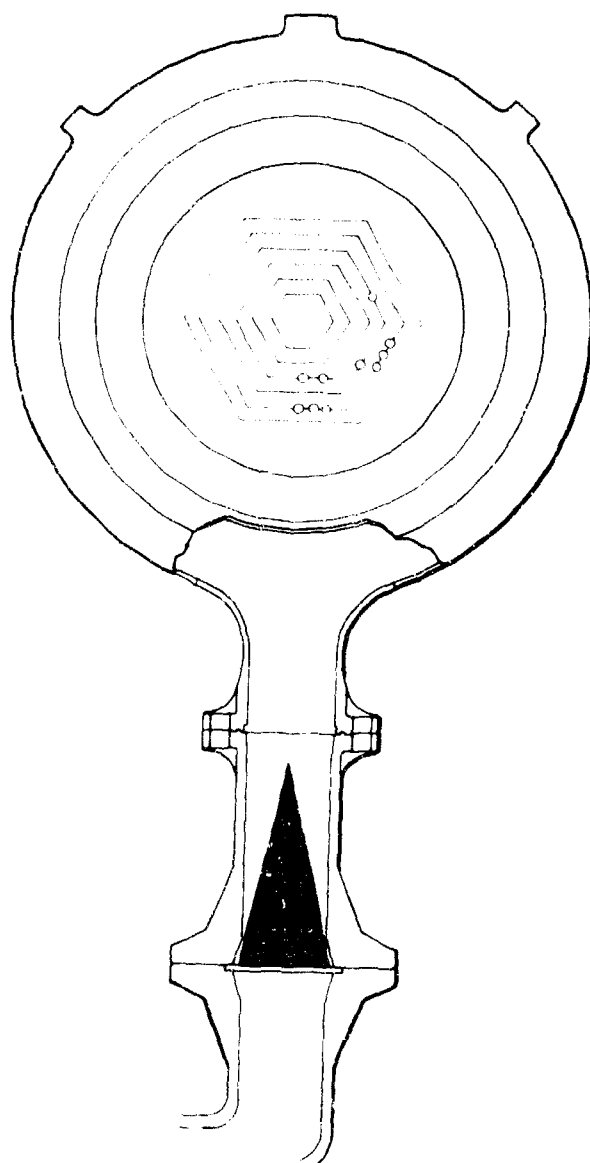


Figure 412. Fuel Filter Close Coupled to Fuel Inlet Horn FD 37332D

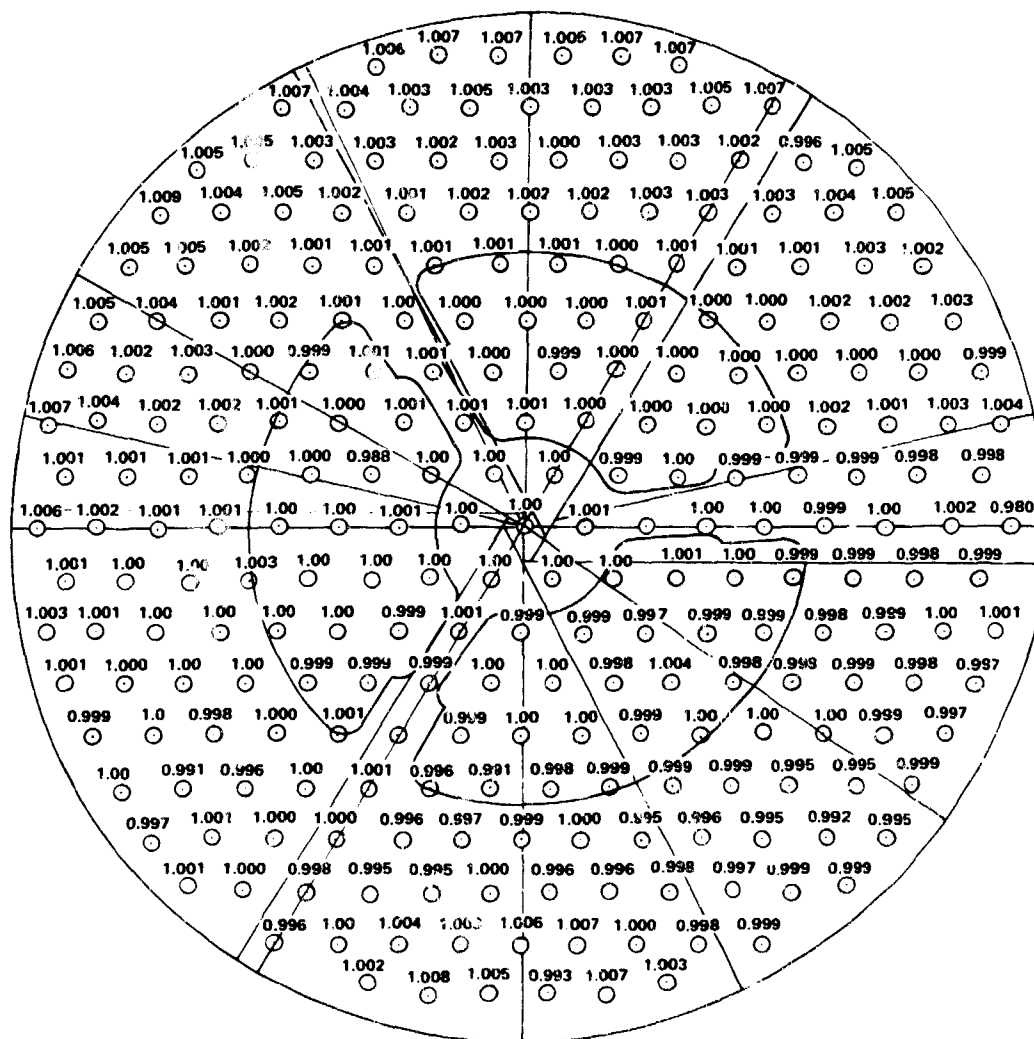


Figure 413. GN₂ On Fuel Injector With Filter Near
Injector - Ratio of Individual Pressure
to Average Pressure

FD 38479

After flow tests were completed, the injector primaries were back-flushed with water at approximately 500 psid to remove trash accumulating during the test series.

The seventh test determined the cleaning effect of the primary back flush. Test 1, a nitrogen back flush of the primaries, was repeated.

Test results were again used to compute a ratio of test 7 gas flow A_{cd} to the preassembly water flow A_{cd} as described in test 1. The shaded areas in figure 414 show locations that are considered blocked (ratios below 0.9) and it is apparent there was a significant reduction in the number of blocked primaries when compared to test 1 results.

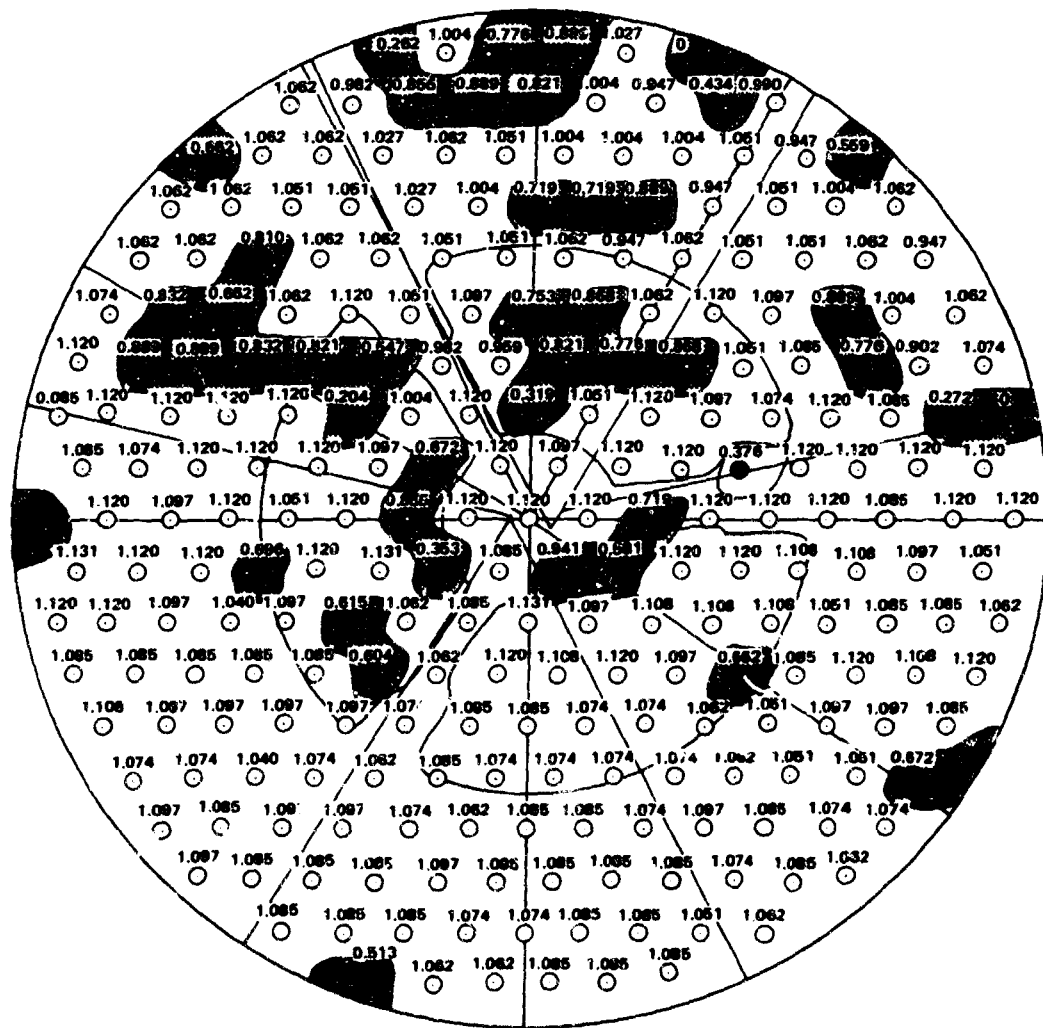


Figure 414. Shaded Areas Showing Locations Considered Blocked

FD 38480A

Conclusions drawn from the injector flow program are:

1. There were blocked and partially blocked primaries which are unacceptable even though there was no correlation with the hot firing combustion temperatures
2. The majority of the primaries were plugged with trash that was removed by back flowing
3. Stand plumbing caused a maldistribution of fuel flow in the injector
4. Installing the high loss stand filter upstream of the injector flattened the fuel maldistribution.

It was then decided to perform hot fire tests that would show the effects of fuel temperature, flowrate, and flowsplit on combustion temperature profile. Action taken to repair or modify the rig for build 4 was:

1. The six elements with blocked primaries were plugged by welding shut the secondary slots and filling the tube with steel rod and seal welded at the tube discharge as seen in figure 415

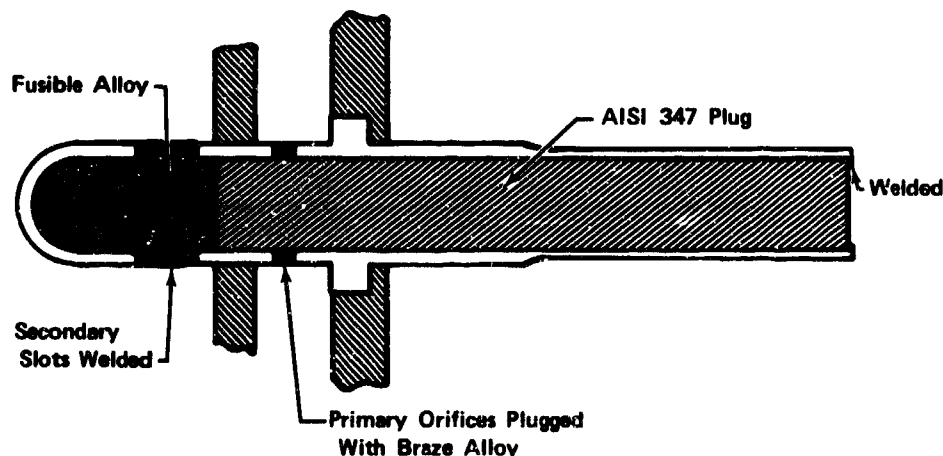


Figure 415. Six Elements With Blocked Primaries Plugged By Welding

FD 37523

2. The transpiration liner assembly was replaced by one with individual compartments within each zone. Each of the 18 compartments within each zone is supplied by a zone orifice. The external and zone orifices were resized so that most of the pressure drop occurs across the zone orifices, thereby reducing the drop across the Rigimesh. These modifications were made in an effort to maintain coolant flow to a given small compartment by a high pressure drop in the compartment supply orifice. The scheme forces a uniform distribution of coolant flow regardless of local variations in either chamber heat flux or Rigimesh porosity

3. The 12 point temperature rakes in the 11 in. plane were omitted because four equally spaced rakes in the 15 in. plane would become the standard for evaluating the profile
4. The facility fuel inlet filter was relocated to prevent maldistribution of fuel in the injector.

The preburner rig was assembled with the described modifications and mounted in E-8 test stand for continued hot firing.

Run 7.01 of build 4 of the preburner test rig was programed for a mixture ratio of 5 at both the 20 and 50% thrust levels. At the 20% level, flowsplit was to be varied from the cycle value of 0.56 to 0.40 and fuel temperature was to be raised from 125°R to 400°R. At 50% thrust, the LO₂ flowsplit was to be varied from 0.10 to 0.40. All excursions were planned to show profile effects as a function of injection conditions.

Run 7.01, conducted on January 31, 1970, was of full duration at 52.9 sec. Inspection of the rig after run 7.01 shows the combustion liner was blued to varying degrees in 12 places, spaced fairly uniformly around the circumference. Metal erosion was not evident in any area. In a number of places, the blueing extended from the upstream edge of the liner through the second transpiration cooling zone, with the third zone remaining clean and the blueing beginning again downstream of the transpiration section on the liner extension. The injector face as well as a typically discolored area of the liner as seen through a mirror is shown in figure 416. The data show that the maximum-to-average combustion temperature at 20% and a mixture ratio of 5 was 215°R. The expected LO₂ flowsplit at 20% and a mixture ratio of 5 cycle condition where the 215°R profile was measured was 38% instead of the programed 56%. This was caused by a leak between the primary and secondary cavity downstream of the preburner oxidizer valve. Because of this leak, no programed flowsplits were attained at 20% thrust and mixture ratio of 5.

The run 7.01 flowsplit excursion at 20% thrust, mixture ratio of 5 ranged from 29 to 38%, showing only a weak correlation, indicating lower combustion temperature profiles with lower flowsplits in this flowsplit range, as can be seen from figure 417 and 418.

During the 20% thrust and mixture ratio of 5 cycle point and the LO₂ flowsplit excursion, some of the combustion liner temperatures downstream of the transpiration section were above the average combustion temperature by approximately 135°R. The hottest liner temperature reached 2200°R at the end of the flowsplit excursions. Figure 419 shows the hottest liner temperature recorded during the run as well as a baseline temperature. The baseline temperature is taken from a thermocouple that remained intact throughout this build.

As fuel flow was increased at 20% thrust and a mixture ratio of 5 to allow a fuel temperature excursion from 125°R to 400°R, while maintaining a combustion temperature no higher than 1350°R, the liner temperature rapidly fell to below average combustion temperature. The maximum-to-average combustion temperature was 133°R at 380°R fuel temperature.

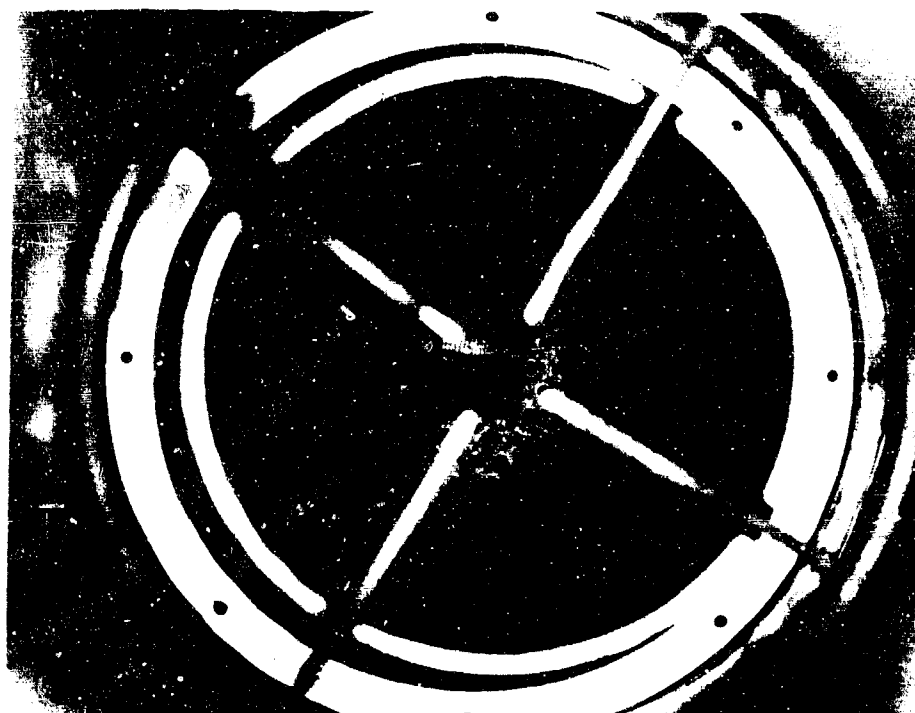


Figure 416. Preburner Discolored Area,
Run 7.01

FE 95379

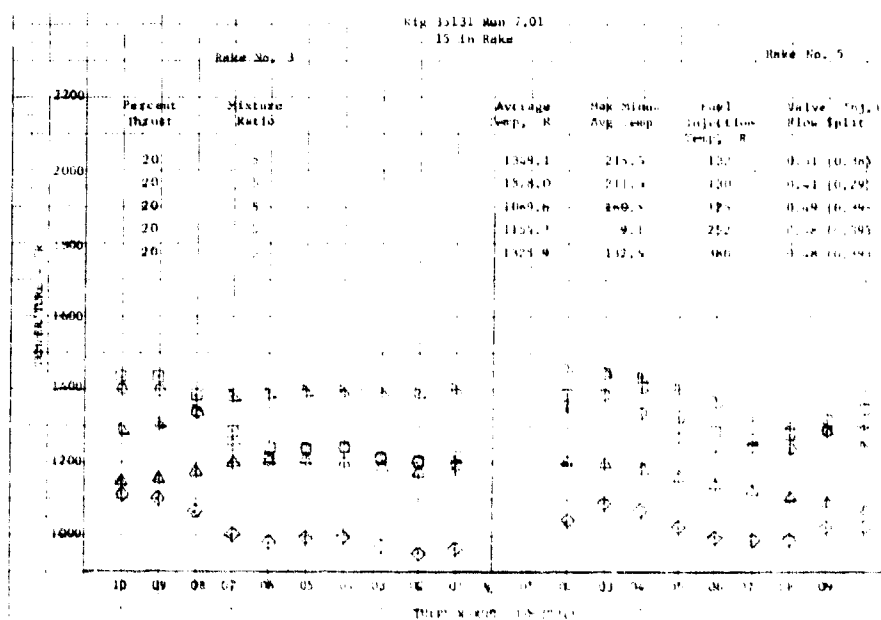


Figure 417. Fixed Area Preburner Temperature
Profile, Run 7.01

DF 78955

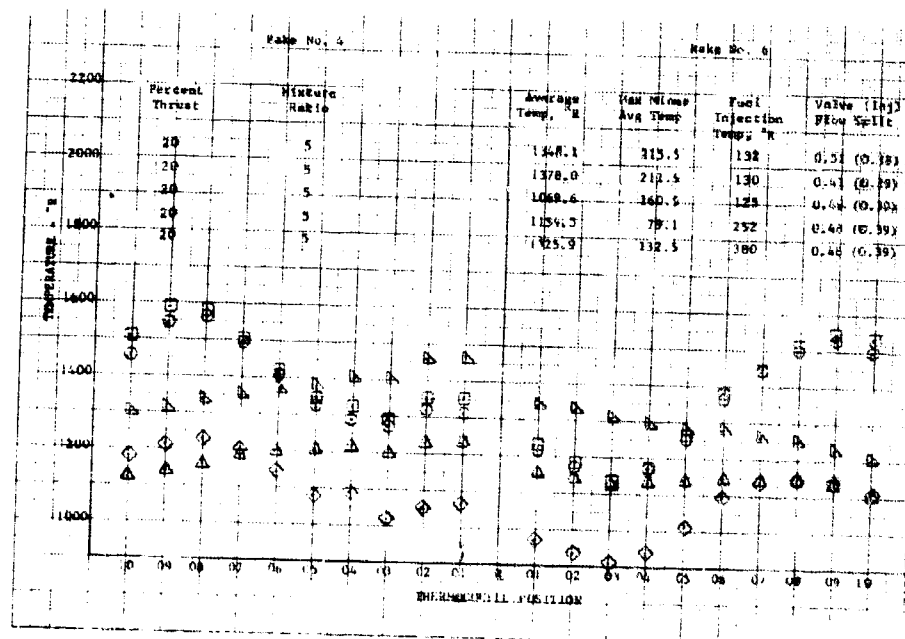


Figure 418. Fixed Area Preburner Temperature Profile, Run 7.01

DF 78956

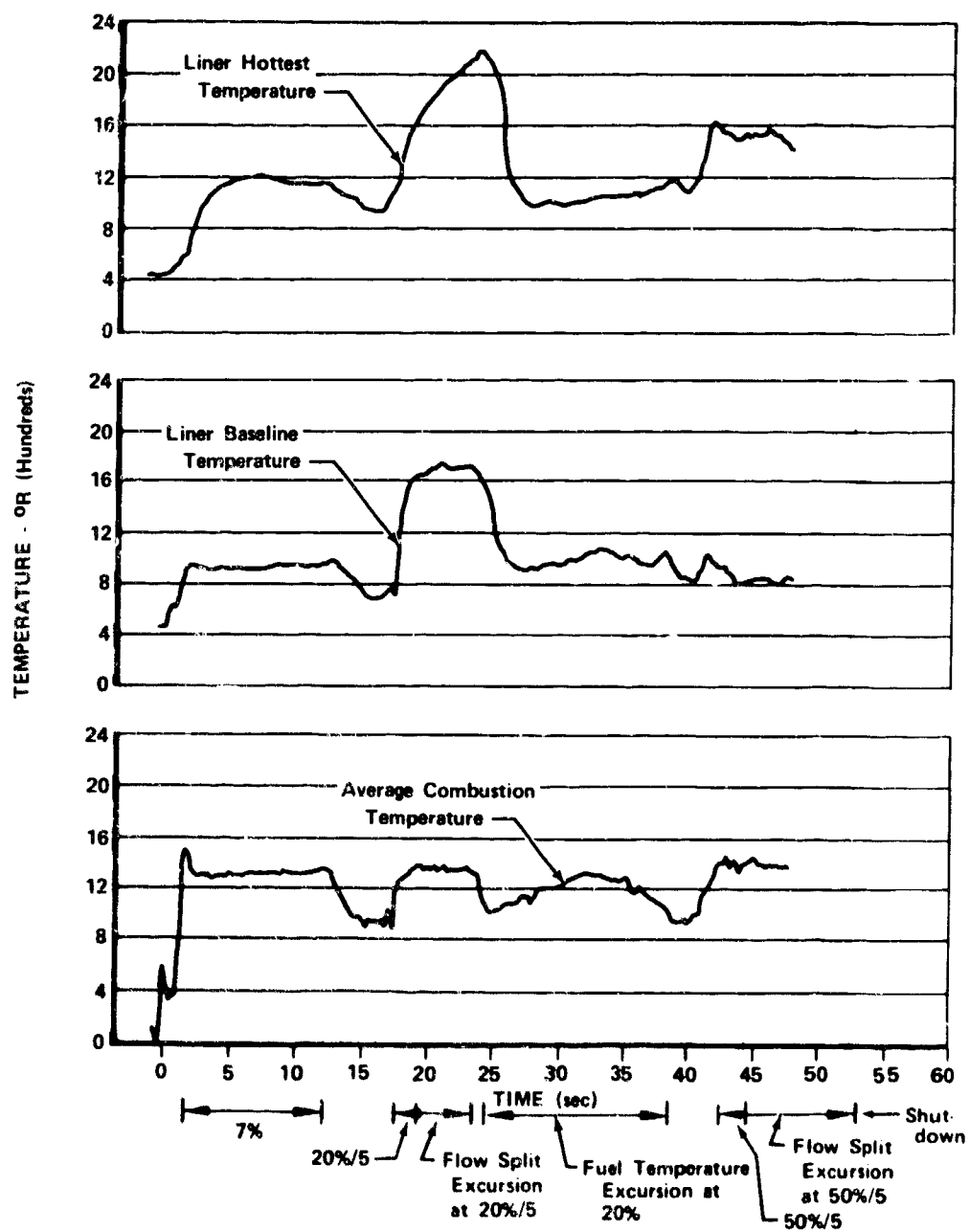


Figure 419. Preburner Scrub Liner and Average Combustion Temperature, Test 7.01

FD 38217A

As the propellants were ramped to the 50% thrust, mixture ratio of 5 condition, the combustion liner temperature, which had been higher than the average combustion temperature at 20% thrust, mixture ratio of 5 cycle conditions, climbed to 100°R above the 1400°R average combustion temperature.

During the ramp to 50% thrust, mixture ratio of 5, the Rosemont temperature probe, by which the GH₂ valve controls fuel temperature, failed and the resulting signal caused the GH₂ valve to close. Since the LH₂ valve is on total flow control (summing LH₂ and GH₂ flow) the total flow to the rig continued to follow the program but the flow was all liquid hydrogen at 102°R. Therefore, all 50% points were at this fuel temperature.

At 50% thrust, mixture ratio of 5 cycle conditions (fuel temperature of 102°R instead of 142°R and LO₂ flowsplit of 23% rather than 26%), the maximum-to-average combustion temperature spread was 190°R. The cycle predicted and attained conditions at 50% thrust are shown in tables XXXXV and XXXXVI. The LO₂ flowsplit was varied from 9% to 32%. During the flowsplit excursion at 50% thrust, mixture ratio of 5 the maximum-to-average temperature spread changed as illustrated in figure 420.

Run 8.02 was programed for 20% thrust and a mixture ratio of 5 with a LO₂ flowsplit excursion that would cause the injected flowsplit to range from 38% to 56% and a reduction of LO₂ flow while at 20% thrust and mixture ratio of 5 to lower the average combustion temperature to approximately 1000°R. The reduction in LO₂ flow simulates the point attained on run 7.01 where fuel flow was increased in preparation for increasing fuel temperature. Propellant flows were scheduled to be increased to 50% thrust and mixture ratios of 5, 6, and 7.

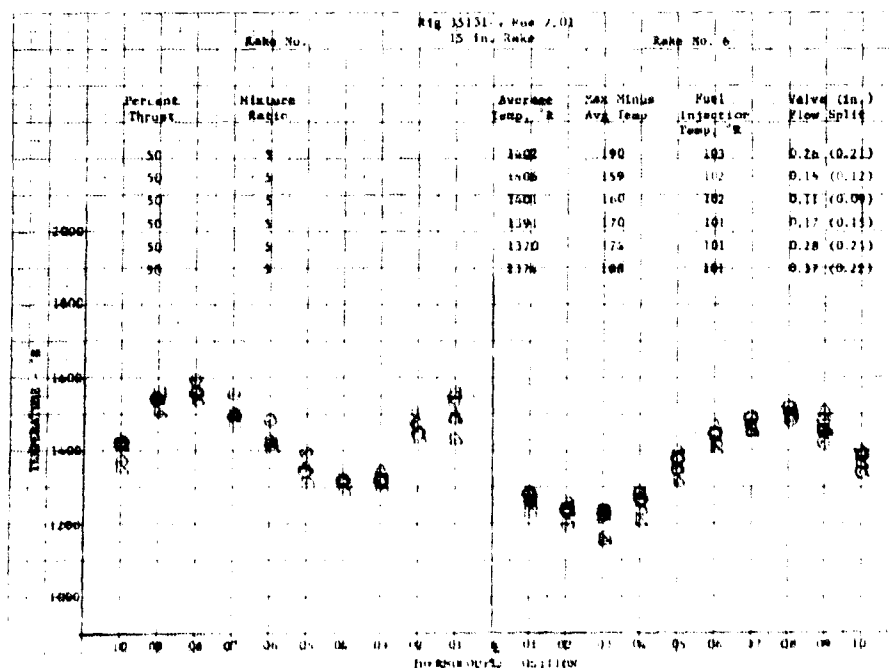


Figure 420. Fixed Area Preburner Temperature Probes

DF 78957

Table XLV. Predicted vs Actual Performance For 50% Thrust,
Engine Mixture Ratio of 5, Rig 35131-4, Run 7.01

Rig No. 33151	Engine Cycle Predicted	Test Results
Chamber Pressure - psia	2.010.1	2020.
Total Oxidizer Flow - lb/sec	28.23	28.71
Oxidizer Primary Flow - lb/sec	7.293	7.48
Oxidizer Secondary Flow - lb/sec	20.94	21.23
Total Fuel Flow - lb/sec	38.07	37.807
Injector Fuel Flow - lb/sec	36.97	36.461
Upper Coolant Liner Flow - lb/sec	0.690***	0.594
Lower Coolant Liner Flow - lb/sec	0.512***	0.386
Injector Mixture Ratio	0.763	0.787
Overall Mixture Ratio	0.742	0.759
Combustion Temperature - °R	1488.	1402.
Flow Divider Valve Position - %	48.2	48.4
Oxidizer Injector Primary ΔP	558.6	344.2*
Oxidizer Injector Secondary ΔP	35.0	47.5*
Fuel Injector ΔP (Plate)	110.	88.1
Oxidizer Injector Temperature - °R	208.	187.
Fuel Injector Temperature - °R	142.0	103.**
Temperature Profile (11 in.) - °R	0.	
Temperature Profile (15 in.) - °R	0.	190.
Average Temperature (11 in.) - °R	1488.	
Average Temperature (15 in.) - °R	1488.	1402.
Oxidizer Primary/Total Flow Split (Valve)	0.2583	0.2604*
Oxidizer Primary Injector A_{cd} - in ²	0.0550	0.0731*
Oxidizer Secondary Injector A_{cd} - in ²	0.6309	0.5589*
Fuel Injector A_{cd} (Overall) - in ²	3.1***	NAV
η_c^* (Based on P_c , WT) - %	100.	99.3
η_c^* (Based on Average Temperature at 11 in.) - %	100.	
η_c^* (Based on Average Temperature at 15 in.) - %	100.	97.5
Transpiration Liner Flow - lb/sec	0.372***	0.366
Fuel Injector A_{cd} (Plate) - in ²	3.3***	3.22

*Note: There is an apparent leak of primary injector flow into the secondary injector cavity. Injector flow split is 0.21.

**At the 50% condition a malfunction in the facility control system shut off the gaseous hydrogen flow driving fuel temperature down.

***Rig Cycle Predictions.

Table XLVI. Predicted vs Actual Performance for 20% Thrust,
Engine Mixture Ratio of 5, Rig 35131-4 Run 10.02

	Rig Cycle Predicted	Test Results
Chamber Pressure - psia	708.7	694.
Total Oxidizer Flow - lb/sec	9.59	8.93
Oxidizer Primary Flow - lb/sec	5.367	4.49
Oxidizer Secondary Flow - lb/sec	4.22	4.44
Total Fuel Flow - lb/sec	13.76	13.81
Injector Fuel Flow - lb/sec	13.38	13.36
Upper Coolant Liner Flow - lb/sec	0.2506	0.2085
Lower Coolant Liner Flow - lb/sec	0.1832	0.1310
Injector Mixture Ratio	0.716	0.663
Overall Mixture Ratio	0.697	0.647
Combustion Temperature - °R	1394.	1349.
Flow Divider Valve Position - %	25.8	26.0
Oxidizer Injector Primary ΔP	310.5	131.*
Oxidizer Injector Secondary ΔP	4.7	7.*
Fuel Injector ΔP (Plate)	35.56	37.
Oxidizer Injector Temperature - °R	200.0	188.2
Fuel Injector Temperature - °R	125.4	128.3
Temperature Profile (11 in.) - °R	0.	NAV
Temperature Profile (15 in.) - °R	0.	196.
Average Temperature (11 in.) - °R	1394.	NAV
Average Temperature (15 in.) - °R	1394.	1348.
Oxidizer Primary/Total Flow Split	0.5596	0.5023*
(Valve)	0.0550	0.0711*
Oxidizer Primary Injector A_{cd} - in ²	0.3509	0.3046*
Oxidizer Secondary Injector A_{cd} - in ²	3.1	NAV
Fuel Injector A_{cd} (Overall) - in ²	100.	103.
η_c^* (Based on P_c , WT) - %		
η_c^* (Based on Average Temperature at 11 in.) - %	100.	NAV
η_c^* (Based on Average Temperature at 15 in.) - %	100.	102.
Transpiration Liner Flow - lb/sec	0.110	0.111
Fuel Injector A_{cd} (Plate) - in ²	3.3	3.14

*Note: There is an apparent leak of oxidizer flow from the primary injector cavity into the secondary cavity. Injector flow split is 0.43.

The LO₂ flow excursion at 20% thrust and mixture ratio of 5 indicated the effect of cycle flowsplits on temperature profile. The programed reduction in LO₂ flow at 20% thrust and mixture ratio of 5 was to show the effect of the decrease of LO₂ flow on liner temperatures while 50% thrust, mixture ratio of 5, 6, and 7 levels would indicate the maximum-to-average temperature at higher average combustion temperatures.

Run 8.02 was conducted on February 6, 1970. The run was automatically advanced after 1.47 sec due to a high combustion liner temperature. Post-test inspection of the rig revealed no damage. It was concluded that LO_2 had accumulated behind the combustion liner during the preignition LO_2 lead and was burned with transpiration coolant.

Run 9.01 was conducted on February 7, 1970 and was a programmed repeat of run 8.02, although a GHe purge of approximately 0.4 lb/sec was introduced through the fuel side of the injector and through the transpiration and outer cooled liners, or 4 sec before the start of the preignition LO_2 lead in an effort to prevent LO_2 from accumulating behind the liner. Run 9.01 was automatically advanced after 1.47 sec because of a high combustion liner temperature. Inspection of the rig after run 9.01 revealed no damage.

Subsequent analysis of data from run 8.02 and 9.01 indicate the combustion liner temperatures were dropping to LO_2 saturation temperatures during the pre-run countdown, indicating a leak in the preburner oxidizer valve prior to the preignition LO_2 lead.

Run 10.02 was scheduled as a repeat of 8.02 except the GHe purge to the fuel line was initiated two minutes before the run to more adequately purge the chamber of puddled LO_2 .

Run 10.02, conducted on February 9, 1970, was automatically advanced after 29.1 sec, just before the end of the fuel ramp to 50% thrust and a mixture ratio of 5, resulting from an erroneously high fuel injector ΔP signal.

During acceleration to 50% flowrates and after shutdown of run 10.02, the chamber pressure tap furnishing the low side pressure to the fuel injector differential pressure remained at the 20% chamber pressure level indicating the tap was plugged. Investigation of the pressure tap after shutdown revealed water in the probe. Since the chamber pressure probe has cold (120°R) fuel circulating around it, ice could have formed in the probe from water created in the combustion process. Inspection of the rig after run 10.02 did not reveal any damage to rig hardware. Figure 421 shows a portion of the injector face and a typical section of the liner as viewed through a mirror. The injector face had experienced one small spot of metal erosion which is in the center of the darkened area seen in the photograph.

For subsequent runs the low side of the fuel injector differential pressure was furnished from an igniter chamber pressure port which was not surrounded with cold fuel. The igniter is turned off upon reaching 20% thrust, and therefore is a good chamber pressure source that does not freeze.

The 20% thrust, mixture ratio of 5 cycle point predicted and attained conditions are generally the same as those previously shown in table VA-15 for run 10.02, except the attained flowsplit was 43%. The LO_2 flowsplit excursion was made across a range of 42% to 52%. The excursion had no effect on either temperature profile or distribution as can be seen from figure 422 and 423. Figure 422 also shows that the reduction of LO_2 flow to get 1098°R average combustion temperature did not affect profile. The combustion liner temperature did not drop off when LO_2 flow decreased average combustion temperature (shown in figure 424) as it had in test 7.01 where average combustion temperature was decreased by increasing fuel flow.



Figure 421. Portion of Injector Face and Typical
Liner Section Viewed Through Mirror

FE 95592

Rig J5131 Test 10.02
15-in. Rake

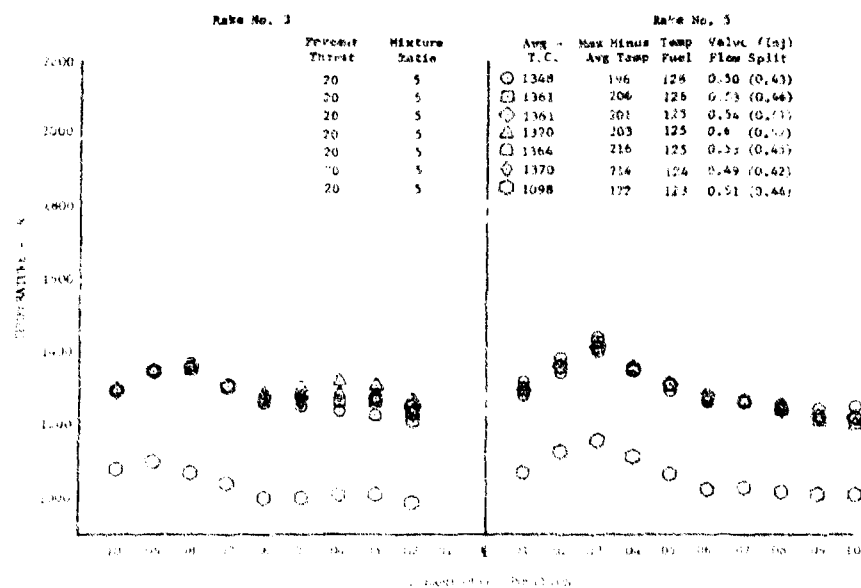


Figure 422. Fixed Area Preburner Temperature
Profile, Test 10.02

DF 79863

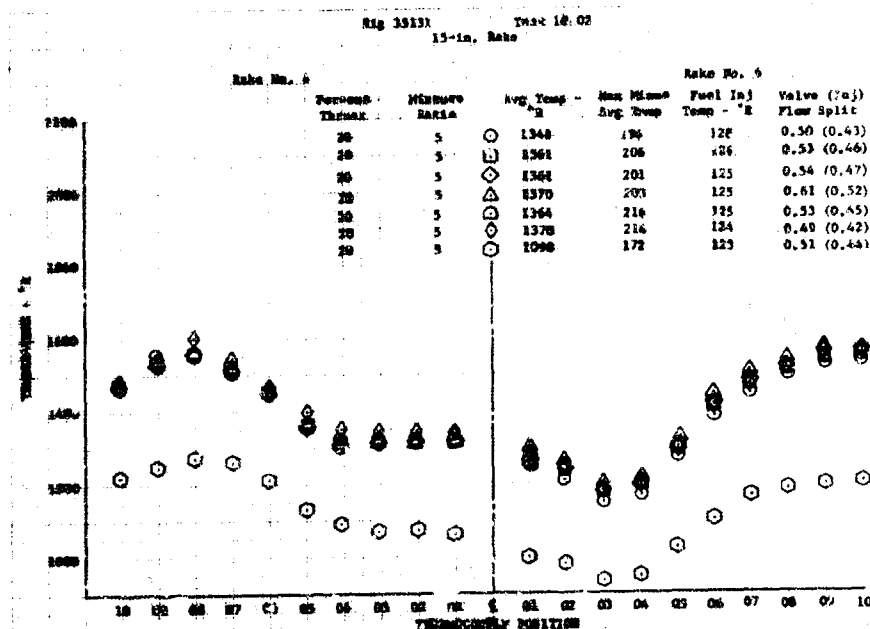


Figure 423. Fixed Area Preburner Temperature Profile, Test 10.02 DF 79864

In an effort to ensure getting the 50% thrust, mixture ratio of 5, 6, and 7 data points, the next test was programed to omit a repeat of the 20% points and ramp directly to 50%.

Run 11.01 was programed for cycle points at 50% thrust, mixture ratio of 5, 6, and 7. The ramp to 50% thrust and mixture ratio of 5 was stopped at 20% long enough to open the preburner oxidizer valve secondary port.

Run 11.01, conducted on February 11, 1970, was a full duration run of 35 sec. Inspection of the rig after shutdown did not reveal any damage. Figure 425 shows the injector face. As can be seen in the photograph, the eroded areas on the injector face do not constitute any problem. Conditions attained on test 11.01 are shown in tables XLVII, XLVIII, and XLIX. The conditions attained are close to prediction except for the leak into the secondary cavity causing an incorrect flowsplit. The temperature profile is an acceptable 173°R maximum-to-average temperature at 2106°R average. The temperature distribution retains the characteristic shape as shown in figures 426 and 427. Liner temperature during the mixture ratio excursion at 50% remained at or near the average combustion temperature, also shown in figure 427.

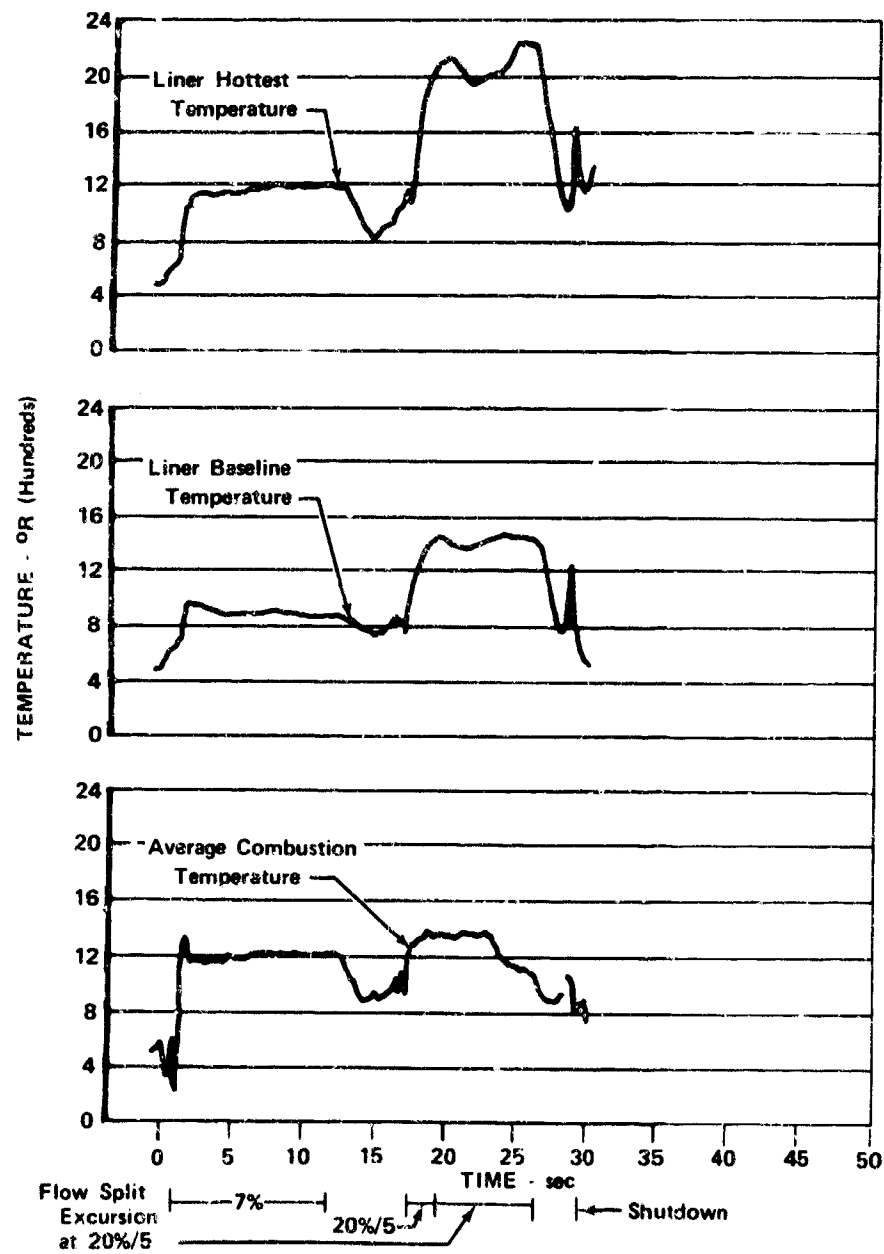


Figure 424. Preburner Scrub Liner and Average Combustion Temperature, Test 10.02

FD 39144A



Figure 425. Injector Face Showing Eroded Areas FE 95672

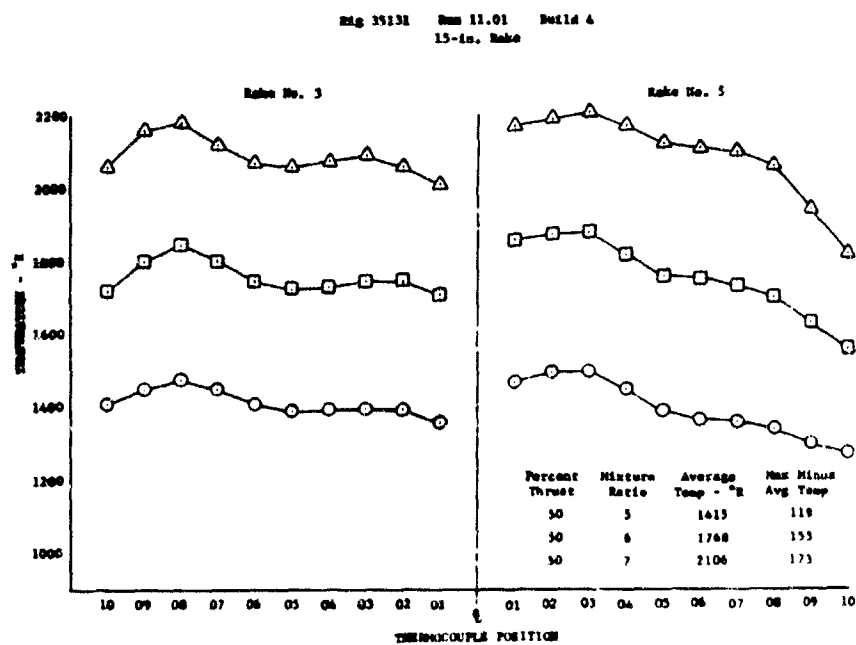


Figure 426. Fixed Area Preburner Temperature Profile, Run 11.01, Build 4 DF 79865

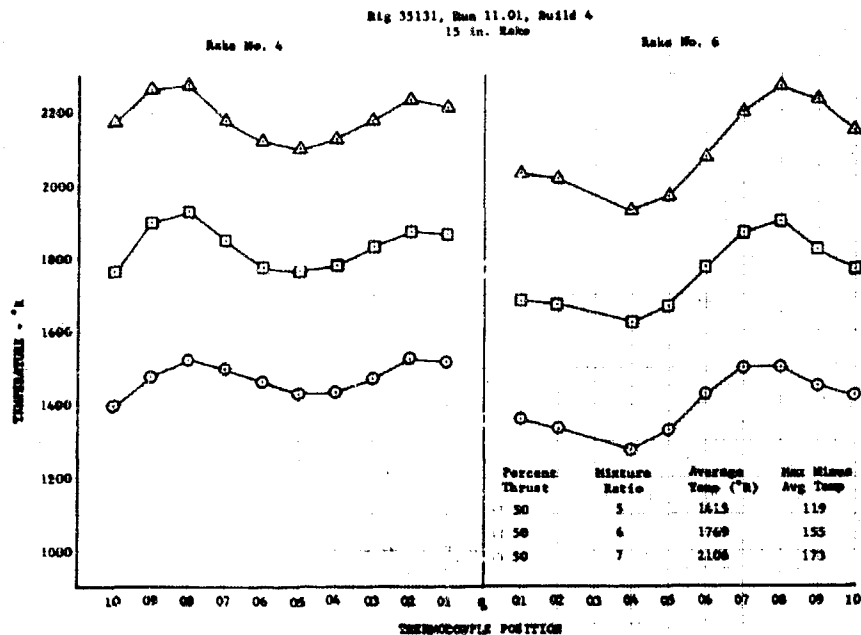


Figure 427. Fixed Area Preburner Temperature Profile, Run 11.01, Build 4

DF 79866

Based on the acceptable combustion temperature profile and distribution at 2106°R average combustion temperature, and liner temperatures that show the transpiration cooling combustion liner to be operating satisfactorily, it was decided to program a run for 100% thrust and a mixture ratio of 7 where the average combustion temperature is the highest in the cycle.

Run 12.01 was programed for 75/7, 100/6, and 100/7 cycle data points. The preburner oxidizer valve was programed to open while the propellant flow was near the 20% level, but still in transient to 75% thrust.

Run 12.01 conducted on February 13, 1970, was manually advanced after 16.4 seconds because of two erroneous high outer combustion liner temperatures. The run was advanced before opening the preburner oxidizer valve secondary ports.

Table XLVII. Predicted vs Actual Performance for
50% Thrust, Engine Mixture Ratio of 5,
Rig 35131-4, Run 11.01

	Engine Cycle Predicted	Test Results
Chamber Pressure - psia	2010.1	203.2
Total Oxidizer Flow - lb/sec	28.23	28.34
Oxidizer Primary Flow - lb/sec	7.293	7.16
Oxidizer Secondary Flow - lb/sec	20.94	21.18
Total Fuel Flow - lb/sec	38.07	38.07
Injector Fuel Flow - lb/sec	36.97	36.64
Upper Coolant Liner Flow - lb/sec	0.690	0.672
Lower Coolant Liner Flow - lb/sec	0.512	0.370
Injector Mixture Ratio	0.763	0.766
Overall Mixture Ratio	0.742	0.745
Combustion Temperature - °R	1488.	1415.
Flow Divider Valve Position - PR	48.2	48.1
Oxidizer Injector Primary ΔP	558.6	347.*
Oxidizer Injector Secondary ΔP	35.0	45.6*
Fuel Injector ΔP (Plate)	110.	124.
Oxidizer Injector Temperature - °R	208.	190.
Fuel Injector Temperature - °R	142.0	142.
Temperature Profile (11 in.) - °R	0.0	NAV
Temperature Profile (15 in.) - °R	0.0	119.
Average Temperature (11 in.) - °R	1488.	NAV
Average Temperature (15 in.) - °R	1488.	1415.
Oxidizer Primary/Total Flow Split (Valve)	0.2583	0.2526*
Oxidizer Primary Injector A_{cd} - in ²	0.0550	0.0697*
Oxidizer Secondary Injector A_{cd} - in ²	0.6309	0.5689*
Fuel Injector A_{cd} (Overall) - in ²	3.1**	NAV
η_{c*} (Based on P_c , wt) - %	100.	99.8
η_{c*} (Based on Average Temperature at 11 in.) - %	100.	NAV
η_{c*} (Based on Average Temperature at 15 in.) - %	100.	98.0
Rigimesh Liner Flow - lb/sec	0.372**	0.384
Fuel Injector A_{cd} (Plate) - in ²	3.3**	3.2

*Note: There is an apparent leak of oxidizer flow from the injector
primary cavity into the secondary cavity. (Injector F.S. = 0.22)

**Rig Cycle Predictions

Table XLVIII. Predicted vs Actual Performance for 50% Thrust,
Engine Mixture Ratio of 6, Rig 35131-4, Run 11.01

	Engine Cycle Predicted	Test Results
Chamber Pressure - psia	1958.1	1985.
Total Oxidizer Flow - lb/sec	29.54	29.79
Oxidizer Primary Flow - lb/sec	7.470	7.29
Oxidizer Secondary Flow - lb/sec	22.07	22.50
Total Fuel Flow - lb/sec	31.58	31.49
Injector Fuel Flow - lb/sec	30.77	30.28
Upper Coolant Liner Flow - lb/sec	0.573	0.583
Lower Coolant Liner Flow - lb/sec	0.420	0.313
Injector Mixture Ratio	0.960	0.974
Overall Mixture Ratio	0.935	0.946
Combustion Temperature - °R	1827	1769.
Flow Divider Valve Position - %	48.2	48.0
Oxidizer Injector Primary ΔP	586.0	386*
Oxidizer Injector Secondary P	38.5	49.3*
Fuel Injector ΔP (Plate)	90.2	103.
Oxidizer Injector Temperature - °R	207.	190.
Fuel Injector Temperature - °R	163.3	166.
Temperature Profile (11 in.) - °R	0°	NAV
Temperature Profile (15 in.) - °R	0°	155.
Average Temperature (11 in.) - °R	1827.	NAV
Average Temperature (15 in.) - °R	1827.	1769.
Oxidizer Primary/Total Flow Split Valve	0.2528	0.2445*
Oxidizer Primary Injector A_{cd} - in ²	0.0550	0.0672*
Oxidizer Secondary Injector A_{cd} - in ²	0.6347	0.5814*
Fuel Injector A_{cd} (overall) - in ²	3.1**	NAV
η_c^* (based on P_c , WT) - %	100.	99.1
η_c^* (based on average temperature at 11 in.) - %	100.	NAV
η_c^* (based on average temperature at 15 in.) - %	100.	97.7
Rigimesh Liner Flow - lb/sec	0.308**	0.306
Fuel Injector A_{cd} (plate) - in ²	3.3**	3.2

*Note: There is an apparent leak of oxidizer flow from the injector
primary cavity into the secondary cavity. (Injector preburner = 0.21)
**Rig Cycle Predictions.

Table XLIX. Predicted vs Actual Performance for 50% Thrust,
Engine Mixture Ratio of 7, Rig 35131-4, Run 11.01

	Engine Cycle Predicted	Test Results
Chamber Pressure - psia	1915.2	1964.
Total Oxidizer Flow - lb/sec	30.60	30.76
Oxidizer Primary Flow - lb/sec	7.596	7.42
Oxidizer Secondary Flow - lb/sec	23.00	23.34
Total Fuel Flow - lb/sec	27.13	27.06
Injector Fuel Flow - lb/sec	26.40	36.04
Upper Coolant Liner Flow - lb/sec	0.493	0.500
Lower Coolant Liner Flow - lb/sec	0.357	0.274
Injector Mixture Ratio	1.159	1.17
Overall Mixture Ratio	1.128	1.137
Combustion Temperature - °R	2157.	2106.
Flow Divider Valve Position - %	48.2	48.0
Oxidizer Injector Primary ΔP	605.8	415.*
Oxidizer Injector Secondary ΔP	41.3	53.0*
Fuel Injector ΔP (Plate)	75.1**	86.5
Oxidizer Injector Temperature - °R	207.	189.
Fuel Injector Temperature - °R	182.8	182.7
Temperature Profile (11 in.) - °R	0°	NAV
Temperature Profile (15 in.) - °R	0°	173.
Average Temperature (11 in.) - °R	2157.	NAV
Average Temperature (15 in.) - °R	2157.	2106.
Oxidizer Primary/Total Flow Split	0.2482	0.2413*
Oxidizer Primary Injector A_{cd} - in ²	0.0550	0.0661*
Oxidizer Secondary Injector A_{cd} - in ²	0.6380	0.5815*
Fuel Injector A_{cd} (Overall) - in ²	3.1**	NAV
c^* (Based on P_{C^*} , WT) - %	100	99.7
c^* (Based on Average Temperature at 11 in.) - %	100	NAV
c^{**} (Based on Average Temperature at 15 in.) - %	100	98.1
Rigimesh Liner Flow - lb/sec	0.264	0.250
Fuel Injector A_{cd} (Plate) - in ²	3.3**	3.1

*Note: There is an apparent leak of oxidizer flow from the injector primary cavity into the secondary cavity.

**Rig Cycle Predictions.

Inspection of the rig after test 12.01 did not reveal any damage. Both the high reading liner thermocouples on which the run was advanced, used during the run could be seen through the nozzle throat. No indication of high temperature was observed near these thermocouples, which were open after the test. Therefore, it was concluded that the thermocouples opened during the test giving an erroneously high temperature reading.

Run 13.01 was programed as a repeat of programed run 12.01. Run 13.01, made on February 13, 1970, was automatically advanced after 25.0 seconds due to an erroneous high outer combustion liner temperature. The advance occurred during the 75% thrust, $r = 7$ data point. Control system gains provided an unprogramed 300-millisecond data point at 75% thrust, $r = 5$.

Inspection of the rig after run 13.01 did not reveal damage as viewed through the nozzle or behind the inner and outer combustion liners as reviewed by borescope inspection, through pulse gun ports. The liner thermocouple that caused the automatic advance was found electrically open inside the rig. It became obvious that liner thermocouples were not durable enough to use outputs as advance sensing parameters. Therefore, run 14.01 was run without liner temperature parameters.

The combustion liner temperature remained satisfactory at 75% thrust, $r = 7$ as can be seen in figure 428. The conditions attained on run 13.01 are shown in tables L, LI, and LII. Two data points are shown at 75% thrust, $r = 7$ because a shift in profile occurred during that data point. The temperature distribution corresponding to the early part of the 75% thrust, $r = 7$ data point is shown in figures 429 and 430. The temperature distribution after the profile shift is shown in figures 431 and 432. Figures 433 and 434 are plots of temperature distribution every 100 milliseconds on run 13.01 between 75% thrust, $r = 5$ and the end of the 75% thrust, $r = 7$ data point. It can be seen that at time 186.5 sec the shift in profile occurred. This is further illustrated by figure 435 which is a plot of thermocouple No. 1 on rake 3. At time 186.5 sec the temperature shifts upward by 250°R. The temperature distribution curve before 186.5 sec is the same as all previous data points at any mixture ratio and thrust level.

The temperature profile at 75% thrust, $r = 7$ before time 186.5 sec was 189°R maximum-to-average at 2250°R. The temperature profile at 75% thrust, $r = 7$ after time 186.5 sec was 244°R at 2268°R average temperature. The shift at time 186.5 sec is a permanent shift affecting the temperature profile and distribution at all subsequent data points on run 13.01 and 14.01.

A cracked fuel faceplate seal, between the injector face and injector housing, was discovered in run 14.01 post-test inspection. It was concluded that the faceplate seal cracked at time 186.5 sec in run 13.01. The cracked seal caused fuel leakage at the chamber outside diameter which robbed fuel from the core causing high combustion temperatures toward the center of the injector. The cracked seal was not found during rig inspection after run 13.01 and run 14.01 was apparently made with a cracked seal.

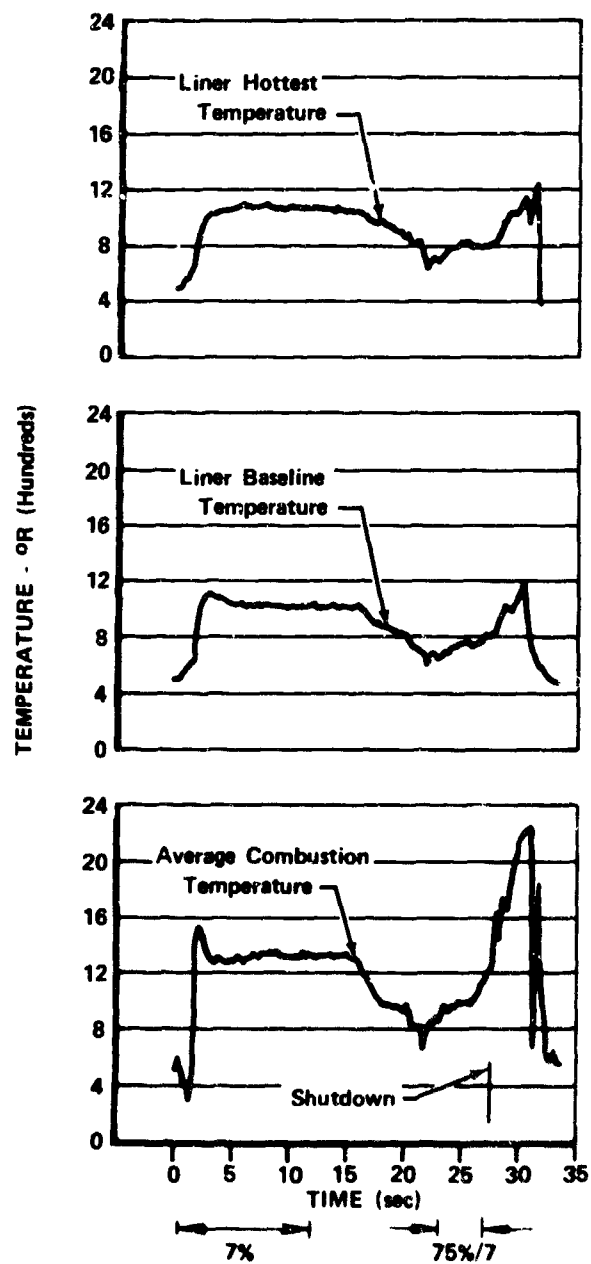


Figure 428. Preburner Scrub Liner and Average Combustion Temperature, Test 13.01

FD 39145A

Table L. Predicted vs Actual Performance for 75% Thrust, Engine
Mixture Ratio of 5, Rig 35131-4, Run 13.01

	Engine Cycle Predicted	Test Results
Chamber Pressure - psia	3281.0	3283
Total Oxidizer Flow - lb/sec	50.20	50.07
Oxidizer Primary Flow - lb/sec	9.117	7.60
Oxidizer Secondary Flow - lb/sec	41.08	42.47
Total Fuel Flow - lb/sec	58.05	57.74
Injector Fuel Flow - lb/sec	56.36	55.64
Upper Coolant Liner Flow - lb/sec	1.053**	0.990
Lower Coolant Liner Flow - lb/sec	0.791**	0.559
Injector Mixture Ratio	0.891	0.891
Overall Mixture Ratio	0.865	0.867
Combustion Temperature - °R	1713	1692
Flow Divider Valve Position - %	63.8	64.3
Oxidizer Injector Primary ΔP	854.5	372.9*
Oxidizer Injector Secondary ΔP	113.3	134.7*
Fuel Injector ΔP (Plate)	214**	252.3
Oxidizer Injector Temperature - °R	221	187
Fuel Injector Temperature - °R	159.8	186
Temperature Profile (11 in.) - °R	0	NAV
Temperature Profile (15 in.) - °R	0	150
Average Temperature (11 in.) - °R	1713	NAV
Average Temperature (15 in.) - °R	1713	1692
Oxidizer Primary/Total Flow Split (Valve)	0.1816	0.1516*
Oxidizer Primary Injector A_{cd} - in ²	0.0550	0.0713*
Oxidizer Secondary Injector A_{cd} - in ²	0.6810	0.6631*
Fuel Injector A_{cd} (Overall) - in ²	3.1**	NAV
η_c^* (Based on P_c , WT) - %	100	98.7
η_c^* (Based on Average Temperature at 11 in.) - %	100	NAV
η_c^* (Based on Average Temperature at 15 in.) - %	100	98.7
Rigimesh Liner Flow - lb/sec	0.575**	0.552
Fuel Injector A_{cd} (Plate) - in ²	3.3**	3.3

*Note: There is an apparent leak of oxidizer flow from the primary
cavity into the secondary cavity. (Injector FS = 0.13)

**Rig Cycle Predictions

Table LI. Predicted vs Actual Performance for 75% Thrust, Engine
Mixture Ratio of 7, Rig 35131-4, Run13.01, Before Pro-
file Shift

	Engine Cycle Predicted	Test Results
Chamber Pressure - psia	3006.6	2993
Total Oxidizer Flow - lb/sec	49.29	49.46
Oxidizer Primary Flow - lb/sec	7.283	7.26
Oxidizer Secondary Flow - lb/sec	42.07	42.20
Total Fuel Flow - lb/sec	42.00	41.89
Injector Fuel Flow - lb/sec	40.91	40.40
Upper Coolant Liner Flow - lb/sec	0.762**	0.701
Lower Coolant Liner Flow - lb/sec	0.560**	0.422
Injector Mixture Ratio	1.205	1.213
Overall Mixture Ratio	1.174	1.181
Combustion Temperature - °R	2235	2250
Flow Divider Valve Position - %	63.8	64.3
Oxidizer Injector Primary ΔP	550.5	366.3*
Oxidizer Injector Secondary ΔP	114.0	137.4*
Fuel Injector ΔP (Plate)	135**	158.9
Oxidizer Injector Temperature - °R	211	185
Fuel Injector Temperature - °R	190.4	205
Temperature Profile (11 in.) - °R	0	NAV
Temperature Profile (15 in.) - °R	0	189
Average Temperature (11 in.) - °R	2235	NAV
Average Temperature (15 in.) - °R	2235	2250
Oxidizer Primary/Total Flow Split (Valve)	0.1477	0.147*
Oxidizer Primary Injector A_{cd} - in ²	0.0550	0.0759*
Oxidizer Secondary Injector A_{cd} - in ²	0.6975	0.6277*
Fuel Injector A_{cd} (Overall) - in ²	3.1**	NAV
η_c^* (Based on P_c , WT) - %	100	99.6
η_c^* (Based on Average Temperature at 11 in.) - %	100	NAV
η_c^* (Based on Average Temperature at 15 in.) - %	100	99.4
Fuel Injector A_{cd} (Plate) - in ²	3.3**	3.2
Rigimesh Liner Flow - lb/sec	0.416**	0.368

*Note: There is an apparent leak of oxidizer flow from the primary
cavity into the secondary cavity (Injector Flow Split = 0.13)

**Rig Cycle Predictions

Table LII. Predicted vs Actual Performance for 75% Thrust, Engine
Mixture Ratio of 7, Rig 35131-4, Run 13.01, After Pro-
file Shift

	Engine Cycle Predicted	Test Results
Chamber Pressure - psia	3006.6	2982
Total Oxidizer Flow - lb/sec	49.29	49.49
Oxidizer Primary Flow - lb/sec	7.283	7.12
Oxidizer Secondary Flow - lb/sec	42.07	42.37
Total Fuel Flow - lb/sec	42.00	41.95
Injector Fuel Flow - lb/sec	40.91	40.42
Upper Coolant Liner Flow - lb/sec	0.762**	0.718
Lower Coolant Liner Flow - lb/sec	0.560**	0.428
Injector Mixture Ratio	1.205	1.213
Overall Mixture Ratio	1.174	1.180
Combustion Temperature - °R	2235	2268
Flow Divider Valve Position - %	63.8	64.3
Oxidizer Injector Primary ΔP	550.5	378.1*
Oxidizer Injector Secondary ΔP	114.0	142.5*
Fuel Injector ΔP (Plate)	135**	170.2
Oxidizer Injector Temperature - °R	211	186
Fuel Injector Temperature - °R	190.4	201
Temperature Profile (11 in.) - °R	0	NAV
Temperature Profile (15 in.) - °R	0	244
Average Temperature (11 in.) - °R	2235	NAV
Average Temperature (15 in.) - °R	2235	2268
Oxidizer Primary/Total Flow Split (Valve)	0.1477	0.1437*
Oxidizer Primary Injector A_{cd} - in ²	0.0550	0.0664*
Oxidizer Secondary Injector A_{cd} - in ²	0.6975	0.6451*
Fuel Injector A_{cd} (Overall) - in ²	3.1**	NAV
η_c^* (Based on P_c , wt) - %	100	100.1
η_c^* (Based on Average Temperature at 11 in.) - %	100	NAV
η_c^* (Based on Average Temperature at 15 in.) - %	100	99.9
Rigimesh Liner Flow - lb/sec	0.416**	0.383
Fuel Injector A_{cd} (Plate) - in ²	3.3**	3.1

*Note: There is an apparent leak of oxidizer flow from the primary
cavity into the secondary cavity (Injector flow split = 0.13)

**Rig cycle predictions

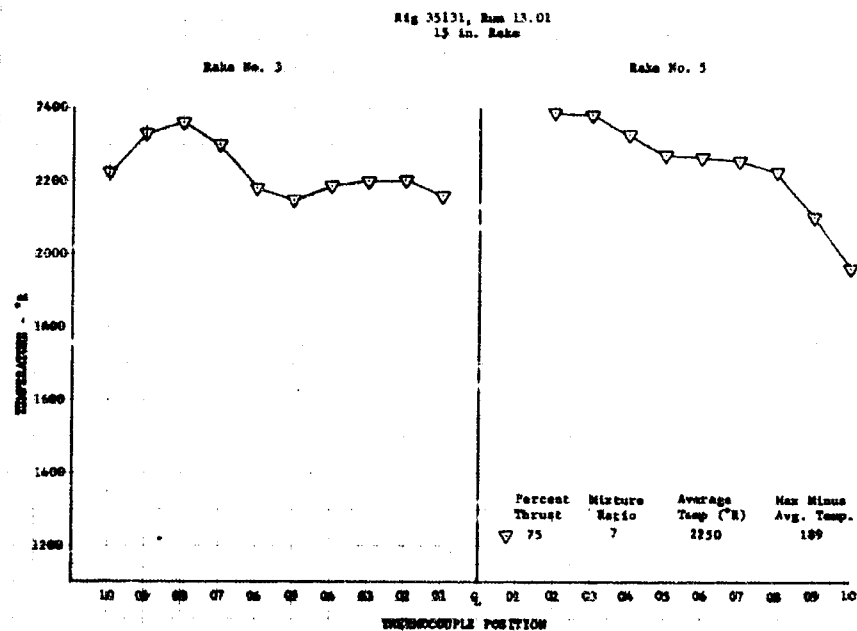


Figure 429. Fixed Area Preburner Temperature Profile, Run 13.01

DF 79867

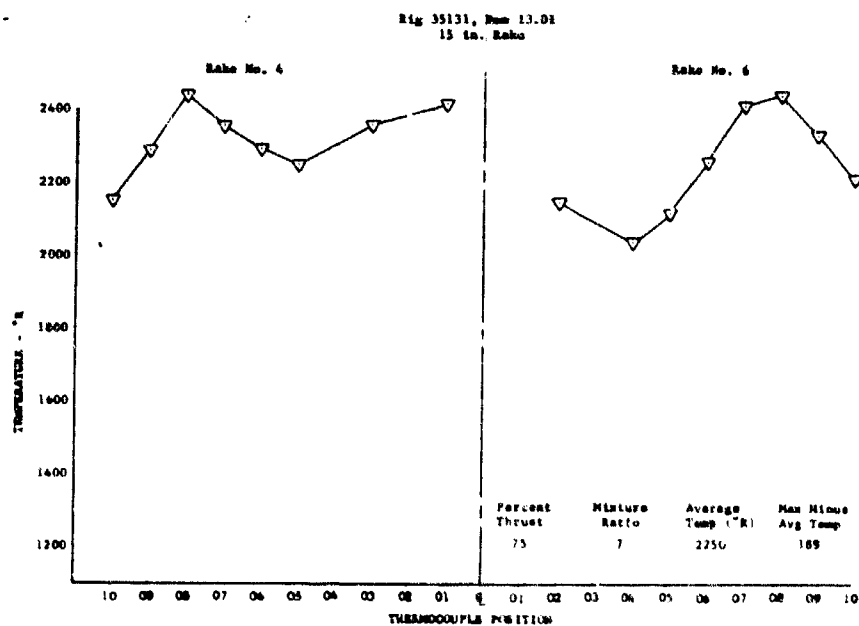


Figure 430. Fixed Area Preburner Temperature Profile, Run 13.01

DF 79868

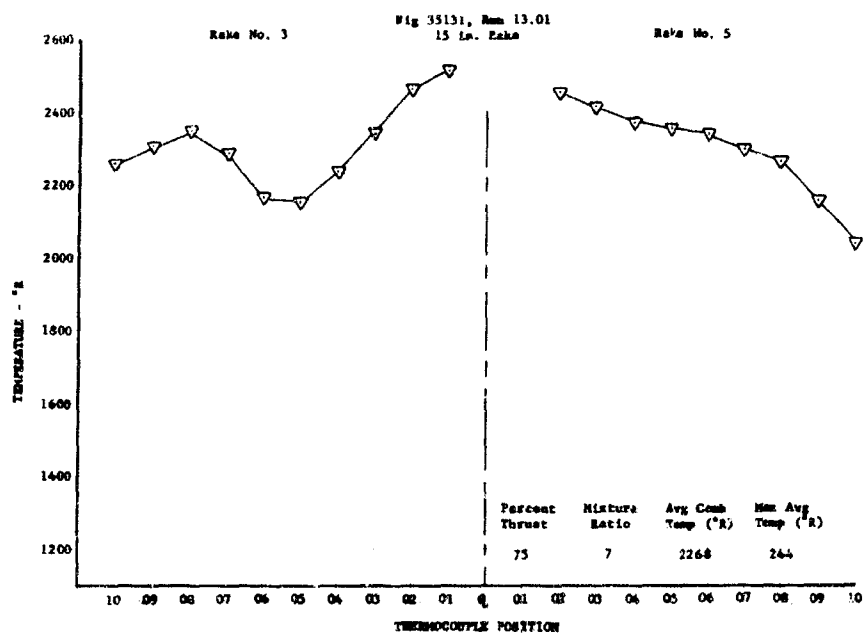


Figure 431. Fixed Area Preburner Temperature Profile, Run 13.01

DF 79869

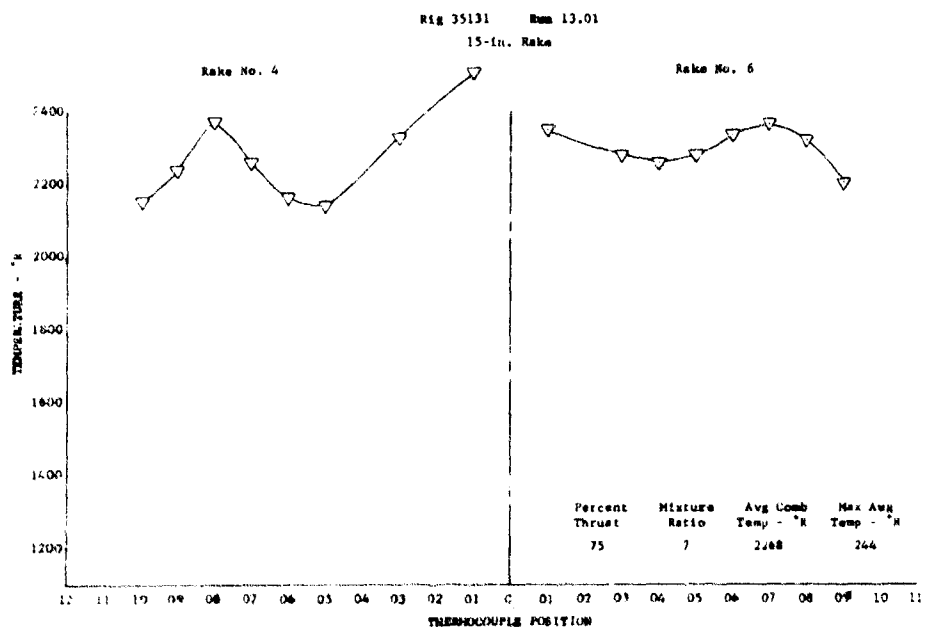


Figure 432. Fixed Area Preburner Temperature Profile, Run 13.01

DF 79870

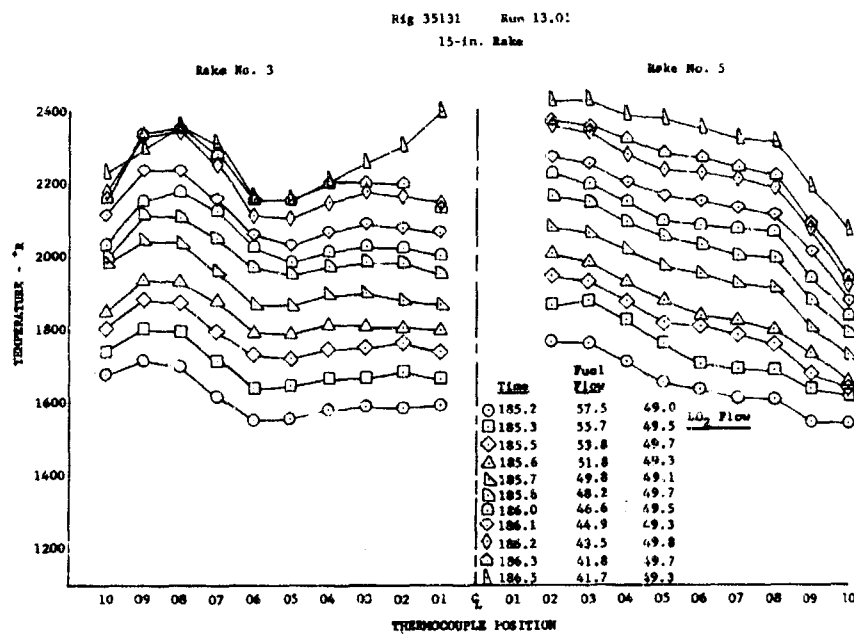


Figure 433. Fixed Area Preburner Temperature Profile, Run 13.01

DF 79871

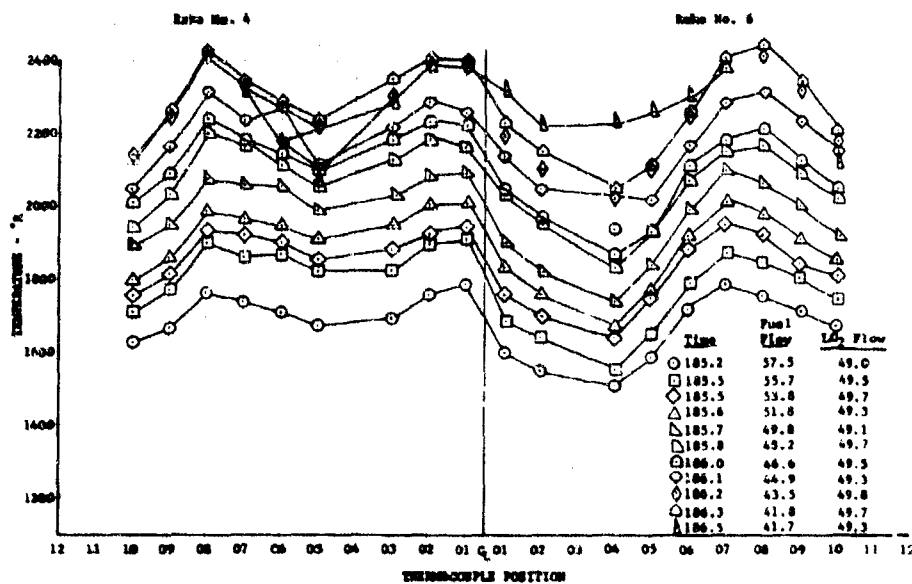


Figure 434. Fixed Area Preburner Temperature Profile, Run 13.01

DF 79872

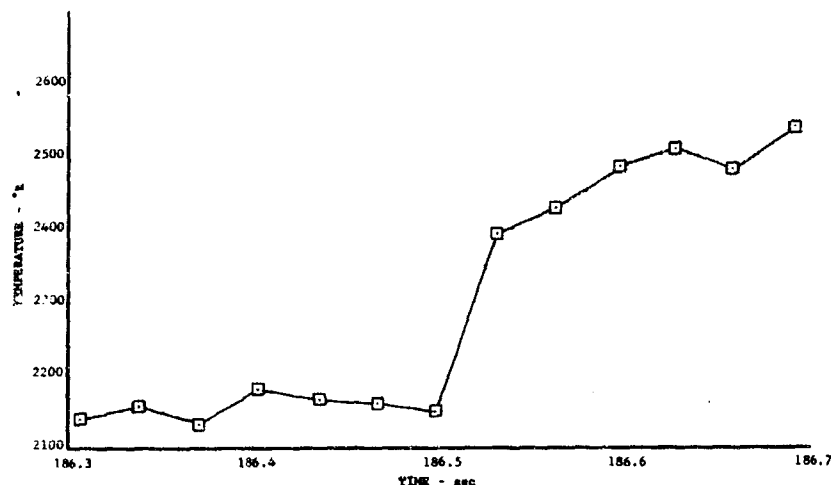


Figure 435. Profile Shift of PCT 301, Run 13.01 DF 79873

Run 14.01 was programed as a repeat of programed run 12.01. Run 14.01, made on February 14, 1970, was manually advanced during the 100% thrust, $r = 6$ data point, at 30.5 sec due to fuel leaks on the test stand. Visual inspection of the rig on the test stand revealed no damage. A post-run 14.01 injector face photograph is shown in figure 436 which reveals that the injector face remained in good condition.

The conditions attained on run 14.01 are shown in tables LIH and LIV. It can be seen that the temperature profile at 75% thrust, $r = 7$ was 318°R maximum-to-average at an average temperature of 2260°R . Figure 437 and 438 show the temperature distribution. The shape of the distribution at 75% thrust, $r = 7$ and 100% thrust, $r = 6$ on run 14.01 and the 75% thrust, $r = 7$ after time 186.5 sec on run 13.01 temperature distributions are like one another but different than the typical shapes that have been exhibited on all other thrust points on previous runs of build 4.

Motion pictures taken of run 14.01 revealed substantial fuel leaks emitting from the rig during the run, which lit off just at shutdown, causing an overboard fire. Leak check of the rig failed to account for all of the leaks observed earlier, hence the rig could not be run again. With obviously large unaccounted for leaks, the rig was pulled from the test stand for teardown inspection.

Teardown inspection of the rig revealed the following:

1. The outer two rows of the fuel faceplate tang braze joints were broken from approximately 3 to 7 o'clock allowing the faceplate to bend toward the chamber approximately 0.090 in.
2. The sheet metal seal between the fuel faceplate and injector housing was cracked in 3 places. One crack extended for three-fourths the circumference. This explains why there was a temperature distribution shift during run 13.01.

3. The preburner oxidizer valve leaked when closed due to seal seat damage explaining the LO₂ puddling behind the combustion liner on prestart.
4. Five of eight scrub-liner support tabs shown in figure 439 were cracked or broken.

To make a failure analysis of the faceplate braze joints, the failed joints were masked with wax to protect the fracture faces at the tang joints and the remaining sound joints were etched away in an acid solution.

Visual examination was conducted on both the Rigimesh plate and the injector oxidizer elements after faceplate removal. No information was gained from the Rigimesh plate as the area was inaccessible to visual examination. Visual and binocular examination of the braze joint location on the oxidizer element was in general very difficult if not impossible due to the configuration of the part. As there was this hinderance to direct observation, those areas which appeared to show the most promise by visual examination were replicated with plastic for easier access. These replicas of the areas of the failed joints were examined both by light microscopy and electron microscopy. One condition observed on all the samples was evidence of etching or corrosion, indicating that the protective wax masking was not completely effective.



Figure 436. Injector Face Shown After Run 14.01

FE 95748

Table LIII. Predicted vs Actual Performance for 75% Thrust, Engine
Mixture Ratio of 5, Rig 35131, Run 14.01

	Engine Cycle Predicted	Test Results
Chamber Pressure - psia	3006.6	2967
Total Oxidizer Flow - lb/sec	49.29	49.37
Oxidizer Primary Flow - lb/sec	7.283	3.62
Oxidizer Secondary Flow - lb/sec	42.07	45.75
Total Fuel Flow - lb/sec	42.00	42.01
Injector Fuel Flow - lb/sec	40.91	40.43
Upper Coolant Liner Flow - lb/sec	0.762*	0.714
Lower Coolant Liner Flow - lb/sec	0.560*	0.431
Injector Mixture Ratio	1.205	1.208
Overall Mixture Ratio	1.174	1.175
Combustion Temperature - °R	2235	2260
Flow Divider Valve Position - %	63.8	91.6 ²
Oxidizer Injector Primary ΔP	550.5	152.6 ⁴
Oxidizer Injector Secondary ΔP	114.0	147.8 ⁴
Fuel Injector ΔP (Plate)	135.0*	146.6 ¹
Oxidizer Injector Temperature - °R	211	191.4
Fuel Injector Temperature - °R	190.4	196.0
Temperature Profile (11 in.) - °R	0	NAV
Temperature Profile (15 in.) - °R	0	318
Average Temperature (11 in.) - °R	2235	NAV
Average Temperature (15 in.) - °R	2235	2260
Oxidizer Primary/Total Flow Split	0.1477	0.0732 ⁴
Oxidizer Primary Injector A_{cd} - in ²	0.0550	0.0530 ⁴
Oxidizer Secondary Injector A_{cd} - in ²	0.6975	0.6822 ⁴
Fuel Injector A_{cd} (Overall) - in ²	3.1*	NAV
η_c^* (Based on P_c , wt) - %	100	98.9 ³
η_c^* (Based on Average Temperature at 11 in.) - %	100	NAV
η_c^* (Based on Average Temperature at 15 in.) - %	100	100.0
Rigimesh Liner Flow - lb/sec	0.416*	0.441
Fuel Injector A_{cd} (Plate) - in ²	3.3*	3.312

- Notes: 1. This run was possibly made with a broken injector fuel face plate seal.
2. The flow divider valve was not in the correct position.
3. There was a leak out of the preburner chamber.
4. There was an apparent leak of oxidizer flow from primary to secondary cavities (Injector flow split = 0.073)

*Rig cycle predictions.

Table LIV. Predicted vs Actual Performance for 100% Thrust, Engine
Mixture Ratio of 6, Rig 35131, Run 14.01

	Engine Cycle Predicted	Test Results
Chamber Pressure - psia	4367.2	4276
Total Oxidizer Flow - lb/sec	71.45	69.35
Oxidizer Primary Flow - lb/sec	7.483	4.50
Oxidizer Secondary Flow -	63.97	64.85
Total Fuel Flow - lb/sec	66.23	65.6
Injector Fuel Flow - lb/sec	64.23	63.1
Upper Coolant Liner Flow - lb/sec	1.201*	1.130
Lower Coolant Liner Flow - lb/sec	0.897*	0.662
Injector Mixture Ratio	1.112	1.087
Overall Mixture Ratio	1.079	1.057
Combustion Temperature - °R	2086	2054
Flow Divider Valve Position - %	85.5	100.7(2)
Oxidizer Injector Primary ΔP	571.4	265.6(4)
Oxidizer Injector Secondary ΔP	245.0	273.6(4)
Fuel Injector ΔP (Plate)	270.0	260.3(1)
Oxidizer Injector Temperature - °R	220	182.3
Fuel Injector Temperature - °R	183.2	177.7
Temperature Profile (11 in.) - °R	0	NAV
Temperature Profile (15 in.) - °R	0	259
Average Temperature (11 in.) - °R	2086	NAV
Average Temperature (15 in.) - °R	2086	2054
Oxidizer Primary/Total Flow Split	0.1047	0.0648(4)
Oxidizer Primary Injector A_{cd} - in. ²	0.0550	0.050(4)
Oxidizer Secondary Injector A_{cd} - in. ²	0.7184	0.7107(4)
Fuel Injector A_{cd} (Overall) - in. ²	3.1*	NAV
η_{c*} (Based on P_c , wt) - %	100	98.7(3)
η_{c*} (Based on Average Temperature at 11 in.) - %	100	NAV
η_{c*} (Based on Average Temperature at 15 in.) - %	100	100.0
Rigimesh Liner Flow - lb/sec	0.695*	0.695
Fuel Injector A_{cd} (Plate) - in. ²	3.3*	3.35

Notes:

- (1) This run was possibly made with a broken injector faceplate seal.
- (2) The flow divider valve was not in the correct position.
- (3) There was a leak out of the preburner chamber.
- (4) There was an apparent leak of oxidizer flow from primary to secondary cavities (injector flow split = 0.068)

* Rig Cycle Predictions

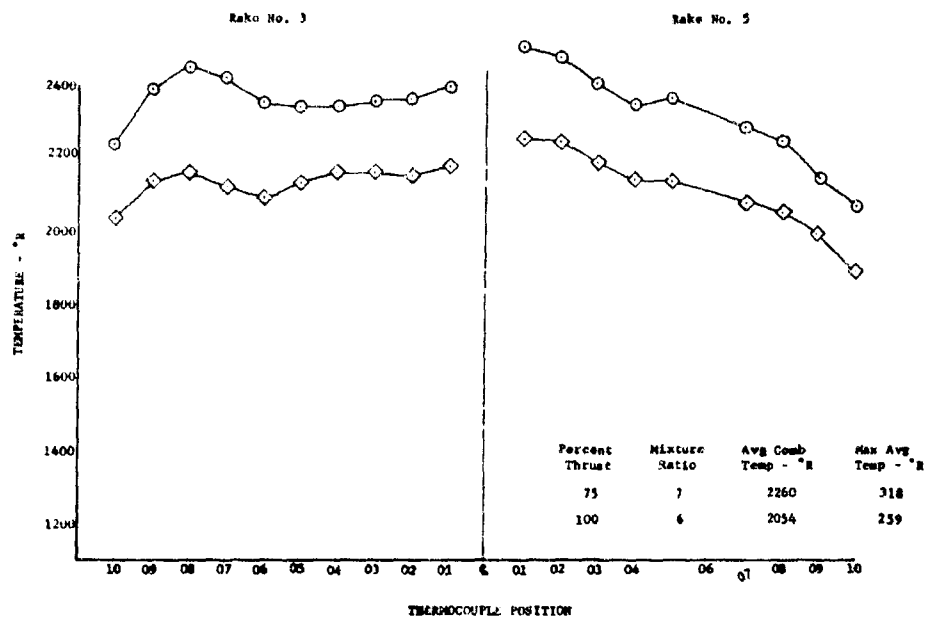


Figure 437. Fixed Area Preburner Temperature Profile, Run 14.01 DF 79874

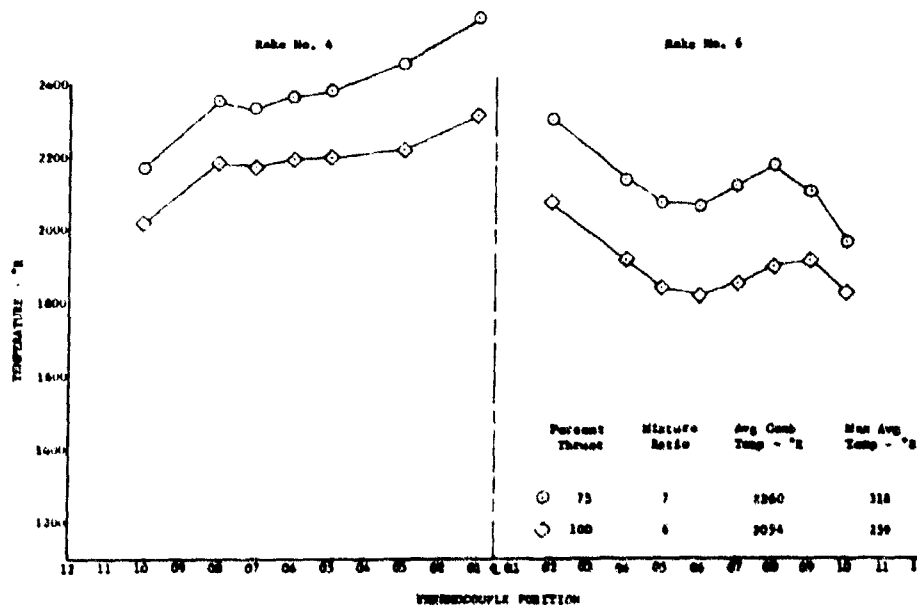


Figure 438. Fixed Area Preburner Temperature Profile, Run 14.01 DF 79875

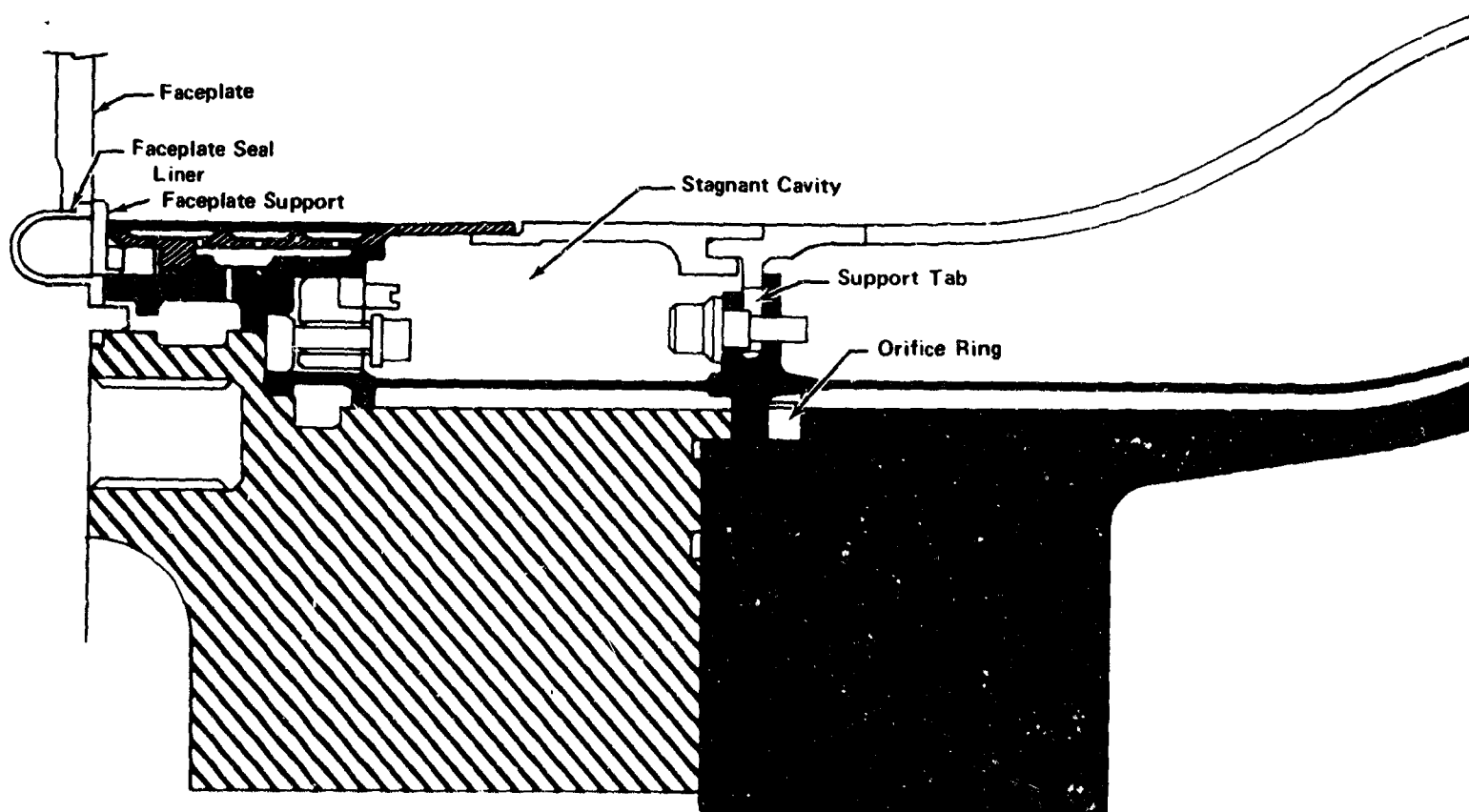


Figure 439. Uncooled and Cooled Liner Configuration

A

Uncooled Liner

Cooled Liner

FD 40253

455/456

All of the replicas examined exhibited areas which appeared to be tensile failures although these areas were not very clear. The failure dimples were relatively equiaxed and not the elongated dimples which are associated with shear failures. Two of the fracture faces exhibited areas which were relatively flat and had some very faint traces suggestive of fatigue.

Although the evidence is not conclusive, there is a tendency to suspect that fatigue was a factor in the separation of the Rigimesh to element joints.

The failure of the Rigimesh-to-oxidizer element joints occurred adjacent to the location where the seal between the OD of the Rigimesh and injector had extensive fatigue cracking, as explained in the following paragraph.

The fuel faceplate sheet metal seal was machined from the injector assembly and sectioned for failure analyses. It was found that the three cracks in the seal were fatigue failures. The thickness in one of the three cracks was 0.012 in. undersized. The material thickness in the area of the other two cracks was as required. It was determined that the material conformed to the hardness and composition requirements.

Failure analysis of the scrub liner support tabs showed a fatigue failure which progressed from both edges toward the center.

It is probable that the fatigue failures experienced during the last rig build were caused by the low frequency (600 Hz) combustion oscillations that are experienced during a hot firing. The combustion oscillations are caused by the presence of helium in the secondary oxygen injector cavity during the acceleration to 20% thrust level. Subsequent preburner testing was made with revised test procedures, as described later in this report, to shorten the length of time when the oscillations are present.

The preburner rig was rebuilt as rig 35133, build 2 for further testing with the second preburner injector, a revised preburner liner that provides support for the outer perimeter of the fuel faceplate, and an uncooled liner vibration damper.

The second injector has a stronger faceplate seal and scarfed elements as described in the fabrication section. To proof check the faceplate braze joint and liner support system load carrying capability, the second injector was water flowed, using the preburner liner support, to the equivalent of 745 psid faceplate differential pressure. In addition, the elements of the injector were individually GN₂ flowed, as described on the cold flows of the first injector after run 6.01, and no blocked elements were found. Figure 440 shows the revised liner faceplate support. The outer edge of the fuel faceplate rests on the upper edge of the liner, which takes some of the load off of the outer elements which were the highest loaded elements. The outer element load is the limiting factor for setting allowable operating faceplate differential pressure. The liner faceplate support scheme allows approximately 100 psid higher differential pressure.

The modifications that strengthen the injector faceplate seal and faceplate attachment lower the operating stress and thus increase the fatigue life.

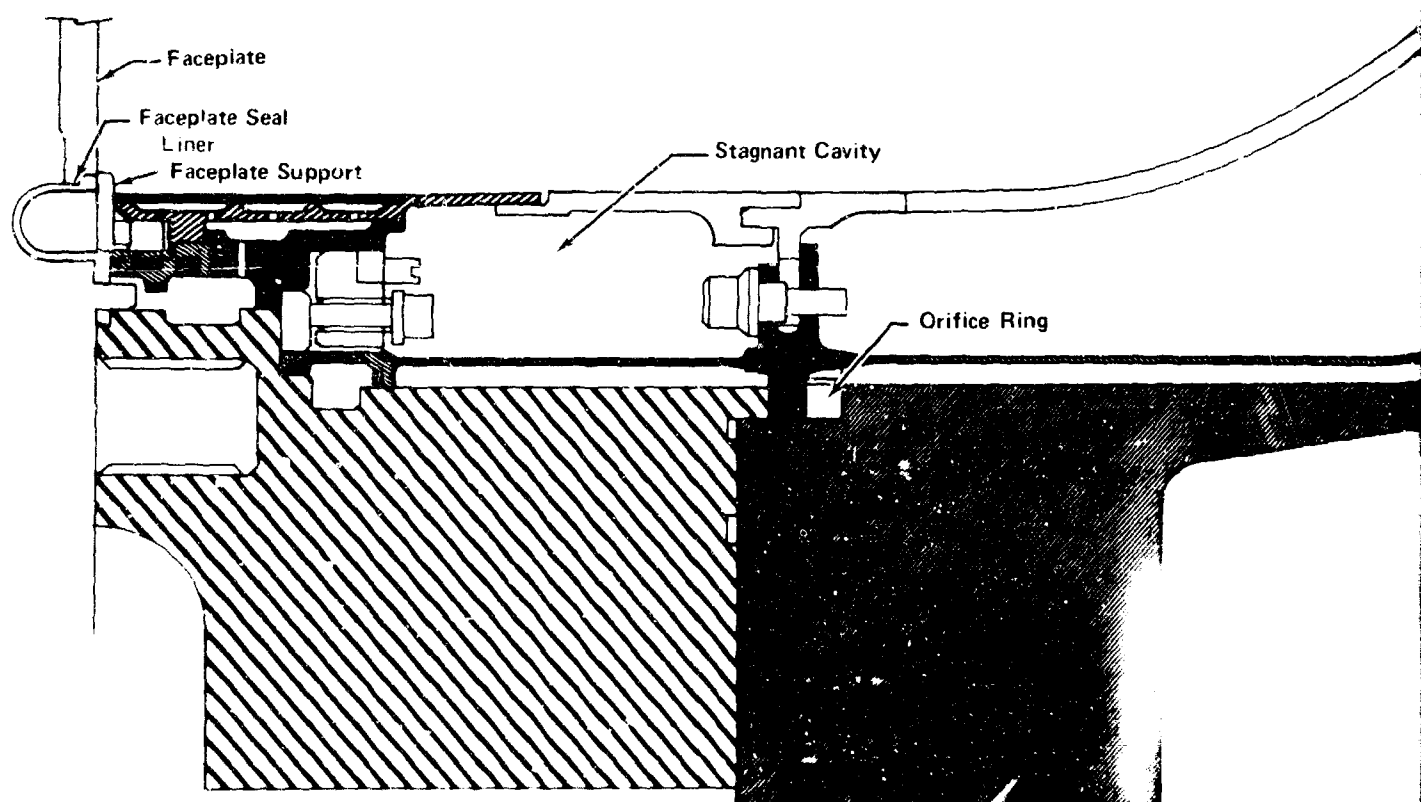


Figure 4b. Cooled Liner Configuration With Uncooled Liner Vibration Damper

Uncooled Liner

Rear Support

Cooled Liner

FD 10251

150 / 460

BLANK PAGE

The uncooled liner vibration damper is shown in figure 440. The dampening scheme consists of supporting the liner at the downstream end with a bolt and clevis at six locations. The bolt and clevis limits the liner movement in the axial, radial, and circumferential directions while allowing axial growth.

The preburner rig was mounted on E-8 and eight tests were made. The preburner rig with the second injector is designated as rig 35133, build 2.

Run 1.01 was programed for 20% thrust, $r = 5$ and 50% thrust, $r = 5$ data. The 20% thrust, $r = 5$ and 50% thrust, $r = 5$ data points were chosen because the preburner liner had previously sustained no damage at these levels, thus the temperature profile could be evaluated prior to committing the rig to high combustion temperatures. During start up of the rig while the fuel tank was being pressurized at the steady-state 7% level, a GN_2 purge to the secondary cavity was programed to replace the GHe purge. The GHe purge was returned and the GN_2 purge closed for the acceleration to 20% thrust, $r = 5$. The GN_2 replacement purge was used in an effort to reduce or eliminate the 600 Hz combustion frequency which is known to be caused by the GHe purge, thus reducing the likelihood of fatigue failures to rig hardware.

Run 1.01 was a full duration run of 28.36 sec. The rig conditions and temperature profiles attained on runs 1.01 through 8.01 are shown in the table XXXVII.

Visual inspection of the rig after run 1.01 showed no damage. There were local blued spots on the liner extension downstream of the transpiration section and minor metal erosion had occurred. Figures 441 and 442 show the prerun injector face and 12 o'clock liner condition for comparison to post-run 1.01 conditions as shown in figures 443 and 444. The injector face had two areas where metal was eroded during run 1.01. These eroded metal spots did not progress to any larger size in subsequent firings.

The data revealed that the 600 Hz combustion frequency was present with the GHe purge, but at a lower amplitude than previously seen, and that the 600 Hz goes away when GN_2 is substituted for GHe.

The conditions that were predicted and attained for run 1.01 are shown in table LV and table LVI. The temperature profile on the second injector was acceptable and the profile was comparable to the first injector during runs 7.01 through 14.01. The temperature distribution for run 1.01 is shown in figures 445 and 446.

The inner combustion liner was instrumented with eight thermocouples placed every 45 deg in a plane 2.3 in. from the injector face. The hottest liner temperature on run 1.01 was at the top of the liner (12 o'clock position) and is shown in figure 447. This liner temperature was 525 to 550°R hotter than average combustion temperature at both 50% thrust, $r = 5$. The top liner temperature was at its maximum at 50% thrust, $r = 5$ where combustion temperature was the highest. It was decided to commit the rig to a run to 20% thrust, $r = 7$ since the automatic and manual liner temperature advances would be adequate indication to shut down the rig if liner distress developed.

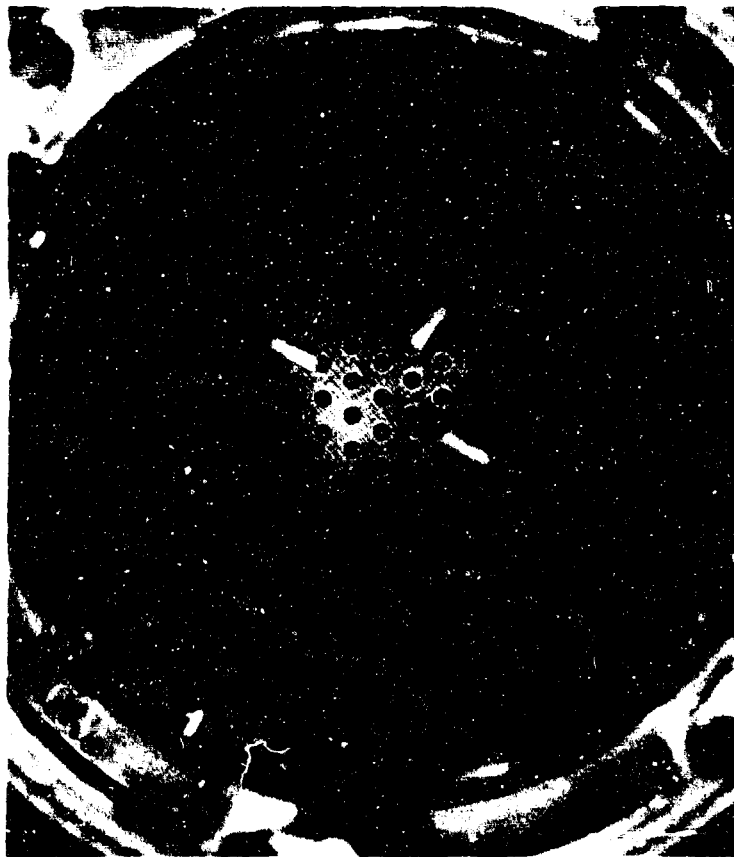


Figure 441. Injector Face Before Run 1.01

FE 96963

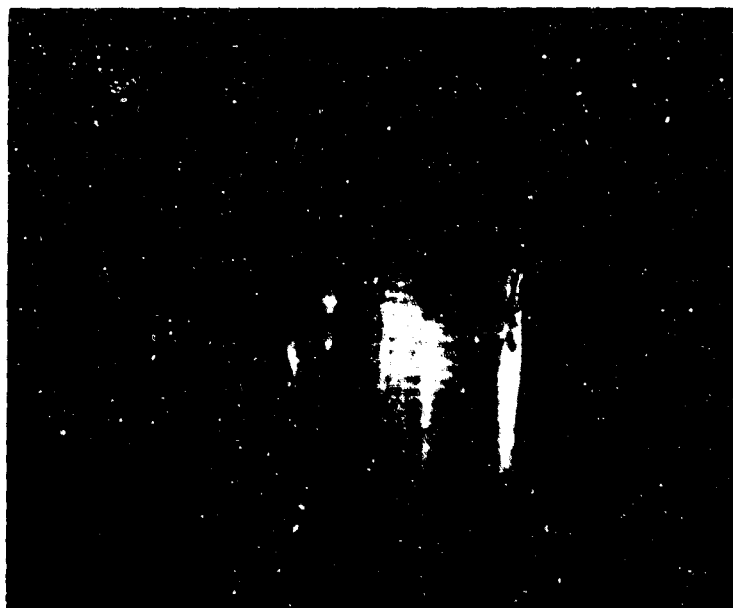


Figure 442. Liner Condition Before Run 1.01

FE 97119

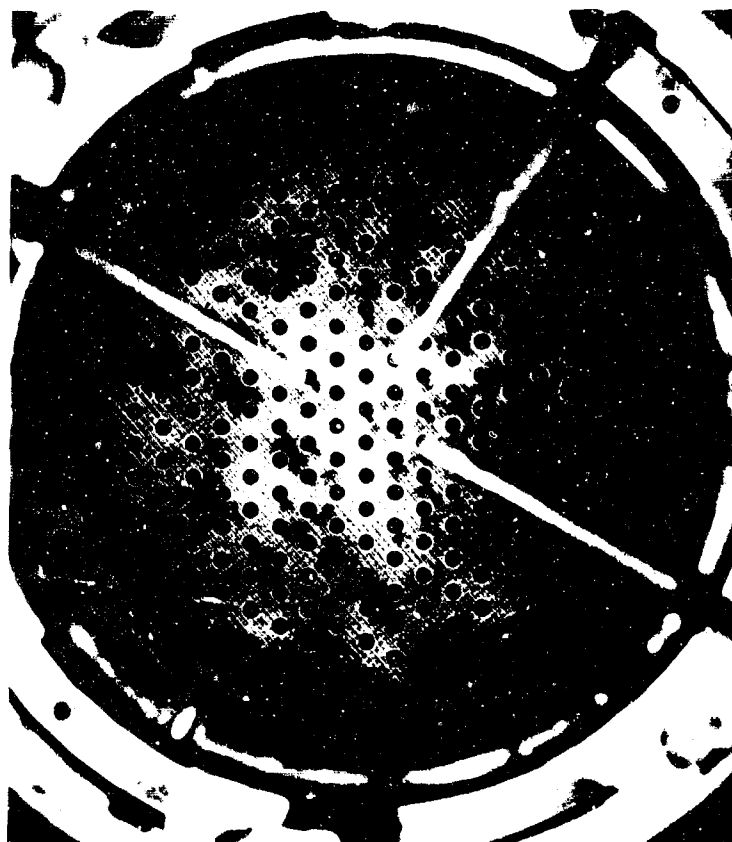


Figure 443. Injector Face After Run 1.01

FE 97210



Figure 444. Liner Condition After Run 1.01

FE 97201

Table LV. Engine Thrust Level 20%, Engine Mixture Ratio 5, Rig No. 35133, Run No. 1.01

	Predicted Engine Cycles	Test Results
Chamber Pressure - psia	732.4	724.4
Total Oxidizer Flow - lb/sec	9.59*	0.947
Oxidizer Primary Flow - lb/sec	5.782*	5.69
Oxidizer Secondary Flow - lb/sec	3.808*	3.77
Oxidizer Primary/Total Flow Split	0.6029*	0.602
Total Fuel Flow - lb/sec	13.38	13.82
Injector Fuel Flow - lb/sec	13.38	13.32
Upper Coolant Liner Flow - lb/sec	NAV	0.2558***
Lower Coolant Liner Flow - lb/sec	NAV	0.1348***
Rigimesh Liner Flow - lb/sec	NAV	0.111
Injector Mixture Ratio	0.716	0.7046
Overall Mixture Ratio	0.716	0.6847
Oxidizer Injector Temperature - °R	200.0	188.6
Fuel Injector Temperature - °R	125.4	127.7
Temperature Profile - °R	0°	280.1
Average Temperature - °R	1394	1344.
Oxidizer Injector Primary ΔP	274.5	127.2**
Oxidizer Injector Secondary ΔP	7.425*	13.06**
Fuel Injector Plate ΔP	25.0	32.70
Oxidizer Primary Injector $A_{cd} - in^2$	0.63*	0.0920**
Oxidizer Secondary Injector $A_{cd} - in^2$	0.2526*	0.1903**
Fuel Injector Overall $A_{cd} - in^2$	3.48	2.6
Fuel Injector Plate $A_{cd} - in^2$	3.7	3.26
Flow Divider Valve Position - %	25.0*	25.6
η_c^* (Based on P_c , wt) - %	100	102.8
η_c^* (Based on Average Temperature) - %	100	99.3

Comments:

- * Rig Cycle Predictions
- ** There is an apparent leak of oxidizer flow from primary to secondary cavities. (injector flow split = 0.415)
- *** Due to either a leak or faulty instrumentation, liner flows could not be determined. Number given are based on percentages of total flows from previous runs.

Table LVI. Engine Thrust Level 50%, Engine Mixture Ratio 5, Rig No. 35133, Run No. 1.01

	Predicted Engine Cycles	Test Results
Chamber Pressure - psia	2010	2071
Total Oxidizer Flow - lb/sec	28.23*	28.30
Oxidizer Primary Flow - lb/sec	7.856*	8.02
Oxidizer Secondary Flow - lb/sec	20.37*	20.28
Oxidizer Primary/Total Flow Split	0.2783*	0.283
Total Fuel Flow - lb/sec	36.97	38.21
Injector Fuel Flow - lb/sec	36.97	36.83
Upper Coolant Liner Flow - lb/sec	NAV	0.7069*****
Lower Coolant Liner Flow - lb/sec	NAV	0.3726*****
Rigimesh Liner Flow - lb/sec	NAV	0.306
Injector Mixture Ratio	0.763	0.7621
Overall Mixture Ratio	0.763	0.7406
Oxidizer Injector Temperature - °R	208.2*	190.1
Fuel Injector Temperature - °R	142.0*	144.5
Temperature Profile - °R	0°	155.
Average Temperature - °R	1488	1427.
Oxidizer Injector Primary ΔP	493.9*	308.8**
Oxidizer Injector Secondary ΔP	38.00*	37.1**
Fuel Injector Plate ΔP	89.6	120.9
Oxidizer Primary Injector $A_{cd} - in^2$	0.063	0.0822**
Oxidizer Secondary Injector $A_{cd} - in^2$	0.5897	0.6012**
Fuel Injector Overall $A_{cd} - in^2$	3.48	NAV***
Fuel Injector Plate $A_{cd} - in^2$	3.7	3.25
Flow Divider Valve Position - %	46.5	47.6
η_c^* (Based on P_c , wt) - %	100.	100.6
η_c^* (Based on Average Temperature) - %	100.	98.5

Comments:

- * Rig cycle predictions
- ** There is an apparent leak of oxidizer flow from primary to secondary cavities. (Injector flow split = 0.215)
- *** The fuel injector high pressure data is not good.
- **** Due to either a leak or faulty instrumentation, liner flows could not be determined. Numbers given are based on percentages of total flows from previous runs.

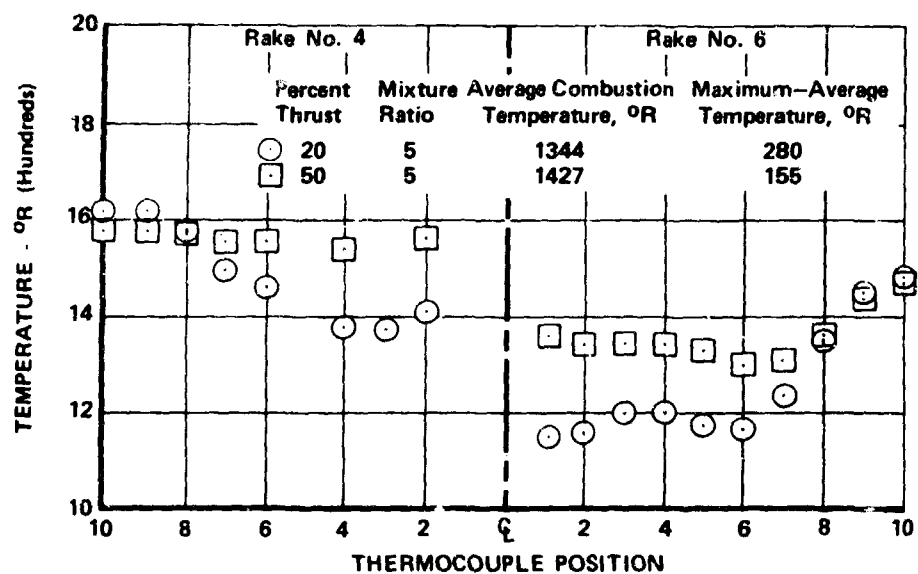


Figure 445. Temperature Distribution for Run 1.01 FD 44044

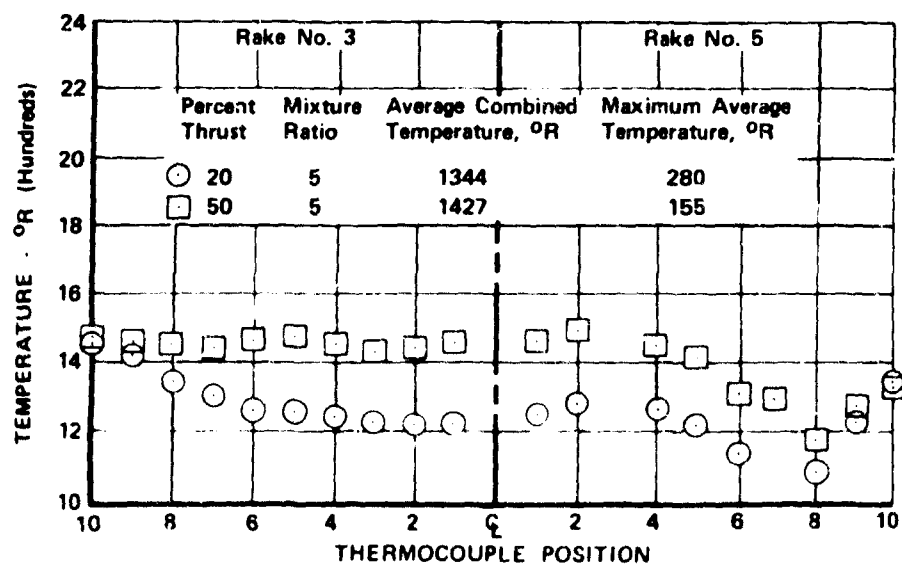


Figure 446. Temperature Distribution for Run 1.01 FD 44045

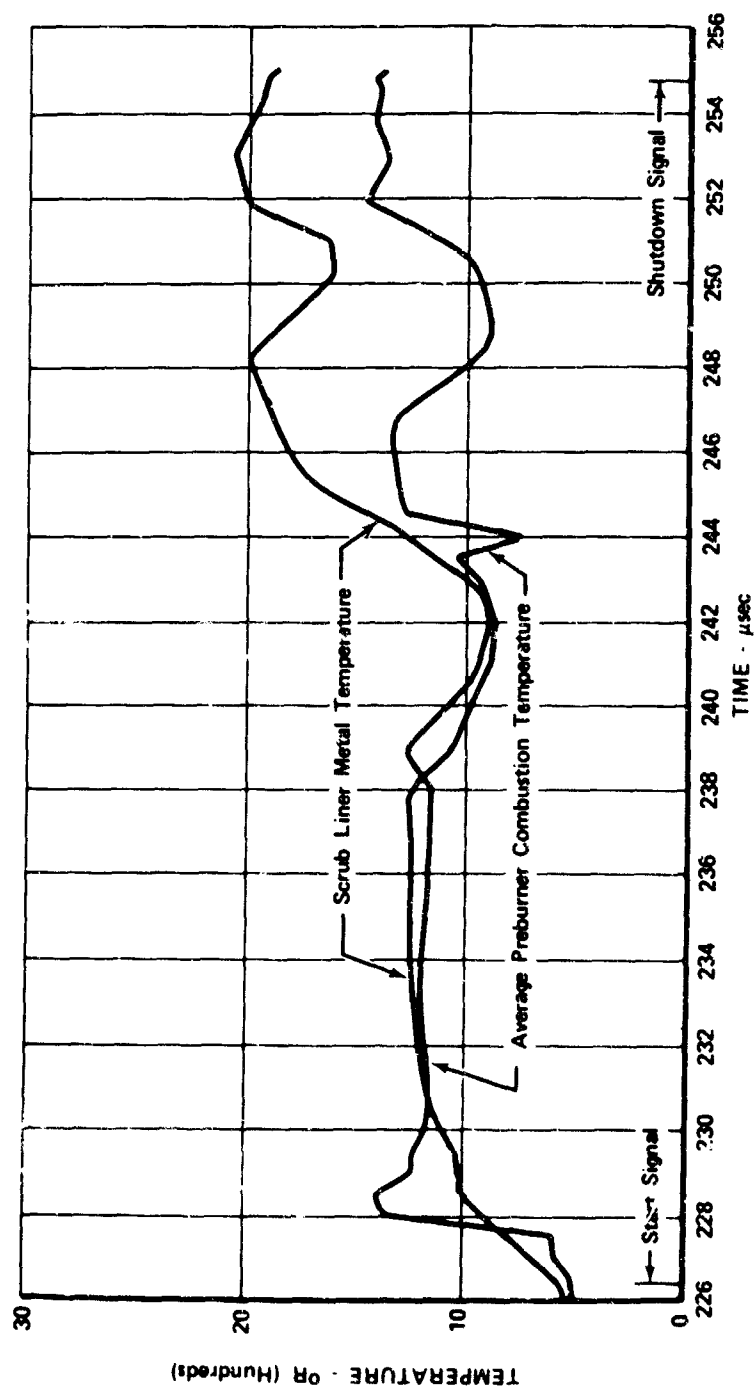


Figure 447. Scrub Liner Temperature

FD 42872

Run 2.01 was programed for 20% thrust, $r = 5, 6$, and 7 and 50% thrust, $r = 5, 6$, and 7. The GHe purge was as in run 1.01 except a combined GHe and GN_2 purge was used during the acceleration to 20% thrust, $r = 5$. The attained flowrate of GN_2 on run 1.01 was lower than expected so it was not desirable to run the transient from 7% to 20% with GN_2 only. It was decided to use both GN_2 and GHe purges in the transient to assure adequate pressure, yet eliminate the 600 Hz combustion frequency.

Run 2.01 was automatically advanced at 17.53 sec due to a sequencer patching error. The automatic advance was triggered by low GHe supply pressure. The low GHe supply trigger circuit was programed to stop sampling when the GHe supply valve was closed, but was erroneously patched to start sampling when the GHe supply valve closed. Therefore, when the GHe valve closed it caused the supply pressure to fall which triggered the run to advance.

Run 3.01 was a quick turnaround rerun of the 2.01 program with the low GHe and GN_2 trigger circuits disarmed. Run 3.01 was automatically advanced after 6.77 sec due to erroneous high scrub liner temperature advance. The advance level was set at 1490°R instead of 2640°R as requested. The rig was in good condition after the run.

Review of the data from run 2.01 and 3.01 shows that the GN_2 purge is warping the combustion temperature profile, causing the rakes that are away from the GN_2 entrance port to be hot. Since this is undesirable, the GN_2 purge during start was eliminated.

Run 4.01 was a repeat attempt at the 2.01 run program without use of the GN_2 purge. Run 4.01 was advanced 0.10 sec before SSV up because of low igniter combustion temperature. Disassembly of the igniter revealed a piece of copper seal in the oxidizer supply orifice restricting oxidizer flow.

Run 5.01 was a repeat of 4.01. The run was full duration which is 44.01 sec. Inspection of the rig revealed 0.70 in. diameter sized high temperature eroded area in zone 1 of the Rigimesh section of the combustion liner at about the 7 o'clock position. The Rigimesh liner however, was not burned through. The uncooled liner extension had two metal eroded areas. One was at the tip of the No. 3 pulse gun at about the 7 o'clock position and the other was at the end of the chamber pressure tap (PBCP10) at 5:30 o'clock position. The chamber pressure tap was melted closed. Neither of these two eroded areas constituted a problem to further testing. Figures 448 and 449 show the injector face and the 12 o'clock liner position after run 5.01. Note that the that the injector face conditions remain the same as after run 1.01.

PBCP10 read normally during the acceleration to 20% thrust. On the acceleration to 50%, PBCP10 did not respond to the chamber pressure change indicating that the pressure tap was melted closed during the 20% condition. It is presumed that all the liner damage was sustained when the chamber pressure tap was melted and further that the tap was melted after the 20% thrust, $r = 5$ level since no damage was sustained at this point on run 1.01.



Figure 448. Injector Face Condition After Run 5.01 FE 97318

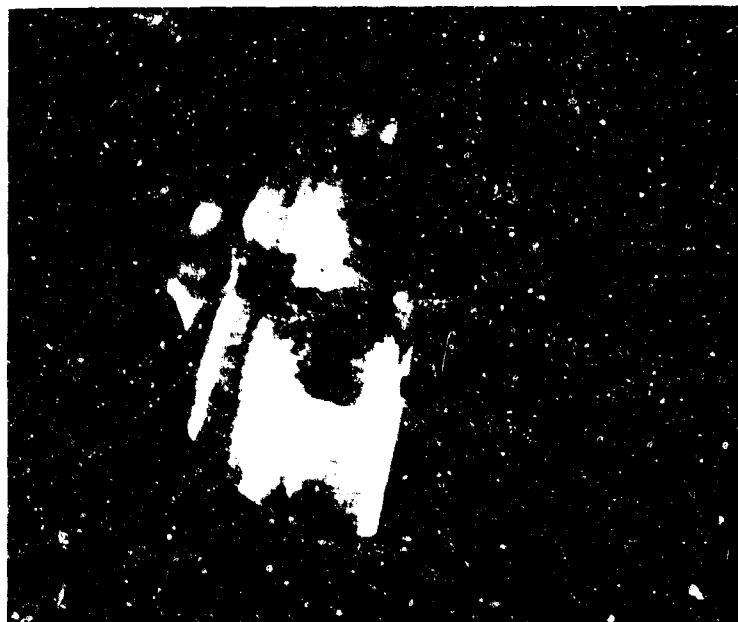


Figure 449. Liner Position (12 o'clock) After Run 5.01 FE 97308

The conditions that were predicted and attained for run 5.01 are shown in tables LVII through table LXII. Figures 450 through figure 453 show the temperature distribution during run 5.01. It can be seen that there is a slight improvement in profile and distribution with an increase in thrust level.

Table LVII. Engine Thrust Level 20% Engine Mixture
Ratio 5, Rig No. 35133, Run No. 5.01

	Predicted Engine Cycles	Test Results
Chamber Pressure - psia	732.4	707.2
Total Oxidizer Flow - lb/sec	9.59*	9.30
Oxidizer Primary Flow - lb/sec	5.782*	5.48
Oxidizer Secondary Flow - lb/sec	3.808*	3.822
Oxidizer Primary/Total Flow Split	0.6029*	0.589
Total Fuel Flow - lb/sec	13.38	13.70
Injector Fuel Flow - lb/sec	13.38	13.22
Upper Coolant Liner Flow - lb/sec	NAV	0.2426
Lower Coolant Liner Flow - lb/sec	NAV	0.1292
Rigimesh Liner Flow - lb/sec	NAV	0.103
Injector Mixture Ratio	0.716	0.6976
Overall Mixture Ratio	0.716	0.6787
Oxidizer Injector Temperature - °R	200.0*	187.4
Fuel Injector Temperature - °R	125.4*	127.4
Temperature Profile - °R	0°	207.
Average Temperature - °R	1394.	1368
Oxidizer Injector Primary ΔP	274.5*	125.7**
Oxidizer Injector Secondary ΔP	7.425*	32.9**
Fuel Injector Plate ΔP	25.0	35.11
Oxidizer Primary Injector $A_{cd} - in^2$	0.63*	0.0888**
Oxidizer Secondary Injector $A_{cd} - in^2$	0.2526*	0.121**
Fuel Injector Overall $A_{cd} - in^2$	3.48	2.31
Fuel Injector Plate $A_{cd} - in^2$	3.7	3.15
Flow Divider Valve Position - %	25.0*	26.0
η_c^* (Based on P_c , wt) - %	100.	101.9
η_c^* (Based on Average Temperature) - %	100	100.7

* Rig cycle predictions

** There is an apparent leak of oxidizer flow from primary to secondary cavities. (Injector flow split = 0.422)

Table LVIII. Engine Thrust Level 20% Engine Mixture
Ratio 6, Rig No. 35133, Run No. 5.01

	Predicted Engine Cycles	Test Results
Chamber Pressure - psia	719.2	708.4
Total Oxidizer Flow - lb/sec	10.42*	10.27
Oxidizer Primary Flow - lb/sec	6.112*	6.02
Oxidizer Secondary Flow - lb/sec	4.308*	4.25
Oxidizer Primary/Total Flow Split	0.5866*	0.586
Total Fuel Flow - lb/sec	10.97	11.31
Injector Fuel Flow - lb/sec	10.97	10.90
Upper Coolant Liner Flow - lb/sec	NAV	0.2090
Lower Coolant Liner Flow - lb/sec	NAV	0.1102
Rigimesh Liner Flow - lb/sec	NAV	0.084
Injector Mixture Ratio	0.950	0.9351
Overall Mixture Ratio	0.950	0.9087
Oxidizer Injector Temperature - °R	200.3*	189.6
Fuel Injector Temperature - °R	147.5*	147.3
Temperature Profile - °R	0°	258.
Average Temperature - °R	1795.	1765.
Oxidizer Injector Primary ΔP	306.4*	155.6**
Oxidizer Injector Secondary ΔP	8.395*	33.0**
Fuel Injector Plate ΔP	22.1	29.82
Oxidizer Primary Injector $A_{cd} - \text{in}^2$	0.063	0.0881**
Oxidizer Secondary Injector $A_{cd} - \text{in}^2$	0.2686	0.126**
Fuel Injector Overall $A_{cd} - \text{in}^2$	3.48	2.42
Fuel Injector Plate $A_{cd} - \text{in}^2$	3.7	3.10
Flow Divider Valve Position - %	25.2*	26.0
η_c^* (Based on P_c , wt) - %	100.	100.7
η_c^* (Based on Average Temperature) - %	100.	99.6

* Rig cycle predictions

** There is an apparent leak of oxidizer flow from primary to secondary cavities. (Injector flow split = 0.415)

Table LIX. Engine Thrust Level 20% Engine Mixture
Ratio 7, Rig No. 35133, Run No. 5.01

	Predicted Engine Cycles	Test Results
Chamber Pressure - psia	710.1	708.4
Total Oxidizer Flow - lb/sec	11.08*	10.90
Oxidizer Primary Flow - lb/sec	6.316*	6.39
Oxidizer Secondary Flow - lb/sec	4.764*	4.510
Oxidizer Primary/Total Flow Split	0.5701*	0.586
Total Fuel Flow - lb/sec	9.35	9.63
Injector Fuel Flow - lb/sec	9.35	9.28
Upper Coolant Liner Flow - lb/sec	NAV	0.1633
Lower Coolant Liner Flow - lb/sec	NAV	0.0963
Rigimesh Liner Flow - lb/sec	NAV	0.065
Injector Mixture Ratio	1.185	1.166
Overall Mixture Ratio	1.185	1.132
Oxidizer Injector Temperature - °R	200.1*	190.7
Fuel Injector Temperature - °R	166.5*	167.8
Temperature Profile - °R	0°	275.
Average Temperature - °R	2181.	2145.
Oxidizer Injector Primary ΔP	327.0*	178.4**
Oxidizer Injector Secondary ΔP	9.092*	39.2**
Fuel Injector Plate ΔP	19.2	26.24
Oxidizer Primary Injector A_{cd} - in ²	0.063*	0.0874**
Oxidizer Secondary Injector A_{cd} - in ²	0.2853*	0.132**
Fuel Injector Overall A_{cd} - in ²	3.48	2.49
Fuel Injector Plate A_{cd} - in ²	3.7	3.04
Flow Divider Valve Position - %	25.8	26.0
η_c * (Based on P_c , wt) - %	100.	100.7
η_c * (Based on Average Temperature) - %	100.	99.4

* Rig cycle predictions

** There is an apparent leak of oxidizer flow from primary to secondary cavities. (Injector Flow Split = 0.415)

Table LX. Engine Thrust Level 50% Engine Mixture
Ratio 5, Rig No. 35133, Run No. 5.01

	Predicted Engine Cycles	Test Results
Chamber Pressure - psia	2010.	2042.
Total Oxidizer Flow - lb/sec	28.23*	28.08
Oxidizer Primary Flow - lb/sec	7.856*	7.72
Oxidizer Secondary Flow - lb/sec	20.37*	20.36
Oxidizer Primary/Total Flow Split	0.2783*	0.275
Total Fuel Flow - lb/sec	36.97	37.93
Injector Fuel Flow - lb/sec	36.97	36.47
Upper Coolant Liner Flow - lb/sec	NAV	0.7073
Lower Coolant Liner Flow - lb/sec	NAV	0.3674
Rigimesh Liner Flow - lb/sec	NAV	0.380
Injector Mixture Ratio	0.763	0.7405
Overall Mixture Ratio	0.763	188.2
Oxidizer Injector Temperature - °R	208.2*	144.3
Fuel Injector Temperature - °R	142.0*	144.3
Temperature Profile - °R	0°	203.
Average Temperature - °R	1488	1429.
Oxidizer Injector Primary ΔP	493.9*	302.**
Oxidizer Injector Secondary ΔP	38.00*	NAV***
Fuel Injector Plate ΔP	89.6	122.9
Oxidizer Primary Injector $A_{cd} - in^2$	0.063*	0.080**
Oxidizer Secondary Injector $A_{cd} - in^2$	0.5897*	NAV***
Fuel Injector Overall $A_{cd} - in^2$	3.48	2.32
Fuel Injector Plate $A_{cd} - in^2$	3.7	3.21
Flow Divider Valve Position - %	46.5*	48.3
η_c^* (Based on P_c , wt) - %	100.	100.0
η_c^* (Based on Average Temperature) - %	100.	98.6

* Rig cycle predictions

** There is an apparent leak of oxidizer flow from primary to secondary cavities.

*** The downstream tap of secondary ΔP is bad.

Table LXI. Engine Thrust Level 50% Engine Mixture
Ratio 6, Rig No. 35133, Run No. 5.01

	Predicted Engine Cycles	Test Results
Chamber Pressure - psia	1958.	1998.
Total Oxidizer Flow - lb/sec	29.54*	29.44
Oxidizer Primary Flow - lb/sec	8.047*	8.07
Oxidizer Secondary Flow - lb/sec	21.49*	21.38
Oxidizer Primary/Total Flow Split	0.2724*	0.274
Total Fuel Flow - lb/sec	30.77	31.41
Injector Fuel Flow - lb/sec	30.77	30.22
Upper Coolant Liner Flow - lb/sec	NAV	0.5836
Lower Coolant Liner Flow - lb/sec	NAV	0.3068
Rigimesh Liner Flow - lb/sec	NAV	0.295
Injector Mixture Ratio	0.960	0.9649
Overall Mixture Ratio	0.960	0.9375
Oxidizer Injector Temperature - °R	207.4*	188.9
Fuel Injector Temperature - °R	163.3*	164.4
Temperature Profile - °R	0°	216.6
Average Temperature - °R	1827.	1797.
Oxidizer Injector Primary ΔP	518.1*	341.4**
Oxidizer Injector Secondary ΔP	41.59*	NAV***
Fuel Injector Plate ΔP	73.7	100.0
Oxidizer Primary Injector A_{cd} - in ²	0.063*	0.0786**
Oxidizer Secondary Injector A_{cd} - in ²	0.5947*	NAV***
Fuel Injector Overall A_{cd} - in ²	3.48	2.45
Fuel Injector Plate A_{cd} - in ²	3.7	3.17
Flow Divider Valve Position - %	47.1*	48.3
η_c * (Based on P_c , wt) - %	100.	99.7
η_c * (Based on Average Temperature) - %	100.	98.9

* Rig cycle predictions

** There is an apparent leak of oxidizer flow from primary to secondary cavities.

*** The downstream tap of secondary ΔP is bad.

Table LXII. Engine Thrust Level 50% Engine Mixture
Ratio 7, Rig No. 35133, Run No. 5.01

	Predicted Engine Cycles	Test Results
Chamber Pressure - psia	1915.	1964.
Total Oxidizer Flow - lb/sec	30.60*	30.39
Oxidizer Primary Flow - lb/sec	8.182*	8.32
Oxidizer Secondary Flow - lb/sec	22.42*	22.075
Oxidizer Primary/Total Flow Split	0.2674*	0.274
Total Fuel Flow - lb/sec	26.40	26.90
Injector Fuel Flow - lb/sec	26.40	25.89
Upper Coolant Liner Flow - lb/sec	NAV	0.5016
Lower Coolant Liner Flow - lb/sec	NAV	0.2647
Rigimesh Liner Flow - lb/sec	NAV	0.241
Injector Mixture Ratio	1.759	1.163
Overall Mixture Ratio	1.159	1.130
Oxidizer Injector Temperature - °R	206.8*	188.5
Fuel Injector Temperature - °R	182.8*	181.5
Temperature Profile - °R	0°	267.
Average Temperature - °R	2157.	2133.
Oxidizer Injector Primary ΔP	535.6*	370.5**
Oxidizer Injector Secondary ΔP	44.61*	NAV***
Fuel Injector Plate ΔP	64.2	94.72
Oxidizer Primary Injector $A_{cd} - \text{in.}^2$	0.063*	0.0778**
Oxidizer Secondary Injector $A_{cd} - \text{in.}^2$	0.5989*	NAV***
Fuel Injector Overall $A_{cd} - \text{in.}^2$	3.48	2.51
Fuel Injector Plate $A_{cd} - \text{in.}^2$	3.7	3.13
Flow Divider Valve Position - %	47.7*	48.2
η_c^* (Based on P_c , wt) - %	100.	99.9
η_c^* (Based on Average Temperature) - %	100	99.2

* Rig cycle predictions

** There is an apparent leak of oxidizer flow from primary to secondary cavities.

*** The downstream tap of secondary ΔP is bad.

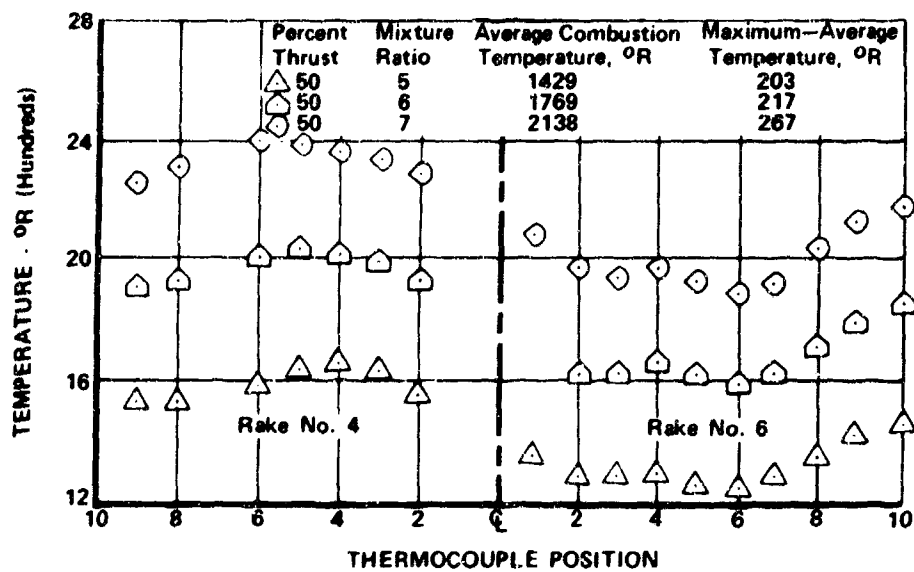


Figure 450. Temperature Distribution During Run 5.01

FD 44046

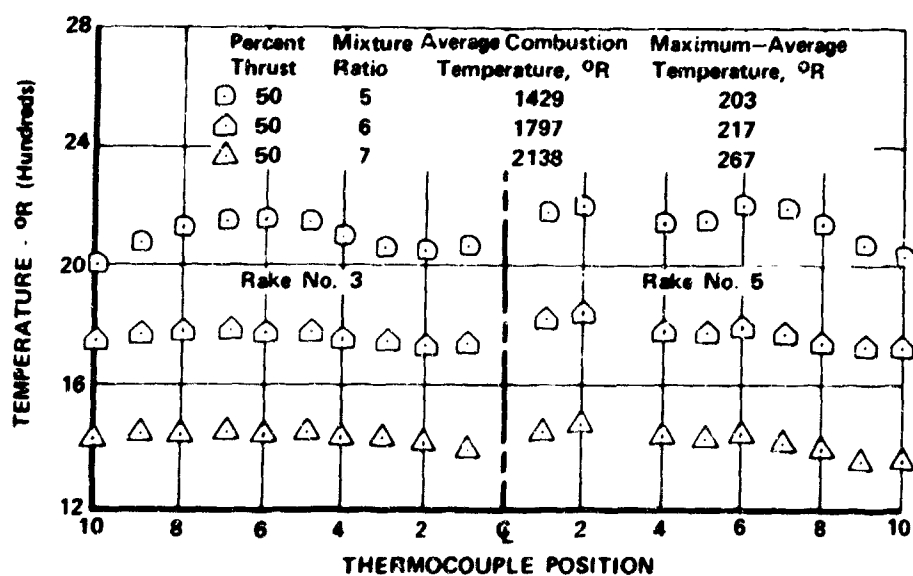


Figure 451. Temperature Distribution During Run 5.01

FD 44047

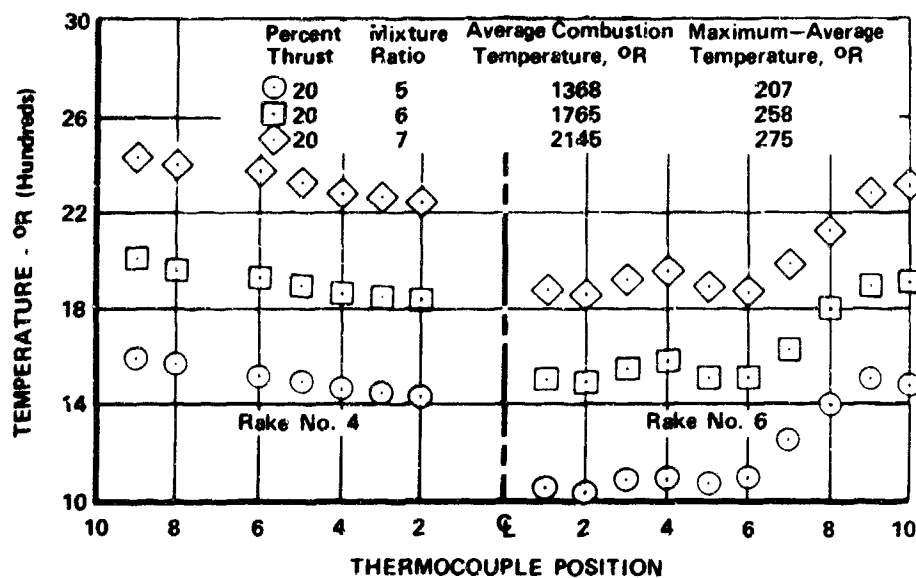


Figure 452. Temperature Distribution During Run 5.01

FD 44048

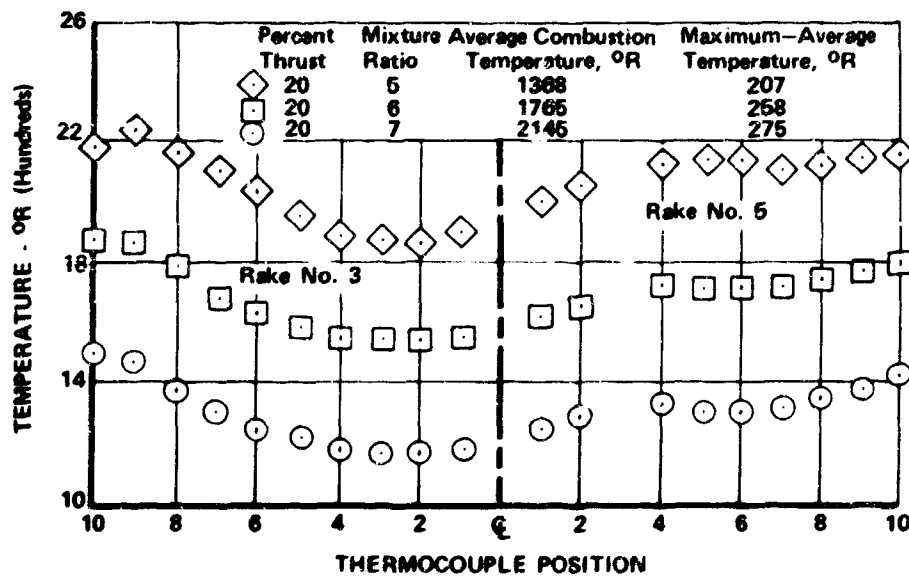


Figure 453. Temperature Distribution During Run 5.01

FD 44049

The data from run 5.01 showed that the liner temperature located at 12 o'clock was again the highest one. At 20% thrust, $r = 7$ this liner temperature was at its hottest level of 2400°R which is 350°R above average combustion temperature. At 50% thrust, $r = 7$ the 12 o'clock liner temperature was 2093°R and still was the hottest one. A plot of the 12 o'clock liner temperature is shown in figure 454.

Run 6.01 was programed for 75% thrust, $r = 7$, 100% thrust, $r = 6$, and 100% thrust, $r = 7$. The run was automatically advanced after 23.72 sec by high combustion temperature which is before reaching the first data point. The high combustion temperature was false even though the advance system functioned properly. The high temperature advance circuit had a faulty patch pin connection that caused a variable resistance in the trigger circuit which indicated a false high temperature signal.

Inspection of the rig after run 6.01 revealed no problems.

The program for run 7.01 was a repeat of run 6.01. The run was automatically advanced at 26.37 sec because of low combustion temperature which is just after the 75% thrust, $r = 7$ data point. The indication of low combustion temperature was false because the sensing thermocouple opened up during the run and caused a signal that looked like low combustion temperature. The rig remained in good condition after run 7.01.

The conditions that were predicted and attained are shown in table LXIII and the temperature distribution is shown in figures 455 and 456. Again, there is a slight improvement in temperature profile with increasing thrust level.

The hot combustion liner temperature in run 7.01 was again at 12 o'clock as shown in figure 457. The maximum temperature is 1670°R at 75% thrust, $r = 7$ which is 520°R below average combustion temperature. The hottest liner temperature is decreasing with increasing thrust level.

Run 8.01 was a repeat of the programed 6.01 run. Run 8.01 was manually advanced at 28.24 sec, which is on the ramp to 100% thrust, $r = 6$, after the 75% thrust, $r = 7$ data point, because of a stand fire.

Inspection of the rig revealed a crack in the lower cooled chamber liner at the downstream end of the liner. The transpiration liner and injector face remained in good condition.

The rig was pulled from the test stand and delivered to the assembly floor for teardown. Figures 458 and 459 show the injector face and liner conditions after teardown.

Teardown inspection of the rig revealed that the Rigimesh portion of the transpiration liner was bowed inward, as well as the cracked lower cooled liner.

The conditions that were predicted and attained are shown in table LXIV. Figures 460 and 461 show the temperature distribution during run 8.01. The hot combustion liner temperature during run 8.01 was again at 12 o'clock as shown in figure 462.

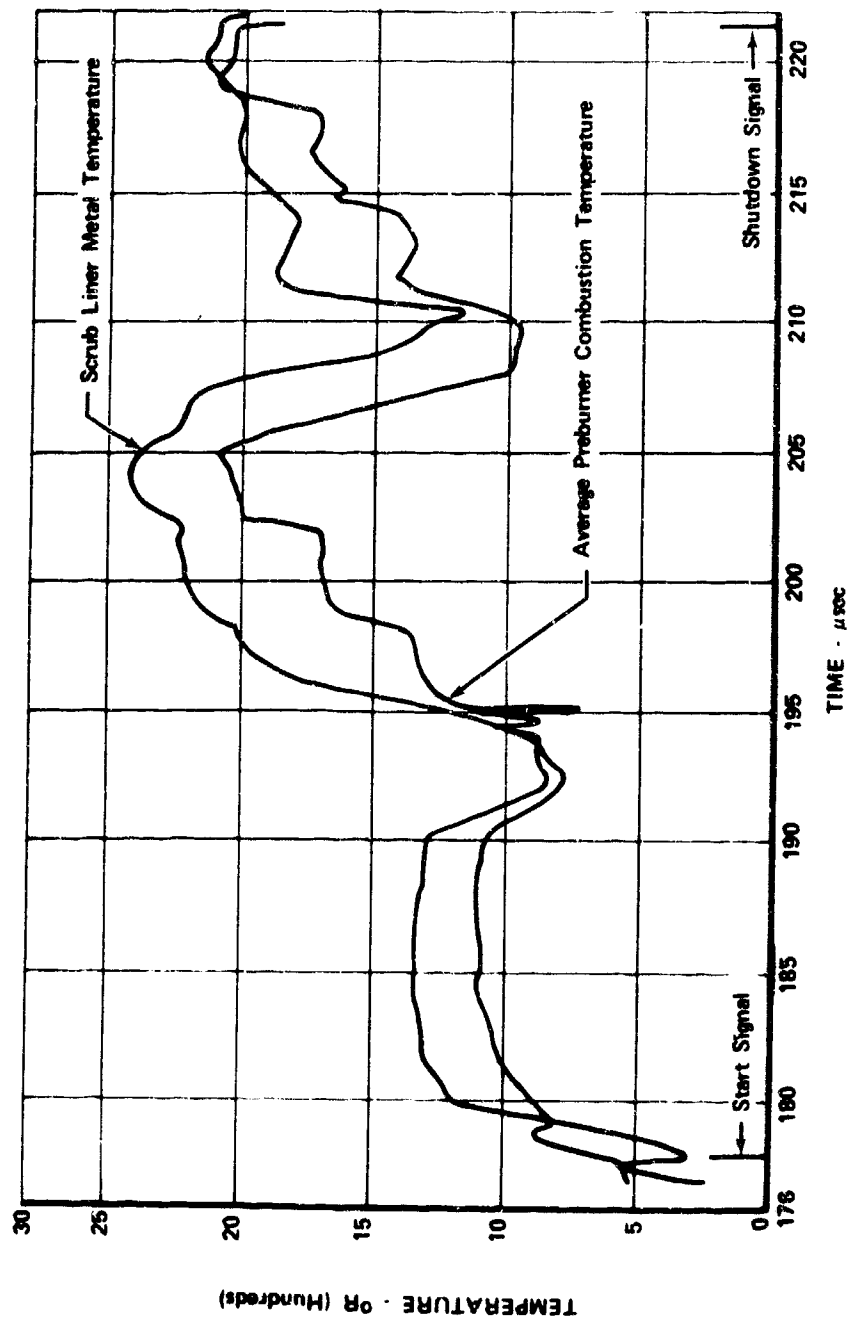


Figure 454. Scrub Liner Temperature, Run 5.01

FD 42871

Table LXIII. Engine Thrust Level 75% Engine Mixture
Ratio 7, Rig No. 35133, Run No. 7.01

	Predicted Engine Cycles	Test Results
Chamber pressure - psia	3007.	2957.
Total oxidizer flow - lb/sec	49.29*	49.30
Oxidizer primary flow - lb/sec	7.843*	8.33
Oxidizer secondary flow - lb/sec	41.45*	40.97
Oxidizer primary/total flow split	0.1591*	0.169
Total fuel flow - lb/sec	40.91	42.06
Injector fuel flow - lb/sec	40.91	40.53
Upper coolant liner flow - lb/sec	NAV	0.7780
Lower coolant liner flow - lb/sec	NAV	0.4101
Rigimesh liner flow - lb/sec	NAV	0.336
Injector mixture ratio	1.205	1.206
Overall mixture ratio	1.205	1.172
Oxidizer injector temperature - °R	211.2*	190.1
Fuel injector temperature - °R	190.4*	193.3
Temperature profile - °R	0°	252.
Average temperature - °R	2235.	2190.
Oxidizer injector primary - ΔP	486.7*	376.3**
Oxidizer injector secondary - ΔP	116.5*	120.6**
Fuel injector plate - ΔP	112.0	151.7
Oxidizer primary injector $A_{cd} - \text{in}^2$	0.063*	0.0769**
Oxidizer secondary injector $A_{cd} - \text{in}^2$	0.6813*	0.6687**
Fuel injector overall $A_{cd} - \text{in}^2$	3.48	NAV***
Fuel injector plate $A_{cd} - \text{in}^2$	3.7	3.25
Flow divider valve position - %	63.9	64.3
η_c * (Based on P_c , wt) - %	100.	98.8
η_c * (Based on average temperature) - %	100.	98.6

* Rig cycle predictions

** There is an apparent leak of oxidizer flow from primary to secondary cavities. (Injector flow split = 0.1350)

*** Horn pressure used for overall fuel injector A_{cd} is bad. Due to either a leak or faulty instrumentation liner flows could not be determined. Numbers given are based on percentages of total flows from previous runs.

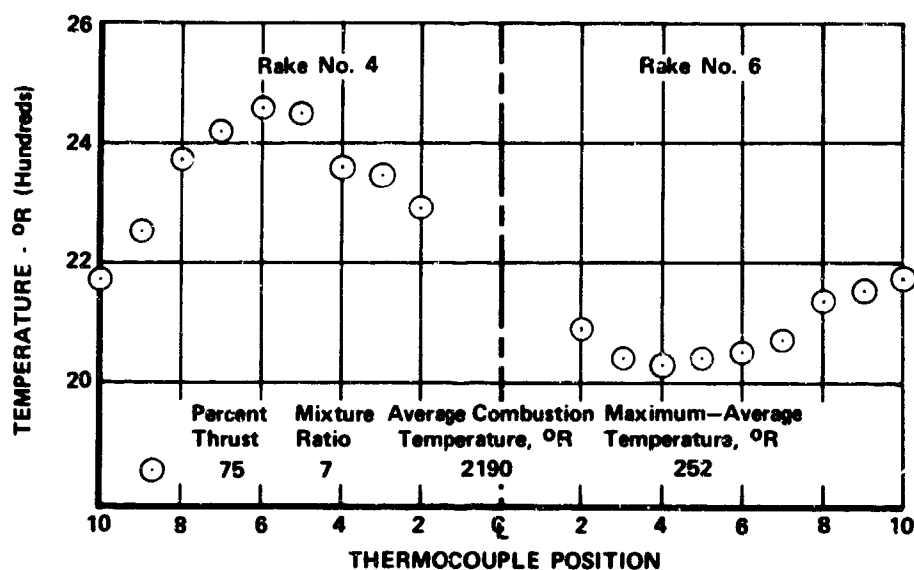


Figure 455. Temperature Distribution, Run 7.01 FD 44050

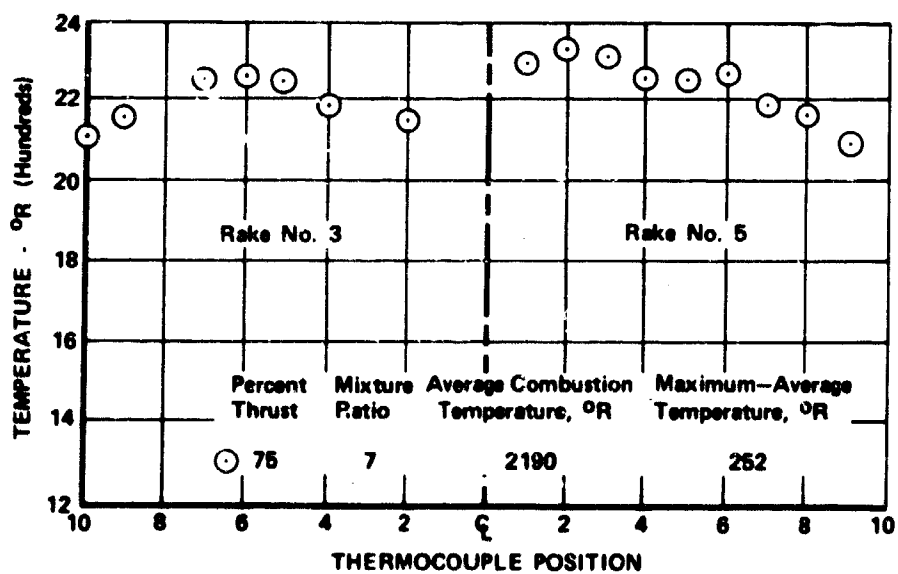


Figure 456. Temperature Distribution, Run 7.01 FD 44051

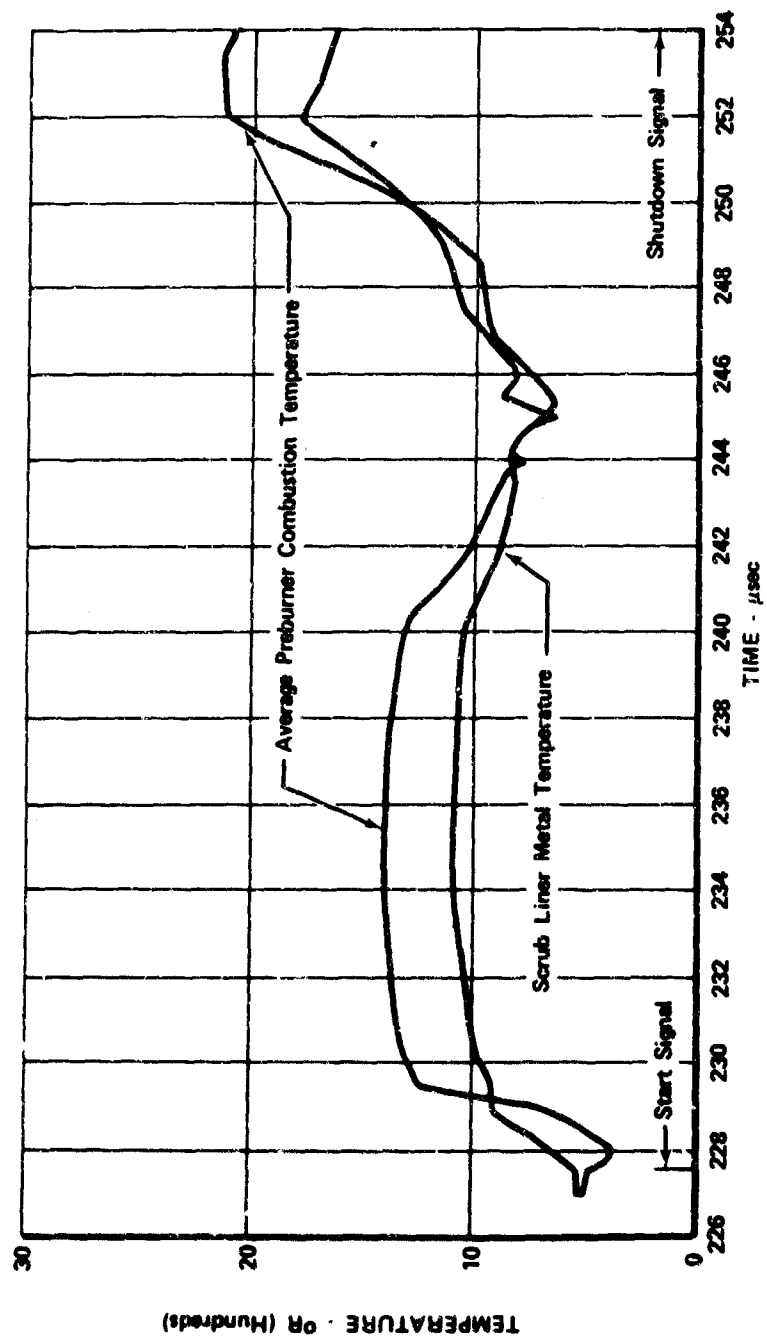


Figure 457. Scrub Liner Temperature, Run 7.01

FD 42874

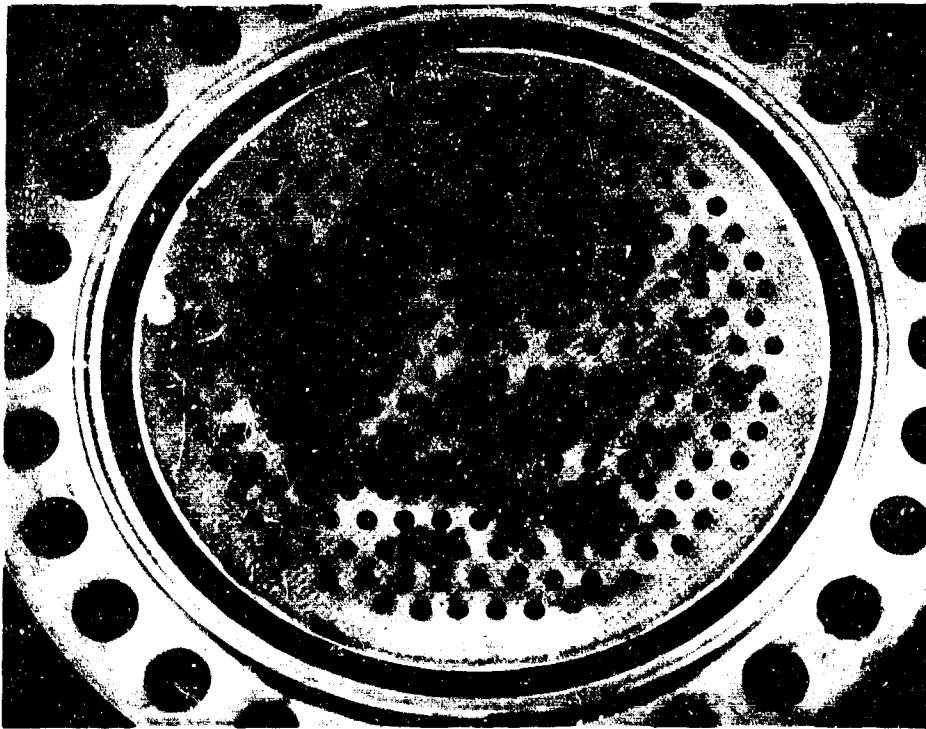


Figure 458. Injector Face Condition After Teardown FE 97485



Figure 459. Liner Condition After Teardown FE 97501

Table LXIV. Engine Thrust Level 75% Engine Mixture
Ratio 7, Rig No. 35133, Run No. 8.01

	Predicted Engine Cycles	Test Results
Chamber Pressure - psia	3007.	2964.
Total Oxidizer Flow - lb/sec	49.29*	48.89
Oxidizer Primary Flow - lb/sec	7.843*	8.37
Oxidizer Secondary Flow - lb/sec	41.45*	40.53
Oxidizer Primary/Total Flow Split	0.1591*	0.171
Total Fuel Flow - lb/sec	40.91	42.38
Injector Fuel Flow - lb/sec	40.91	40.84
Upper Coolant Liner Flow - lb/sec	NAV	0.7840****
Lower Coolant Liner Flow - lb/sec	NAV	0.4132****
Rigimesh Liner Flow - lb/sec	NAV	0.339
Injector Mixture Ratio	1.205	1.187
Overall Mixture Ratio	1.205	1.154
Oxidizer Injector Temperature - °R	211.2*	191.2
Fuel Injector Temperature - °R	190.4*	196.3
Temperature Profile - °R	0°	258.
Average Temperature - °R	2235.	2203.
Oxidizer Injector Primary ΔP	436.7*	364.8**
Oxidizer Injector Secondary ΔP	116.5*	119.7**
Fuel Injector Plate ΔP	112.0	155.1
Oxidizer Primary Injector A_{cd} - in ²	0.063*	0.0785**
Oxidizer Secondary Injector A_{cd} - in ²	0.6813*	0.6650**
Fuel Injector Overall A_{cd} - in ²	3.48	NAV***
Fuel Injector Plate A_{cd} - in ²	3.7	3.26
Flow Divider Valve Position - %	63.9*	64.2
η_c * (Based on P_c , wt) - %	100.	99.3
η_c * (Based on Average Temperature) - %	100.	99.4

* Rig cycle predictions

** There is an apparent leak of oxidizer flow from primary to secondary cavities. (Injector flow split = 0.135)

*** Horn Pressure used for overall fuel injector A_{cd} is bad.

**** Due to either a leak or faulty instrumentation, liner flows could not be determined. Numbers given are based on percentages of total flows from previous runs.

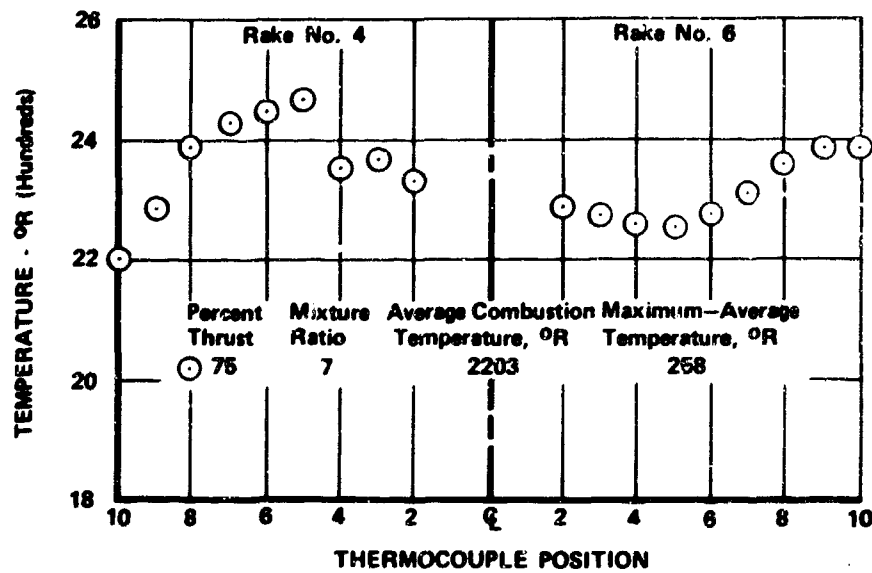


Figure 460. Temperature Distribution During Run 8.01

FD 44052

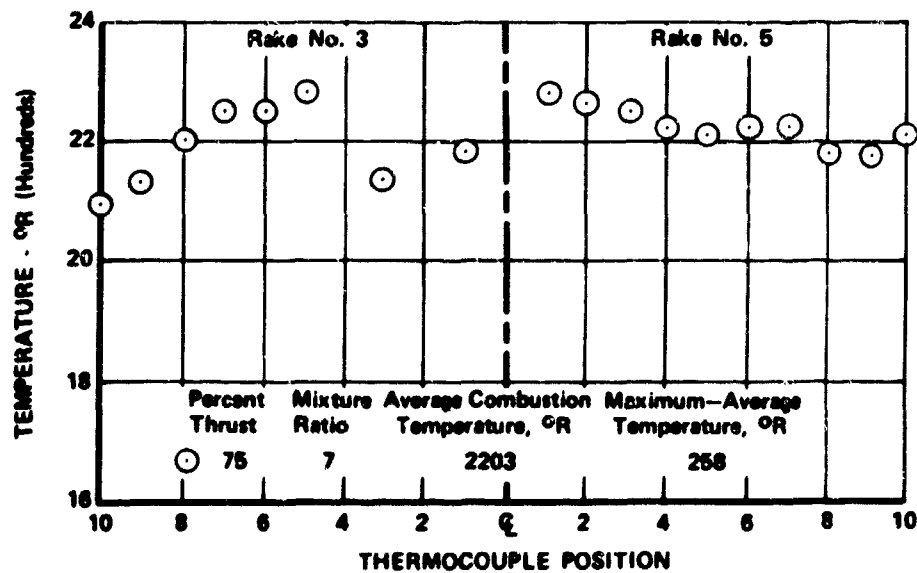


Figure 461. Temperature Distribution During Run 8.01

FD 44053

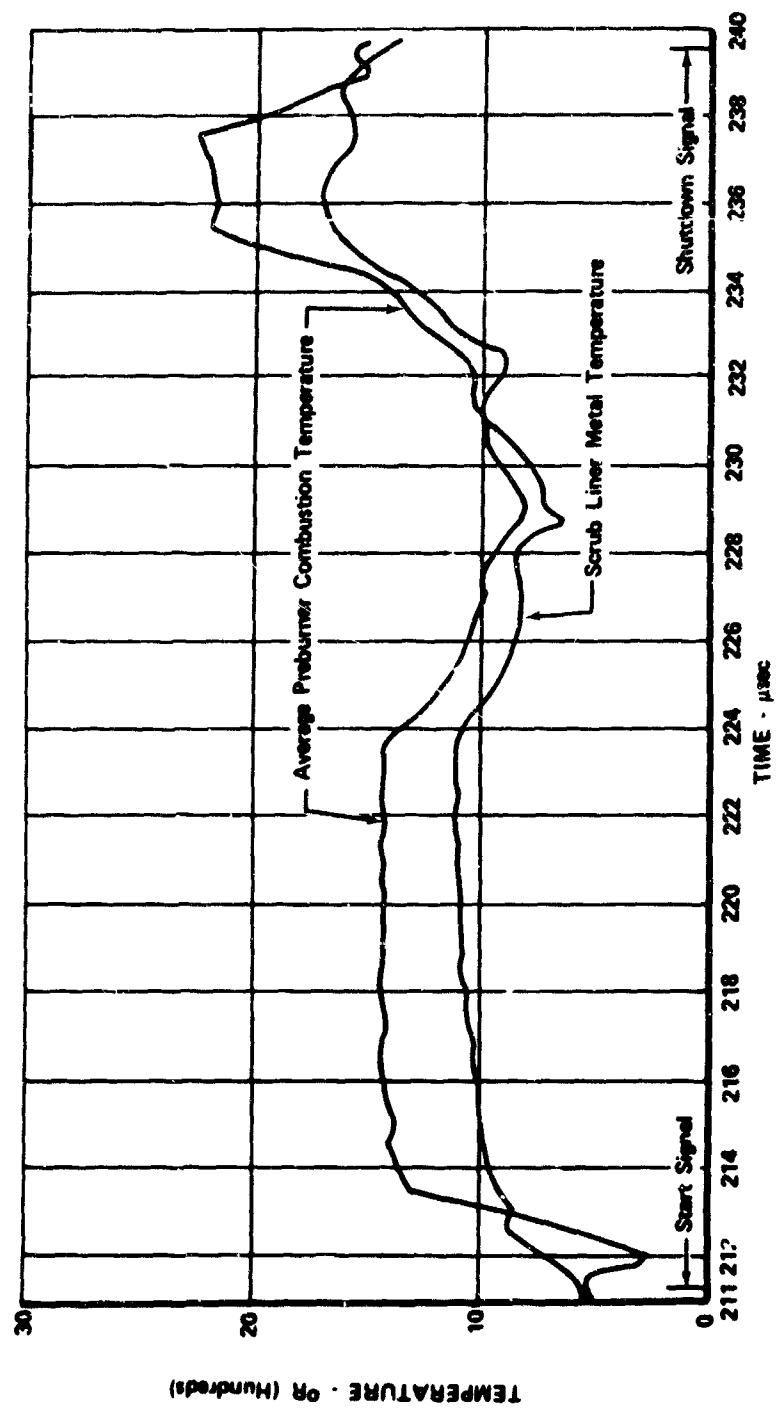


Figure 462. Scrub Liner Temperature, Run 8.01

FD 42873

Failure analysis by zygo and binocular examination revealed that the lower cooled chamber liner which was fabricated from Hastelloy X Material (AMS 5536) failed circumferentially only the liner/ring weld in three locations approximately 16 in., 1-1/4 in., and 1/2 in. in length. In two locations the cracks branched out axially through the liner and the weld (figure 463). Fracture through the 1-1/4 in. circumferential crack revealed fatigue progressing from numerous origins on the ID and OD surfaces of the skirt (figure 464).

Microexamination of a section through the 1/2 in. long circumferential indication revealed a single, transgranular crack progressing through the liner side heat affected zone of the liner/ring weld (figure 465). The grain size was ASTM 5-7, AMS 5536 requires ASTM 4 or finer. The structure appeared normal for welded and stress relieved AMS 5536.

Spectrographic analysis identified the material as being similar to required AMS 5536. The hardness across the liner, heat affected zone, and weld was RB 95-98 (converted). Thickness of the liner in the vicinity of the weld was 0.042 to 0.044 in.; drawing requires 0.045 in. minimum.

It is concluded that the circumferential cracking in three locations was due to fatigue which progressed from numerous origins on both the ID and OD surfaces of the liner. Material conformed to composition requirements.

It is probable that the fatigue cracking experienced was caused by low frequency (600 Hz) combustion oscillations that are experienced during a hot firing as explained previously in this report.

The bulged Rigimesh transpiration liner was sectioned, and examination of the section revealed that the electron beam had locally missed the land, as shown in figure 466 during fabrication when the Rigimesh transpiration liner was electron beam welded to the Rigimesh support. The electron beam weld serves not only as a structural means of preventing the Rigimesh transpiration liner from collapsing, but also provides a seal between coolant zones. Thus, when the Rigimesh liner bulged, the fuel coolant became maldistributed axially (zone to zone) and circumferentially causing over cooling in some areas and overheating in others. The result was local hot spots on the Rigimesh liner, in addition to the bulging.

The general conclusions that can be made from the preburner rig tests are:

1. The temperature profile is acceptable for driving the fuel pump turbine.
2. The addition of the transpiration cooled section of the preburner liner will allow operation of the preburner at any cycle condition above 20% thrust. The preburner liner temperatures show a decrease in operating level as thrust is increased even at high average combustion temperatures. The preburner can be operated at 20% thrust, $r = 5$ with no distress to the liner. It is expected that increasing the cooling flow will allow satisfactory operation at 20% thrust, $r = 6$ and 20% thrust, $r = 7$ conditions.



Figure 463. View of Large End of Liner Showing Large Circumferential Crack Along Ring Weld and Crack Branched Out Through Weld and Liner

FAL 18260

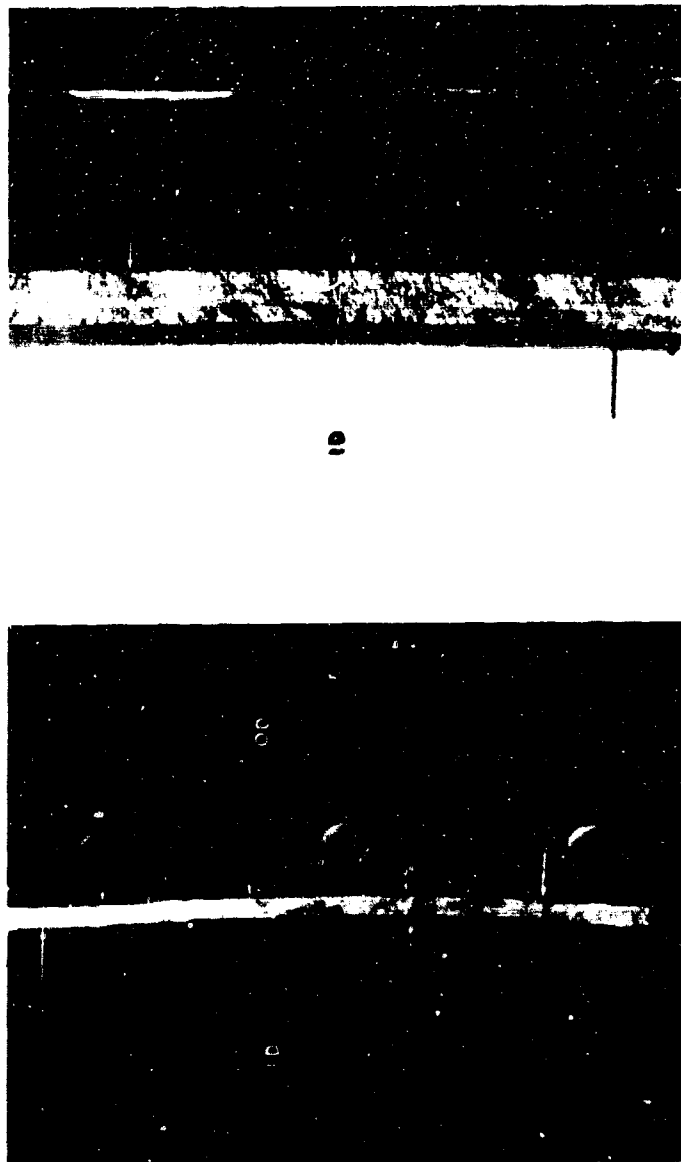


Figure 464. Close-Up of Fracture Through 1-114 in. Long Circumferential Crack Showing Fatigue
Progressing From Numerous Origins On Both the ID and OD of the Liner

FAL 18261

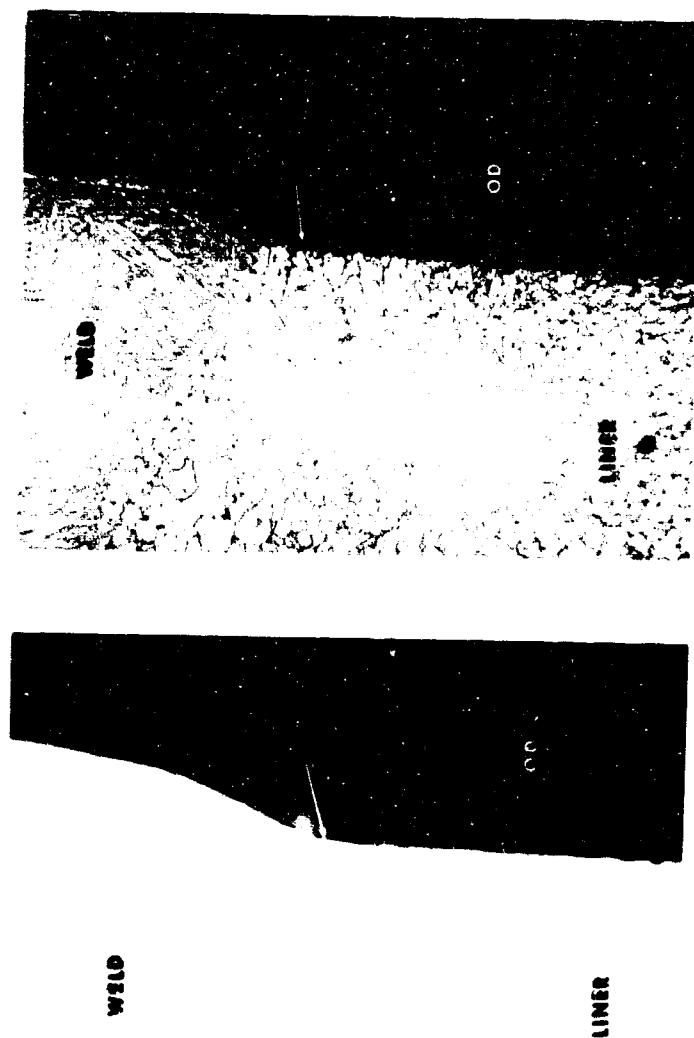


Figure 465. Photomicrographs of Section Through 1/2 in. Long Circumferential Indication Showing a Single, Transgranular Crack Progressing Through the Liner FAM 42498

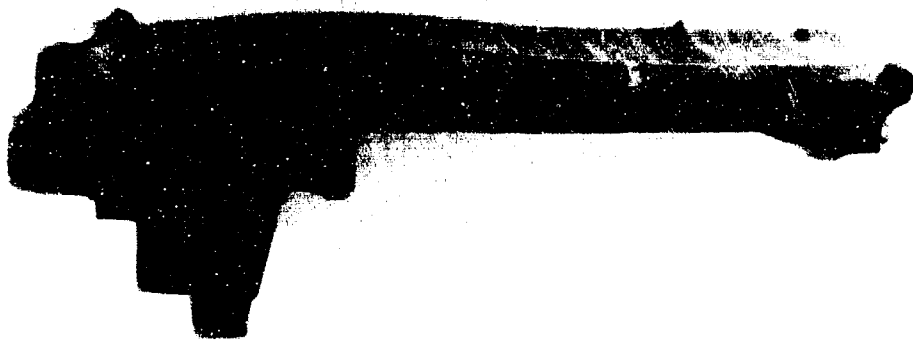


Figure 466. Section of Transpiration Liner Showing FE 99694
Where Electron Beam Missed the Land

Since the temperature profile is satisfactory and the preburner liner is adequate above 20% thrust it was decided to run the preburner injector in the hot gas system test rig.

e. Preburner Torch Igniter Testing

(1) Test Setup

Two new preburner torch igniter assemblies, which were designed for use in the transition case during hot gas system tests, were mounted in B-7 test stand as shown in figure 467. In addition to the bill-of-material igniter assemblies, other hardware included a phase I spark plug and exciter, a new 110v, 400Hz spark plug and exciter, and a test stand adapter which simulated the igniter housing on the transition case. This adapter permitted the igniter to be hot fired with the same cooling flow path used with the igniter as installed in the transition case for hot gas system testing. Also, an annular flame enclosure which simulated a transition case preburner duct scrub liner was mounted in series with the igniter discharge to determine the effects of direct igniter torch impingement on the transition case preburner duct scrub liner.

The igniter rig instrumentation is shown in figure 468. These parameters were incorporated to monitor possible hardware distress, determine cooling characteristics, and to provide sufficient data for performance evaluation. Data recording consisted of strip charts, oscillograph, and digital print out.

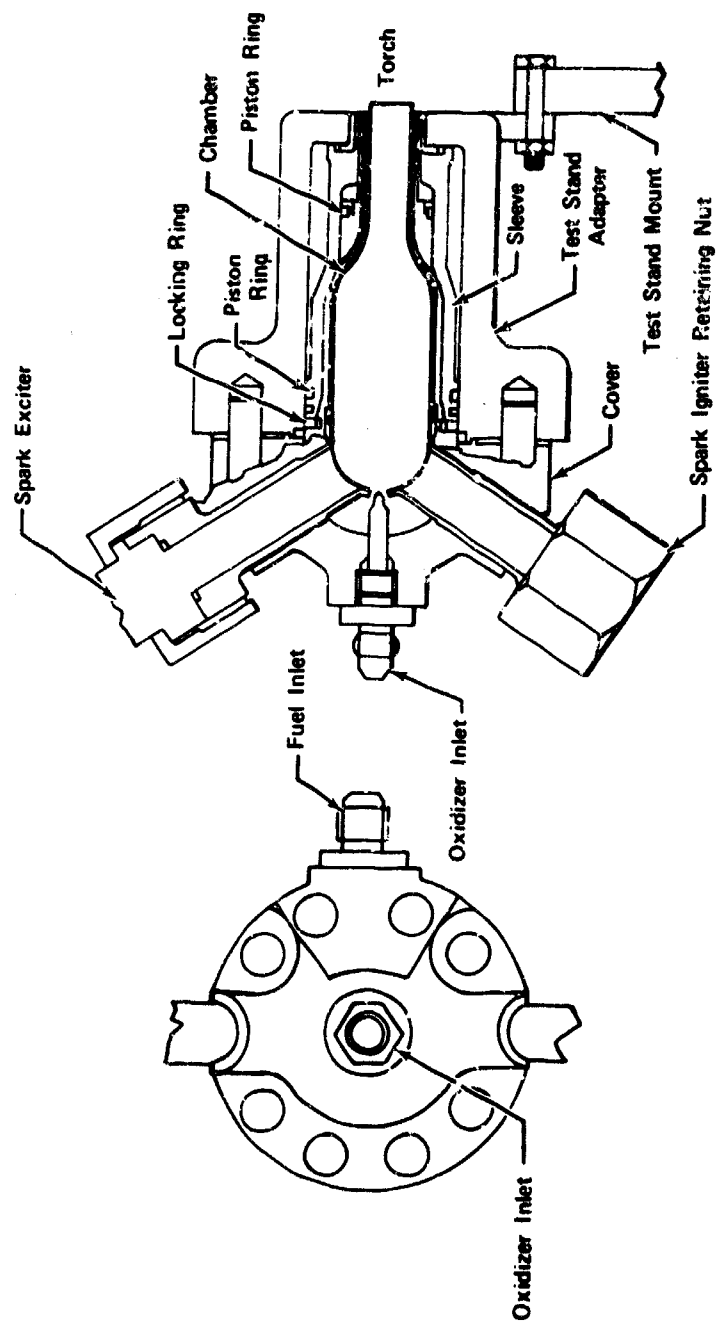


Figure 467. Preburner Torch Igniter Assemblies Mounted in B-7 Test Stand

FD 40256

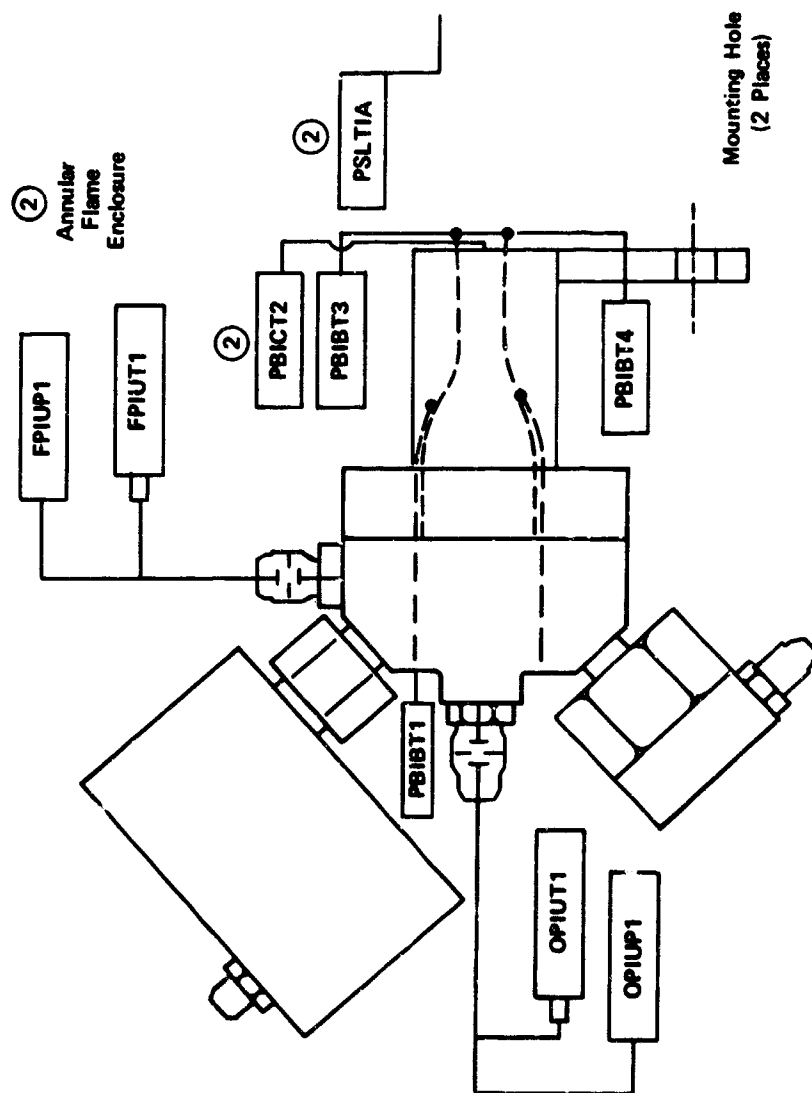


Figure 468. Igniter Instrumentation

FD 40255

(2) Hot Firings

The igniter assemblies were hot fired as separate rigs prior to being installed in the transition case to define operational characteristics and to provide a reliable torch ignition system for the transition case during hot gas system and hot turbine fuel pump testing. Twenty-three successful firings were made on the No. 1 igniter with hot time totaling 688.9 sec.

Figure 469 shows a typical igniter firing. The No. 2 igniter was fired five times accumulating 161.4 sec hot time. Significant parameters from successful tests on both igniters are shown in table LXV. The first 20 tests were made using the spark plug and exciter from phase I testing. The remaining tests were made with the No. 1 115v 400 Hz spark plug and the exciter ignited the rig satisfactorily during use.



Figure 469. Typical Igniter Firing

FE 98738-4

The first series of hot firings, test 1.02 through 10.02, on the No. 1 igniter assembly were programmed to determine the fuel flow split; i.e., \dot{W}_f Coolant/ \dot{W}_f total, and to verify purge, propellant, and spark on-off timing sequences based on phase I igniter operation.

A mixture ratio of 1 producing an average combustion temperature of 2300°R was programmed for test 1.02. This combustion temperature was low enough to prevent hardware distress even if the coolant flow was found to be much lower than the design target. Mixture ratio of the tests was increased, test by test to ensure the igniter assembly could be operated at a target design mixture ratio of 2 without hardware distress.

Table LXV. Summary of Igniter Test Data

Test No.	Hot Time, sec	W_f total, sec	W_o , sec	P_o/T_o , psia/R	P_f/T_f , psia/R	$T_o/O/F$, °R	T_o/T_a^2 , R/°R	T_g/T_g^4 , R/°R	T_{liner} , R	W_f Cool, W_f Total	Comments
1.02	22.0			325/550	750/550		820/-	895/780			Combustion temp (Tc) not operated.
2.01	22.0	0.00454	0.000234	388/540	750/540	1380/0.45	775/-	775/720			Temp shift from 1380°R to 1540°R due to foreign material in GDX orifice.
	8.0	0.00154	0.000281	388/540	750/540	1540/0.54	775/-	760/740			Temp shift from 1540°R to 1910°R due to GDX purge.
6.01	25.0	0.00454	0.000390	500/540	750/540	1910/0.75	860/-	830/770			Target O/F = 1.4
7.01	31.3	0.00448	0.000221	550/555	755/555	2920/1.40	1070/-	1040/940			Target O/F = 1.6, GDX orifice partially plugged.
8.01	31.7	0.00440	0.000270	625/560	775/555	2880/1.36	1070/-	1010/920			Target O/F = 1.8, GDX orifice partially plugged.
9.01	31.6	0.00449	0.000276	715/565	780/545	2850/1.35	1035/-	970/910			Return of 8.01 with clean GDX orifice.
10.02	31.5	0.00464	0.000822	710/540	770/540	3120/1.54	1150/-	1080/1070			Design point O/F = 2.0.
11.02	31.3	0.00451	0.000879	690/560	760/555	3350/1.71	1205/-	1180/1090		0.887	Target O/F = 1.8.
12.01	31.4	0.00459	0.000985	780/570	760/560	3600/1.98	1255/-	1240/1145		0.884	120° of design flows.
13.01	32.1	0.00555	0.001202	945/560	915/550	3570/1.88	1205/-	1170/1110		0.883	80° of design flows.
14.01	31.3	0.00373	0.000805	625/545	620/540	3105/1.53	1080/-	1100/1000		0.858	Repeat of 13.01.
15.01	31.4	0.00368	0.000820	630/540	610/540	3150/1.57	1090/-	1095/1085	1330	0.859	Simulated liner 9 in. from igniter discharge. Design flows.
16.01	31.6	0.00468	0.000977	760/550	750/550	3090/1.52	1175/-	1065/1050	1075	0.857	Simulated liner 4.5 in. from igniter discharge. Design flows.
17.01	31.5	0.00654	0.000965	765/550	760/550	3050/1.49	1160/-	1065/1050	900	0.855	Simulated liner 4.5 in. from igniter discharge. 120° of design flows. T _{liner} has not reached steady state.
18.01	6.6	0.00549	0.001202	930/545	915/545	3290/1.67	1125/-	1000/965		0.869	Repeat of 17.01.
19.01	32.0	0.00565	0.001212	935/540	920/540	3120/1.54	1105/-	1015/990	1115	0.860	Simulated liner full distance from igniter discharge. 120° of design flows.
20.01	31.9	0.00554	0.001212	930/535	915/535	3130/1.55	1120/-	1045/1020	1260	0.860	Flame out test. Initial steady state data presented. Flamed out at approximately 2200°R.
21.01	13.3	0.00654	0.001010	785/550	760/550	2980/1.44	1035/-	990/-		0.845	Flame out test. Initial steady state data presented. Flamed out at approximately 2200°R.
22.01	12.2	0.00653	0.000989	765/545	755/545	2850/1.35	-/1045/-	950/-		0.840	Tc spiked above 3650°R at ignition. Settled out at 3460°R.
23.01	32.3	0.00641	0.00189	605/535	385/535	3460/1.79	-/1200/-	1260/1230		0.811	Target O/F = 1.25.
24.01	30.9	0.00275	0.001022	785/535	375/530	4230/2.44	-/1305/-	1400/1365		0.815	Target O/F = 1.50.
25.01	33.1	0.00646	0.000655	510/550	780/550	2685/1.24	-/985/-	1005/964		0.885	Target O/F = 2.0. T _g noisy.
26.01	34.4	0.02465	0.000801	620/545	775/545	3050/1.49	-/1010/-	910/900		0.884	Target O/F = 2.0. T _g 3 high and noisy. Flow split low.
27.01	1.0	0.00665	0.000752	810/540	770/535	3650/1.95	Not Steady			0.884	Repeat of 28.03.
28.03	31.2	0.00646	0.000404	310/535	800/535	1160/0.355	-/480/-	1450/775		0.751	No comment.
29.01	32.3	0.00668	0.000392	305/550	785/550	1225/0.370	670/690	780/800		0.773	Tc damaged. Tc determined from T _g .
30.01	32.6	0.00660	0.000694	535/550	770/550	2700/1.25	1060/1120	1170/1100		0.881	
31.01	32.4	0.00667	0.000872	675/545	780/545	3245/1.64	1165/1215	1200/1220		0.886	
32.01	32.5	0.00670	0.001058	815/540	780/540	3630/1.93	1260/1265	1250/1310		0.883	

**Installed 110u - 400 cpa Spark Plug and Exciter Box Assembly

- W_f Total - Coolant plus combustion fuel flow rate
- P_o - Pressure supplied to GDX external orifice
- T_o - Orificer flow rate
- T_g - Temperature at GDX external orifice
- T_f - Pressure supplied to fuel external orifice
- T_i - Temperature at fuel external orifice
- T_c - Combustion temperature
- O/F - Igniter chamber mixture ratio
- T_g through T_g - Igniter barrel temperatures
- T_{liner} - Temperature of simulated transition case liner
- W_f Cool - Fraction of total fuel flow that is used as barrel coolant
- W_f Total

Mixture ratio was controlled by regulating fuel and gaseous oxygen upstream pressures as set flowing through the rig before ignition. Purge and propellant valve and spark timing sequences were controlled by a programmed digital sequencer.

From the beginning of the test series, problems with plugging the orifice on the gaseous oxygen supply caused the actual mixture ratio to be lower than target. In addition, plugging of the fuel coolant flow orifices, which causes low mixture ratio, was experienced. Tests 1.02 through 9.01 experienced gaseous oxygen orifice plugging and some degree of fuel coolant orifice plugging, causing the combustion temperature to be lower than target.

In those tests experiencing partial plugging of the gaseous oxygen external orifice, mixture ratio was determined from combustion temperature as gaseous oxygen flow could not be calculated, igniter fuel flow split was calculated in later testing. Igniter barrel temperature, T_{B1} or T_{B3} was found to be a linear function of combustion temperature and the igniter barrel temperature was used in determining average combustion temperature in tests, in which the combustion temperature probe was overscaled or otherwise inoperative.

The approximate design mixture ratio was reached on run 11.01. A visual inspection of the rig made after each test revealed no hardware distress. Runs 12.01 through 14.01 were made to show the durability of the igniter with flowrates 20% above and below the design flowrates.

Runs 15.01 and 16.01 were made with the igniter discharge directed at a simulated transition case preburner duct scrub liner at a design distance of 9 in. and a shorter-than-design distance of 4.5 in. respectively, at approximate design flows. Runs 17.01 through 19.01 were a repeat of tests 15.01 and 16.01 except flows were 20% higher than design flows. These tests demonstrated direct impingement of the igniter discharge on the simulated lines caused no distress of the liner at the design or higher than design propellant flowrates.

Runs 20.01 and 21.01 were made to determine the lower mixture ratio limit for sustained combustion once the igniter was lit and running. The igniter flamed out at approximately 2200°R. The fact that the igniter would not continue burning down to the combustion temperature levels experienced in run 2.01 and the subsequent runs 28.03 and 29.01 on the No. 2 igniter were not investigated or explained.

Run 24.01 was made to show durability of the igniter at combustion temperatures higher than design. The igniter was run at a combustion temperature of 4230°R for 31 sec, and inspection of the igniter after this test did not indicate any distress.

The No. 1 igniter was disassembled and flushed after run 24.01 because the changing coolant flow split showed the fuel coolant slots were becoming progressively more plugged. To correct this problem, the facility lines were thoroughly blowdown, and all lines, valves, and filters were cleaned. After cleaning the No. 1 igniter, runs 25.01, 26.01, and 27.01 were made to determine if the fuel coolant slot blockage had been removed. The flow split had returned to the original level of 88% of the total fuel flow going through the coolant metering orifices. The No. 1 igniter was dismantled and inspected with no problem areas noted.

The No. 2 igniter was mounted, checked, and fired up to design flowrates during runs 28.01 through 32.01. The No. 2 igniter was dismantled and inspected. No indications of hardware distress or other problems were noted. These tests concluded the test work done on the preburner igniters.

6. Facilities

a. E-8 Test Stand

This test stand was provided by United Aircraft Corporation to support the Phase I full scale preburner and staged combustion test programs, and a plot plan is shown in figure 470. The addition of this large capacity pressurized facility to the existing FRDC facilities has allowed testing of 250,000 lb thrust preburners at pressures in excess of 5000 psi. The facility consists of a 2400 gallon, 6600 psi hydrogen tank, and a 900 gallon, 6600 psi oxygen tank. These liquid run tanks are pressurized with gaseous hydrogen and gaseous nitrogen, supplied from seven 9000 psi cylinders with a total storage volume of 4185 cu ft. The facility includes twin 10,000 psi hydrogen gas compressors and 10,000 psi nitrogen vaporizer pumps for charging the tank pressurization bottles. The liquid and gas capacity enables testing the 250,000 lb thrust preburner, at design operating pressure, for 7 sec, and staged-combustion tests for 15 sec. The thrust measurement system is sized for 350,000 lb thrust and will allow accurate thrust measurement with a precision error of less than $\pm 1\%$ over a 10 to 1 thrust range. A liquid-gas mixer is provided to supply hydrogen to the rig at any temperature between that of liquid hydrogen and room temperature to simulate engine operating conditions. In addition, separate hydrogen systems are available for chamber and nozzle coolants. Control of propellants to the test rig is accomplished by using 23 electrohydraulic commercial control valves in the gas and liquid systems. These control valves, many of which are in parallel, allow a pressure flow control range of 450 to 1.

The facility control system is based around an analog computer, allowing for closed loop control of the electrohydraulic servovalves plus associated mathematical computation and nonlinear function generation. Figures 471 and 472 show the E-8 control consoles and analog computer. The computer system consists of the following components:

- 200 coefficient potentiometers
- 160 Philbrick dc operational amplifiers
- 20 EAI multipliers
- 26 variable diode function generators
- 26 voltage comparators
- 1 NLS digital voltmeter
- 1 NLS digital printer
- 1 NLS digital frequency counter

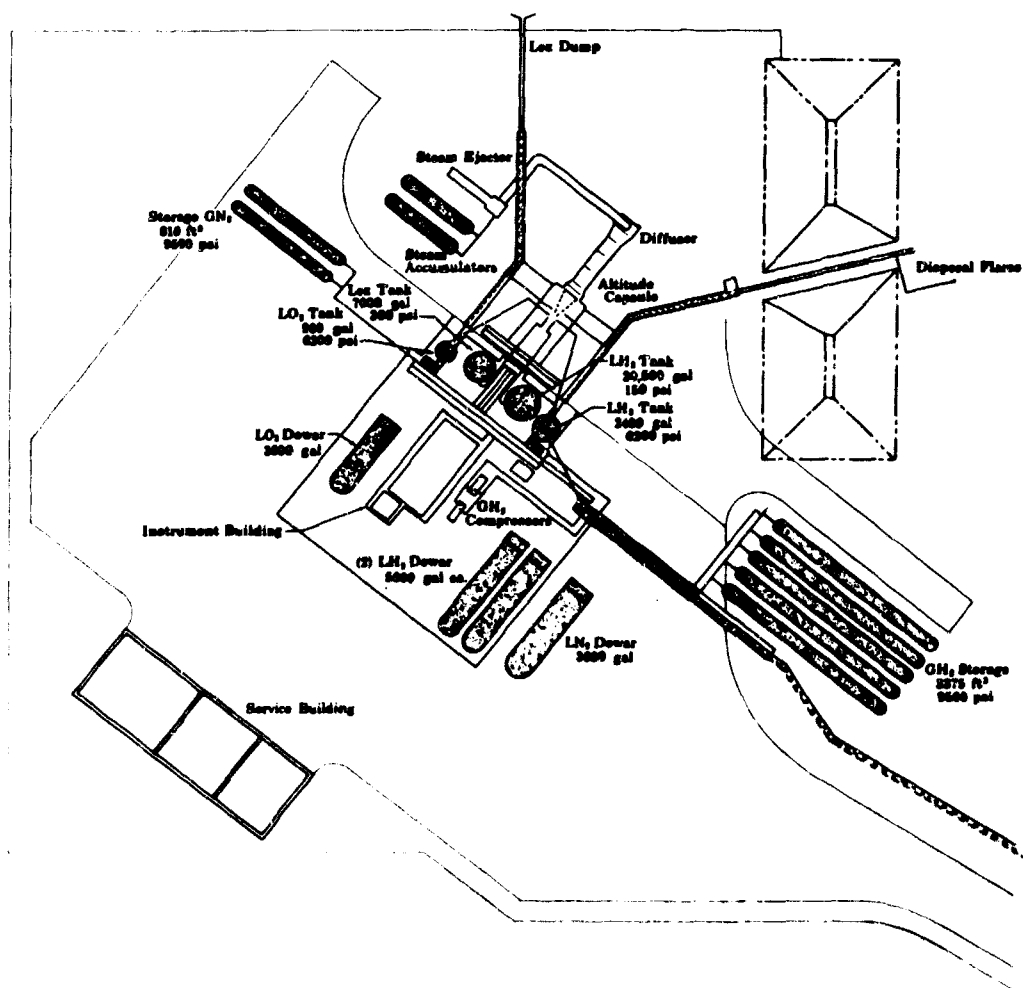


Figure 470. E-8 Test Stand Plot Plan

FD 21139

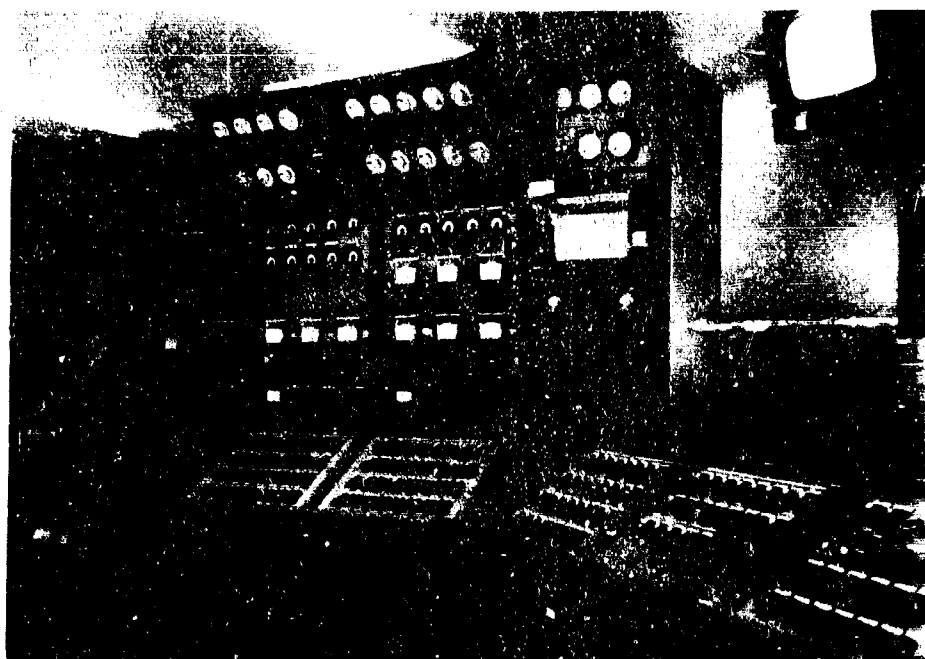


Figure 471. E-8 Control Console

FC 14114

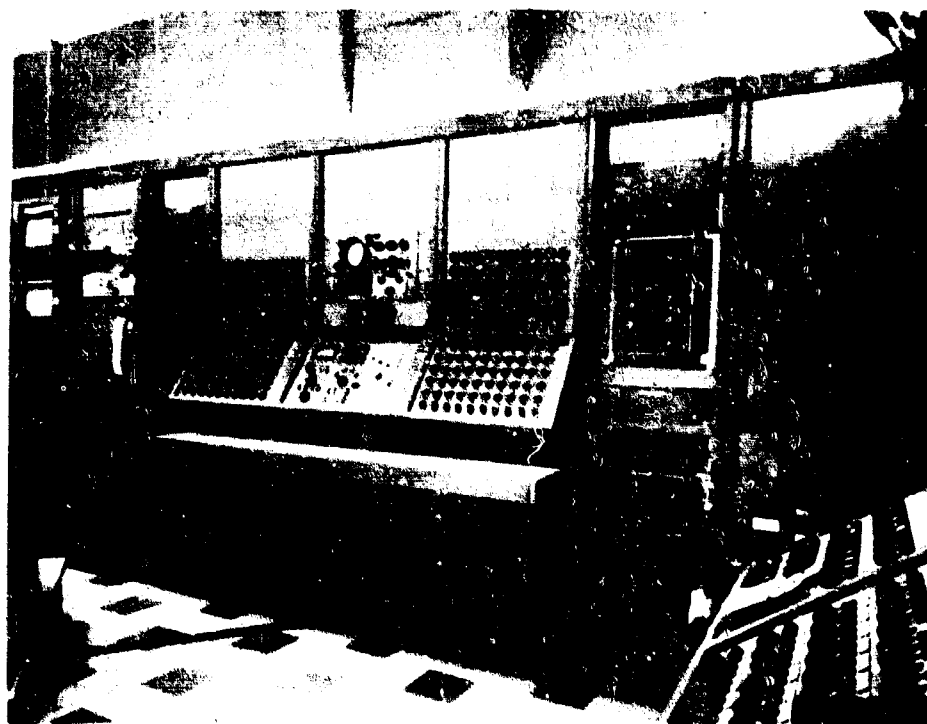


Figure 472. E-8 Analog Computer

FC 13694

24 Astrodata differential amplifiers

1 Vidar voltage-to-frequency converter

1 Wavitek function generator

5 Vidar frequency-to-voltage converters

1 hp dual trace oscilloscope

Test program events are controlled by an electronic digital sequencer. This unit converts a constant frequency pulse train into time controlled switch operations according to a predetermined program sequence. These switches can be operated in series, parallel, cascade, and time delayed sequence. Event timing can be scheduled in 1 msec intervals on any one of 60 relay channels between the time limits of ± 999.999 sec. In conjunction with the analog computer, the sequencer provides for prefiring and post-firing valve operation, initiation, and shutdown of test, and timing of controlled parametric changes during the test. The sequencer is programed to interrogate, in conjunction with voltage comparators, certain parameters at specific time interval, thus providing a go-no-go indication for the test to proceed, advance to a preprogramed controlled shutdown, or abort. During the test program this engine parameter interrogation system has proved invaluable in the protection of rig hardware from damage due to program error, controller, or valve malfunction.

Control system input as well as data recording is handled through a 200 channel digital data system with a sampling rate of 6666 samples per sec. (See figure 473). The transmission and signal conditioning system has the capacity to handle the following:

Pressures (individual power supplies)	72 channels
Thrust	12 channels
Resistance temperature bulbs	24 channels
Flow and rpm	12 channels
Flow multipliers	15 channels
Thermocouples, C-A	48 channels
Thermocouples, C-C	48 channels
Vibrations	18 channels
Dynamic pressures	6 channels

The data are presented using:

Strip charts	28 channels
Oscillograph	36 channels

Analog tape	24 channels
Digital recording	200 channels
Oscillograph (control parameters)	18 channels

In addition there are nine high speed camera locations and closed circuit TV for test monitoring.



Figure 473. 300-Channel Digital Data System

FC 12357

The 250,000 lb thrust preburner is tested to optimize the temperature profile and investigate the effect changes in fuel inlet temperature and momentum ratio have on the temperature profile. The control configuration used for preburner testing is shown in figure 474. In this configuration, the operating level of the preburner is determined by power level, which schedules the oxidizer and fuel flowrates.

Power level also schedules the desired valves of preburner liquid oxygen and hydrogen flows.

The measured valves of these flows are fed to the control system and are then compared with the desired levels, which are functions of the power level.

The preburner starting sequence is accomplished by diverting the required fuel and oxidizer flows from a preset overboard condition to the injector and allowing them to stabilize. Preburner combustion pressure is 7% at this point

and the oxidizer valves are on flow control and the fuel valves are on position control. The liquid fuel valves are then switched to total flow control. On total flow control the flow signal from the liquid and gaseous hydrogen flow meters are summed. The gaseous hydrogen valves are on temperature control; sensing the temperature at the mixer exit. Preburner flows are ramped to the desired equivalent thrust level and combustion temperature.

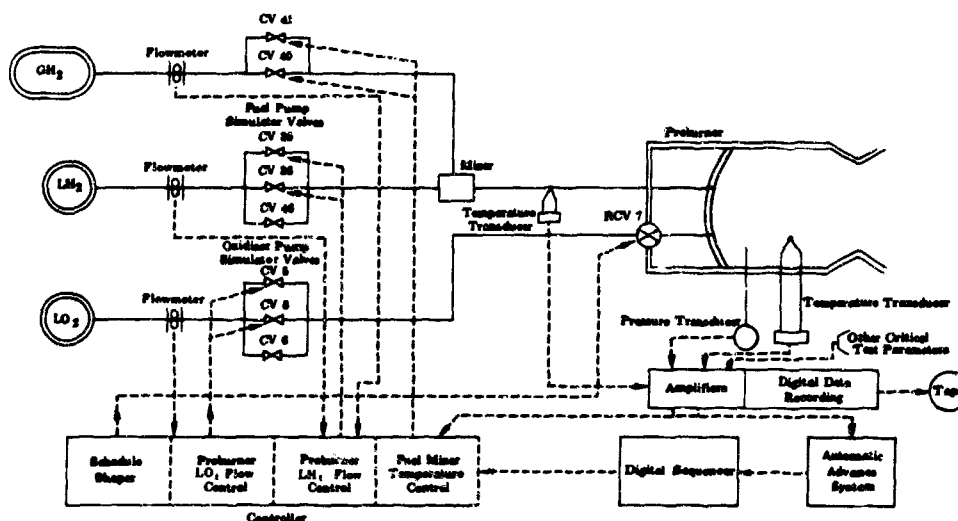


Figure 474. Preburner Rig Control System

FD 21136C

Test conditions, other than those scheduled by power level, are programmed in and out of the control by the digital sequencer to set starting flows, provide automatic changes of flow level, and provide automatic excursions in test conditions to acquire performance data.

b. Injector Calibration B-21 Test Stand

Injector calibrations were obtained through the use of the closed loop water blowdown facility B-21 stand. The water flow loop consists of a 2100 gallon run tank, which when filled is pressurized to the required level from a 5000 psi nitrogen source. The tank is capable of supplying 1500 psi water to the inlet of the test item at flowrates from 1% to 100% of the equivalent 250K main oxygen flowrate. The water passes through electrohydraulic control valves that will set the preprogrammed flow versus pressure ramp to the test item. A 20 channel analog computer is used for this purpose. The water through the test section flows into a catch tank to recover the working fluid. The recovered water is then pumped back to the run tank for reuse. The internal surface of the flow system is stainless steel, and demineralized water allows for the test component to be maintained in a LO₂ clean condition. Turbine flowmeters are used for flow measurement, and data are recorded on strip charts and on an 18 channel oscillograph. A minimum test duration of 30 sec is attainable with this system when operating at the maximum flowrate.

B. TRANSITION CASE

1. Introduction

The transition case serves as the mounting structure for three major engine components; the preburner, oxidizer pump, and fuel pump. It contains internal ducting that routes preburner discharge gases through the fuel and oxidizer pump turbines and to the main burner injector. A machined boss for installing the preburner igniter is located on the preburner sphere. With incorporation of the preburner injector and turbopump components, the transition case is a self-contained powerhead, capable of supplying the main burner chamber and nozzle with the high pressure propellant necessary to produce the design thrust. Figure 475 shows the transition case location and figure 476 shows how the components are attached or plugged in the transition case. It also serves as the primary combustion stage for the staged combustion cycle. The gimbal spherical ball sea socket and retainer is incorporated in the upper end of the outer case so the outer case also serves as a structural member that transmits thrust from the main burner to the gimbal ball.

The design analysis of the transition case was substantiated by subscale transition case model tests that assisted in the evaluation of the selected design. Following the model testing and consideration of five intersecting sphere configurations, a design concept of coplanar intersecting spheres was selected for the transition case. A detailed description of the model testing and design studies is presented in the Demonstrator Engine Design Report, AFRPL-TR-70-6. A lightweight, high strength materials requirement placed upon the outer case fabrication material predicated selection of Inconel 718. Rings were forgings, and the shell was hydroformed flat plates. The case cooling liners and preburner discharge gas flow ducts (although not an integral part of the outer case structure) including a centerbody where the flow split resulted, were essential elements of the overall concept. The internal ducting of the transition case splits the hot, fuel rich gases from the preburner to provide adequate gas flow into each turbine, the fuel turbine requiring approximately twice that required to drive the oxidizer turbine. Cooling liners between the outer case and the hot gas flowpath keep the outer case temperature below 540° R.

The gimbal thrust ball, an assembly external to the transition case, provides for engine attachment to the vehicle while permitting engine gimbaling in the pitch and yaw axes.

2. Summary Conclusions and Recommendations

The coplanar design was selected over the canted components version after completing design studies and model testing. The coplanar design was selected because it offered the best solutions regarding the inner duct design, cooling, thrust load handling, assembly and manufacturing problems.

Inconel 718 ring forgings were used to provide a high strength assembly in the high stress areas. These were welded to the main sphere and later finish machined. The main sphere was composed of two Inconel 718 hydroformed welded hemispheres.

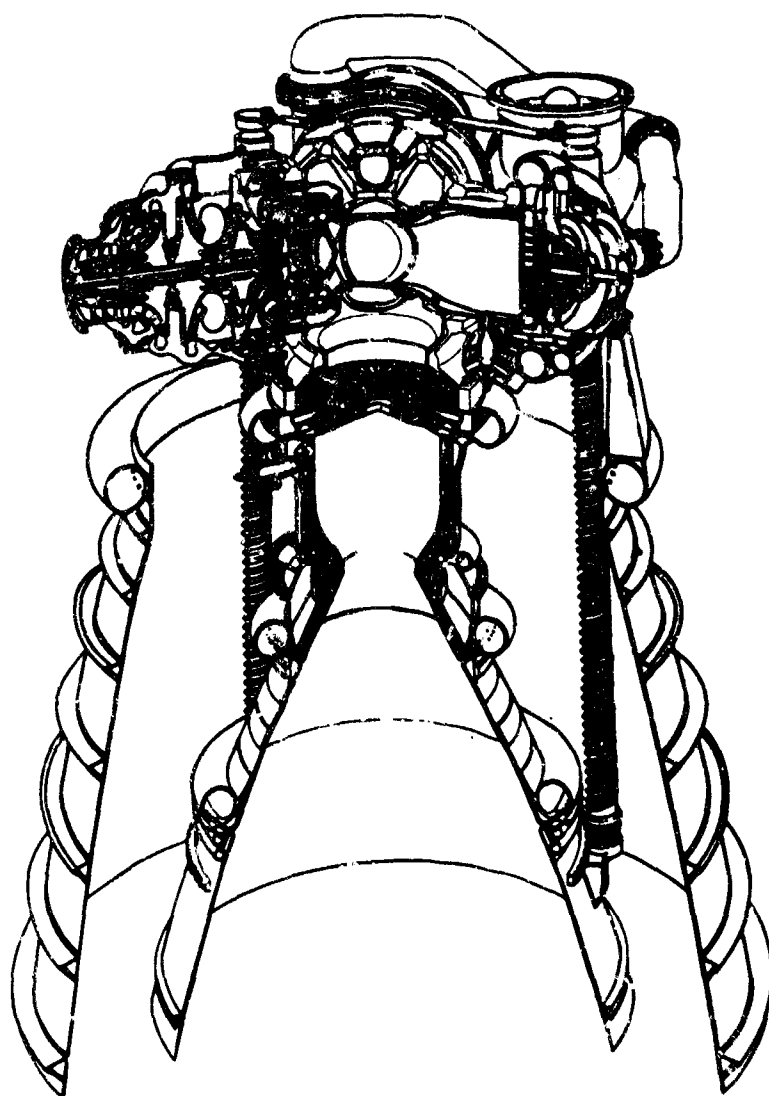


Figure 475. XLR129 Reusable Rocket Engine

FD 31415

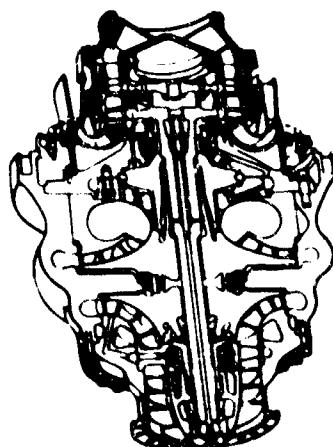
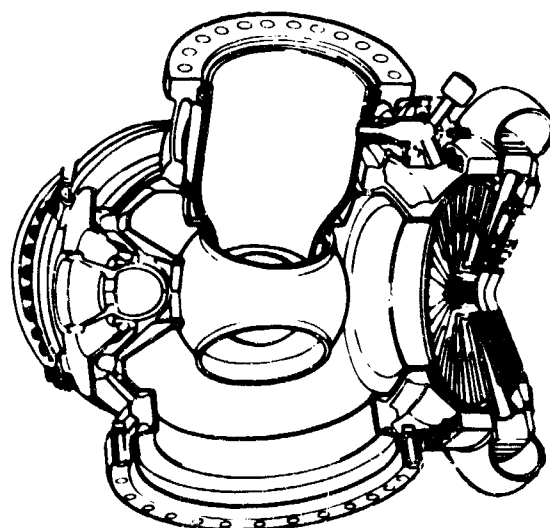
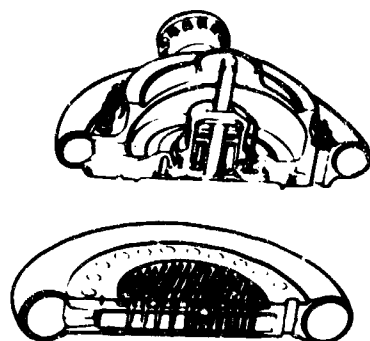


Figure 476. Plug-In Concept

FD 33179A

Hand welding methods were used in the fabrication of the transition case. A study of welded specimens was conducted showing that hand welding was superior to machine welding when cost, quality and consistency were considered.

The porous cooling liner that routes the coolant to the outer case was installed in subassembly sections in the outer case. The liners were fabricated by a vendor and were formed to the case contour. Because the coolant flowrates, after forming, proved from tests to be unpredictable, the flow was tailored by a flame spraying process. Studies show the flow can be tailored as required and the pure nickel spray bonding is permanent under extreme conditions. The gimbal ball uses a uniball joint to distribute thrust and side loads into the transition case. This eliminates the need for a standard cross pin universal joint and provides a simpler, lighter and more stable joint.

The centerbody, a sphere intersected by three cylindrical rings, provides the shortest possible plumbing for the intersection of the fuel, oxidizer and preburner duct, and provides the sealing surfaces for the piston rings that are installed as part of the individual duct assemblies. The outer shell of the centerbody is a porous liner that protects the structure of the centerbody from the hot turbine exhaust gases. The centerbody is supported by the transition case at the gimbal support cone through a threaded joint. Coolant supply to the centerbody from the transition case flows through this threaded joint, cooling the gimbal area before entering the centerbody.

For the initial preburner-transition case testing, turnaround caps that closely simulate the fuel and oxidizer turbines were planned. Where possible, actual turbine parts were designed into the cap assemblies. These ducts and the preburner duct that plugs into the centerbody form the plug-in concept.

The preburner duct serves as a combustion chamber and discharges combustion products into the centerbody. The duct design considerations used include cycle life, strength and weight. Inconel 625 material, offering good cycle life, was selected for the internal detail of the liner. Because the duct assembly is also a structural duct, Inconel 718 was selected for the outer duct detail. Coolant passages are formed when the two details are joined and oven brazed. The coolant flows the length of the duct discharging into the gas flow stream through the centerbody liners.

The transition case details were successfully proof pressure tested to 120% of their hot run stresses and recommended for testing with the preburner injector. Section VII describes these tests.

3. Hardware Description

The transition case assembly, illustrated in figure 477, is composed of the outer case, cooling liner, preburner flow duct, and centerbody.

a. Outer Case

The preburner injector, oxidizer pump, fuel pump, and main burner injector are flange mounted to a common duct, and the method of intersecting these flanged components defines the engine package. The outer case is the mounting structure for these components and in operation contains combustion products. The outer case and cooling liner are illustrated in figure 478.

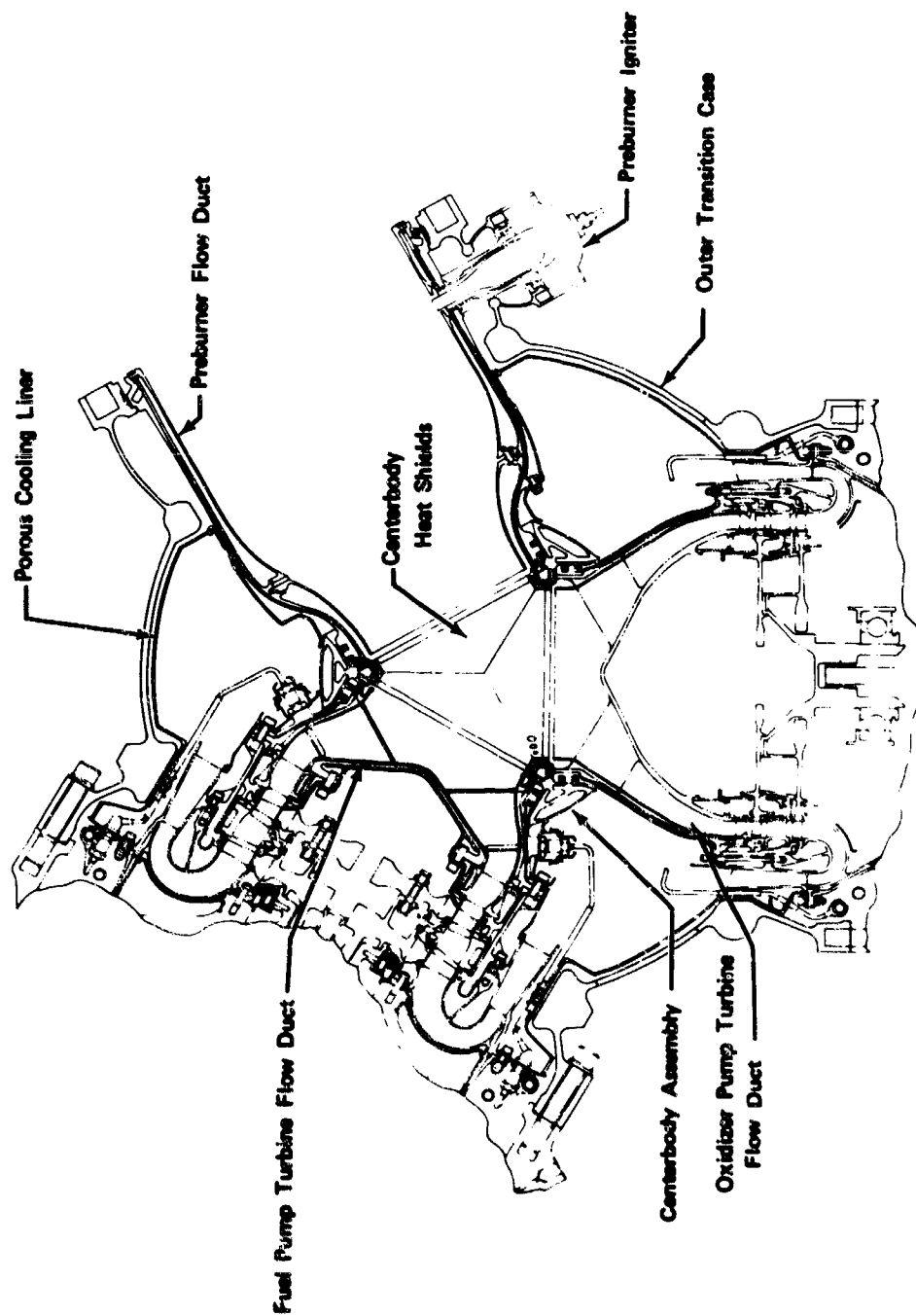


Figure 477. Transition Case Assembly

FD 29115C

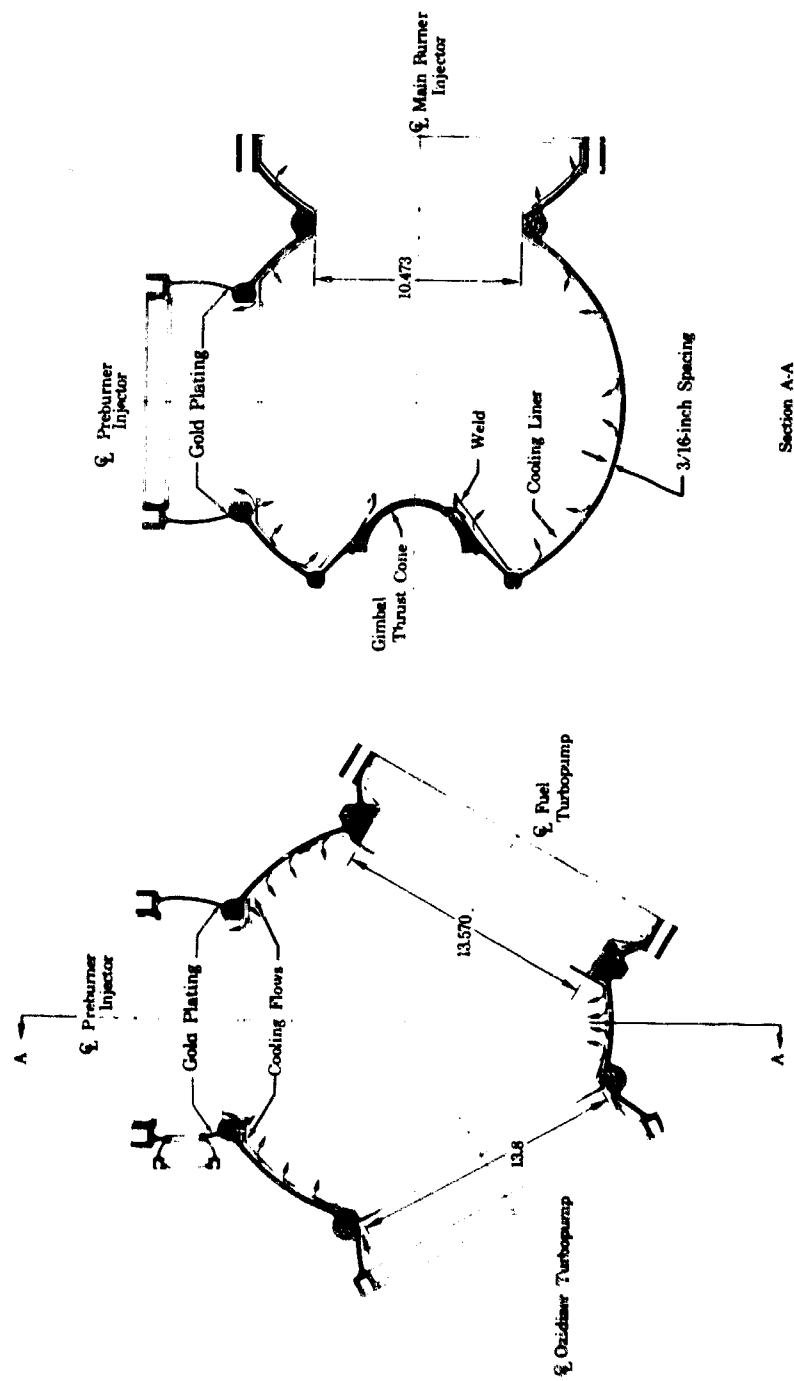


Figure 478. Outer Case and Cooling Liner

FD 29116A

To minimize weight and maintain a compact engine package, a spherical vessel was selected as the basic case building block and is intersected by four flanged, spherical segments.

The overall case envelope was determined by the area of the main burner injector proportioned to the area of the ring at the lower sphere ring intersection. The individual components determined the overall size of the component spheres. Shell material thickness supported by a stiffening ring maintains equal deflection at the intersection points; therefore, bending stresses occurring at the point of highest stress in the case (the main burner injector flange-to-shell intersection) determined the shell thickness requirement of 0.185 in. The thrust load is applied through the center sphere of the transition case by intersecting it with an inverted cone and gimbals. The outer case is designed for an internal operating pressure of 4500 psi (including a safety factor of 1.5) and a thrust load of 250,000 lb.

b. Cooling Liner

The cooling liner shields the outer case structure from the high temperature turbine exhaust gases as they flow from the turbines to the main burner injector. The liner is hydrogen transpiration-cooled, and prevents the case external skin from exceeding 540°R. The inside of the outer case preburner segment has gold plating (0.0001 in.) that reduces preburner flow duct radiation from increasing the temperature of the outer case structure in this area.

The liner takes the shape of the outer case and is assembled into the outer case by welding together preformed spherical segments fabricated from sintered wire mesh, creating a porous metal barrier between the outer case and turbine exhaust products. Hydrogen passes through the liner forming an insulating boundary.

Design studies indicate that a spherical Rigimesh liner that uniformly follows the outer case contour is optimum for providing the best flow properties. This will ensure there is no severe maldistribution of coolant caused by the quantity or location of coolant supply points. The liner was set at a liner-to-outer-shell proximity of 0.170 to 0.190 in. to minimize volume because the volume behind the Rigimesh strongly affects liner pressure differential during a transient. The selected liner was designed for a 10 psi pressure differential under design conditions, providing a Rigimesh liner differential pressure of 4 psi at minimum thrust and maximum mixture ratio conditions. Therefore, a design point steady-state drop of less than 10 psi could lead to poor coolant distribution at off-design conditions. Stiffening rings fabricated from L-605 (AMS 5759) are installed at the mounting flanges for the mounting of the two pumps and the main burner injector. The liner is 0.057 in. thick and has a porosity of 21 scfm ambient air at a 2 psid pressure. The liner is flame sprayed in local areas as required to ensure the proper flowrate.

Coolant supply is obtained downstream of the transpiration supply heat exchanger and is supplied to the transition case through the fuel and oxidizer turbopump flanges. Coolant is supplied at 450°R and a flowrate of 1.2 lb/second.

c. Gimbal Thrust Ball

The function of the gimbal thrust ball assembly, shown in figure 479, is to provide for engine attachment to the vehicle while permitting engine gimbaling in the pitch and yaw axes, to distribute thrust and side loads uniformly into the transition case, and to distribute the thrust load uniformly to the vehicle structure through a cone intersecting the ball. Ball size was determined in terms of the highest stress point at the intersection of the cone and sphere. The thickness was kept uniform around the ball except at the torsion pin boss.

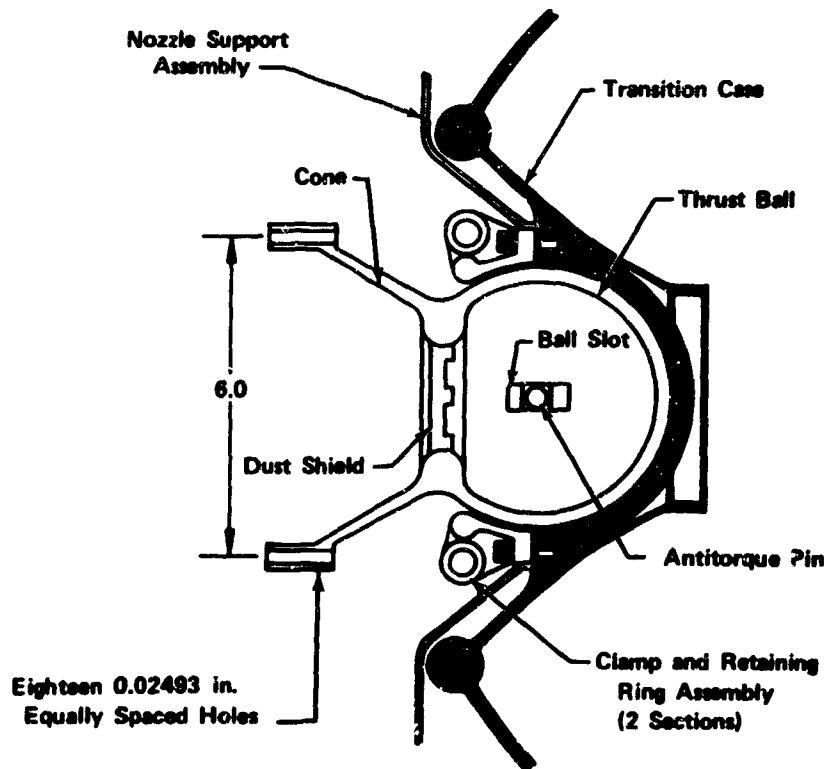


Figure 479. Gimbal Thrust Ball Assembly

FD 31020A

Bearing stresses and pin shear stresses are minimized by using a uniball joint to distribute the thrust and side loads into the transition case. This eliminates the need for the standard cross pin universal joint, thereby affording a simpler, lighter, more stable joint. The load thus distributed to the transition case is transmitted uniformly in shell fashion, thereby minimizing stress concentrations and bending.

A low friction, easily replaceable liner is used between the ball and socket. The material is a composition of teflon, fiberglass, and epoxy, and is bonded to the socket.

An antitorque pin used between the ball and socket resists torsion, enabling the ball to rotate about the pin axis, but preventing axial twisting. A slot in the ball permits the ball to rotate normally to the pin.

d. Preburner Flow Duct

The preburner flow duct is composed of a cooled structural duct, a hot gas scrub liner, and an outer heatshield. The preburner flow duct is illustrated in figure 480.

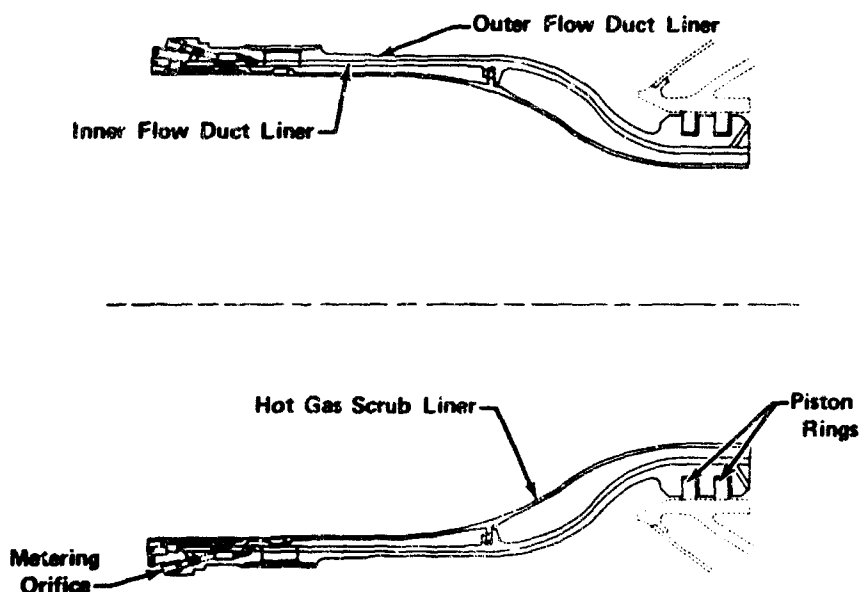


Figure 480. Preburner Flow Duct

FD 29138B

The small end of the preburner duct outer structural wall has a ring into which two grooves are machined. These grooves are part of a three piece piston ring seal design, which is shown in figure 481. The piston rings (AMS 5759) are backed by a spring which provides ring set centering during the blind assembly and provides positive, radial outward load at starting. The rings have a small radial wall dimension to allow pressure to more readily conform the ring to the seal diameter. A three piece ring has proved better than a one or two piece ring because of its bidirectional sealing capability. The area of contact is three times larger than the gap area to ensure the seal does not pivot. The piston rings are loaded by the 1800 to 2000 psi differential pressure across them. The maximum leakage calculated for the three ducts is approximately 0.1 lb/sec at 1800°R and 1800 psid, assuming one ring per duct and a leakage gap of 0.001 in.

The hot gas scrub liner protects the structural duct by preventing hot combustion gas from scrubbing directly against the cooled inner wall of the duct. The first 2 in. of the liner utilizes a porous liner to provide film cooling in that area of the combustion chamber considered most susceptible to burning damage. In addition, film carryover cools downstream for a distance onto the uncooled liner. This transpiration section is a cylinder of sintered wire mesh, electron-beam welded into a support member which has three coolant feed annuli. This assembly is shrink fitted into the preburner duct, with a tight fit at each end of the porous material section to provide seals for a fuel supply manifold. Figure 482 shows details of the cooled liner assembly.

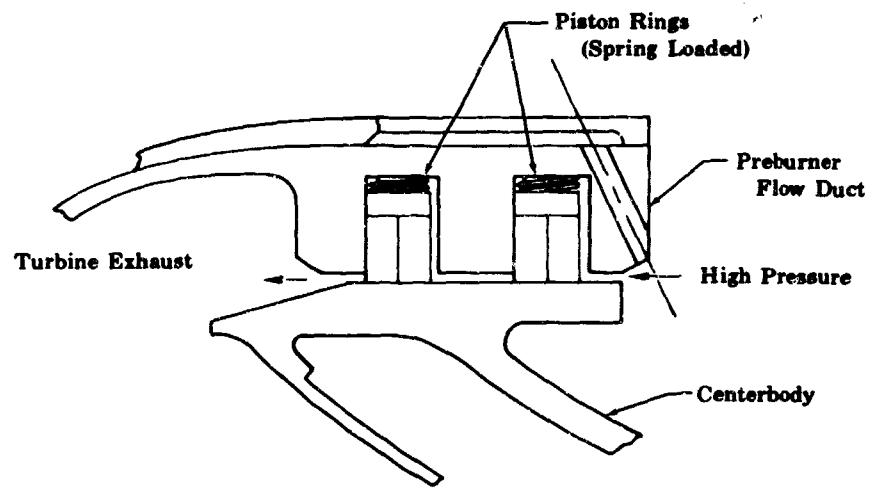


Figure 481. Preburner Flow Duct to Centerbody
Piston Ring Connection

FD 29139



Figure 482. Details of Cooled Liner Assembly

FE 97227

The initial transpiration cooled liner design and the design iterations leading to the final design are covered in paragraph 4. b. The final design included a porous liner with a porosity of 43 scfm at a pressure drop of 2 psi and orifices of 0.028 in. (18 holes) and 0.0205 in. (36 holes) in diameter. Because of continued erosion of the porous liner during the hot gas system rig (35139) hot tests, the flowrate through the porous liner was increased for the hot turbine fuel pump rig (35155) hot tests. A new cooled liner was fabricated with a porosity of 76 scfm and orifices of 0.042 in. (18 holes) and 0.034 in. (36 holes) in diameter. Additionally, after sectioning the cooled liner used in the hot gas system rig, poor electron-beam weld penetration was apparent. To ensure a permanent bond of the porous liner to the carrier, the electron-beam welds between coolant zones were reinforced with heliarc plug welds 0.375 in. long by 0.045 in. wide.

The uncooled liner is a single piece that bayonet joints into the preburner duct approximately 5 in. behind the igniter. This portion of the liner serves to reduce the temperature gradient through the cooled duct, enhancing the low-cycle fatigue life of the duct. This joint provides a metal-to-metal seal loaded by a differential pressure, and is a minimum leakage seal allowing small amounts of combustion products to aspirate behind the liner.

Material selected for the duct and liners are:

1. Cooled Duct - Inconel 718 and Inconel 625
2. Transpiration cooled liner
 - a. Porous material - L-605
 - b. Support - Inconel 718
 - c. Extension - Hastelloy X
3. Uncooled liner - Haynes 188.

Duct and liner cooling flow comes from 28 injector pilot holes into a manifold. Eight metering plugs feed the manifold providing cooling for the preburner duct structure. The transpiration cooled liner flow is controlled by the carrier orifice sizes.

The rear section of the scrub liner has axial restrainer tangs that engage slots in the inner duct liner as shown in figure 483.

The front end of the preburner flow duct is supported by the transition case flange and preburner injector as shown in figure 484. A metal ring seal on the front of the duct prevents coolant from leaking into the combustion chamber.

The purpose of the outer heatshield is to prevent hot turbine exhaust gases from scrubbing the outside of the duct structural wall, adversely affecting low-cycle fatigue life. Very small gaps at the front and rear ends of the heatshield prevent gas flow behind the shield. The outer heatshield is held by shoulder bolts through a slotted hole. The loose fit permits thermal flange and shield growth independent of the duct. The rear of the shield grows outward against the centerbody piston ring ramp at a high thrust and mixture ratio, and the front

of the shield grows outward against the transition case line-to-duct seal support. The center flange has four holes for shutdown venting.

The centerbody, illustrated in figure 485, is composed of the structural body, the outer porous cooling liner, and the inner liner assemblies. The structural body is a sphere intersected by three cylindrical rings. These rings are equally spaced around the equator of the sphere and are the sealing surfaces for the piston rings installed as part of the individual duct assemblies.

An outer porous liner encloses the structural shell and ring assembly to protect the assembly from hot turbine exhaust gases. This porous liner is flame sprayed with pure nickel to tailor the flowrate as required.

The centerbody liner divides the preburner gas flow between the two turbo-pumps and also prevents the preburner gas flow from scrubbing the inside structural walls.

The centerbody inner liner is cooled by the preburner duct coolant flow. The coolant discharges from the preburner duct into the area between the centerbody outer structure and the supporting segments. The coolant flows around the entire inner spherical surface to the side opposite the preburner duct and is discharged into the turbine inlet hot gas stream. A portion of the coolant flow (1.2 lb/sec) supplied to the transition case porous liner flows into this cavity through sixteen 0.375 in. diameter holes in the gimbal thrust cone, cooling the gimbal area. The coolant flows into the area between the outer porous liner and the centerbody outer structure and discharges through the porous liner into the turbine exhaust gases.

The estimated weight of the transition case was 277 lb, excluding the gimbal and pump ducts. The actual weight is 304 lb.

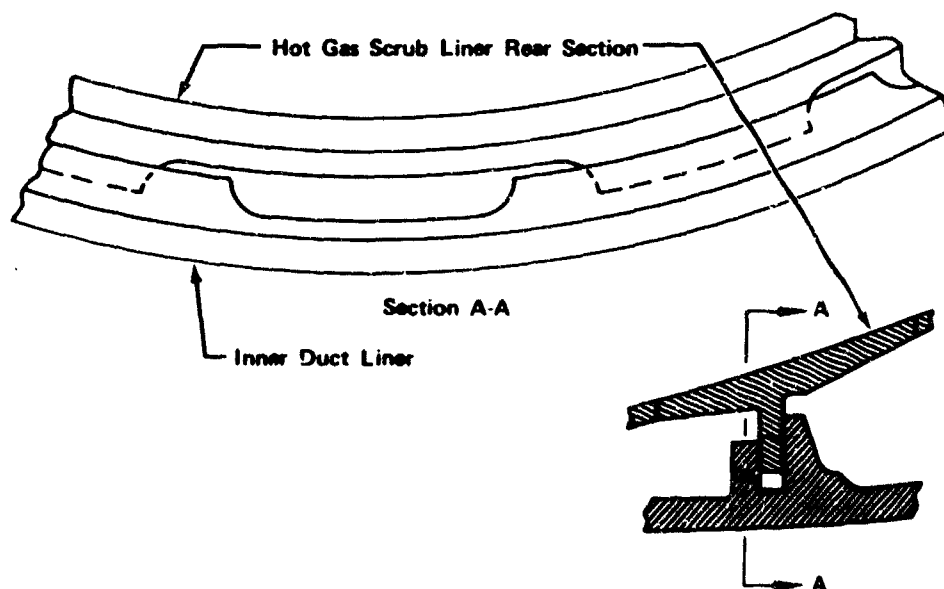


Figure 483. Connection of Front and Rear Section of Hot Gas Scrub Liner FD 29140A

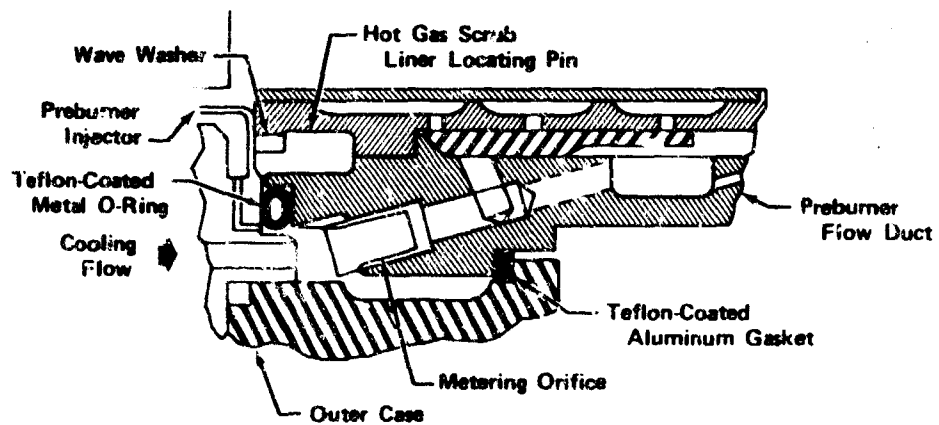
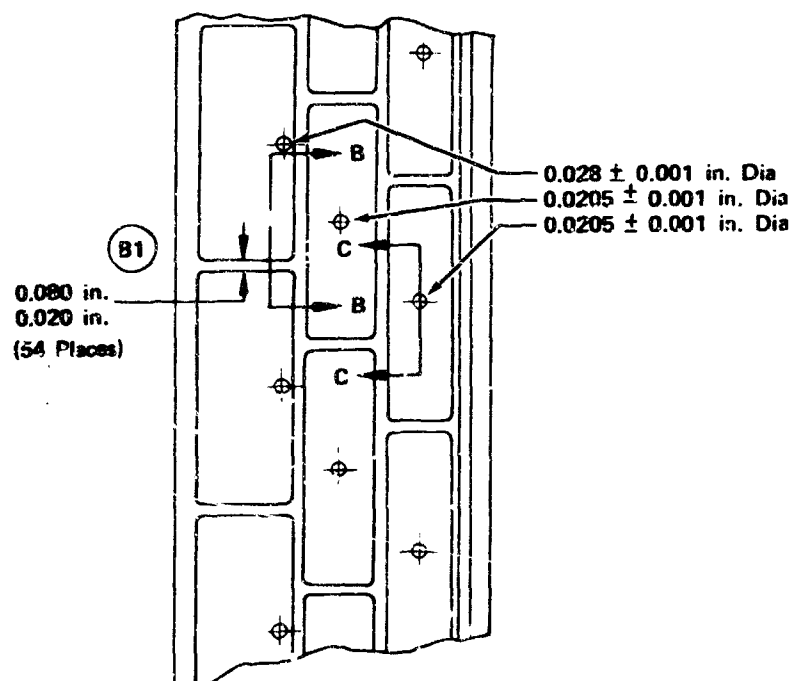


Figure 484. Preburner Flow Duct Front Support FD 45717

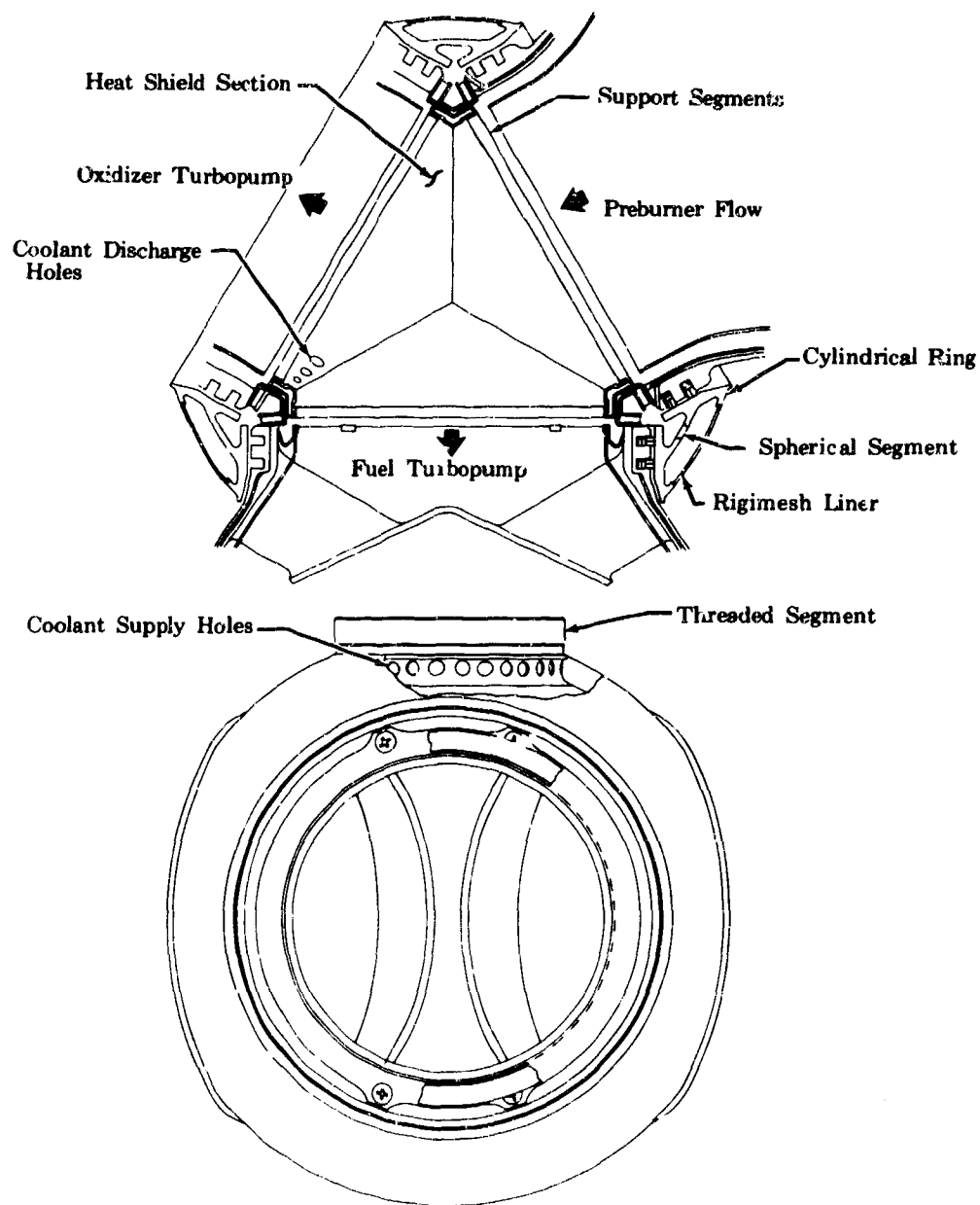


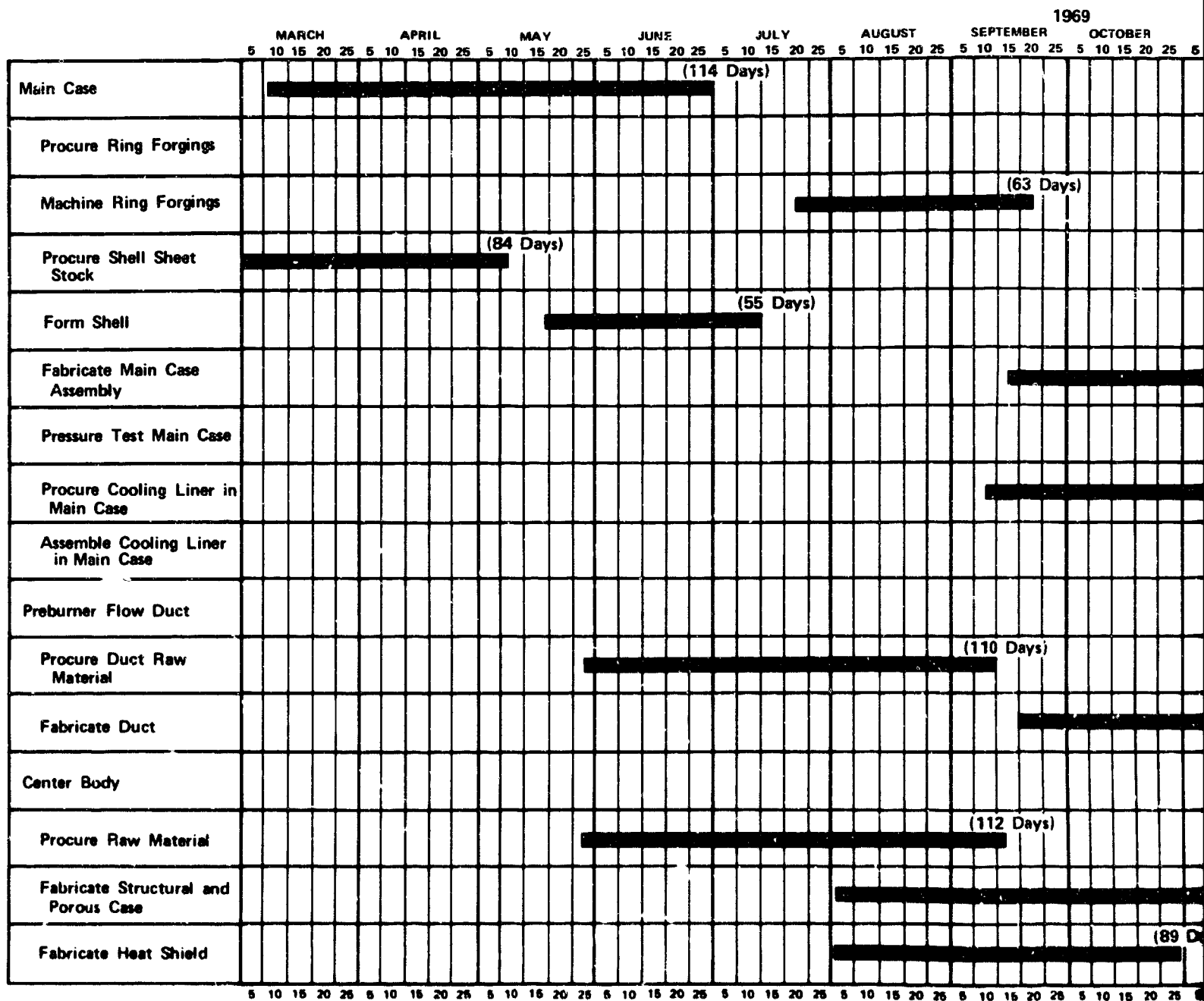
Figure 485. Transition Case Centerbody

FD 29179

4. Fabrication

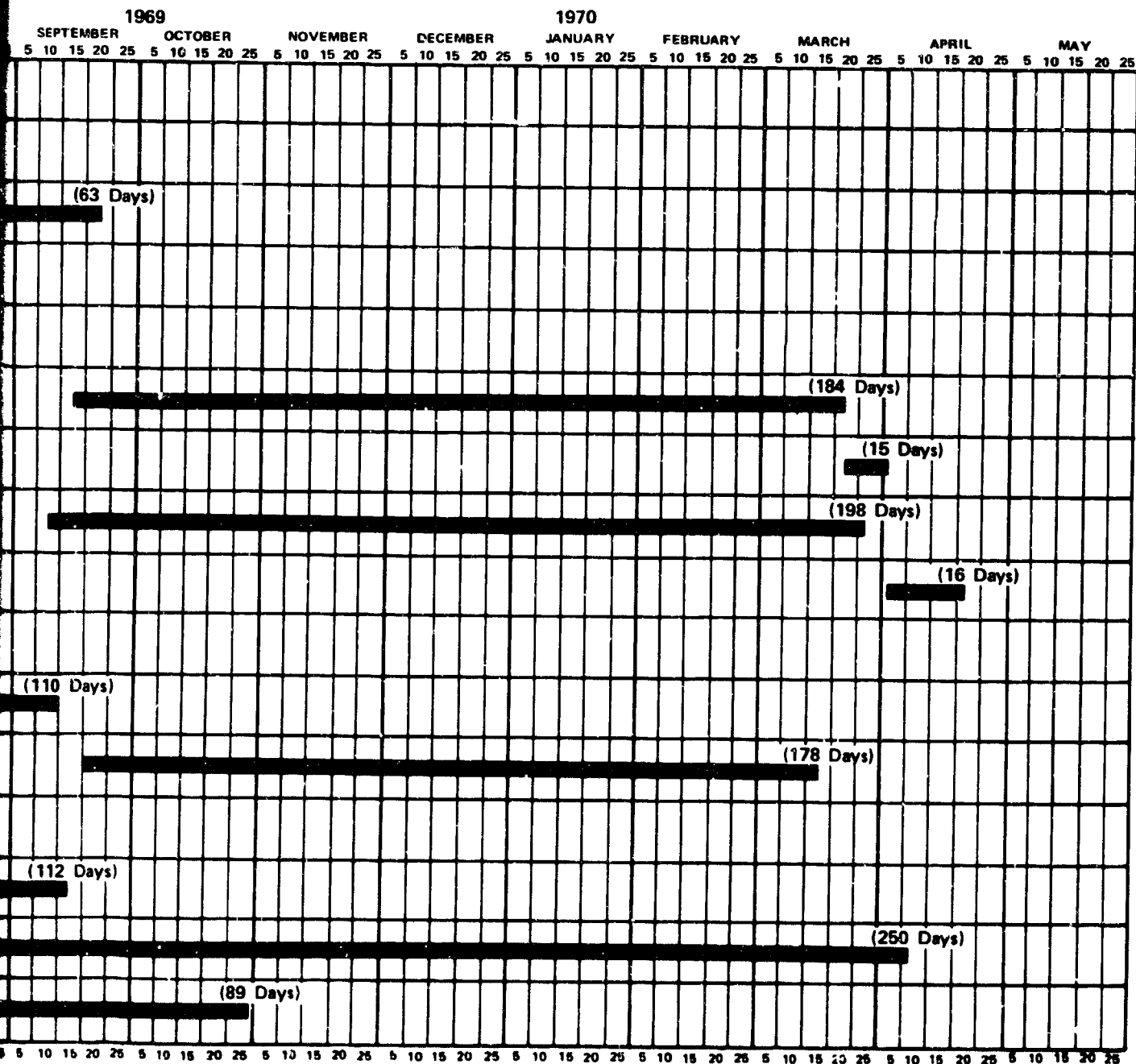
The component manufacturing timetable is shown in table LXVI which shows the procurement and manufacturing time required for the principal subcomponents of the transition case.

Table LXVI. Component Manufacturing Time



A

onent Manufacturing Timetable



FD 44682

13

a. Outer Case

The outer case is a weldment consisting of a major sphere, fabricated by hydroforming Inconel 718 plate, to which are welded four flanged spherical segments and one pancake segment machined from cylindrical forgings.

To verify the weld efficiency used in the case design, a weld tensile strength test program was conducted. The material used was heat treated Inconel 718. The welds were patterned after the transition case welds, which included both butt and T-intersecting welds. Both manual and machine welding methods were utilized in fabricating specimens.

Machine welding methods are superior to manual welding primarily because of weldment uniformity. However, when close control was exercised in the manual welding method, the results were equal to those of the automatic welds. Because of high tooling cost for the machine welding method, the manual method was selected. The results obtained, which are shown in tables LXVII and LXVIII for machine and manual welds respectively, showed that when the weld tolerance closely conformed to the limits specified in the layout, the ultimate tensile strength met or exceeded 180,000 psi.

For correlation, specimens were run that were out of the layout specified range for mismatch and bead height. No appreciable reduction of tensile strength was noted as a result. The maximum deviations were a mismatch of 0.070 and a bead height of 0.070. The blueprint mismatch tolerance is ± 0.005 and the bead height tolerance is 0.010-0.030. The lowest ultimate tensile strength recorded on any specimen was 169,000 psi. Severe conditions were noted when the cross sectional area was abruptly changed, when variations such as sudden increase or decrease of weld bead were encountered. All specimens were inspected by X-ray and zygo techniques before testing to ensure that cracks or voids were not present. These were manually repaired when detected. Tensile strengths of the repaired specimens were within acceptable limits and were not measurably affected as a result of the repair.

All forgings to be used for outer case fabrication were inspected before machining by X-ray, sonic and zygo techniques, to ensure that the material was free from detrimental flaws. In addition, all Inconel 718 used had spot metallographic examination performed to ensure the NiC_3 strengthening constituent had not precipitated during forging to the undesirable eta phase, eliminating it as the strengthening gamma prime phase.

Upon receipt of the hydroformed hemispheres to be used for the major sphere, it was determined that explosive forming would be required to bring the sphere within the required dimensions. A die was fabricated and the shells formed. The hemispheres were trimmed, scarfed for welding, and hand welded using heliarc welding and Inconel 718 rod. Figure 486 shows the fixtured sphere before welding.

Upon completion of the major sphere, the five semifinished forgings were individually welded to the sphere. Figure 487 shows the sphere fixture with two of the component segments welded and the other component segments before welding.

Table LXVII. Machine Welded Specimens

No.	Mismatch	Bead Height/ Penetration	Zygo	X-ray	Ultimate Tensile Strength	0.2% Offset Yield Strength	Elongation (%)	Comments
1a	0.027	0.020/0	OK	OK	191,800	162,000	7.5	
1b	0.027	0.015/0	OK	Small Void	221,000	167,900	8.0	
1c	0.027	0.015/0	OK	Imperfection at Edge of Weld of Void	231,000	166,200	12.0	
2a	0.019	0.030/0	OK	OK	180,900	164,200	5.0	
2b	0.019	0.025/0	OK	OK	192,800	169,300	6.5	
2c	0.019	0.070/0.049	Crack	OK	177,500	165,400	5.5	Weld Bead Was Not Machined Down
3a	0.016	0.015/0	OK	OK	213,000	168,000	10.0	
3b	0.016	0.015/0	OK	OK	234,000	169,500	12.0	
3c	0.016	0.010/0	OK	Small High Density Incl.	188,800	163,200	7.5	
4a	0.022	0.030/0	OK	OK	184,400	157,600	7.0	
4b	0.022	0.030/0	OK	OK	190,600	164,500	8.0	
4c	0.022	0.020/0	OK	Small Void	194,400	166,400	8.5	

Table LXVIII. Hand Welded Specimens

No.	"B" Butt "A" Angle T-Welds	Mismatch			Zyglo	X-ray	Fabrication Research	Ultimate Tensile Strength	0.2% Offset Yield Strength		Elongation (%)	Comments
		1	2	3								
1	B	0.026	0.050	0.010	Lack of filler at inter- section	Lack of filler noted	Lack of filler	169,000	154,600		2.0	Lack of filler caused reduc- tion in surface area
2	A	0.0035	0.0195	0.08	OK	OK		179,100	148,400		4.0	Small area in percent mate- rial where welds meet
3	A	0.044	0.017	0.025	OK	OK	4 welds in seam	197,200	163,100		5.0	
4	A	0.040	0.006	0.049	OK	OK		195,700	163,900		4.5	
5	A	0.037	0.060	0.030	Crack along short weld	Crack noted		185,100	147,100		4.5	
6	A	0.029	0.070	0.039	OK	OK	Undercut Weld - 3 welds in seam	190,200	135,200		8.0	
7	A	0.047	0.0025	0.035	Crack along short weld	Crack noted		189,200	160,000		4.5	
8	B	0.033	0.011	0.040	OK	OK	Undercut Weld	178,800	156,700		4.5	Undercut Weld



Figure 486. Sphere Welding Fixture

FE 89598

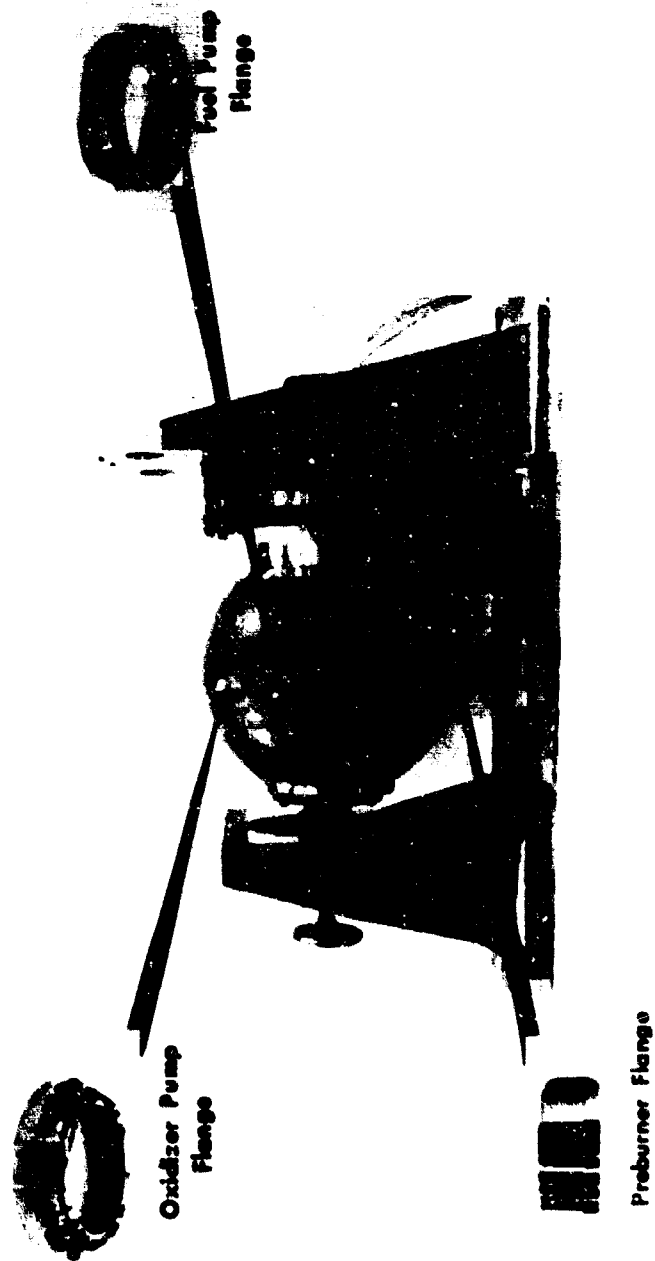


Figure 487. Sphere Showing Two Segments Welded in Position

GS 13236

After completion of welding the oxidizer pump, fuel pump, gimbal socket, preburner, and main chamber segments, the weld bead areas were X-ray inspected. Evaluation of X-rays revealed several spots of porosity in the welds ranging up to 0.040 in. diameter. Repair was initiated by drilling into the porous spots and rewelding. This process was continued until all welds were acceptable. During the weld process, each weld rod was cleaned before use by vapor degreasing in trichloroethylene. However, it was theorized because of the number of porosity spots, that oxidation still may have existed on the weld rod after cleaning. Before welding the second transition case, all weld rods were cleaned by immersing in a 70% nitric acid, 10% hydrofluoric, and 20% water solution. Welds of the second transition case showed improvement in lack of porosity when compared to the initial weldments.

Following welding, the unfinished flanged segments were finished machined, except for approximately 0.100 in. excess material on the flange face to allow a stress relief margin. This operation was later accomplished on a tracing vertical turret lathe. The case was then solution heat treated in a hydrogen atmosphere at 2360°R for one hour followed by aging at 1860°R for 8 hr and an additional 8 hr at 1560°R. The finished flange dimensions were cut and bolt holes were completed in the flanges. Figure 488 shows the case during bolt hole drilling and figure 489 shows the case in the mockup stage with the preburner injector and fuel pump housing installed. Following fabrication, the case was successfully proof pressure/thrust tested under conditions exceeding normal test levels. Figure 490 shows the case during testing, with stress coat to indicate areas of high stress.

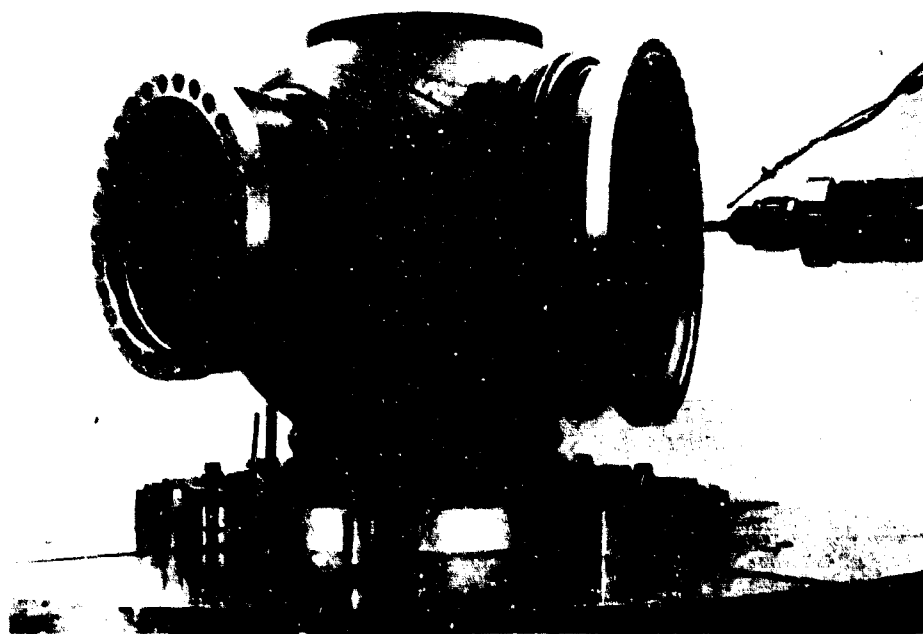


Figure 488. Transition Case Bolt Hole Drilling
Fixture

FE 95740



Figure 489. Transition Mockup Assembly Showing Preburner Injector and Fuel Pump Installation FE 96289

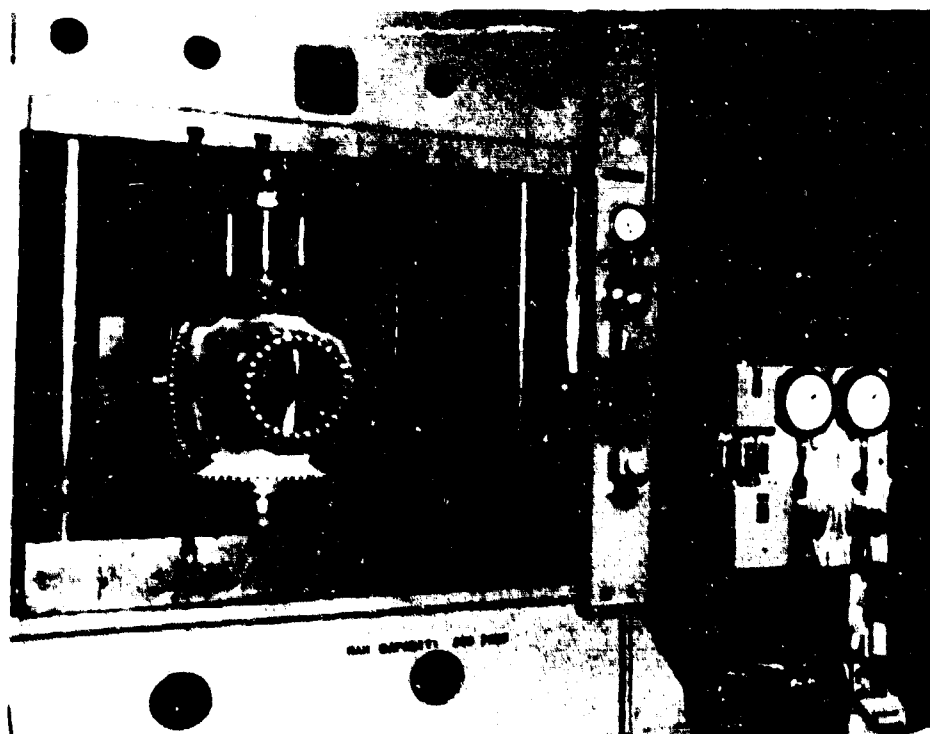


Figure 490. Hydrostatic Proof Test of the Transition Case FE 96989

The pressure test included a complete stress coating of the assembly so that the highest stress areas could be pinpointed. The stress coating was then washed from the assembly and strain gages were applied to the areas of highest stress. Strain gages applied for the test included 42 two-gage rosettes at various outer locations that were matched by 42 two-gage rosettes on the shell inside diameter. Additionally, 4 two-gage rosettes external and 1 three-gage rosette internal were also included. Figures 491 through 498 show the locations of the strain gages.

The transition case was then placed in a 350 ton hydraulic press as shown in figure 499. Pressure/thrust tests were conducted to 120% of the design level for both normal engine operating conditions and normal pressure/low thrust conditions that duplicated the preburner tests described in Section VIII. To simulate the preburner conditions, the case was loaded in 15% increments to a maximum level of 3600 psig and 48,000 lb. During the first cycle, strain data was recorded at each increment. For the second cycle, the case was loaded in 30% increments up to the same maximum level recording highest strains only at each increment.

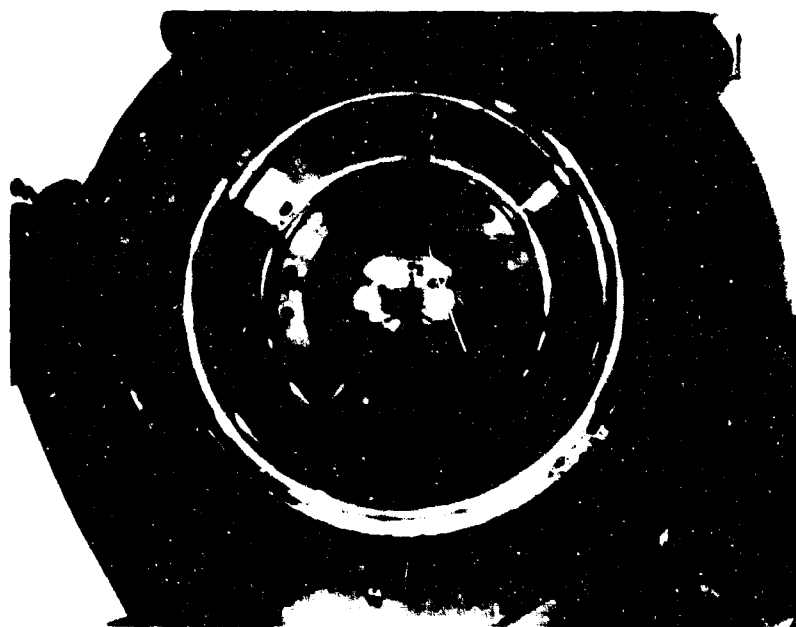


Figure 491. Advanced Propulsion XLR129
Preburner Outer Case Showing
Locations of Strain Gage Rosettes
No. 1 through No. 10. Strain
Gage Rosette No. 47 Located In-
side Case. (2147902 S/N 1)

FMDL 14837-3

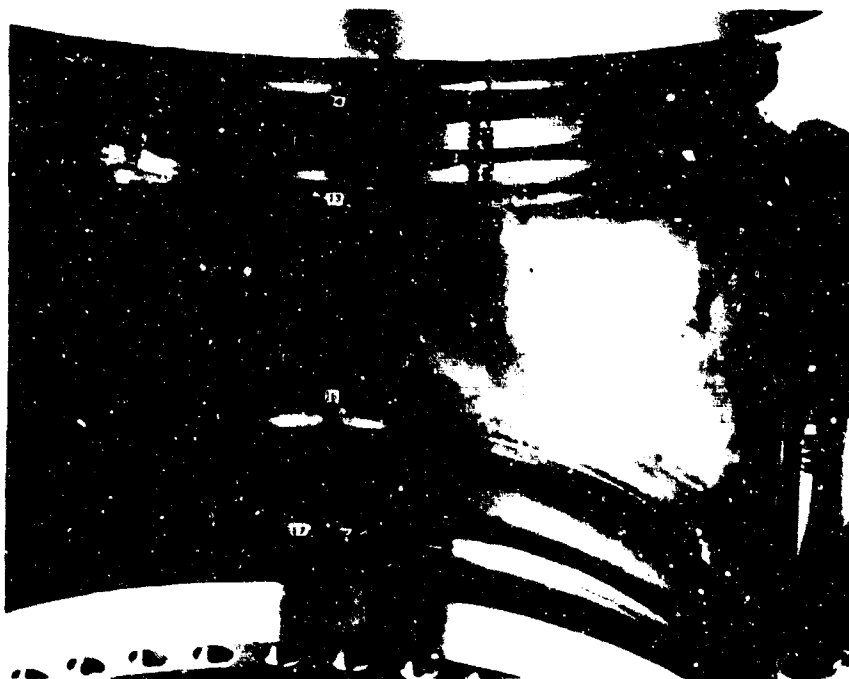


Figure 492. Advanced Propulsion XLR129
Preburner Outer Case Showing
Locations of Strain Gage
Rosettes No. 12 Through 18,
36, and 44 (2147902 S/N 1)

Figure 493. Advanced Propulsion XLR129
Preburner Outer Case Showing
Locations of Strain Gage
Rosettes No. 11, 29 Through
33, 40, 41, and 43
(2147902 S/N 1)



Figure 494. Advanced Propulsion XLR129
Preburner Outer Case Showing
Locations of Strain Gage Rosettes
No. 20 through 24, 37, 38, 39, and
42. (2147902 S/N 1)

FMDL 14837-6

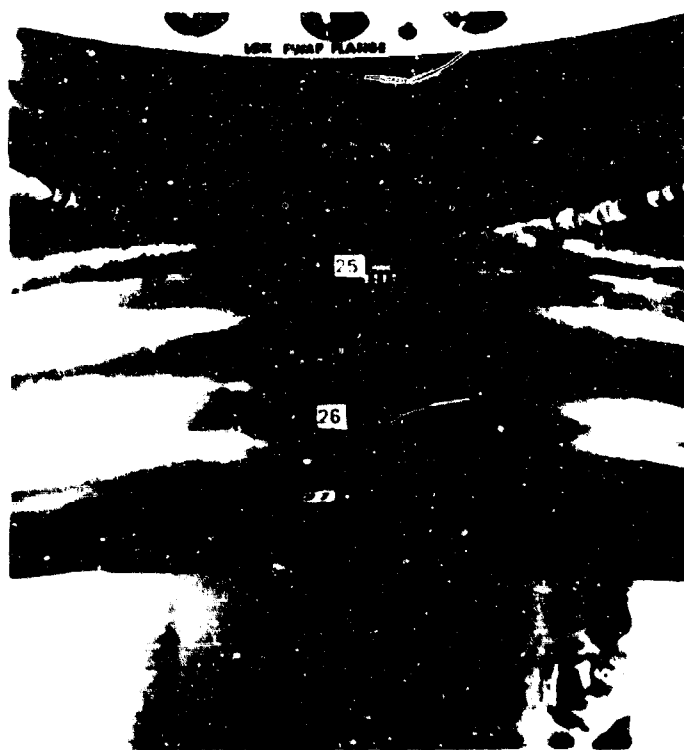


Figure 495. Advanced Propulsion XLR129
Preburner Outer Case Showing
Locations of Strain Gage Rosettes
No. 19, 25, 26, and 27
(2147902 S N 1)

FMDL 14837-7

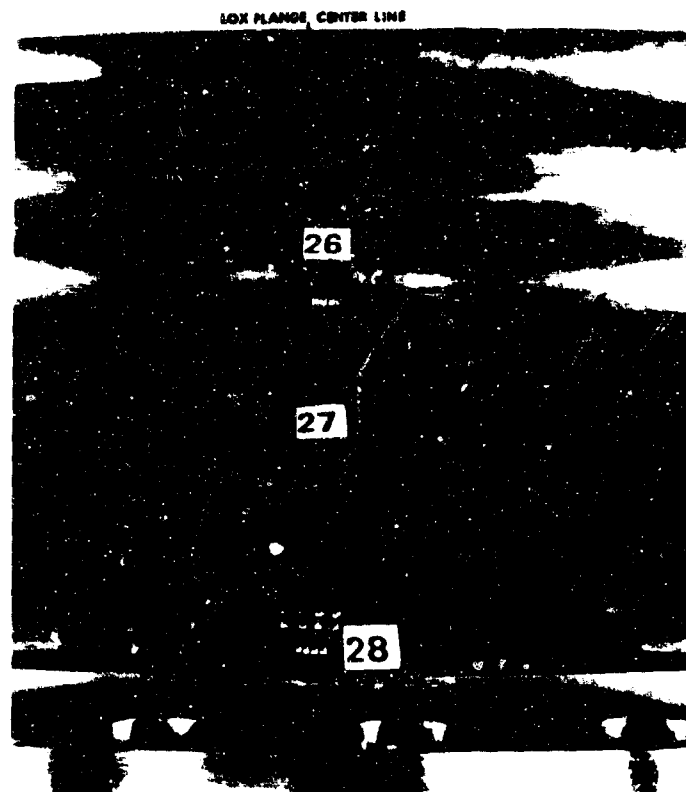


Figure 496. Advanced Propulsion XLR129 FMDL 14837-8
Preburner Outer Case Showing
Locations of Strain Gage Rosettes
No. 26, 27, and 28. (2147902 S/N 1)



Figure 497. Advanced Propulsion XLR129 FMDL 14837-9
Preburner Outer Case Showing
Locations of Strain Gage Rosettes
No. 34, 35, and 36 (2147902 S N 1)



Figure 498. Advanced Propulsion XLR129
Preburner Outer Case Showing
Locations of Strain Gage Rosettes
No. 45 and 46. (2147902 S/N 1)

FMDL 14837-10

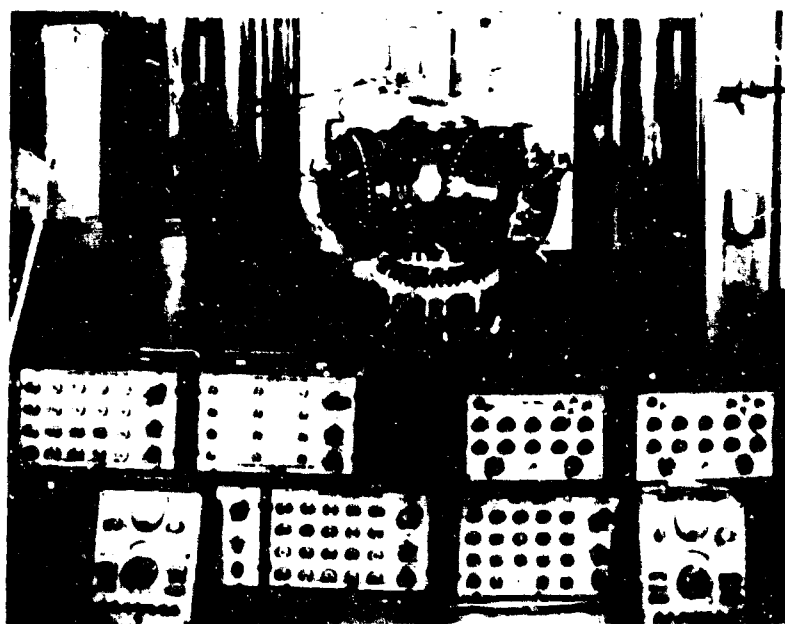


Figure 499. Transition Case Showing Setup for
Experimental Stress Analysis and
Internal Pressure - Thrust Proof
Test

FMDL 14837-1

A maximum tensile biaxial strain of 19,550 $\mu\text{in./in.}$ (approximately 2%) with 0.7% offset occurred at strain gage location 18 under combined 3600 psig internal pressure and 48,000 lb thrust load. This is equivalent to a uniaxial strain of 11,900 $\mu\text{in./in.}$ Biaxial yield strain was approximately 7700 $\mu\text{in.}$ (biaxial stress of 273,400 psi) which is equivalent to uniaxial yield strain of 4500 $\mu\text{in.}$ (uniaxial stress of 135,000 psi). Strain and stress data are listed in table LXIX. Biaxial and equivalent uniaxial strain data for strain gage number 18 are plotted in figure 500. Biaxial strain data for strain gage number 20A are plotted in figure 501.

To simulate the engine conditions, the case was loaded in 15% increments to a maximum level of 3150 psig and 262,500 lb (105%) recording strain data at each increment. For the second cycle, the case was loaded in 30% increments to a maximum level of 3600 psig and 300,000 lb. Only the highest strains were recorded at each increment except at the 120% level where all strain data were recorded.

A maximum tensile biaxial strain of 15,250 $\mu\text{in./in.}$ with 0.34% offset occurred at strain gage location 16 under combined 3150 psig internal pressure and 262,500 lb thrust load. This is equivalent to a uniaxial strain of 9190 $\mu\text{in./in.}$ Biaxial yield strain was approximately 8200 $\mu\text{in.}$ (biaxial stress of 288,700 psi) which is equivalent to uniaxial yield strain of 5000 $\mu\text{in.}$ (uniaxial stress of 141,500 psi). Strain and stress data are listed in table LXX. Biaxial and equivalent uniaxial strain data for strain gage number 16 are plotted in figure 502. Biaxial strain data for strain gage number 20A are plotted in figure 501.

The high tensile biaxial strains of 15,250 and 19,550 $\mu\text{in./in.}$ at strain gage locations 16 and 18 were caused by combined P/A and bending at the intersecting weld between the case shell and the oxidizer sphere. The bending resulted from a mismatch between the oxidizer ring and the main sphere. This mismatch occurred because the rings were machined symmetrical while the main sphere was 0.040 in. out of round and had a thickness variation resulting from the forming operation. A high stress point was also seen at a local weld area of the igniter boss, adjacent to the preburner sphere flange.

A post-test zygo inspection showed the case to be free of surface deviations.

Following the proof pressure test, the preburner sphere area of the assembly was gold coated to reduce radiation effects from the preburner duct. Instrumentation to monitor conditions in the cavity between the outer case and porous cooling liner were applied to the case as shown in figure 503.

b. Cooling Liner

The porous cooling liner that routes the coolant to the outer case was installed in the outer case in sections. Liners were fabricated and formed to the outer case contour by outside vendors. Because the porosity of the liner was proved to be locally unpredictable (porosity varied from 73 scfm to 167 scfm) after forming, the flow was tailored by flame spraying nickel over local areas to reduce porosity. This process allowed the liner porosity to be controlled to within $\pm 10\%$ of the desired value.

Table LXIX. Strain and Elastic Stress Data XLR129 Transition Case Under Combined Internal Pressure and Thrust Loads (Preburner Ratio)

Point No.	Strain (in. in.) for Combined Pressure Thrust Loads (psig. lb) of:	Elastic Stress (psi) for Combined Pressure Thrust Loads (psig. lb) of:																Membrane Stress at Max Load	Bending Stress at Max Load
		150	300	450	600	750	900	1050	1200	1350	1500	1650	1800	1950	2100	2250	2400		
1	1	150	300	450	600	750	900	1050	1200	1350	1500	1650	1800	1950	2100	2250	2400	3600	4800
1A	1	150	300	450	600	750	900	1050	1200	1350	1500	1650	1800	1950	2100	2250	2400	3600	4800
2	1	150	300	450	600	750	900	1050	1200	1350	1500	1650	1800	1950	2100	2250	2400	3600	4800
2A	1	150	300	450	600	750	900	1050	1200	1350	1500	1650	1800	1950	2100	2250	2400	3600	4800
3	1	150	300	450	600	750	900	1050	1200	1350	1500	1650	1800	1950	2100	2250	2400	3600	4800
3A	1	150	300	450	600	750	900	1050	1200	1350	1500	1650	1800	1950	2100	2250	2400	3600	4800
4	1	150	300	450	600	750	900	1050	1200	1350	1500	1650	1800	1950	2100	2250	2400	3600	4800
4A	1	150	300	450	600	750	900	1050	1200	1350	1500	1650	1800	1950	2100	2250	2400	3600	4800
5	1	150	300	450	600	750	900	1050	1200	1350	1500	1650	1800	1950	2100	2250	2400	3600	4800
5A	1	150	300	450	600	750	900	1050	1200	1350	1500	1650	1800	1950	2100	2250	2400	3600	4800
6	1	150	300	450	600	750	900	1050	1200	1350	1500	1650	1800	1950	2100	2250	2400	3600	4800
6A	1	150	300	450	600	750	900	1050	1200	1350	1500	1650	1800	1950	2100	2250	2400	3600	4800
7	1	150	300	450	600	750	900	1050	1200	1350	1500	1650	1800	1950	2100	2250	2400	3600	4800
7A	1	150	300	450	600	750	900	1050	1200	1350	1500	1650	1800	1950	2100	2250	2400	3600	4800
8	1	150	300	450	600	750	900	1050	1200	1350	1500	1650	1800	1950	2100	2250	2400	3600	4800
8A	1	150	300	450	600	750	900	1050	1200	1350	1500	1650	1800	1950	2100	2250	2400	3600	4800
9	1	150	300	450	600	750	900	1050	1200	1350	1500	1650	1800	1950	2100	2250	2400	3600	4800
9A	1	150	300	450	600	750	900	1050	1200	1350	1500	1650	1800	1950	2100	2250	2400	3600	4800
10	1	150	300	450	600	750	900	1050	1200	1350	1500	1650	1800	1950	2100	2250	2400	3600	4800
10A	1	150	300	450	600	750	900	1050	1200	1350	1500	1650	1800	1950	2100	2250	2400	3600	4800
11	1	150	300	450	600	750	900	1050	1200	1350	1500	1650	1800	1950	2100	2250	2400	3600	4800
11A	1	150	300	450	600	750	900	1050	1200	1350	1500	1650	1800	1950	2100	2250	2400	3600	4800

Table LXIX. Strain and Elastic Stress Data XLR129 Transition Case Under Combined Internal Pressure and Thrust Loads (Preburner Ratio) (Continued)

Rosette No.	Strain (μ in./in.) for Combined Pressure Thrust Loads (psig/lb) of:										Elastic Stress (psi) for Combined Pressure Thrust Loads (psig/lb) of:										Membrane Stress at Max Load											
	450	900	1350	1800	2250	2700	3150	3600	4050	4500	Zero	450	900	1350	1800	2250	2700	3150	3600	4050	4500	Zero	450	900	1350	1800	2250	2700	3150	3600	4050	4500
12 ϵ_1	370	720	1090	1430	1770	2100	2390	2640		16000	31200	47100	61900	76800	91300	104700	117100					16000	31200	47100	61900	76800	91300	104700	117100			
12 ϵ_2	440	860	1290	1710	2130	2550	2980	3450		17600	34300	51500	68200	84800	101300	117800	135200					17600	34300	51500	68200	84800	101300	117800	135200			
12A ϵ_1	*									*																						
12A ϵ_2	490	950	1410	1850	2320	2770	3240	3760		19400	39400	59400	79000	98200	117900	138900	159600	101500				19400	39400	59400	79000	98200	117900	138900	159600	101500	58100	
13 ϵ_1	480	980	1480	2090	2560	2990	3460	3970		18300	36500	54900	73600	92400	110500	128700	148200	131900				18300	36500	54900	73600	92400	110500	128700	148200	131900	16200	
13 ϵ_2	430	850	1280	1710	2150	2570	3000	3460		5300	9900	14600	18800	23700	29100	35400	43400	101500				5300	9900	14600	18800	23700	29100	35400	43400	101500	-58100	
13A ϵ_1	30	40	60	80	120	190	300	350		14600	29100	43000	57000	71200	85300	99700	115700	131900				14600	29100	43000	57000	71200	85300	99700	115700	131900	-16200	
13A ϵ_2	450	900	1330	1770	2210	2640	3070	3540		14600	28500	43100	57600	72700	86300	99700	113100	81300				14600	28500	43100	57600	72700	86300	99700	113100	31700	81300	
14 ϵ_1	340	740	1120	1500	1890	2240	2580	2900		11900	23300	35600	47200	59500	71100	83000	96600	29500				11900	23300	35600	47200	59500	71100	83000	96600	67100	29500	
14 ϵ_2	260	510	780	1030	1300	1560	1830	2160		-6400	-13100	-18600	-25300	-31900	-37200	-44700	-49600	-81300				-6400	-13100	-18600	-25300	-31900	-37200	-44700	-49600	-81300	-29500	
14A ϵ_1	-270	-540	-780	-1050	-1320	-1550	-1860	-2100		4700	8500	13300	17000	21200	26000	30700	37600	67100				4700	8500	13300	17000	21200	26000	30700	37600	67100	-81300	
14A ϵ_2	230	430	650	850	1060	1280	1520	1810		23200	45000	67900	90400	114000	137500	159300	180300	114000				23200	45000	67900	90400	114000	137500	159300	180300	66200	114000	
15 ϵ_1	650	1260	1900	2530	3190	3850	4450	5020		14500	28300	42700	56700	71600	86200	100900	115900	78300				14500	28300	42700	56700	71600	86200	100900	115900	78300	37500	
15 ϵ_2	260	510	770	1020	1290	1550	1830	2130		-5700	-11500	-16300	-22600	-27900	-33900	-41400	-47800	66200				-5700	-11500	-16300	-22600	-27900	-33900	-41400	-47800	66200	-114000	
15A ϵ_1	-250	-500	-720	-990	-1210	-1470	-1780	-2070		5300	9900	15100	19300	24100	25000	34600	40800	78300				5300	9900	15100	19300	24100	25000	34600	40800	78300	-37500	
15A ϵ_2	240	460	690	900	1120	1350	1600	1900		*												*										
16 ϵ_1	850	1640	2430	3190	3920	4670	5820	7540	1340																							
16 ϵ_2	*																															
16A ϵ_1	-500	-950	-1370	-1820	-2270	-2730	-3320	-4040		-11200	-21000	-29800	-39800	-49600	-59500	-73800	-91500					-11200	-21000	-29800	-39800	-49600	-59500	-73800	-91500			
16A ϵ_2	490	970	1450	1900	2380	2880	3350	3900		10800	21800	33100	43100	54100	65700	75000	85700					10800	21800	33100	43100	54100	65700	75000	85700			
17 ϵ_1	1190	2280	3350	4350	5450	6600	8060	9620	1140	42000	80700	118700	154300	193300	233900	284700	341000	158200				42000	80700	118700	154300	193300	233900	284700	341000	158200	182700	
17 ϵ_2	430	840	1250	1640	2050	2470	2910	3600	160	25100	48600	71900	93900	117400	141800	169800	206700	146000				25100	48600	71900	93900	117400	141800	169800	206700	146000	60600	
17A ϵ_1	700	1330	1950	2540	3180	3850	4710	5610		20200	38600	56700	73600	92200	111700	136700					20200	38600	56700	73600	92200	111700	136700					
17A ϵ_2	-380	-710	-1000	-1370	-1620	-1770	-1970	-2170	540	-8300	-15000	-20600	-29000	-33200	-34000	-33500	-24500	158200				-8300	-15000	-20600	-29000	-33200	-34000	-33500	-24500	158200	-182700	
17A ϵ_2	490	800	1150	1530	1930	2340	2730	3200	130	9100	18700	28000	35700	46000	57600	69100	85400	146000				9100	18700	28000	35700	46000	57600	69100	85400	146000	-60600	
17A ϵ_2	1460	2890	4410	6010	7870	10330	13800	19550	7120	51000	101000	154000	209500	273400				116050				51000	101000	154000	209500	273400				116050	157350	
17A ϵ_2	470	930	1410	1980	2360	2830	3300	4180	190	28900	57300	87100	117400	150400				103950				28900	57300	87100	117400	150400				103950	46450	
17A ϵ_2	560	1700	2600	3550	4660	6160	8320	11500		25000	49400	75400	102900	135200								25000	49400	75400	102900	135200						
17A ϵ_2	10150								7480																							
17A ϵ_2	1260								200																							
17A ϵ_2	-340	-780	-1170	-1600	-2020	-2500	-3050	-3820	-700	-7300	-15400	-23300	-32700	-41300	-52100	-65000	-84100	116050				-7300	-15400	-23300	-32700	-41300	-52100	-65000	-84100	116050	-157350	
17A ϵ_2	500	990	1460	1910	2410	2880	3370	3940	70	12300	24100	35300	45600	57500	67900	78200	89000	103950				12300	24100	35300	45600	57500	67900	78200	89000	103950	-46450	
17A ϵ_2	-510	-1020	-1520	-2020	-2540	-3100	-3700	-4450																								
19 ϵ_1	430	950	1490	2040	2560	3140	3620	4240		18800	40100	62800	85300	106800	130600	150800	177300	88600				18800	40100	62800	85300	106800	130600	150800	177300	88600	88600	
19 ϵ_2	530	1030	1600	2120	2640	3190	3710	4410		21000	41900	65200	87100	108600	131700	152900	181100	162600				21000	41900	65200	87100	108600	131700	152900	181100	162600	18500	
19A ϵ_1	-40	-250	-420	-660	-860	-1070	-1260	-1490		3200	3000	3300	700	100	-600	-700	0	88600				3200	3000	3300	700	100	-600	-700	0	88600	-88600	
19A ϵ_2	600	1150	1740	2270	2880	3500	4130	4970		18400	34300	51400	66000	83600	101300	119600	144100	162600				18400	34300	51400	66000	83600	101300	119600	144100	162600	-18500	
20 ϵ_1	-370	-870	-1220	-1540	-1860	-2160	-2430	-2690		-16600	-30600	-43000	-54400	-65900	-76600	-860																

Table LXIX. Strain and Elastic Stress Data XLR129 Transition Case Under Combined Internal Pressure and Thrust Loads (Preburner Ratio) (Continued)

Load No.	Strain (in. in.) for Combined Pressure Thrust Loads (psig. lb) of:										Elastic Stress (psi) for Combined Pressure Thrust Loads (psig. lb) of:										Membrane - Bending Stress at Max Load	
	450	900	1350	1800	2250	2700	3150	3600	4050	4500	4950	5400	5850	6300	6750	7200	7650	8100	8550	9000	3600	48000
22	170	350	530	710	890	1070	1250	1430	1610	1790	1970	2150	2330	2510	2690	2870	3050	3230	3410	3590	3600	48000
22A	170	350	530	710	890	1070	1250	1430	1610	1790	1970	2150	2330	2510	2690	2870	3050	3230	3410	3590	3600	48000
23	170	350	530	710	890	1070	1250	1430	1610	1790	1970	2150	2330	2510	2690	2870	3050	3230	3410	3590	3600	48000
23A	170	350	530	710	890	1070	1250	1430	1610	1790	1970	2150	2330	2510	2690	2870	3050	3230	3410	3590	3600	48000
24	170	350	530	710	890	1070	1250	1430	1610	1790	1970	2150	2330	2510	2690	2870	3050	3230	3410	3590	3600	48000
24A	170	350	530	710	890	1070	1250	1430	1610	1790	1970	2150	2330	2510	2690	2870	3050	3230	3410	3590	3600	48000
25	170	350	530	710	890	1070	1250	1430	1610	1790	1970	2150	2330	2510	2690	2870	3050	3230	3410	3590	3600	48000
25A	170	350	530	710	890	1070	1250	1430	1610	1790	1970	2150	2330	2510	2690	2870	3050	3230	3410	3590	3600	48000
26	170	350	530	710	890	1070	1250	1430	1610	1790	1970	2150	2330	2510	2690	2870	3050	3230	3410	3590	3600	48000
26A	170	350	530	710	890	1070	1250	1430	1610	1790	1970	2150	2330	2510	2690	2870	3050	3230	3410	3590	3600	48000
27	170	350	530	710	890	1070	1250	1430	1610	1790	1970	2150	2330	2510	2690	2870	3050	3230	3410	3590	3600	48000
27A	170	350	530	710	890	1070	1250	1430	1610	1790	1970	2150	2330	2510	2690	2870	3050	3230	3410	3590	3600	48000
28	170	350	530	710	890	1070	1250	1430	1610	1790	1970	2150	2330	2510	2690	2870	3050	3230	3410	3590	3600	48000
28A	170	350	530	710	890	1070	1250	1430	1610	1790	1970	2150	2330	2510	2690	2870	3050	3230	3410	3590	3600	48000
29	170	350	530	710	890	1070	1250	1430	1610	1790	1970	2150	2330	2510	2690	2870	3050	3230	3410	3590	3600	48000
29A	170	350	530	710	890	1070	1250	1430	1610	1790	1970	2150	2330	2510	2690	2870	3050	3230	3410	3590	3600	48000
30	170	350	530	710	890	1070	1250	1430	1610	1790	1970	2150	2330	2510	2690	2870	3050	3230	3410	3590	3600	48000
30A	170	350	530	710	890	1070	1250	1430	1610	1790	1970	2150	2330	2510	2690	2870	3050	3230	3410	3590	3600	48000
31	170	350	530	710	890	1070	1250	1430	1610	1790	1970	2150	2330	2510	2690	2870	3050	3230	3410	3590	3600	48000
31A	170	350	530	710	890	1070	1250	1430	1610	1790	1970	2150	2330	2510	2690	2870	3050	3230	3410	3590	3600	48000
32	170	350	530	710	890	1070	1250	1430	1610	1790	1970	2150	2330	2510	2690	2870	3050	3230	3410	3590	3600	48000
32A	170	350	530	710	890	1070	1250	1430	1610	1790	1970	2150	2330	2510	2690	2870	3050	3230	3410	3590	3600	48000

Table LXIX. Strain and Elastic Stress Data XLR129 Transition Case Under Combined Internal Pressure and Thrust Loads (Preburner Ratio) (Continued)

Rosette No.	Strain (μin./in.) for Combined Pressure/Thrust Loads (psig/lb) of:										Elastic Stress (psi) for Combined Pressure/Thrust Loads (psig/lb) of:										Membrane + Bending Stress at Max Load	
	450/6000	900/12000	1350/18000	1800/24000	2250/30000	2700/36000	3150/42000	3600/48000	Zero	450/6000	900/12000	1350/18000	1800/24000	2250/30000	2700/36000	3150/42000	3600/48000					
33 ϵ_1	-70	-140	-190	-230	-260	-290	-320	-350	-380	-2700	-5600	-7700	-9600	-11100	-11500	-10500	-8000	63500	-71500			
33 ϵ_2	-50	-120	-170	-240	-290	-340	-370	-400	-430	-2300	-5200	-7200	-9200	-11200	-13300	-13900	-14000	7700	-21700			
33A ϵ_1	600	1190	1780	2350	2910	3450	3920	4350	-170	18900	37200	55400	72800	90100	106900	121600	135000	63500	71500			
33A ϵ_2	-20	-80	-140	-220	-280	-320	-350	-380	-30	5100	8800	12600	15500	18900	22800	26300	29500	7700	21700			
34 ϵ_1	320	640	1000	1340	1700	2050	2400	2820		15200	30100	46700	62600	79000	95500	111900	131400	106000	25400			
34 ϵ_2	520	1020	1550	2080	2600	3160	3700	4340		19600	38600	59000	79100	99100	120300	140900	165300	160800	4400			
34A ϵ_1	160	300	450	560	700	860	1030	1160		10500	20100	30000	38800	48600	59000	70100	80600	106000	-25400			
34A ϵ_2	560	1100	1640	2190	2750	3300	3900	4560		19400	37900	56600	75100	94300	113400	134100	156400	160800	-4400			
35(2) ϵ_1	*	*	*	*	*	*	*	*		*	*	*	*	*	*	*	*	*				
35(2) ϵ_2	430	880	1320	1780	2230	2700	3160	3670		9300	16900	24500	30900	38400	45900	53600	61200					
35A ϵ_1	140	230	320	380	460	540	630	700		17600	34100	50900	66400	83400	100800	117900	136400					
35A ϵ_2	510	1000	1500	1970	2480	3000	3510	4070		5600	13200	21500	30400	38800	48000	56200	66100	64300	1700			
36 ϵ_1	40	140	260	400	520	660	770	920		14700	30300	46500	62800	78900	96200	112800	131500	130900	500			
36 ϵ_2	450	910	1380	1850	2320	2820	3310	3850		10000	18500	26500	32700	40400	48400	55900	62600	64300	-1700			
36A ϵ_1	170	300	410	470	570	670	760	810		16900	32800	48500	63400	79700	96600	112700	130400	130900	-500			
36A ϵ_2	480	940	1400	1850	2330	2830	3310	3850		21400	42700	63800	84900	106200	128700	151100	174600					
37 ϵ_1	550	1100	1640	2180	2730	3310	3890	4500		18300	36000	54200	72100	90200	109100	127700	146900					
37 ϵ_2	410	800	1210	1610	2010	2430	2840	3260		18300	36000	54200	72100	90200	109100	127700	146900					
37A ϵ_1	*	*	*	*	*	*	*	*		*	*	*	*	*	*	*	*	*				
37A ϵ_2	420	830	1230	1600	2000	2430	2840	3260		16000	30600	45600	58900	73700	88300	102500	116300	118100	-1800			
38 ϵ_1	430	810	1200	1540	1920	2290	2660	3010		11800	23700	36000	47500	60100	72900	84400	96700	93700	2900			
38 ϵ_2	240	500	770	1030	1310	1600	1850	2130		16300	30700	44700	57300	72000	87600	103900	120000	118100	1800			
38A ϵ_1	450	830	1200	1530	1920	2330	2770	3200		11000	22000	33100	43000	54400	66900	78400	90800	93700	2900			
38A ϵ_2	210	440	680	890	1130	1400	1630	1890		23700	45300	68500	90400	112200	135800	159500	187300	107800	79400			
39 ϵ_1	620	1210	1790	2360	2930	3550	4180	4930		19000	37400	55400	73200	90800	109500	127600	147800	126000	21800			
39 ϵ_2	410	810	1200	1590	1970	2370	2750	3160		4000	7100	10800	13500	17200	21300	25300	28400	107800	-79400			
39A ϵ_1	0	-20	-20	-50	-50	-50	-50	-100		13400	25600	38100	49900	62300	75700	89100	104200	126000	-21800			
39A ϵ_2	420	810	1200	1580	1970	2390	2810	3300		33200	66500	100000	134200	168600	208100	255200	322600	140600	182000			
40 ϵ_1	910	1820	2740	3680	4630	5730	7070	9030	1660	1660	33200	45800	68600	91600	114400	139900	167300	202300	60300			
40 ϵ_2	440	890	1330	1770	2200	2670	3130	3640	110	15200	30500	45900	61600	77600	96000	118600	152100	141900				
40A ϵ_1	520	1050	1580	2100	2670	3300	4100	5250		-3300	-8200	-12100	-16700	-20300	-24500	-31500	-41400	140600	-182000			
40A ϵ_2	-230	-500	-740	-1030	-1230	-1490	-1830	-2270	-400	11200	21000	31200	41100	51300	62200	71700	81600	141900	-60300			
41 ϵ_1	150	320	490	670	860	1050	1260	1570	50	9200	18900	28400	38500	49700	59300	70400	84800	63900	20800			
41 ϵ_2	460	910	1340	1790	2230	2700	3160	3640		16100	32100	47400	63400	79300	96100	112700	131000	115200	15800			
41A ϵ_1	110	190	240	310	370	440	460	460		3600	10200	15600	20200	27430	33300	38400	43100	63900	-20800			
41A ϵ_2	10	430	830	1080	1630	2020	2480	2980		1400	15500	28700	37400	55500	68600	83400	99400	115200	-15800			
42 ϵ_1	410	920	1430	1990	2510	3070	3590	4250		17800	38800	59800	82500	104000	126900	148600	175600	153000	22600			
42 ϵ_2	490	990	1490	2000	2510	3040	3580	4200		19500	40300	61200	82800	104000	126200	148600	174500	112700	61700			
42A ϵ_1	470	950	1410	1900	2370	2890	3400	3970		16300	32400	47600	63600	79100	96000	112700	130400	153600	-22600			
42A ϵ_2	140	220	280	320	270	410	460	410		9000	16100	22400	28400	34400	40700	47200	51000	112700	-61700			
43(2) ϵ_1	520	1000	1470	1930	2410	2680	3340	3820		20700	40100	59000	77800	96900	116100	134700	154100					
43(2) ϵ_2	430	860	1270	1700	2110	2540	2960	3380		18700	37000	54500	72600	90800	108500	126300	144200					

Table LXIX. Strain and Elastic Stress Data XLR129 Transition Case Under Combined Internal Pressure and Thrust Loads (Preburner Ratio) (Concluded)

Rosette No.	Strain (μ in. in.) for Combined Pressure/Thrust Loads (psig/lb) of:										Elastic Stress (psi) for Combined Pressure/Thrust Loads (psig/lb) of:										Membrane + Bending Stress at Max Load	
	450	900	1350	1800	2250	2700	3150	3600	4050	450	900	1350	1800	2250	2700	3150	3600					
+4(2)	590	1170	1740	2340	2920	3540	4140	4740		22800	45300	67300	90300	112800	136600	159700	182400					
45	420	840	1240	1650	2070	2490	2900	3280		19000	38000	56200	75000	93900	113200	132000	149800					
	-10	-20	-20	0	30	110	200	250	80	5600	10800	16100	22800	29900	39900	52800	68700					
46	620	1200	1780	2380	3030	3810	4860	6350	1880	19700	38100	56400	75800	96800	122500	156900	204900					
	420	810	1200	1590	2010	2500	3180	4150		12100	23400	34700	46000	58300	72600	92100	120400					
46(2)	1110	2270	4570	7160	*					39900	81200	168900	*									
	470	930	2430	*						25600	51300	121100										
47A	-20	-50	-80	-140	-170	-200	-240	-280		-500	-2100	-3400	-5800	-6700	-8300	-8600	-8800					
	-10	-50	-80	-140	-160	-200	-230	-270		-800	-2100	-3700	-5800	-7000	-8300	-9600	-11100					
48	-10	-50	-80	-140	-160	-200	-200	-200														

* Gages are inside back-to-back locations.

* Instrumentation failure.

(1) Strain data plotted in figure

(2) Location of flaws

(3) Second cycle data are tabulated for rosette 18 and plotted in figure

ϵ_1 Strain is perpendicular to welds or radii

ϵ_2 Strain is perpendicular to welds or radii

ϵ_3 is equivalent uniaxial strain.

Elastic stresses calculated using Young's Modulus $E = 29.0 \times 10^6$ psi.

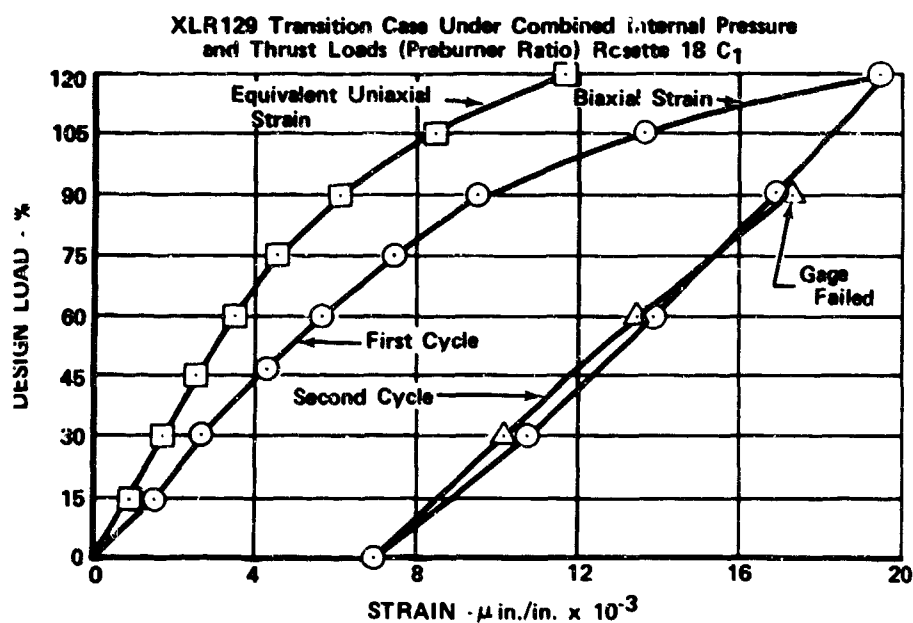


Figure 500. Strain Gage Data, Gage No. 18

FD 45724

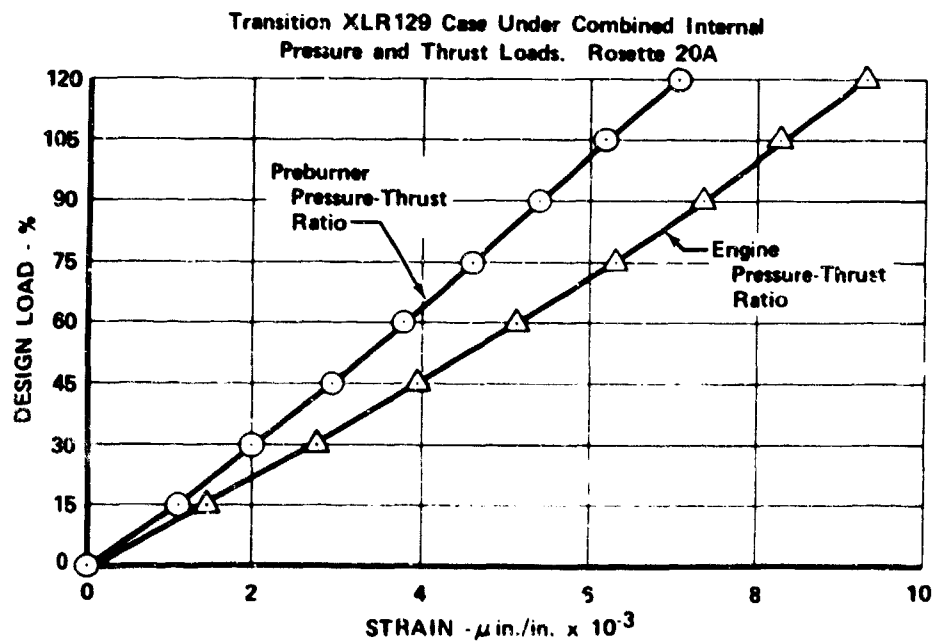


Figure 501. Biaxial Strain Data, Gage No. 20A

FD 45726

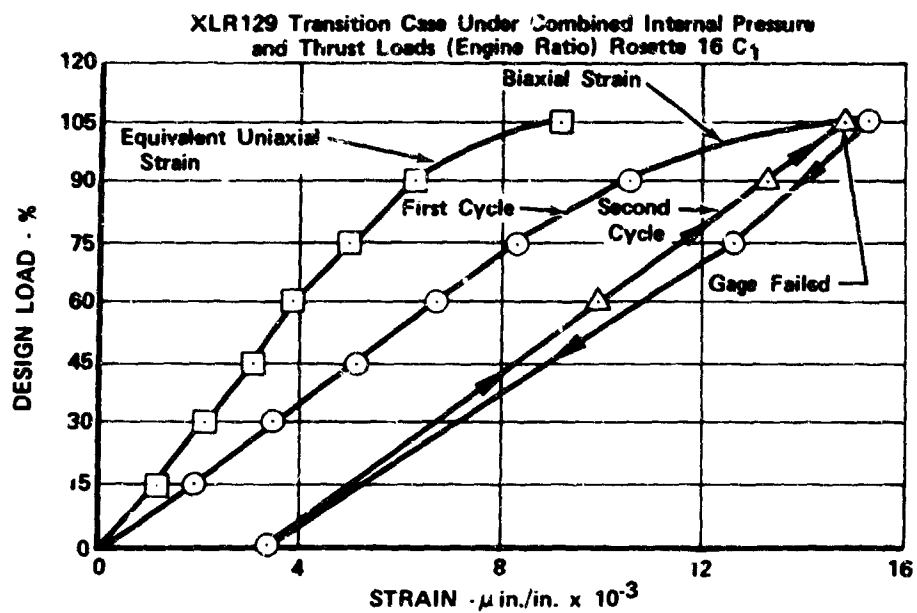


Figure 502. Strain Gage Data, Gage No. 16

FD 45725



Figure 503. Outer Case and Porous Cooling Liner
Instrumentation

FE 97307

Table LXX. Strain and Elastic Stress Data XLR129 Transition Case Under Combined Internal Pressure and Thrust Loads (Engine Ratio)

Rosette No.		Strain (in. in.) for Combined Pressure Thrust Loads (psig/lb) of:										Elastic Stress (psi) for Combined Pressure/Thrust Loads (psig/lb) of:										Membrane + Bending Stress at Max Load	
		450	900	1350	1800	2250	2700	3150	3600	300000(5)	450	900	1350	1800	2250	2700	3150	3600	300000(5)				
1	1	-170	-450	-730	-1000	-1290	-1590	-1900	-2280	-2280	-5900	-14700	-23500	-31900	-41100	-50600	-60200	-71400	12360	-83700			
2	2	-50	-40	-20	0	0	10	40	60	60	-3200	-5800	-7600	-9600	-12300	-14900	-16900	-19700	11700	-51400			
3	3	350	700	1020	1300	1710	2090	2500	2870	2870	11430	23100	33700	43000	56800	69200	83300	96100	12390	83700			
4	4	260	510	750	1000	1230	1460	1700	1930	1930	7900	15600	22900	30700	37800	44900	52400	59500	66000	31400			
5	5	-40	-70	-100	-120	-150	-170	-190	-210	-210	1300	2600	4000	5700	7000	8500	10200	11900	-2300	49900			
6	6	-120	-270	-430	-610	-720	-880	-1020	-1220	-1220	-4000	-8800	-14200	-20400	-27400	-33800	-40300	-47000	14100	-49900			
7	7	-20	-20	-50	-100	-110	-140	-140	-150	-150	-1800	-3200	-5700	-9000	-10400	-12900	-14200	-16400	-2300	-14100			
8	8	200	500	740	1000	1250	1510	1700	2100	2100	6600	15600	22500	30400	37900	45800	51300	63500	66000	40700			
9	9	-40	-40	-110	-150	-200	-240	-300	-360	-360	2500	3500	3600	4800	5600	6800	6700	8600	22700	6300			
10	10	0	0	-160	-240	-270	-340	-410	-580	-580	1000	2000	4400	-7200	-8000	-10400	-12500	-19000	22700	-40700			
11	11	160	400	600	830	1030	1250	1470	1650	1650	6000	13400	19600	26900	33300	40100	47100	53100	18000	-5300			
12	12	-20	-100	-190	-270	-320	-400	-460	-470	-470	4400	6100	7300	9500	11400	12900	15000	17400	2900	35100			
13	13	50	200	380	520	630	770	940	1100	1100	1700	3000	3000	3000	3000	3000	3000	3000	14400	-35100			
14	14	-20	-50	-110	-160	-200	-250	-300	-350	-350	-200	300	100	-100	-400	-600	-600	-600	10100	-10700			
15	15	80	150	200	250	320	380	440	520	520	3000	5700	5100	10200	13200	15600	18100	20800	25300	6300			
16	16	50	100	180	230	310	360	430	440	440	2500	4600	7600	9700	12900	15100	17900	19600	10100	-10700			
17	17	-90	-180	-270	-360	-450	-550	-630	-700	-700	-2900	-6100	-8700	-114200	-143200	-175700	-219500	-295600	25300	-6300			
18	18	-40	-10	-20	-50	-50	-60	-70	-80	-80	-170	-10700	-18600	-25700	-32800	-41500	-51000	-63800	25300	-6300			
19	19	-650	-1270	-1850	-2420	-3020	-3710	-4630	-6230	-6230	-18900	-36800	-53600	-70100	-87700	-107500	-134300	-19500	25300	-6300			
20	20	400	830	1220	1610	2060	2310	2500	3000	3000	-12900	-26700	-39300	-51800	-66100	-74000	-80100	-85700	87100	-182800			
21	21	-10	-30	-40	-50	-50	-40	-40	-10	-10	60	-4100	-8900	-12900	-17000	-21300	-25200	-29000	33800	-62800			
22	22	1800	2880	3850	4820	5810	6740	7590	8310	8310	53800	89700	121800	153800	186400	217000	245200	270000	182800	62800			
23	23	-370	-220	-90	20	130	230	350	540	540	5400	20500	33900	46700	59700	71800	83700	96700	33800	62800			
24	24	1340	2090	2600	3210	3830	4420	4950	5370	5370	38900	57900	75300	93000	111000	128100	143500	155700	162800	62800			
25	25	90	210	310	430	550	670	830	1050	1050	8100	17100	25100	33800	42800	51100	61100	73000	38500	34500			
26	26	550	1090	1590	2100	2640	3110	3620	4140	4140	18400	36700	53600	71000	89400	105500	123300	142000	9900	34500			
27	27	-150	-300	-430	-570	-710	-840	-950	-1130	-1130	400	600	1400	1800	2400	2900	4100	4000	35500	-34500			
28	28	540	1060	1580	2090	2620	3100	3600	4180	4180	15800	30900	46200	61200	76700	90800	105600	122400	132200	-9800			
29	29	700	1400	2060	2710	3370	3960	4680	5170	5170	880	25700	51800	76100	100150	124600	147000	174100	112500	103400			
30	30	350	750	1090	1440	1800	2140	2680	3380	3380	590	17800	37300	54400	71800	89600	107300	130000	149400	103400			
31	31	400	800	1190	1570	1950	2330	2700	3350	3350	11700	23500	34500	45400	55500	66400	78300	97000	149400	12700			
32	32	-190	-360	-520	-690	-820	-940	-1020	-1100	-1100	-1200	-1900	-2400	-3300	-4200	-5000	-5800	-6600	112500	-103400			
33	33	510	1000	1440	1960	2460	2990	3670	4620	4620	14400	28400	42200	55900	70500	86300	107200	136700	149400	-12700			
34	34	240	540	770	1000	1230	1460	1700	2100	2100	10100	19300	27900	36600	45400	54000	62700	71200	112800	-12700			
35	35	120	250	350	490	630	800	1040	1370	1370	6500	1300	18500	25200	32800	42700	56400	73600	73600	-12700			
36	36	150	390	450	620	790	1000	1280	1670	1670	•	•	•	•	•	•	•	•	•	•			
37	37	1120	2300	3420	4530	5670	7200	9830	•	•	•	•	•	•	•	•	•	•	•	•			
38	38	•	•	•	•	•	•	•	•	•	•	•	•	•	•	•	•	•	•	•			
39	39	•	•	•	•	•	•	•	•	•	•	•	•	•	•	•	•	•	•	•			

Table LXX. Strain and Elastic Stress Data XLR129 Transition Case Under Combined Internal Pressure and Thrust Loads (Engine Ratio) (Continued)

Table LXX. Strain and Elastic Stress Data XLR129 Transition Case Under Combined Internal Pressure and Thrust Loads (Engine Ratio) (Continued)

Rocette No.	Strain (in. in.) for Combined Pressure				Elastic Stress (psi) for Combined Pressure-Thrust Loads (psi) lb. of:												Membrane - Bending Stress at Max Load
	450	900	1350	1800	2250	2700	3150	3600	4050	4500	4950	5400	5850	6300	6750	7200	
21	1.30	2.20	3.20	4.30	5.30	6.30	7.30	8.30	9.30	10.30	11.30	12.30	13.30	14.30	15.30	16.30	-13500
21A	1.30	2.20	3.20	4.30	5.30	6.30	7.30	8.30	9.30	10.30	11.30	12.30	13.30	14.30	15.30	16.30	-13500
22	1.30	2.20	3.20	4.30	5.30	6.30	7.30	8.30	9.30	10.30	11.30	12.30	13.30	14.30	15.30	16.30	-13500
22A	1.30	2.20	3.20	4.30	5.30	6.30	7.30	8.30	9.30	10.30	11.30	12.30	13.30	14.30	15.30	16.30	-13500
23	1.30	2.20	3.20	4.30	5.30	6.30	7.30	8.30	9.30	10.30	11.30	12.30	13.30	14.30	15.30	16.30	-13500
23A	1.30	2.20	3.20	4.30	5.30	6.30	7.30	8.30	9.30	10.30	11.30	12.30	13.30	14.30	15.30	16.30	-13500
24	1.30	2.20	3.20	4.30	5.30	6.30	7.30	8.30	9.30	10.30	11.30	12.30	13.30	14.30	15.30	16.30	-13500
24A	1.30	2.20	3.20	4.30	5.30	6.30	7.30	8.30	9.30	10.30	11.30	12.30	13.30	14.30	15.30	16.30	-13500
25	1.30	2.20	3.20	4.30	5.30	6.30	7.30	8.30	9.30	10.30	11.30	12.30	13.30	14.30	15.30	16.30	-13500
25A	1.30	2.20	3.20	4.30	5.30	6.30	7.30	8.30	9.30	10.30	11.30	12.30	13.30	14.30	15.30	16.30	-13500
26	1.30	2.20	3.20	4.30	5.30	6.30	7.30	8.30	9.30	10.30	11.30	12.30	13.30	14.30	15.30	16.30	-13500
26A	1.30	2.20	3.20	4.30	5.30	6.30	7.30	8.30	9.30	10.30	11.30	12.30	13.30	14.30	15.30	16.30	-13500
27	1.30	2.20	3.20	4.30	5.30	6.30	7.30	8.30	9.30	10.30	11.30	12.30	13.30	14.30	15.30	16.30	-13500
27A	1.30	2.20	3.20	4.30	5.30	6.30	7.30	8.30	9.30	10.30	11.30	12.30	13.30	14.30	15.30	16.30	-13500
28	1.30	2.20	3.20	4.30	5.30	6.30	7.30	8.30	9.30	10.30	11.30	12.30	13.30	14.30	15.30	16.30	-13500
28A	1.30	2.20	3.20	4.30	5.30	6.30	7.30	8.30	9.30	10.30	11.30	12.30	13.30	14.30	15.30	16.30	-13500
29	1.30	2.20	3.20	4.30	5.30	6.30	7.30	8.30	9.30	10.30	11.30	12.30	13.30	14.30	15.30	16.30	-13500
29A	1.30	2.20	3.20	4.30	5.30	6.30	7.30	8.30	9.30	10.30	11.30	12.30	13.30	14.30	15.30	16.30	-13500
30	1.30	2.20	3.20	4.30	5.30	6.30	7.30	8.30	9.30	10.30	11.30	12.30	13.30	14.30	15.30	16.30	-13500
30A	1.30	2.20	3.20	4.30	5.30	6.30	7.30	8.30	9.30	10.30	11.30	12.30	13.30	14.30	15.30	16.30	-13500
31	1.30	2.20	3.20	4.30	5.30	6.30	7.30	8.30	9.30	10.30	11.30	12.30	13.30	14.30	15.30	16.30	-13500
31A	1.30	2.20	3.20	4.30	5.30	6.30	7.30	8.30	9.30	10.30	11.30	12.30	13.30	14.30	15.30	16.30	-13500

Table LXX. Strain and Elastic Stress Data XLR129 Transition Case Under Combined Internal Pressure and Thrust Loads (Engine Ratio) (Continued)

The outer case cooling liner was fabricated from L-605 sintered woven wire matrix, 0.057 in. thick with a targeted porosity of 21 sefm. The liner was designed to conform to the outer case shape and is spaced a distance of 0.170 to 0.190 in. from the outer case. The liner was fabricated in core-like segments and preformed. After the proof pressure check of the outer case, the liner was welded into the case. Figure 504 shows the cooling liner details and subassemblies. Figure 505 shows the cooling liner after installation into the transition case.

c. Thrust Gimbal

The thrust gimbal ball arrangement uses a uniball joint to distribute thrust and side loads into the transition case. This eliminates the need for a standard cross pin universal joint, thus providing a simpler, lighter, more stable joint.

The assembly consists of a hollow thrust ball machined from an Inconel 718 forging (AMS 5663), which is intersected by an integrally machined flanged cone. The thrust ball is mated to the outer case socket and held in place by a bolted two-piece clamped retaining ring, fabricated of Inconel 718 (AMS 5662). A low friction liner, composed of Teflon, fiberglass, and epoxy, was applied and baked to the ball. Two ball assemblies have been fabricated, and one is shown in figure 506.

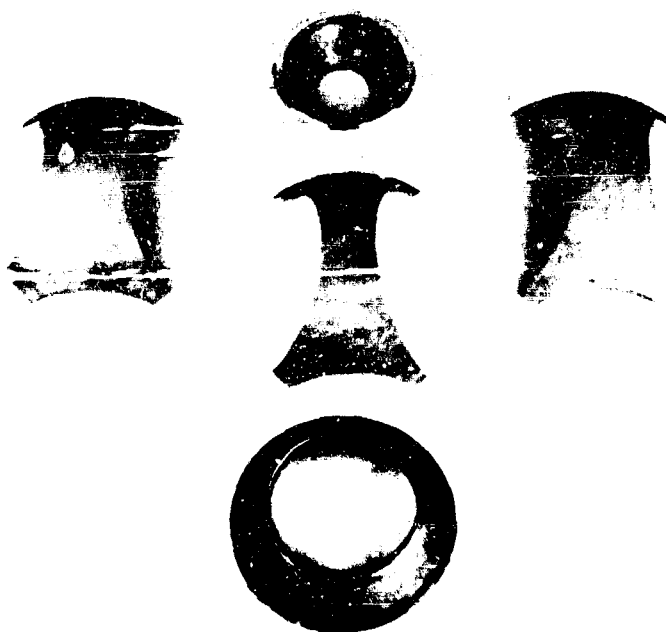


Figure 504. Formed Case Cooling Liner Segments FE 97227

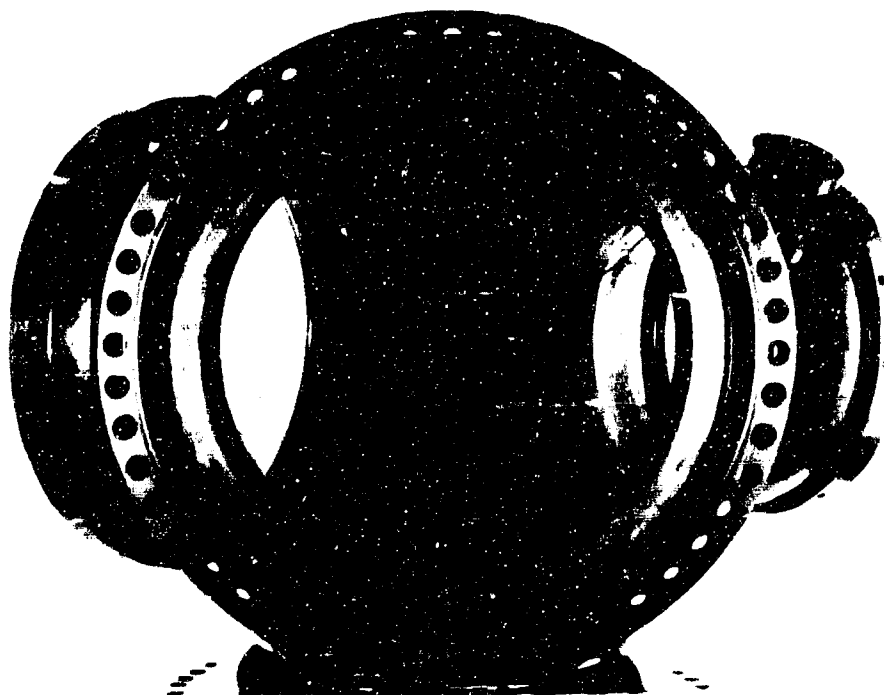


Figure 505. Transition Case With Cooling Liner FE 97599



Figure 506. Gimbal Ball

FE 96107

d. Preburner Flow Duct

The subassembly that completes the preburner duct is a hydrogen transpiration cooled liner composed of a 2 in. cylindrical porous section, which is electron-beam welded into a manifold and support member. The support member (Inconel 718) has three feed annuli to support coolant to the porous liner.

An uncooled liner (Haynes 188) is located immediately downstream of the transpiration cooled section. This is a single piece liner that bayonet-joins into the preburner duct approximately 5 in. behind the igniter. This joint provides a metal-to-metal seal, and is loaded by differential pressure.

The uncooled liner is a weldment assembly consisting of the upstream liner detail, bayonet-joint detail, and downstream liner detail. The upstream and downstream liners were fabricated from sheet stock which was rolled and spun to the correct contour. The bayonet-joint was machined from a Haynes 188 ring.

The preburner duct serves as a combustion chamber that discharges combustion products to the centerbody. The duct design consideration included cycle life, strength, and weight. Inconel 625 (AMS 5599 and AMS 5666) material, which offers good cycle life, was selected for the internal detail of the liner. The duct assembly is also a structural duct, and Inconel 718 (AMS 5662) was selected for the outer duct detail. Coolant passages are formed when these two details are oven-brazed. The coolant flows the length of the duct, and discharges into the gas flow stream through centerbody liners. Both ducts are fabricated from forgings.

The inner liner contains 60 longitudinal coolant passages approximately 0.260 in. wide x 0.060 in. deep, contour-milled into the outer surface. Before mating the inner and outer duct to form the major portion of the preburner duct, each duct was silver flashed (AMS 2666) to provide braze material. After assembly of the inner duct to the outer duct, which is a tight fit, the assembly was oven brazed. The slots that were milled in the inner duct formed cooling passages. The inner and outer ducts are shown before brazing in figure 507. Because the braze is loaded in compression, it is not critical as far as strength and coverage are concerned. Flow checks indicated the slots to be unobstructed, and braze coverage, where desired, exceeded 90%. Figure 508 shows the brazed assembly.

e. Centerbody

The centerbody provides the shortest possible plumbing for the intersection of the fuel, oxidizer and preburner ducts. The centerbody is a sphere intersected by three cylindrical rings. It provides the sealing surfaces for the piston rings that are installed as part of the individual duct assemblies. The centerbody is functionally divided into two sections; the outer structural sphere, and the internal hot flow duct.

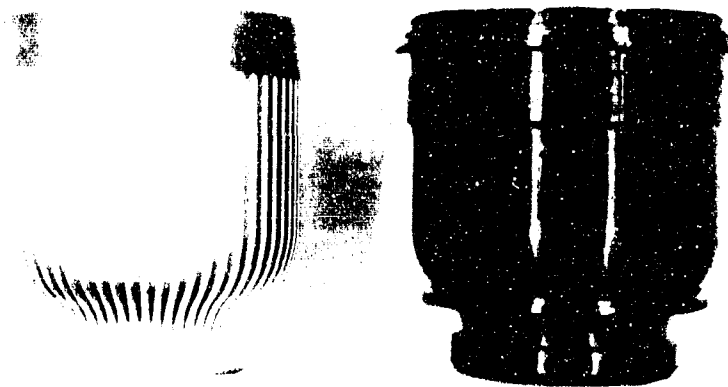


Figure 507. Preburner Combustor Duct and Inner
Coolant Liner

FE 95743



Figure 508. Preburner Combustor Duct Braze
Assembly

FE 95742

The outer structural sphere is an Inconel 718 weldment similar to the outer transition case except for smaller size. This sphere is also formed by welding two hydroformed hemispheres. Three equally spaced holes are then machined into the sphere and a cylindrical ring welded into each port. The cylindrical rings are machined from ring forgings. They provide the sealing surfaces for the piston rings, which are installed as part of the individual duct assemblies. The rings also serve to strengthen the shell at the location of the three holes. A taper is machined at the outside edge of each cylindrical ring to form a diverging section to provide a lead in ramp for the piston rings.

To provide good corrosive and oxidation resistance, the internal hot flow duct sections of the centerbody are fabricated of 0.040 in. thick L-605, a cobalt base material.

There are two separate sets of liners that compose the liner sections; an inner and an intermediate. The function of the inner liner sections is to divide the preburner gas flow between the two turbopumps and to prevent the hot preburner gases from scrubbing the inside structural walls of the centerbody. The intermediate liner is incorporated as a radiation shield to protect the cooler surfaces of the centerbody from the hot liners. These liners control the coolant that is discharged from the preburner duct and provide holes to discharge the coolant back into the preburner gas stream.

The liner details are manufactured by spinning. The intermediate liner is in three sections, one each of which is placed through one of the openings in the centerbody. The inside end of each section is mitered to allow the three adjacent segments to intersect at a simple butt joint. Each section incorporates a support segment at the outer diameter that serves for mechanically attaching the section to the centerbody. The inner heatshield (a y-section that is inserted first) is aligned when all three intermediate sections are installed.

The outermost shell is a porous liner similar to the outer case cooling liner. Its purpose is to protect the structure of the centerbody from the hot turbine exhaust gases. The centerbody is supported by the transition case at the gimbal support cone through a threaded joint. Coolant supplied to the centerbody from the transition case flows through this threaded joint, cooling the area of the gimbal before entering the centerbody. A spherical volume is provided between the cooling liner and structure to allow coolant flow to circulate and discharge into the flow stream. Similar to the transition outer case porous cooling liner, the coolant liner flow is tailored by flame-spraying to allow the designed flow rate and pressure differential. The structural sphere and rings are composed of Inconel 718. The outer porous liner is made of N-155 wire. Subassembly of the structural segment and cooling liner details are shown in figure 509. A complete centerbody assembly is shown in figure 510, installed in the outer case.

For the initial preburner/transition case testing, turnaround caps simulating the fuel and oxidizer turbines shown in figure 511 were used rather than fuel turbines. Where possible, actual turbine parts were used in the design and fabrication. These ducts, and the preburner duct that plugs into the centerbody complete the plug-in concept. Figures 512 and 513 show the simulator assemblies installed in the outer case and centerbody as viewed through the main burner port. Figure 514 shows the completed fuel simulator, and figure 515 shows the completed oxidizer simulator.

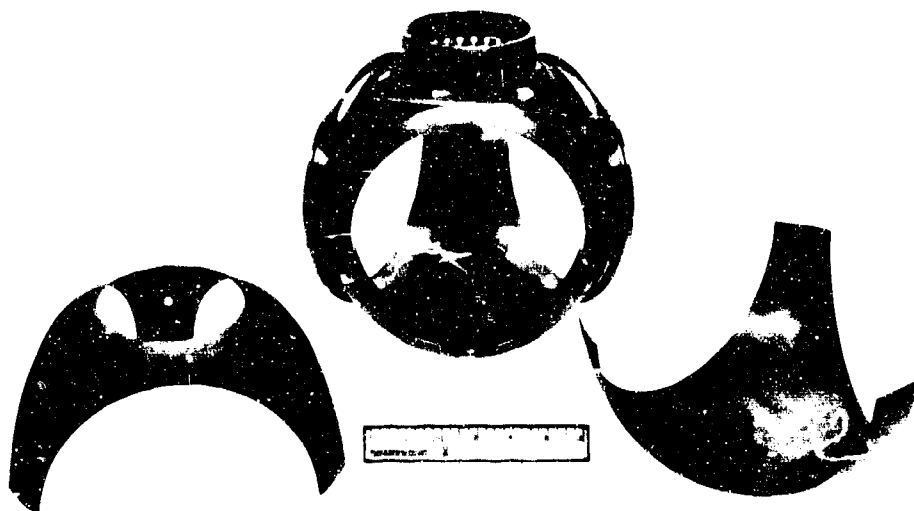


Figure 509. Centerbody and Formed Outer Liners FE 93696



Figure 510. Transition Case With Centerbody Installed FE 97796

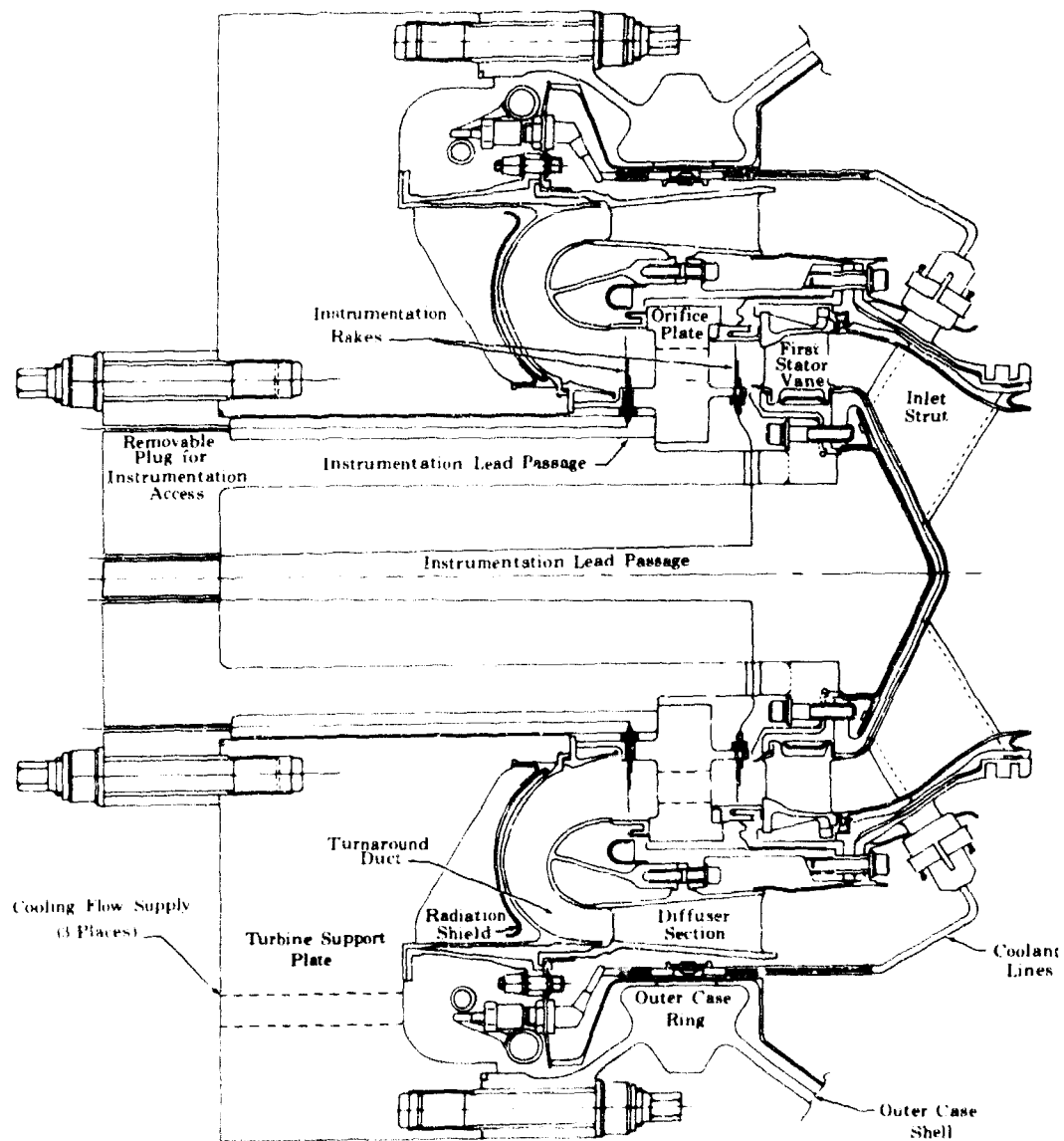


Figure 511. Turbine Simulator Cap

FD 33030



Figure 512. Transition Case Assembly Viewed Through Main Injector Flange

FE 98040

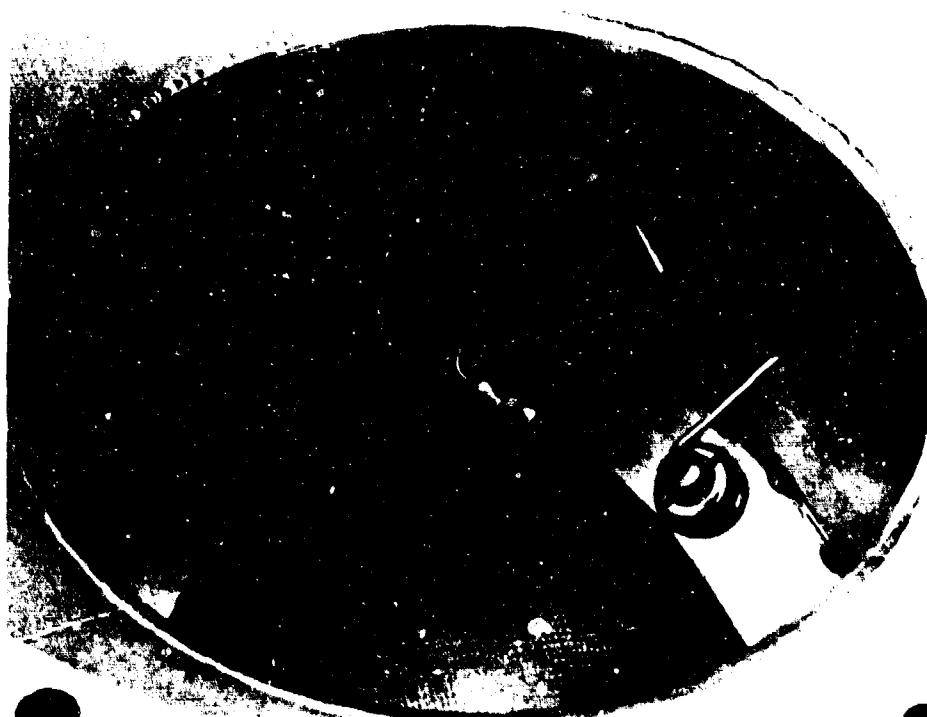


Figure 513. Turbine Ducts Viewed Through the Main Injector Flange

FE 98041

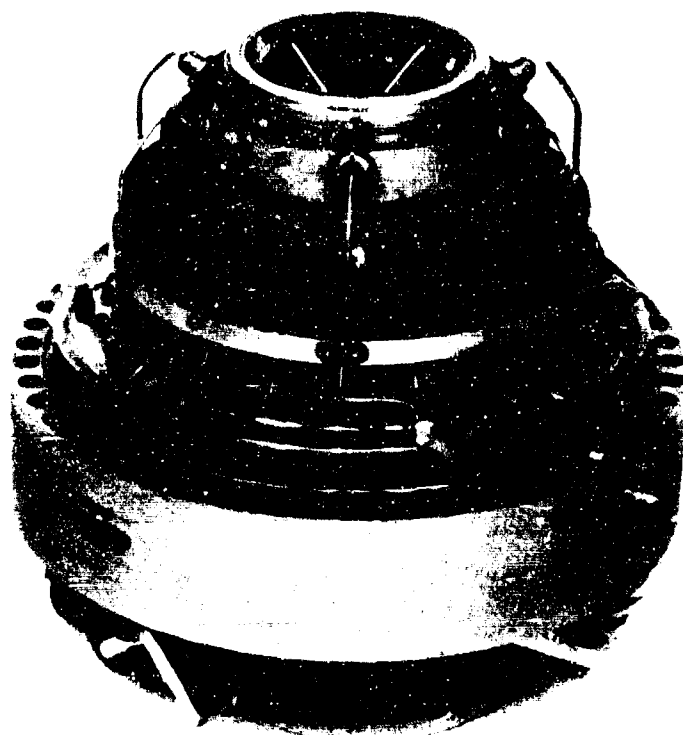


Figure 514. Fuel Turbopump Duct and Turbine Simulator Assembly

FE 97979

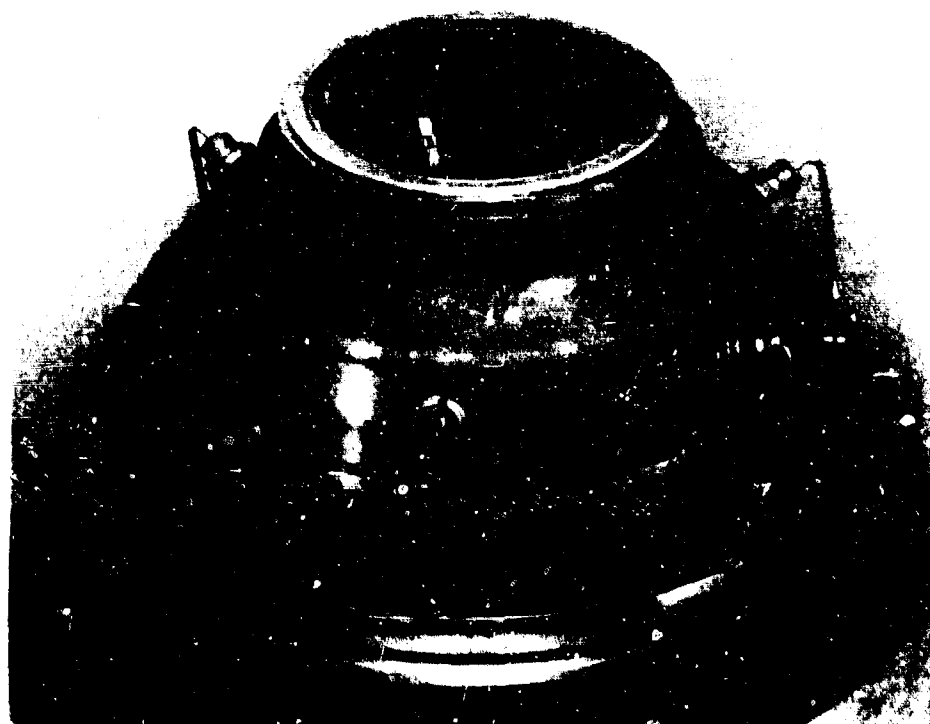


Figure 515. Oxidizer Turbopump Duct and Turbine Simulator Assembly

FE 97983

The first preburner/transition case/turbine simulator assembly, designated F-35139 build 1, was completed and the rig was delivered to the E-8 test stand on 2 May 1970. Figure 516 shows the assembly mounted in the test stand prior to its initial test. Section VII describes the preburner/transition case testing.



Figure 516. Transition Case Mounted In E-8 Test Stand Before Test FE 97733

C. MAIN BURNER INJECTOR

1. Introduction

The main burner injector introduces and atomizes liquid oxygen with hot, fuel rich, preburner combustion and turbine discharge products so that efficient and stable combustion is achieved over the full operating range of thrust and mixture ratios. Turbine discharge gases flow around injector elements and spraybars into the Rigimesh injector faceplate. Part of these gases flows through the Rigimesh faceplate for cooling; however, the major portion of the gases flows through openings machined in the faceplate around the oxidizer elements. The main burner ignition system consists of a hydrogen cooled, continuous burning, oxygen-hydrogen torch. Double sparkplug igniters are provided having separate exciter boxes for system redundancy. The spark igniters ignite the torch, which ignites the main burner chamber propellant mixture.

2. Summary, Conclusions, and Recommendations

Design of the main burner igniter was completed, and it was concluded that to develop a durable, lightweight, easily fabricated injector design, as compared to the Phase I main burner injector, the following concepts must be pursued:

1. Individual tapered tube spraybars offer the lightest weight element manifold having an increased hot gas flow area compared to other concepts
2. Individual spraybars are adaptable to a cast fabrication technique, but until actual temperature measurements are obtained during hot tests, spraybars will be fabricated by machine fabricating wrought material for increased ductility and longer life
3. A one-piece, self supporting Rigimesh faceplate will eliminate thermal incompatibility of the injector with the supporting structure, and reduce the limitation on life.

A detailed description of the design task is presented in the Demonstrator Engine Design Report AFRPL-TR-70-6.

Finish machined spraybars were fabricated for two assemblies. Final fabrication of the main burner injector was terminated because of program re-direction.

3. Hardware Description

The main burner injector, shown in figures 517 and 518 consists of four major components: (1) the oxidizer manifold and housing, (2) the spraybar-type internal manifolds, (3) the oxidizer injection elements, and (4) the porous faceplate.

a. Oxidizer Manifold and Housing

The main injector housing consists of the oxidizer inlet horn, the oxidizer manifold, and the crossover passages to the spraybars. Liquid oxygen enters the main burner injector from the single inlet horn into the wraparound manifold (figure 519). The injector housing forms the crossover passages to the spraybars, and contains the injector spraybars, which contain the individual oxidizer elements.

The configuration of the inlet flange is based on design criteria believed to yield optimum proportions for flange deflection, sealing requirements, and current bolt technology. Flange dimensions are consistent with the analytical method established for flange and seal design during this program.

The oxidizer inlet horn has a 3 in. ID and has a 90 deg turn. It intersects the wraparound manifold, which has a constant 2.5 in. ID. The flange, inlet horn, and manifold are fabricated from Inconel 718 (AMS 5662).

The injector housing is fabricated of Inconel 718 (AMS 5662). It is attached to the engine between the main burner chamber outer pressure shell forward flange and the transition case with forty-eight 9/16 in. diameter bolts fabricated

of Inconel 718 (AMS 5662). Slots, connecting the wraparound manifold and spraybars then passing between bolt holes, form the oxidizer spraybar crossover manifold, as shown in figure 520.

b. Spraybar Internal Manifolds

Forty-eight individually machined spraybars (figure 521) are brazed to the oxidizer housing and are individually supported at the outside diameter, thus permitting free thermal growth.

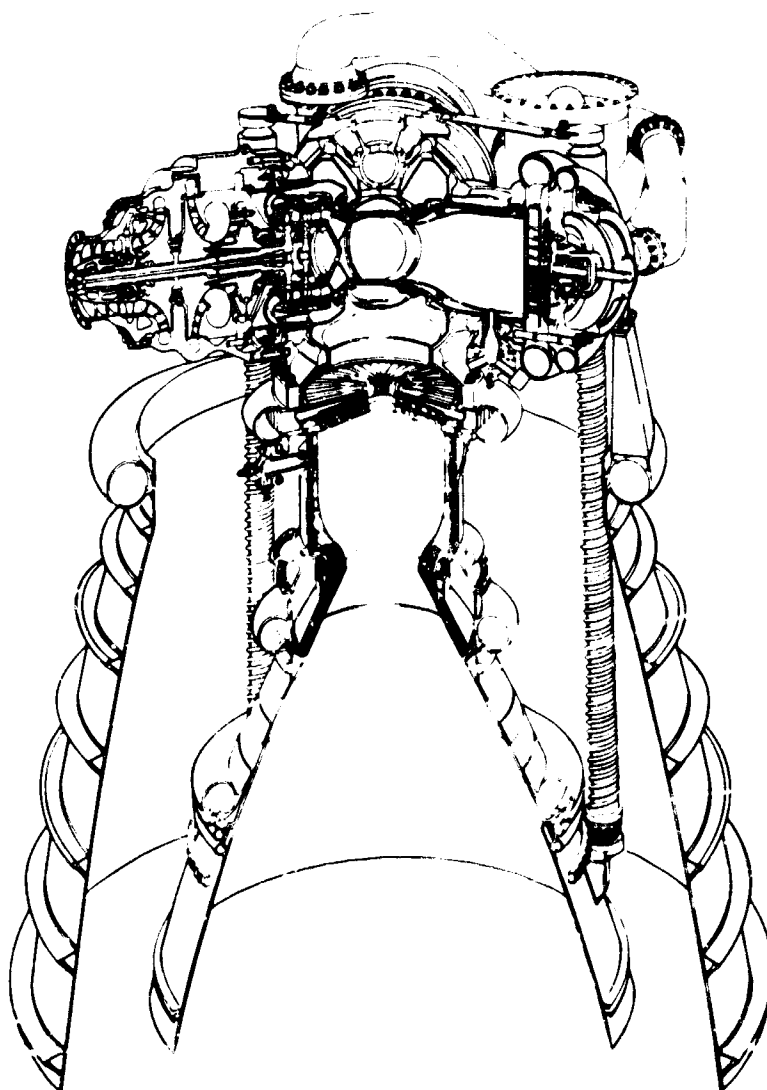


Figure 517. Main Burner Injector and Torch Location

FDC 31493A

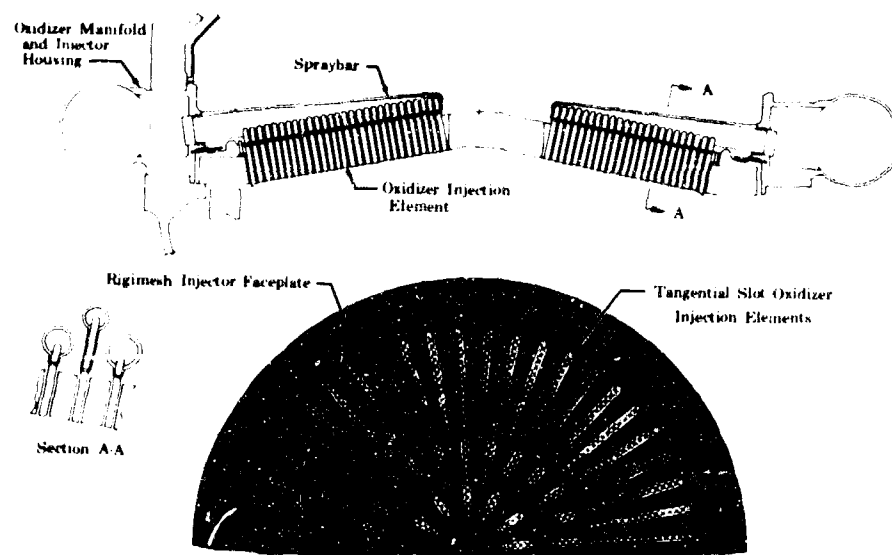


Figure 518. Main Burner Injector

FD 25641A

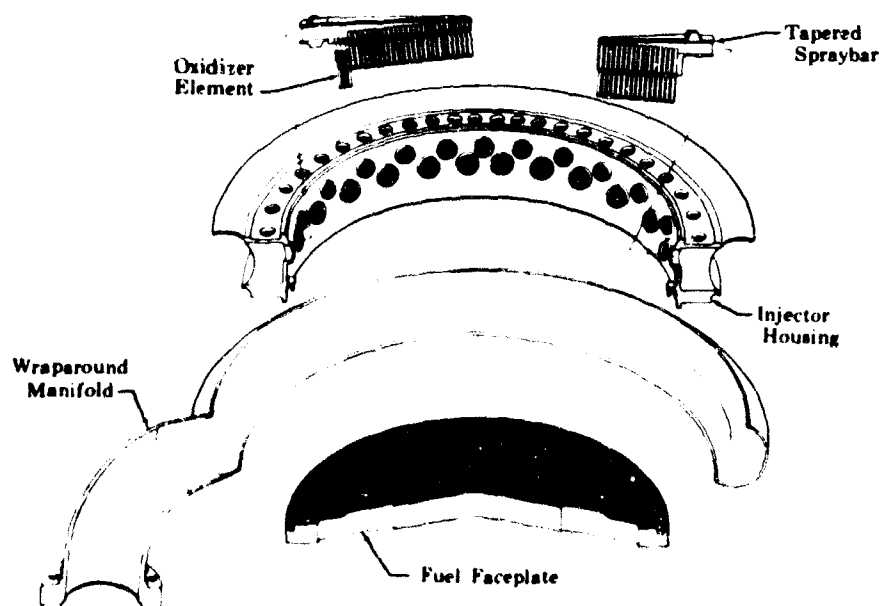


Figure 519. Segmented Injector Concept

FD 33005

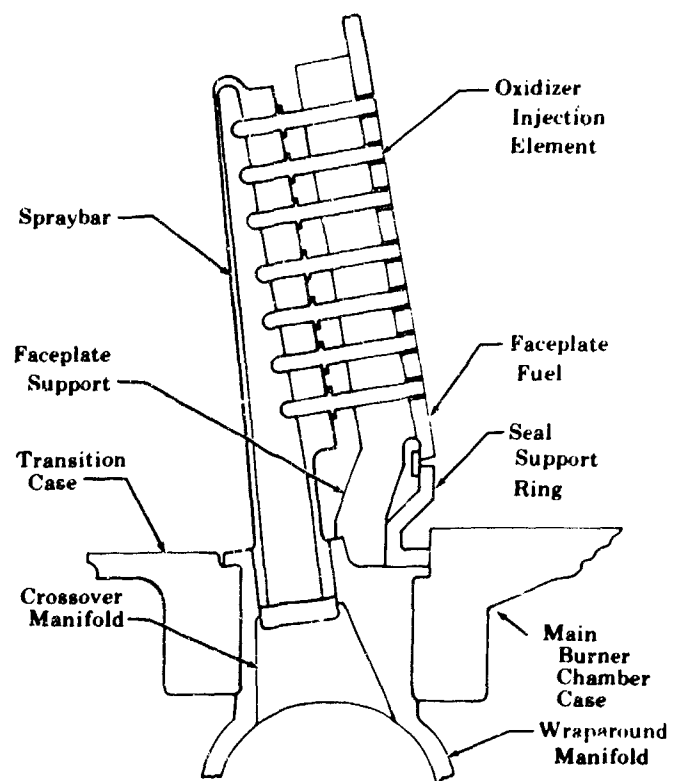


Figure 520. Typical Main Burner Injector Cross Section FD 25360A

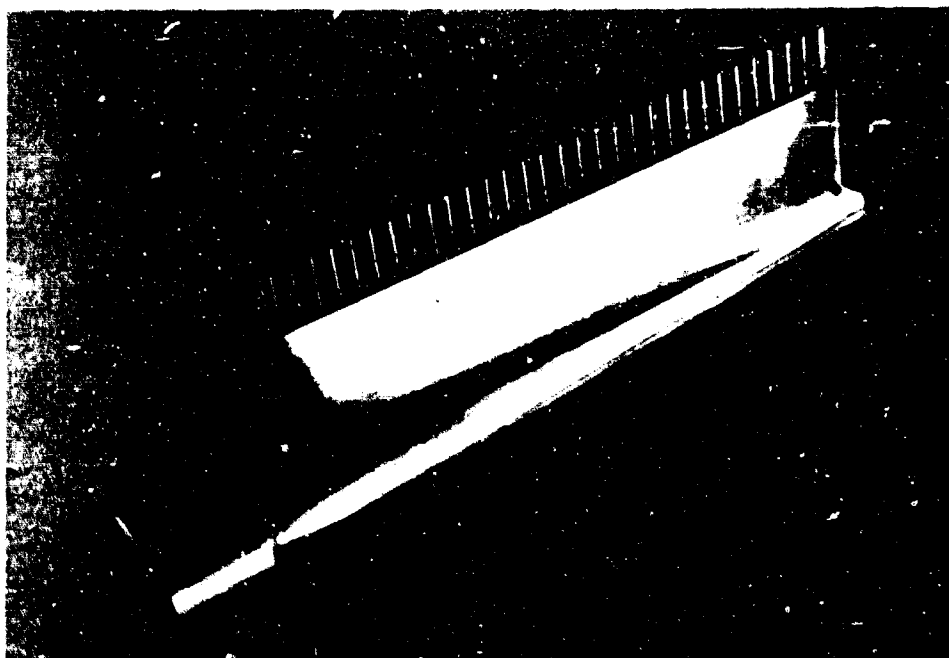


Figure 521. Typical Spraybar FD 34503

The spraybars are arranged in three configurations: 12 long spraybars equally spaced around the circumference; 12 medium spraybars equally spaced between the long spraybars; and 24 short spraybars equally spaced between the medium and long spraybars. This overall arrangement provides the maximum number of spraybars consistent with such mechanical considerations as main bolt hole spacing and spraybar wall thickness and results in good oxidizer element density and uniform radial flow distribution. The tapered spraybars have respective inlet diameters of 0.735, 0.655, and 0.525 in. ID for the long, medium and short spraybars. All bars have a tip ID of 0.265 in. Spraybars are axially offset, as previously shown in figure 519, to minimize the hot gas pressure loss in the flowpath between spraybars. The fuel hot gas flow area is 82.6 in². The spraybar material is Inconel 625 (AMS 5666B), selected because of its ability to withstand high thermal gradients, and it exhibits good low-cycle fatigue life.

c. Oxidizer Injector Elements

Self atomizing injection elements, shown in figure 522, are spaced closely along the spraybars, resulting in fine oxidizer atomization and good distribution. There are 996 oxidizer elements, each having a 0.1166 in. ID. The elements have flow ports machined tangential to the tube ID, which causes the flow to leave the element in a hollow cone swirl and enter the main burner chamber. Oxidizer element A_{cd} is controlled to uniformly inject the oxidizer mass flow across the face, and divide flow into three classes that form seven groups across the face. Element A_{cd} is controlled by sizing of the slot area. To prevent the spray cone from impinging on the chamber wall, the outer elements are cut at a 45 deg angle, as previously shown in figure 520. Adjacent elements are counter swirled for uniformity of injection pattern.

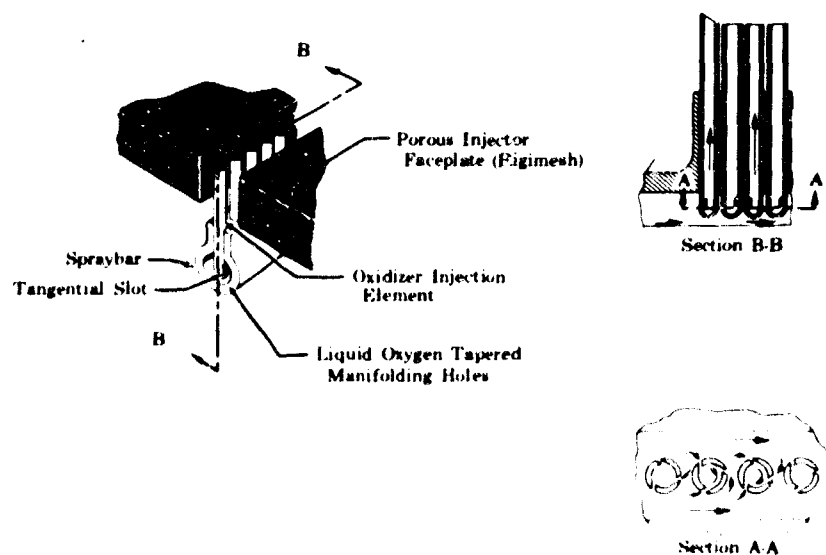


Figure 522. Main Burner Injector Spraybar Cross Section

FD 20688C

d. Porous Faceplate

The fuel faceplate mounts between the injector and the main chamber, and forms the fuel injection side of the injector assembly. To meet low cycle fatigue life requirements, a self supporting Rigimesh face was selected for design (figure 519). Rigimesh is a sintered, woven wire matrix forming a porous structure. The design has 44 layers of L-605, plain dutch weave wire rolled to a 1 in. thickness. The Rigimesh will admit air flow at approximately 320 scfm at 2 psid. At this thickness, the working stress is predicted to be 65% of the material yield strength.

The fuel faceplate directs approximately 92% of the hot, fuel rich, preburner combustion gases through slots surrounding the oxygen injection elements. The slot width is shaped to supply an amount of fuel at a given location consistent with the classed oxidizer flow, and create a uniform mixture ratio. The radial slots in the faceplate permit differential radial thermal growth between the hot faceplate and the lower temperature spraybars. The radial layout of both spraybar and fuel slot is in line with radial thermal growth, thus reducing misalignment of the elements inside the fuel slots. The incorporation of a 1 in. thick Rigimesh faceplate renders the slot gap seals used in Phase I ineffective in the new design. The fuel will be redistributed in the 1 in. length while crossing from the upstream to the discharge edges of the faceplate.

e. Main Burner Torch Igniter

The main burner torch assembly consists of a cover and chamber assembly shown in figure 523.

The cover, with attached chamber, bolts to the mounting flange on the pressure shell of the main burner chamber perpendicular to the main burner axis. In addition, two offset dowel pins, shown in figure 524, position the cover when it is bolted to the mounting flange and ensure assembly in the correct position. The cover is fabricated from Inconel 718 (AMS 5662) and contains two spark igniter tubes, an oxidizer element and a fuel fitting. Removable orifice plugs are also contained in these fittings. Each spark igniter tube houses a spark igniter plug attached to the cover by a lockwired nut. The cylindrical section of the chamber is fabricated from copper (AMS 4500), and is brazed directly to the bottom of the cover. The chamber has a throat size of 0.0952 in.². A stainless steel (AMS 5646) piston ring is a carrier for an Inconel Y-750 (AMS 5667) piston ring seal with circumferential bearing on the internal wall of the main chamber flange. This permits igniter chamber axial and transverse thermal growth, and is brazed to the chamber at the nozzle end. Propellants are distributed (figure 524) in the same manner as preburner torch propellants; however, cooling passage dimensions and arrangement differ.

4. Fabrication

a. Housing

The main burner injector housing and wraparound manifold are fabricated from Inconel 718 (AMS 5662) wrought forgings. The housing is machined to finish dimensions and spraybars are brazed in position. After brazed joint inspection, the manifold closure is welded to the housing using Inconel 718 weld rod.

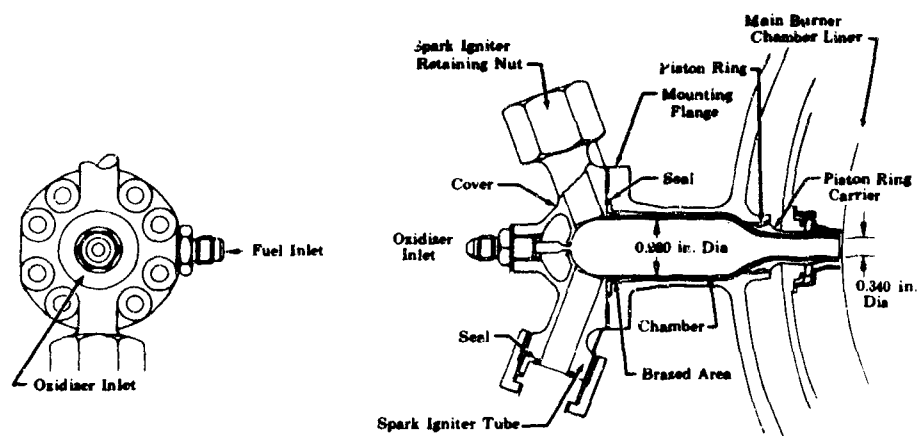


Figure 523. Main Burner Torch Assembly

FD 31817

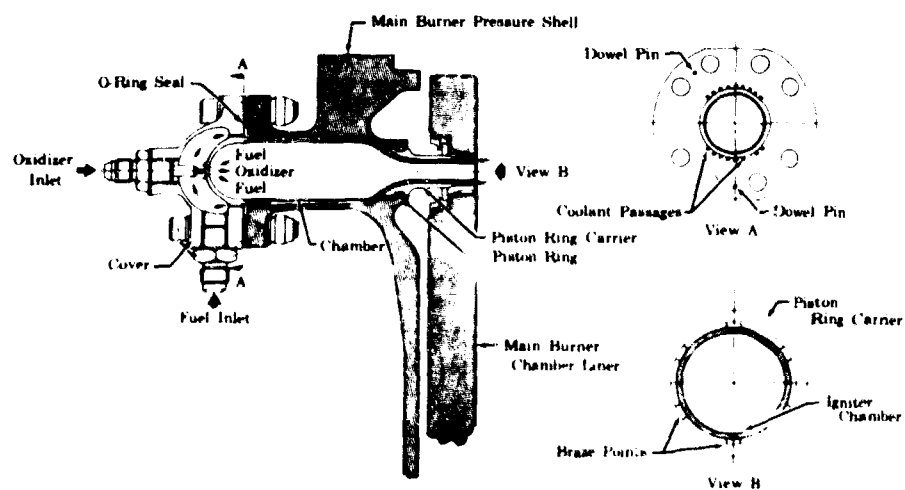


Figure 524. Main Burner Torch Assembly, Propellant Flow, Mounting and Sealing

FD 31818

Table LXXI presents the procurement and manufacturing time required for the main burner injector.

Table LXXI. Component Manufacturing Timetable

Component	Lead Time (weeks)
Housing - Ring Forging	16
Manifold - Ring Forging	8
Inlet Flange - Bar Forging	13
Inlet Elbow - Bar Forging	6

b. Spraybar

One typical main burner injector spraybar was fabricated and tested to substantiate the design and to obtain the following experimental data and fabrication experience:

1. Machining of the spraybar
2. Braze technique of the injection element to the spraybar
3. Braze technique of the spraybar to the housing
4. Pressure loss through the spraybar as determined by water flow test
5. Natural frequency of the assembly.

Material selected for the test spraybar was Inconel 718 (AMS 5662). Injection element material was type 347 stainless steel because TD nickel tubing was not available within the time allowed for fabrication.

The spraybar was contour milled, and the flow passage step drilled and taper reamed. The injection elements were water flowed for A_{cd} determination and gold-nickel brazed into the spraybar. X-ray revealed approximately two-thirds of the joints had little or no braze penetration. All joints had a large braze fillet formed at the contact point of the element shoulder and spraybar body. It was concluded that if gold-nickel braze were used, it would be necessary to fabricate additional test spraybars to establish a fit that would allow braze penetration without molten braze running through the joint and plugging the element entry slots. The spraybar was then silver brazed into a simulated housing. The silver was plated in the joint area and did not depend on flowing to penetrate. The braze joint was satisfactory, having over 90% internal coverage and a continuous fillet on both sides. Figure 521 shows the finished test spraybar.

The test spraybar assembly was water flowed to determine pressure loss coefficients inside the spraybar. As shown in figure 525 the mathematical prediction of pressure losses inside the spraybar needs only minor adjustment to coincide with test data. The test spraybar was then removed from the flow block and installed on a shaker table to determine the natural frequency of the injection

element and support platform combination. Results indicate a natural frequency of 313 Hz. This is not in the range of the combustion system noise and, therefore, will not present a problem.

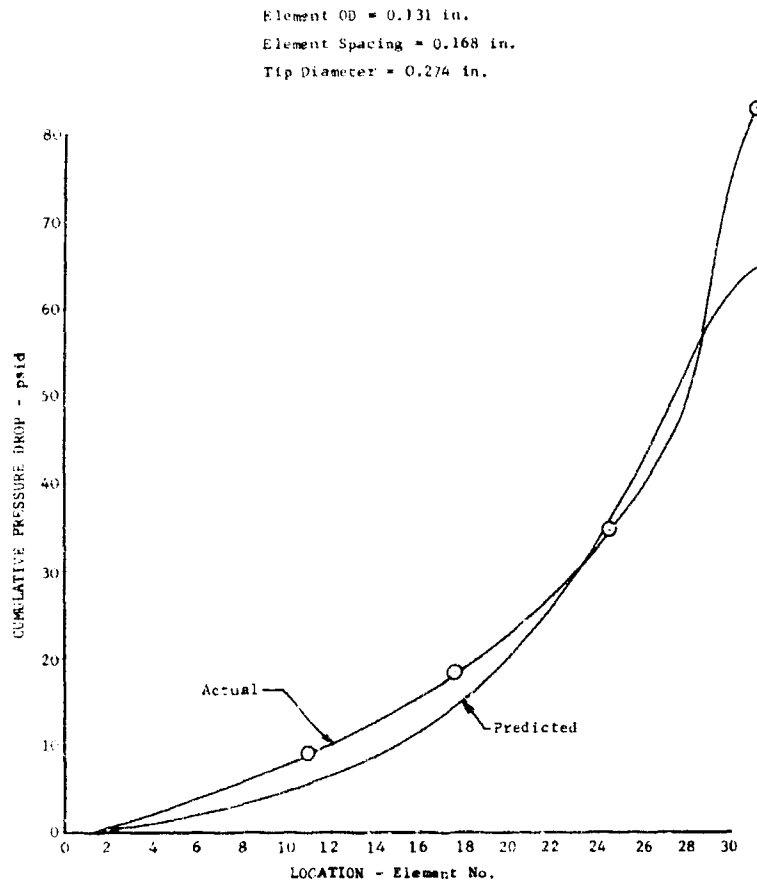


Figure 525. Comparison of Predicted and Actual Flow Data DF 70088

(1) Copper Braze Test Program

When Inconel 625 (AMS 5666B) was selected as the spraybar material for the main burner injector, copper braze, according to AMS 2671, was considered as a braze candidate because it was used successfully on the Phase I injector. Copper braze can be plated, and does not depend on flow to obtain a good joint. In the element spraybar assembly, the braze material must not run completely through the joint and out onto the tangential feed slots in the elements. Plated copper braze material can be stopped from running into the tangential feed slots by plating with nickel just below the copper.

Three copper braze test spraybars were fabricated using existing Phase I main injector TD nickel-oxidizer elements. Details and braze information are

shown in table LXXII. The first copper braze spraybar was made in accordance with the Phase I main injector copper braze cycle and element configuration indicated on table LXXII. The other two spraybars were changed based on the results of the first. Comments on the three brazed test spraybars are listed below:

(a) Braze No. 1

1. X-ray inspection erroneously indicated the braze joint was void of braze material; therefore, the inspection was not acceptable. The density of copper is almost identical to Inconel 625 and TD nickel so the braze was not discernible by X-ray.
2. Microscopic examination by the Materials Development Laboratory revealed good bonding between the copper plated on the oxidizer element before braze, and the TD nickel oxidizer elements. In some cases, the bond between the copper braze material and the simulated spraybar was not sufficient for sealing and strength. There appeared to be an oxide film, possibly an improperly cleaned part, on the spraybar hole interface which would have prevented proper bonding. In some places, braze material did not flow 0.060 to 0.040 in. below the shoulder as prescribed (see table LXXII).
3. Pry testing of two randomly selected elements was performed which a chisel and a hammer. One element was easily pried from the platform, indicating an inadequate bond. Inspection of this element and the vacated hole indicated approximately 20 to 30% bonding. Reasonable force was applied in an attempt to pry the second element loose. The bond was assumed good because the element did not loosen.
4. Fillets around each element were continuous and had approximately a 0.025 in. minimum radius. Also, bridging of braze material between each element to 0.060 in. above the bottom of the element shoulder was observed.

From the above test observations it was concluded that a poorly bonded element was caused by improperly cleaned surfaces. In the second braze test, each hole was individually cleaned with a swab using PMC 9015. A decision was also made to extend the copper plate to the top of the element shoulder and eliminate the added machining cost of the undercut step diameters in the plated areas. The braze material exterior coverage was changed as shown in table LXXII to displace some of the copper braze that caused bridging between elements. X-ray indicated all braze joints were void of braze, and microscopic examination revealed good bonding on some elements. The feasibility of using X-ray as a means of determining braze joint quality was also investigated on the next test spraybar.

Table LXXII. Braze Detail Tabulation

[illegible]

(b) Braze No. 2

To verify apparent discrepancies in the first X-ray analysis, spraybar No. 2 was assembled and X-rayed several times prior to brazing. The X-ray procedure was recorded so it could be duplicated after brazing.

1. After brazing, spraybar No. 2 was X-rayed several times to duplicate X-rays made of the assembled part prior to brazing. Comparison of both sets of X-rays indicated no apparent differences between X-rays before and after brazing. Microscopic examination revealed the brazed joint did contain copper braze material, but did not contain noticeable voids. X-ray analysis of these parts in the brazed condition is not warranted; therefore, X-raying of succeeding braze samples was discontinued.
2. Microscopic examination revealed very good bonding between the elements and the simulated spraybar. The braze coverage was estimated to be between 90 and 100%.
3. Pry testing of two elements selected at random revealed that neither element was easily removed from the test spraybar. Examination of these elements and the vacated holes indicated the bond was very good.
4. Fillets around each element were continuous and had an approximate 0.025 in. minimum radius. Bridging between elements also occurred, but was slightly reduced (approximately 0.035 in. above the bottom of the shoulder) compared to braze No. 1.

(c) Braze No. 3

Spraybar No. 3 was constructed with a pressurization manifold on the upstream side of the element which simulated the spraybar oxidizer manifold. When the manifold is pressurized the element is loaded in the same way it would be in the injector. Results were as follows:

1. The spraybar was successfully hydrostatically pressure tested to 1500 psig, simulating the injection pressure (hold time was 5 minutes). The spraybar was also submerged in water and successfully pressure tested to 1500 psig using GH_4 (hold time was 5 minutes). This pressure, 1500 psig, is approximately 65% greater than operating pressure. No leaks were detected.
2. Microscopic examination revealed good bonding between the elements and the simulated spraybar, but not as good as brazed spraybar No. 2, because braze coverage was approximately 10% less. The braze coverage was estimated to be between 80 and 90%.
3. Pry testing of two elements selected at random revealed that neither element was easily removed from the test spraybar. Examination of a dislodged element and the vacated hole revealed a small discontinuous area in the exposed surface, revealing the absence of bonding in this area. The estimated

80 to 90% coverage revealed by microscopic examination was verified.

4. Fillets around each element were continuous and had approximately a 0.025 in. minimum radius. Bridging also occurred between elements the same as in brazing spraybar No. 2.

It was concluded that copper braze, when used as shown in table LXXII (spraybars 2 and 3) qualifies as an acceptable method of joining the injection elements to the spraybars to provide a reliable, leak free joint.

(2) Silver Braze Test Program

A braze test program was also conducted to substantiate the spraybar-to-housing joint. Silver brazing per procedure PWA 85 was the only candidate braze considered on this particular braze cycle. The lower braze temperature required by silver provides a considerable margin of safety in preventing a remelt of the first braze cycle. Silver braze material, like copper, has an advantage over braze alloys because silver braze material can be plated directly on either or both of the parts to be joined. This advantage ensures braze coverage to any desirable depth by plating braze material to the dimensions desired. Such a joint is the spraybar-to-injector housing joint, which requires absolute sealing in addition to reliable strength.

A total of five silver brazed spraybar assemblies were fabricated. Each assembly consisted of two pieces. One piece simulated the spraybar, while the other simulated the injector housing into which a spraybar was to be brazed. Electrolytic nickel plating was used in all pieces. The spraybar pieces were then silver plated. In the bill-of-materials hardware, the spraybar enters the injector housing at an 11 deg angle below the horizontal plane of the injector. This angle was simulated in the brazing of the spraybar assemblies. Complete fabrication details of the samples are listed in table LXXIII. Changes in fabrication are also noted and reasons are given below.

(a) Braze No. 1

1. X-ray inspection revealed the absence of detectable voids in the braze joint (X-ray personnel estimate a 0.002 in. void would be clearly detectable).
2. Microscopic examination of a sectioned sample revealed good bonding in the braze joint. There was also good penetration of braze material from the circular braze loop into the joint at the shoulder interface. This examination revealed several minute voids in the braze joint. The voids appeared isolated and discontinuous. The fact that the voids were not continuous was substantiated by the X-ray inspection. It was estimated that total braze coverage was at least 90%.
3. The fillet around the shoulder was continuous and varied in size from top to bottom as installed in the braze fixture. The fillet was leaner at the bottom vertical centerline because of 11 deg clockwise rotation. It was noted that a small continuous fillet was formed at the base of the spraybar inside the housing joint.

Table LXXIII. Fabrication Detail Tabulation

Sheet Number	Insulated Section	Insulated Section	Assembly	Basic Material	Core	Remarks
Page 1	<p> A 1.425 1.485 diameter before plating B 1.425 1.485 diameter after the plate C 1.425 1.475 diameter after Ag plate D 1.425 1.475 diameter after Ag plate E 1.425 1.475 diameter after Ag plate F 1.425 1.475 diameter after Ag plate G 1.425 1.475 diameter after Ag plate H 1.425 1.475 diameter after Ag plate I 1.425 1.475 diameter after Ag plate J 1.425 1.475 diameter after Ag plate K 1.425 1.475 diameter after Ag plate L 1.425 1.475 diameter after Ag plate M 1.425 1.475 diameter after Ag plate N 1.425 1.475 diameter after Ag plate O 1.425 1.475 diameter after Ag plate P 1.425 1.475 diameter after Ag plate Q 1.425 1.475 diameter after Ag plate R 1.425 1.475 diameter after Ag plate S 1.425 1.475 diameter after Ag plate T 1.425 1.475 diameter after Ag plate U 1.425 1.475 diameter after Ag plate V 1.425 1.475 diameter after Ag plate W 1.425 1.475 diameter after Ag plate X 1.425 1.475 diameter after Ag plate Y 1.425 1.475 diameter after Ag plate Z 1.425 1.475 diameter after Ag plate </p>	<p>Material Insulated 718</p> <p> A 1.485 1.485 diameter before plating B 1.485 1.475 diameter after the plate C 1.485 1.475 diameter before plating D 1.485 1.475 diameter after the plate E 1.485 1.475 diameter after the plate F 1.485 1.475 diameter after the plate G 1.485 1.475 diameter after the plate H 1.485 1.475 diameter after the plate I 1.485 1.475 diameter after the plate J 1.485 1.475 diameter after the plate K 1.485 1.475 diameter after the plate L 1.485 1.475 diameter after the plate M 1.485 1.475 diameter after the plate N 1.485 1.475 diameter after the plate O 1.485 1.475 diameter after the plate P 1.485 1.475 diameter after the plate Q 1.485 1.475 diameter after the plate R 1.485 1.475 diameter after the plate S 1.485 1.475 diameter after the plate T 1.485 1.475 diameter after the plate U 1.485 1.475 diameter after the plate V 1.485 1.475 diameter after the plate W 1.485 1.475 diameter after the plate X 1.485 1.475 diameter after the plate Y 1.485 1.475 diameter after the plate Z 1.485 1.475 diameter after the plate </p>	<p>0.001-0.0010 Loose on diameter</p>	<p>One hoop of 0.040 diameter PWA 704 sleep braun were Note For this run 0.040 were not available and 0.034 diameter were used individually</p>	<p>All details checked thoroughly with PNC 9015 checked. Based on 1790 100272 for 10.15 minimum in hydrogen atmosphere As checked in laser</p>	<p>"Q" received 11 degrees to its insulative position as installed in S/O/S inspector Note No. 1 White OD surface did not require N₂ plate insulation and was acceptable for plating all surfaces ready</p>
Page 2	<p>Same as No. 1</p>	<p>Same as No. 1</p>	<p>Same as No. 1</p>	<p>Same as No. 2</p>	<p>Same as No. 1</p>	<p>Sample with not fast welding in base fixture and did not minimum 11 degrees for condition</p>
Page 3	<p>Same as No. 1</p>	<p>Same as No. 1</p>	<p>0.004-0.0020 Loose on diameter</p>	<p>Same as No. 2</p>	<p>Same as No. 1</p>	<p>"Q" received 11 degrees to its insulative position as installed in S/O/S inspector</p>
Page 4	<p>Same as No. 1</p>	<p>Same as No. 1</p>	<p>Same as No. 4</p>	<p>Same as No. 2</p>	<p>Same as No. 1</p>	<p>Measured welding in base and to fixture position</p>

Minute voids in the braze joint were assumed to have been caused by fabrication of the parts. As noted in table LXXII, these parts were totally nickel plated per AMS 2404 (electroless). This process was in the development stage and several plating and stripping operations were required to obtain a good bond between the nickel and parent materials, and to meet blueprint dimensions. Repeating these operations resulted in pitting the surfaces of the simulated spraybar. It was assumed the pitted condition of the simulated spraybar had led to voids detected in the braze joint. Based on this, new simulated spraybars were fabricated in the same manner as spraybar No. 1.

(b) Braze No. 2

Two errors occurred in the fabrication of this spraybar assembly. The spraybar had no nickel or silver plating on the larger diameter or on the inside face of the shoulder. When brazed, the silver braze material from the circular braze loop did not wet on the simulated spraybar, but spread on the exterior surface of the simulated injector housing. In addition, the sample was not properly installed in the braze fixture designed to hold the part in the 11 deg clockwise rotation during brazing. During brazing the part rotated back to an upright position.

As a result of these errors, no examination was made of this assembly because information regarding a fillet around the shoulder and penetration into the joint was considered invalid for this investigation.

(c) Braze No. 3

The simulated spraybar for this assembly was erroneously fabricated without nickel or silver plating on the large diameter and inside face of the shoulder. The sample was tack welded in the fixture and brazed in the same way as spraybar No. 1.

The results of the shoulder fillet and joint penetration were identical to that of spraybar No. 2

Microscopic examination revealed approximately 80 to 90% braze coverage in the joint. It was also noted that small voids, like those obtained in spraybar No. 1, were not present, and bonding appeared to be good.

Pry testing, with a hammer and chisel, was also performed to determine the strength quality of the joint. After several attempts, it was found that the parts could not be separated.

Because the results of brazed spraybar assemblies No. 2 and 3 were incomplete, two additional assemblies were fabricated. As can be seen in table LXXII, two additional spraybar assemblies were fabricated with several changes. The changes are described below:

1. The simulated spraybar for assemblies No. 4 and 5 was fabricated in the same basic configuration spraybar assemblies as No. 1, 2, and 3. The previous assemblies required pressing the parts together. It is believed the pressing action scraped and marred the plated parts. To reduce this damage and allow easier assembly, the base of the spraybar was chamfered.

The chamfer provided a guide for inserting the piece in the simulated injector housing, and it reduced the sharpness of the leading edge. The base of the cap of the spraybar was also chamfered. This allowed the circular loop of braze wire to seat in the chamfered area. This was intended to promote capillary action at the cap and housing interface.

2. To aid in assembly, the simulated injector housing received chamfers at both ends of the inside diameter. Both ends were chamfered so the simulated spraybar could be inserted from either end to avoid possible errors in assembly. The chamfer ensured the spraybar was seated flat and it provided a volume for an additional fillet that added to the sealing capability.
3. To increase the braze fit, the clearance between mating parts was increased. From the 0.0001 to 0.001 in. allowable difference in diameters of the simulated injector housing and spraybar of the first three assemblies, the allowable difference was increased to 0.0004 to 0.002 in. The increased difference served to aid in assembly while remaining within allowable clearances for silver brazing.

(d) Braze No. 4

1. X-ray inspection did not reveal any detectable voids in the brazed joint. Braze coverage was greater than 90%.
2. Microscopic examination revealed 100% bonding in the braze joint. There was full penetration from the braze loop into the joint at the shoulder interface and the inner fillet was filled with braze material. Voids were not visible under microscope.
3. The fillet around the shoulder was continuous. As in assembly No. 1, the amount of fillet material varied from top to bottom.

Assembly No. 4 was used to verify the changes made from the previous test spraybar assemblies. The added chamfers made assembly easier and reduced the damage to the plated surface. The increased clearance between the mating parts also made assembly easier, and the braze coverage remained complete.

(e) Braze No. 5

The X-ray and microscopic examination revealed the same results as those obtained in No. 4. X-ray did not reveal any voids, and examination by the Materials Development Laboratory rated the braze coverage at 100%. All fillets were completely filled and continuous and the only variation was caused by gravity flow. This variation was slight.

Assembly No. 5 underwent a pressure test designed to simulate the operating conditions in the injector. After brazing, a manifold was welded to the back side of the simulated housing piece. The sample then underwent two pressure tests. The pressure load was against the base of the simulated spraybar and approximately 65% greater than the operating ΔP . The first test was a hydrostatic test

at 1500 psig for 5 minutes, and the second was the same conditions, but with gaseous helium as the pressurizing medium. Neither test revealed signs of leaks or failure.

It was concluded that to obtain complete braze coverage achieved in samples No. 4 and 5, the following braze procedure used on these assemblies should be followed.

1. Silver braze is acceptable as a braze medium in the second braze cycle; however, nickel plating of all braze surfaces is a prerequisite for silver brazing
2. The 0.0004 to 0.002 in. variation in diameters of mating parts allows ease in assembling while providing good braze coverage
3. The chamfer on the leading edge of the hole in the injector housing guides the spraybar into the hole and provides an additional fillet for strength and sealing
4. Chamfers on the edges of the spraybar base also serve to guide the piece into the injector housing while reducing the possibility of damage to the plated surfaces. Chamfers also provide a seat for the braze material to form fillets.

Because of different coefficients of thermal expansion associated with two different metals, Inconel 718 housing and Inconel 625 spraybar, and the bulk temperature differential between the two created during operation, the silver braze joint experiences a tensile force of 13,000 lb. A test program was run to verify the braze joint could withstand the expected tensile stresses.

Nine test plates were fabricated simulating the spraybar and housing configuration. Plates of Inconel 718, shown in figure 526, received a hole identical to that specified for the injector housing to accept the medium spraybar. Disks of Inconel 625 were cut to the identical outside diameter for the medium spraybar. All plates and disks were nickel plated and then braze material was applied to the disks by silver plating according to blueprint specifications for the spraybar detail. The disks were placed in the holes of the plates, and brazed in a manner simulating the injector braze cycle.

No extra silver wire material had been placed adjacent to the braze joint on the test sample, as will be done on the injector, because a fillet was not desired on the test samples. This differed from the injector specifications because uniform braze thicknesses and flat surfaces were necessary for test specimens to accurately determine the stressed area. The result of this deletion was the creation of voids because of lack of braze material in the joint. This was repaired by an addition of braze wire and a second similar braze cycle. This repair created an end result that was representative of the braze in the injector.

Each brazed specimen was machined to the typical tensile specimen configuration shown in figure 527. Two brazed regions remained in the gage section of each specimen. The region was not more than 45 deg of the braze joint. The arc was kept small to create mainly tensile forces and nearly eliminate shear forces on the joint when the specimen was located in tension. In the first series of tests, two equal braze sections received identical stress loads and only the

weaker section failed. Thus, with each data point obtained, there was a second point of equal or greater strength.

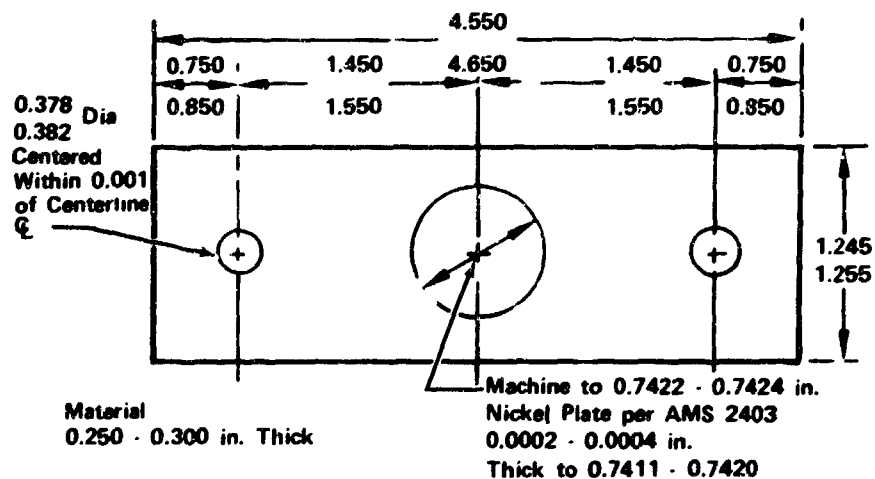


Figure 526. Plates of Inconel 718 Machined to Accept Medium Spraybar

FD 46629



FE 88091

Joint Location - Spraybar to Housing
Braze Material - Pure Silver
Method of Application - Plating
Leak Checked - 1500 psid (GHe)

Figure 527. Spraybar Braze Technique Substantiated

GS 12310

The first tests were made to determine the ultimate tensile strength of the braze joint at room temperature and 1060°R. Two specimens were run at room temperature, and each tested at two joints. The lowest ultimate tensile strength of four braze joints was 54,800 lb. At 1060°R, the lowest ultimate tensile strength of four specimens was 36,820 lb, which is nearly three times the expected stress load.

Tensile specimens were created from each tested braze joint. The remaining joints had undergone stress loads that had failed their sister joints, and the ultimate tensile strength of the remaining joints was high. The specimens were tested at 760°R and 1260°R. Figure 528 shows a plot of all data from the tensile specimens.

The qualified specimens were used to examine the effect of cyclic loading. The spraybar-to-housing braze joint must withstand 13,000 lb tensile load for 300 cycles. Three specimens were tested repeatedly at various stress loads of 23, 30, and 33 K psi while at 1060°R. A fourth specimen was run at 23 K psi, but at 1260°R. The loads were cycled until the braze joint failed in fatigue. The test data shown in figure 529 shows the design point is well within the safe region.

The use of silver braze to join Inconel 625 to Inconel 718 provides a strong joint. This joint withstood expected stress of a one time extreme stress load and repetitive stress loads present in actual operation.

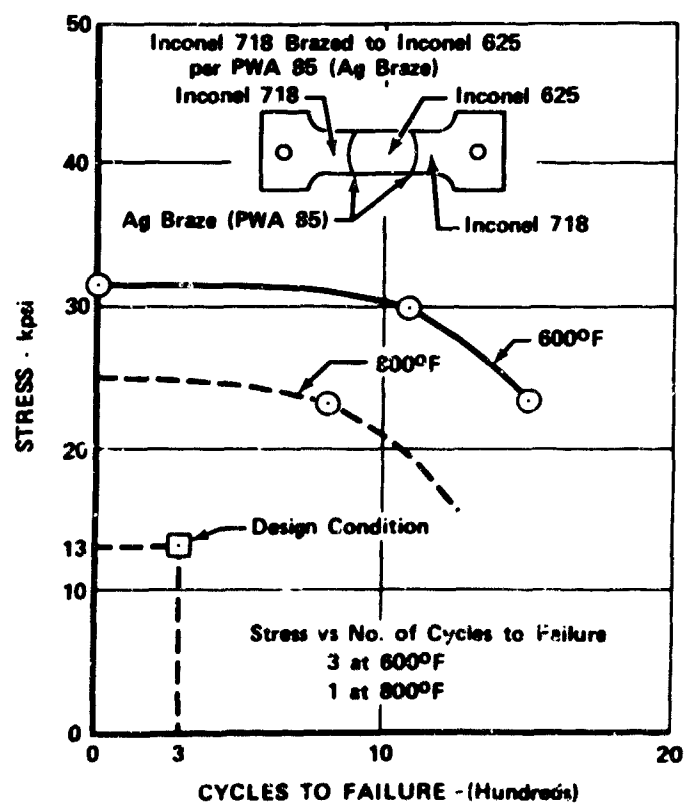


Figure 528. Tensile Specimen Data Plot

FD 46630

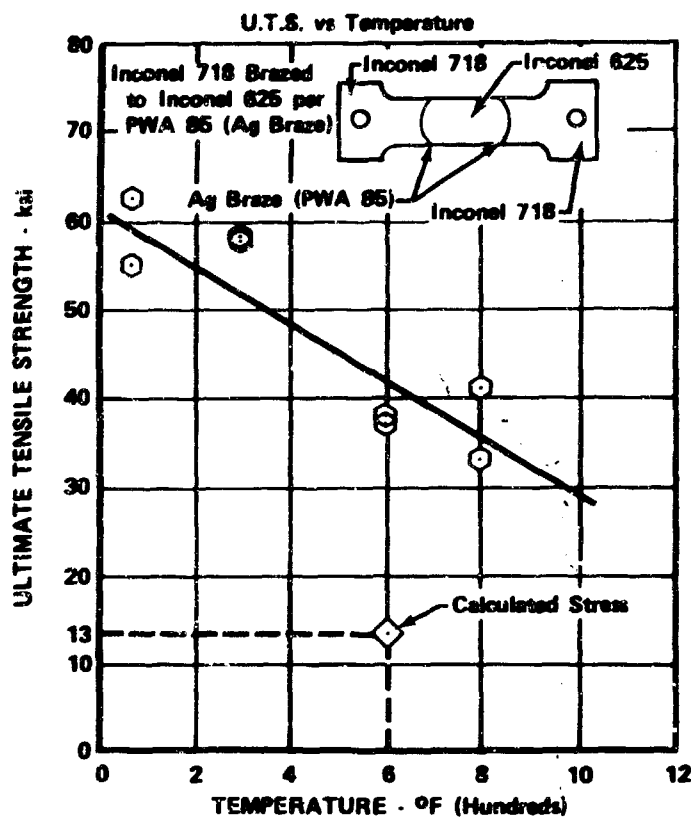


Figure 529. Cyclic Loading Tensile Specimen Data FD 46631

Bill-of-material spraybars were placed on order and the following quantities received:

Long Spraybars	28
Medium Spraybars	28
Short Spraybars	54

c. Injection Elements

Consistent with Phase I main burner injection element experience, TD nickel was chosen for high strength and high thermal conductivity as the element material. Raw tubing was procured from which the finished elements would be fabricated.

d. Porous Faceplate

To substantiate the main burner injector faceplate design, experimental data on thick Rigimesh were required. A test program was defined and sample 18 in. x 18 in. x 1 in., thick plates were ordered from Aircraft Porous Media. The plate consisted of 44 layers of L-605 plain dutch weave wire. The target flowrate of this Rigimesh is approximately 350 scfm at 2 psid. A total of four pieces of Rigimesh is necessary for complete property evaluation. The material properties that are needed are shown in table LXXIV. The first sheet of Rigimesh would be used to complete the minimum tests shown in the chart. The information

from the minimum tests as well as the flowrate through the test sample allows an early judgment on the predicted strength and flowrate of the Rigimesh prior to fabricating the remaining three Rigimesh pieces. If either flowrate or strength were too low, the remaining pieces of Rigimesh could be changed by increasing or decreasing the number of layers of wire. Increasing the number of layers increases the strength while decreasing the flowrate.

Table LXXIV. Rigimesh Material Property Program

Property	Temperature and/or Direction	Minimum Test	Complete Test
Tensile	Perpendicular weave	1	3
	45 deg weave	1	3
	Parallel weave	1	3
	1760° R	-	4
	2060° R	1	4
		<u>4</u>	<u>17</u>

Tensile will obtain 0.2% yield strength, ultimate, and modulus.
Sample size 13-1/4 x 2-1/4 x 1 in.

Compression	Room Temperature	1	4
	2060° R	1	4
		<u>2</u>	<u>8</u>

Compression will obtain 0.2% yield strength and modulus. Sample size 5 x 1-1/4 x 1 in.

10 hr Stress Rupture	2060° R	1	4
-------------------------	---------	---	---

Sample size 13-1/4 x 2-1/4 x 1 in.

Flex Bending	1760° R	1	4
--------------	---------	---	---

Sample size 6-1/4 x 1-1/2 x 1 in.

Shear	1760° R	1	4
-------	---------	---	---

Sample size 2-1/4 x 2-1/4 x 1 in.

Total minimum test 9 pieces

Total complete test 37 pieces

To expedite evaluation of the 1 in. thick Rigimesh, the first sample was ordered using N-155 material instead of L-605 because the N-155 was on hand. The first plate was received and air flow tested to determine if porosity was uniform. The data indicated that flow varied from 204 to 264 scfm at 2 psid. This level showed uniformity that was acceptable, but density was higher than requested.

Visual examination of the Rigimesh (N-155) revealed numerous cracks on one side of the Rigimesh plate. The cracks were irregular in shape, size and direction. The opposite face of the plate has fewer cracks and generally were confined to the edges of the plate. The cracks are as deep as 3/32 in., which crosses approximately four layers of wire. X-ray of the Rigimesh (N-155) plate indicates the cracks are on the outer surfaces only, with no hidden cracks inside the plate. One surface of the plate had some areas near the edge of the plate that lacked porosity. This lack of porosity was caused by incipient melting during the sintering process.

Neither of the two conditions described appear insurmountable. The rolling process must be adjusted to avoid outer layer cracking and the sintering time and temperature process must be corrected to avoid incipient melting.

The Rigimesh (N-155) plate will not be used for material property testing. The plate was returned to the vendor and further work was terminated because of the program redirection.

e. Main Burner Torch Igniter

Fabrication of the main burner torch igniter was withheld because of the program redirection.

D. MAIN BURNER CHAMBER

1. Introduction

Main burner thrust chamber design is based on the copper wafer transpiration cooled thrust chamber demonstrated during Phase I (Contract AF04(611)-11401).

A design study of the transpiration cooled wafer liner was conducted to provide an outer case and chamber liner that would meet the weight limitations of Phase II and eliminate the radial pressure load on the combustion chamber inherent in the Phase I design. A number of main burner chamber liner configurations were studied and the selection of the best design was based on the criteria of heat transfer and pressure drop, structural and mechanical integrity, and weight.

The selected design included internal coolant passages in the cylindrical section that eliminated the buckling load present in the Phase I design.

The incorporation of this internally cooled design, permitting a reduction in liner wall thickness, reduced the outer shell-to-injection flange bolt circle diameter. This resulted in a reduction of Phase I hardware weight to meet the Phase II contractual weight requirements.

2. Summary, Conclusions, and Recommendations

The design of the main burner chamber was completed, procurement of raw material initiated and fabrication started on the long lead time items.

Structural and heat transfer studies indicated a cylindrical copper chamber in the forward section, externally manifolded for cooling, would solve the buckling problems of Phase I and reduce weight because of a smaller bolt circle. It was

determined that a liner having metering orifices axially installed, and accessible from the rear of the cylindrical liner, was more desirable than one having orifices installed radially. Removal and replacement of the radial orifices necessary during flow optimization, would require prior removal of other engine and rig hardware. The axially attached orifice scheme selected consisted of 95 orifices. Each orifice discharged into a coolant tube brazed internally to the liner. Welding these tubes to the chamber endplate provided additional structural support to the stackup. Further refinements in the heat transfer study indicated that a 60 orifice axial design was sufficient to produce equal coolant distribution in the chamber and was selected for the final design.

A weight reduction, compared to Phase I hardware, resulted because the heat exchanger wall thickness was reduced from that used in Phase I. This was possible because the radial pressure loading of the copper chamber coolant was eliminated.

Design considerations of the throat and rear sections were basically unchanged from Phase I hardware because Phase I incorporated internally cooled manifold passages in the throat and rear sections. Major changes were the number of coolant zones and the heat exchanger wall thickness. The coolant zones, numbering 24 in Phase I, were increased to 28 in Phase II to permit more selective cooling in local areas. For detailed information refer to mechanical description section of the Design Milestone Report AFRPL-TR-70-6.

Because of the difficulty in etching satisfactory spiral grooves in the wafer plate during Phase I, special attention was given while etching spiral grooves during Phase II. Several vendors were contacted for price quotations on etched wafer plates and they were requested to furnish product samples having deep etching. Phase I and 50K photo masters were provided to those vendors indicating interest in fabrication. Requirements included consistency of spiral grooves on both the individual plates and from plate-to-plate. Grooves consistent in size and shape were required to display accuracy in the cross sectional flow area determination. The 50K plate samples were desirable because tooling was available to individually flow these plates. This flow tooling provided an excellent check for consistency of accuracy in spiral grooves. The basic drawback encountered by vendors was inexperience with deep etching and other associated problems such as slot side etching.

The fabrication authorization of Phase II hardware was issued and procurement of raw material was initiated. To provide a high-strength material outer case, Inconel forgings were purchased. Copper plate was purchased with a smooth finish on one side to afford good reproduction of the photo masters.

3. Hardware Description

The main burner chamber, whose location is shown in figure 530, consists of two main components: an outer pressure shell shown in figure 531 fabricated of Inconel 718 (AMS 5662) and a transpiration cooled copper (AMS 4501) chamber liner, shown in figure 532. In addition to functioning as the primary structural member, the outer pressure shell, shown in figure 533, provides coolant flow-paths to the chamber liner and also serves as a mount for attaching two sections of the chamber liner. Forward and rear flanges are provided for attaching the assembly to the transition case duct, main burner injector, and primary nozzle. The copper cylindrical wafers forming the chamber liner are divided into 28 zones.

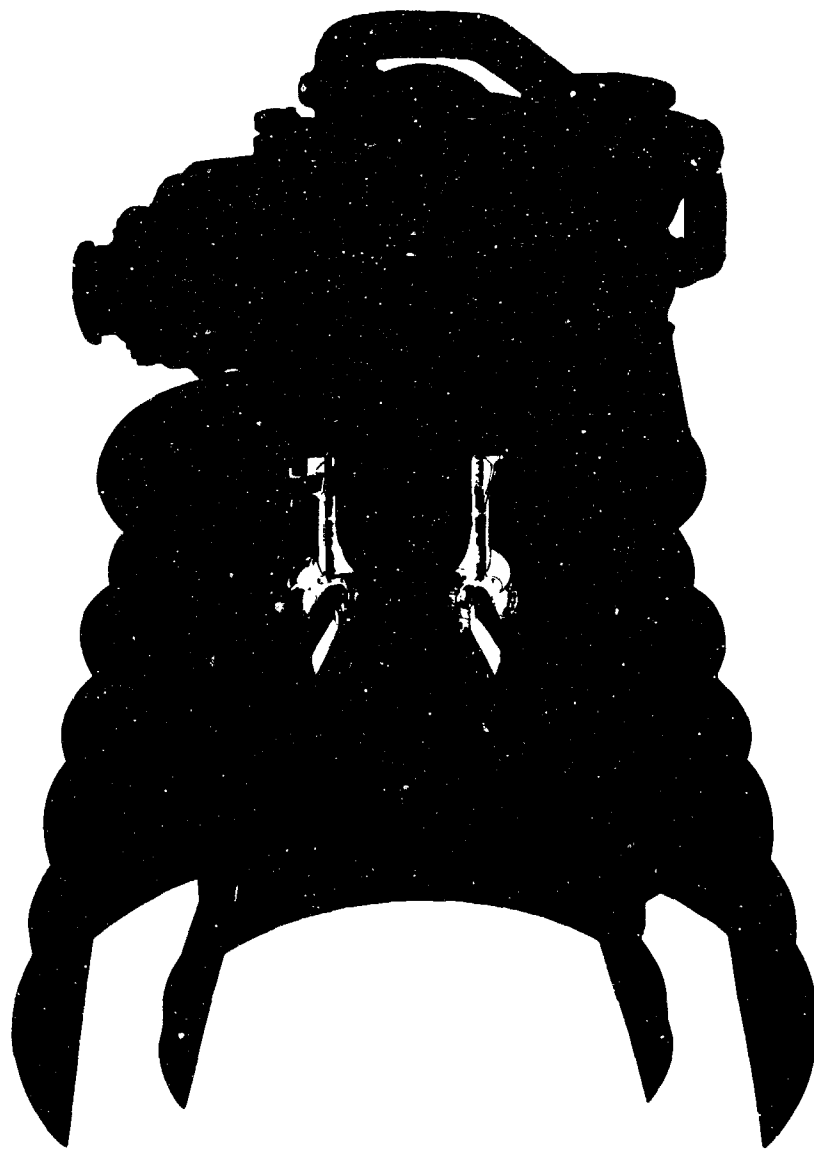


Figure 530. Location of Main Burner Chamber Assembly

FD 31413

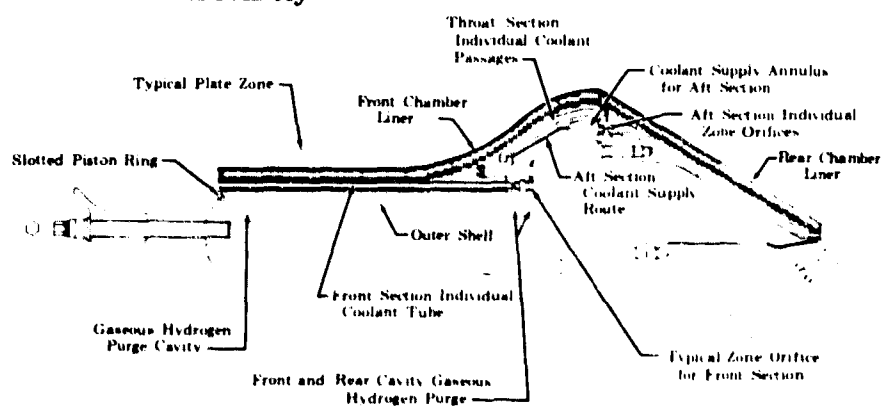


Figure 531. Main Burner Chamber Assembly, Side View

FD 31972A

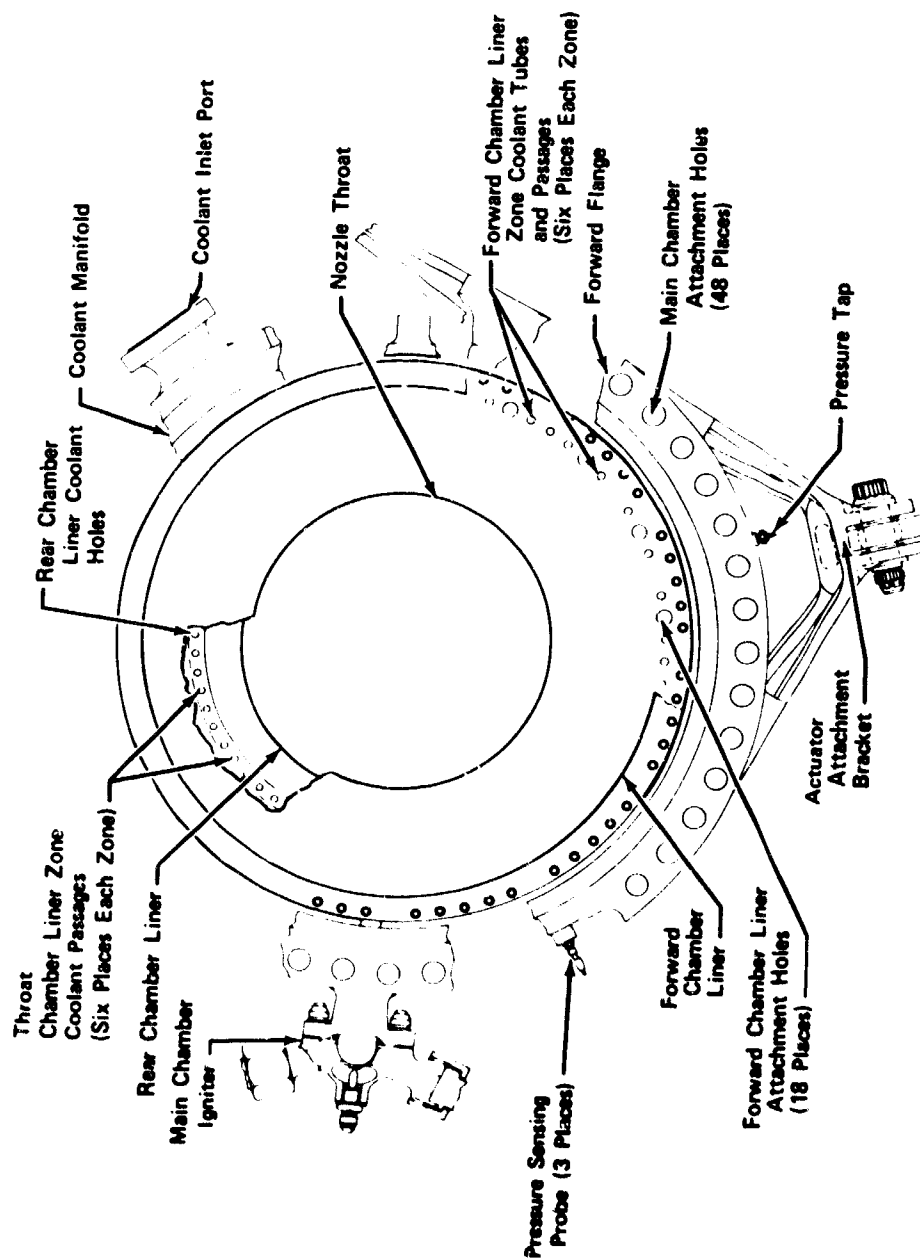


Figure 532. Main Chamber Assembly, View Aft

FD 31362B

Item	Function	No.
A	Forward Chamber Liner Coolant Supply, Zones 11 Through 17	42 Places
B	Forward Chamber Liner Coolant Supply, Zones 1 Through 10	60 Places
C	Rear Chamber Liner, Coolant Distribution Ring Coolant Supply, Zones 18 Through 28	12 Places
D	Rear Chamber Liner, Throat Plane Orifices, Zones 18 Through 28	66 Places

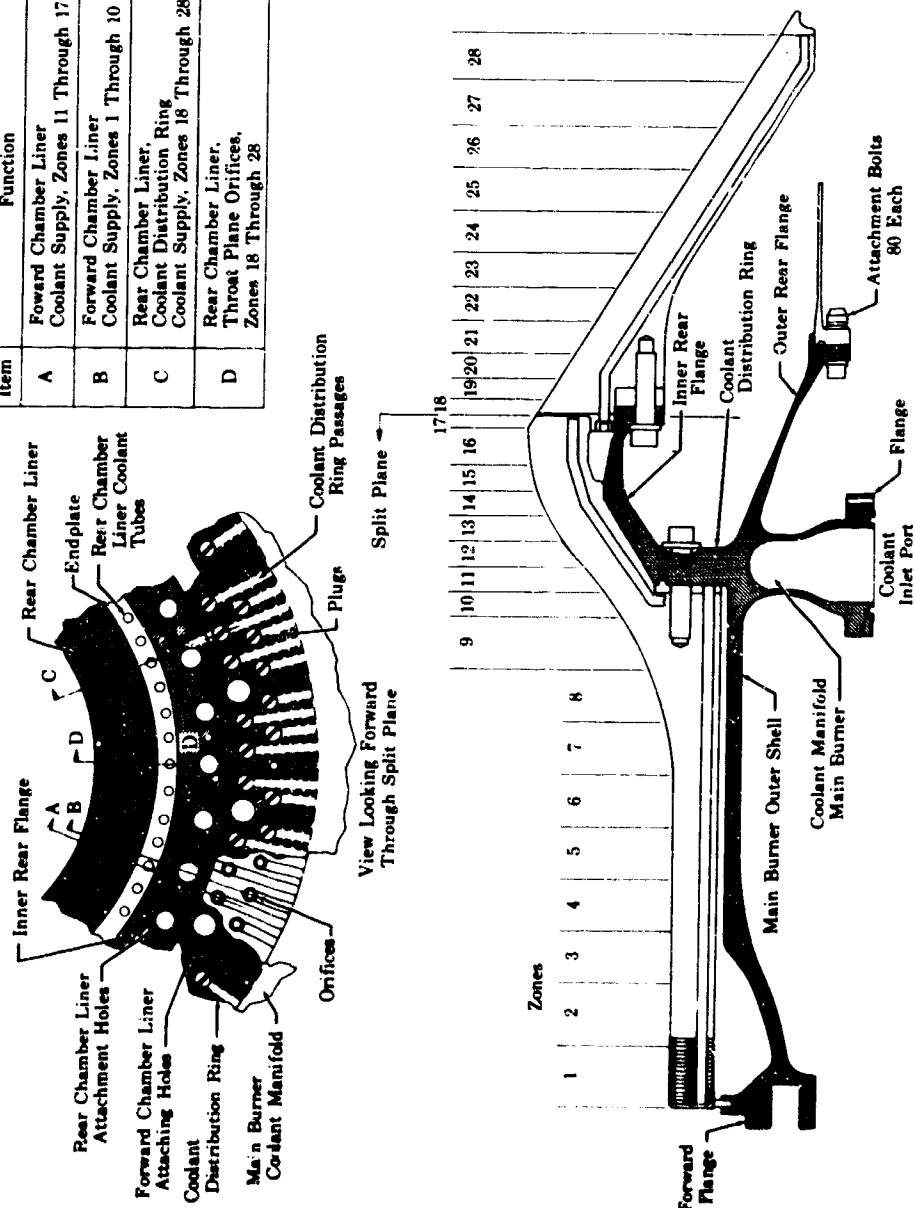


Figure 533. Main Burner Chamber, Side View

FD 31359

One zone is a collection of wafers fed by interconnecting zone coolant manifolds. Each wafer consists of a front and a back plate. Coolant is supplied to a zone coolant manifold from the main chamber coolant manifold in the outer shell, and routed through coolant tubes or passages internal to the liner.

Instrumentation for evaluating performance consists of a chamber pressure tap in the forward flange of the chamber shell and three Kistler dynamic pressure transducers. The instrumentation locations are isolated in various zone sections so that flow cooling in the region of the tap can be locally controlled. Two taps are in zone 2. One is in the zone 2 igniter sector and the other in a sector 180 deg from the igniter. The third transducer is in zone 6. Zone 6 wafers are dammed to isolate the probe for local evaluating. Like the igniter, dynamic pressure transducers penetrate the chamber shell and liner.

Temperature instrumentation consists of thermocouples imbedded in the heat exchanger to measure metal temperature at one-third and three-quarters of the distance from the hot wall to the heat exchanger outside diameter. Six plates contain these thermocouples, and their data are used to determine thermal gradients. The cold wall temperature is measured by thermocouples attached to the liner in two locations. The hot side wall of the liner is coated with temperature indicating metallic coatings.

In addition to liner instrumentation, the inner surfaces of the chamber shell are coated with temperature indicating metallic coatings. Thermocouples are also installed to check the adequacy of purge gas flow in maintaining the wall temperature below 540°R.

a. Outer Case

The main burner chamber coolant manifold was sized for the allowable pressure drop stated in the design criteria. This manifold feeds coolant to passages in the coolant distribution ring. The coolant distribution ring, which supports the transpiration cooled chamber liner, contains orifice plugs that control the coolant flow to the passages in the forward section of the chamber liner (figures 534 and 535). Orifices in the front section are accessible by removing the primary nozzle and then removing the plugs that back up the orifices in the coolant distribution ring. Orifice plugs controlling the pressure in the rear section of the chamber liner (figures 536 and 537) can be changed by removing the primary nozzle and the rear section of the chamber liner. Changing the rear section supply orifices requires removal of the front section in addition to the components.

Loads on the inner rear flange, upon which the rear section of the liner chamber is bolted, cause an increased closing deflection at the seal; thus, a flat-face flange is sufficient at this location.

Two gimbal actuator links are welded to the outer shell 90 deg apart. The load is transferred into the forward flange and the coolant distribution ring, passing close to the centroids to minimize twist. The gimbal actuator load is considered a distributed load whose summation equals four times the maximum axial load absorbed by the case. Using this conservative assumption, the low stress value in this area indicates a capability to withstand actual loading conditions.

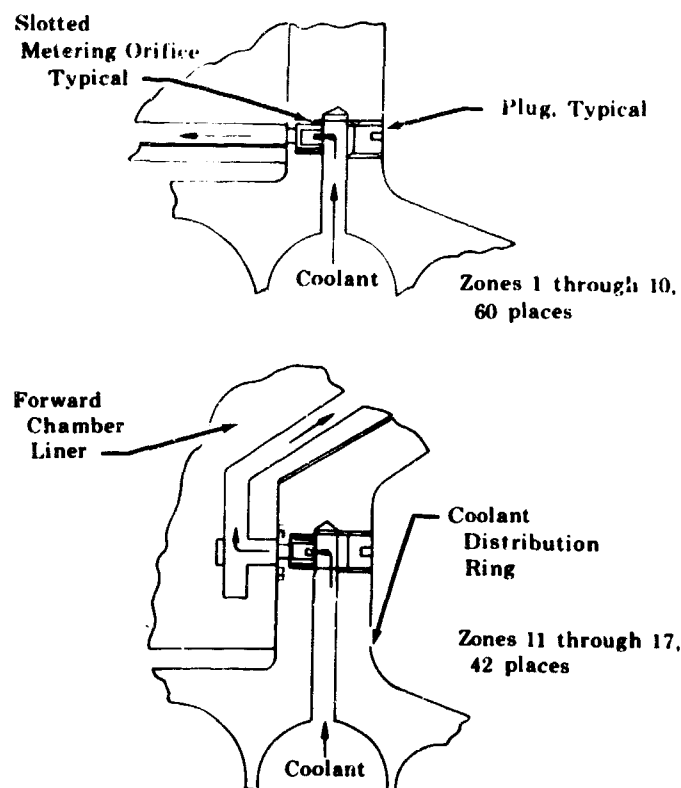


Figure 534. Forward Chamber Coolant Metering FD 31367

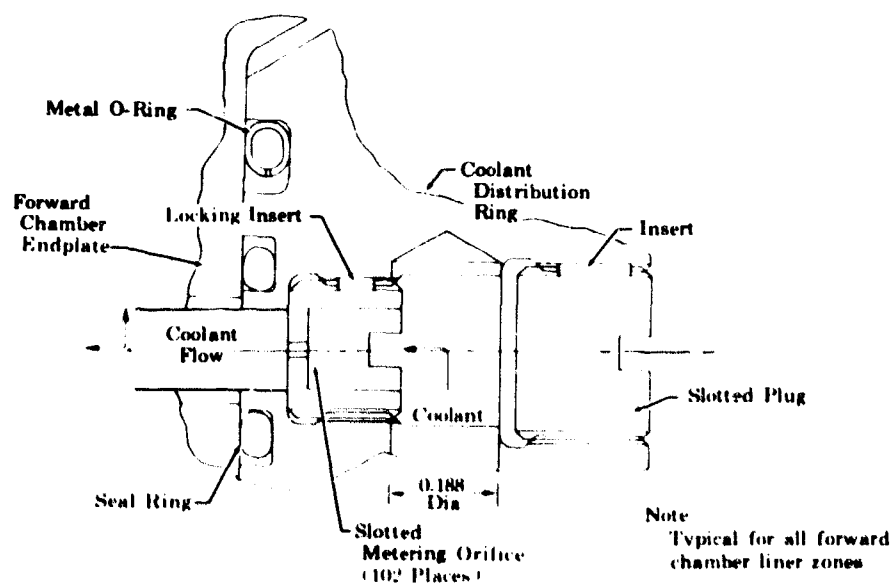


Figure 535. Forward Chamber Liner Coolant Metering Installation, Side View FD 31364

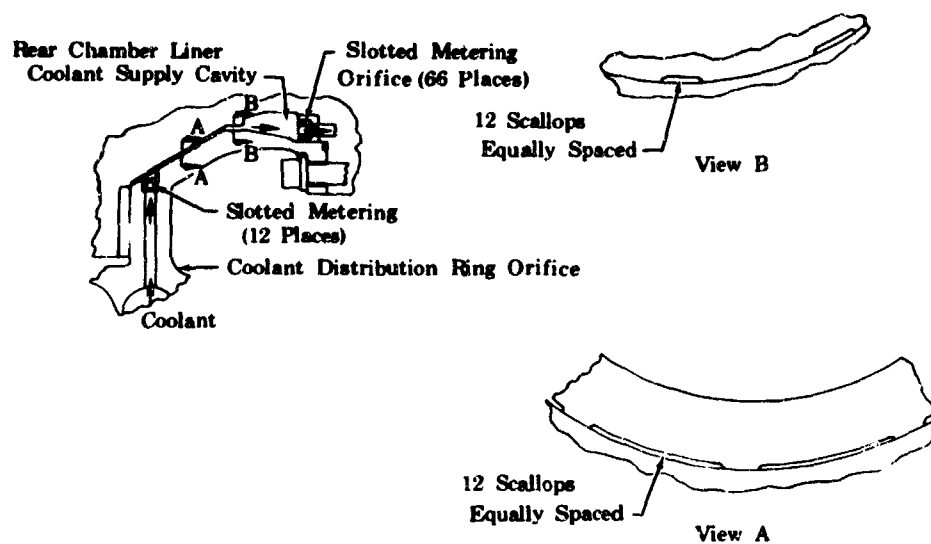


Figure 536. Rear Chamber Liner Coolant

FD 31365

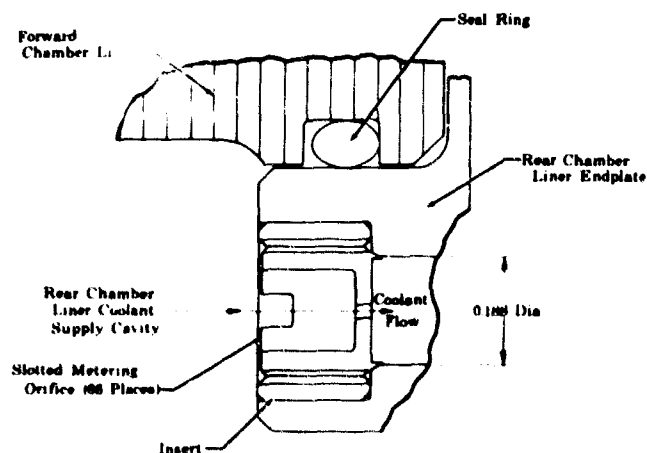


Figure 537. Rear Chamber Liner Coolant Metering, Side View

FD 31363

To maintain the outer pressure shell temperature at the required maximum of 540°R, combustion gases from the main burner chamber are prevented from entering the annular gap, between the front combustion chamber liner and the outer shell, by a purge gas flow entering through an orifice in the coolant manifold. If the magnitude of the circumferential pressure gradient is such that purge gas flow alone will not prevent hot gas circulation, a slotted piston ring forming a flow resistance will be employed.

This purge gas flow is also employed in the annular gap between the rear combustion chamber liner and the outer shell. However, because the pressure required for purge gas flow is low in this area, a spring type of seal attached to the primary nozzle is used. This seal, acting as a check valve, prevents hot gas circulation and permits purge gas venting.

b. Transpiration Cooled Liner

In addition to forming the main burner chamber contour with the inside diameter of the brazed wafer liner, each individual wafer functions as a porous heat exchanger (figure 538). Spiral groove patterns photoetched into one side of each wafer half provide the path from the zone coolant manifold to the inside diameter of the chamber where they open into the main burner chamber. Coolant is supplied to a zone coolant manifold through six passages each having an individual orifice at the coolant distribution ring. The manifold distributes coolant circumferentially to spiral grooves beginning on the inside diameter of the annular manifold and continuing to the inside diameter of the chamber.

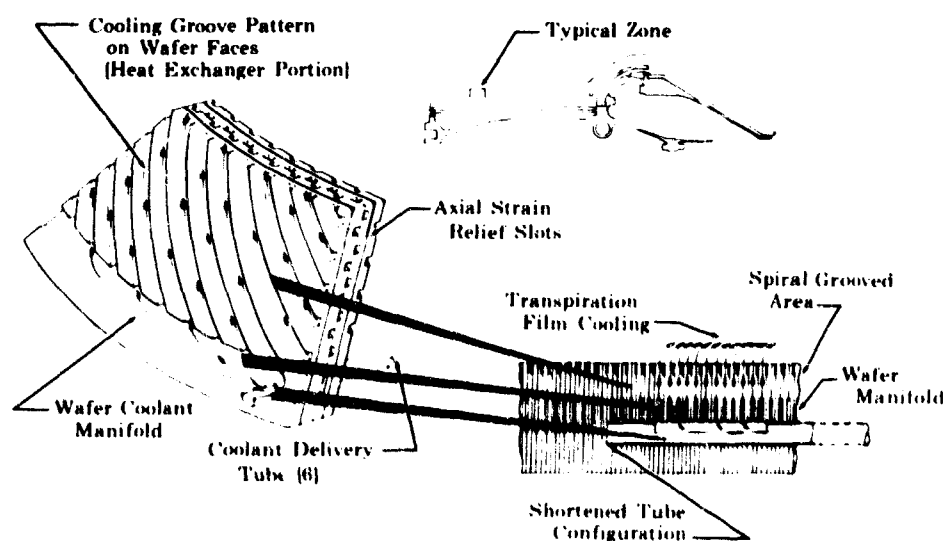


Figure 538. Typical Cylindrical Wafer

FD 31356

The spiral grooved area forms the heat exchanger. The spiral is logarithmic with an entrance angle of 6 deg. This small angle allows the coolant to be injected into the chamber so that it tends to remain along the hot surface rather than immediately mixing with the hot gas stream, thereby reducing the heat transferred to the wall and promoting the coolant film effect. The effective internal heat transfer coefficient is also enhanced by the turbulence caused by arranging the wafers so

that adjacent spiral grooves at the wafer interface run in opposite directions. The small angle also results in maximum internal surface area per unit volume of material.

The combustion chamber section has 10 zones fed by 60 stainless steel, type 347 (AMS 5575) tubes brazed to the liner. This eliminated buckling pressure which occurred during Phase I of Contract AF04(611)-11401, by moving the manifolding function to within the copper chamber liner. The tubes have the inner half of their cylindrical section removed along the axial distance, coinciding with the width of the zone they feed. Zone coolant manifolds or slots connected to the coolant manifolds intersect the tubes in this area where the inner half of the tubes are removed to form the flowpath for the coolant. The remainder of the forward section of the chamber liner contains seven zones fed by 42 drilled passages. The drilled coolant passages terminate at the aft end of the zone they feed. Slots intersect the coolant passages to form the flowpath to the zone coolant manifold.

The rear section of the chamber liner coolant distribution pattern is similar to that previously described, with 11 zones fed by 66 drilled passages. Coolant pressure is controlled by 66 orifice plugs in the front endplate. Twelve orifice plugs in the coolant distribution ring control manifold pressure feeding these 66 orifice plugs.

A minimum heat exchanger radial thickness of 0.3 in. was chosen because a thinner heat exchanger would require additional material on the heat exchanger outside diameter to compensate for the lower strength of heated copper. Also, as radial thickness is decreased less than 0.2 in., coolant mass flux requirements increase greatly. As radial thickness is increased, the liner diameter increases, thus increasing the bolt circle diameter and the weight of the chamber housing.

Because it was mechanically difficult to insert the main burner igniter torch through the transition case, the igniter torch enters the main burner chamber radially through the outer shell (figure 539) and the front section of the liner. To keep performance losses associated with the required coolant overflow of the penetrated zone to a minimum, the igniter torch region is isolated from the rest of the zone so that only a small percentage of the zone requires over-cooling. This is accomplished by including narrow radial dams across the spiral grooves to form a 60 deg sector (figure 540) when photoengraving the grooves. The igniter boss is also designed to accept a pulse gun, figure 541. During staged combustion testing, the chambers will be pulsed to evaluate combustion stability.

4. Fabrication

a. Outer Case

A one-piece outer case serves as the outer structural shell for the forward transition-cooled liner and also is used to support the rear liner. In addition, the outer case contains the coolant distribution manifold for liner coolant and supports the primary and two-position nozzle.

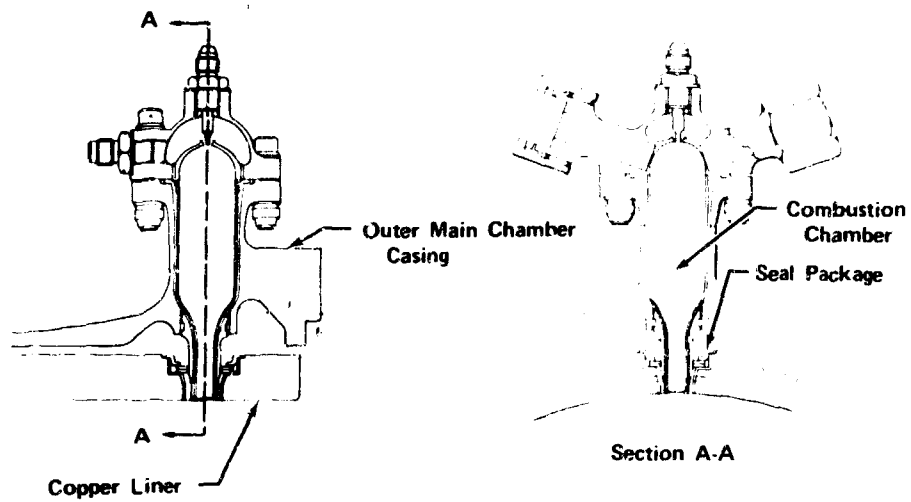


Figure 539. Igniter Incorporated In Main Chamber Wall FD 33026A

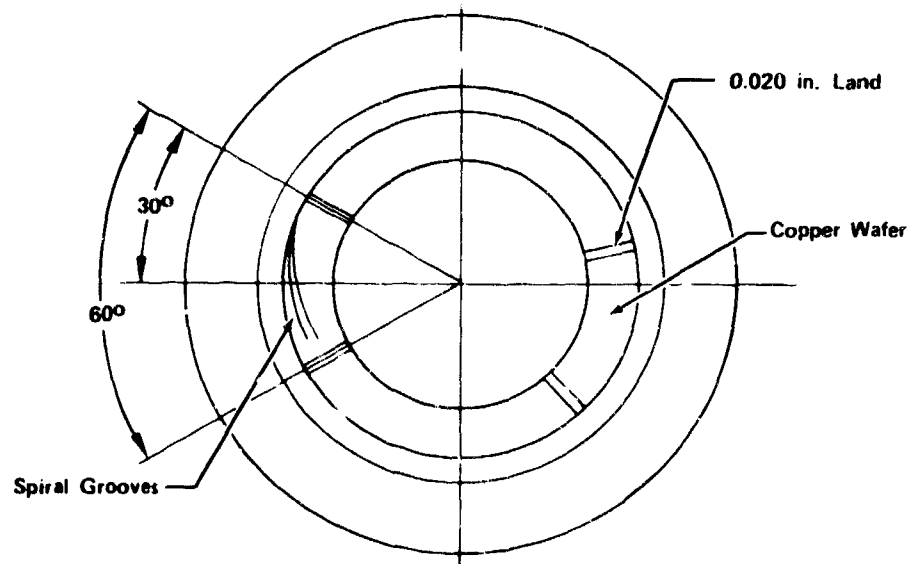


Figure 540. Location of Lands on Chamber Wafer FD 35254

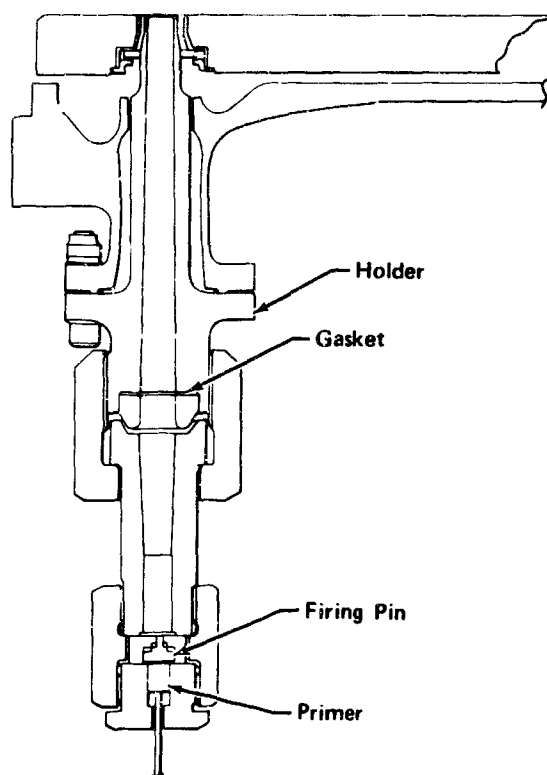


Figure 541. Pulse Gun Installation In Igniter Boss FD 35431

The outer case has four locating flanges. The forward flange of the outer pressure shell is fastened to the transition case and main injector flange by 48 Inconel 718, 9/16-in. diameter studs. The outer rear flange is fastened to the primary nozzle with 80 Inconel 718, 1/4-in. diameter bolts. The inner rear flange is fastened to the rear transpiration liner sections by 36 3/8-in. Inconel 718 bolts. The forward transpiration liner attaches to the coolant manifold ring bolt circle.

In order to provide a high strength outer case and ensure a lightweight design, an Inconel 718 forging was selected as the housing material. The design of the case included a lightweight line-of-action flange at the main burner injector interface. This was advantageous over a standard cantilever flange from the standpoint of weight savings. In addition, the line-of-action flange reduces flange twist by passing the shell load approximately through the centroid of the flange cross sectional area. Because the case is a spherical configuration immediately downstream of the main injector, an increased section is provided between the spherical and downstream cylindrical sections of the liner to take the additive hoop load.

The manifold is formed by welding an outer manifold, segment ring to a matching manifold segment ring that was part of the main housing forging.

The gimbal actuator arms attach to gimbal actuation links which are welded to the outer shell in two positions 90-deg apart. Each actuator link is machined from a one-piece forging.

Procurement of outer case details was initiated for Phase II designed hardware as outlined in the hardware description of this report. Table LXXV tabulates the material delivery dates.

Table LXXV. Material Delivery Dates

Item	Placement	Delivered	Quantity
Copper Wafer	8-7-69	12-30-69	2025
Outer Case Forgings	8-1-69	2-11-70	3
Coolant Manifold Ring Forging	8-1-69	9-17-69	3
Coolant Manifold Flange	8-14-69	9-4-69	1
Igniter Boss Forging	8-14-69	9-15-69	1

The outer case forgings were manufactured and received. Three forgings were procured, and two were required for Phase II testing. Because the forging is a long lead time item, the third piece ordered was intended for future engine testing. In the meantime, it serves as a backup for rig testing. Machining of the forgings was deferred, consequently this material was stored for future use. Ring forgings for the outer manifold segment, coolant manifold flange, and outer case igniter boss were also received but not machined.

b. Transpiration-Cooled Liner

The main burner chamber transpiration-cooled chamber liner is fabricated by stacking 512 0.040-in. thick etched copper wafer halves on brazing fixtures in two assemblies and oven brazing at 1920°R in a hydrogen atmosphere. The front assembly takes 322 wafer halves and the rear assembly 190. Silver is used for braze material and is applied on every second wafer by a plating process. Raw material for each plate is a 0.040-in. thick, 20-in. square (OFHC) oxygen free copper sheet. To produce spiral passages on the wafers, each plate half is photoengraved and etched on one side in a predetermined spiral groove. Slot etching is a chemical milling process where an etchant, generally ferric chloride with additives, is splashed on each copper wafer to remove metal from unprotected surface areas. Control of the etch rate and a balanced chemical solution is required for consistently acceptable results. An uncontrolled procedure would result in wafer plates in assorted slot sizes and flow rates. Areas of the plates to be etched are outlined by photomasters that are produced with photographic equipment. Flawless photomasters and controlled procedures are necessary to produce grooves having acceptable accuracy. Any defect on the photomaster would be reproduced on the etched plates. Because the depth of both the spiral grooves and manifold are the same, the same photomaster can be used and etching is simultaneously accomplished.

The two plate halves forming each full wafer are brazed in the stackup at the unetched centerplane. The front of the wafer halves have a thermal relief slot etched 0.001 in. deep and for a distance of approximately 0.1 in. from the inside edge of the wafer. By locating the slot in this plane, the heat exchanger

BLANK PAGE

spiral grooves on the opposite face are not affected. Zones 1 through 24 incorporate the thermal relief slots to ensure cycle life. Because thermal gradients of zones 25 through 28 are not excessive, cycle life can be met without use of thermal relief slots.

Wafers selected for a given zone are picked on the basis of the flow requirements of that zone and flow compatibility with other plates. Flow of individual wafers is checked by a fixture specifically designed and fabricated for this purpose. The fixture uses a hydraulic pressure ram to load a seal plate against the wafers etched side for accurate flow measurement. Flow media can be air or gaseous nitrogen.

Each wafer selected for the stackup is individually silver plated. Following the braze cycle, the brazed assembly is dipped in molten wax to keep the passages and slots free of chips during the subsequent machining. Following final machining and removal of the wax, the assembly is flow checked to ensure that all passages are free of obstructions.

Copper was procured for two and one half sets. The additional 50% was purchased to replace wafers that were not acceptable. Other parts pertaining to the chamber liner such as endplates, orifice plugs and seals were not ordered.

Photomasters required for Phase II wafers were completed and sent to the vendor.

The vendor began photoetching on the copper wafers and forwarded three plates produced with Phase II photomasters. These were evaluated and found to be unacceptable because of inconsistency between plates in the flow area. This was not considered a major problem, but one that required manufacturing adjustments. Because fabrication of the main chamber was deferred shortly after the three plates were produced, the vendor was unable to adjust his technique to produce acceptable wafer plates. Vendor production was halted and the raw material was returned to FRDC.

E. NOZZLES

1. Introduction

The nozzle assembly for the demonstrator engine consists of two fixed sections forming the primary nozzle and a lightweight translating section as the two position nozzle. The primary nozzle attaches to the main burner chamber at an area ratio of 5.3 and extends to an area ratio of 35. The two position nozzle extends from an area ratio of 35 to an area ratio of 75. Nozzle locations are shown in figures 542 and 543 and the XLR129 demonstrator engine nozzle assembly is illustrated in figure 544. The objective of this subtask was to design and fabricate the primary nozzle, the two position nozzle, and the two position nozzle translating mechanism.

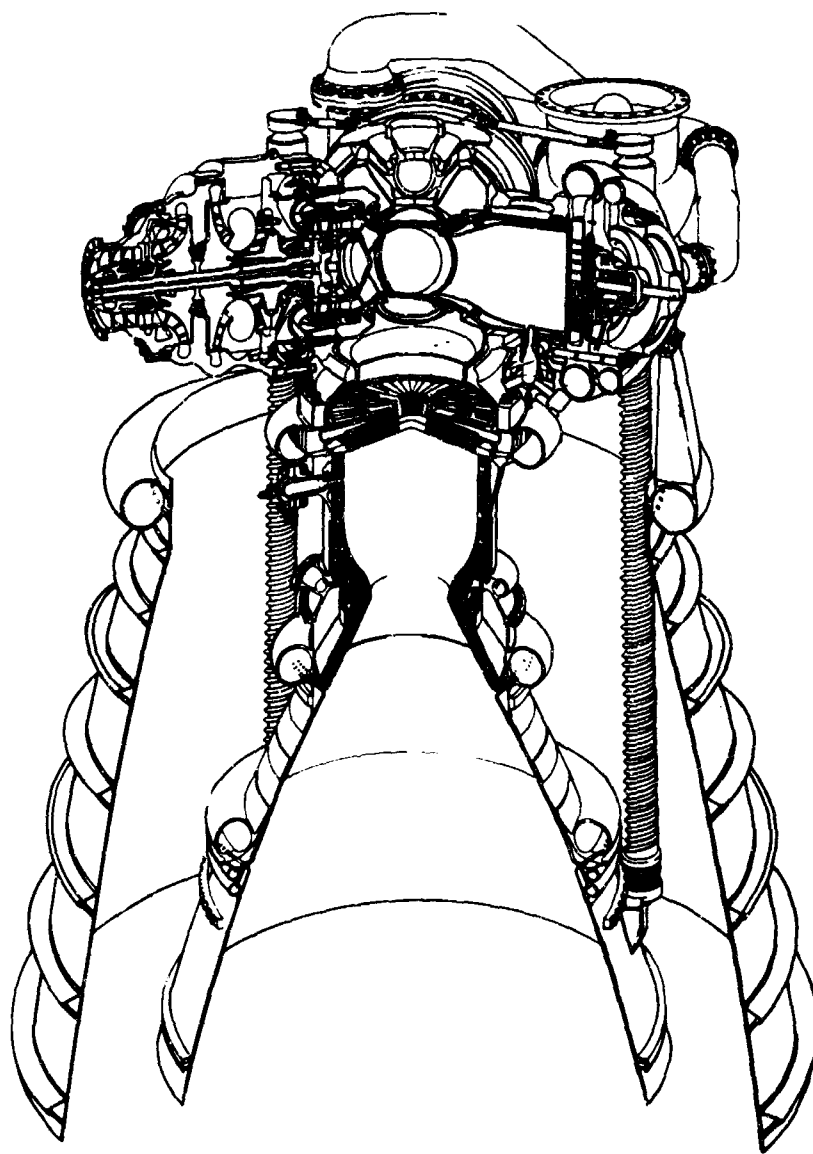


Figure 542. Location of Primary Nozzle

FD 33370

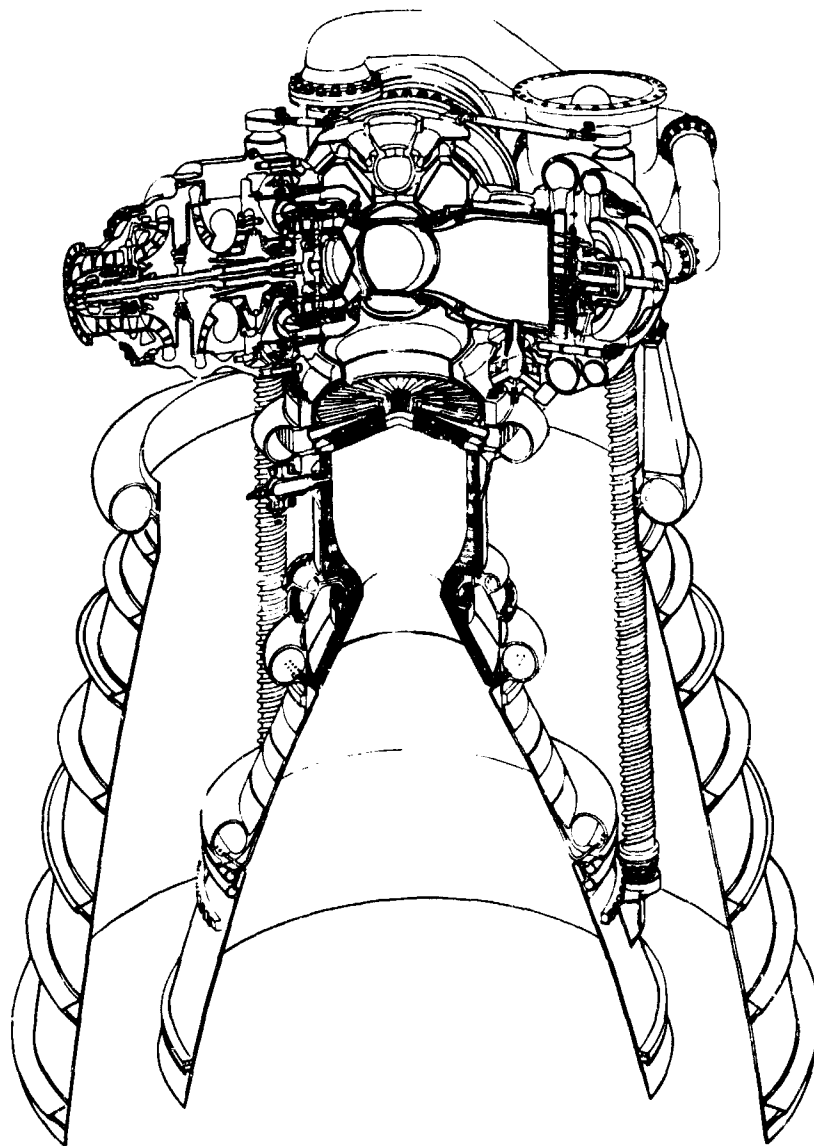


Figure 543. Location of Two-Position Nozzle and Translating Mechanism FD 33369

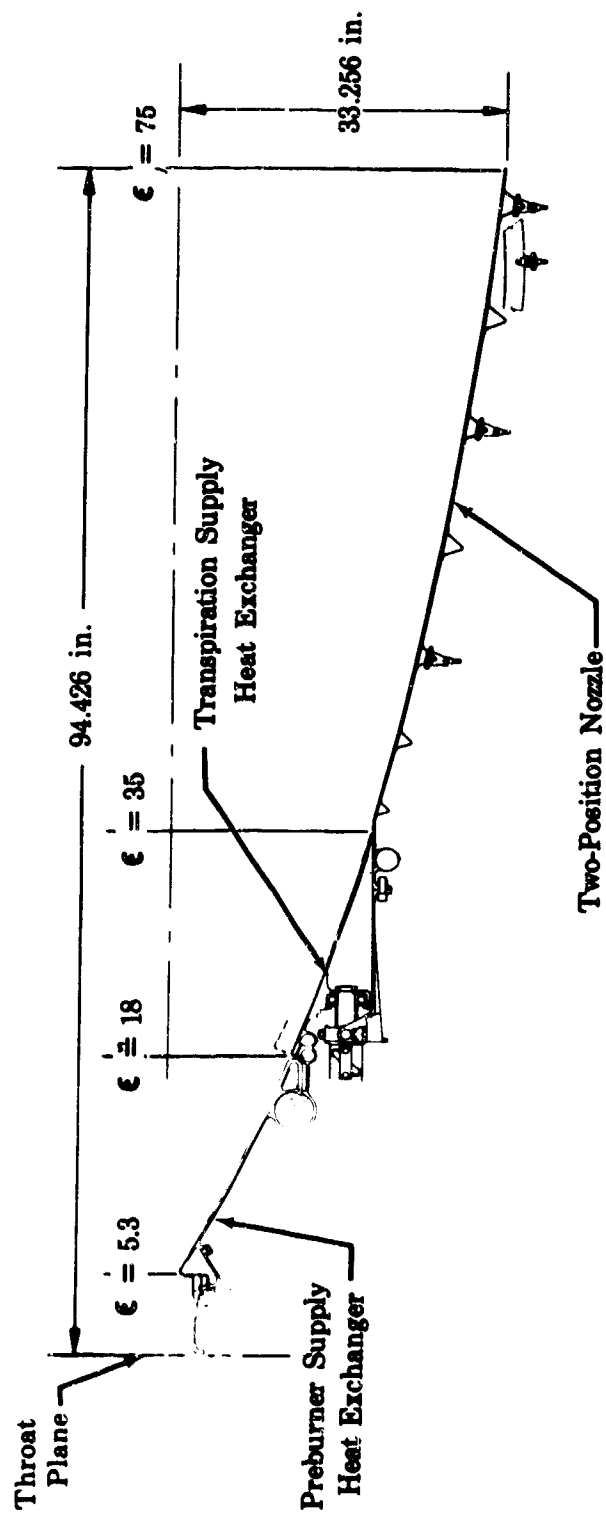


Figure 544. Nozzle Assembly

FD 25573A

2. Summary, Conclusions, and Recommendations

- a. The design indicates the primary regeneratively cooled nozzle is mechanically feasible. The recommended primary nozzle design has a single-pass heat exchanger at the inlet end and a double-pass heat exchanger at the exit end.
- b. The design indicates the two position nozzle is mechanically feasible. Two position nozzle coolant passages are designed to transfer coolant at a flowrate that will keep the inner skin of the nozzle at as high a temperature as possible in the axial direction to absorb maximum energy in the flow stream. The skin temperature in the inlet region is limited to avoid low cycle fatigue over the required life of the engine.
- c. The outer skin of the two position nozzle will have a high circumferential thermal gradient because of corrugated flow passages and the fin cooled weld flats. Thermal stresses imposed on the outer skin by the gradient will be taken out in hoop tension.
- d. The outer skin of the two position nozzle will be smooth. This design has three advantages. The stiffening bands can have an uninterrupted bonding surface. The outer skin thickness is based on strength requirements instead of thermal requirements. The corrugation cannot be constricted by thermal expansion.

3. Hardware Description

a. Primary Nozzle

The primary nozzle consists of two heat exchangers; a double-pass transpiration supply heat exchanger, and a single-pass preburner supply heat exchanger.

The nozzle and exhaust flowpaths are shown schematically in figure 545. High-pressure hydrogen from the main fuel pump is supplied to the two regeneratively cooled portions of the primary nozzle. The downstream tubular heat exchanger is double pass, and supplies hydrogen to the hydrogen inducer turbine and transpiration cooled main burner chamber. The upstream section is single-pass and cools the nozzle from an area ratio of approximately 5.3 to 18 using the remainder of the pump discharge hydrogen flow prior to delivery to the preburner injector.

The primary nozzle is illustrated in figure 546.

Regenerative heat exchangers are shaped from tubes forming the desired nozzle contour. The tube design along the heat exchanger length was determined by the heat flux that could be transferred while maintaining adequate structural integrity of the tube material. Tube pressure loss vs tube weight trade studies established the tube internal geometry. Figures 547 and 548 show the thrust and pressure distribution within the nozzles for maximum chamber

pressure. Figure 547 shows the accumulative thrust (starting at exit and progressing towards throat) experienced by the primary nozzle and caused by the axial pressure exerted on the nozzle walls. Because the two position nozzle is attached to the primary nozzle through brackets, ballnut, jackscrew and then the bearing journal of the jackscrew, the thrust exerted on the two-position nozzle when it is extended must be absorbed by the primary nozzle at its attachment point. Figure 548 shows the wall static pressures experienced by the primary nozzle.

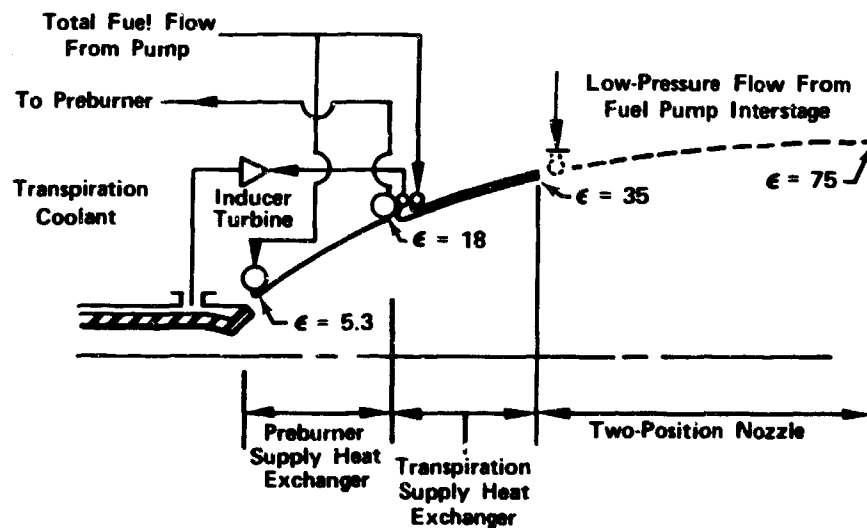


Figure 545. Regeneratively Cooled Primary Nozzle FD 25647A

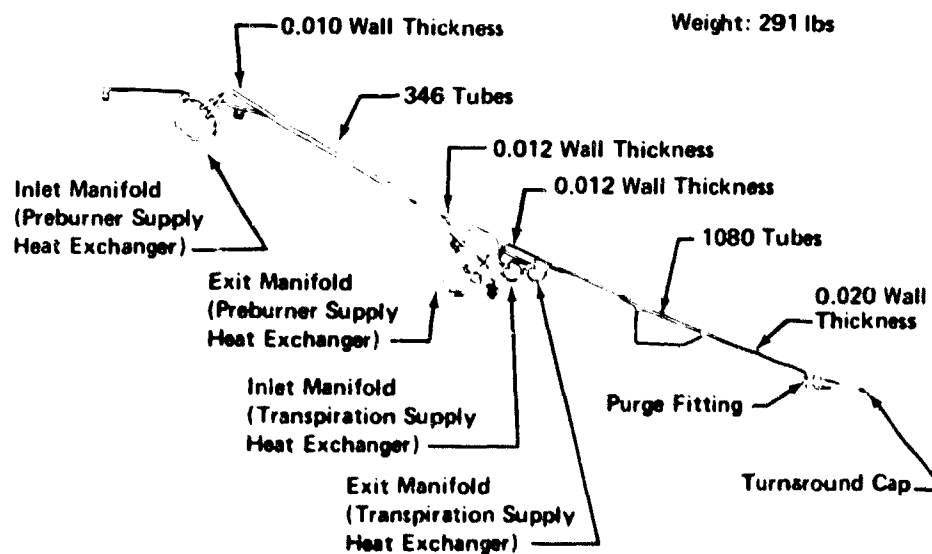


Figure 546. Primary Nozzle Configuration

FD 31783A

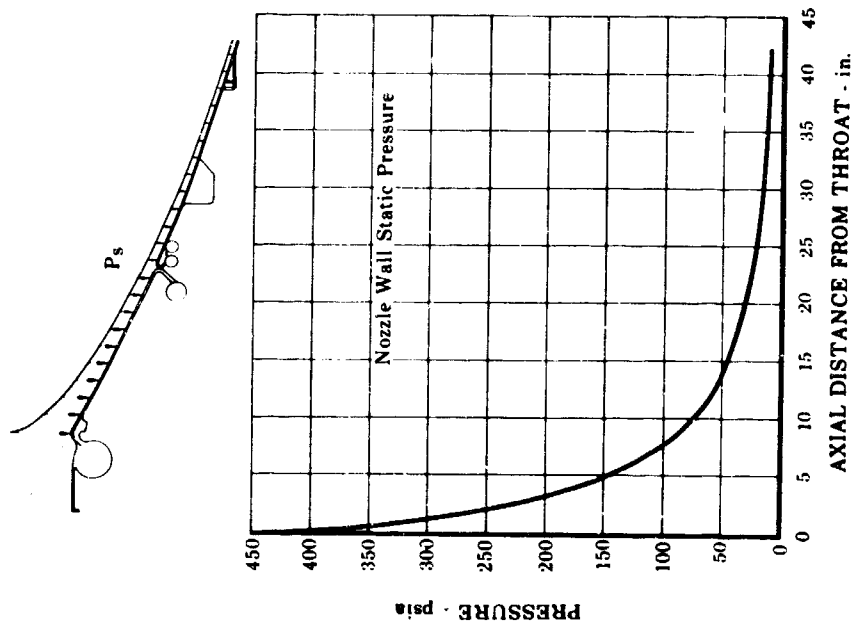
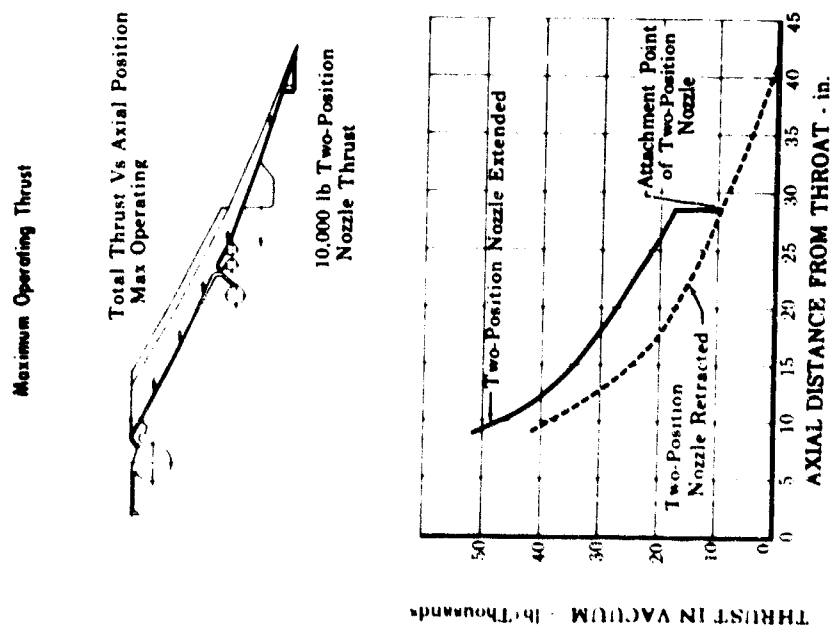


Figure 547. Total Thrust vs Axial Position FD 33187B Figure 548. Nozzle Wall Static Pressure FD 33188

The forward end of the preburner supply heat exchanger, figure 549, attaches to the rear flange of the main burner chamber with 80 Inconel 718, 0.25 in. diameter bolts. This bolted flange is designed to withstand maximum seal, gimbal, maneuver, thrust, and internal pressure loads while fulfilling the maximum deflection criterion of 0.002 in.

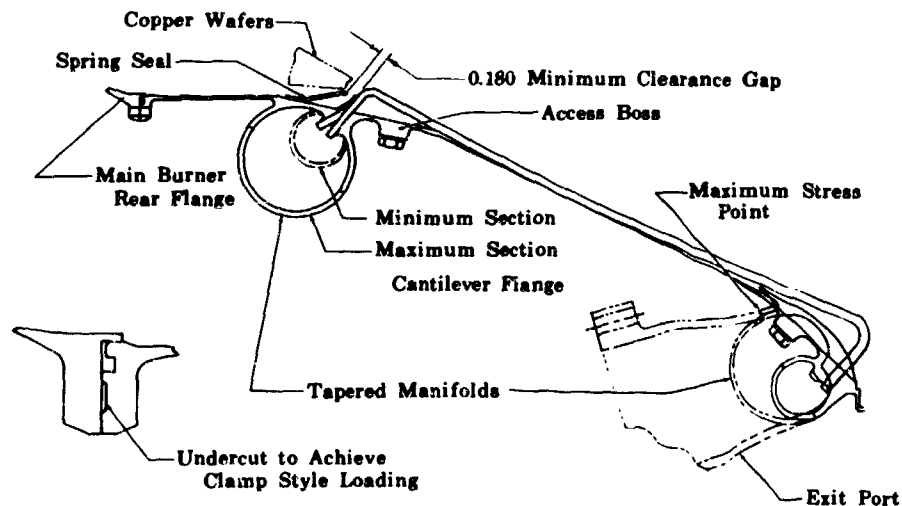


Figure 549. Preburner Supply Heat Exchanger

FD 33189

This heat exchanger was designed to minimize pressure drop, because any pressure drop in the preburner supply heat exchanger represents a decrease in total engine performance. A number of provisions are incorporated to minimize pressure drop: (1) the inlet and exit manifold are tapered to avoid unwanted expansion and contraction flow losses, (2) the manifold ports maintain a constant flow area to avoid flow pressure drops, and (3) a minimum number of bends is used in the arrangement of the heat exchanger tubes and manifolds. The tapering of the preburner supply heat exchanger manifolds not only decreases flow pressure losses, but also minimizes the manifold weight. The lightest manifolds were achieved by positioning them in such a manner as to obtain the smallest possible mean torus.

The maximum stress point in the manifolds occurs where the inlet and exit ports are welded to the manifolds. This area has been strengthened to maintain the stresses below the 0.2% yield point for 1.5 proof pressure at its operating temperature.

Flanges on the inlet and exit ports are the high-pressure cantilever style and meet the 0.002 in. maximum deflection criterion.

Based upon low cycle fatigue data provided later in this section, Inconel 625 was selected as the heat exchanger tube material. To ensure brazing adjacent tubes, the sides of each are spanked to produce a 0.030 in. flat. The braze between tubes is checked to ensure that combustion products flowing in the nozzle do not leak into the cavity between the back side of the tubes and the support jacket. Moisture must be kept from this cavity to prevent ice formation, and

resultant damage to the tubes. To prevent ice formation during sea level operation, fittings are provided to facilitate evacuation, drying, and inert gas pressurization of the cavity. During engine test, pressure relief valves are attached to these fittings for venting any unforeseen high-pressure coolant leaking into this cavity.

During fabrication, tubes are positioned against the outer jacket with a mandrel, and the entire assembly is then placed in a furnace for silver brazing. Braze repairs are made with a low temperature hand braze.

Inconel 625 is used for the jackets and the transpiration and preburner heat exchangers because it maintains thermal compatibility with the tubes for brazing, and is the strongest of the non-hardenable nickel alloys. This material is easily welded, and it may be used after welding without any subsequent heat treatment. Visual inspection of the tube-to-manifold braze joints is possible because the manifold caps can be welded into place after brazing.

Tubes forming the nozzle contours are analytically treated as possessing no structural strength for resisting nozzle hoop loads. The outer shell (jacket) must support all hoop pressure loads, and the strength of the tubes considers only the distribution of axial and bending moments. The limiting design loads for the nozzle jacket occurs during simulated altitude ignition on a sea level test stand, wherein the nozzle is evacuated to 0.5 psia while the nozzle exterior is exposed to 14.7 psia ambient pressure; therefore, a continuous jacket is necessary to prevent buckling and collapse of the nozzle. A flight nozzle would not be exposed to this buckling condition, because the inside has the greater pressure causing the nozzle to be loaded in the hoop direction only. Therefore, an alternate flight type nozzle design has been provided, saving 7.6 lb in the preburner heat exchanger, and 9.3 lb in the transpiration supply heat exchanger, by incorporating lightening holes throughout the outside jacket surrounding the tubes.

The clearance gap between the main burner copper wafers and the forward section of the preburner nozzle (area ratio 5.3:1) is kept minimal to prevent separation of the boundary layer from the tubes at this junction. Loss of the boundary layer would cause an abrupt increase in tube wall temperature. Additional increase in tube wall temperature will occur if the combustion gases flow into the cavity behind the copper wafers. Therefore, a purge flow is supplied to this cavity to prevent intake of combustion gas. This purge flow cools the back wall of the copper liner supplying film cooling for the heat exchanger tubes. A spring loaded seal between the heat exchanger and main burner copper liner is used to maintain the purge at 0.025 lb/sec.

The purge flow control spring consists of two conical Inconel 625 sheet metal rings slotted in 60 places, and positioned with slots offset causing the rings to form a tight seal when deflected. The portion of the seal bearing against the copper liner is treated with a dry film lubricant as a wear resistant surface. If during engine abort, the pressure behind the copper wafers exceeds the chamber pressure by more than 15 psia, the spring loaded seal will open and prevent buildup of a high buckling pressure across the copper liner.

For test stand convenience, the preburner and transpiration supply heat exchangers are connected by a bolted flange shown in figure 550. For flight engine application the two heat exchangers would be welded together forming one

large assembly. Flange elimination will save approximately 5 lb, and has been designed to meet the zero leakage criteria. The flange is sized to withstand the translating system jackscrew loads providing axial compression of the metal O-ring seal. Flange joint stresses have been limited to 0.2% yield strength at room temperature, and deflection is limited to 0.002 in. for both. The flange is bolted with 120 Inconel 718 bolts of 3/16 in. diameter.

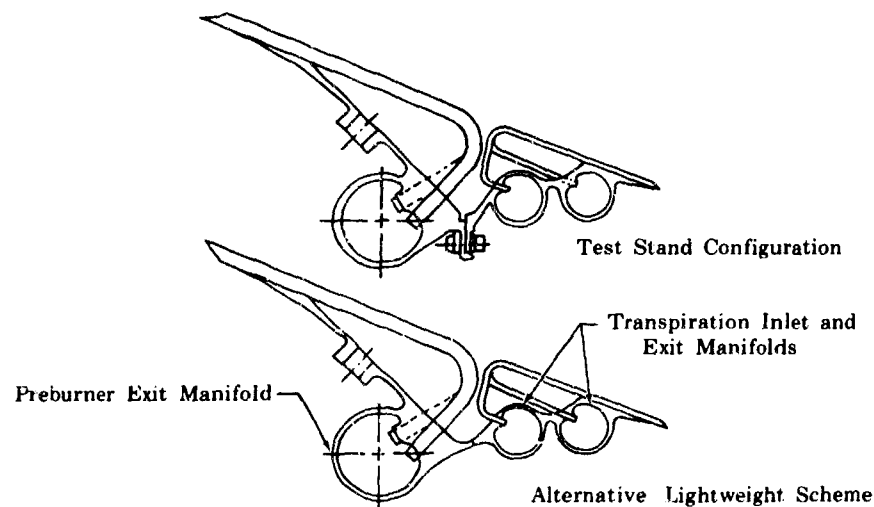


Figure 550. Preburner to Transpiration Heat Exchanger Flange FD 33190A

Because pressure loss was not a limiting criterion in transpiration supply heat exchanger design, shown in figure 551, the manifolds were not tapered around the nozzle circumference, and the nozzle was made as a two pass heat exchanger. A two pass heat exchanger provides a better packaging scheme because the envelope defined by the translating two position nozzle must clear both the inlet and discharge plumbing of the heat exchanger. Tapering the manifolds would have afforded a weight savings of 2 lb but would result in considerable manufacturing expense. The transpiration supply heat exchanger manifolds meet the 1.5 proof pressure at operating temperatures without exceeding the 0.2% yield strength of Inconel 625.

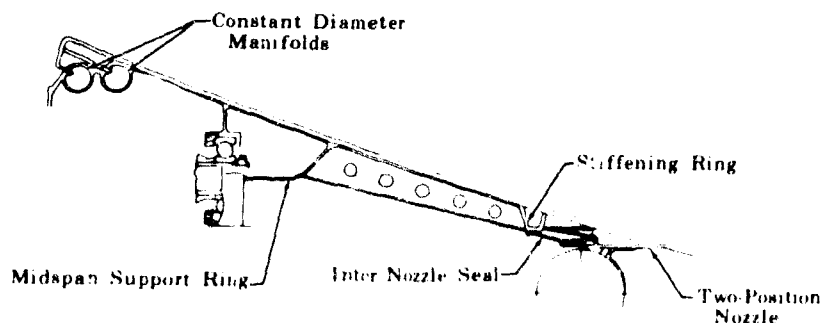


Figure 551. Transpiration Supply Heat Exchanger FD 33191

An important function of the transpiration heat exchanger is to provide support for the two position nozzle. The rear thrust bearings for the jackscrew actuators are supported in a circumferential ring at the midspan of the transpiration heat exchanger. This ring is sized to distribute the two position nozzle loads into the transpiration heat exchanger. Because this ring is also a bearing support, it was necessary to limit deflections to a minimum. The torsional rigidity of the support ring was increased by spanning axial stiffeners between the midspan ring and a stiffening ring at the aft end of the transpiration heat exchanger.

Stresses in the midspan ring are very low, except for those points where the bearing supports are welded into the stiffening ring. Because local punch loads are transferred into the ring by a system of shear webs, combined stresses at these points are limited to the 0.2% yield for use of Inconel 625.

Maximum bearing loads occur at altitude with the engine operating at maximum thrust, and while under gimbal and maneuver loads. The bearings will also absorb stall torque effect of the actuation motor as the two position nozzle first starts to retract from extended position.

A circumferential ring at the transpiration heat exchanger aft end serves as a seal land, stiffens the nozzle exit, is sized to withstand test stand buckling pressure, and is required to withstand buckling loads occurring during sea level flight. The outer diameter of the band is a seal land for the seal between the transpiration heat exchanger and dump nozzle when extended.

The turnaround manifold cross section at the exit of the transpiration heat exchanger has been reduced to minimize step in flowpath between the regenerative heat exchanger and dump nozzle, and meets 1.5 times proof pressure criterion.

b. Two Position Nozzle

The two position nozzle consists of a circumferential coolant distribution manifold, a smooth nozzle outer skin with circumferential stiffening bands, and longitudinally corrugated nozzle inner skin, which forms longitudinal coolant passages.

The nozzle has an overall area ratio of 75 with a baseline contour produced by truncating a nozzle shape designed to turn the exit flow axial at an area ratio (A_D) of 110. This contour starts at an area ratio 35, extends to an area ratio of 75, and is a compromise between a minimum surface nozzle contour and a maximum performance nozzle contour.

The two position nozzle, figure 552, is designed to be cooled with low pressure hydrogen, taken from the fuel pump interstage. (During sea level and low altitude operation with the nozzle skirt retracted, coolant flow is not required.) The coolant is expanded through small nozzles at the trailing edge of the nozzle. The expansion of this warm hydrogen gas produces a specific impulse comparable to main stream specific impulse.

Figure 553 illustrates a typical nozzle shell configuration. The inner skin passages are resistance seam welded to the inside surface of the outer skin between corrugations. Voids between the outer and inner skins formed by this method of construction become longitudinal coolant passages. Coolant enters

these passages at the forward end of the nozzle from the radial feed holes in the base of the coolant distribution manifold. After traveling the length of the nozzle, coolant is discharged into the exhaust stream. Figure 554 describes the two position nozzle configuration.

The geometry of the passageways at various positions along the nozzle is shown in figure 555. The required exit area for the coolant passages is obtained by partially closing the end of each passage by means of a spherical inward dimple in the outer skin.

The coolant distribution manifold is of toroidal shape and is brazed to the nozzle outer skin at the forward (upstream) end. Weldment flanges are provided at three nearly equally spaced locations for the purpose of attaching mounting brackets to the manifold. Coolant enters from the supply line and is then circumferentially distributed about the nozzle through radial feed holes in the manifold base (one feed hole per nozzle coolant passage). The feed holes in the base of the manifold have a cross sectional area over twice that of the local coolant passages.

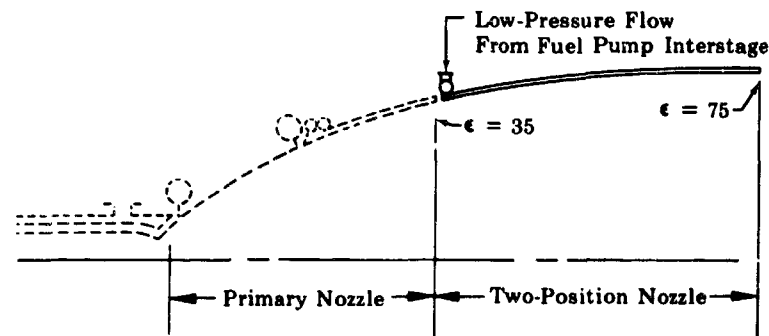


Figure 552. Two-Position Nozzle

FD 25646

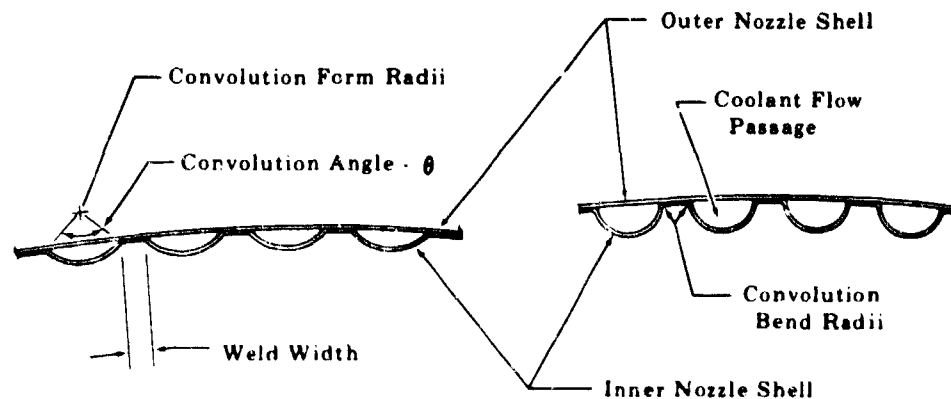


Figure 553. Typical Nozzle Shell Configuration

FD 21098A

Material	Inconel 625
Outer Sheet	Smooth
Outer Sheet Thickness	0.016
Inner Sheet	Corrugated
Inner Sheet Thickness	0.010 in.
Number Corrugations	360
Inlet Dia	45 in.
Exit Dia	66 in.
Length	50 in.
Weight (Sea Level)	227 lb
Weight (Altitude)	186 lb

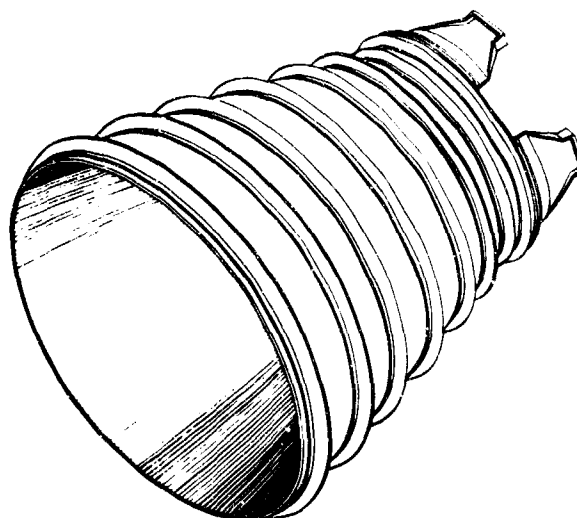


Figure 554. Design of Two-Position Nozzle Complete

GS 12309

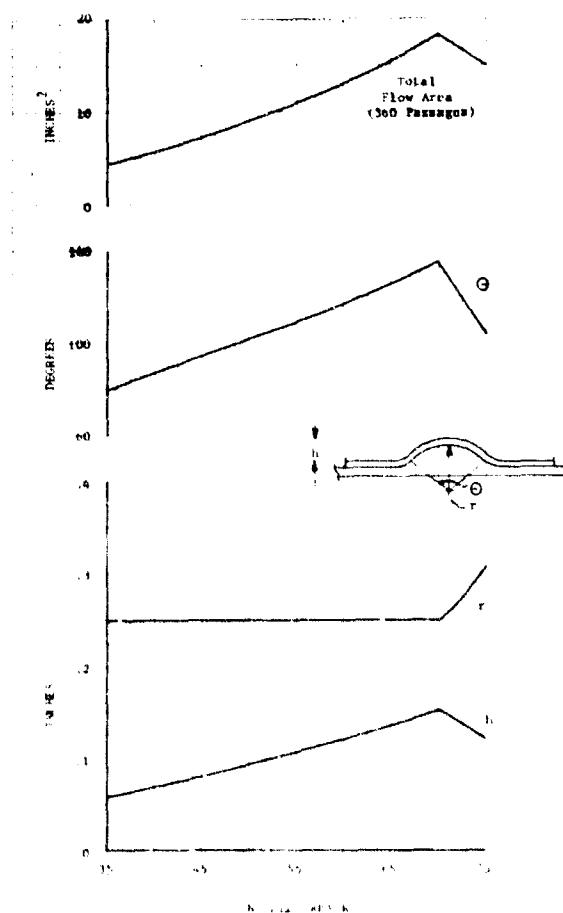


Figure 555. Two-Position Nozzle Geometry

DF 77228

The nozzle outer skin mating holes are slightly larger than those in the manifold base to provide for axial and circumferential misalignment. The coolant distribution manifold is sized as a deflection limited structural member to minimize the clearance gap between the primary nozzle and the two position nozzle. With the nozzle in the extended position, the manifold is outboard and slightly forward of the primary nozzle turnaround manifold. This orientation results in a short constant diameter section in the two position nozzle. The constant diameter section helps establish smooth coolant flow before the corrugations become exposed to exhaust stream temperature.

Three mounting brackets attach the two position nozzle and manifold assembly to the three jackscrews forming the translation system. Each bracket has the form of a truncated pyramid as shown in figure 556, with its based curved to fair tangentially into the coolant distribution manifold. This bracket is formed from a 0.040 in. sheet of Inconel 625. The truncated top of the bracket is faired into a rectangular shaped flange that mates to one provided on the jack-screw ball-nut assembly.

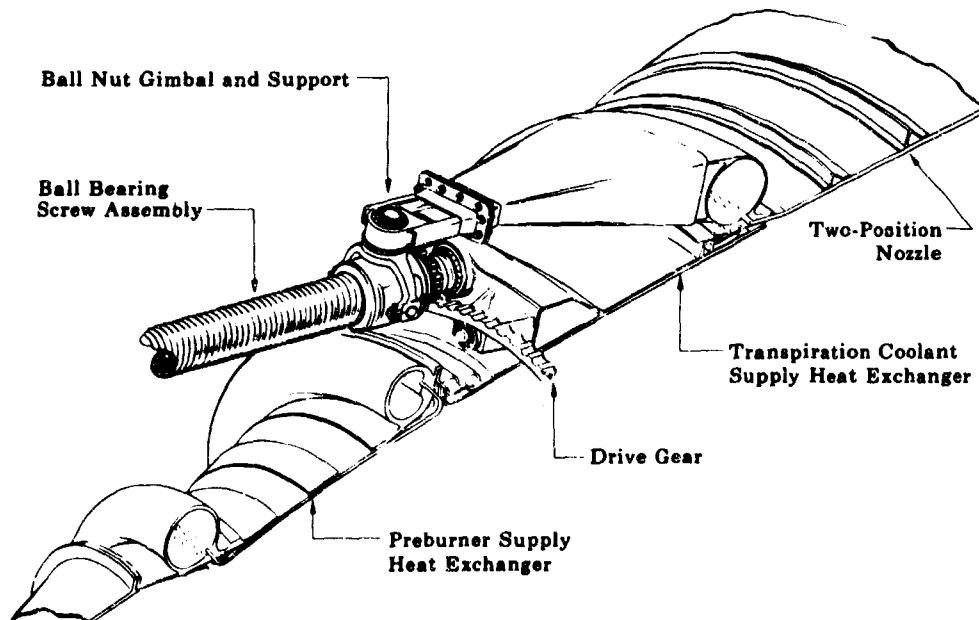


Figure 556. Translating Mechanism

FD 31787A

The mounting brackets straddle the manifold so that loads transmitted through their inner and outer walls are tangentially directed into the toroidal manifold shell. This tangential transition joint places the load on the manifold in shear modulus eliminating bending at the point of application. Manifold radial and axial deflections are minimized when any applied loads are evenly distributed about the manifold circumference because the manifold is a primary structural member. Packaging requirements limit each bracket foot print to a 45-deg included angle of approximately 19.5 in. arc length on the manifold. Deflections are acceptable resulting from loading into 38% of the manifold circumference. Each bracket is structurally adequate to transmit the combination of imposed axial, bending, and torsional loads during flight, sea level testing, or altitude simulation testing.

Circumferential stiffening bands, V-shaped in cross section, are brazed to the outer surface of the smooth outer skin. There are 16 equally spaced holes longitudinally through each band for the attachment of external supports during simulated altitude testing. Reinforcement washers welded around each hole, one on each side of the band, prevent tearout. The small stiffening band nearest the manifold is provided with holes to attach a two-piece diffuser seal ring for the simulated altitude test.

The circumferential stiffening bands are sized and spaced for sea level and simulated altitude test conditions. For sea level testing, nozzle buckling loads require a larger moment of inertia obtained by increasing band height and cross sectional area. The nozzle is therefore 25 lb heavier than the altitude design.

c. Translating Mechanism

The translating mechanism (figure 556) extends and retracts the two position nozzle during engine operation and provides precision positioning in the extended and retracted positions. Positive locking devices maintain the nozzle position when the engine is not operating.

The two position nozzle is gimbaled to a ball nut at three locations. The ball nuts are translated by rotation of three ball screw assemblies, which are secured at their aft end to the primary nozzle, and at their forward end by adjustable support linkages attached to the engine gimbal thrust ball retainer. The ball screws are synchronized and driven at their aft ends by a ring gear internally supported by bearings mounted on the outer periphery of the primary nozzle. The ring gear is driven by a 21.2 hp hydraulic drive unit through an offset gearbox, and a drive shaft system which maintains a 1:1 drive ratio between the motor and the ball screws.

Deceleration is accomplished with variable flow valves controlled by cam-actuated plungers. Approximately 2 in. from the end of each stroke, hydraulic fluid flowrate through the motor is reduced by a cam-actuated valve to obtain a final translation speed of 0.75 in./sec. The nozzle at the end of the stroke is seated by motor stall torque into spring located stops integrally mounted on the ball screw shafts.

The nozzle is locked in either the extended or retracted position by a spring loaded friction clutch, energized when hydraulic pressure is removed from the motor to prevent rotation of the motor shaft in the absence of hydraulic pressure.

The ball bearing screw assembly converts rotary motion of the drive system into linear motion to translate the two position nozzle, and is the supporting structure between nozzle and engine.

The ball bearing screw assembly has large diameter, thin wall, ball screw shafts. Each shaft has a 3.125 in. ball circle diameter and 0.250 in. diameter balls. This is the largest shaft providing adequate ball nut clearance from the exit manifold for the preburner supply heat exchanger, with adequate clearance between the ball nut stop and the two position nozzle seal ring. The shaft bore fabrication limit has 0.195 in. wall thickness beneath the ball grooves.

One of the double threads is used as a race for the ball nut bearings while the other is nonfunctional, but provides lighter grooves and can be used as an alternate race to extend the shaft life by switching the ball nut bearings to the alternate thread.

The drive gear system transmits power from the hydraulic motor to the ball screw shaft and synchronizes the three jack screw shafts. Power from a hydraulic motor is transmitted through an idler shaft which is engaged into a small 22 tooth drive gear (figure 557) which drives a larger synchronizing ring gear having 331 teeth (figure 557), which is supported by 13 small ball bearings (figure 556) that pilot the ring gear in an internal groove. This ring gear transmits power to three small driven 22 tooth gears engaged on each of the three jack screws. As these jack screws are rotated, they cause the ball nuts and the two position nozzle to axially translate.

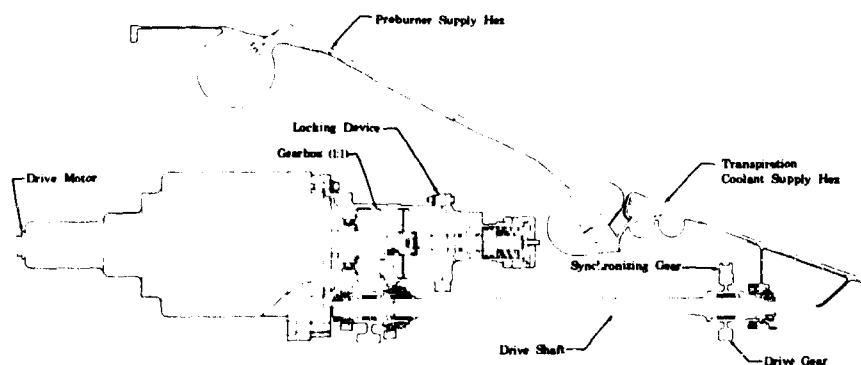


Figure 557. Drive Motor, Gearbox and Locking Device For Translating Mechanism

FD 33017

The control and drive system, which is commercially available and not lightweight for the demonstrator program, (figure 557), provides the power required to translate the two position nozzle, limits the loads imposed on the engine by translation of the nozzle, and positions and secures the nozzle during engine operation. A friction clutch lock is also provided to secure the nozzle when the engine is not operating.

The ball nut gimbal is the connecting link between the ball nut and the two position nozzle support structure. The gimbal (figure 558) provides 2 deg of swivel to prevent failure by the transfer of bending moments from the nozzle support structure to the ball nut.

Each ball screw shaft is supported at its forward end by adjustable two-bar linkages attached to a support plate (figure 559), which is fastened to the transition case at the engine gimbal thrust ball retainer. The support plate is constructed of aluminum and is adequately sized to withstand lateral buckling stress. Zinc chromate primer provides galvanic corrosion resistance for the aluminum.

The translating system weights are shown in table LXXVI.

4. Fabrication

a. Primary Nozzle

Two braze samples were fabricated to establish a repair procedure in the event braze voids are experienced after the initial furnace braze. The first repair braze sample revealed that hand braze repair in the manifold tube socket area is feasible with either high temperature or low temperature brazing material. X-ray and microanalysis of the test samples detected no indication of tube cracking caused by stress alloying. A second repair braze sample was hand brazed, but has not been inspected for stress alloying.

The semifinished tubes for the regeneratively cooled nozzle were placed on order with tentative delivery promised in 20 weeks. The requirements for forgings and raw material necessary to fabricate the nozzle assemblies were established, the purchase orders issued, and the raw material received.

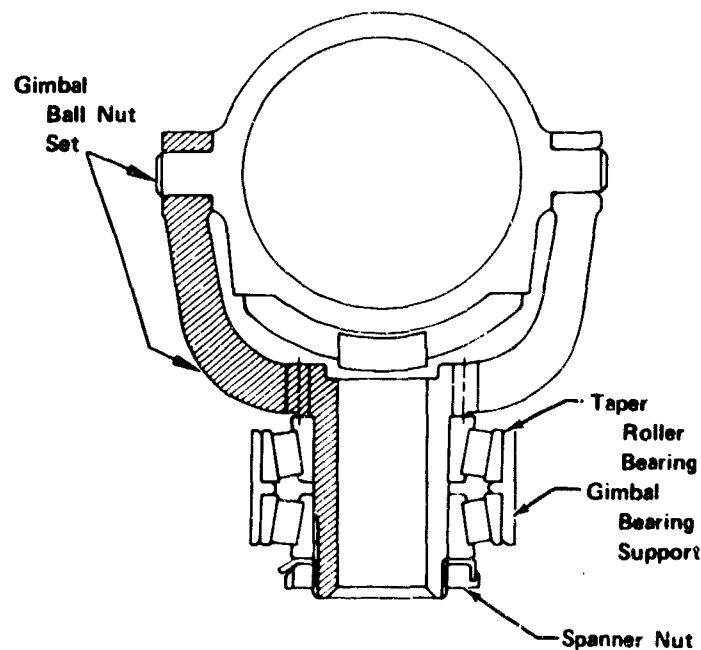


Figure 558. Ball Nut Gimbal and Support

FD 23199A

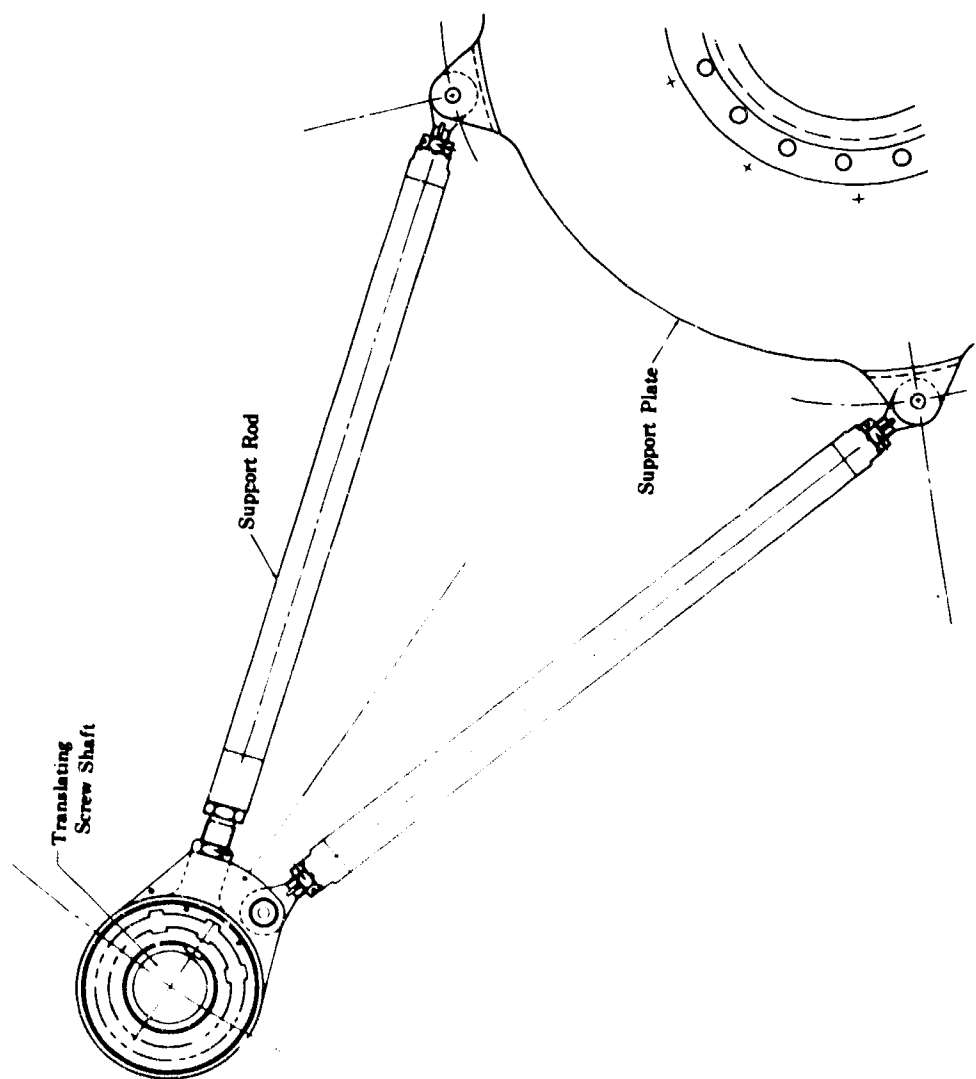


Figure 559. Translating Mechanism Forward Supports

FD 33201

Table LXXVI. Translating System Weights

Item	Weight (lb)
Ball Screw Shaft Gears and Rear Support	17.5
Ball Bearing Screw Assembly	129.6
Ball Screw Forward Support and Stop	17.7
Lock, Drive System, Two Position Nozzle	6.2
Gearbox, Nozzle Extension Drive	8.7
Ball Nut Gimbal and Support	17.6
Translation System Total Weight	197.3*
*Hydraulic motor, motor mounts, and control valves are not included in flight system weight.	

b. Two Position Nozzle

The raw material and forging requirements necessary to fabricate two nozzle assemblies were established, purchase orders issued, and material received. The design of the two position nozzle specifies eight annular Inconel 625 stiffening bands brazed to the flat outer skin. These bands resist internal hoop and external buckling of the corrugated skin panels. Because of a possible 14.7 psi buckling pressure differential on the nozzle during shutdown of the engine in the altitude diffuser, the method of band attachment is important. Because the band-to-skin junction would place the braze in a peel resisting load, tests were conducted to substantiate the braze peel characteristics. The all braze configuration would be the simplest to fabricate and the lowest in cost. Tests of braze peel strength for the support bands were conducted with the following results indicating adequate strength for the configuration selected because the required strength was 40 lb load/in. (figure 560).

1460°R - Pure Silver Braze - Failed at 511 lb load/in.

1460°R - Gold-Nickel Braze - Failed at 2542 lb load/in.

1460°R - Pure Silver Braze - Failed at 546 lb load/in.

1460°R - Pure Silver Braze (removed fillet) - Failed at 480 lb load/in.

1460°R - Gold-Nickel Braze (removed fillet) - Failed at 2103 lb load/in.

1660°R - Pure Silver - Failed at 266 lb/in.

1660°R - Gold-Nickel - Failed at 1737 lb/in.

1860°R - Gold-Nickel - Failed at 973 lb/in.

1260°R - Gold-Nickel - Failed at 3330 lb/in.

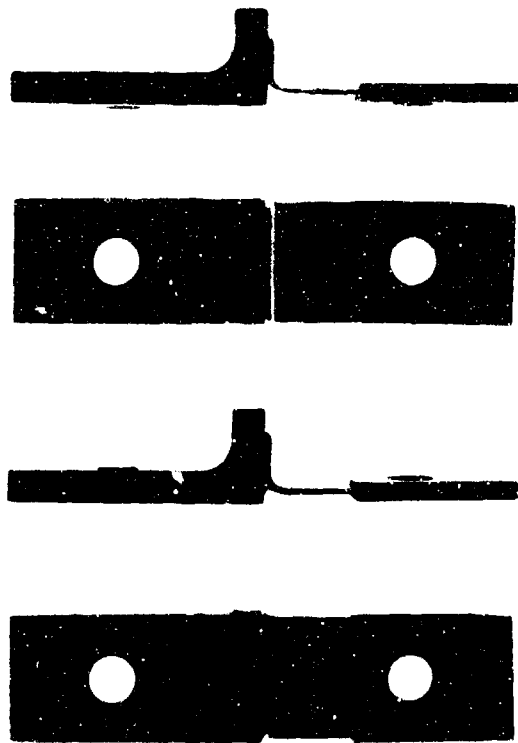


Figure 560. Braze Peel Test Specimens

FE 84164

c. Translating Mechanism

The long lead bearings and the long lead forgings required to fabricate two nozzle assemblies were determined, purchase orders were issued, and the material was received.

5. Subcomponent Testing

At the lower area ratio, where wall temperature and thermal cycles govern design, a maximum hoop stress of 29,000 psia ($r = 5$) and maximum wall temperature (with maximum tube wall thickness) of approximately 1700°R ($r = 7$) are predicted.

In engine operation, the regenerative nozzle has a large thermal gradient between the hot combustion side of the tube and the cold backside of the tube. This gradient causes a strain in the axial direction on the hot side of the tube as the hot side expands and the cold side decreases in length. The continued cycling of these conditions repeatedly causes the hot side to go into plastic strain, and eventually to fatigue, crack and fail. This type of tube failure is called thermal low cycle fatigue.

Thermal low cycle fatigue studies were conducted to optimize tubular, regeneratively cooled nozzle tube designs (figure 561). Tube operating conditions are simulated in test rig by restraining one side of the tube with a brazed rigid bar of the same material as the tube. The rigid bar side of the tube is held at liquid nitrogen temperature (approximate temperature of the cold side of the tube during operation) while the hot sidewall of the tube is heated by an electrical induction heating element to a temperature approximating operation temperatures of the nozzle tube. The tube is pressurized to provide a predetermined stress level in the tubes. As the hot sidewall is heated, it tends to grow axially while being restrained by the opposite side of the tube, which tends to decrease in length because of the liquid nitrogen temperature. The inside pressure is held constant as the heating element is cycled on and off. The cyclic frequency is selected so the hot sidewall temperature varies from approximately liquid nitrogen temperatures to elevated temperatures simulating an operating hot side tube wall temperature. This causes the hot side plastic deformation, which causes fatigue failure after repeated cycles. Low cycle fatigue testing results at equivalent cycle tube hoop stress levels are shown in figure 562. The predicted operating temperature and stress at the nozzle inlet ($\epsilon = 5.3$) based on nominal wall thickness and $r = 7$, shown in figure 562, indicates a life greater than 300 cycles is attained. If maximum allowable wall thickness, which is the worst LCF condition, is considered, the tube wall temperature increases to 1707°R ($r = 7$) and the stress decreases to 22,000 psia. Figure 563 shows a typical predicted temperature gradient for a tube having maximum wall thickness in the primary nozzle preburner supply section near the coolant inlet manifold.

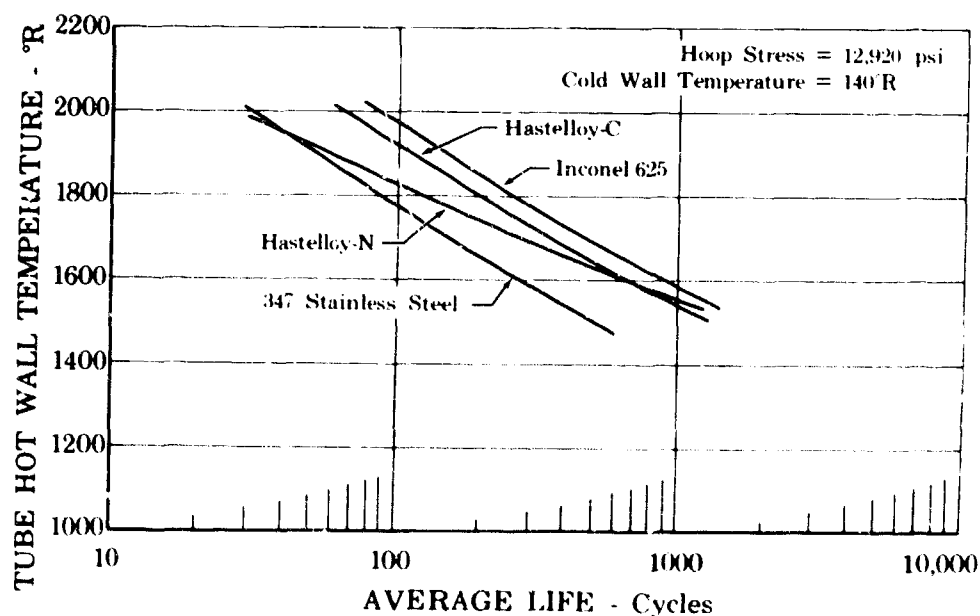


Figure 561. Inconel 625 Provides Highest Average Cycle Life

FD 21090

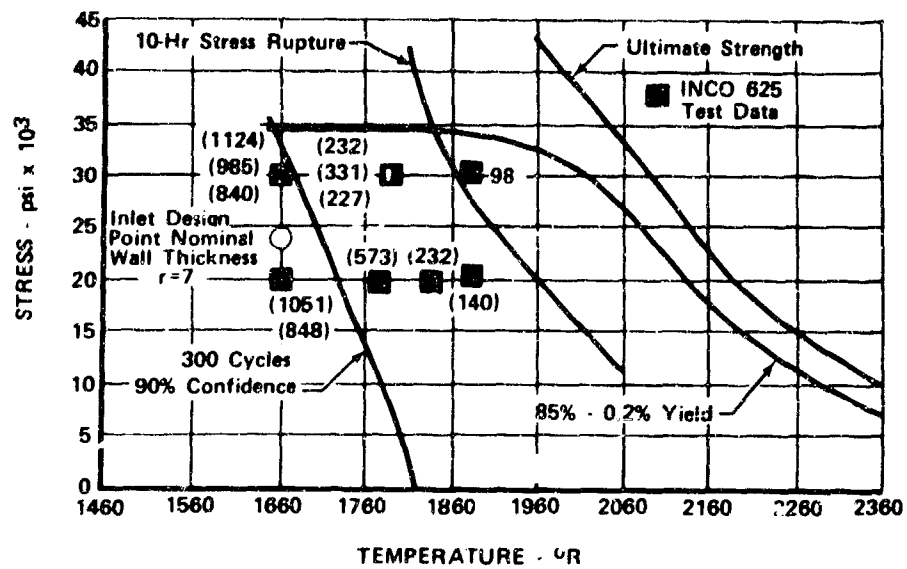


Figure 562. Primary Nozzle Meets Life Requirements FD 27521A

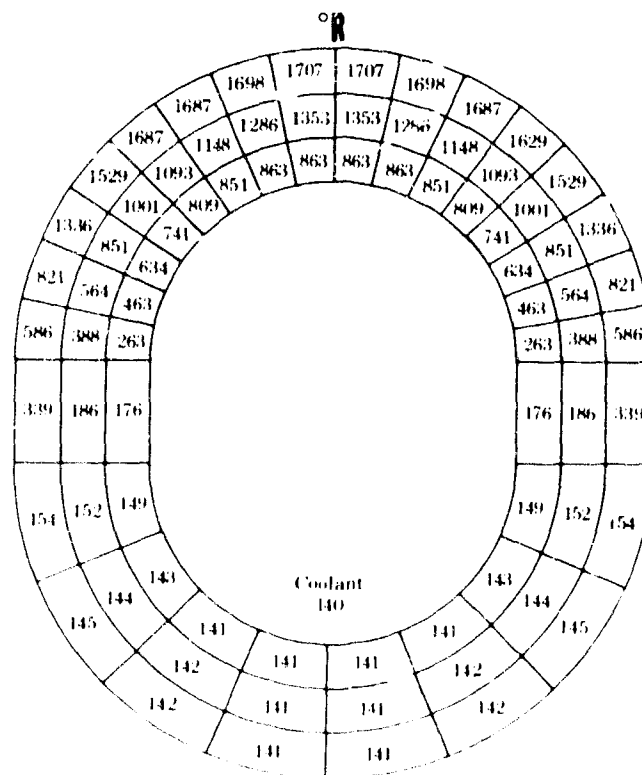


Figure 563. Predicted Thermal Gradient of Regenerative Nozzle Tube Nearest Throat FD 33021A

F. FUEL TURBOPUMP

1. Introduction

The fuel turbopump provides high pressure hydrogen required by the engine cycle. This turbopump is a single shaft unit with two back-to-back, centrifugal pump stages driven by a two-stage, pressure compounded turbine. The turbopump shaft is radially aligned by two roller bearings, and axially by a double acting thrust balance piston. The fuel turbopump delivers liquid hydrogen at a flowrate of 91.3 lb/sec and a pressure of 5654 psia at the design point (engine 100% thrust, with a mixture ratio of 5). The two stage turbine delivers approximately 49,000 horsepower to the pump and operates at a maximum inlet temperature of 2325° R at 100% thrust and a mixture ratio of 7.0. The fuel turbopump assembly is located as illustrated in figure 564 and a cross-sectional view is illustrated in figure 565.

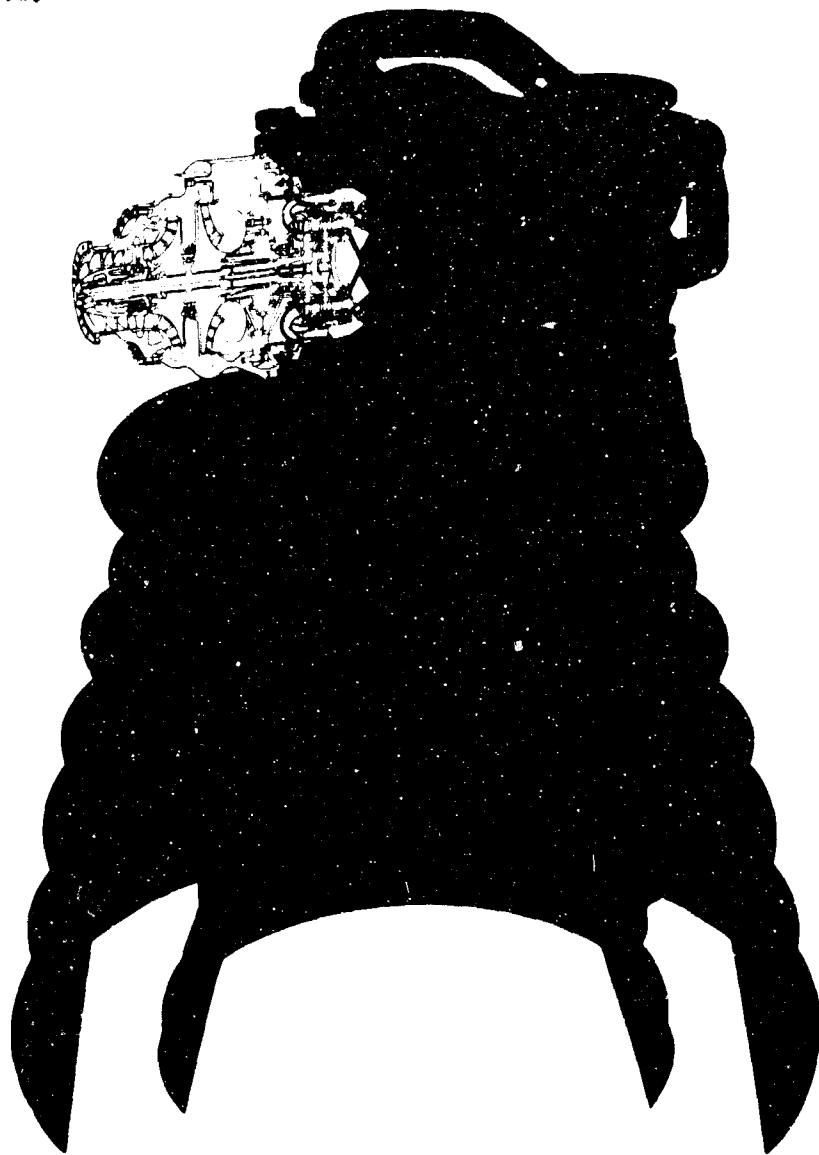


Figure 564. Fuel Turbopump Location

FD 31416

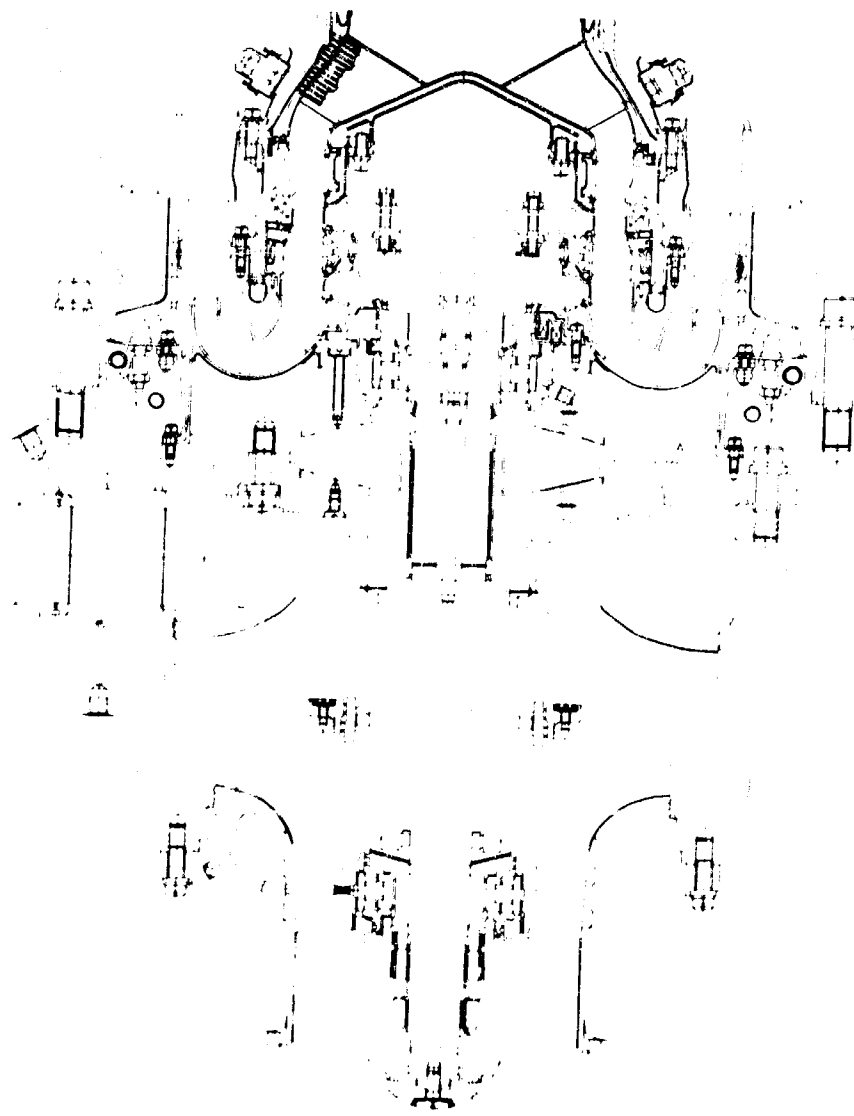


Figure 565. Fuel Turbopump Assembly

FD 29206

2. Summary, Conclusions and Recommendations

a. Summary

(1) Design

The fuel turbopump design was completed and fabrication drawings were released to Manufacturing. A detailed description of the design studies is presented in the Demonstrator Engine Design Report, AFRPL-TR-70-6.

(2) Fabrication

Two complete turbopumps and one spare rotor were fabricated.

(3) Tests

Subcomponent tests were conducted in the following areas:

1. Rotor spin tests
2. Blade vibration tests
3. Main housing proof pressure tests
4. Lift off seal tests
5. Turbine stator calibration tests
6. Critical speed evaluation tests.

Three fuel turbopump rig builds were completed and a series of 13 pump tests was conducted to evaluate the pump performance axial thrust balance and mechanical integrity. The pump performance exceeded the design goals in efficiency, pressure rise, and NPSH capability. Axial thrust balance was satisfactory over the pump operating range. Mechanical integrity was demonstrated by operation at speeds as high as 48,136 rpm and discharge pressure levels as high as 6705 psia. Following these tests the turbopump was mounted on the transition case for hot turbine tests. These tests are discussed in Section VII.

b. Conclusions

Based on subcomponent tests completed and turbopump testing the following conclusions are made:

1. Subcomponent tests indicate that design objectives have been achieved or exceeded in all except the lift off seal subcomponent areas. This unit failed after 2525 cycles during an endurance test to demonstrate 10,000-cycle life durability. Static leakage measurements on this unit were within the specification 10 secs gaseous nitrogen at 50 psid. A similar unit was incorporated for the first pump performance test series because the 2525 cycle life demonstrated on the first lift off seal tested was several orders of magnitude greater than that required for the first pump performance test series.

2. The initial pump performance test series indicates that pump performance is approximately 2 to 3 percentage points better in overall efficiency than predicted, overall head rise is approximately 8% better than predicted, and the turbopump is capable of stable operation over the wide flow range required to satisfy the demonstration engine cycle. Although the liftoff seal failed during the first test series creating high vibration levels, subsequent pump tests with a revised liftoff seal bellows configuration were satisfactory and the pump was operated to a maximum speed of 48,136 rpm. Pump operation with vibration levels less than $\pm 5g$ was demonstrated at speeds up to 47,000 rpm with $\pm 8.8g$ vibration at the maximum speed level.

c. Recommendations

It was recommended that pump tests be continued in conjunction with the preburner and transition case to map turbopump performance and to demonstrate suitability of the component for use on the XLR129 demonstration engine. The tests are reported in Section VII.

3. Hardware Description

Major components of the fuel turbopump are pump, turbine, rotor assembly, and housings, and are described in detail in the following paragraphs.

a. Pump Section

The pump section of the fuel turbopump includes the high speed inducer, both bearings and mount system, both impellers, and the thrust balance system.

(1) High-Speed Inducer

The high-speed inducer shown in figure 566 has three helical blades equally spaced at 120 degrees. The inducer is fabricated from A-110 titanium, selected because of its high strength-to-weight ratio.

The inducer has an internal spline that engages mating splines on the shaft loading nut and the front bearing carrier shown in figure 567. The inducer is secured to the rotor assembly shaft by a nut torqued to 5500 lb-in. at the forward end. The spline attachment is designed to transmit maximum torque of 2340 lb-in. from the front roller bearing carrier to the inducer. The spline engagement between the inducer and the shaft loading nut is not designed to transmit torque but is provided for nut locking only. Maximum stresses in the high-speed inducer hub and blades at design point conditions are previously shown in figure 566.

The front face of the inducer has provisions for 20 balance plugs which provide a 0.507 oz-in. maximum balance capability.

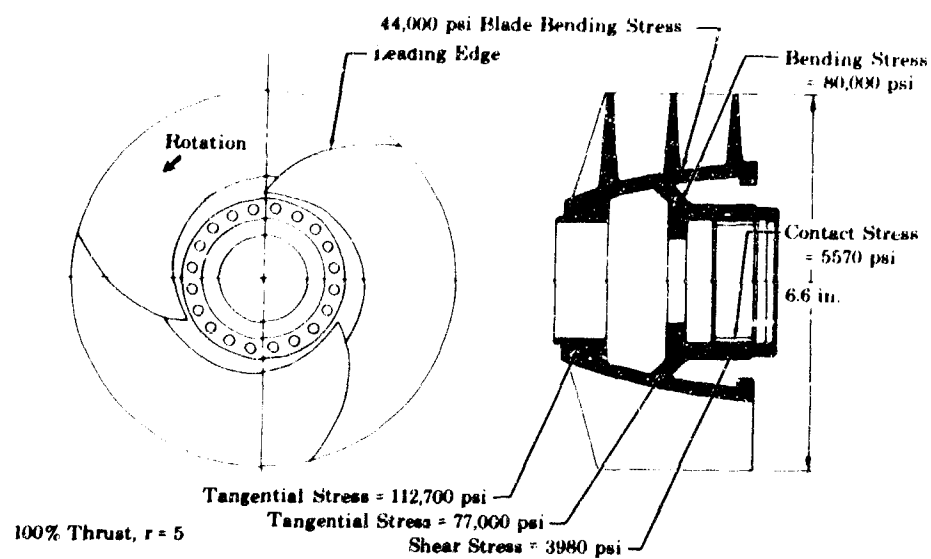


Figure 566. High-Speed Inducer

FD 31656

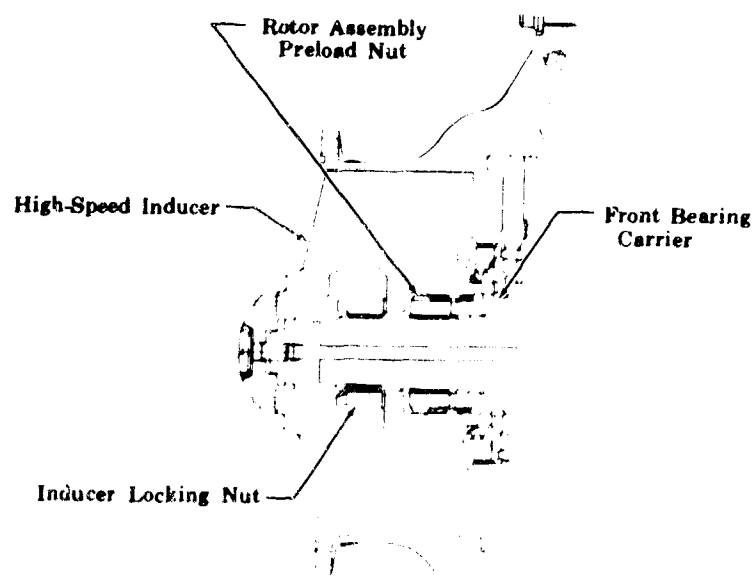


Figure 567. High-Speed Inducer Attachment

FD 31618

(2) Front Bearing and Mount Assembly

The front bearing axial location is between the high-speed inducer and the 1st-stage impeller shown in figure 568. The bearings are 55 x 96.5 mm roller bearings that operate at a DN^* of 2.64×10^6 . The roller bearing configuration is shown in figure 569. The stainless steel rollers are single crown rollers with a length-to-diameter ratio of 1. The outer race is fabricated from carbon steel. The inside diameter of the outer race is carburized to a depth of approximately 0.040 to 0.050 in. and hardened to a value of R_a 81 to 85. The core of the outer race is maintained at a hardness value of R_c 30 to 40. This configuration offers a hardware resistant roller track and puts the inside diameter in compression to minimize the effects of bearing loads. The inner race is fabricated from stainless steel and has a hardness value of R_c 56 to 62. The roller bearing design has an outer race, guided Armalon cage, roller end-to-side rail clearance of 0.020 in., and a negative internal clearance of 0.0044 in. at assembly. The front bearing mount spring rate is calculated to be 1.8×10^6 lb/in.

The front bearing (figure 570) is radially positioned between the bearing carrier and the front bearing support. The bearing carrier is press fit on the rotor assembly shaft and has an external spline at the forward end that engages the high-speed inducer internal spline, and two slots at the aft end that engage tangs on the 1st-stage impeller. The spline and the two tang slots are designed for a maximum torque of 2340 lb-in. transferred to the inducer. The rotor assembly preload of 120,000 lb is transmitted through the bearing carrier to the 1st-stage impeller. This prevents imposing the preload on the bearing inner race, which would result in bearing internal clearance problems resulting from Poisson's effect. The bearing carrier is fabricated from carbon steel, hardened to R_c 30 to 40, and chrome coated.

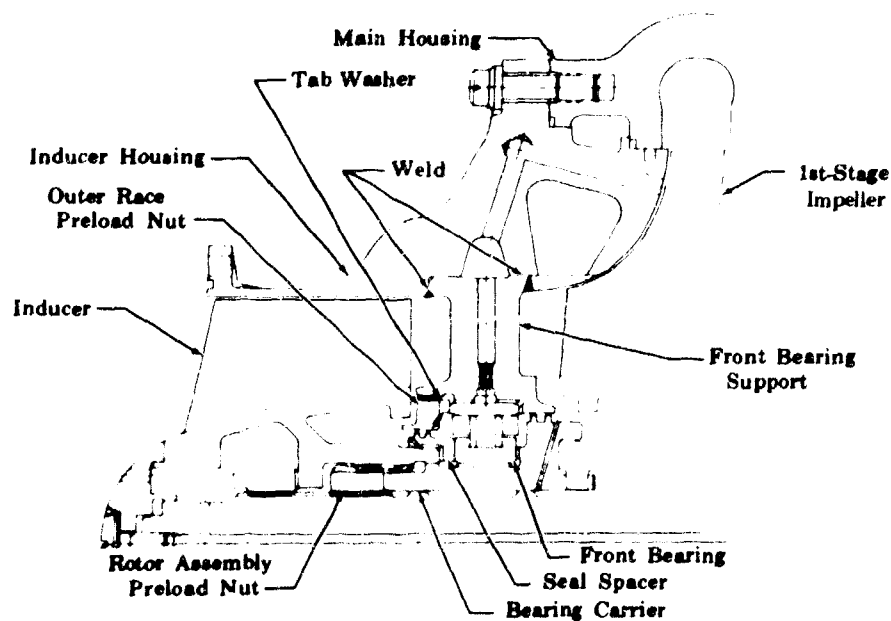


Figure 568. Front Bearing and Mount Assembly

FD 31619A

* DN = inner diameter of race (mm) times rotational speed (rpm).

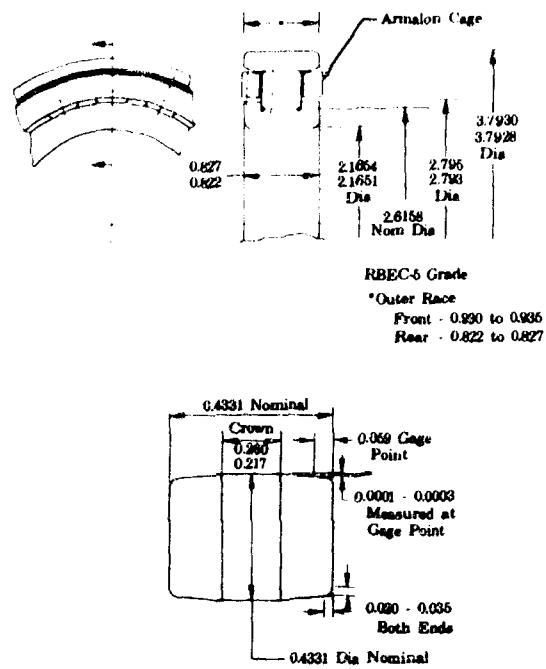


Figure 569. Roller Bearing Configuration

FD 31632

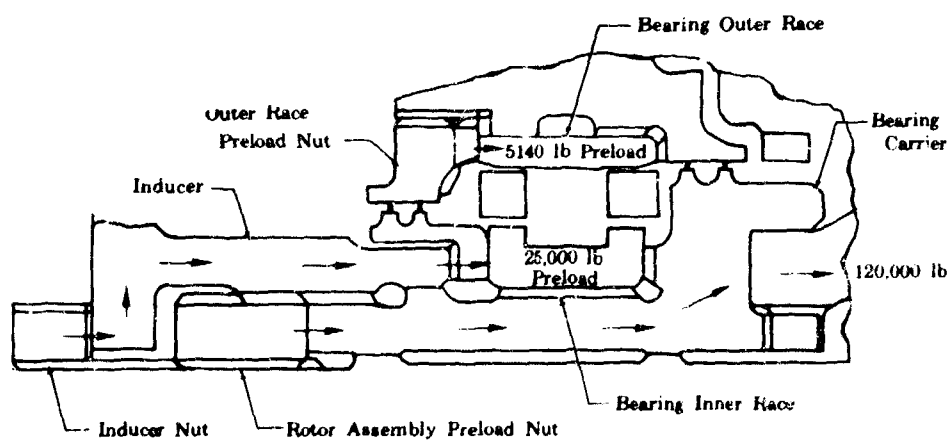


Figure 570. Front Bearing Preloading

FD 31655

The bearing inner race is loaded by the inducer nut torque of 5500 lb-in. which results in a preload of 25,000 lb. The outer race is loaded by an externally threaded nut on the front bearing support rim which is torqued to 5000 lb-in. using a washer with locking tabs.

Bearing internal fits, outer race-to-housing clearance, and inner race-to-bearing carrier clearance were established to obtain the same roller bearing operating conditions as successfully demonstrated during the bearing test program. Compatible materials were used so that differences in the coefficient of expansion would not relax the assembled parts and permit outer race spinning. Also, the preload nut has a left-hand thread that tends to tighten if the outer race rotates.

The bearing support has seven equally spaced struts extending through the main fuel flowpath. The bearing support rim distributes the bearing load to the inducer housing. The front bearing support is fabricated from carbon steel and is welded to the Inconel 600 inducer housing as previously shown in figure 568. The seven struts are positioned at an angle of 43 deg to align with the direction of inducer discharge flow. Four of the struts are used to distribute bearing coolant flow and two struts have provisions for temperature probes for measuring bearing outer race temperature.

The bearing coolant flow shown in 571 is supplied by four inlet passages drilled in the contoured surface of the inducer housing. The coolant flows into an annular manifold, which provides equal pressure distribution to the metering orifices located in the four struts. This provides a high-pressure source for the bearing coolant supply that prevents pressure variations from greatly affecting the metering orifice discharge flowrates. The 0.067 in. diameter stainless steel, removable metering orifices regulate the bearing coolant flow. The coolant cools the outer race and flows into the cavity between the rollers and the bearing carrier labyrinth seal (0.016 in. clearance). A flow of 0.098 lb/sec passes through this labyrinth seal and into the 1st-stage impeller inlet. The total bearing coolant flowrate is 9.35 lb/sec at a mixture ratio of 5 and 100% thrust (highest speed). The flowrate through the rollers is 0.275 lb/sec, which is controlled by using the front labyrinth seal clearances 0.030 in. as an orifice. The remaining 0.075 lb/sec coolant passes under the inner race and flows through eight slots in the seal spacer. Both flows vent into the main fuel flow downstream of the inducer.

(3) Pump Impellers

The back-to-back 1st- and 2nd-stage impellers are shown in figure 572. Both impellers have 24 equally spaced curved blades, which are divided into groups of six long blades, six medium length splitter blades, and 12 short splitter blades. Impellers are fabricated from A-110 titanium forgings. This material was selected because of its high strength-to-weight ratio.

The 2nd-stage impeller turbine side has an internal drive spline that engages an external spline on the rotor assembly shaft. The two impellers are connected by a face type spline, and the 1st-stage impeller inducer side engages two tangs in the front bearing carrier. Torque is transmitted from the 2nd-stage impeller drive spline through the inter-impeller spline, and through the front bearing carrier to the inducer.

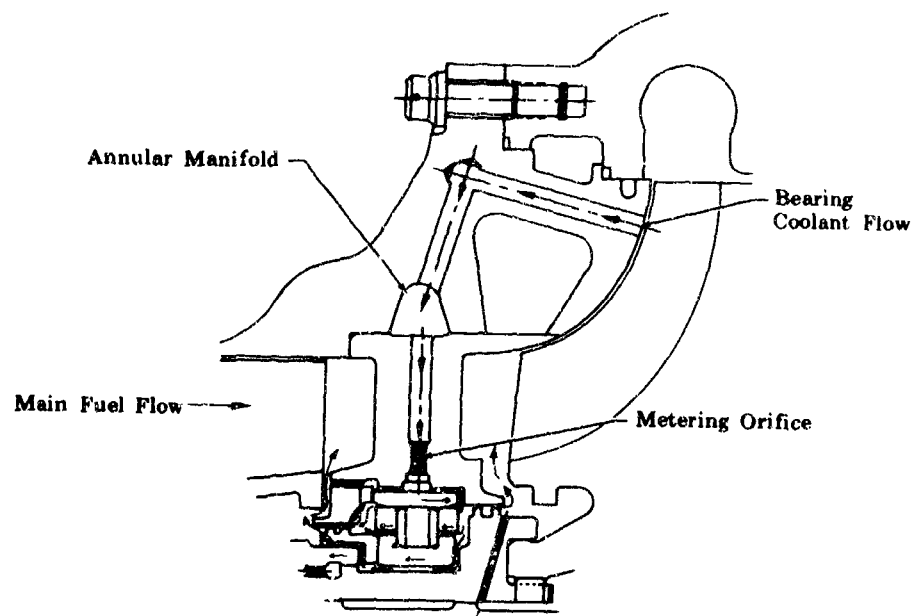


Figure 571. Front Bearing Coolant Flowpath

FD 31620A

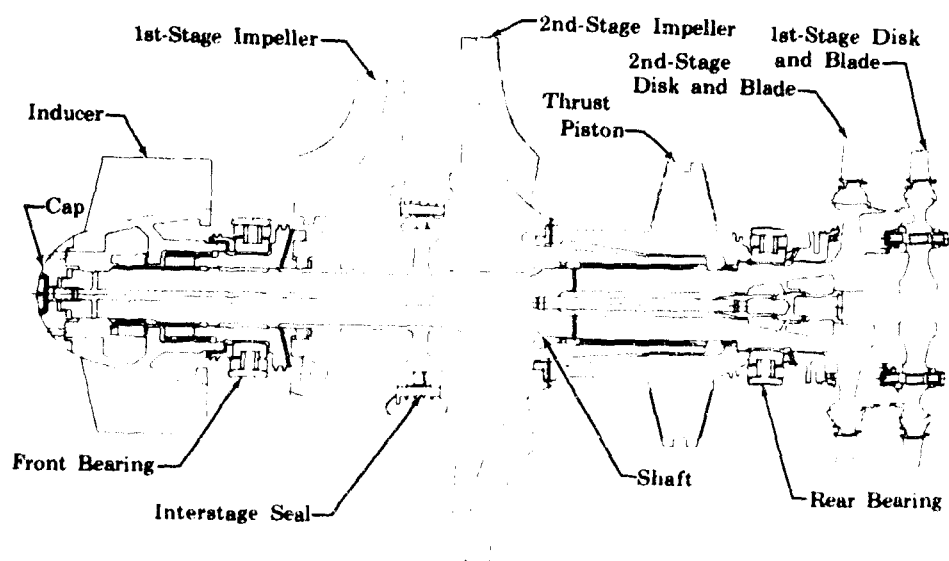


Figure 572. Rotor Assembly

FD 31659

Centrifugal forces at operating speed cause impeller bores to grow. This necessitates a very tight fit with the mating shaft to maintain the pilot between these parts. The burst margin of the impeller would also be reduced if the torque transmission splines were in the impeller bore, because splines would cause stress concentration at the bore. To eliminate both of these problems, extended necks are used at each spline location to provide the pilot diameter that mates with the shaft. The pilot diameter is then independent of the impeller bore growth avoiding stress concentrations in the bore.

(a) 1st-Stage Impeller

The 1st-stage impeller is designed without backvanes, but is designed to permit machining backvanes if test results indicate this is required for axial thrust balance. The impeller has an average tangential stress of 86,000 psia. This provides a 1.36 burst margin at 128°R average disk temperature. Blade root stresses are 32,000 psia at the inlet, 130,400 psia at the midpoint, and 98,400 psia at discharge.

(b) 2nd-Stage Impeller

The 2nd-stage impeller has an average tangential stress of 96,000 psia, providing a 1.27 burst margin at 160°R average disk temperature. Blade root stresses are 136,000 psia at the inlet, 142,000 psia at the midpoint, and 84,500 psia at discharge.

(4) Thrust Balance System

The thrust balance system shown in figure 573 is designed to compensate for the net axial imbalance during turbopump operation. The system provides a force of 50,000 lb with 2100 psi differential pressure across the piston. The thrust balance system is composed of the thrust piston, the thrust piston housing, and the rear bearing housing.

The thrust piston, fabricated from Inconel 718, has an internal spline that engages two lugs on the rotor shaft at the turbine end. Piston force loads are transmitted to the shaft through a compression face as previously illustrated in figure 573. The piston outer seal radius is 3.4 in. and the inner seal radius is 1.99 in. This provides a 23.8 in.² pressure face area.

Both sides of the thrust balance piston are supplied with high pressure fuel (2nd-stage discharge) from a common manifold. Flow is distributed through 12 drilled passages in the rear bearing housing to the piston turbine side, and through 12 drilled passages in the thrust piston housing to the piston impeller side. The flow is regulated by 0.075 in. diameter orifices press fit in the leaded bronze rub inserts. Thrust piston flow is discharged to the 2nd-stage impeller inlet. The fluid flowpath is illustrated in figure 574.

(5) Rear Bearing and Mount Assembly

The rear bearing axial location is between the thrust piston and the turbine 2nd-stage disk as shown in figure 575. The roller bearing configuration is the same as previously described for the front bearing, illustrated in figure 569, except the width of the outer race is the same as the inner race. This narrow outer race was used to improve the rotor critical speed, which is very sensitive

to the amount of turbine overhang. The bearing is radially positioned between the rotor assembly shaft and the bearing radial spring.

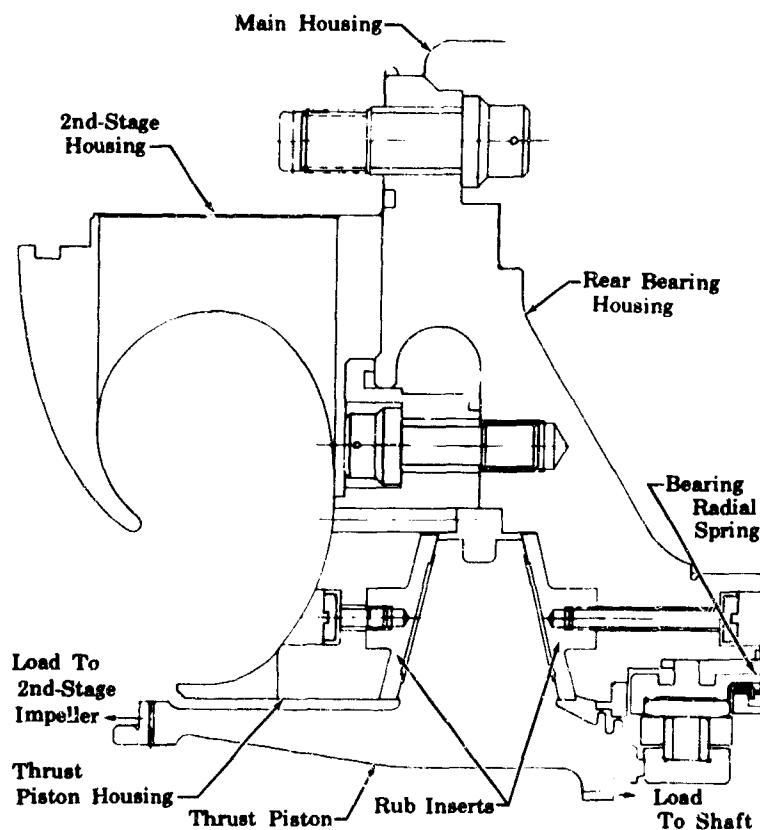


Figure 573. Thrust Balance System

FD 31621

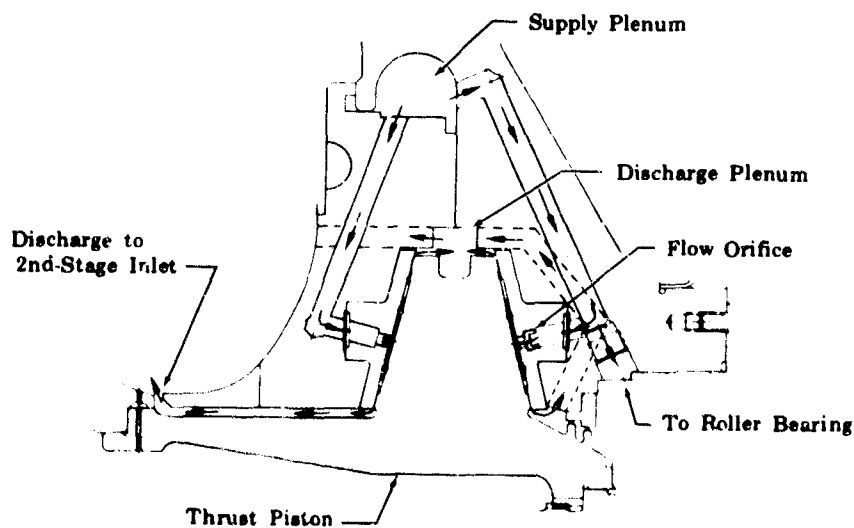


Figure 574. Thrust Piston Fluid Supply and Discharge

FD 31622

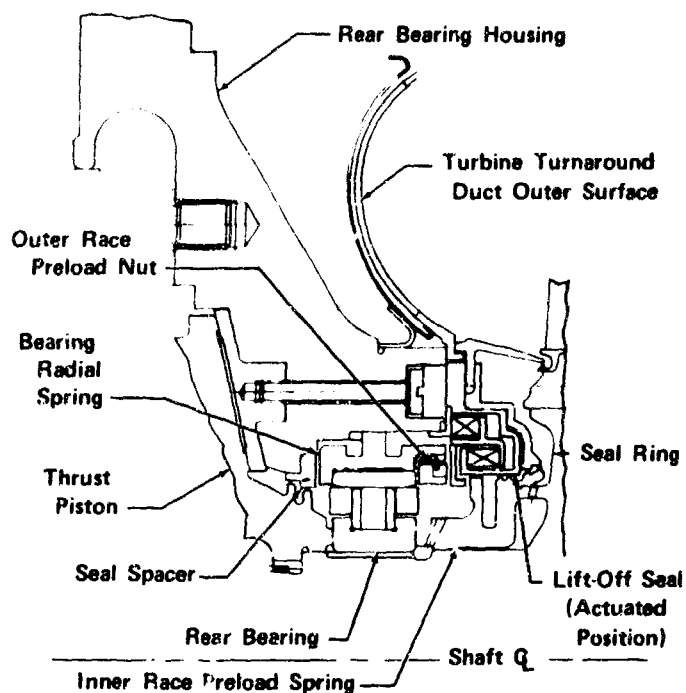


Figure 575. Rear Bearing and Mount Assembly

FD 31623A

The bearing outer race is preloaded by an externally threaded nut on the bearing radial spring and torques to 110 lb-in., which results in a preload of 10,500 lb at operating temperature because of thermal contraction of the Inconel 718 radial spring relative to the carbon steel bearing race. The inner race preload of 25,000 lb is established by splitting the 120,000 lb rotor assembly preload between the rotor assembly preload between the rotor shaft-to-thrust piston mating surface and thrust piston-to-inner race mating surface. This is accomplished by the stackup fit of the inner race preload spring. This arrangement is illustrated in figure 576.

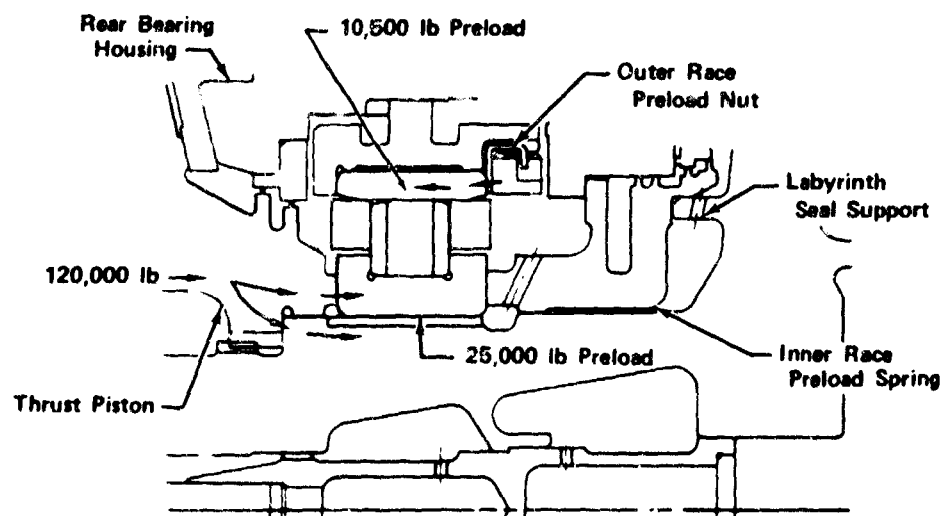


Figure 576. Rear Bearing Preloading

FD 31552A

The bearing coolant flow shown in figure 577 is supplied by extending the 12 thrust piston supply passages in the rear bearing housing to the bearing cavity. Threaded supply orifices of 0.046 in. diameter total coolant supply to the cavity between the bearing and thrust piston. Flow of 0.43 lb/sec passes through the labyrinth seal into the thrust balance piston discharge flow. The total bearing coolant flowrate is 0.59 lb/sec at a mixture ratio of 5 and 100% thrust (highest speed). The flow split between the rollers and inner race is controlled by the relative resistance between the forward labyrinth seal on one side, and the rollers and metering resistance on the other. The flowrate through the roller is 0.26 lb/sec. The remaining 0.33 lb/sec of coolant passes under the inner race and flows through eighteen 0.095 in. diameter holes in the inner race preload springs. Both flows are discharges into the turbine turnaround duct. This flow is sealed by the liftoff seal before engine start.

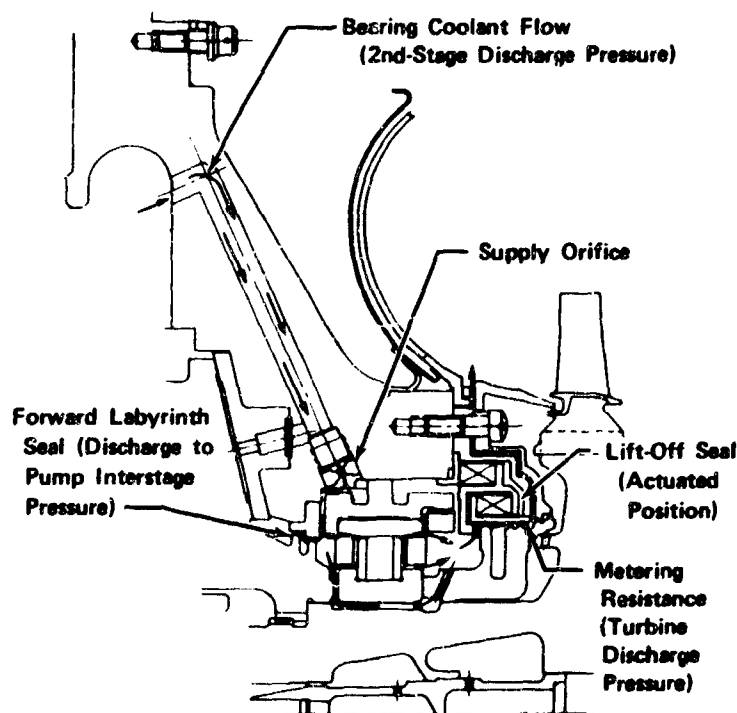


Figure 577. Rear Bearing Coolant Flow

FD 31624A

During the time the fuel turbopump is filled with propellant before start, the liftoff seal restricts leakage to less than 10 sccs. Just before ignition, 1500 psia helium is applied to the liftoff seal to compress the bellows and move the seal face forward from the inner race preload spring. The liftoff seal assembly is shown in figure 578. The seal surfaces of the liftoff seal are spray coated with layer coats of Teflon to a thickness of 0.003 to 0.005 in. Teflon provides a good sealing surface because it will compress to the form of minute imperfections in the opposing interface under the 100 lb minimum sealing loads.

b. Turbine Section

The 2nd-stage turbine previously shown in figure 572 is cantilevered from the rear bearing assembly and, in addition to the two turbine stages, consists

of the inlet ducting, support structure, turnaround manifold and exit diffuser, turbine coolant manifolding, and the two stator stages.

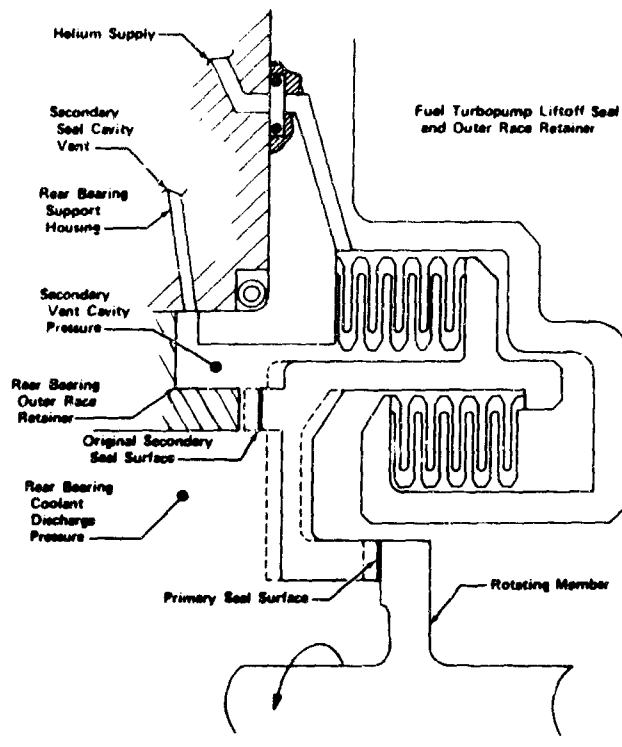


Figure 578. Fuel Turbopump Liftoff Seal

FD 38349A

(1) Turbine Inlet Duct

The turbine inlet duct shown in figure 579 is designed to mate with the transition case centerbody. The outer duct coolant distributor contains two spring loaded piston rings that permit blind assembly with the transition case centerbody. The piston rings are identical to those described in Section VIB for the transition case preburner duct. The inlet duct is the flow path structure for the transition case, hot gas discharge to the turbine, and is a one-piece housing consisting of an inner diameter bullet joined by six struts to the outer diameter wall. The inlet duct is machined from Inconel 718 and is protected from hot gas scrubbing by a heat shield fabricated from Haynes 188.

The inner and outer heat shields determine the flowpath area and are designed to provide a constantly decreasing area in the direction of the turbine. The area occupied by six struts crossing the flowpath, and their heat shields are designed as a modified airfoil to minimize turbulence and drag. These heat shields are attached to the inner and outer heat shields by intermittent welds at assembly, which will provide venting and limit to 50 psi the differential across the heat shields.

The inner heat shield has two circumferential slots that permit compressing the outside diameter so the heat shield can pass through the inlet edge of the housing at assembly. The slots are welded and abraded flush after installation. The outer heat shield is fabricated in six sections and welded together at assembly.

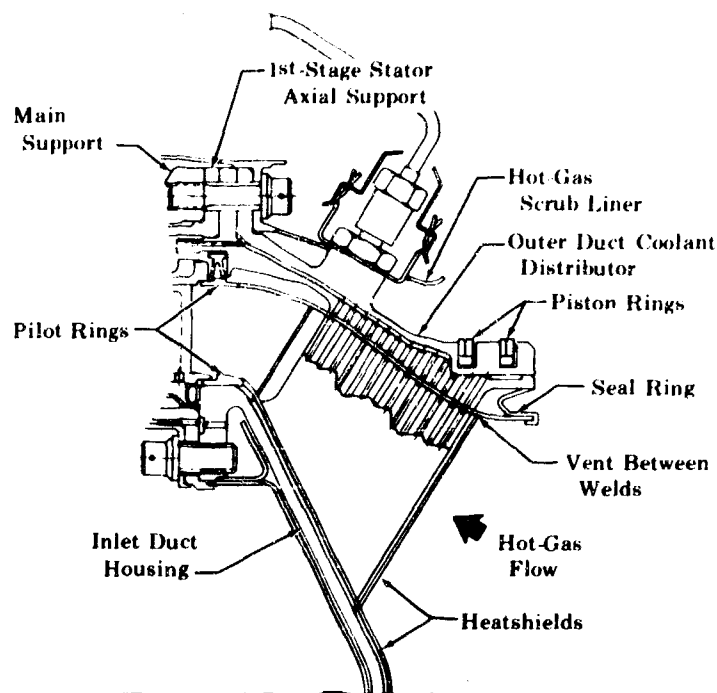


Figure 579. Turbine Inlet Duct

FD 31626

Assembled heat shields provide a still air gap of 0.050 in. for thermal insulation. The seal ring welded to the outer heat shield consists of a double Belleville washer and is designed to conform to the housing circumference after ignition. The seal closes when the heat shield temperature reaches 860°R. Before reaching this temperature, this gap allows hot gas to enter on both sides of the heat shield, causing the heat shield to expand more rapidly with less distortion. The seal ring also locates the heat shield concentrically with the housing, prevents oscillation caused by buffeting, stiffens the outer edge of the heat shield, and prevents local bulking in the area between the struts.

The inner and outer heat shields are welded to pilot rings at assembly. The entire heat shield assembly is fabricated from Haynes 188 and does not require post-weld heat treatment.

The inlet duct housing, outer duct coolant distributor, 1st-stage stator axial support, and the turbine discharge, hot gas scrub liner are sandwiched and bolted to the turbine main support by 24 bolts. Torque and axial loads of the turbine inlet duct and the 1st- and 2nd-stage stators are transmitted to the diffuser case by the turbine main support.

(2) 1st-Stage Stator and Support

The 1st-stage stator consists of integrally cast vanes, a continuous inner shroud ring, and individual vane outer shroud platforms. The 1st-stage stator is cast from IN100 (AMS 5397), and the 22 vanes are supported at each shroud in both axial and tangential directions.

The inner shroud is a complete ring from which the vanes extend outward in a radial direction. Eight radial slots, equally spaced on a flange below the

flowpath surface and near the stator inlet, engage lugs on the inlet duct housing to locate the inner shroud during all thermal conditions (Figure 580.) Torque or tangential loads from the ring are transmitted to the inlet duct housing through these lugs. A second flange below the flowpath, the outer shroud or exit is designed to transmit the axial load of the inner ring to the inlet duct through the stator retaining cylinder. This flange also has a snap provided to mount a one piece seal shim. Shim thickness is determined at assembly to provide vane axial support at 100% thrust and a mixture ratio of 7.

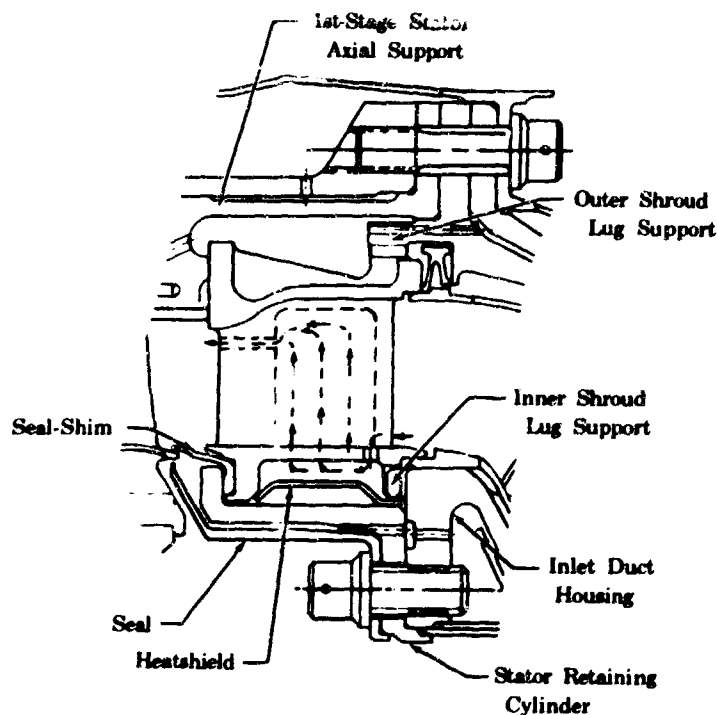


Figure 580. 1st-Stage Stator Installation

FD 31627

The inner shroud ring has twenty-two 0.11 in. diameter holes near the stator inlet to supply hot gas flow to the root of the cored vane. The gas flow enters the vane core and exits through two 0.0750 in. diameter holes near the vane tip on the pressure side of the airfoil. The purpose of this flow through the vane is to reduce the severity of thermal shock during start and shutdown transient conditions by applying gas stream temperature to both sides of the vane wall. Vane wall thickness is not less than 0.050 in. Very little change in chord along the vanes length occurs although there is some twist. Maximum bending stress under maximum temperature is 17,284 psi at the vane leading edge, giving a 10 hour, 2% stress rupture margin.

The Inconel 718, 1st-stage, stator retaining cylinder, which carries the stator axial load, bolts to a flange on the inlet duct inner bullet. There is also an approximate 100 psid pressure drop across the cylinder. Therefore, the cylinder thickness is sized as a pressure vessel as well as a tension member. The inside diameter is in contact with the turbine coolant flow and the outside diameter is protected from hot gas scrubbing by a three piece Haynes 188 heat shield.

The outer shroud is split between each vane because of the thermal incompatibility of a cool outer ring joined to a hot inner ring. The gap is 0.060 in. maximum at the outer surface and is covered by a flat strip seal trapped in a slot perpendicular to the radial split. On top of each vane platform toward the stator inlet is a lug that transmits the tangential load at this support into the inlet duct housing. All of the vane axial load is transmitted to the 1st-stage stator axial support until the inner diameter axial support seals because of thermals and local deflections at 100% thrust and $r = 7$.

Flow area changes may be accomplished on both turbine vane stages if required for turbine matching on the engine. To increase the flow area, the trailing edges of the vanes may be trimmed back 0.10 in. on both stages to obtain an approximate 10% flow area increase. To reduce the flow area, castings with reduced blade height are used to obtain 10% flow area reduction on the 1st-stage and 5% reduction in flow area on the 2nd-stage.

(3) 1st-Stage Blade and Disk

The 1st-stage turbine blade is approximately 1.2 in. long with an uncooled solid airfoil approximately 0.7 in. long. The blade is cast from SM200, a nickel base alloy. The blade castings are directionally solidified to obtain a preferred grain orientation in the direction of the predominant stress. A rectangular platform is provided at the airfoil base with sufficient width and length to isolate the attachment, disk, and shafting from the main gas path.

A four-toothed (two on each side) fir tree is provided to transfer the blade centrifugal load into the disk by means of mating slots axially cut through the disk rim. The blade is restrained from axial movement by an integral lug extending below the disk slot profile to bear on the upstream side of the disk rim, and by a retaining pin through a hole in the blade root to bear against the downstream side of the disk rim.

A small clearance between adjacent platforms, necessary to tolerate thermal incompatibilities between the cool disk and the hot platforms, is covered by a thin sealing strip. Attached to the sealing strip is a weight that, as a result of a centrifugally induced load, will press on the inside surfaces of adjacent platforms to provide damping of blade vibrations. The seal strip, damper weight, and retainer pin are made of Inconel 600. The forward and aft edges of the platform have closely machined features to complement knife edges on the adjacent nonrotating turbine parts in achieving effective labyrinth-type seals.

The 1st-stage disk is fabricated from modified Waspaloy. Stepped seal lands are provided on the forward side of the disk to complement mating knife edges on the 2nd-stage stator seal diaphragm. A short projection is also provided on the forward side to serve as a support pilot at the rotor shaft flange to 1st-stage disk attachment. The disk is secured to the rotor shaft by 10 bolts. A self locking nut on the forward side is torqued to 55 lb-in. and the aft nut, available in several weight classes for dynamic balance corrections, is torqued to obtain a 0.0044 to 0.0046 in. bolt stretch. This establishes a bolt preload of 4500 lb. This preload is affected significantly by the range of coefficient of friction and is reduced by Poisson's effect during rotation. The bolts have an axially drilled hole through the center to maintain a minimum temperature gradient between the bolts and the disk during start and shutdown transients. Ten holes are provided in the disk for balance pins. Initial disk unbalance can also be corrected by interchanging

blades and dampers, and small corrections can be made by grinding the overhung portion of the nut.

The 1st-stage turbine blade shroud, fabricated from Inconel 625, is radially controlled by the 1st-stage stator axial support shown in figure 581. The shroud is a split ring and has a 0.005 in. tight outside diameter fit with the stator support. As the temperature of the turbine gases increase, the shroud tends to increase in diameter. Because the shroud is restrained diametrically by the cooled support structure, the split in the ring closes due to thermals without overstressing the shroud. The 1st-stage blade tip-to-shroud clearance at assembly is 0.0185 to 0.0285 in.

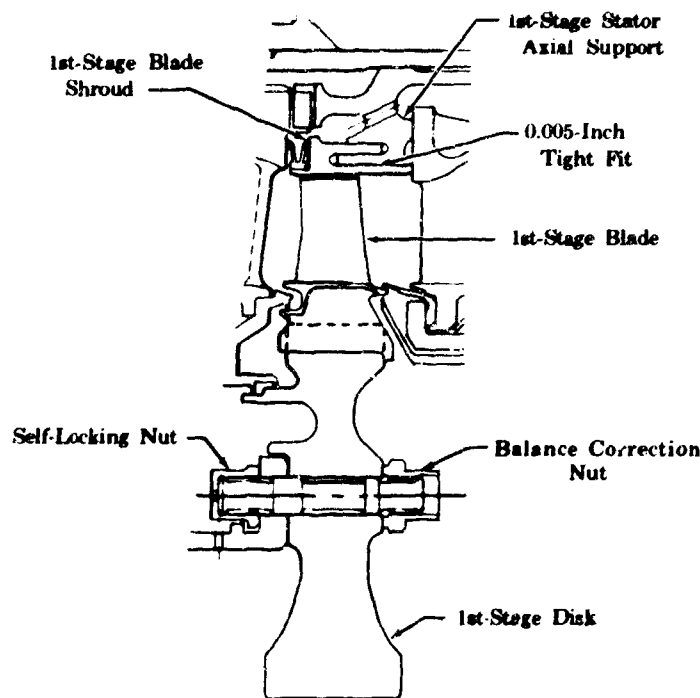


Figure 581. 1st-Stage Disk, Blade and Shroud Installation

FD 31628A

(4) 2nd-Stage Stator and Support

The 2nd-stage stator consists of integrally cast vanes, a continuous outer shroud ring, and individual vane inner shroud platforms. The 2nd-stage stator is cast from IN100. The 36 vanes are supported at the outer shroud in both axial and tangential directions.

The outer shroud is a complete ring from which the vanes extend inward in a radial direction. Eight equally spaced radial slots on the outer ring engage lugs on the 1st-stage stator axial support to locate the outer shroud at all thermal conditions, as previously shown in figure 582. Torque or tangential loads from the vanes and seal diaphragm are transmitted to the 1st-stage stator axial support through these lugs. The 2nd-stage stator axial loads are transmitted to the turbine main support.

The outer shroud ring has thirty-six 0.058 in. diameter holes to divert mainstream hot gas to the flow guide as shown in figure 582. The flow is directed along each heavy end section of the casting to minimize the steady-state gradient. The flow is then directed to the core to equalize the temperatures across the vane wall and then to the inner shroud. The flow guide, illustrated in figure 583, is a two-piece ring design and is fabricated from Inconel 625. The gap in the flow guide is covered by an Inconel 625 seal strip held in place by two Inconel 600 (AMS 7232) rivets on one side of the gap. The flow guide is positioned radially by an L-605 pin inserted into a vane core opening approximately 180 deg from the gap. The outer shroud has a Waspaloy cover to separate the mainstream hot gas flow from the turbine coolant flow. Because the cover will loosen during shutdown transients, an axial pinch seal is on one end, and an L-605 piston ring on the other.

The vanes have a variable chord and they have twist. Under the worst conditions, the maximum stress at the tip leading edge is 37,900 psia and provides an approximate 7% margin based on a 10 hour stress rupture. The original vane wall thickness was 0.050 in. but was thinned to 0.040 in. at the root to provide more flow area to reduce the pressure drop of the core flow.

The inner shroud is split between each vane. These gaps close under operating conditions permitting a restricted hot gas flow on the inside of the shroud to reduce the thermal gradient across the shroud. This engagement provides radial centering or support of the seal diaphragm. The inner shroud has a stop that provides axial restraint for the seal diaphragm axial load. The spline retention permits thermal growth of the 2nd-stage stator without imposing stresses in the cooler diaphragm seal.

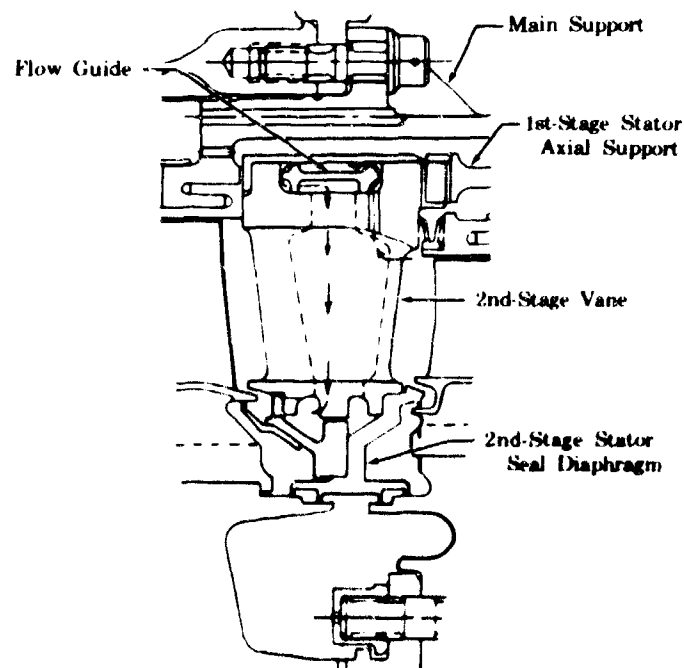


Figure 582. 2nd-Stage Stator Installation

FD 31629

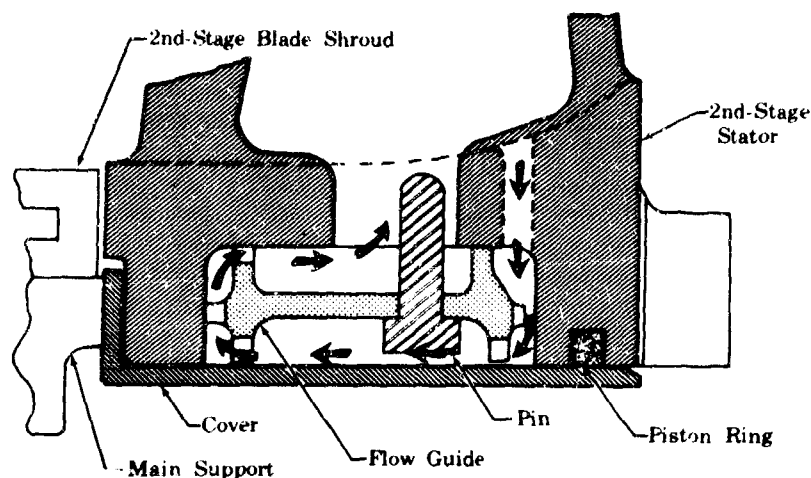


Figure 583. 2nd-Stage Stator Flow Guide

FD 31630

The 2nd-stage stator diaphragm seal is illustrated in figure 584. The diaphragm consists of three parts riveted together: the front cone, the rear cone, and a single labyrinth seal plate. The parts are fabricated from Waspaloy. The front cone is designed to carry the 5000 lb differential pressure load and has five labyrinth seal lips. The rear cone, which holds the single labyrinth seal, has the radial centering and support spline and, when riveted to the front cone, holds the diaphragm to the stator casting.

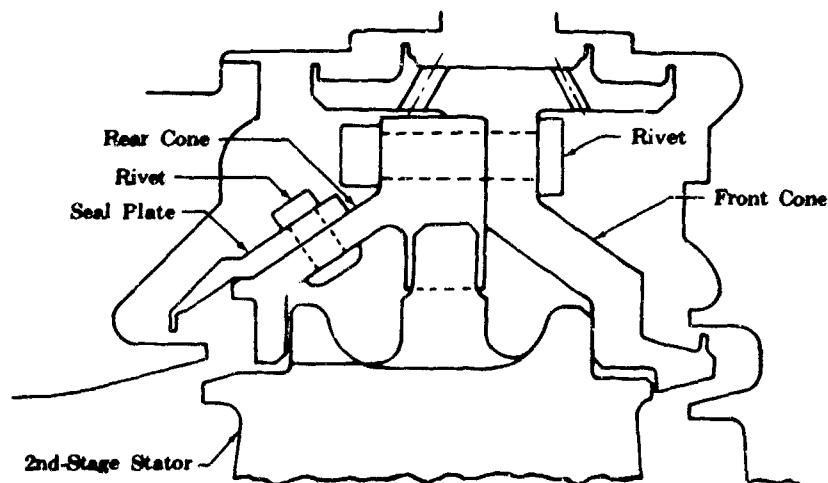


Figure 584. 2nd-Stage Stator Seal Diaphragm

FD 31740

The rear cone has 36 reliefs that provide approximately 0.07 in.^2 flow area to permit the vane core hot gas flow to exit at the root of the 2nd-stage blade. One spline tooth has offset width to prevent the entire diaphragm assembly from being incorrectly assembled.

The diaphragm assembly is designed so that differential pressure exerts less than 1 lb tensile load in the rivets. Maximum stresses in the seal are nominally 26,000 psi and the rotation of the seal cylindrical section is 0.009 radians, which will impose only a minor load on the rivets.

(5) 2nd-Stage Blade and Disk

The 2nd-stage turbine blade is approximately 1.7 in. long with an uncooled solid airfoil approximately 1.0 in. long. The blade is cast from SM200, (a nickel base alloy). Blade castings are directionally solidified to obtain a preferred grain orientation in the direction of predominant stresses. A rectangular platform is provided at the airfoil base with sufficient width and length to isolate the attachment, disk, and shafting from the hot main gas path. The forward and aft ends of the blade platform have machined features to mate with nonrotating seal ring and 2nd-stage stator seal diaphragm to achieve labyrinth type seals. At assembly the 2nd-stage blade tip-to-shroud clearance is 0.021 to 0.030 in.

The 2nd-stage disk is integral to the rotor assembly shaft and is fabricated from modified Waspaloy. Stepped seal lands are provided on the aft side of the disk rim to complement mating knife edges on the 2nd-stage stator seal diaphragm. A short projection is provided on the shaft side of the disk to serve as a support pilot for the rotor element of the labyrinth seal, refer to figure 576. This projection also receives a small portion of the shaft axial stackup load transmitted through the rear bearing inner race. A flange is provided on the aft side of the disk for attaching the 1st-stage disk.

The disk operates at higher than cryogenic temperatures while the rear bearing is maintained at cryogenic temperature. The design isolates the resulting temperature gradients in the portion of the shaft between the disk and rear bearing. Isotherms ($^{\circ}\text{R}$) are shown in figure 585.

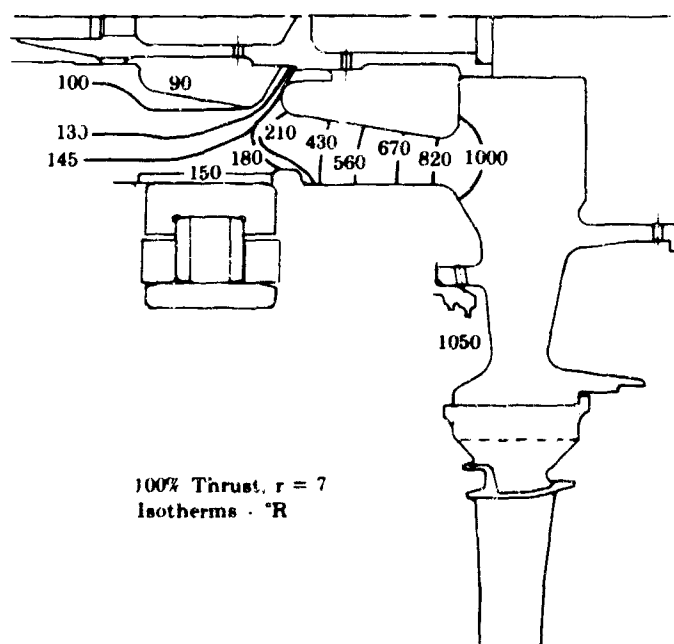


Figure 585. Rotor Assembly Shaft Transition Section Isotherms

FD 31662

(6) Turnaround Manifold

The turnaround manifold, illustrated in figure 586, consists of a seal rig, a baffle assembly, and an inner duct guide. This manifold provides a constantly decreasing area flowpath. The turnaround manifold is coupled to a straight walled diffuser section that discharges turbine hot gases into the transition case. The turbine exit area to diffuser entrance area is 0.89 during operation and the diffuser has a 10 deg included angle with an effective area ratio of 1.91.

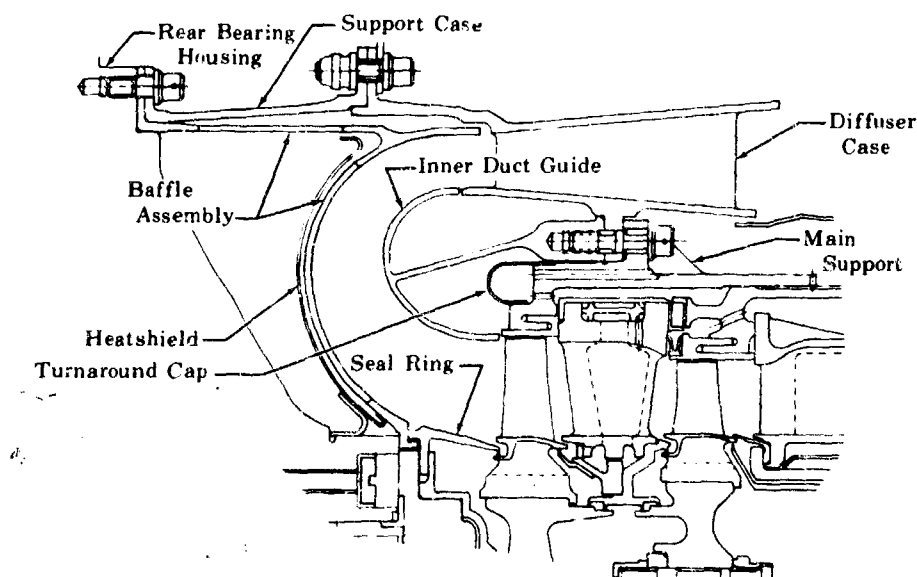


Fig. 586. Turbine Discharge Turnaround Manifold

FD 31631

The seal ring provides 1) a knife edge seal for sealing the 2nd-stage blade platform, 2) a method of discharging rear bearing coolant flow and 2nd-stage disk coolant flow, and 3) the initial turnaround manifold contour.

The complete seal ring is composed of two pieces; an outer seal ring, and an inner retainer ring. The outer seal ring is separate from the inner ring because of the severe thermal stresses present in a one piece design. Positioning and retention of this ring is accomplished by six close tolerance slots in the inner ring, which permits radial growth of the outer seal ring. The inner ring is mounted on the liftoff seal housing by fillister head screws. Slots are provided in 22 places on both pieces for the disk and rear bearing coolant flows.

The baffle assembly is fabricated from Inconel 625. The baffle assembly outer flange, which is bolted with the outer support case to the rear bearing housing, shields the outer support case from hot gases. The resulting cavity is vented to turbine discharge. The inner flange is positioned by slots in the seal ring, and has axial slots that vent the cavity between the baffle assembly and the rear bearing housing. Venting minimizes bending stresses occurring in the turnaround baffle. An Inconel 625 heat shield is provided to insulate the adjacent pump housing from the heat radiating from the turnaround baffle assembly.

The diffuser case, cast from IN100, has 40 struts which tie the inner and outer walls. These struts are load carrying members and have no aerodynamic function. The turbine torque and axial loads are transmitted to the diffuser case by 24 radial lugs sandwiched between the turbine main support and the inner duct guide. The total load is transferred to the main pump housing by the Inconel 625 outer support case.

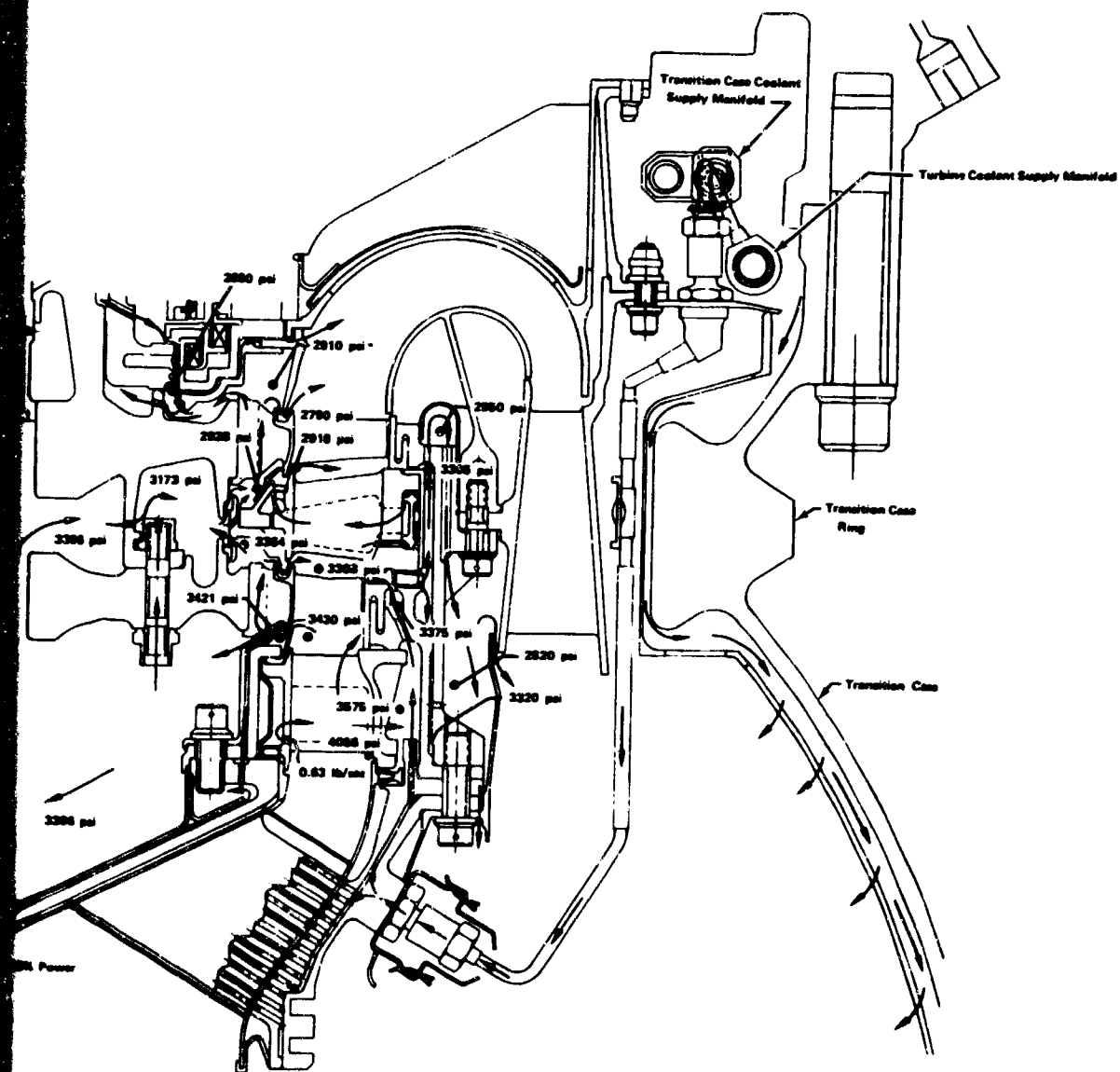
The Waspaloy inner duct guide completes the internal flowpath of the turnaround manifold. Because the duct guide is uncooled, hot turbine discharge gases are allowed to enter the static cavity behind the contoured surface. This effect results in virtually uniform temperature throughout the guide, thereby greatly reducing thermal stresses.

(7) Turbine Cooling

The transition case and turbine coolant supply manifolds are located in a cavity formed by the main fuel pump housing, the transition case, the turbine turnaround duct, and the diaphragm seal as shown in figure 587. The transition case manifold is supplied with coolant from the transpiration coolant supply heat exchanger and discharges this coolant into the cavity through four fixed metering jets located approximately 90 deg apart. Metering jets are positioned to discharge outboard and tangentially to increase circulation within the cavity and to prevent direct impingement of the coolant on the structural walls. Coolant flows from this cavity into the gap between the transition case wall and the cooling liner.

The turbine coolant supply manifold is connected to six bulkhead fittings on the diaphragm seal. The diaphragm seal provides a support for the manifold and also provides sealing necessary to prevent loss of the transition case coolant. During assembly, the outer perimeter of the seal contacts the mating seal surface of the transition case liner and is deflected 0.060 in. to provide initial seal loading. During normal engine operation this is a pressure loaded seal. The turbine coolant, supplied from pump discharge, flows to the inlet duct coolant distributor through six supply tubes. This coolant is used to cool the entire turbine inlet structure and ultimately cools the rotating and nonrotating turbine parts shown in figure 587.

Coolant is supplied through six 0.125 in. OD tubes to the outer duct coolant distributor. The Inconel 718 distributor forms a 0.040 in. thick concentric coolant passage with the outside diameter of the inlet duct housing. Spot welded baffles on the duct housing route the coolant to thirteen 0.050 in. diameter holes in each of the six struts. Coolant discharges into a coolant passage formed by the stainless steel bullet coolant distributor. Coolant is collected at the bullet outer diameter behind the 1st-stage stator retaining flange and discharges through thirty 0.050 in. diameter flange holes into an annulus formed by the 1st-stage stator retaining cylinder and the 1st-stage blade inner labyrinth seal. The coolant enters a chamber formed by the two seals. The inner diameter seal forms a 0.040 in. gap with the 1st-stage blade platform on the flowpath side to permit hot gas to enter the mixing chamber. The labyrinth seal forms a 0.050 in. gap on the inside 1st-stage blade platform through which mixed coolant is discharged to be charged to cool disks and blade roots.



FD 31660C

635/636

1

BLANK PAGE

A 0.020 in. magnesium zirconate coating is applied to the first inlet duct bullet flange and lugs that contact the 1st-stage stator inner shroud. This reduces the temperature gradient through the thick section of the ring.

To prevent a large temperature difference between the 2nd-stage disk coolant and the rear bearing coolant from imposing large temperature gradients in the shaft and/or disk, the shaft section between the bearing region and the disk was made as narrow and as long as possible, so that the major portion of the gradient would occur in the noncritical section. Part of the turbine disk coolant flow is diverted along the pump side of the 2nd-stage disk to uniformly cool the disk on each side. This coolant is vented through a labyrinth seal and vents into the turbine discharge through slots in the seal ring.

Coolant from the outer duct coolant distributor is also discharged through eleven 0.050 in. diameter holes in the duct housing outer diameter torque lugs into a chamber formed by the 1st-stage stator axial support and the 1st-stage stator outer shroud. Hot gas enters this chamber through two holes in each intervane strip seal. This coolant mixture is used to maintain blade tip clearance by cooling the shroud support structure. To prevent uncontrolled hot gas from entering this mixing chamber, a K-type seal is provided between the 1st-stage stator outer shroud and the flange of the inlet duct housing.

Coolant discharges from the mixing chamber through thirty-six 0.087 in. diameter holes into the cavity behind the 1st-stage stator axial support, then the coolant flows into the cavity behind the 1st-stage blade shroud. A K-type seal is provided between the 1st-stage blade shroud and the 2nd-stage stator shroud to minimize coolant leakage for this cavity. The 1st-stage stator axial support is scalloped between the engagement slots for the 2nd-stage stator to permit coolant to flow around the 2nd-stage stator and through forty-eight 0.064 in. diameter holes in the main support to the turnaround cap. The coolant leaves the turnaround cap through forty-eight 0.072 in. diameter holes to the cavity between the diffuser case and main support structure. To efficiently cool the 1st-stage stator axial support, a small flow is directed between the main support and the 1st-stage stator axial support. This coolant is vented to the cavity between the main support and diffuser case through ten 0.059 in. diameter holes. Coolant is routed to the diffuser discharge pressure via scallops in the aft flange.

System orifices provide a programmed pressure drop, so as flow progresses along the various stages in the turbine, the pressure differential between coolant flow and mainstream flow is relatively small. This prevents excessive coolant leakage and reduces buckling pressure loads on the various components.

c. Rotor Assembly

The rotor assembly is illustrated in figure 588. The modified Waspaloy shaft consists of the 2nd-stage turbine disk with a flanged protrusion on one side for the 1st-stage turbine disk, and a splined section with a tie bolt extension on the other side. At assembly, the tie bolt is loaded to 120,000 lb tensile force, creating a stress level of 102,500 psia in the tie bolt. This load is required to ensure the rotor stackup remains tight at design speed when the unbalanced forces act on the impellers tending to stretch the tie bolts. Also, as the impeller increases in speed, hoop stresses increase and the impeller grows in diameter and results in a decrease in impeller axial length equivalent to Poisson's ratio of axial to radial deflection. This effect tends to reduce bolt load. As the temperature is lowered, the tie bolt contracts much faster than the stacked parts, therefore

increasing bolt load, which is caused by the higher coefficient of thermal expansion of the steel tie bolt versus the lower coefficient for the titanium impellers. These interactions were considered when bolt preload requirements were predetermined.

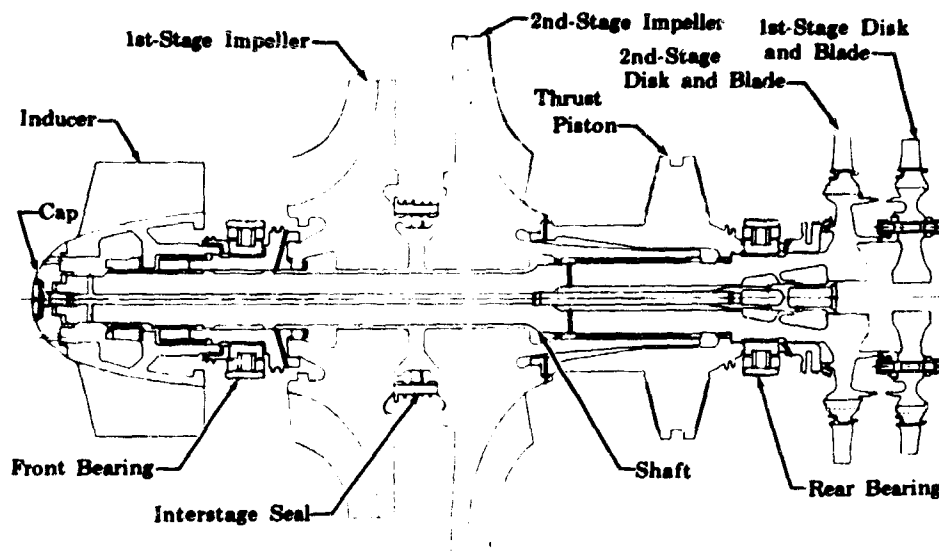


Figure 588. Rotor Assembly

FD 31659

The shaft spline has 30 teeth that engage the 2nd-stage disk. The teeth are designed having a straight face on the pressure side. This design was selected because the torque load is always in the same direction and radial deflections can be tolerated with this tooth shape.

A conical section, between the spline and the turbine disk, is used to transition from hot to cold areas in the turbopump. Coolant flow from the 2nd-stage impeller inlet flows through six 0.045 in. diameter holes in the 2nd-stage impeller and thrust piston, around the 2nd-stage impeller spline, and along the outside diameter of the shaft to provide impeller bore cooling before exiting into the area ahead of the 1st-stage impeller. Cooling flow is illustrated in figure 589. Some coolant is directed through two 0.069 in. diameter holes toward the rear bearing area and is directed through four 0.063 in. diameter holes to the center of the shaft. This flow is discharged through two 0.117 in. diameter holes in the shaft and through four 0.175 in. diameter holes in the cap to pump inlet. This coolant scheme creates a thermal barrier between the rear bearing and the 2nd-stage turbine disk. Low temperatures exist on the bearing side and higher temperatures prevail on the turbine side with a thermal gradient along the conical section in the middle. Figure 585 illustrates the isotherm cross section in the transition section.

d. Housings

The fuel pump housings are illustrated in figure 590. The Inconel 600 inducer housing is designed for a bearing load of 1500 lb, an aggregate of the impeller pressure load distribution, seal loads, inlet pipe bending moment and blowoff load, and inducer pressure distribution. This housing material

was selected because of the high modulus of elasticity minimizing housing deflection and to obtain a thermal coefficient of expansion similar to that of the carbon steel front bearing support. The extra ring section was incorporated in the housing to carry the hoop load, thereby limiting the deflection of the housing so bearing and seal deflections can be held to a minimum, and impeller clearances can be maintained.

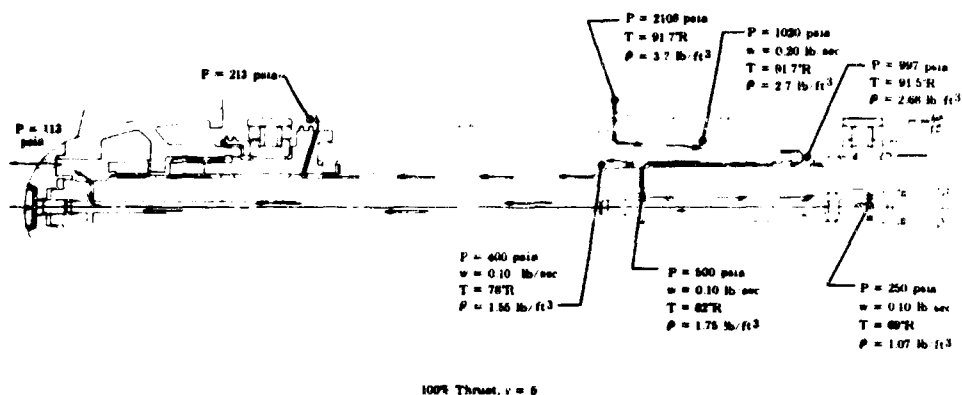


Figure 589. Rotor Assembly Coolant Flows

FD 31661

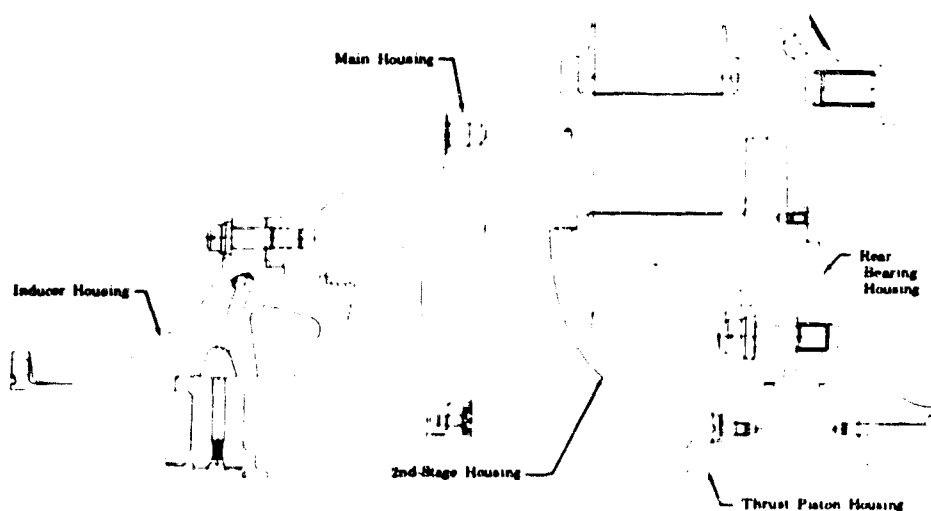


Figure 590. Fuel Turbopump Housings

FD 31666

A double static seal arrangement was used on the inducer housing so the inner cavity would be vented to the low pressure pump inlet. This scheme prevents a condition of having a potential high-pressure overboard leak. Vent flow is vented downstream of the 1st-stage impeller inlet preventing impeller inlet flow distortion. Fuel leakage from the liftoff seal is also vented into the same low-pressure cavity.

The inducer housing inlet flange is a cantilever design having a 0.001 in. calculated deflection at the seal location under a worst-case operating condition.

The large flange is not a cantilevered design because of the potential increase in the housing deflection.

The initial test inducer housing has provisions for mounting the following instrumentation:

1. Inducer discharge static pressure (1)
2. Bearing outer race temperature (2)
3. Speed (2)
4. Impeller discharge static pressure (2)
5. Various impeller pressures (2).

The Inconel 718 main housing, between the inducer housing and the transition case, encloses the two stage centrifugal pump and forms a rigid outer body to which the bearing support structures are attached. Each pump stage has a constant velocity collection system and two discharge diffuser horns. Two interstage tubes are welded to the housing to eliminate possible leak sources of static seals and to minimize weight and envelope. Interfaces are provided in the housing to accommodate thrust piston supply flow, transition case liner coolant flow, and helium liftoff seal supply pressure. The main housing has mounting provisions for the following instrumentation:

1. Pump discharge pressure (2)
2. Pump discharge temperature (2)
3. Turbine inlet pressure (1)
4. Turbine inlet temperature (1)
5. Turbine discharge pressure (1)
6. Turbine discharge temperature (1)
7. Thrust piston pressure - pump side (1)
8. Thrust piston pressure - turbine side (1)
9. 2nd-stage inlet temperature (2).

On the initial test housing, 35 additional pressure and temperature bosses have been provided. Interfaces for auxiliary flows from the fuel low speed inducer to the two position nozzle are incorporated in one of the interstage tubes.

The Inconel 718 thrust piston and rear bearing housings provide a multifunctional capability. The rear bearing housing provides a high radial spring rate for the rear bearing support and contains the bearing coolant supply manifold. The combined housings enclose the rear end of the pump and provide a high axial spring rate for the thrust piston reaction faces. The thrust piston reaction faces are leaded bronze (Bearing B-10) inserts which provide a

compatible rub surface for the thrust piston if rubbing should occur during a transient condition. The housings contain the thrust piston supply manifold and have interfaces to accommodate thrust piston flow, bearing coolant flow, and the helium liftoff seal supply pressure.

The 2nd-stage housing is fabricated from aluminum because this part is primarily used to provide the desired flowpath for the 2nd-stage impeller and because it is not a highly stressed pressure vessel. Use of aluminum instead of Inconel 718 saves approximately 12 lb turbopump weight. Housing deflections and stress are illustrated in figure 591.

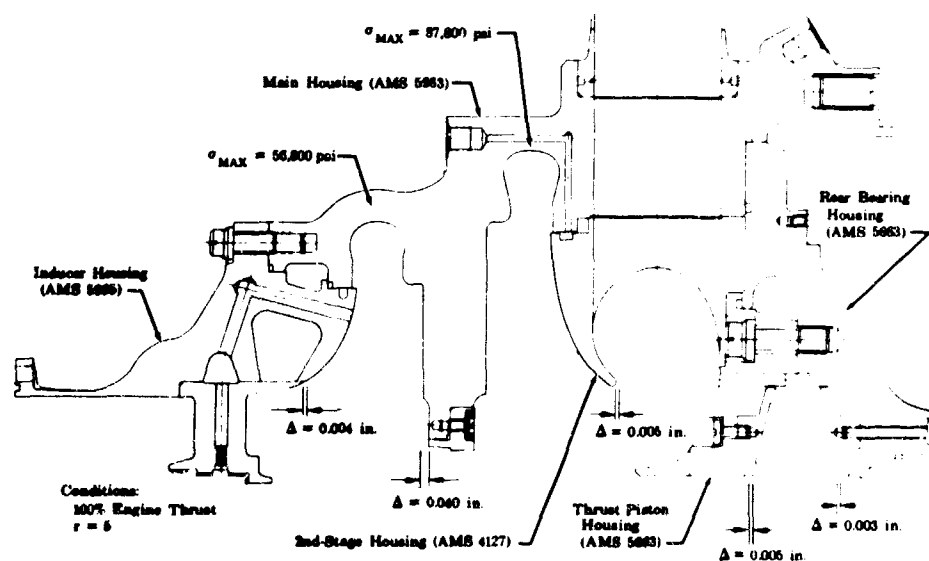


Figure 591. Maximum Stresses and Deflections in Critical Areas of the Housings FD 31667

The fuel turbopump calculated weight is 565 lb including the manifolds for the transition case liner cooling and approximately 10 lb additional instrumentation bosses that will not be required after the original pump rig testing. It is also anticipated that approximately 19 lb may be removed from subsequent main housings following the proof pressure tests. Additional material was allowed in some areas of the housing because of the inability to accurately calculate stresses having very complicated load paths. The actual weights are 587 lb and 590 lb for the two turbopumps fabricated.

The XLR129 fuel turbopump predicted performance and actual performance for inlet flow parameters vs pressure rise is shown in figure 592.

4. Fabrication

Table LXXVII lists the turbopump parts procurement time for major turbopump parts.

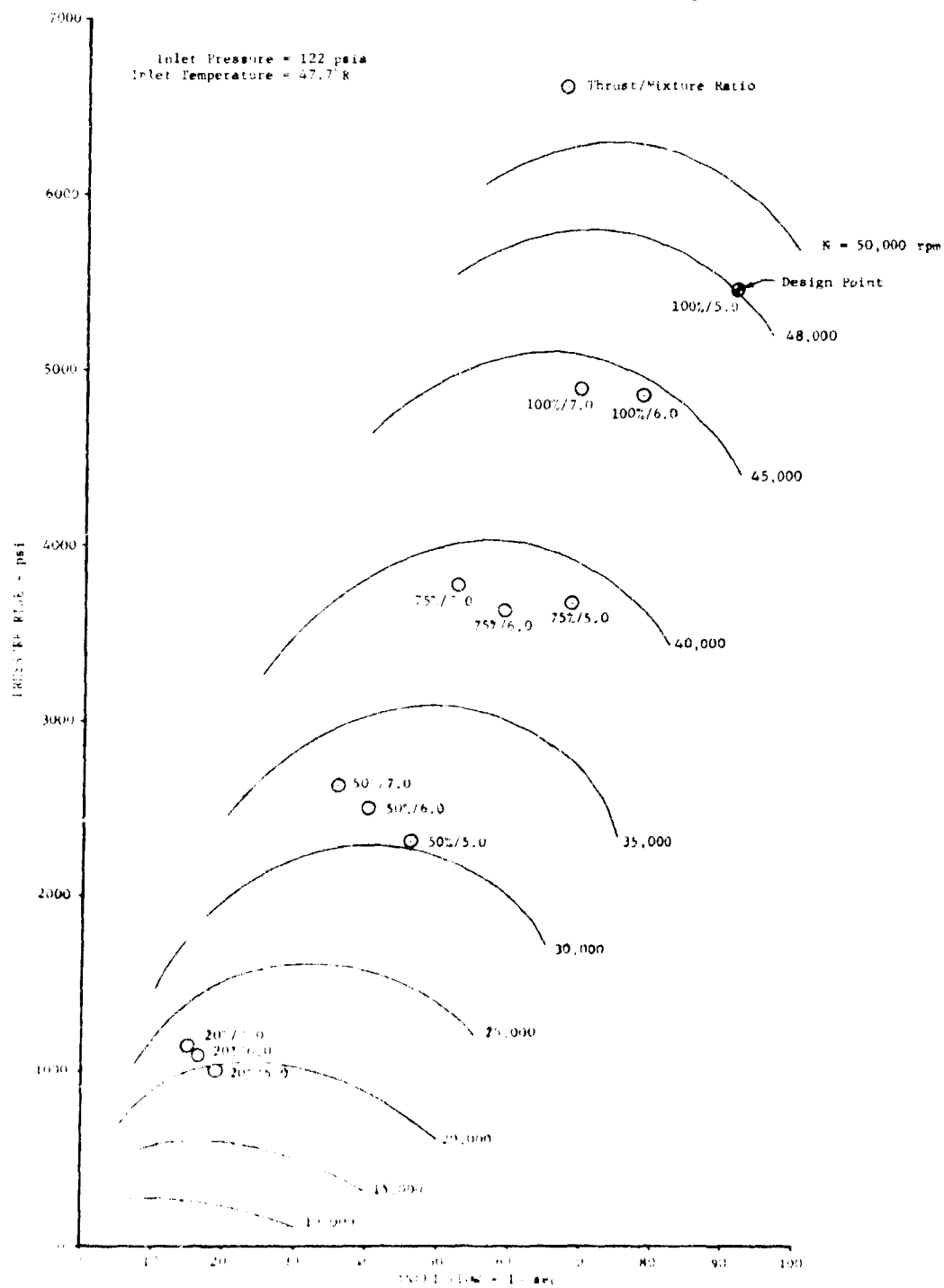


Figure 592. Fuel Turbopump Inlet Flow vs Pressure Rise DF 71765

Table LXXVII
XLR129 Fuel Turbopump Parts Procurement Time

	Material	Raw Material	Fabrication
Inducers and Impellers	Titanium Forgings	21 wks	16 wks
Housings	Inconel Forgings	16 wks	26 wks
Thrust Balance Set	Inconel Forgings	10 wks	22 wks
Turbine Disks	Waspaloy Forgings	11 wks	20 wks
Turbine Blades	D. S. Nickel Base Castings	23 wks	6 wks
Turbine Stators & Exit Diffuser	Nickel Base Castings	20 wks	5 wks
Bearings	AISI440C	----	35 wks

a. Rotor

(1) Inducer

The inducers were fabricated from A-110 titanium pancake forgings having radial grain flow. The blades are machined with a three-dimensional pantograph milling machine controlled by a double size duplicating master. The master was constructed to duplicate one full blade (or blade set in the case of the impellers) and indexed to reproduce the blades over 360 deg. Individual blade and hub outside contours were hand finished to attain the smooth surfaces required. Internal hub contours were fabricated using standard machining techniques, excepting the second impeller shaft spline which was machined using the single point tool technique. Figure 593 shows the inducer as viewed from the inlet end.

(2) Impellers

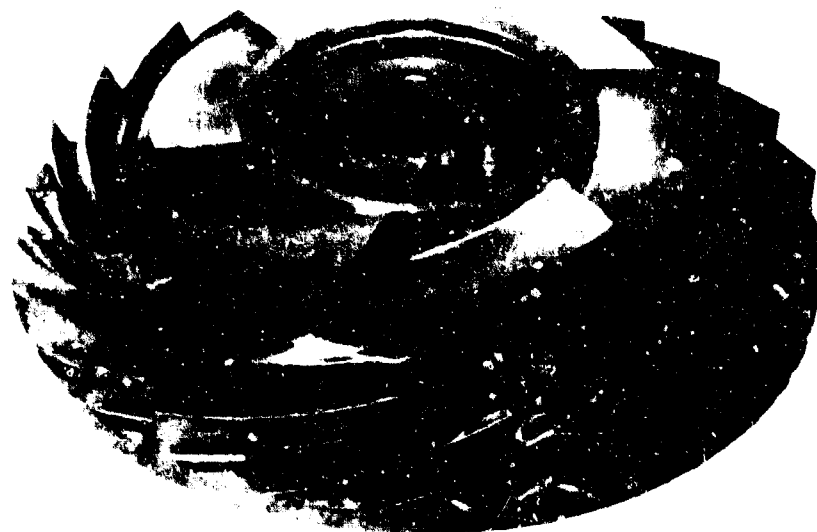
Impellers for the 1st- and 2nd-stages are fabricated from A-110 titanium closed-die forgings with grain flow orientation following the hub and blade contour. Machining techniques are the same as those employed for the inducer. Figures 594 and 595 show the 1st- and 2nd-stage impellers, respectively, as viewed from the inlet end.



FL 88099

Figure 593. High-Speed Inducer

FD 38321



FL 88100

Figure 594. 1st-Stage Impeller

FD 38322



Figure 595. 2nd-Stage Impeller

FE 80641

FD 38323

(3) Thrust Balance Piston

The thrust balance piston was fabricated from a closed die Inconel 718 forging using conventional machining practices. The part was rough machined in the solution heat treated condition. Final grinding of the critical surfaces and the cutting of the internal splines were performed after solution and precipitation heat treatment. Figure 596 shows a finished machined thrust balance piston unit.



Figure 596. Thrust Balance Piston

FE 80641

FD 38324

(4) Turbine Disk and Blades

The 1st-stage turbine disk was fabricated from a closed die modified Waspaloy forging using conventional machining practices. Axial blade attachment fir tree slots were broached. Machine capacity and broach design flexibility permitted each fir tree to be completely broached in a single pass, thereby minimizing setup errors. Before the actual broaching operation in the turbine disk, test coupons were broached and inspected relative to the design specification, and by the actual turbine blade fir tree profiles to ensure a proper load distribution.

The 2nd-stage turbine disk, being integral with the shaft, required optimized properties. The part was fabricated from a modified Waspaloy forging and grain size and orientation requirements met using a controlled forging process. The 0.250 in. diameter centerbore was gun drilled after solution heat treatment, and the part given conformal stabilization and aging heat treatment. Conventional machining practices were employed. Splines were single-point machined, and the fir tree blade attachment slots were broached in the disk as described above for 1st-stage fabrication.

Turbine blade operating environment and high operating stresses required parts with superior ductility achieved only in materials having controlled grain orientation. Directionally solidified blade castings from nickel base alloy similar to SM200 were selected, based on experience acquired in several turbo-jet applications. Considerable development time was required by the casting vendor to adapt the processes and techniques of directional solidified castings to the small sizes required for the fuel turbopump blade. Primary casting problems encountered were unpredictable grain growth, microshrinkage and inclusions. The grain problem was investigated and the grain was found to be sensitive to the length of the base stock or distance of the usable mass from the chill plate initiating nucleation of the grains. Mold-to-mold variations were found to be critical and required stringent process controls to achieve a predictable yield. Microshrinkage, especially critical on small parts or parts with thin sections, was minimized by incorporation of excess metal attachments (fences) on the affected surfaces to feed the voids formed by the solidification process. The shrinkage problem also requires development of a particular gating arrangement and the position of the feed was found to be extremely critical. Once a suitable blade pattern and gating arrangement was established, parts were poured in molds with clusters of 24 blades. The end result provided acceptable blade castings, and one finished blade of each stage is shown in figure 597. Figures 598 and 599 show the 1st- and 2nd-stage turbine blade and rotor assemblies, respectively.

(5) Roller Bearings

The roller bearing inner race and rollers are fabricated from AISI 440C stainless steel. The outer race details are machined from carbon steel carburized on the inside diameter to a depth of 0.040 to 0.050 in. and case hardened to a value of R_a 81 to 85. The bearing cages are fabricated from Armalon, Grade 405C-116, which is a spiral wrapped glass cloth laminate having a teflon resin binder. The roller pockets are broached in FRDC shops. Final machining of the bearing races to establish critical fits is performed at the FRDC shops using conventional grinding techniques. Figure 600 shows a typical fuel turbopump roller bearing.



1st-Stage

2nd-Stage

FE 00112

Figure 597. Turbine Blades

FD 38325

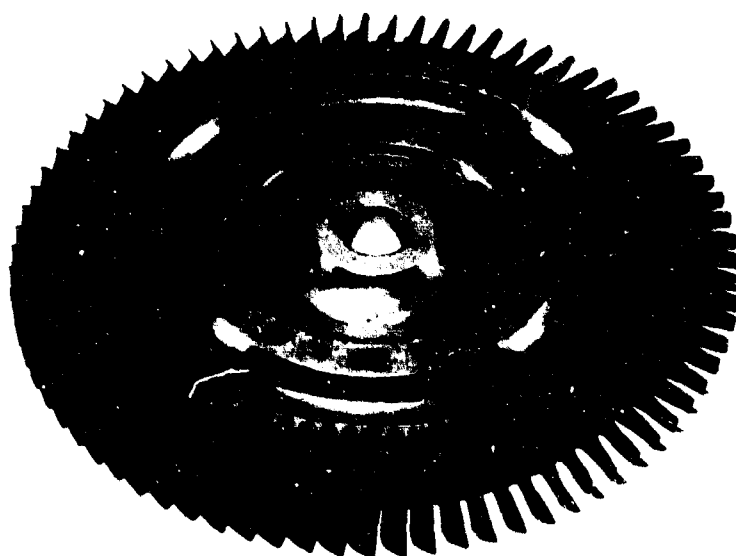


**Figure 598. 1st-Stage Turbine Blade and Rotor
Assembly**

FE 92198

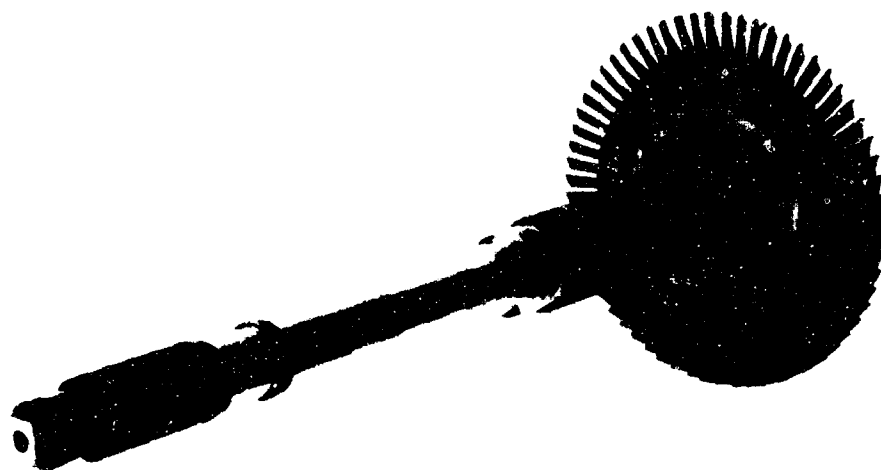


Figure 599. 2nd-Stage Turbine Blade and Rotor Assembly

KFE 92191

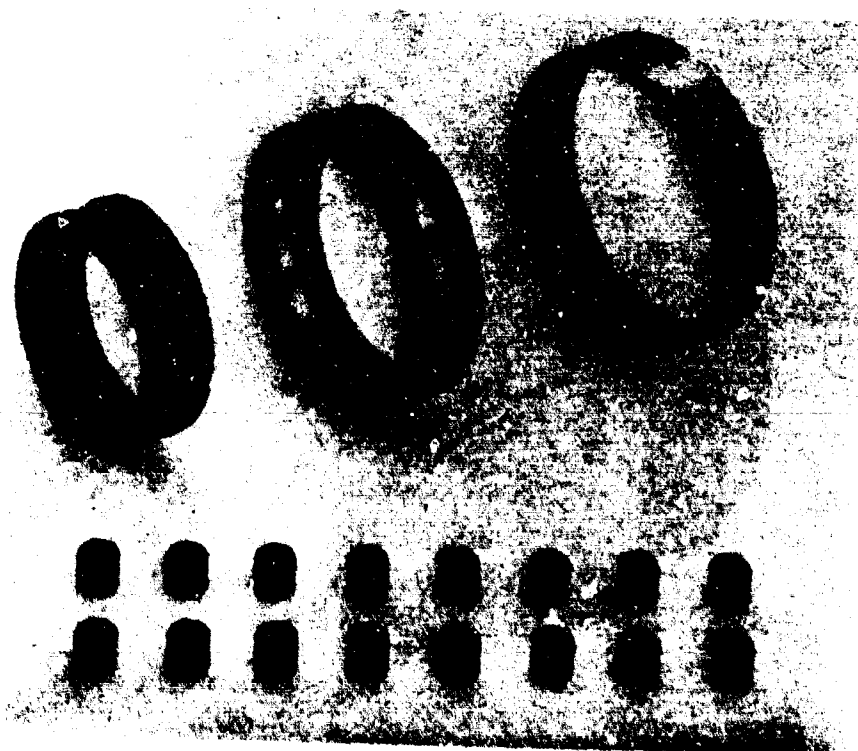


Figure 600. Fuel Turbopump Bearing (Typical)

FE 95610

b. Housings

(1) Inducer Housing assembly

The inducer housing consists of two major parts; the inducer housing and the front bearing support structure. The inducer housing was fabricated from an Inconel 600 forging to provide axial grain flow orientation. The bearing support was machined from an alloy steel pancake forging to provide radial grain flow in the area of the support struts transitioning to axial orientation at the center hub.

The inducer housing was machined using conventional techniques. The 1st-stage pumping contour was formed using a template and tracer lathe. The bearing support structure was machined using conventional techniques except for the struts formed by tracer milling. After completion of rough machining the part was heat treated to obtain the desired hardness of $R_c 35$. Interface diameters were machined to provide a 0.001 to 0.002 in. interference fit. After assembly the details were joined by circumferential heliarc welds using Waspaloy filler rod. The part was then finished machined and the bearing support structure was electroless nickel plated on all exposed surfaces. Figures 601 and 602 show the inducer housing assembly.

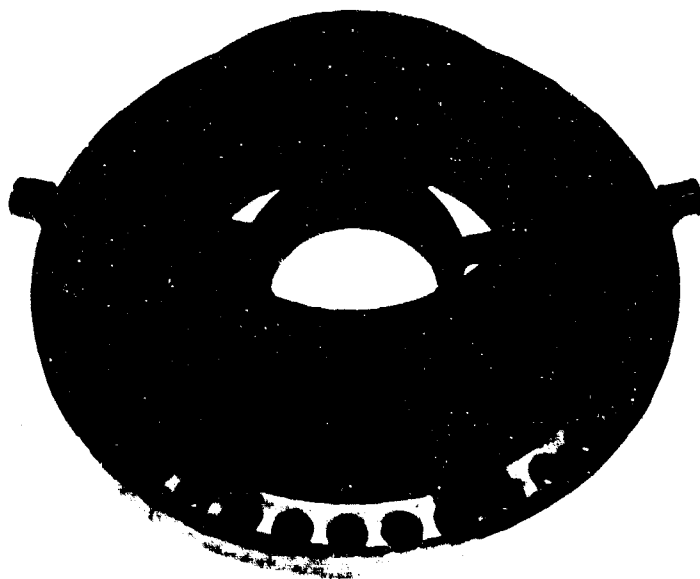


Figure 601. Inducer Housing Assembly (View 1)

KFE 95608



Figure 602. Inducer Housing Assembly (View 2)

KFE 95609

(2) Main Housing

Main housings were fabricated from closed die Inconel 718 forgings. A wood duplicating master of the main housing outside contour was fabricated. With this master, the outside contour including the instrumentation bosses was milled to 0.003 in. tolerance of the final dimension as shown in figure 603. The outside contour was finished by hand barbering. During the barbering operation, the milling and indexing ridges were removed and the outside contour brought to final size by hand grinding. Depth indexing marks were used to guide the polishers during hand grinding operations. Before machining the volute sections, the vendor machined a test ring to qualify his EDM process. The test ring was sectioned and both dimensionally and metallurgically inspected. The inspections revealed the recast layer was less than 0.003 in. depth and approximately 0.010 in. finish stock remained for final polishing and blending. The four volutes were then machined using the EDM process and guided by tracer templates. All other operations utilized conventional machining practices.

Tubing, for the fuel pump interstage was difficult to manufacture because of the small bend radius, relatively heavy wall, allowable thin-out (approximately 20%), ovality and rippling limitations, specified for the design. Many aircraft tubing vendors were asked to submit a quote and only one responded. The vendor had three basic processes for tube forming; i.e., the conventional bend process, pressure assist method, and the pressure bending process. The latter process was selected because it was the only process that would satisfy existing tube

design requirements and had demonstrated a 20% thin-out or less. However, this process required a precision die form not available in time to achieve part delivery to the machining and welding vendor. The vendor commenced an accelerated development program to improve the pressure assist bending method to meet P&WA requirements. Wall thin-out with this process was 35%. As a result of the vendor program, tube details were fabricated that held thin-out less than 20%, rippling was held to 0.003 in., and ovality was less than 2%. Upon delivery of the formed tubes to the machining vendor the interstage tube subassemblies were fabricated.



Figure 603. Main Turbopump Housing Milling Operation

FE 88086

After rough machining of the housing was completed, the interstage tube subassemblies and the discharge diffuser sections were welded to the housing, shown in figure 604. The part was then solution heat treated and aged. Final machining included hand polishing the volute sections to remove the recast surface layer associated with the EDM process, drilling and tapping the bolt holes, and finishing the critical inside faces and diameters. Figure 605 shows the main housing in the finish machined condition.

The finish machining operations on the first part required considerable time because hardened Inconel 718 volutes are extremely difficult to hand

polish and it is also difficult to drill and tap bolt holes in the metal. Measurements were made on the first part before and after heat treatment in order to determine the extent of distortion. In addition, samples of the volute EDM surfaces were analyzed to determine the depth of the recast layer. Results of these checks were applied to the machining plan for the second part. Volute machining was increased to within approximately 0.003 in. of the high limit, and bolt holes were finished before heat treatment with the bolt circle diameters adjusted for the measured shrinkage. The finish machining stock on the inside surfaces was held to a minimum. Final dimensional inspection of the second part confirmed that finish machining operations before heat treatment were within print limits and that heat treatment distortion between parts was repeatable.

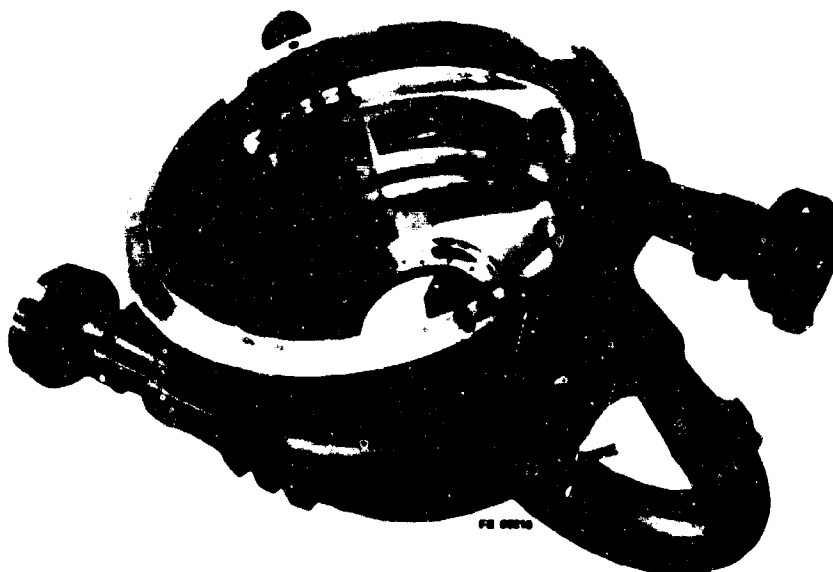


Figure 604. Main Housing After Completion of Welding and Heat Treatment

FD 38332

(3) 2nd-Stage Housing

The 2nd-stage housings were fabricated from aluminum pancake forgings. The kidney shaped internal contour was generated from a tracer model. All other machining was completed using conventional machining techniques. Figure 606 shows the 2nd-stage housing after completion of machining.

(4) Thrust Balance Piston Housing

Thrust balance piston housings were fabricated from Inconel 718 closed die forgings with the grain orientation lines following the basic part contour and utilizing conventional machining practices. Figures 607 and 608 show both sides of the thrust balance piston housing.



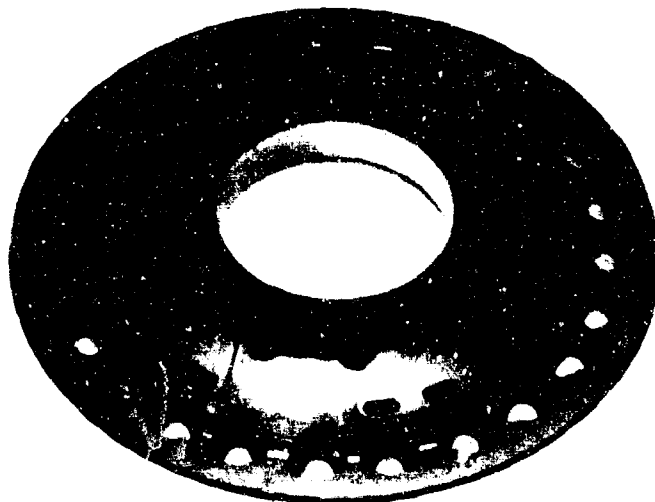
Figure 605. Main Turbopump Housing Machined
to Dimension

FE 90918



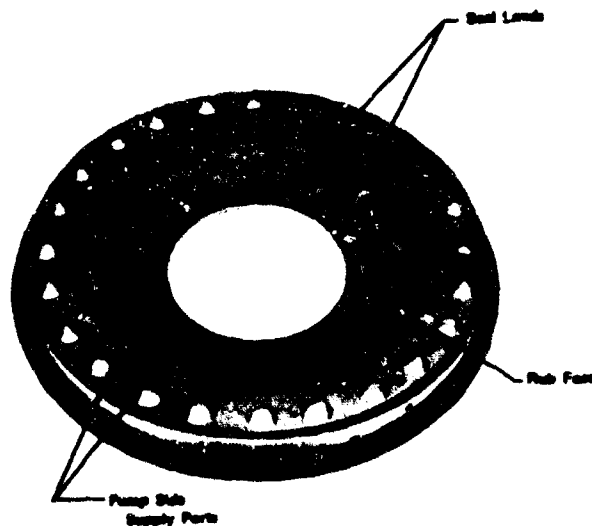
Figure 606. 2nd-Stage Housing After Machining
Operations

FE 92134



FE 08042

Figure 607. Front Thrust Balance Piston Housing - FD 38335
Pump Side Up



FE 08041

Figure 608. Front Thrust Balance Piston Housing - FD 38336
Rear Side Up

(5) Rear Bearing Support

The rear bearing support structure, which also serves as the rear thrust balance piston housing, is fabricated from Inconel 718 (AMS 5663) closed die forgings. Conventional machining practices were employed except for the small diameter radial instrumentation holes and the thrust piston and rear bearing supply passages that were gun drilled. Figures 609 and 610 show views of the

front and rear of the rear bearing support housing. In figure 609 the finish machined rear thrust balance piston rub face can be seen.

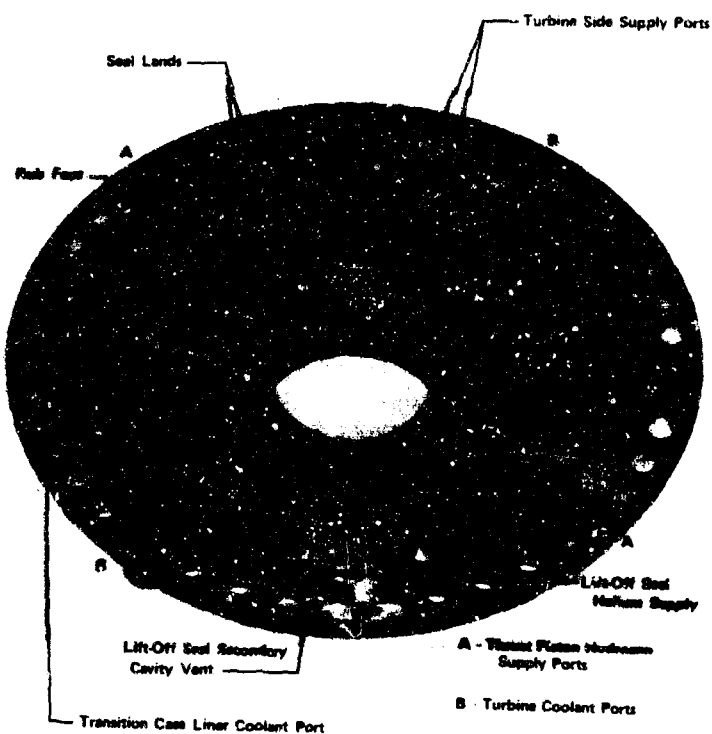


Figure 609. Rear Bearing Support and Rear Thrust Piston Housing - Front Side Up FD 38337

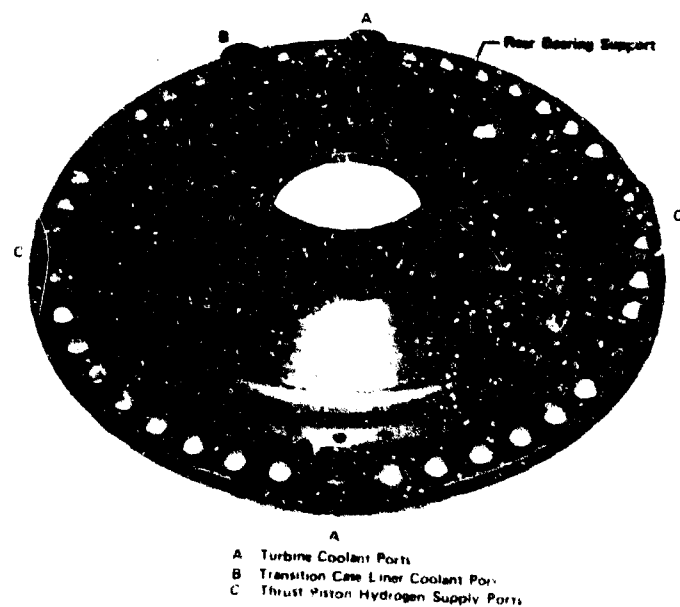


Figure 610. Rear Bearing Support - Turbine Side Up FD 38338A

(6) Lift-off Seal

Two lift-off seal bellows arrangements were fabricated during the fuel turbopump test program. The initial bellows configuration was a 0.020 inch wall thickness machined convolution arrangement. All details of the liftoff seal assembly are fabricated from Inconel 718 (AMS 5663) bar stock. The bellows convolution details are turned on a lathe from disks. The initial machining operation is to turn the outside diameter to the finish size. With the disk piloted on the outside diameter, the convolution section is initially formed by a radial cut from the outside surface. The side faces and the inside diameter are then finish machined. The individual convolutions are stacked in a fixture with an ID mandrel and electron beam butt welded into bellows assemblies. The bellows assemblies are then electron beam welded to the machined support pieces. The bellows subassemblies are X-ray inspected to evaluate the quality of the convolution welds and the bellows spring rate is checked on a mechanical spring rate tester. The details are assembled into a complete liftoff seal unit by TIG welding. The critical primary seal unactuated position is then achieved by final machining of the mounting flange support face. The completed liftoff seal assembly is final inspected to determine the amount of seal travel and leak checked to 1500 psig. Figure 611 illustrates the completed liftoff seal assembly.

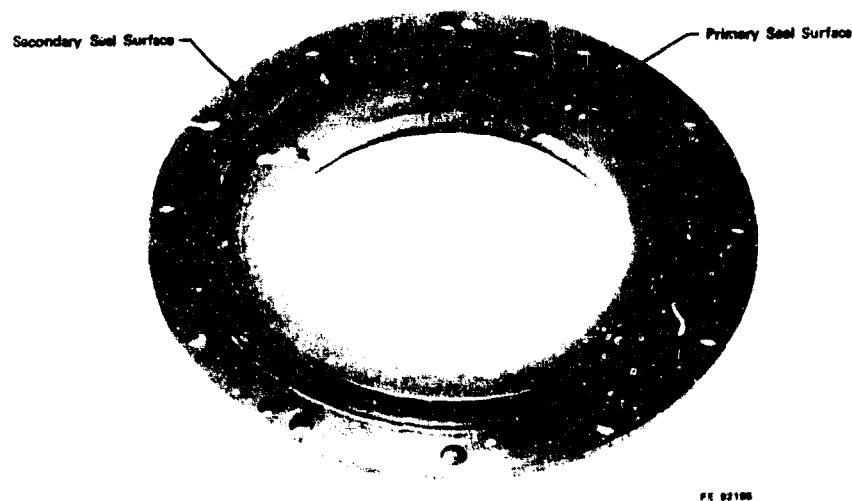


Figure 611. Liftoff Seal Assembly

FD 38339

Evaluation tests of the machined bellows liftoff seals revealed that in addition to an excessive spring rate of 100,000 lb/in. (design spring rate 50,000 lb/in.) the parts could not satisfy the cycling life requirement due to quality control problems associated with the machined convolutions and the welds. The vendor then changed the bellows design to a formed convolution arrangement fabricated from 0.016 in. thick Inconel 718 (AMS 5663) disks. The individual convolution disks were electron beam weld assembled on the inside and outside diameters. The bellows spring rate attained with this configuration was 66,600 lb/in.

c. Turbine Stationary Parts

(1) Turbine Inlet Duct Assembly

The turbine inlet duct assembly consists of the duct structure and the permanently attached flow duct heat shields. The duct was fabricated from an Inconel 718 (AMS 5663) semiclosed die forging. The billet was selected oversized for the closed die form and the hammer stroke was limited. This resulted in an outflow of metal between the hammer and the die face that provided radial grain flow for the outer flange. The strut and internal duct contours were machined on a three dimensional pantograph milling machine by tracing a duplicating master. The thirteen 0.050 in. diameter flow passages were installed in the struts using the EDM method. This method was selected, instead of gun drilling, to maintain the alignment of the holes near the bottom of tool penetration. All 13 holes in each strut were machined in a single pass. This and other machining operations utilized conventional processes. Figures 612 and 613 show the inlet and discharge sides of the turbine inlet duct after completion of final machining.



Figure 612. Turbine Inlet Duct - Inlet End at Top FD 38340

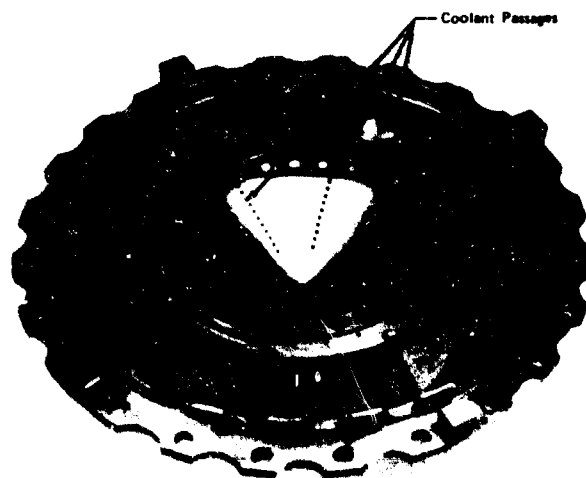
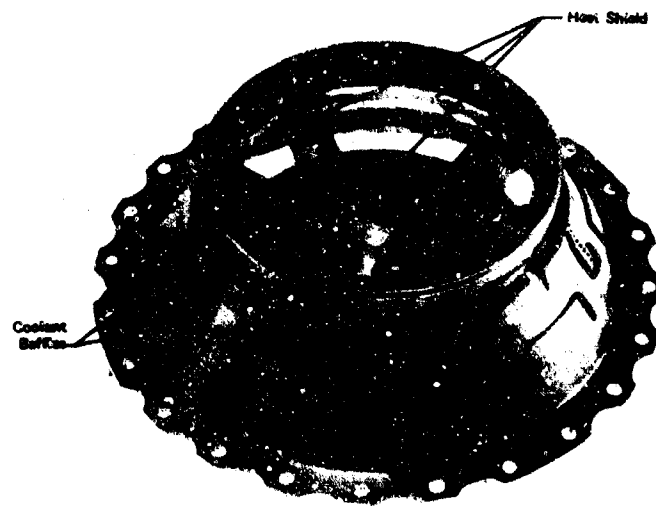


Figure 613. Turbine Inlet Duct - Discharge End at Top FD 38341

The heat shield details of the inlet duct were fabricated from Haynes 188 cobalt alloy sheet stock. This material was selected for its high temperature stability and because it does not require stress relief heat treatment after welding. The heat shield details which serve as the flowpath ducts were spin formed to their final contour. The strut slots were then cut into the parts to prevent deformation during installation in the inlet housing. After the heat shield details were installed they were heliarc weld assembled. The strut shields were assembled to the duct shields using stitch welds. This assembly technique was required to provide venting areas through the heat shield assembly to minimize differential pressure and temperature across the heat shield walls during turbopump operation. Figures 614 and 615 show the inlet and discharge sides of the turbine inlet duct assembly. The square coolant baffles seen on the outside surface of turbine inlet duct, figure 614 are fabricated from Inconel 600 (AMS 5540) wire and are welded to the duct.



FE 92196

Figure 614. Turbine Inlet Duct Assembly With Heat Shields Installed - View 1

The turbine inlet duct cover housing, shown in figure 616 was fabricated from Inconel 718 (AMS 5663) using conventional machining techniques. The inside conical surface was sized to contact the square wire coolant baffles on the outside surface of the inlet duct, thereby directing the coolant flow path. Figure 616 shows the turbine coolant supply bosses on the outside conical section and the seal ring grooves near the inlet end which seal on the transition case fuel turbine duct.

(2) Stators

Turbine stators were designed as single piece castings with integrally cast vanes. Both parts were cast from IN 100 (AMS 5397) nickel base alloy in a vacuum chamber. Because of the inherent casting problems associated with IN 100, shrinkage and hot tearing, and because this alloy does not lend itself to weld repair of defects, two orders were placed for the stators. Uncored parts were ordered for use on the pump test stand which used hydrogen drive gas at 800°R turbine inlet temperature. Concurrent with production of the solid parts, work was started by the casting vendor to develop mold arrangements

and casting techniques for pouring the cored pieces required for turbopump testing with the preburner and transition case. Casting of the 1st-stage stators was complicated by the required integrally cast T-slot arrangement between each vane in the outer ring and the cantilevered core arrangement suspended from the inside diameter.

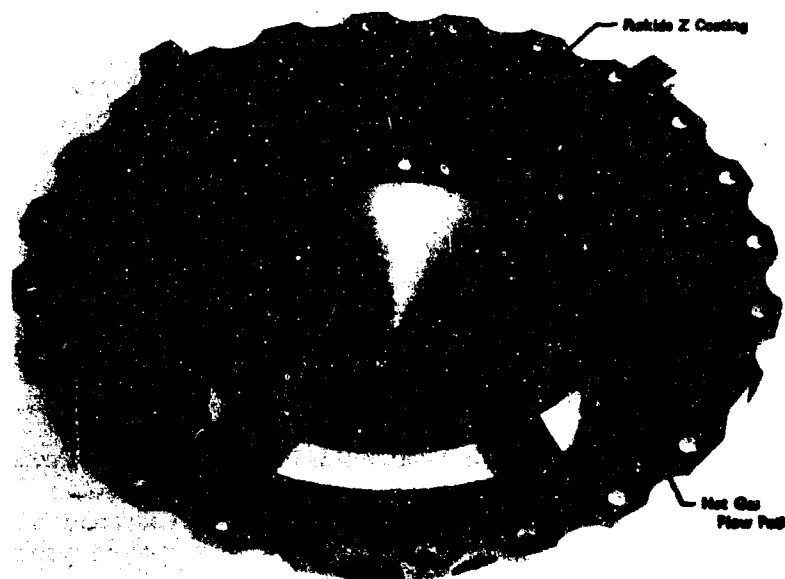


Figure 615. Turbine Inlet Duct Assembly With Heat Shields Installed - View 2 FD 38353

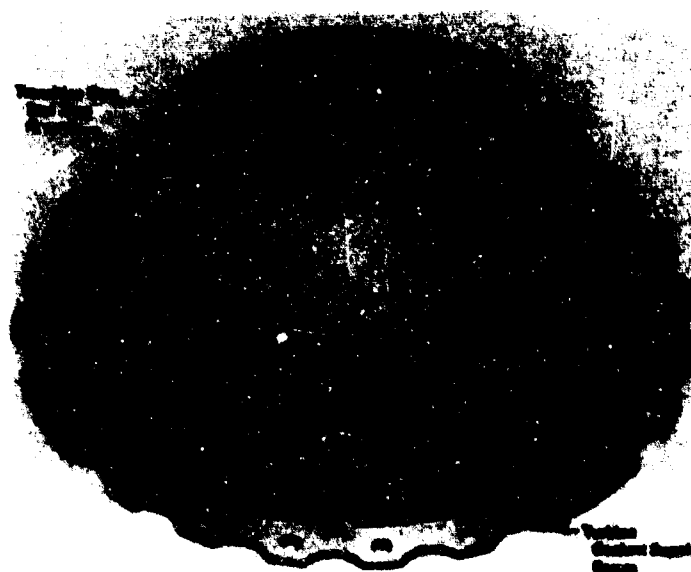


Figure 616. Turbine Inlet Cover Housing

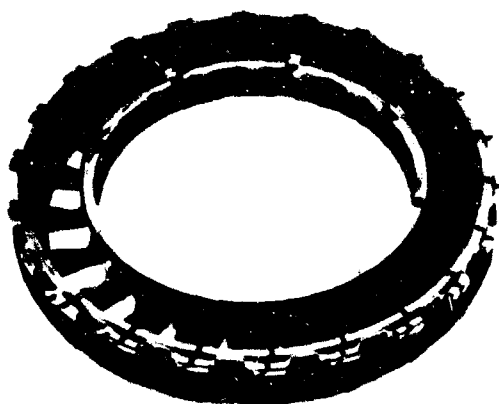
FD 38354

Preliminary casting development was centered around the temperature of the melt and the mold preheat. Once the temperatures were optimized, hot tearing problems were eliminated and shrinkage problems remained to be solved. Gating arrangements were then adjusted until an adequate feeding system was attained.

Molds were formed using wax patterns. The patterns were shot as individual vane segments from dies designed for either the solid or cored vanes. Wax segments were hand assembled into continuous stator rings. Molds were made using the wet dip process with each ceramic layer dehydrated in an oven.

Once the mold dipping was completed, the wax pattern was removed by an oven melting process. When the part was ready for pouring, the melt was prepared in a vacuum furnace and the mold conditioned in a preheat oven. When the melt had attained the desired temperature, and the mold had soaked at the preheat temperature, the mold was placed in the vacuum pouring chamber and the part cast. The part remained in the vacuum until it solidified. Stator castings, acceptable for both rig and hot turbine testing, were all of good quality and did not display any indications of hot tearing and minimal shrinkage.

After finish machining of the stator inside and outside diametral surfaces and faces, final dimensional inspection is completed. The stators are then eloxed to split one of the rings. The first stator outer shroud is split in the planes of the T-slots. The cast tangential arms of the slots were designed to accommodate seal strips to minimize leakage. The 2nd-stage stator inner shroud was slit between each of the 36 vanes. The finish machined 1st-stage stator of the cored configuration is shown in figure 617. A finish machined, 2nd-stage stator of the cored configuration is shown in figure 618.



FE 95643

Figure 617. 1st-Stage Cored Stator

FE 95643

(3) Turbine Exit Diffuser

The turbine exit diffuser, like the stators, was a single piece vacuum casting from IN 100 (AMS 5397) nickel base alloy. A separate vendor had responsibility for the turbine exit diffuser.

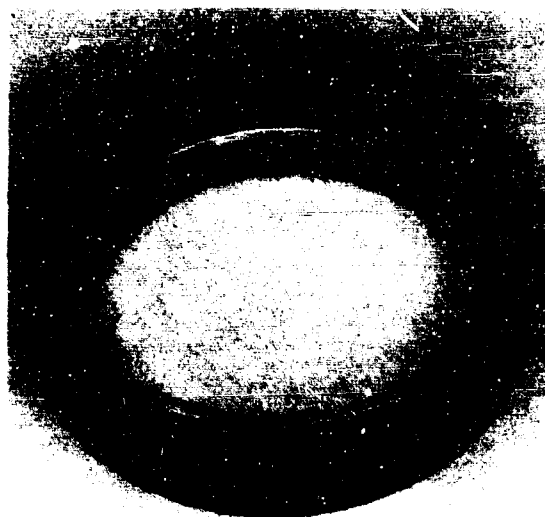


Figure 618. 2nd-Stage Cored Stator

FE 94175

Different mold arrangements, mold material, and melt temperatures compared with the stator castings were used by this vendor. The resulting castings showed no improvement after two months of development in terms of hot tearing and microshrinkage problems. At this time, the stator casting vendor had developed solid stator casting techniques and was in the process of fabricating good quality parts. Because of time limitations, a threefold effort was begun to obtain a part for the first turbopump test rig. The turbine exit diffuser casting vendor was requested to cast a part from Inconel 718 concurrent with continued development of IN 100 casting techniques. Wax patterns were also supplied to the stator casting vendor to determine if his casting techniques were applicable to the exit diffuser design. The primary vendor poured two Inconel 718 parts and one was acceptable for machining and subsequent pump testing (800°R turbine inlet temperature).

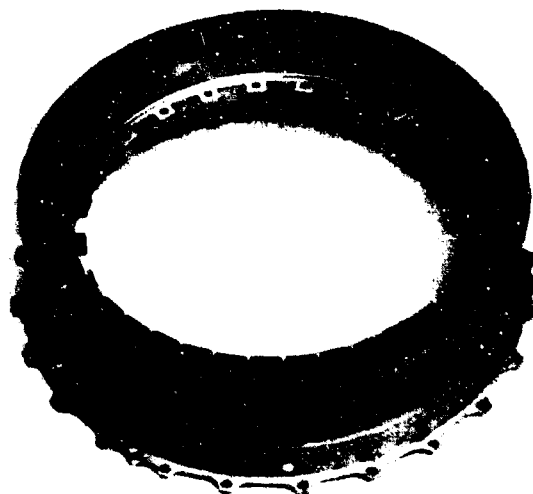
The secondary vendor cast a good quality part on the first attempt; however, layout dimensional inspection revealed the part was considerably undersized due to a difference in mold shrinkage between the two vendor processes. At this time the order for the IN 100 exit diffuser castings was transferred to the secondary vendor. The wax die tooling was shipped to the new vendor and was reoperated to compensate for the vendor's mold shrinkage. After this tooling modification, the vendor delivered excellent quality IN 100 castings required to satisfy the turbopump requirements. Figures 619 and 620 show respective views of an IN 100 turbine exit diffuser from the inlet and discharge sides.



FE 01122

Figure 619. Turbine Exit Diffuser - Inlet Side

FD 38344



FE 01122

Figure 620. Turbine Exit Diffuser Discharge Side

FD 38343

During development of the exit diffuser castings the original vendor expended considerable effort, but was unsuccessful in developing a weld repair technique for IN 100 casting defects. Efforts included electron beam welding which, except for nonstructural fillerwelds, was not successful. Severe weld problems were detected revealing cracking in the parent material adjacent to the weld or in the weld itself. Filler weld samples revealed microcracks radiating from the weld.

(4) Turnaround Ducts

The inside turnaround duct detail was fabricated as a single piece from a Waspaloy (AMS 5709) ring forging. Conventional machining techniques were employed except for the shaped duct contour machined on a tracer lathe as guided by a template. Figure 621 shows the inside turnaround duct after machining.

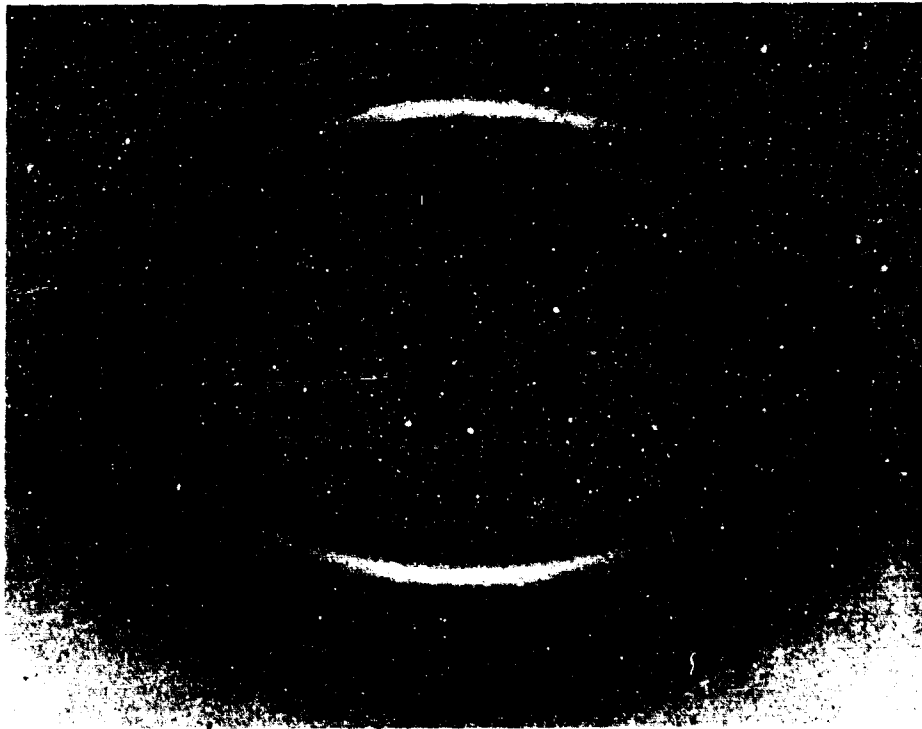


Figure 621. Inside Turnaround Duct

FE 90833

The outside turnaround duct detail is a give piece welded assembly. The three ring details were machined from Inconel 625 (AMS 5666) and the support ring and duct details were fabricated from Inconel 625 (AMS 5599) sheet stock. Conventional machining techniques were used except for the contoured duct detail which was spin-formed on a wooden model. Figure 622 shows the completed outside turnaround duct detail.

(5) Miscellaneous Turbine Stationary Parts

Turbine stationary parts not previously discussed were fabricated using conventional machining techniques and equipment. Figure 623 shows the turbine support ring which carries the stator and turbine inlet duct loads. This part was machined from an Inconel 718 (AMS 5662) ring. The top bolt circle in figure 623 attaches the support ring to the exit diffuser. Figure 624 shows the outside heat shield that protects the turbine support ring and turbine inlet duct cover from the hot gas discharging from the exit diffuser. This part was fabricated from Inconel 625 (AMS 5599) sheet stock using appropriate spinning and stamping techniques.

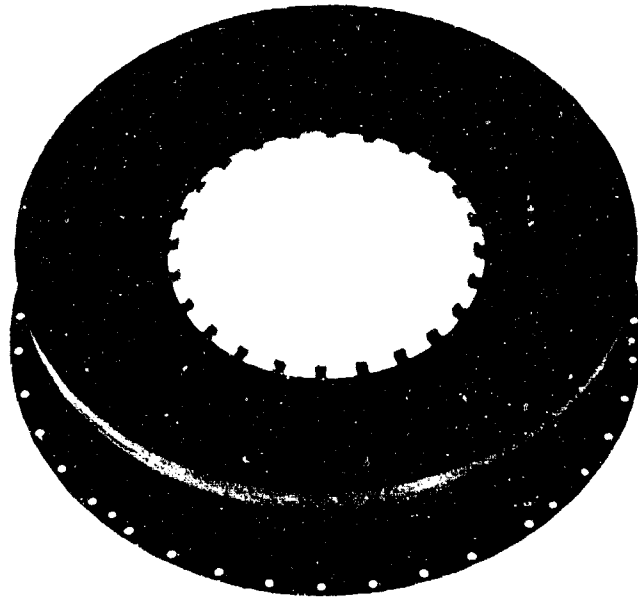


Figure 622. Outside Turnaround Duct

FE 90986



Figure 623. Turbine Support Ring

FE 90982

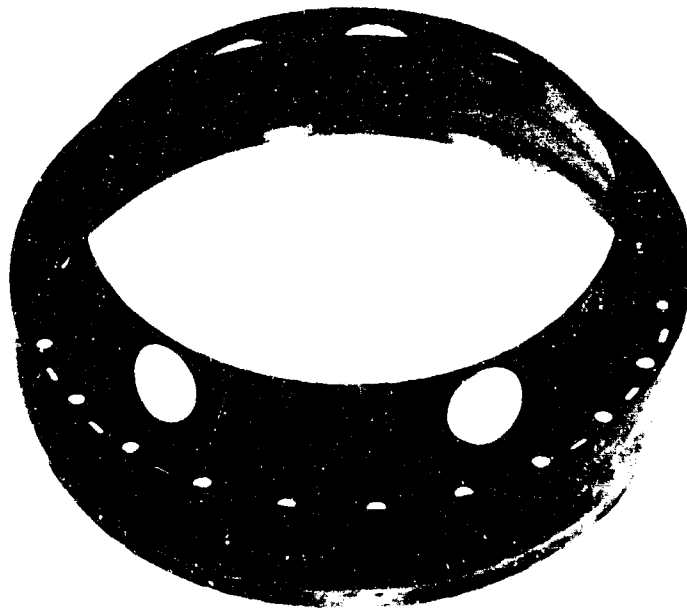


Figure 624. Turbine Outside Heat Shield

FE 92192

5. . Testing

a. Subcomponent Tests

(1) Rotor Spin Testing

All major details of the fuel turbopump rotor assembly were subjected to spin tests demonstrating structural integrity of the parts. The spin test speed was established by analysis of the area of highest stresses and then determining the ambient temperature rotational speed causing limited plastic deformation. This is the equivalent of an overspeed condition during normal operation, varying with part geometry and operating environment. Measurements taken before and after spin testing verified the parts had the desired yield strength and elongation properties. In addition, the parts were sprayed with fluorescent penetrant while at maximum spin test speed. A fluorescent penetrant inspection was completed immediately following the spin tests to detect cracks that may have developed during the spin tests. Rotor details that were spin tested and the respective ambient temperature rotational speeds are listed in table LXXVIII.

(2) Turbine Blade Vibration Tests

Damping of turbine blade vibration in the fuel turbopump is accomplished by placing platform dampers between adjacent blades. Centrifugal force moves the dampers outward against the bottom side of the blade platforms of the two adjacent blades, thereby damping the relative vibration between these two blades. This type of damping arrangement will not limit blade resonant frequency amplitudes if adjacent blades have similar natural resonance frequencies.

Table LXXVIII. Rotor Ambient Spin Test

Part Description	Rotational Speed (rpm)	Bore Growth	
		Measure (in.)	Allowable (in.)
Inducer	24,000	N/A	N/A
First Impeller	36,700	0.0000	0.0010
Second Impeller	34,900	0.0000	0.0010
Thrust Balance Piston	41,900	0.0000	0.0000
Second Turbine Disk	*54,000	0.0001	0.0002
First Turbine Disk	*55,000	0.003	0.003

*Dummy blades were used to simulate blade loads at operating conditions. All parts were successfully tested at the speeds indicated and were found to be free from microstructure defects during the subsequent fluorescent penetrant inspection.

All turbine blades were tested to determine their first (easy-wise) bending mode resonant frequency so that turbine blade placement in the disks would achieve optimum damping capabilities. One blade in each stage was also mode-shape signed using holographic techniques. Holograms accurately describe the blade mode shapes at the resonance frequencies occurring within the critical frequency range of the pump.

Each 1st-stage turbine blade was inserted in a test block broached to the disk fir tree configuration. The blade was loaded outward against the fir tree with a set screw in the bottom of the broach block. The exciter, attached to the broach block, was then driven with a sinusoidal sweep from 2000 to 4000 Hz. An optical probe was used to sense blade tip response and pinpoint the resonance frequency. The setup is shown in figure 625. The first set of blades tested showed the first bending mode within the frequency range of 2566 to 3608 Hz, while the second set of blades were within the 2329 to 3320 Hz range. Fifteen of the blades were repeat tested with resulting frequencies within ± 16 Hz of original test data. These data also indicated that variations in fir tree dimensions greatly affected the first bending resonance frequency because the mode shape extended through the platform into the extended neck and fir tree.

Each 2nd-stage turbine blade (P/N 2150492) was cast into a grind fixture shuttle block with Cerrobend, which covered the entire fir tree on each blade. Care was taken to control the height of Cerrobend on the extended neck of the blade because variations would have induced a large percentage of error in test results. Shuttle blocks were clamped in a fixture attached to the shaker table, and the optical probe was again used to determine resonance frequencies. The setup is shown in figure 626. Two groups of blades were tested. The first bending mode occurred within the ranges of 2304-2820 Hz for the first set of blades, and 2714-2955 Hz for the second set. Twenty percent of the 2nd-stage blades were repeat tested and showed a ± 5 Hz variation from original test data.

These test data are used to select the location of the 1st- and 2nd-stage blades in their respective disks so that adjacent blades have differing frequencies.



Figure 625. 1st-Stage Turbine Blade Vibration
Test Setup

FE 89973

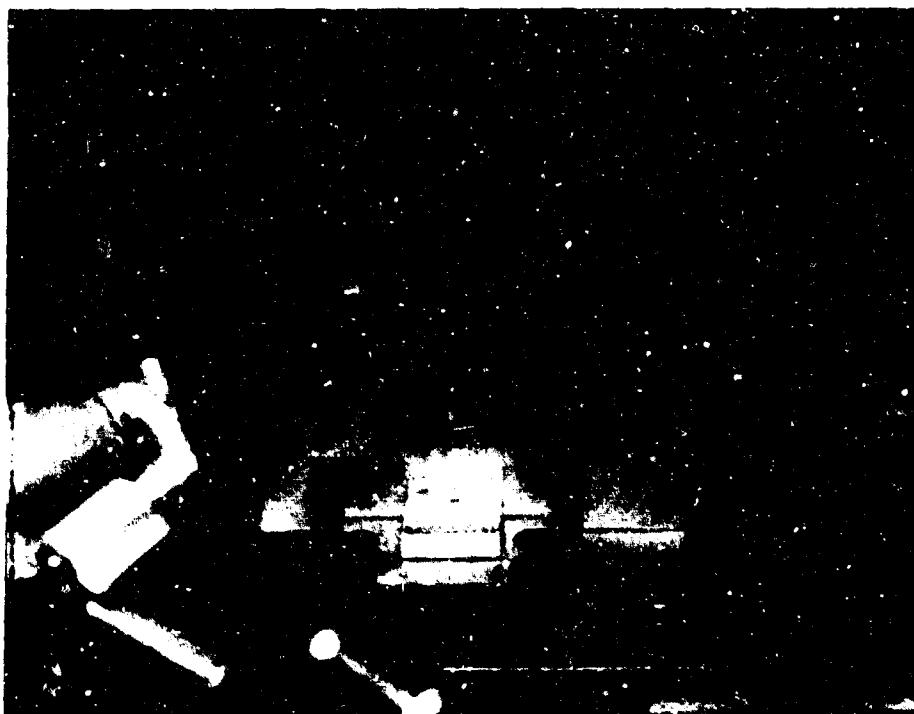


Figure 626. 2nd-Stage Turbine Blade Vibration
Test Setup

FE 93469

Representative 1st- and 2nd-stage turbine blades were mode shape signed using the holographic technique. Each blade was cemented into a broach block using dental cement to ensure maximum contact on the loading attachment. A set screw was also used to load against the bottom of the fir tree. The blade and broach block were then attached to an exciter and the blade profile was aligned in the holographic setup as shown in figures 627 and 628.

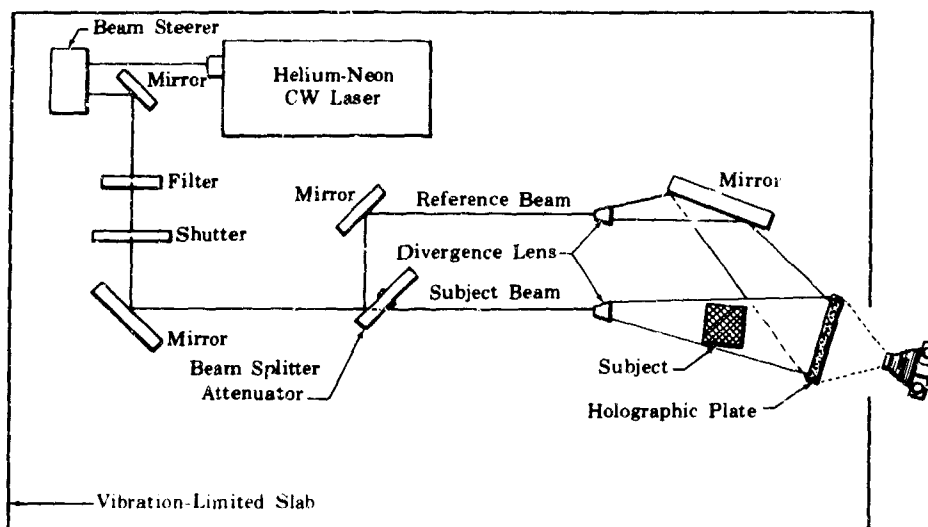


Figure 627. Holographic Test Schematic

FD 33589

The modes of the 1st-stage blade between 100 Hz and 20,000 Hz are first bending, first torsional (leading edge), and first torsional (trailing edge). The same modes were evaluated for the 2nd-stage blades plus second bending and second torsional. It was found for both types of blades that the mode shapes extended into or through the platform, thereby making the resonance frequencies dependent on the loading. The holographic photographs of both blades mode shapes and corresponding frequencies are shown in figure 629 and 630. These test data provide a better understanding of the blade mode shape and help to identify some of the coupled modes that affect the prediction of blade frequencies and modes.

(3) Main Housing Proof Pressure Test

The integrity of the main housing was verified before incorporating it in the turbopump test rig, by a 150% equivalent operating condition proof pressure test. The complexity of the main housing structure and the load systems operating in the volute and diaphragm areas required the proof test to be conducted as two separate tests to subject all critical areas to the combined stresses and deflections sustained at 150% equivalent operating pressure.

Proof test fixtures were designed to provide four compartments shown in figure 631. Close tolerance fits were established between the fixtures and housing to maintain static seals and to ensure that fixtures do not introduce undesirable loads. The area of highest predicted stress is the 2nd-stage cutwater. This stress results from two sources: (1) the interstage diaphragm deflection caused by the differential pressure between the rear of the 1st- and 2nd-stage impellers and (2) the hoop stress from the pressure in the 2nd-stage volute.

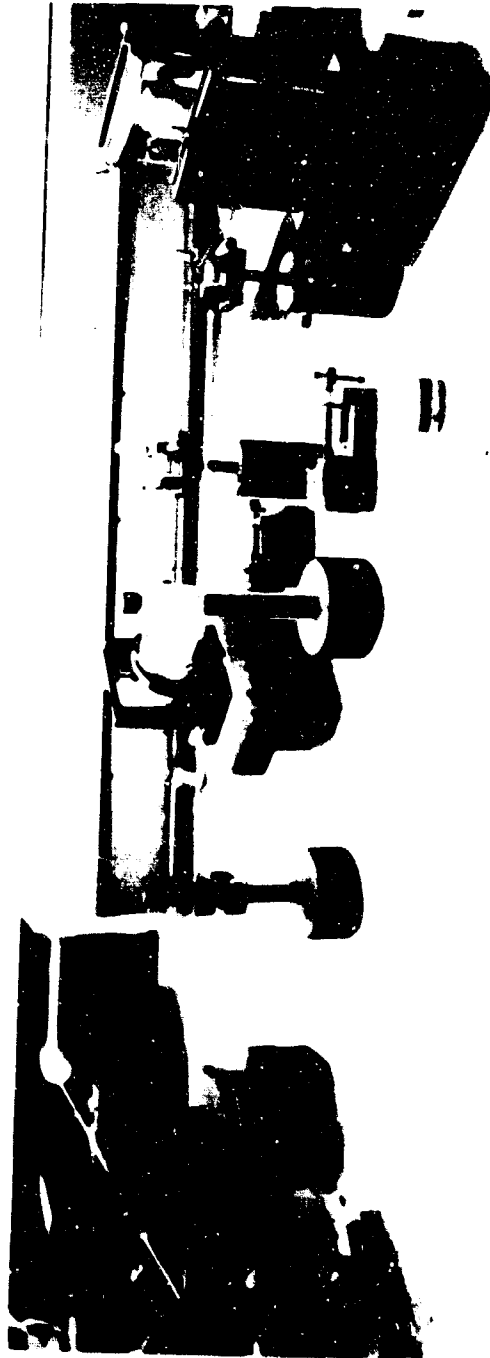


Figure 628. Hologram Test Setup Used for Turbine Blade Mode Shape Determination

FD 38484

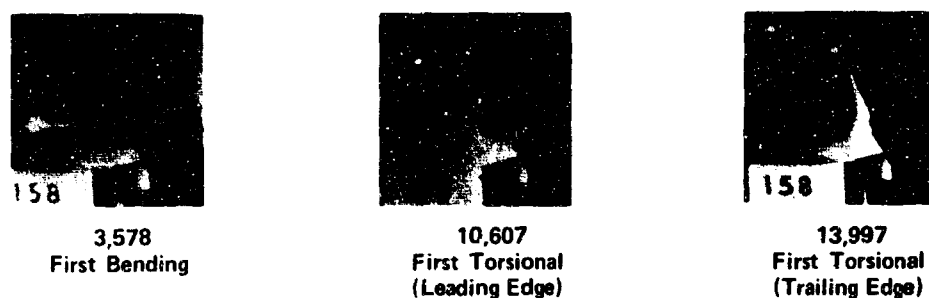


Figure 629. Mode Shapes at the Resonance Points of FD 38485
The XLR129 1st-Stage Turbine Blade

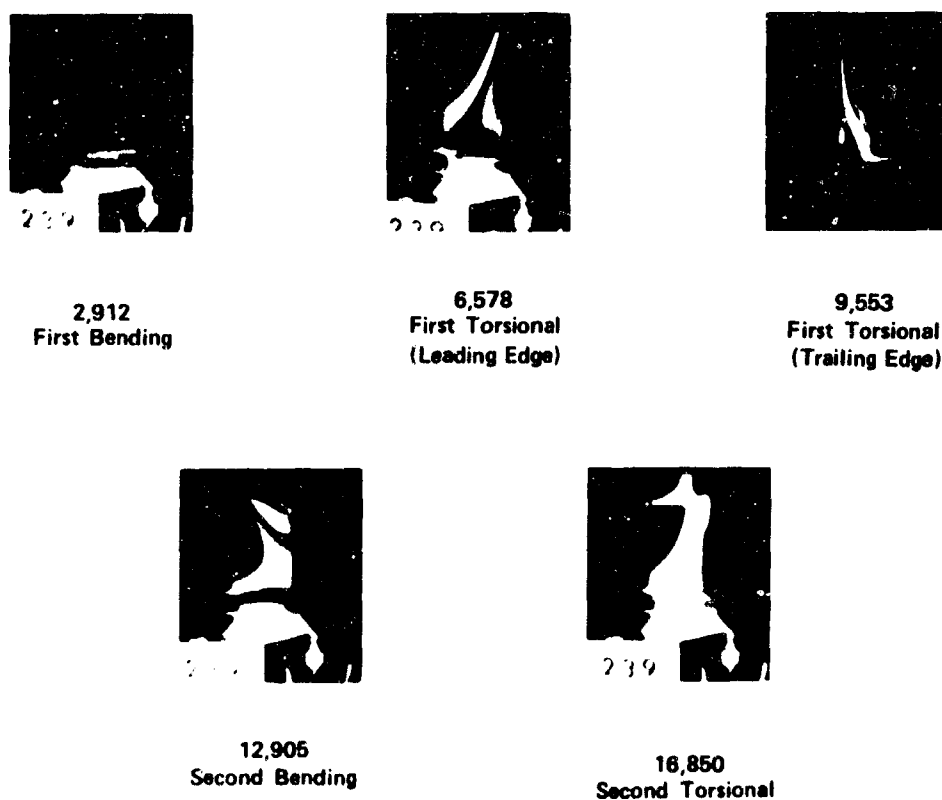
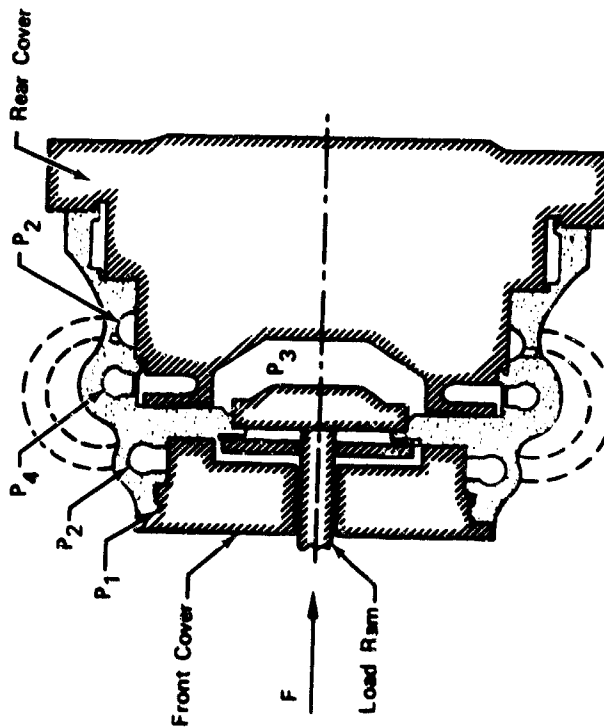


Figure 630. Mode Shapes at the Resonance Points of FD 38486
of the XLR129 2nd-Stage Turbine Blade

Strain gages were attached to the cutwater leading edges, volutes, and at several strategic locations along the wall between the second volute and the rear flange as shown in figure 632.

 Housing
 Fixture



Test	Compartment	Pressure/Load
1	P ₁	895 psig
	P ₂	2820 psig
	P ₃	3960 psig
	P ₄	7420 psig
	F	90,300 lb
2	P ₁	0
	P ₂	0
	P ₃	3960 psig
	P ₄	7420 psig
	F	90,300 lb

Figure 631. Main Housing Proof Test Verified Design

FD 38345

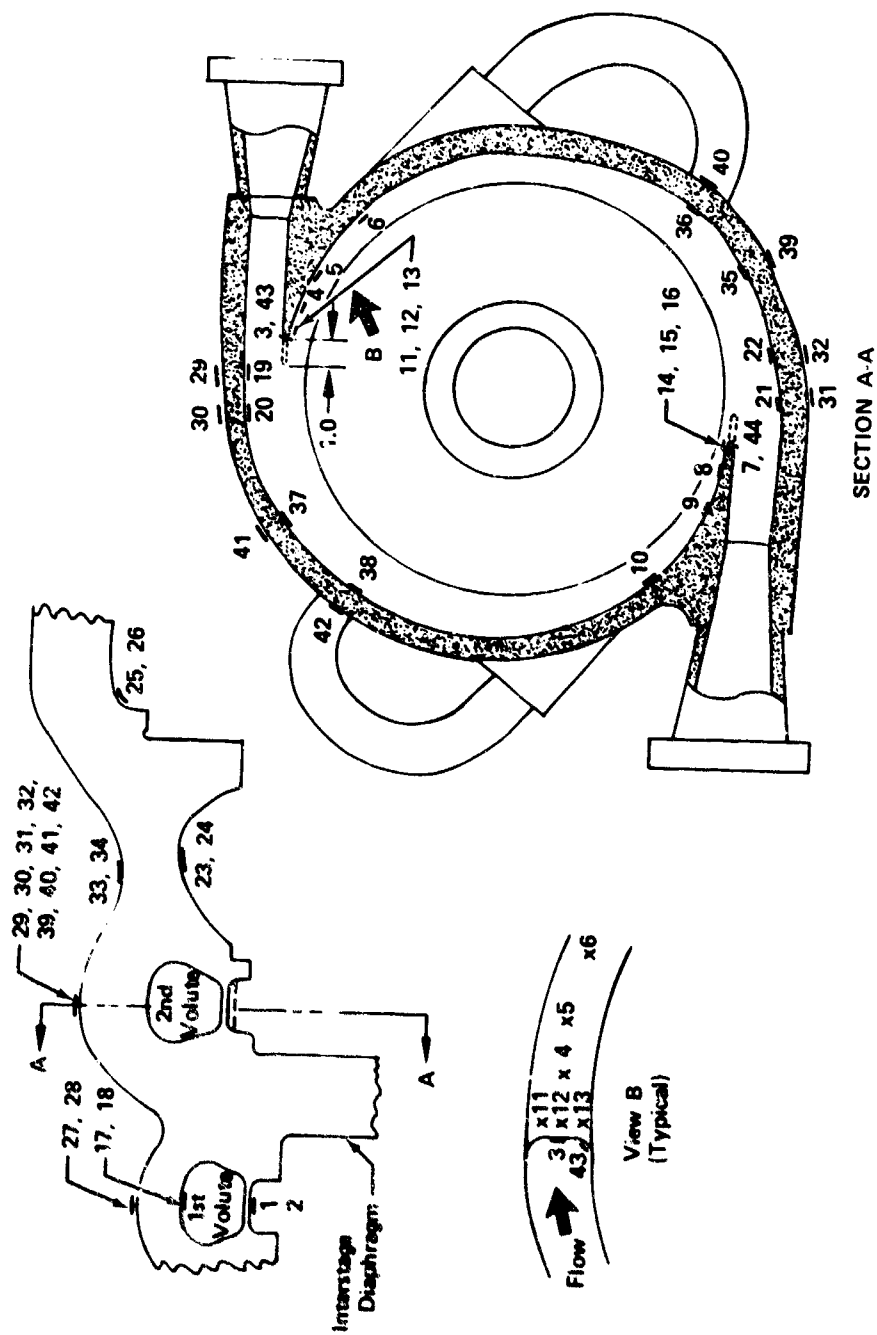


Figure 632. Locations of Strain Gages Installed on the Main Fuel Turbopump Housing for Hydrostatic Proof Pressure Tests

FD 38346

The proof test program was divided into two tests. The first test was accomplished with all fixtures attached to the housing. The front cover restrains the interstage diaphragm deflection in this case and the 2nd-stage cutwater stress is less severe than the actual operating condition. However, this test does subject both the 1st- and 2nd-stage volute areas to the desired hoop stress. The second test was run with the front cover removed and pressure loads applied only to compartments P₃ and P₄. This second test subjected the 2nd-stage volutes and cutwater sections to combined loads equivalent to the most severe stress conditions experienced during pump operation. The 90,000 lb load applied by the load ram during both tests, coupled with the pressure in compartment P₃, provides the required shear and deflection on the interstage diaphragm. Figure 631 defines the two tests and the corresponding pressures and load in each compartment. These pressures at ambient temperature provide stresses and deflections equivalent to a 150% pump operating pressure.

The design objective was to limit the value of strain in the main housing to 1% maximum at 150% equivalent operating pressure to ensure no permanent deformation of the housing. The initial proof pressure test verified the maximum strain was occurring at the 2nd-stage volute cutwater leading edges, as predicted; however, 1% total strain was recorded at 120% equivalent operating pressure. Proof testing was terminated and the 2nd-stage cutwater sections were machined back 1 in. Because this condition had been anticipated in the original housing design, a straight section was incorporated ahead of the diffuser and the repositioning of the cutwater did not affect the discharge diffuser sections. Upon completion of the cutwater machining the proof test was repeated. The initial test cycle after cutwater rework was halted at the 120% level because of failure of the separator static seal between compartments P₃ and P₄. Because seal failure appeared to be associated with the interstage diaphragm deflecting away from the seal, the rear cover was reoperated to permit the seal groove to deflect with the diaphragm. Testing was then resumed and two cycles to 150% equivalent operating pressure showed the maximum total strain, corrected for offset, to be 0.87% at gage location (16) on the 2nd-stage cutwater, shown in figure 633. The next highest value of strain recorded was also on the 2nd-stage cutwater leading edge at gage location (12) and the level was 0.61% total strain. Tables LXXIX and LXXX show the measured strain values and the calculated stress values, respectively for the first cycle to 150% equivalent operating pressure (cycle 2). This test was conducted without the front cover and subjects the 2nd-stage cutwater volute and cutwater sections to the most severe conditions experienced during pump operation.

(4) Liftoff Seal Testing

The liftoff seal for the fuel turbopump is designed to allow the turbopump to be filled with propellant before starting and to restrict leakage of this propellant to less than 10 std cm³/sec (scs). The seal is actuated before pump rotation by 1500 psig helium pressure, causing the primary seal face to lift off the rotating seal face and resulting in contact at the secondary seal face, as shown in figure 634. The secondary seal is designed to create an unbalanced P/A force on the bellows seal arm that helps keep the seal in the actuated position when pressure in the pump rear bearing cavity exceeds the 1500 psig actuation pressure. Calibration and cycling tests were conducted on the first machined bellows unit received from the vendor to evaluate primary and secondary seal leakages at various operating conditions, to determine bellows spring rates, P/A relationships, and to demonstrate the cyclic life goal of 10,000 cycles.

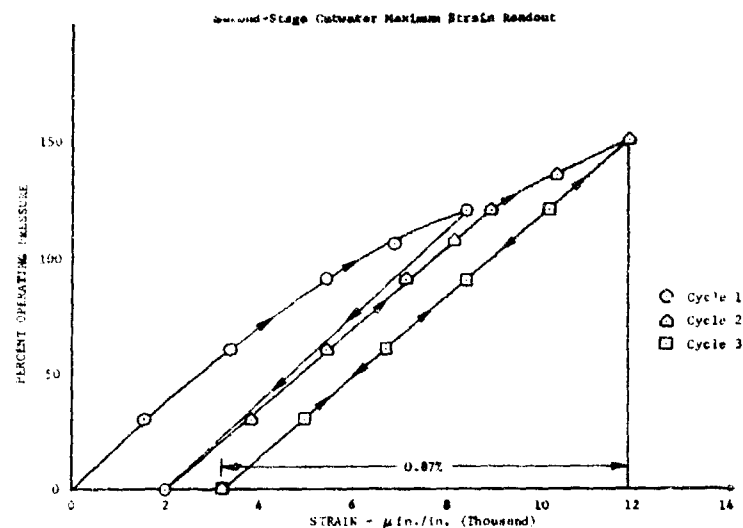


Figure 633. 2nd-Stage Cut Water Maximum Strain Readout

DF 78879

Table LXXIX. Strain Data: XLR129 Fuel Turbopump Housing (2150805), 1 in. Cutback, Proof Pressure Test Cycle 2

Strain (Micro-in./in.) for Percent of Equivalent Operating Pressure						
Strain Gage Locations		30%	60%	90%	120%	150%
1 Axial		-340	-640	-870	-1060	-1200
2 Axial		-570	-880	-1220	-1580	-2100
3 Axial		1080	2140	3200	4340	5760
4 Axial		820	1610	2370	3150	3800
5 Axial		670	1350	2000	2620	3210
6 Axial		630	1250	1820	2400	2950
7 Axial		1100	2100	3050	4040	4910
8 Axial		690	1360	2000	2660	3280
9 Axial		660	1290	1850	2420	2860
10 Axial		760	1500	2020	2560	3070
11 Axial		860	1740	2650	3550	4330
12 Axial		1020	2180	3330	4540	6080
13 Axial		Instrumentation Failure				
14 Axial		800	1610	2310	3050	3620
15 Axial		1000	2010	2950	3980	5000
16 Axial		1810	3410	5080	6920	9830
17 Hoop		130	250	400	570	730
17 Axial		-220	-400	-530	-780	-1010
18 Hoop		190	370	560	770	980
18 Axial		-440	-820	-1150	-1510	-1970
19 Hoop		Instrumentation Failure				
19 Axial						

Table LXXIX. Strain Data: XLR129 Fuel Turbopump Housing (2150805),
1 in. Cutback, Proof Pressure Test Cycle 2 (Concluded)

		Strain (Micro-in./in.) for Percent of Equivalent Operating Pressure				
Strain Gage Locations		30%	60%	90%	120%	150%
20	Hoop	-60	-20	-60	-110	-100
	Axial	670	1280	1920	2600	3200
21	Hoop	50	70	0	-30	-200
	Axial	550	1140	1760	2390	3010
22	Hoop	30	20	10	-70	-170
	Axial	630	1260	1920	2560	3160
23	Hoop	0	0	30	70	100
	Axial	40	-110	-160	-210	-300
24	Hoop	10	20	70	130	220
	Axial	-10	-60	-100	-140	-210
25	Hoop	0	20	30	50	80
	Axial	-20	-20	-10	20	40
26	Hoop	0	0	10	30	60
	Axial	-10	-10	-20	-30	-30
27	Hoop	110	220	370	500	620
	Axial	130	270	400	510	580
28	Hoop	150	340	520	720	900
	Axial	310	540	780	1010	1200
29	Hoop	-60	-100	-130	-170	-230
	Axial	-80	-150	-210	-300	-410
30	Hoop	-90	-140	-190	-250	-310
	Axial	-120	-200	-310	-440	-600
31	Hoop	30	80	160	250	340
	Axial	260	540	820	1100	1400
32	Hoop	20	70	140	200	280
	Axial	310	650	1090	1360	1750
33	Hoop	-80	-110	-140	-180	-220
	Axial	-170	-320	-420	-590	-770
34	Hoop	-80	-120	-150	-200	-350
	Axial	-190	-370	-500	-680	-880
35	Hoop	-80	-130	-160	Instrumentation Failure	
	Axial	590	1180	1680		
36	Hoop	220	320	430	510	560
	Axial	540	1300	2060	2900	3700
37	Hoop	-160	-180	-60	-100	-130
	Axial	1120	2000	2800	3650	4670
38	Hoop	-40	-50	-60	-60	-80
	Axial	530	1100	1730	2420	3030
39	Hoop	-80	-150	-200	-240	-310
	Axial	-200	-400	-570	-780	-1010
40	Hoop	-30	-40	-40	-50	-70
	Axial	-230	-430	-630	-870	-1120
41	Hoop	-80	-110	-160	-200	-230
	Axial	-170	-310	-470	-650	-840
42	Hoop	-30	-40	-30	-40	-70
	Axial	-200	-360	-520	-710	-910
43	Axial	1180	2240	3400	4430	5280
44	Axial	1320	2590	3800	5020	6020

Minus signs indicate compressive strains.

Table LXXX. Elastic Stress Data: XLR129 Fuel Turbopump Housing
(2150805), 1 in. Cutback, Proof Pressure Test Cycle 2

		Stress (psi) for Percent of Equivalent Operating Pressures				
Strain Gage Locations		30%	60%	90%	120%	150%
1	Axial	-9,900	-18,600	-25,200	-30,700	-34,800
2	Axial	-16,500	-25,500	-35,400	-45,800	-61,200
3	Axial	31,300	62,100	92,800	125,900	167,000
4	Axial	23,800	46,700	68,700	91,300	110,200
5	Axial	19,400	39,100	58,000	76,000	93,100
6	Axial	18,300	36,200	52,800	69,600	85,500
7	Axial	31,900	60,900	88,400	117,200	142,400
8	Axial	20,000	39,400	58,000	77,100	95,100
9	Axial	19,100	37,400	53,600	70,200	82,900
10	Axial	22,000	43,500	58,600	74,200	89,000
11	Axial	24,900	50,500	76,800	102,900	125,600
12	Axial	29,600	63,200	96,600	131,700	176,300
13	Axial	Instrumentation Failure				
14	Axial	23,200	46,700	67,000	88,400	105,000
15	Axial	29,000	58,300	85,500	115,400	145,000
16	Axial	52,500	98,900	147,300	*	*
17	Hoop	2,000	4,100	7,700	10,700	13,600
	Axial	-5,800	-10,400	-13,100	-19,400	-25,200
18	Hoop	1,800	4,000	6,900	10,100	12,400
	Axial	-12,200	-22,600	-31,300	-40,800	-53,400
19	Hoop	Instrumentation Failure				
	Axial					
20	Hoop	4,500	11,600	16,400	21,400	27,400
	Axial	20,800	40,600	60,600	81,800	101,000
21	Hoop	6,900	13,100	16,800	21,900	22,400
	Axial	18,000	37,000	56,100	75,900	94,000
22	Hoop	7,000	12,700	18,700	22,200	24,800
	Axial	20,400	40,300	61,300	80,900	99,100
23	Hoop	400	-1,100	-600	200	300
	Axial	1,300	-3,500	-4,800	-600	-8,600
24	Hoop	200	100	1,300	2,800	5,000
	Axial	-200	-1,700	-2,500	-3,200	-4,600
25	Hoop	-200	400	900	1,800	2,900
	Axial	-600	-400	0	1,100	2,000
26	Hoop	-100	-100	100	700	1,600
	Axial	-200	-300	-500	-700	-400
27	Hoop	4,700	9,600	15,600	20,800	25,300
	Axial	5,200	10,700	16,300	21,000	24,400
28	Hoop	7,700	16,000	24,000	32,600	40,200
	Axial	11,300	20,500	29,800	39,100	46,800
29	Hoop	-2,700	-4,600	-6,200	-8,300	-11,200
	Axial	-3,100	-5,700	-7,900	-11,200	-15,300

Table LXXX. Elastic Stress Data: XLR129 Fuel Turbopump Housing
(2150805), 1 in. Cutback, Proof Pressure Test Cycle 2
(Concluded)

		Stress (psi) for Percent of Equivalent Operating Pressures				
Strain Gage Locations		30%	60%	90%	120%	150%
30	Hoop	-4,000	-6,400	-9,000	-12,200	-15,600
	Axial	-4,700	-7,700	-11,700	-16,400	-22,100
31	Hoop	3,400	7,700	12,900	18,500	24,200
	Axial	8,600	18,000	27,700	37,400	47,900
32	Hoop	3,600	8,400	14,900	19,400	25,700
	Axial	10,100	21,400	36,100	45,300	58,400
33	Hoop	-4,200	-6,600	-8,500	-11,400	-14,400
	Axial	-6,200	-11,200	-14,700	-20,500	-26,600
34	Hoop	-4,400	-7,400	-9,600	-12,900	-19,600
	Axial	-6,800	-12,900	-17,400	-23,600	-31,400
35	Hoop	3,100	7,100	11,000	Instrumentation Failure	
	Axial	18,000	36,400	52,000		
36	Hoop	12,200	22,600	33,400	44,000	53,200
	Axial	19,300	44,500	69,800	97,300	123,300
37	Hoop	5,600	13,400	24,900	31,700	40,500
	Axial	34,200	62,000	88,700	115,400	147,600
38	Hoop	3,800	8,900	14,600	21,200	26,400
	Axial	16,500	34,600	54,600	76,500	95,800
39	Hoop	-4,500	-8,600	-11,800	-15,100	-19,500
	Axial	-7,100	-14,200	-20,100	-27,200	-35,200
40	Hoop	-3,200	-5,400	-7,300	-9,900	-12,900
	Axial	-7,600	-14,100	-20,500	-28,200	-36,400
41	Hoop	-4,200	-6,500	-9,600	-12,600	-15,400
	Axial	-6,200	-10,900	-16,500	-22,600	-29,000
42	Hoop	-2,900	-4,700	-5,900	-8,100	-10,900
	Axial	-6,700	-11,900	-16,900	-23,000	-29,700
43	Axial	34,200	65,000	98,600	128,500	153,100
44	Axial	38,300	75,100	110,200	145,600	174,600

#Stresses are calculated from strain data (Table LXXIX) using
Young's Modulus $E = 29.0 \times 10^6$ psi

*Stresses were not computed in the area of high plastic strain
because of limitations of the elastic calculations.

Minus signs indicate compressive stresses

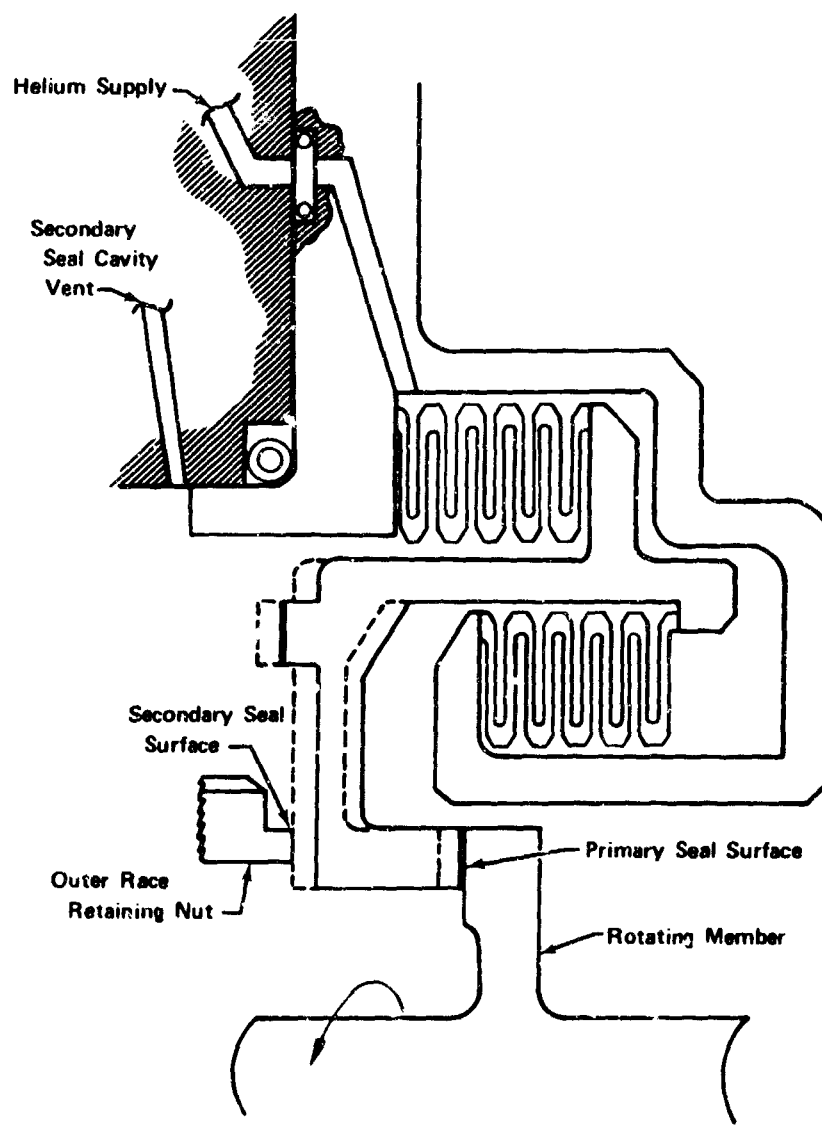


Figure 634. Fuel Turbopump Liftoff Seal

FD 38320

A view of the liftoff seal installed in the liftoff seal test rig is shown in figure 635. Initial testing consisted of 2700 bellows cycling checks with 1500 psig helium at ambient temperatures and periodically measuring primary and secondary seal leakage. After accumulating 25% of the design cycles the leakage was less than 1 sccs gaseous nitrogen on the primary sealing face and 31 sccs on the secondary sealing face with 50 psi differential pressure across the sealing faces. Leakage data are tabulated in table LXXXI.

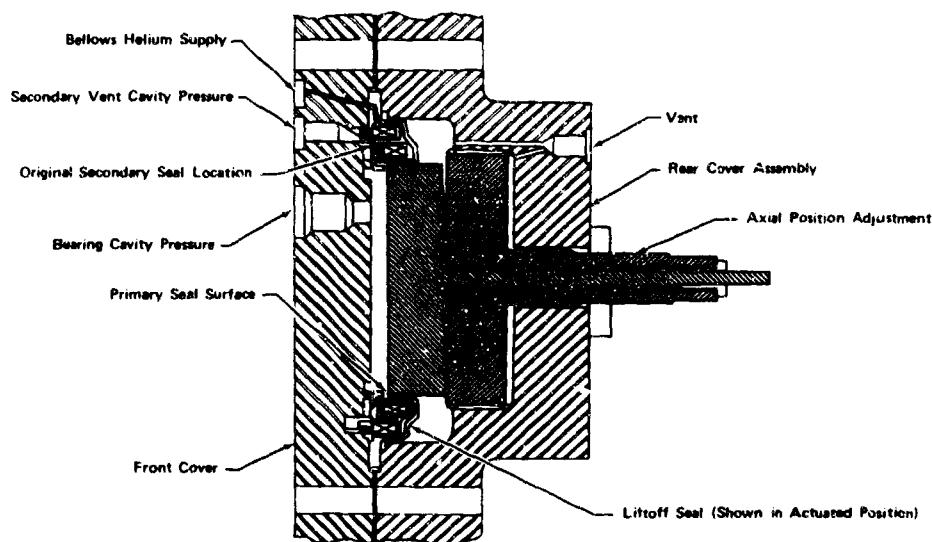


Figure 635. Liftoff Seal Test Rig

FD 38350

Table LXXXI. Liftoff Seal Ambient Leakage Measurements
(Original Secondary Seal Location)

Cycle	Pressure, psid	Primary Seal Leakage, sccs	Secondary Seal Leakage, sccs
1	50	0.1	38.1
100	50	0.1	31.0
300	50	0.1	33.4
800	50	0.1	31.0
1300	50	0.1	28.6
1800	50	0.1	27.4
2700	50	0.1	26.2

After completion of 2700 bellows cycling tests, the test rig was immersed in a bath of liquid nitrogen to permit liftoff seal evaluation in a cryogenic environment. Secondary seal leakage measurements increased significantly indicating the helium actuation force (secondary seal seating force) was insufficient to overcome the increase in bellows spring rate that resulted from temperature effects on the bellows. It was also determined that bearing cavity pressure in excess of 150 psig caused the primary seal to close.

The test rig was modified to move the secondary sealing surface inward from a diameter of 3.76 in. to 3.55 in. also shown in figure 636. This provided an increase in secondary seal force as the bearing cavity pressure is increased. The unit was reinstalled in the test rig and secondary seal face leakage was less than 10 secs at full operating pressure (2800 psig in the bearing cavity). This indicated the desired pressure balance of the seal assembly was achieved with the relocation of the secondary sealing surface. After completion of ambient cycles and leakage checks, cryogenic leakage measurements were made. Results of the leakage tests associated with these 47 cycles are summarized in table LXXXII.

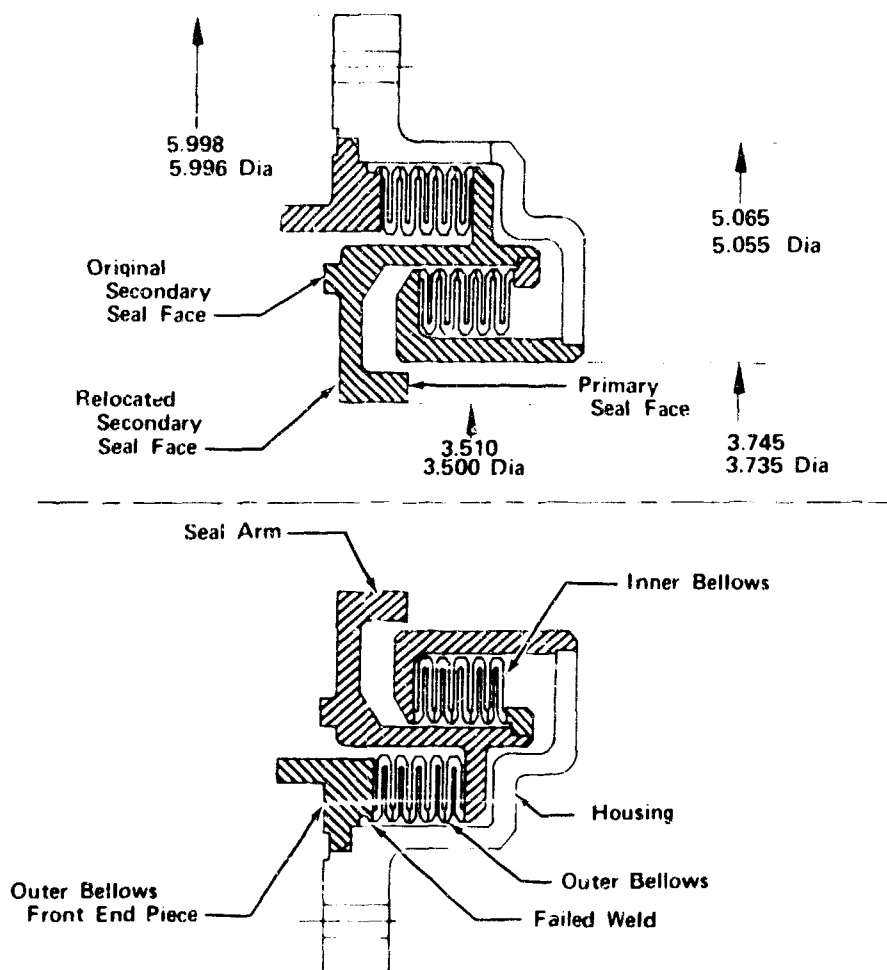


Figure 636. Cross Section of Liftoff Seal Assembly

FD 34997A

Automatic cycling tests were then initiated. The test stand control system was programed to actuate the bellows with 1500 psig helium and then apply 2800 psig gaseous nitrogen pressure to the bearing cavity. The bearing cavity pressure was planned to be vented, followed by venting the bellows actuation pressure. The first automatic cycle (cycle No. 2748) vented the bellows actuation pressure before the bearing cavity pressure and resulted in a bellows differential pressure 87% higher than normal. This abnormal operation resulted from overloading the control circuit operating the test stand valves. Leakage tests performed

on the bellows assembly did not reveal any failures. After 20 manual bellows actuation cycles and 4 pressure cycle tests, the bellows exhibited characteristics indicative of bellows failure. The bellows had accumulated 2772 cycles prior to bellows failure indication. The rig was removed from the test stand and disassembled for inspection. A pressure check determined that outer bellows failure had occurred.

Table LXXXII. Liftoff Seal Leakage Measurements (Relocated Secondary Seal)

Cycle	Environment	Pressure, psig	Primary Seal Leakage, secs	Secondary Seal Leakage, secs
2739	Ambient GN ₂	50	0.1	82.4
	Ambient GN ₂	2800	Not Measured	0.1
2740	Ambient GN ₂	50	3.5	282.0
	Ambient GN ₂	2800	Not Measured	15.9
2746	Liquid Nitrogen	50	0.14	2.35
	Liquid Nitrogen	2800	Not Measured	0.1
2747	Liquid Nitrogen	50	131.6	376.0
	Liquid Nitrogen	2800	Not Measured	65.8

The liftoff seal assembly that failed was X-rayed in an attempt to determine the area of failure. X-rays did not reveal where the seal had failed. The liftoff seal assembly was returned to the vendor for disassembly, and the bellows assembly removed from the housing. The outer bellows failed at the weldment to the front end piece for about 270 deg around the circumference as shown in figure 636. X-ray of the bellows assembly revealed no additional areas of distress. A review of the failure did not disclose the cause or method of failure under normal operating conditions.

The bellows assembly was returned to FRDC and the inner bellows removed for inspection. No visual defects were observed in the inner bellows. The inner bellows were X-rayed and investigation revealed indications of cracks and lack of penetration in the bellows welds. The inner bellows were tested to determine the spring rate and results indicated a spring rate of 43,600 lb/in. The inner bellows were sectioned, and indications of convolution mismatch, poor weld penetration, and cracks were found. See figure 637. The outer bellows were also sectioned for failure investigation as shown in figure 638. This investigation of the outer bellows failure disclosed a tension overstress failure.

From the results of the failure investigation it appeared the cause was over extension of the bellows. With the application of pressure on the secondary seal without the bellows pressurized, the total P/A load seats the primary seal and causes the seal arm to deflect. This action over extends the bellows and results in excessive tensile loads imposed on the bellows end weldments as indicated in figure 639.

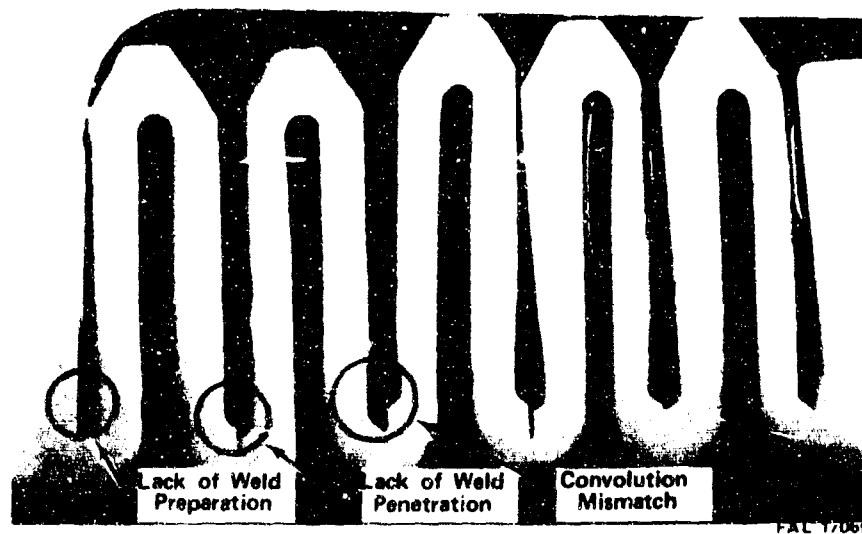


Figure 637. Inner Bellows Section Showing Fabrication Problem Areas

FD 34998A

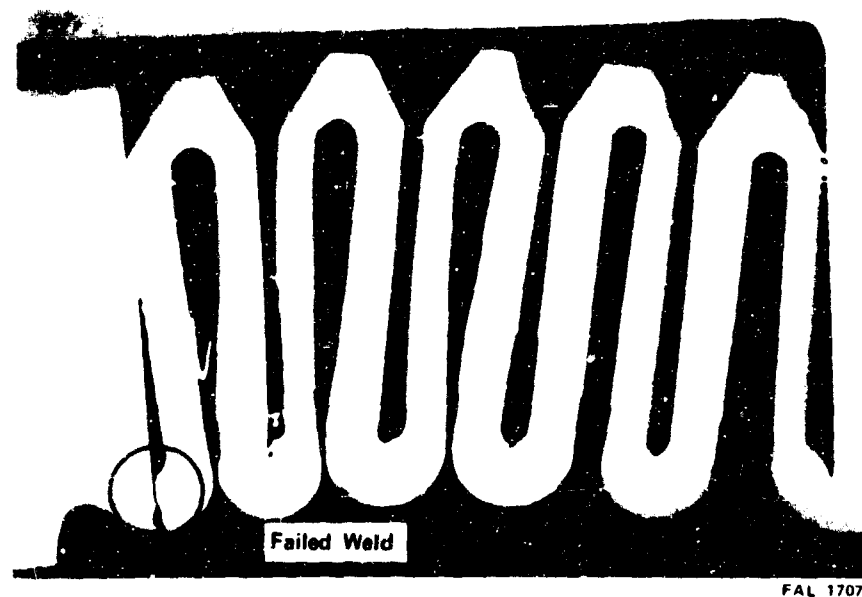


Figure 638. Outer Bellows Weld Fabrication Location

FD 34999A

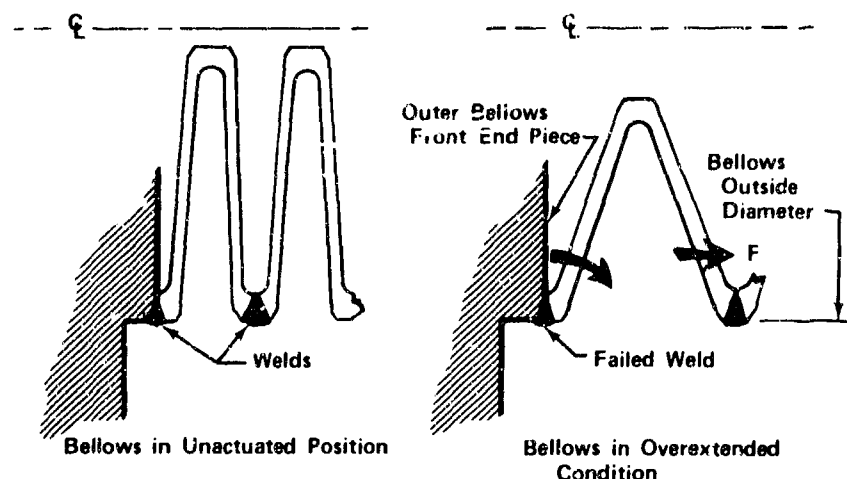


Figure 639. Overextension of Bellows Resulting In Excessive Tensile Loads FD 38348

To prevent recurrence of this failure, the secondary cavity will be vented, as in the engine system, on future tests. Individual spring rate tests will also be performed on the bellows convolution assemblies before installation of end pieces, and X-rays will be made of the convolution assemblies required before installation in the bellows assembly. In addition, a weld transition section on the end pieces is being made. This will allow the weld to be made between two parts with approximately the same thickness to reduce the stress concentration at these points.

The second and third machined bellows liftoff seal units were manufactured simultaneously with the first part that failed during evaluation testing. These units were examined and found to have spring rates and sealing characteristics similar to the first part. Because the first part had exhibited a cycle life in excess of the fuel turbopump rig test requirement, these units were utilized in the fuel turbopump and hot turbine test rigs.

The formed bellows liftoff seal units, which were initiated after the failure examination of the first unit, were not available in time to be evaluated in the fuel turbopump test rig. The first formed bellows unit was calibration tested to determine operational characteristics and was incorporated in the backup fuel turbopump test rig (F35138-3), but this rig was not required in the test program.

(5) Turbine Stator Flow Calibration Tests

Turbine stator flow calibration tests were primarily performed to determine effective flow areas and to establish a basis for acceptance of future castings. Stators were calibrated on a water flow test facility. Stator castings were installed in test adapters simulating the upstream flowpath arrangement of the fuel turbopump turbine. The test item was mounted in the B-21 test stand facility which has a 2000 gal capacity water blowdown system. A schematic of the test facility is shown in figure 640. Flow calibration tests were performed at steady-state flowrates of 400, 550, 850 and 1060 gpm. For each test, values were recorded for upstream static pressure, stator differential pressure, flow and water temperature.

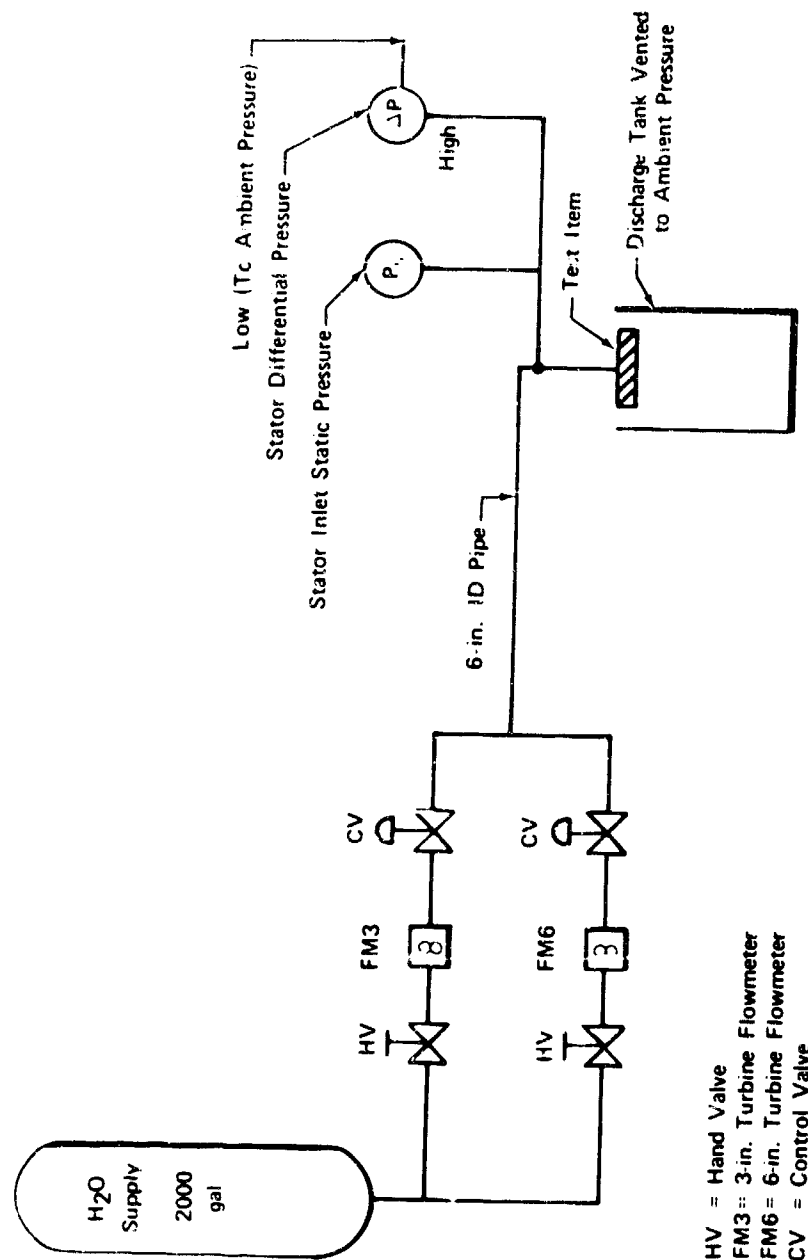


Figure 640. B-2i Test Stand Station Flow Test Arrangement, Block Diagram

Effective flow areas for each stator were calculated from test data and plotted versus water flow and presented in figure 641. Effective flow areas for each stator vary with flow due to discharge coefficient variation with Reynolds number. Test facility limitations precluded flowing the stators at sufficiently high flowrates to eliminate discharge coefficient variation. However, this facility provides a means of acceptance flow testing the castings before finish machining. A correlation will be made between the effective area determined by these tests and the effective area determined during the turbopump testing on E-8 test stand for use in acceptance testing of subsequent stator castings.

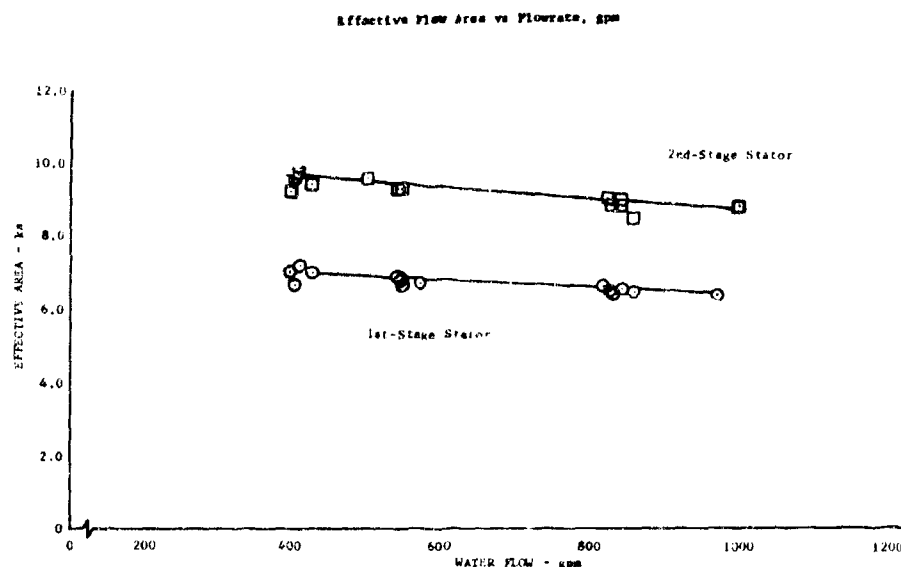


Figure 641. Fuel Turbopump Turbine Stator Flow Calibration DF 78921

(6) Critical Speed Evaluation Tests

The fuel pump assembly critical speeds were predicted by analyzing the rotor natural frequencies alone and when coupled with a support system simulating the pump assembly as shown in figure 642. Predictions were checked by running vibration tests on the rotor alone in the nonrotating free-free state and comparing test results with the predictions to determine shaft lateral stiffness. Spring rate tests were made on the bearing supports and then the pump bearing support configurations were selected based on these predictions. A configuration having only one critical speed (bounce mode) in the pump operating range was selected because 350K fuel pump experience indicated this first (bounce) mode was a stable mode without hydromechanical instability. It was possible to operate through the second (rocking) mode, but a hydromechanical coupling greatly increased the bearing loads.

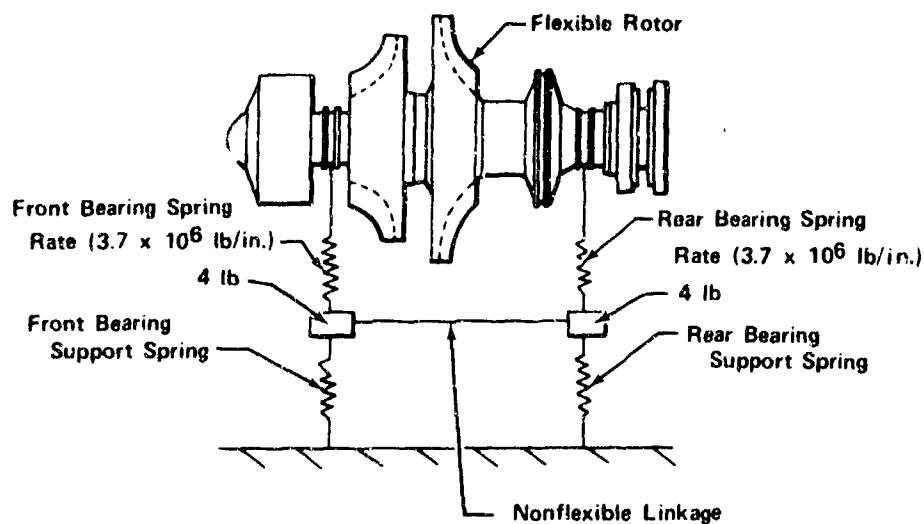


Figure 642. Rotor Support System for Fuel Turbo-pump Critical Speed Analysis FD 38355

The rotor vibration test was set up as shown in figure 643. The rotor, with the tie bolt loaded to 120,000 lb, and with the turbine blades removed, was supported from a beam with elastic cords (10 lb/in. spring rate) at both bearing locations. A drive rod was cemented to the rotor and connected to an MB model C-10 shaker unit. Accelerometers were cemented to the rotor at eight axial locations also shown in figure 643. The shaker was set to automatically sweep the frequency range from 200 to 2000 Hz.

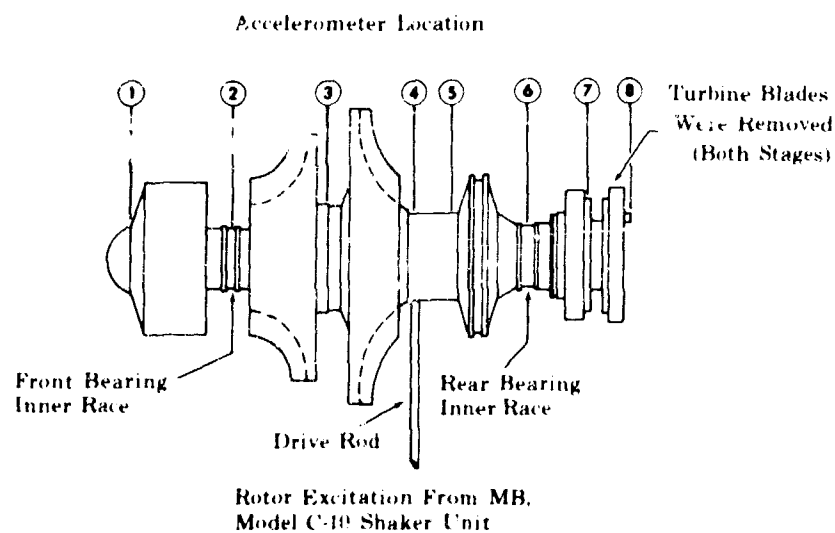


Figure 643. XLR129 Fuel Pump Rotor, Natural Frequency Test FD 33698

The resulting accelerometer data revealed two rotor natural bending frequencies within this frequency range. These frequencies are shown in table LXXXIII.

Table LXXXIII. Natural Bending Frequencies

Rotor Mode	Test Data	Predicted
First Bending	1010 Hz	1000 Hz
Second Bending	1589 Hz	1595 Hz

Rotor mode shapes at these natural frequencies are shown in figures 644 and 645. The solid line on each graph is the predicted rotor deflection shape and the numbered points are the measured deflection points corresponding to the accelerometer locations.

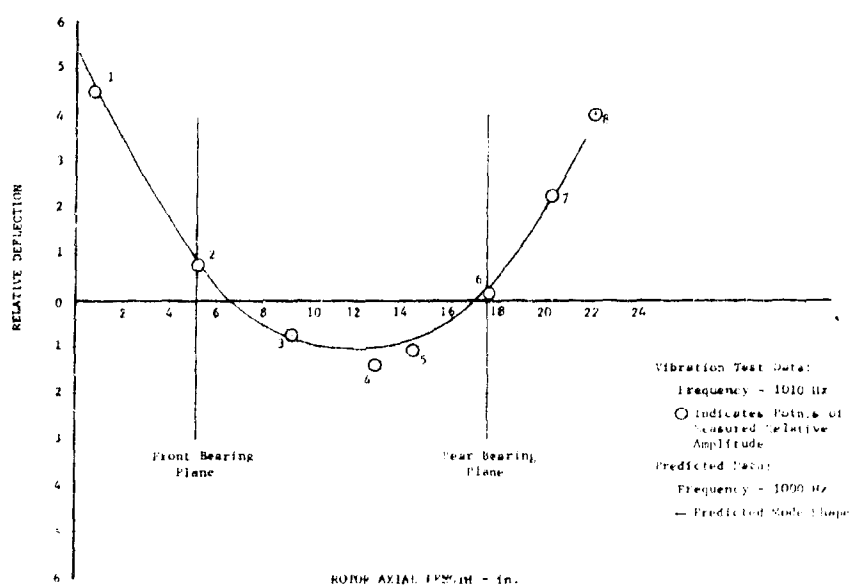


Figure 644. XLR129 Fuel Pump Rotor, Second Bending Mode Predicted and Test Results

DF 76519

Predicted frequencies and mode shapes were computer with no rotational effects and without turbine blades. Turbine blades were not mounted on the rotor assembly because of their loose fit at the disk attachment. This would produce additional noise on the readout making reading of mode shapes difficult.

This test verified the predictions of shaft (rotor) lateral bending stiffness without rotation were accurate within 1%. The stiff bearing critical speed calculation is dependent upon lateral shaft stiffness, gyroscopic stiffness, and the effect of infinitely stiff bearing mounts. The gyroscopic stiffness and effect of infinitely stiff supports are well defined calculations thus leaving rotor lateral bending stiffness as the largest variable in the prediction. Because predictions of lateral stiffness were substantiated, the calculated 1.26 stiff bearing critical speed margin was also substantiated.

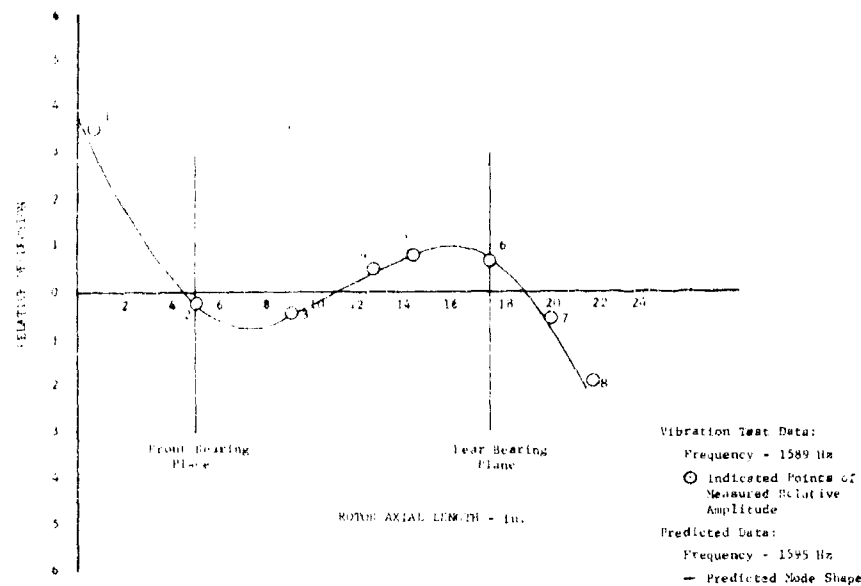


Figure 645. XLR129 Fuel Pump Rotor, First Bending Mode Predicted and Test Results

DF 76520

Vibration tests were conducted on the front and rear bearing supports to determine dynamic and static radial spring rates. These spring rates were used in the determination of the pump predicted critical speeds as previously discussed.

(7) Bearing Support Spring Rate Tests

(a) Front Bearing Support

The front bearing support mounted in the pump front housing completed vibration tests which indicated the static spring rate is 5.4×10^6 lb/in. This rate is much higher than the calculated prediction of 1.8×10^6 lb/in. static spring rate.

The front housing was mounted on the test bed mounting block and connected to the shaker unit shown in figure 646. Accelerometers were mounted as shown in figure 647 to measure the test setup motion.

The vibration test was made with the shaker driving the bearing support with sine wave sweeps from 50 to 400 Hz at ± 0.5 mils displacement and from 400 to 1000 Hz at $\pm g$ acceleration.

The following data were recorded at each accelerometer location:

1. Acceleration/displacement vs frequency
2. Transfer impedance plots - includes dynamic spring rate and effective mass vs frequency

3. Phase angle plots - angular relationship between velocity and force vectors vs frequency.

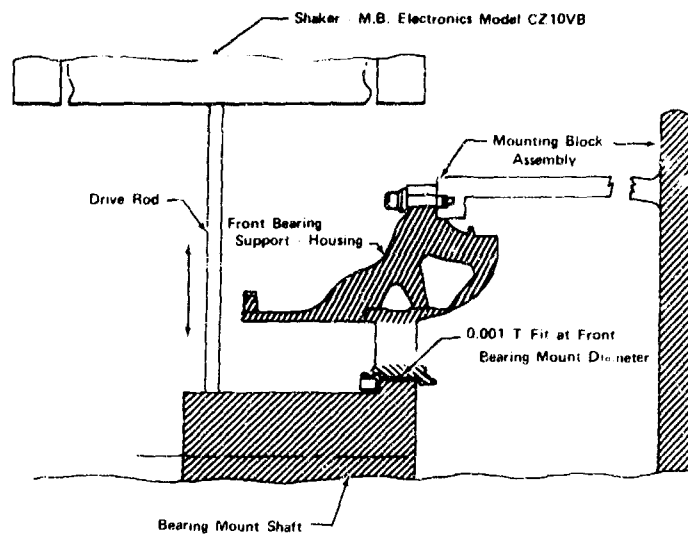


Figure 646. Front Bearing Support Spring Rate Setup

FD 38356



Figure 647. Front Bearing Support Assembly Mounting

FD 90908

The bearing mount shaft, bearing support housing and mounting block act as a series of springs with a dynamic load input shown in figure 648. The deflection vs frequency data were used to determine the relative deflection between each point at a selected frequency and thus determine the dynamic spring rates because the force input was known.

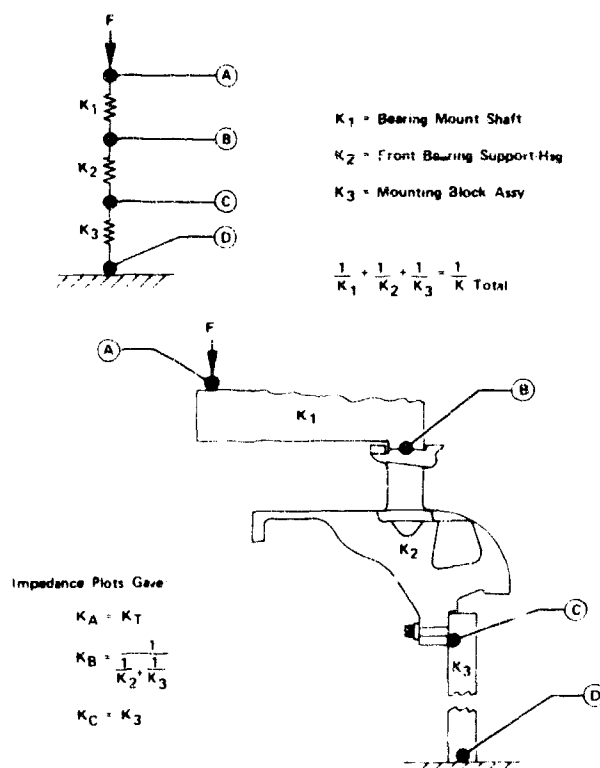


Figure 648. Series Spring Simulation of Front Bearings Support Test Setup

FD 38357

Dynamic spring rates determined from these tests are not similar when the supports are mounted in the pump assembly because of the difference in mount system resonances. These resonances can drastically vary dynamic spring rates at certain frequencies. Because of this variation and the fact that static spring rates are used for critical speed predictions, calculations were made from test data to determine static spring rates. The analysis was made in the following manner.

A spring is considered an ideal static spring when the velocity component leads the force component by 90 deg. Phase angle plots were made to determine when this condition existed during the frequency sweep at each accelerometer location. These plots were superimposed on the impedance plots giving the spring rate at each of the 90 deg lead points. A line through these points yielded the average static spring over the frequency range at each accelerometer location.

Substitution of these values in the series spring formulas yields an average static spring rate for the front bearing support housing of 5.4×10^6 lb/in.

(b) Rear Bearing Support

Vibration tests were performed on two rear bearing support configurations. The initial configuration spring rate was higher than desirable based on the anticipated 1.8×10^6 lb/in. front bearing support spring rate. The rear bearing support was modified to reduce the spring rate; however, this new spring rate was still greater than the desired 2.1×10^6 lb/in. spring rate. Meanwhile, the front bearing spring rate had been tested and was determined to be 5.4×10^6 lb/in. With this high spring rate front support it was determined that a new bearing support spring rate of 9×10^6 lb/in. would place the second critical speed above the maximum pump operating speed. A schematic of the setup for the rear bearing support test is shown in figure 649. Accelerometers were attached at critical locations so systems motion could be described as shown in figure 650.

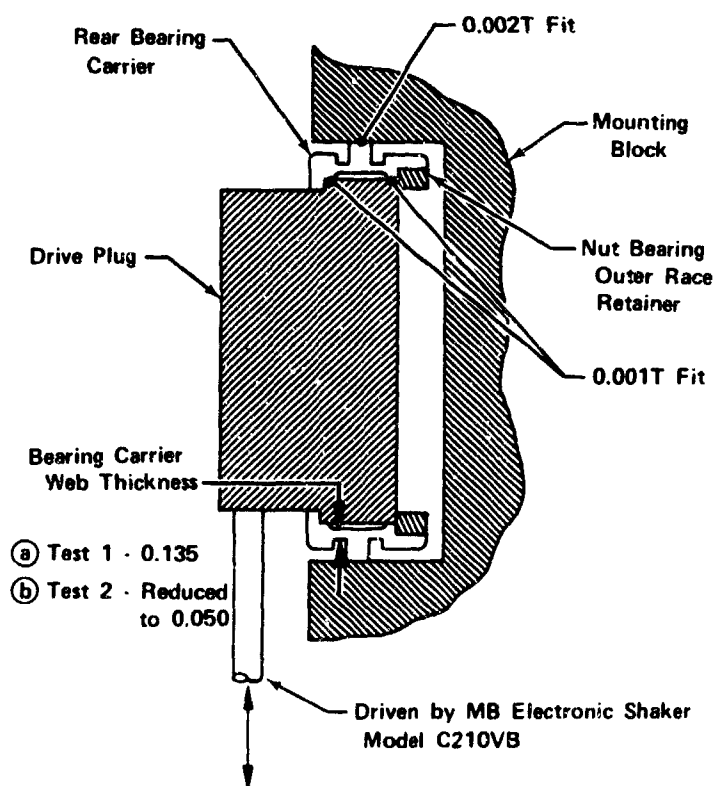


Figure 649. Rear Bearing Support Test Setup

FD 38358

The support was tested by dwelling at several frequency levels within the 100-1000 Hz range and recording accelerometer data. The plug, spring and mount block responded as one unit at all frequencies, indicating the spring was at least as stiff as the mount which had a static spring rate of 10×10^6 lb/in. or greater.

Because this spring rate was too high, the support was modified by reducing the web thickness to 0.050 in. also shown in figure 649.

The same vibration test was repeated with the modified support. This test indicated the support acted as an individual spring leaving a minimum of 8×10^6 lb/in. dynamic spring rate. The minimum dynamic spring rate occurs close to a system resonance and is always much less than the average static spring rate, therefore indicating a static spring rate greater than 8×10^6 lb/in.



Figure 650. Rear Bearing Support Accelerometer FC 19061
Mounting

After the front bearing support was tested and found to have a spring rate of 5.4×10^6 lb/in., a solid rear bearing support was incorporated in the pump to drive the second predicted critical speed above the maximum pump operating speed. This solid support was not tested because the vibration test supporting structure was softer than predicted for the solid bearing support. The static spring rate of this solid rear bearing support is assumed to have a spring rate of at least 10×10^6 lb/in. because this was the spring rate of the first configuration tested, and the solid support is at least as stiff as the first.

Bearing support spring rates determined from vibration tests were used to establish a range of probable rates when mounted in the pump assembly. These ranges were used in the critical speed computer program to predict the expected fuel pump assembly critical speeds. Results of these predictions are listed in table LXXXIV.

(8) Dynamic Rotor Balance

Successful operation of high-speed turbomachinery requires balancing the rotor assembly to minimize centrifugally induced radial forces during pump operation. Turbomachinery designed to operate with the bearings in a liquid hydrogen or liquid oxygen cryogenic environment requires a clean, dry system that greatly restricts or prohibits the use of lubricant. Without a lubricant or a cryogenic atmosphere bearing life is greatly reduced. For this reason, rotation time on the pump bearings for balancing must be held to a minimum so that pump bearing life is not degraded.

Table LXXXIV. Predicted Critical Speeds,
XLR129 Fuel Pump Assembly

Front Bearing Support Spring Rate (lb/in.)	Rear Bearing Support Spring Rate (lb/in.)	First Critical Speed, Bounce Mode (rpm)	Second Critical Speed Rocking Mode (rpm)	Third Critical Speed Bending Mode (rpm)
1.8×10^6 *	2.1×10^6	30,210	37,860	72,200
4×10^6	9×10^6	37,300	47,950	70,500
6×10^6	9×10^6	38,800	48,850	71,650
4×10^6	12×10^6	37,600	49,050	70,500
6×10^6	12×10^6	39,250	49,800	71,650

*Original design configuration.

Fuel turbopump rotor components undergo detail balancing to minimize the force couples generated by the individual parts. This also reduces residual unbalance of the rotor when the detail parts are assembled. In general, the acceptable residual unbalance of the rotor details is 0.02 oz-in. or less at design blade tip speed. Rotor details are assembled and the rotor assembly is supported in the balance machine on the bearing inner races and rotated at 1500 rpm. The rotor assembly is balanced to 0.01 oz-in. in two planes (dynamic balancing). Unbalance correction is accomplished using balance weights installed in the front of the inducer and in the turbine plane by using nuts of varying weights on the turbine tie bolts. Rotor details are alignment marked before disassembly to ensure indexing during reassembly.

After final assembly, the fuel turbopump is installed in a balance machine with the attachment fixture supported on rubber mounts which allow movement in three planes. Dry gaseous nitrogen is directed against the turbine blades by a nozzle arrangement to spin the rotor assembly at 1200 rpm. Before rotation, the liftoff seal is energized and the thrust balance piston is pressurized with dry gaseous nitrogen. The thrust balance piston supply also cools the rear bearing. The front bearing is supplied dry gaseous nitrogen from an external source. Final balancing is performed with a balance machine which utilizes the frequency transposition principle, and has considerably reduced the time required to balance the rotor assembly using roller bearings. Using this principle, alternating potential from the balance pickups, with the frequency predetermined by the revolutions of the test rotor, is transposed to a second alternating potential with a frequency that allows angle and amount of imbalance to be detected independently of line fluctuations or noise.

The turbopump assembly is balanced in the same planes as those used in the rotor balance to a maximum unbalance of 0.01 oz-in. in both planes. Unbalance correction is made similar to that used for the rotor balance, and fine corrections are made by drilling the inducer cover and by grinding material from the turbine tie bolt nuts. The balancing cycle is restricted to one minute of rotation with at least a 3 minute cooling interval between rotation to prevent overheating the bearings. The average rotation time on a turbopump assembly balanced with this machine is less than 10 minutes.

b. Turbopump Tests

(1) Assembly

Assembly of the fuel turbopump begins with the previously detailed balanced rotor parts being assembled for rotor assembled balance. After completion of the rotor assembly balance, all details are alignment marked to ensure proper part-to-part indexing during final assembly in the housings.

The turbine stationary parts forward of the 2nd-stage turbine rotor and the liftoff seal are assembled to the rear bearing support housing, which includes the rear bearing, and the liftoff seal helium system is leak checked. This assembled package is heated to provide a clearance between the rear bearing inner race and the shaft. The shaft and second disk unit is supported on an alignment fixture, turbine end down, and the inner race axial preload spring is then installed. The support fixture is preset to center the thrust balance piston after the housings have been installed. The heated housing and bearing unit is then installed on the shaft and the thrust balance piston, which also has been heating, is immediately installed against the rear bearing inner race and loaded to ensure proper axial positioning until post-cooling interference fits are achieved. Stackup measurements are then taken to assure proper seating of the thrust piston on the shaft.

The thrust balance piston housing is then assembled on the rear bearing support housing with the required seals and bolts. The heated 2nd-stage housing is then installed over the thrust balance piston housing and bolted in place. The heated 2nd-stage impeller is installed on the shaft and bottomed against the end of the thrust balance piston. As the parts cool, measurements are taken to ensure the predetermined stackup measurement requirements have been met. The main housing is heated and lowered over this internal housing and rotor subassembly. The 35 bolts securing the rear bearing support housing to the main housing are installed and tightened. The pump interstage labyrinth seal, 1st-stage impeller and the front bearing inner race support are preassembled. This subassembly is then heated and lowered on the shaft, and the interstage labyrinth seal and splines are mated to the rear of the second impeller. The load nut is installed on the shaft and tightened sufficiently to maintain a load in the rotor stack until the parts are cooled and interference fits are achieved. Stackup measurements are compared a second time against predetermined values. The tie bolt is then stretched using a hydraulic load ram and the nut is torqued to 2100 in. A load of 120,000 lb. was used on the first two pump rigs, and 130,000 lb on the final test rig.

The front bearing is installed in the inducer housing. This housing and bearing subassembly is heated and assembled with the main housing and the shaft. During the initial build, difficulty was encountered during this procedure because of the internal snap fit between the inducer housing and the main housing. Oven heating the inducer housing and bearing subassembly would have caused an increase in the interference fit with the main housing. Therefore, localized heating of the bearing inner race was accomplished by use of heat guns, and heat lamps were directed on the main housing snap diameter to reduce the interference fit with the inducer housing complicating assembly procedures. Analytical predictions based on housing proof pressure test measurements indicates the tight internal fit between the two housings would loosen at design operating conditions, but the bolt loads were sufficient to maintain housing alignment. A redesign of

the front housing was initiated after the first turbopump rig build to eliminate assembly complications and to improve housing alignment under pump operating conditions. The inducer housing was redesigned for an external pilot diameter with the main housing by the addition of an outside diameter support ring electron beam welded to the housing. This inducer housing modification is shown in figure 651.

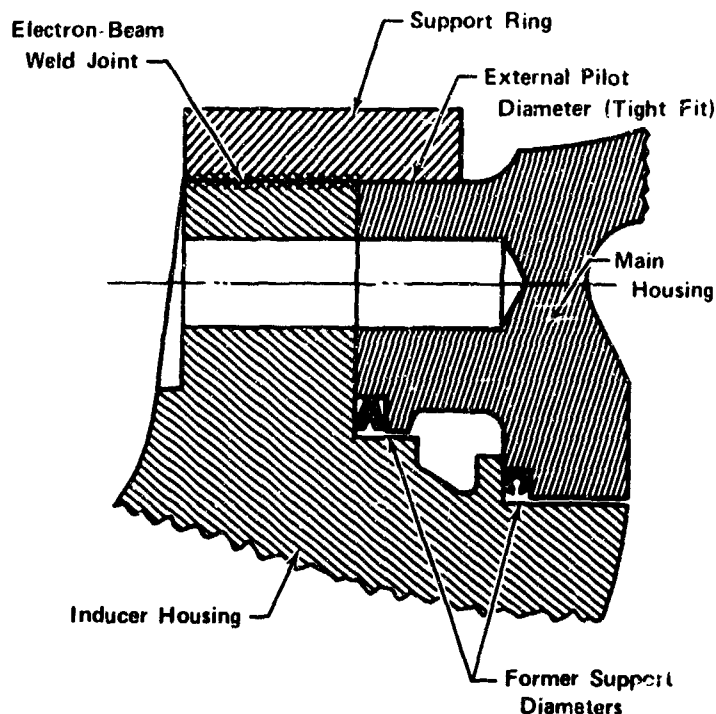


Figure 651. Inducer Housing Modifications

FD 38359

After installation of the inducer housing and front bearing subassembly, the 36 bolts securing the inducer housing to main housing are installed and tightened. The inducer is then heated and installed over the shaft and into the inducer housing. The inducer retaining nut is then tightened and measurements are taken to ensure that rotor detail parts are seated.

The pump assembly is then inverted and mounted in a fixture on the inducer housing. The turbine exit diffuser is bolted to the turbine support case and the turbine inner duct guide is pulled into position with the bolts that secure this duct to the exit diffuser. The 2nd-stage stator and main stator support are also installed on the exit diffuser flange and the bolts are tightened. The 1st-stage turbine rotor is then installed on the second disk flange, and turbine tie bolt nuts are installed and tightened. The 1st-stage turbine blade shroud is installed and retained by the 1st-stage stator axial support that is temporarily bolted to the main stator support.

The pump is rotated to horizontal position and the balance machine support frames are installed. The pump assembly is then installed in the balance machine for final dynamic rotor balancing. After completion of the final assembly balance, which includes the installation of the inducer cap and locking the turbine tie bolt nut locks, the pump is installed in a horizontal support fixture. The temporary

bolts securing 1st-stage turbine blade shroud and 1st-stage static port are replaced with the permanent bolts, and the subassembly of the compressor and turbine inlet housing is installed and the bolts tightened. The turbine coolant manifold is installed and a leak check of the static seals and tube connectors is performed. Then the pump is installed in the test fixture or on the engine transition case, and the interface static seal is leak checked.

(2) Pump Test

Thirteen tests for a total rotational time of 488.7 seconds were completed during three builds of the fuel turbopump rigs on the B-6 test facility. The objectives of these tests were: (1) to map the pump and turbine performance, (2) to evaluate the axial thrust balance system, and (3) to demonstrate the suitability of the turbopump for use on the tests of the powerhead assembly that consists of a preburner, transition case, oxidizer turbine simulator and fuel turbopump. A summary of these tests is shown in table LXXXV.

(a) Rig F35138-1

Five tests for a total rotational time of 142.6 seconds were completed during this first test series. Prior to the initiation of the pump rig tests, six low speed (6000 rpm or less) rotational tests were conducted with liquid nitrogen in the pump and the turbine powered with ambient hydrogen gas to check out the speed signal to the control system. The next two tests (1.07 and 2.01) were facility checkout tests that established the acceleration characteristics of the turbopump on the test facility and provided control and automatic abort system response information.

Test No. 3.01 was conducted on 3 January 1970 and was 61.3 seconds in duration. This was a programed duration test at the 50% speed level (24,000 rpm). A flow excursion was performed to map the pump at this intermediate operating level. Data analysis revealed that all systems operated as expected, axial thrust balance was satisfactory and pump performance was better than predicted. Plots of significant turbopump parameters versus time are shown in figures 652 through 654. Figure 655 is a plot of axial thrust and speed versus time.

Test No. 4.01, conducted on 8 January 1970 was a 45.2 second programed duration test. The objective of this test was to perform a flow excursion at the 40,000 rpm speed level to map pump performance and to evaluate the rotor thrust balance. During the flow excursion at this 83% speed level, the pump discharge bleed valve lost electrical power and the valve went to the fail-open position. This caused a flow excursion at approximately 7% higher than programed flow. Data analysis indicated that pump performance was better than the design predictions, and the thrust balance piston capability was well in excess of the required force. Plots of significant turbopump parameters versus time are shown in figures 656 through 658. Figure 659 is a plot of axial thrust and speed versus time.

Table LXXXV. Fuel Turbopump Test Summary

Test Rig	Test Number	Date of Test	Duration (sec)	Peak Pump Speed (rpm)	Peak Discharge Pressure (psia)	Remarks
35138-2	1.07	12/20/69	5.9	27,730	1862	Facility checkout; high-speed abort.
	2.01	12/30/69	16.4	24,328	1593	Facility checkout; vibration system malfunction.
	3.01	1/03/70	61.3	25,406	2083	Full duration test; flow excursion at 24,000 rpm from 5,700 gpm to 1,800 gpm.
	4.01	1/08/70	45.2	40,400	4380	Full duration test; flow excursion at 40,000 rpm from 10,250 gpm to 8,800 gpm; facility bleed valve failed open.
	5.01	1/13/70	13.6	46,050	5560	Premature shutdown due to excessive vibrations; test terminated after pump had achieved speed set point (46,000 rpm); maximum flow was 11,150 gpm and maximum pump discharge pressure was 5,560 psia.

Table LXXXV. Fuel Turbopump Test Summary (Continued)

Test Rig	Test Number	Date of Test	Duration (sec)	Peak Pump Speed (rpm)	Peak Discharge Pressure (psia)	Remarks
35138-2	6.01	3/5/70	41.6	40,480	5125	Full duration test with flow excursions at 83% and 50% speed levels. All rig components performed as predicted.
	7.01	3/6/70	19.9	46,300	5730	Advanced to shutdown by $\pm 20g$ vibration monitor system at test program speed set point of 46,000 rpm. Vibration was a combination of 1E and another component approximately 0.89E. Indications are second impeller rubbed on the tips as viewed with borescope through discharge horn.
	8.0	3/13/70	18.0	46,260	6398	$\pm 30g$ vibration abort during flow excursion at 96% speed level. Before shutdown, flow excursion completed at 42,500 rpm that demonstrated 100% $r = 6$ & 7 and final data point at the 46,000 rpm level demonstrated 100% $r = 5$. Vibration advance systems ($\pm 20g$ level) disarmed for this test.
	9.01	3/24/70	83.0	32,800	3320	Completed flow excursion at 68% speed level from 7400 gpm to 3800 gpm, and flow excursion at 46% speed level from 2700 gpm to 1600 gpm. Then performed NPSH demonstration at the 22,000 rpm level (1600 gpm). Run was advanced to shutdown at cavitation point, but pump unloaded and sped up to 36,200 rpm before terminated by overspeed abort system. Data indicate thrust piston contacted rear face during the overspeed and part of coast down until pump started pumping again.

Table LXXXV. Fuel Turbopump Test Summary (Continued)

Test Rig	Test Number	Date of Test	Duration (sec)	Peak Pump Speed (rpm)	Peak Discharge Pressure (psia)	Remarks
35136-2	10.01	3/25/70	25.5	42,600	5650	Pump accelerated to the 89% speed level and inlet pressure ramped from 90 psia to 35 psia without pump cavitating. Because cavitation had been anticipated at 46 psia inlet pressure at +19 sec, new (lower) overspeed abort levels were sequenced in at +25 sec because the pump speed was to be reduced to 43% when cavitation occurred at the 89% speed level. Pump pressure rise at the 89% speed level did not indicate desired cavitation level was obtained before the sequencer triggered in the lower advance and abort levels and the run was aborted to shutdown.
	11.01	3/26/70	74.6	42,800	5440	Pump accelerated to the 89% speed level ($Q/N = 0.212$) and inlet pressure was reduced to 26 psia at which time 5% head falloff was attained. Rig then ramped to 20,500 rpm ($Q/N = 0.127$), LH ₂ supply tank pressure reduced to ambient with no significant head falloff.

Pulled rig for teardown inspection on
30 March 1970

Table LXXXV. Fuel Turbopump Test Summary (Concluded)

Test Rig	Test Number	Date of Test	Duration (sec)	Peak Pump Speed (rpm)	Peak Discharge Pressure (psia)	Remarks
35147-1A	1.01	5/28/70	47.3	41,556	5360	Full duration test with flow excursions at 50%, 67%, and 83% speed levels. Rig performance exceeded predicted. Thrust balance satisfactory. Liftoff seal coupled to external control operated satisfactorily.
35147-1A	2.01	6/2/70	36.1	48,136	6705	Full duration test with flow excursions at 67%, 88%, and 100% speed levels. Rig performance better than predicted. Thrust balance satisfactory. Liftoff seal operated satisfactory. All test objectives met. Rig pulled on 6/4/70 for hot turbine testing at E-8 stand.

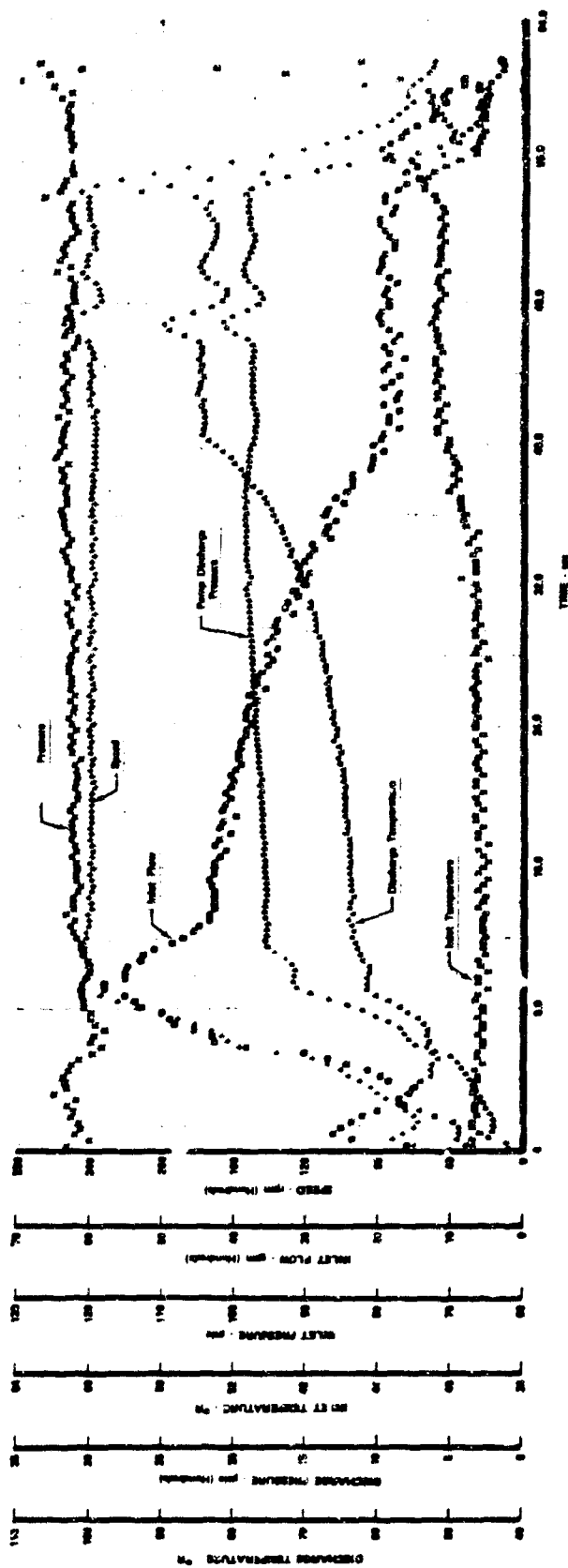


Figure 652. Significant Turbopump Parameters vs Time, Test 3.01, Sheet 1 of 3

FD 37086A

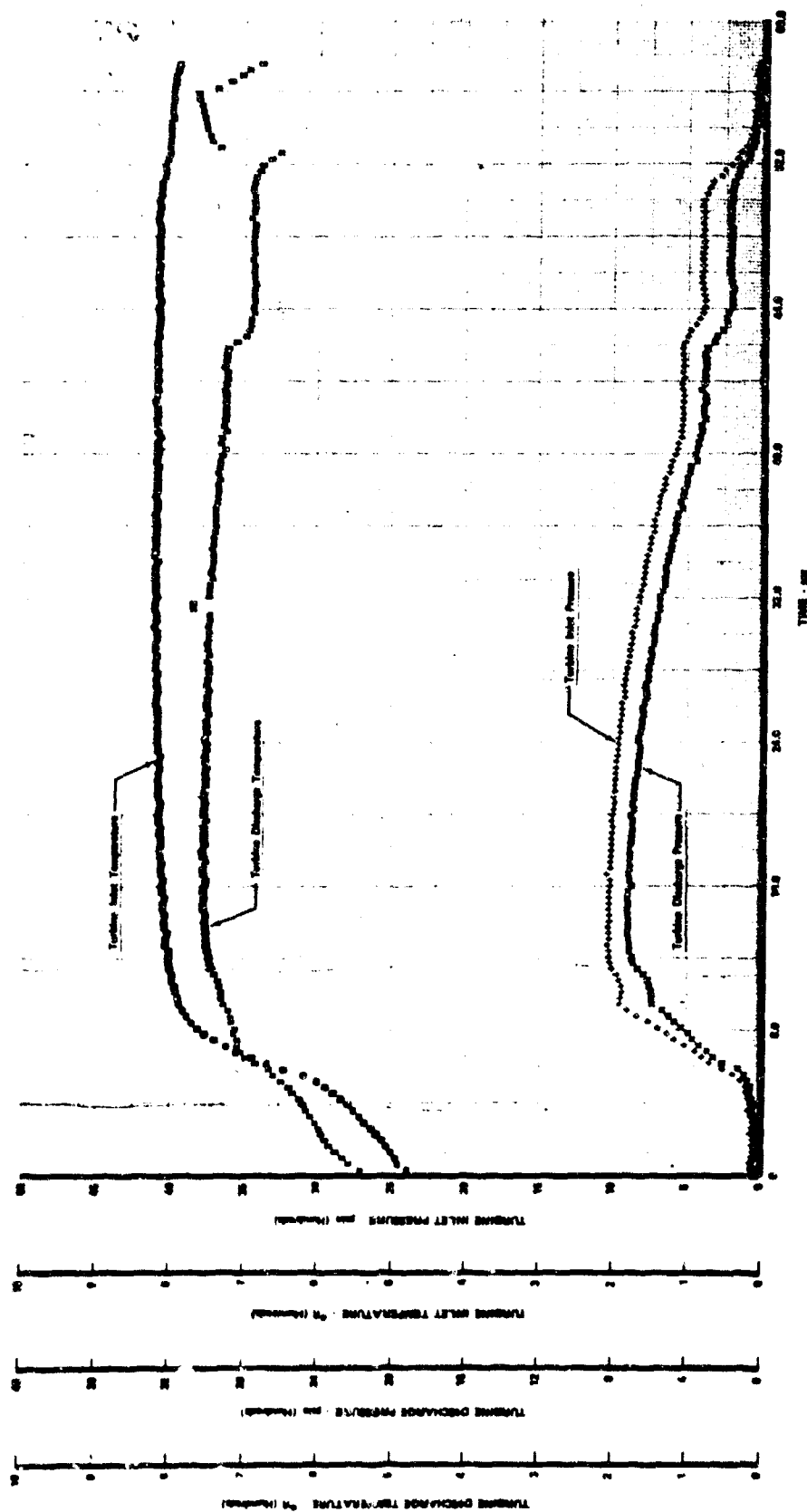


Figure 653. Significant Turbopump Parameters vs Time, Test 3.01, Sheet 2 of 3

FD 37087A

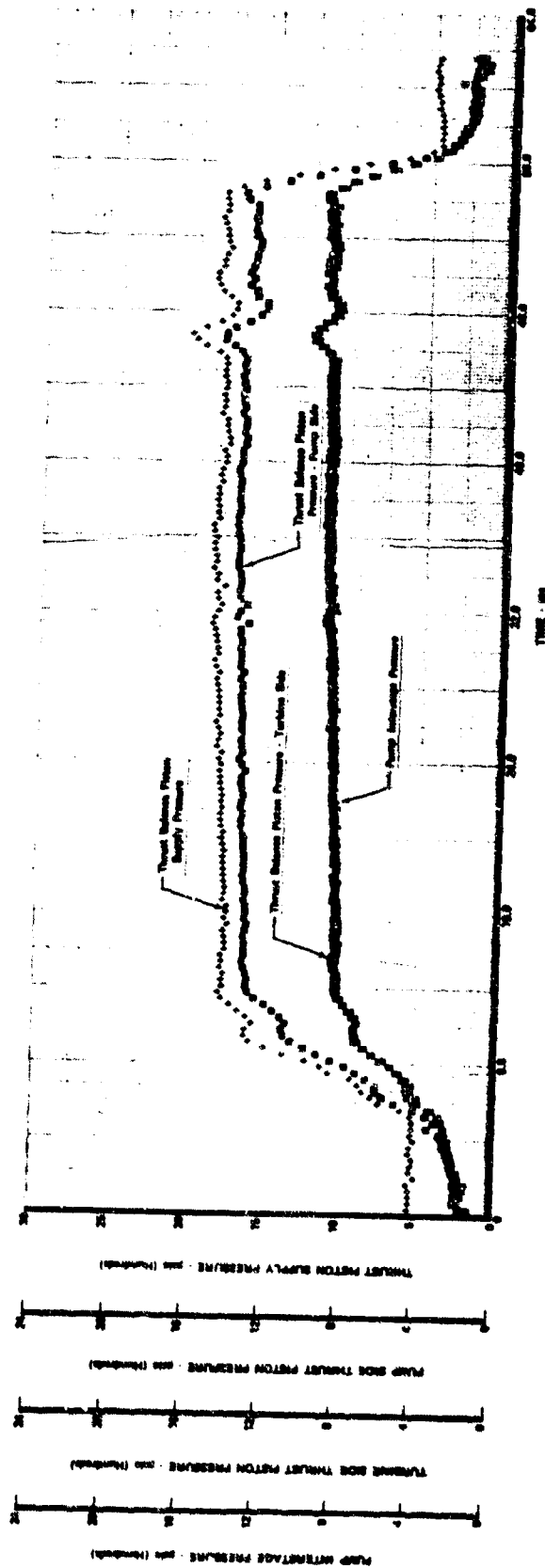
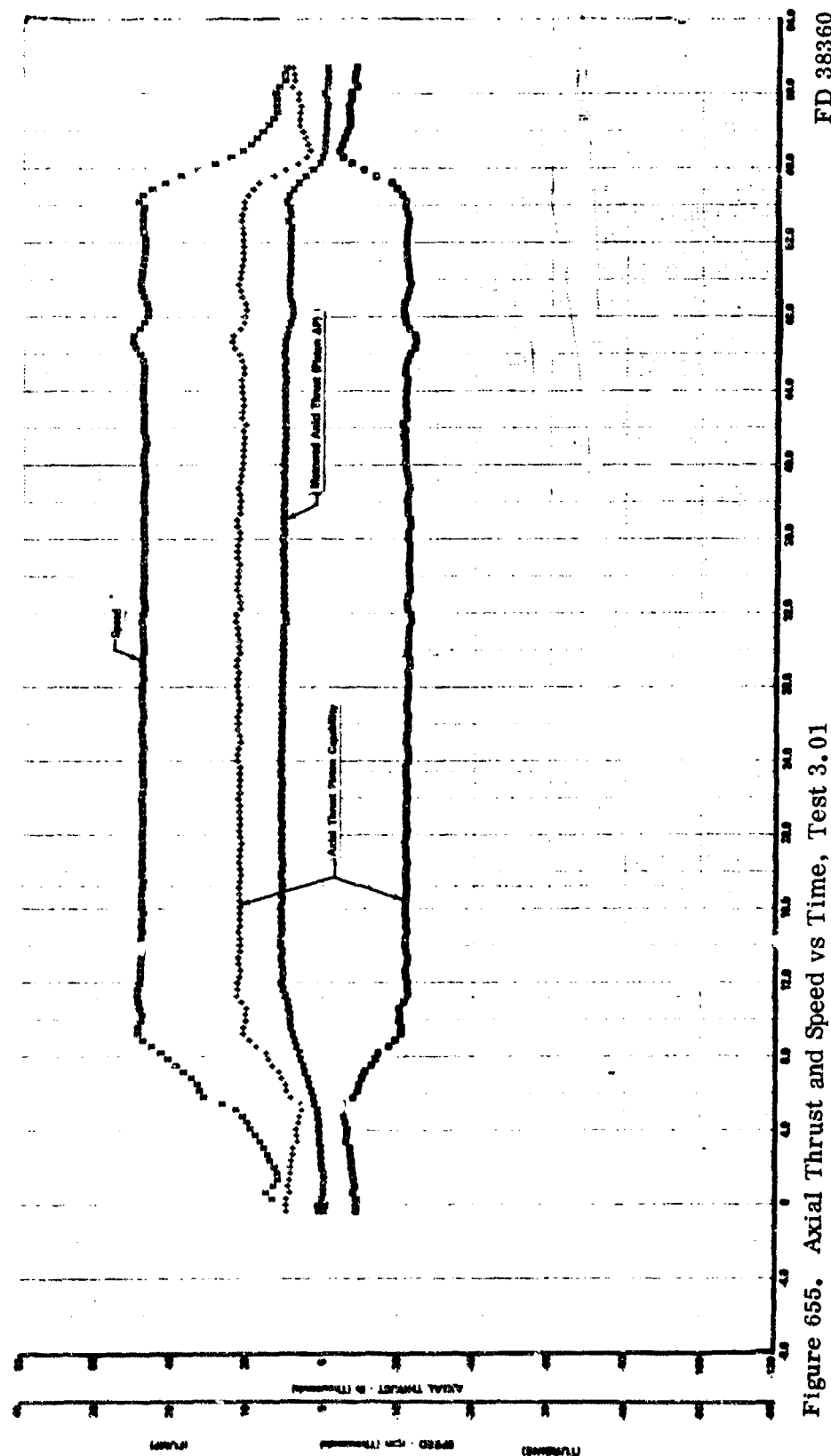


Figure 654. Significant Turbopump Parameters vs Time, Test 3.01, Sheet 3 of 3

FD 37088A



FD 38360

Figure 655. Axial Thrust and Speed vs Time, Test 3.01

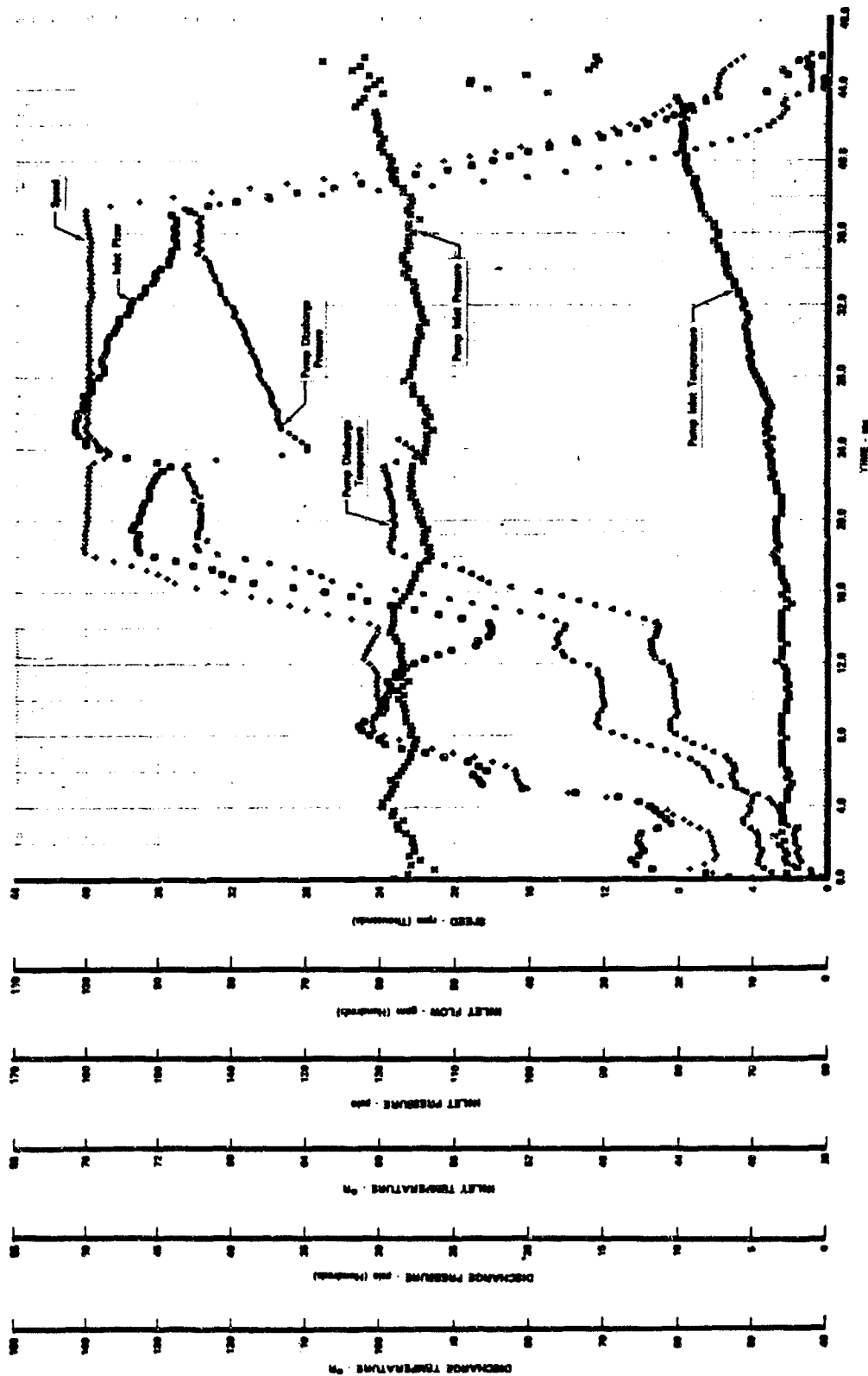


Figure 656. Significant Turbopump Parameters vs Time, Test 4.01, Sheet 1 of 3

FD 37089A

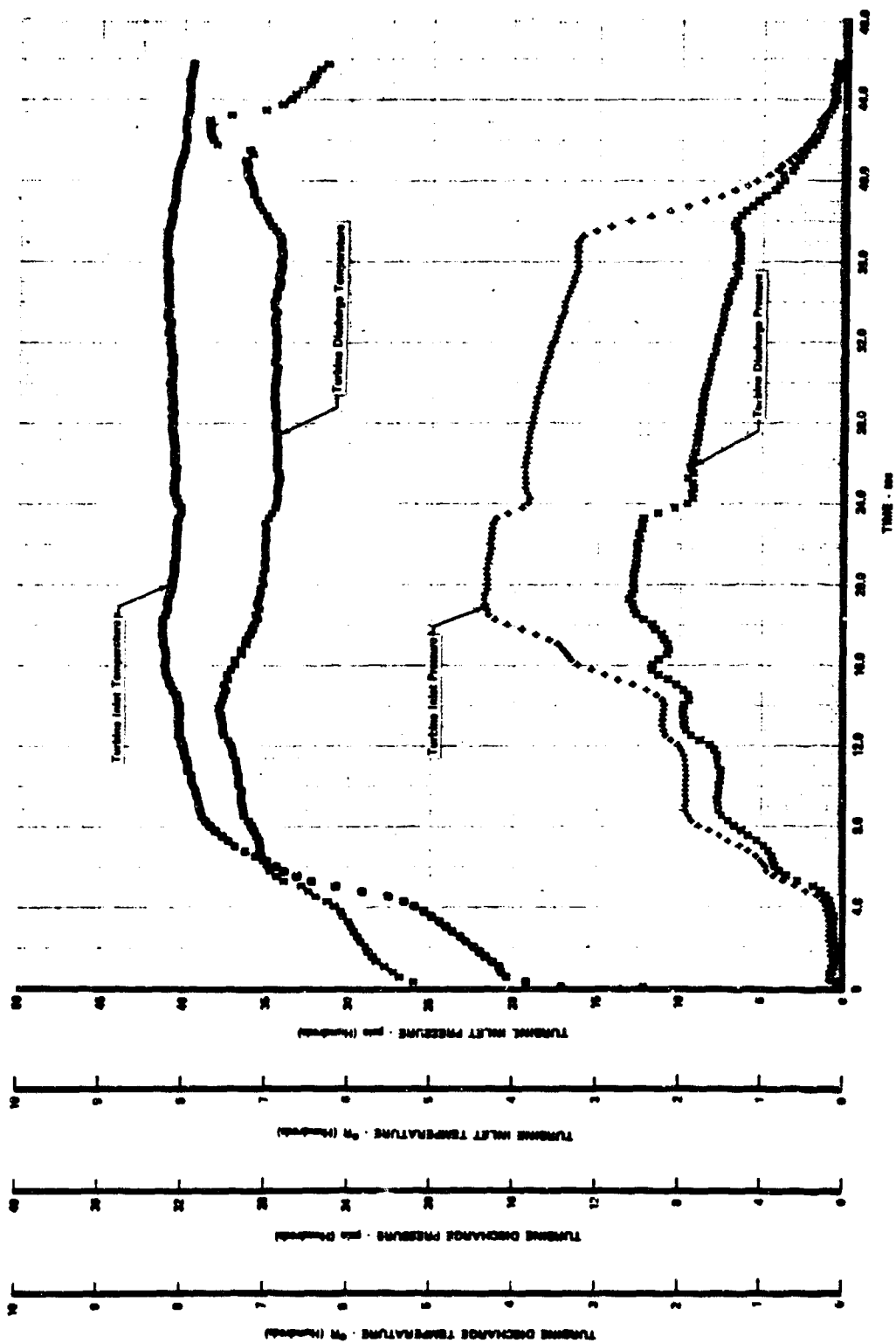


Figure 657. Significant Turbopump Parameters vs Time, Test 4.01, Sheet 2 of 3

FD 37090A

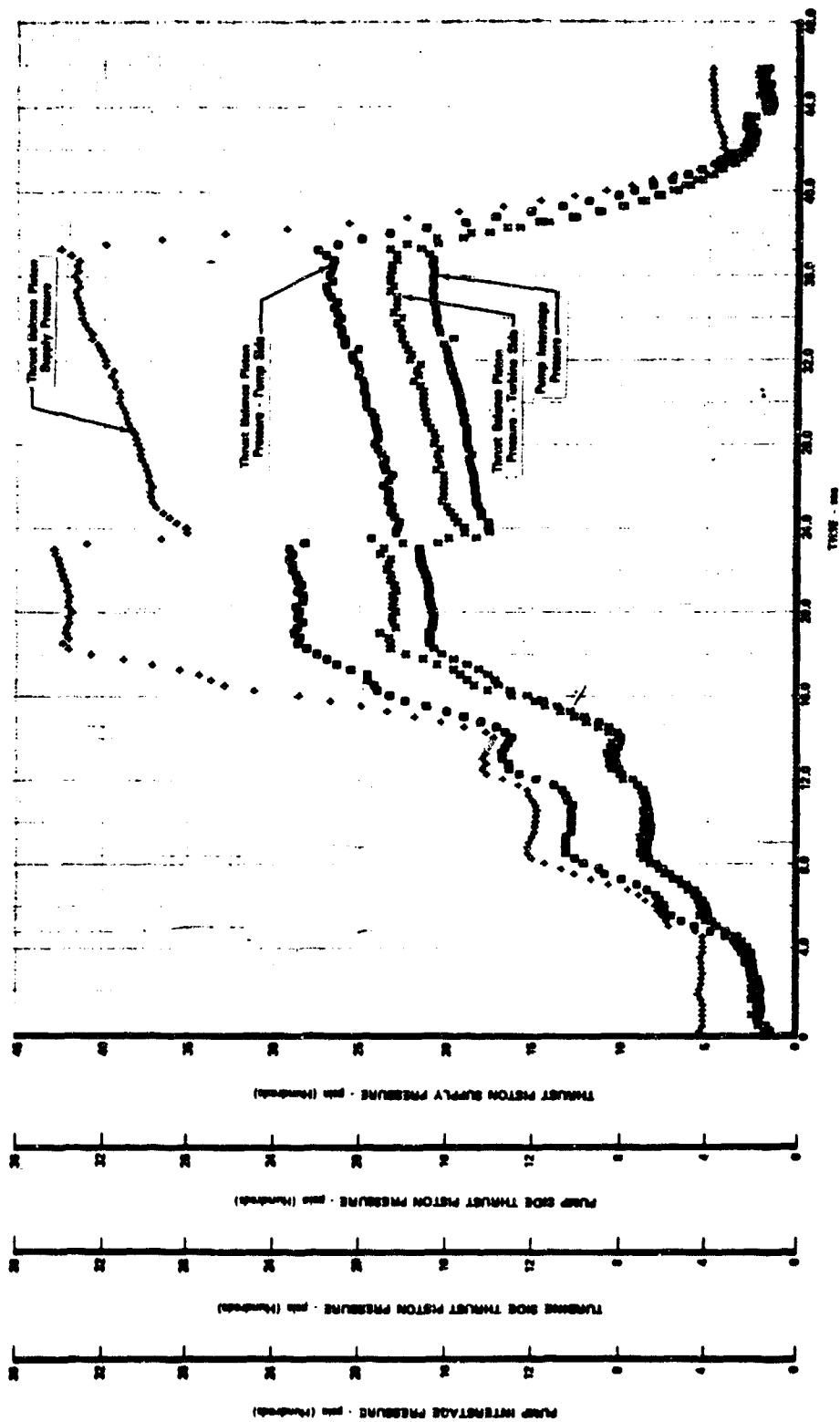


Figure 658. Significant Turbopump Parameters vs Time, Test 4.01, Sheet 3 of 3

FD 37091A

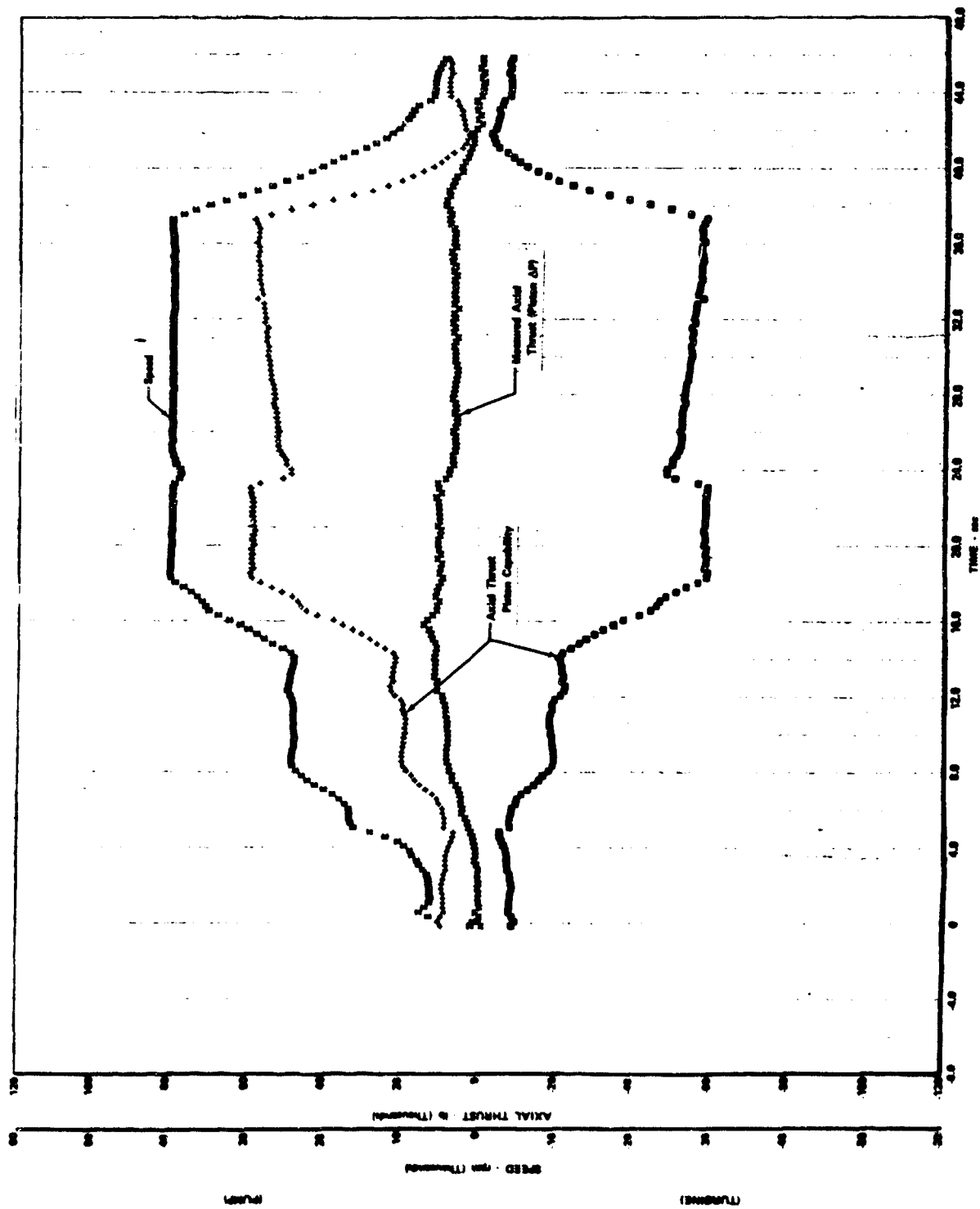


Figure 659. Axial Thrust and Speed vs Time, Test 4.01

FD 38361

The objective of test No. 5.01, was to demonstrate pump performance at design pressure and flow and to conduct flow excursions at 40,000 and 46,000 rpm. Because pump performance demonstrated during the flow excursions of tests 3.01 and 4.01 was better than predicted, the speed set point for test 5.01 was programmed for 46,000 rpm instead of the design speed value of 48,000 rpm. Test 5.01 was conducted on 13 January 1970 and was 13.6 sec in duration. The test was aborted 13.1 sec after start, at 46,000 rpm, because of excessive vibration. The recorded vibration level, shown in figure 660 averaged 5 g peak-to-peak to 44,500 rpm, at which time the vibration levels rapidly increased. This signal is shown as an expanded trace on the same figure. Data analysis indicated low level IE vibration levels (5 g). A 0.91E beat frequency vibration signal, shown in figure 660 and defined in figure 661 was also observed and was the cause of the automatic shutdown. A similar vibration signature on two 350K pump test rigs was attributed to a bearing inner race failure causing random noise that excited both soft bearing natural frequencies causing a beat frequency. Performance data analysis showed the pump operated as predicted and 100% flow and discharge pressure was demonstrated at 46,000 rpm before shutdown. Plots of significant turbopump operational parameters vs time are shown in figures 662 through 664. Figure 665 is a plot of axial thrust and speed versus time.

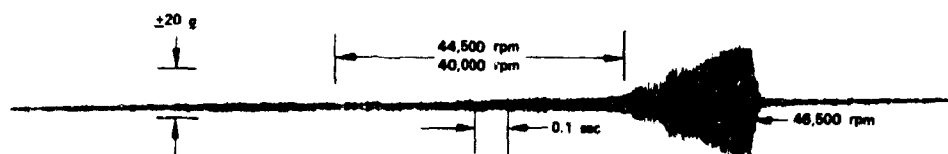


Figure 660. Fuel Pump Vibration Traces, Test Rig 35138-1, Test 5.01 FD 36925B

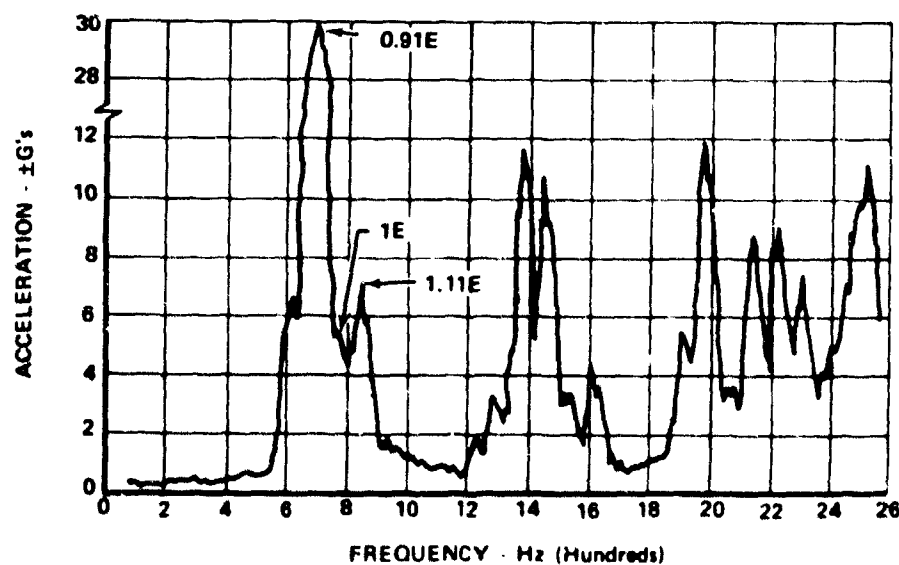


Figure 661. Frequency Analysis of Vibration Data FD 34750

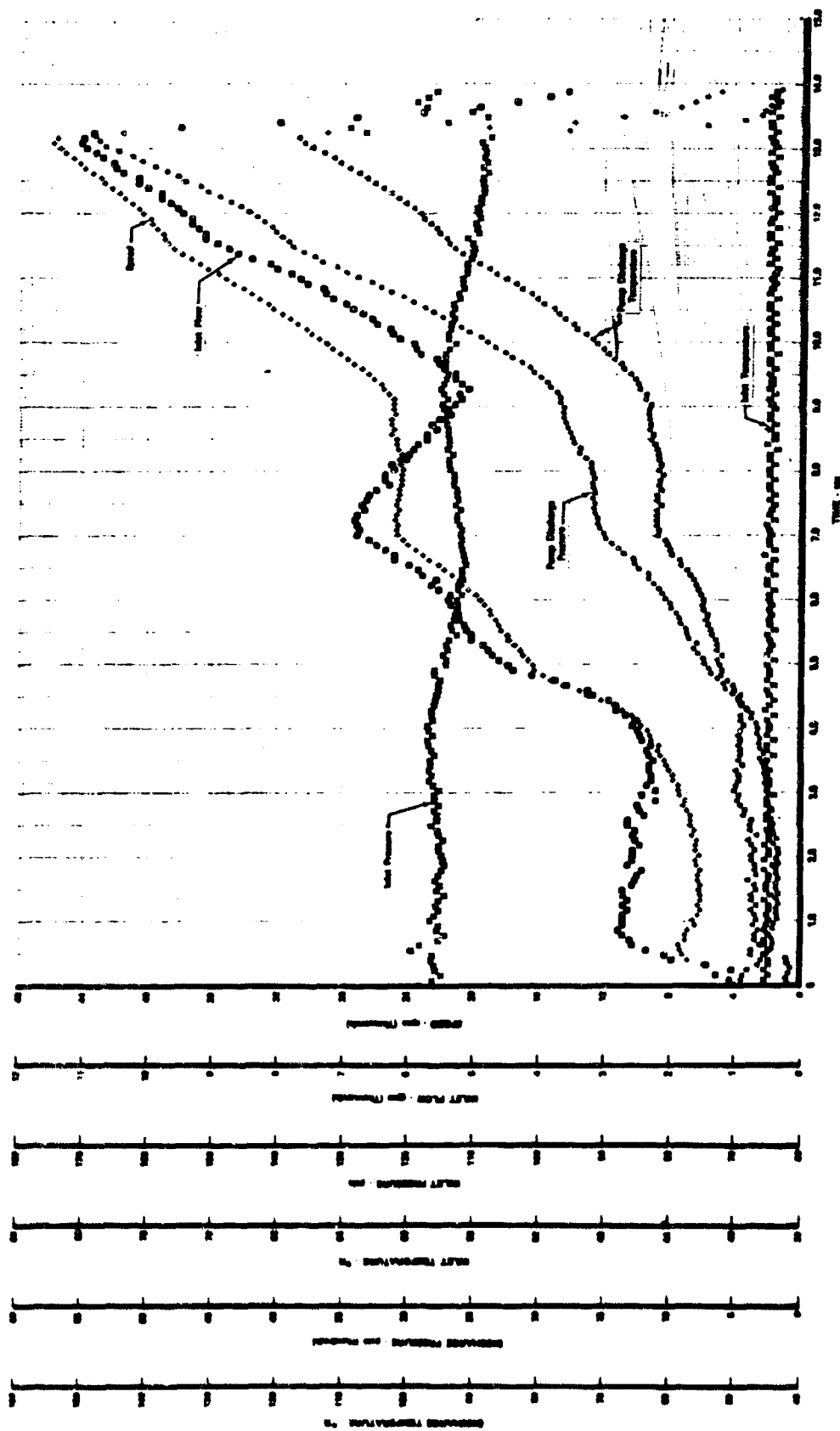


Figure 662. Significant Turbopump Parameters vs Time, Test 5.01, Sheet 1 of 3

FD 37092A

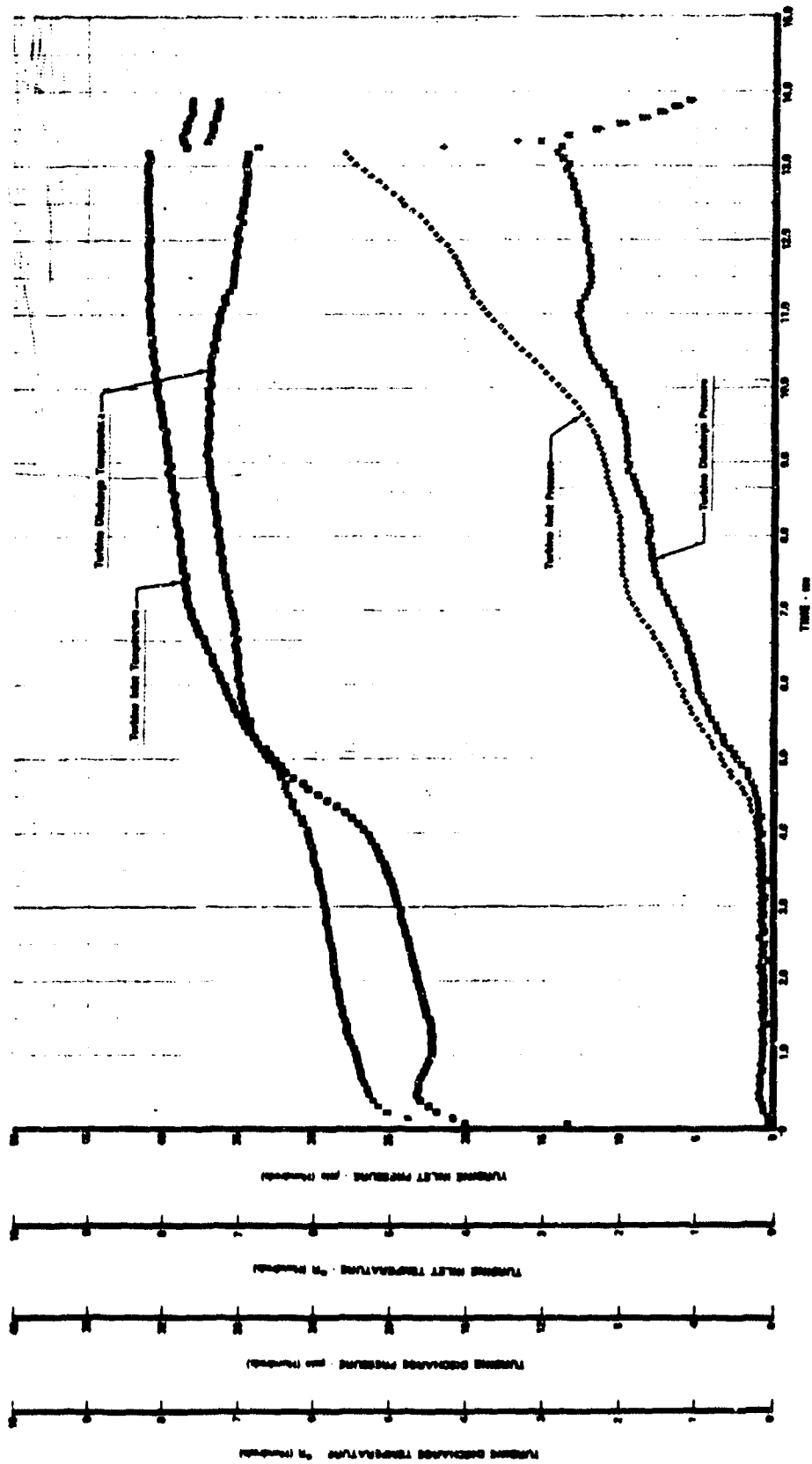


Figure 663. Significant Turbopump Parameters vs Time, Test 5.01, Sheet 2 of 3

FD 37093A

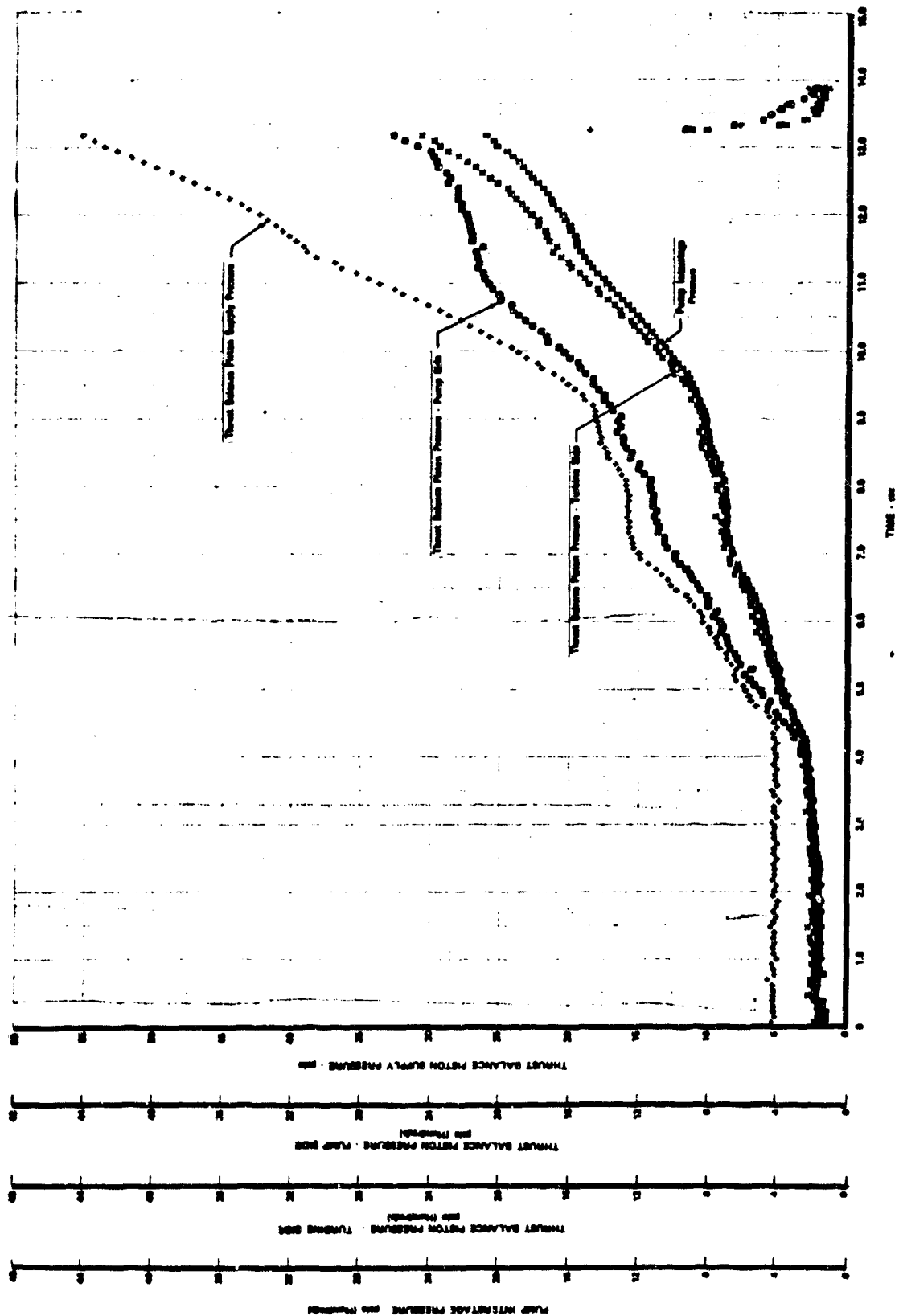


Figure 664. Significant Turbopump Parameters vs Time, Test 5.01, Sheet 3 of 3

FD 37094A

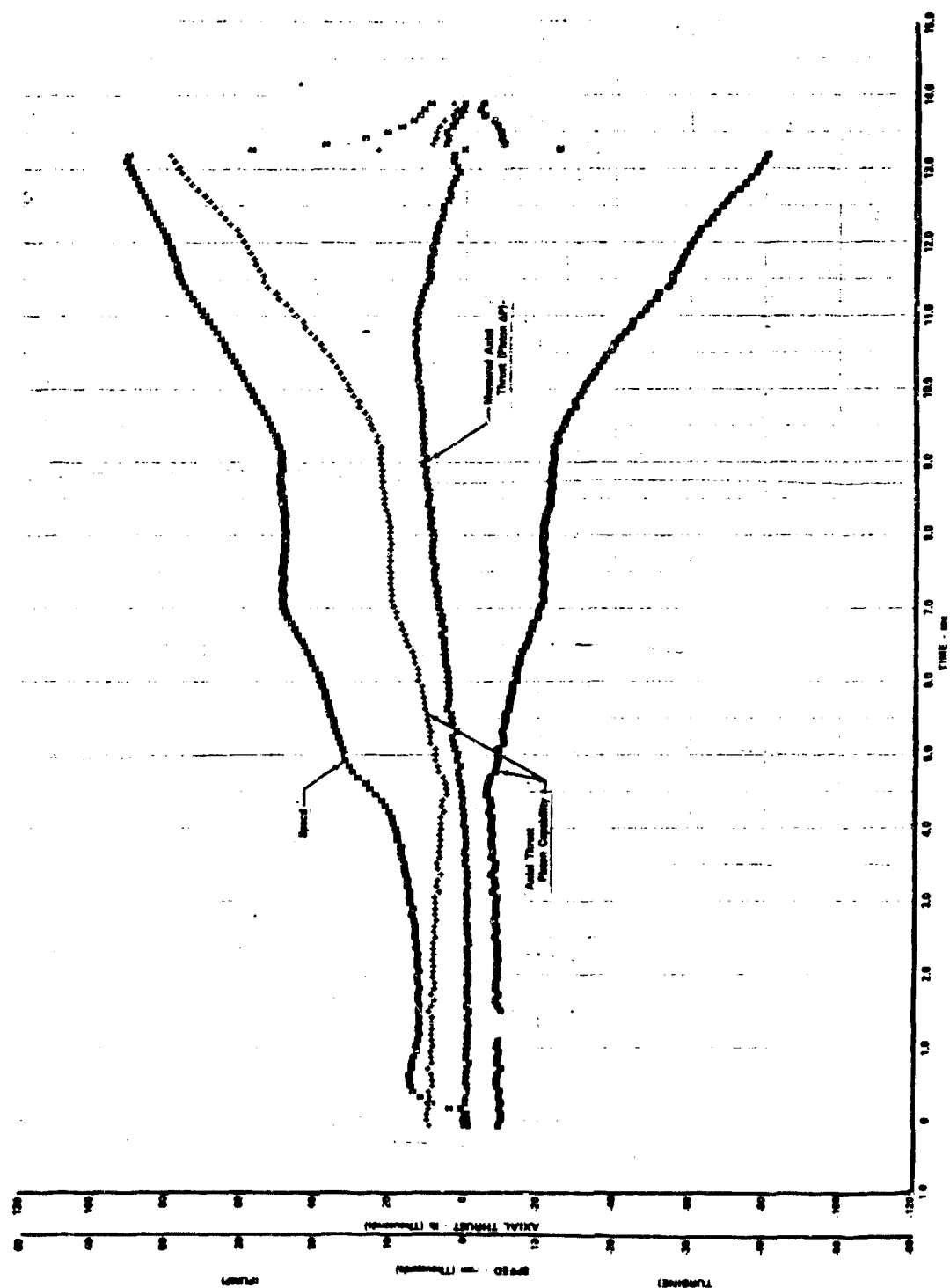


Figure 665. Axial Thrust and Speed vs Time, Test 5.01

FD 38362

The rig was removed from the test stand for post-test inspection, revealing good condition except for failure of the lift-off seal. The lift-off seal apparently closed at the end of the speed ramp causing high vibration indications. Figure 666 shows the rub area on the rotating primary seal surface worn approximately 0.032 in. from contact with the liftoff seal. An additional 0.020 in. was also worn from the primary seal face of the liftoff seal. Roller bearings were in good condition except for minor front side rail scoring. Foreign particle ingestion was noted throughout the pump. Minor thrust balance piston rub face scoring was caused by foreign particles. Nondestructive testing of the parts indicated no defects, except for the liftoff seal failure.



Figure 666. Turbopump Liftoff Seal Wear Results FD 37095

Analysis of the liftoff seal failure indicated the seal had returned to the unactuated position and contacted the rotating rub face. After removal from the fuel pump, the seal was actuated to determine operational capabilities. A stroke of 0.031 in. was recorded at 1000 psig actuation pressure. This is only 10% lower than prebuild test results. The pressure was not increased above this level because of excessive leakage through the failed bellows. The outer bellows was ruptured in two places 180 deg apart in the weld of the second and the fourth convolutions. These failures include approximately 180 deg of the circumference. The inner bellows failed at the weld to the movable end piece. This failure covers approximately 120 deg of the circumference. The bellows were sectioned for further investigation. This investigation revealed incomplete weld penetration, convolution mismatch, and inconsistency in convolution thickness. Figure 667 is a post-test cross sectional photograph of the liftoff seal showing one of the

failed areas, and inconsistency in convolution thickness. A precise cause or time of failure was not determined from review of the data. It is possible that the bellows failed during run 4.01, because there is a short period of test data that indicates a rise in bearing cavity pressure as well as a slight rise in bearing outer race temperature such as would be expected to happen if the liftoff seal closed during pump operation. The failure appears to have resulted from over extension of the bellows because of high pressure over the entire front surface of the seal. This would occur if the pressure in the secondary seal cavity became excessive because of high secondary seal leakage or insufficient venting of this cavity to the lower pressure 1st-stage impeller inlet. The stackup of dimensions also indicates the housing may have deflected to result in the amount of material displaced on the seal face and mating rotor surface.

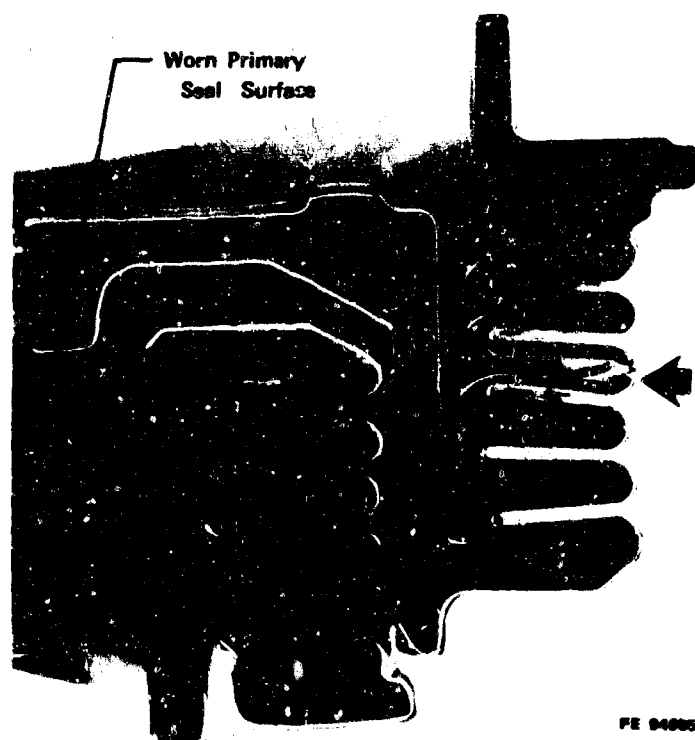


Figure 667. Turbopump Liftoff Seal Failed Bellows Convolution FD 37096

Data analysis of these tests indicated that overall pump performance exceeded the design goals. Figure 668 shows the predicted pump pressure rise versus inlet flow map and test data from the three tests. Figure 669 presents a plot of overall efficiency versus inlet unit flow showing the design point and the predicted off-design characteristic with the test data obtained on these tests. Figures 670 and 671 show the 1st- and 2nd-stage pump efficiencies versus flow coefficient data points and the predicted design points and off design characteristics. Figure 672 shows the overall unit head versus inlet unit flow, design point and engine cycle requirements, and test data from these three tests. The 1st- and 2nd-stage head coefficient versus flow coefficient characteristics of the pump are presented in figures 673 and 674. Figure 675 is a plot of turbine

efficiency versus velocity ratio and the cycle requirement curve and the design point are shown.

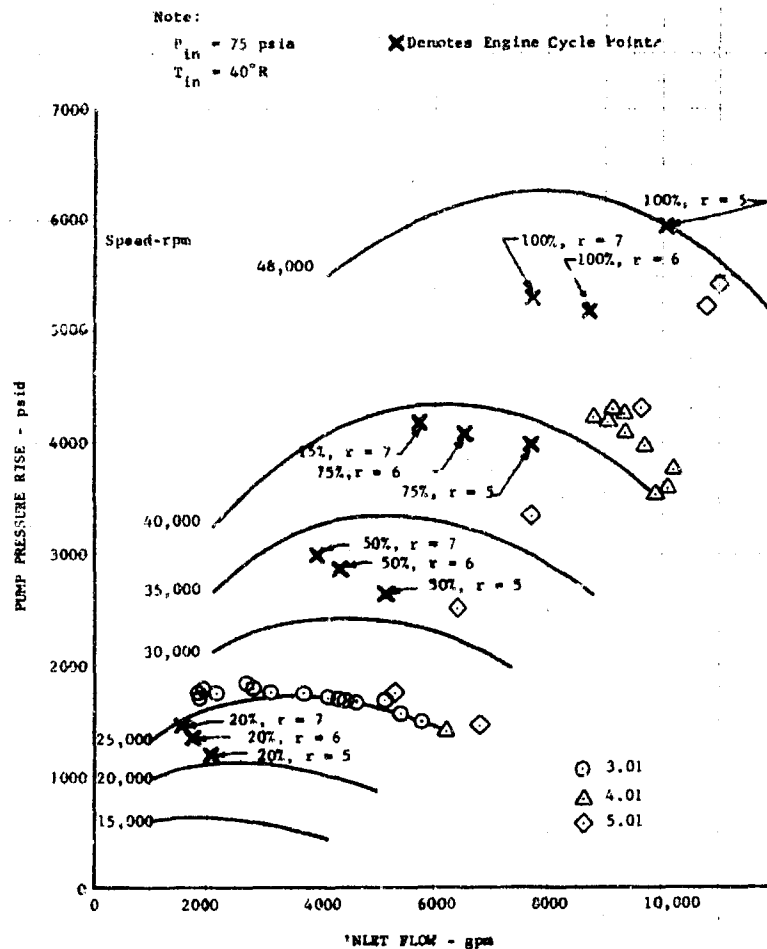


Figure 668. Fuel Turbopump Pressure Rise,
 Rig 35138-1

DF 78386

The axial thrust unbalance of the rotor was toward the pump inlet at all operating levels. The greatest unbalance was at the lowest speed and lowest flow condition and was approximately 50% of the thrust balance piston capability. Thrust unbalance decreased with increased speed and flow conditions on the last two tests, and was less than 10% of the thrust balance piston capability at the maximum speed condition on test 5.01.

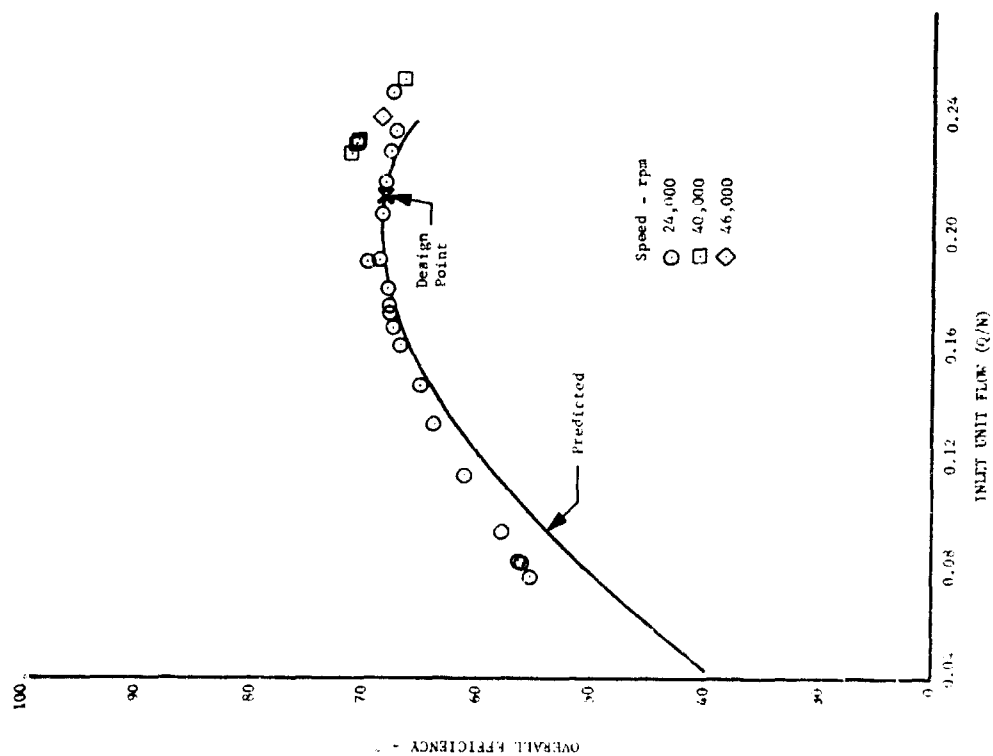


Figure 669. Fuel Turbopump Overall Efficiency, Rig 35138-1

DF 78387

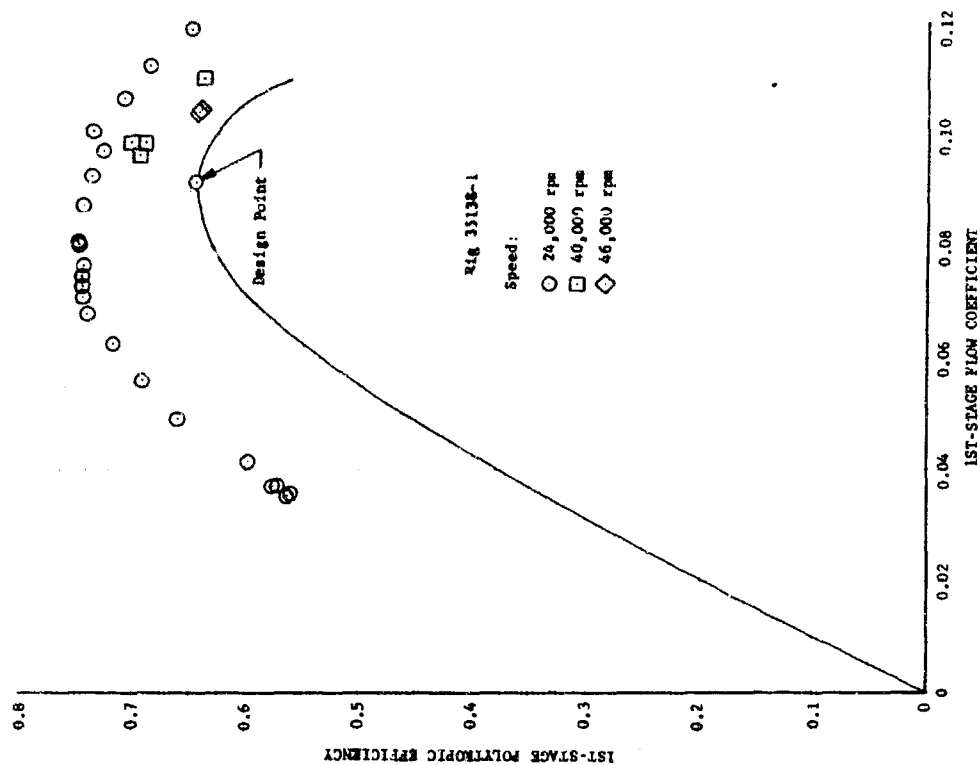


Figure 670. Fuel Turbopump 1st-Stage Polytopic Efficiency, Rig 35138-1

DF 78626

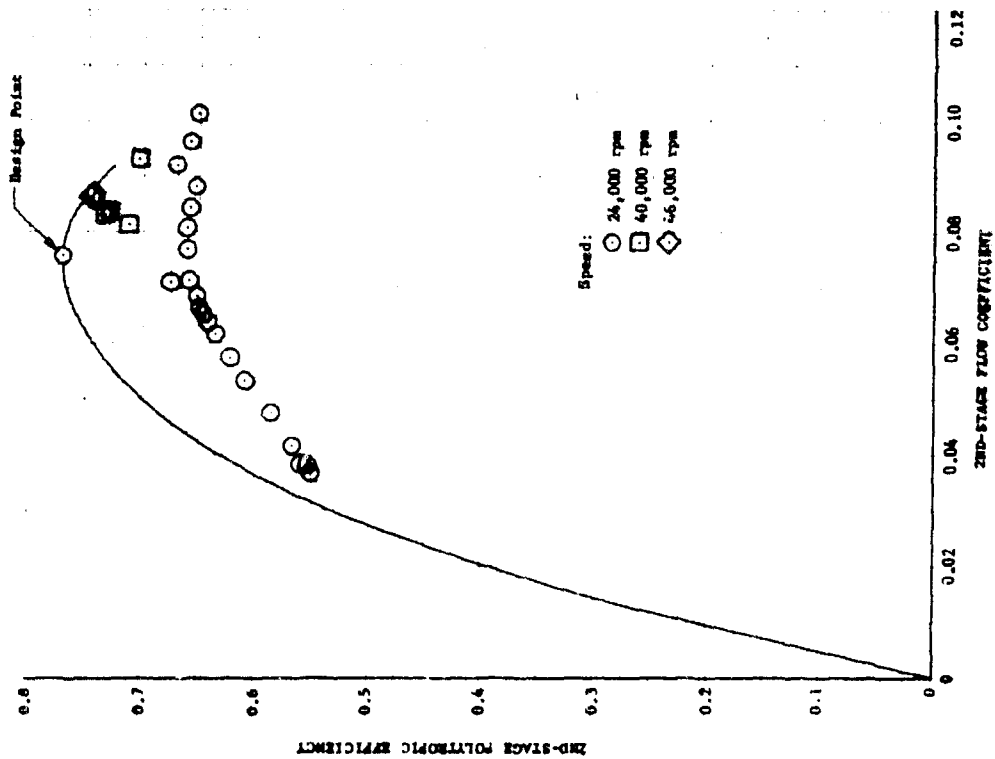


Figure 671. Fuel Turbopump 2nd-Stage Polytropic Efficiency, Rig 35138-1

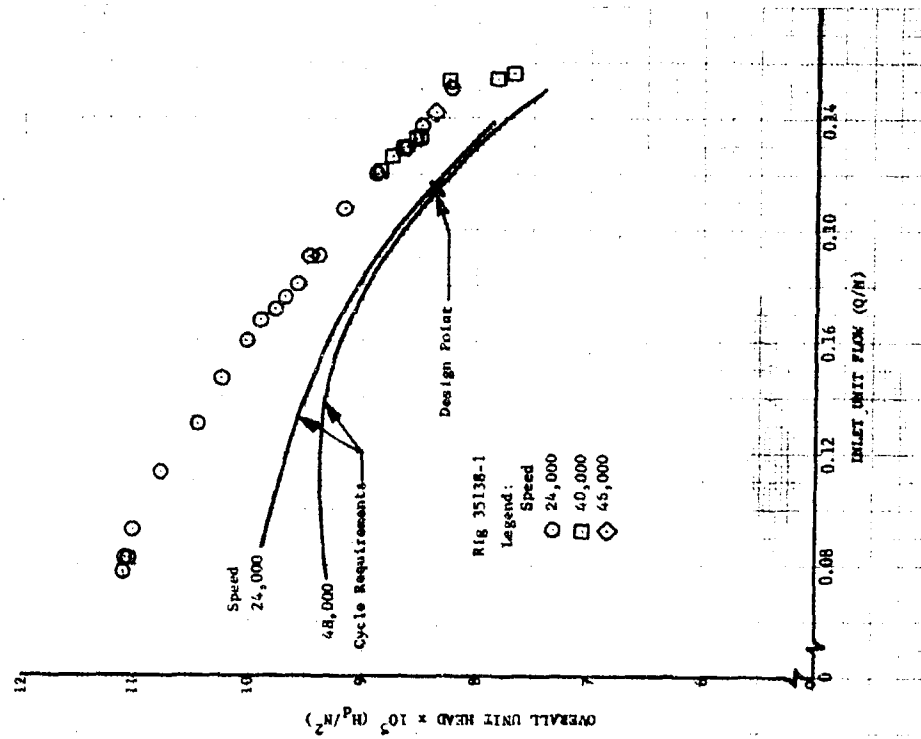


Figure 672. Fuel Turbopump Overall Unit Head, Rig 35138-1 DF 78627 DF 78388

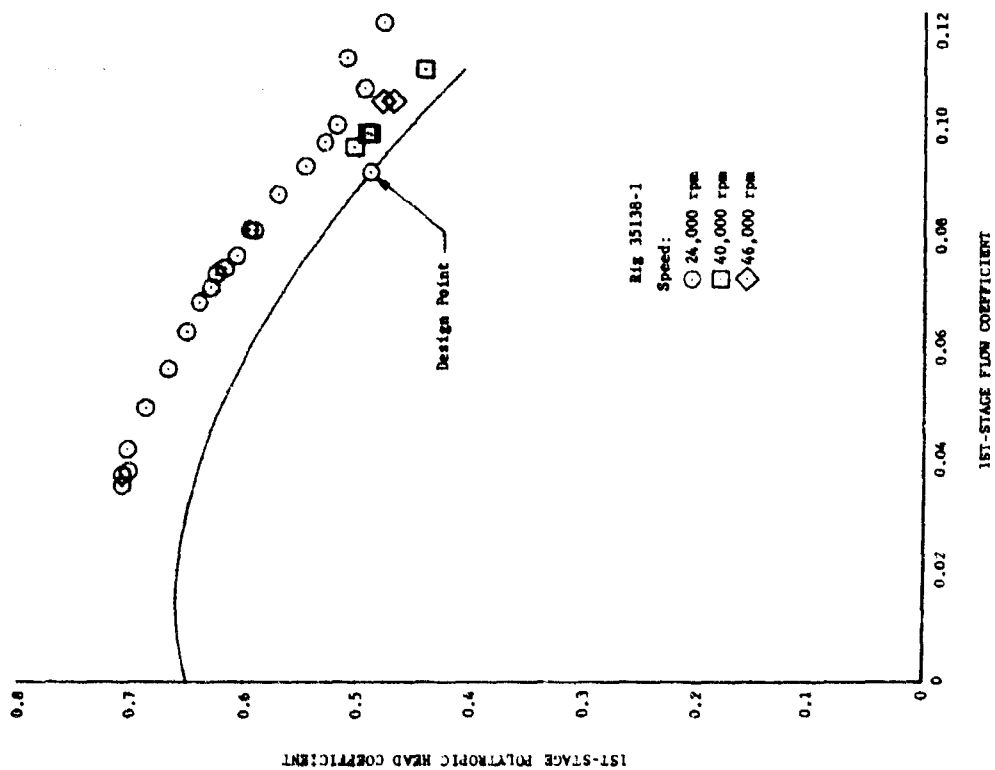


Figure 673. Fuel Turbopump 1st-Stage
Polytropic Head Coefficient,
Rig 35138-1

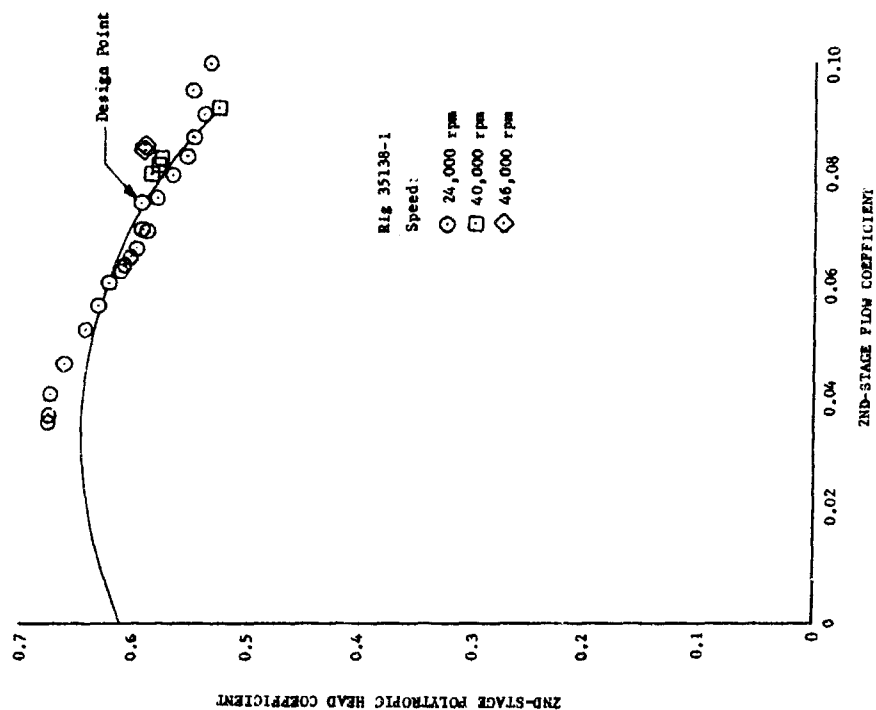


Figure 674. Fuel Turbopump 2nd-Stage
Polytropic Head Coefficient,
Rig 35138-1

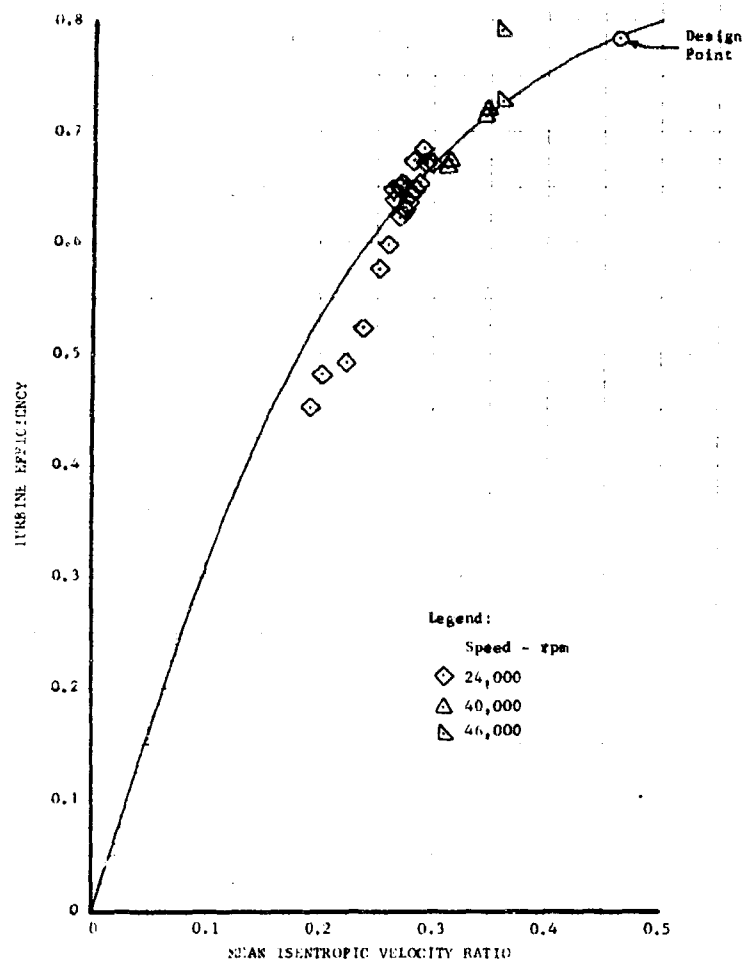


Figure 675. Fuel Turbopump Turbine Efficiency, DF 78044
Rig 35138-1

As a result of the fuel turbopump tests associated with test rig F35138-1, it was concluded:

1. Overall pump efficiency at the design point is estimated to be 3 percentage points higher than predicted. Overall efficiency increased 3 percentage points between 24,000 rpm and 46,000 rpm
2. Overall pressure rise was approximately 8% greater than predicted at design Q/N
3. 1st-stage efficiency is estimated to be 3.5 points higher than predicted at the design point, and was seen to decrease 7 points between 24,000 and 46,000 rpm. The 1st-stage head coefficient is approximately 6% greater than predicted at the design point and decreases 5.5% between the 24,000 and 46,000 rpm speed levels

4. The 2nd-stage efficiency is estimated to be 2 percentage points lower than predicted at the design point, but increased 9 percentage points between 24,000 and 46,000 rpm. The 2nd-stage head coefficient was 5% greater than predicted at the design point and increased 6.5% between 24,000 and 46,000 rpm
5. Thrust piston capability was adequate over the full range tested and would be adequate for engine operating conditions
6. Turbine efficiency closely equaled that predicted
7. Overall turbine effective area was approximately 7% greater than predicted
8. The use of this turbopump in the cycle provides satisfactory engine operation over the full range of thrust and mixture ratio. Maximum preburner combustion temperature is reduced 35°R, and maximum fuel pump speed is reduced 1000 rpm.

(b) Rig F35138-2

This test rig was built to the same configuration as the previous rig (F35138-1) with the following exceptions:

1. The 2nd-stage impeller pumping clearance was reduced by 0.012 in. from 0.050 in. to 0.038 in. for evaluation of the effect on pump performance.
2. A dummy liftoff seal was installed with instrumentation provision to provide supporting test data for the build 1 liftoff seal failure analysis.
3. The inducer housing was modified by electron beam welding a ring on the outer diameter for an external pilot at the main housing interface. This modification was made to facilitate assembly and to ensure alignment with the main housing during pump operation.

During the second test series, six tests that accumulated 262.8 sec of rotation time were conducted on fuel turbopump rig F35138-2. This series of tests defined the pump pressure rise vs flow map and NPSH characteristics.

Test No. 6.01 was completed on 5 March 1970 and was 41.7 sec in duration. This was a programmed duration test with flow excursions from 9660 to 6450 gpm at the 83% speed level (40,000 rpm) and from 2250 to 6550 gpm at the 50% speed level (24,000 rpm). Data analysis revealed that the overall pump operation was satisfactory and pump performance again exceeded the design goals as was seen in build 1 of the test rig. Plots of significant turbopump parameters vs time are shown in figures 676 through 678 and axial thrust vs time for test No. 6.01 is shown in figure 679.

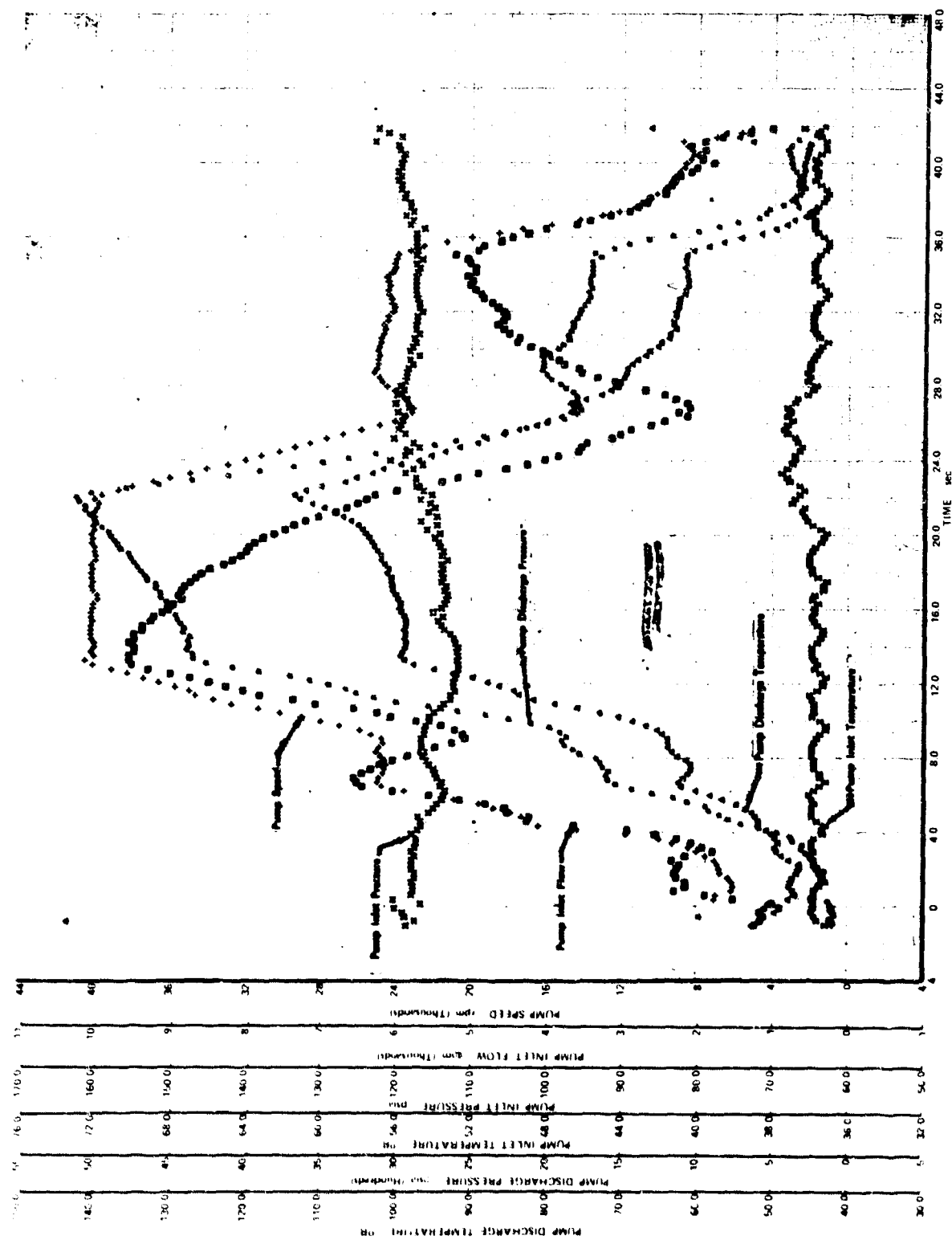


Figure 676. Significant Turbopump Parameters vs Time, Test 6.01, Sheet 1 of 3

FD 38796

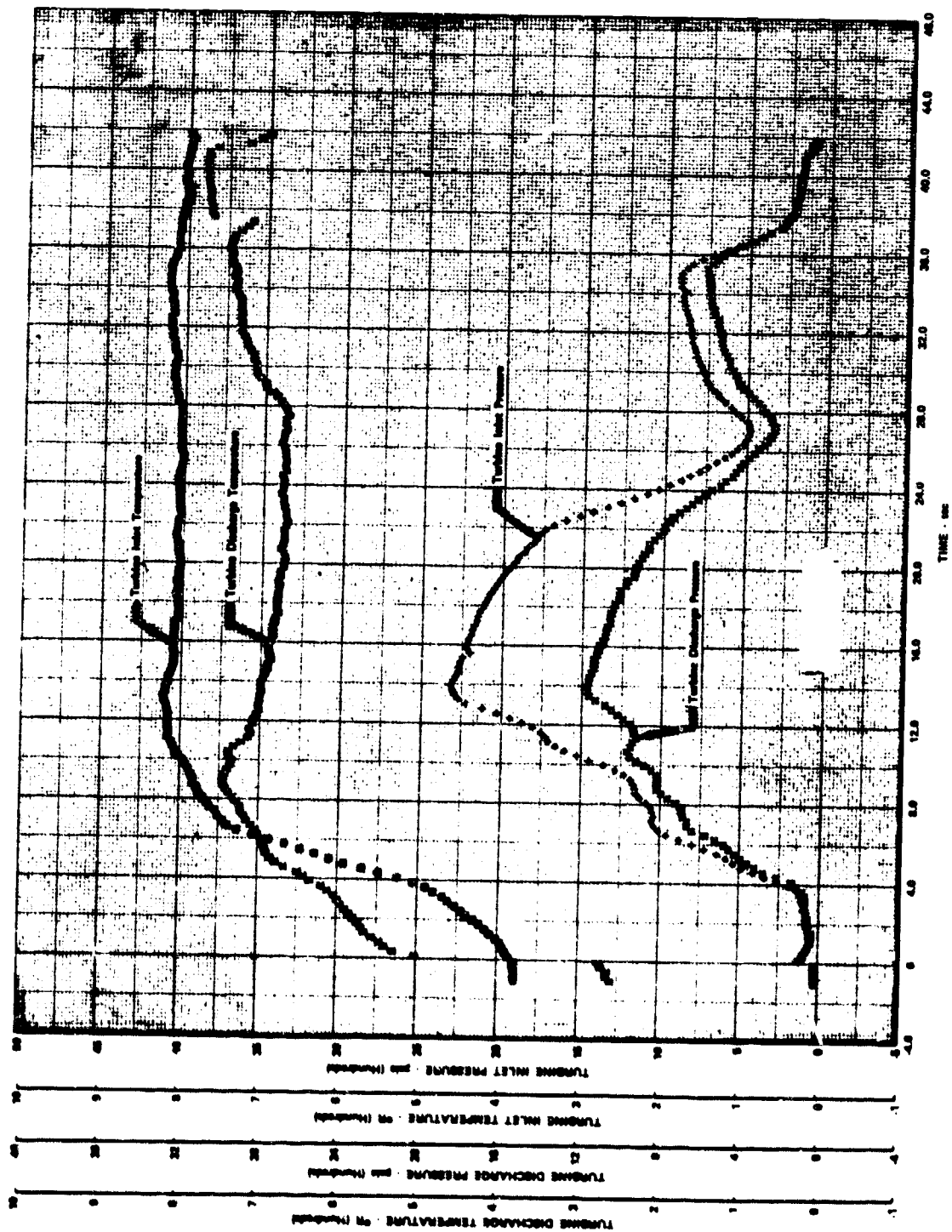


Figure 677. Significant Turbopump Parameters vs Time, Test 6.01, Sheet 2 of 3

FD 38797

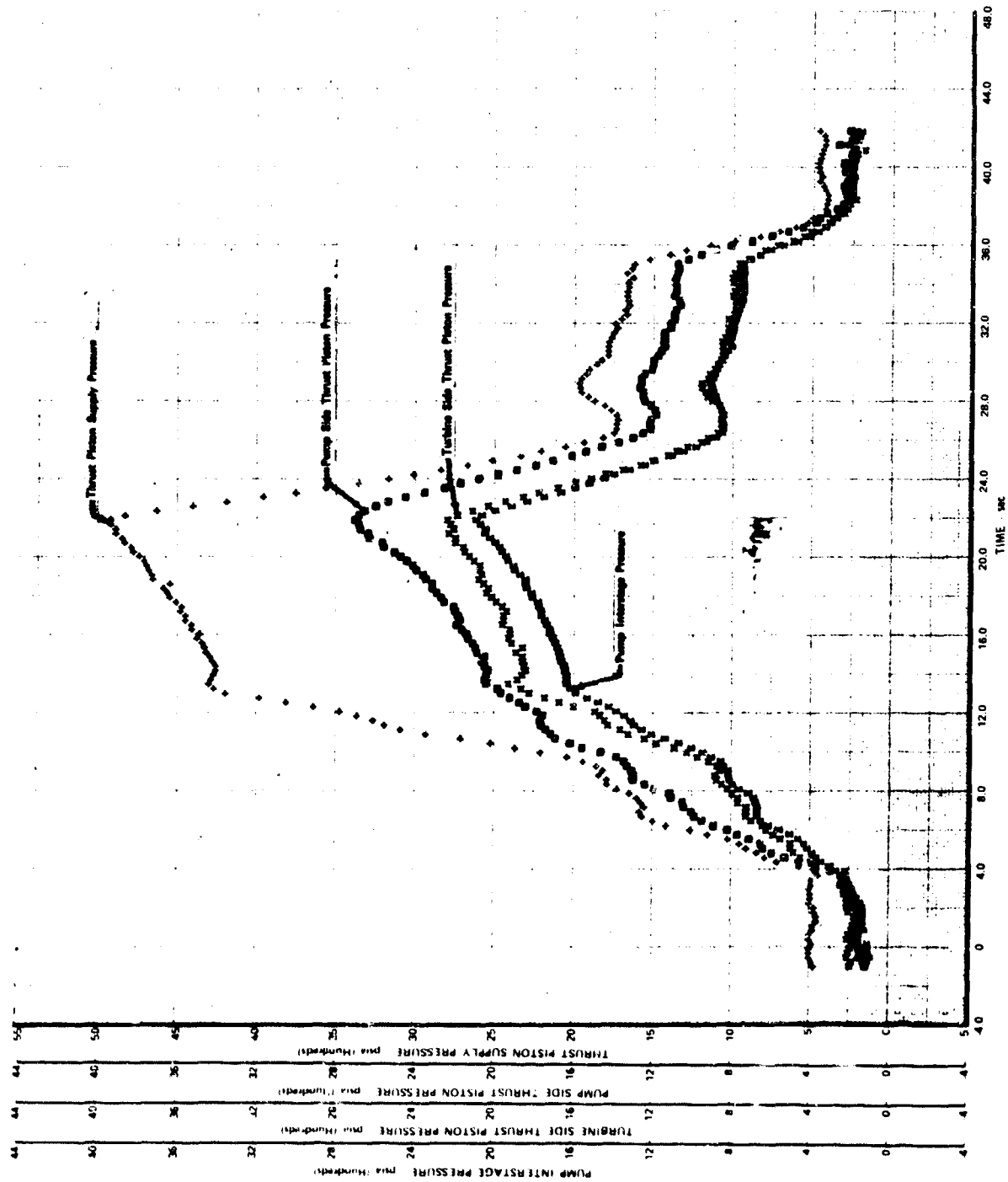


Figure 678. Significant Turbopump Parameters vs Time, Test 6.01, Sheet 3 of 3

FD 38798

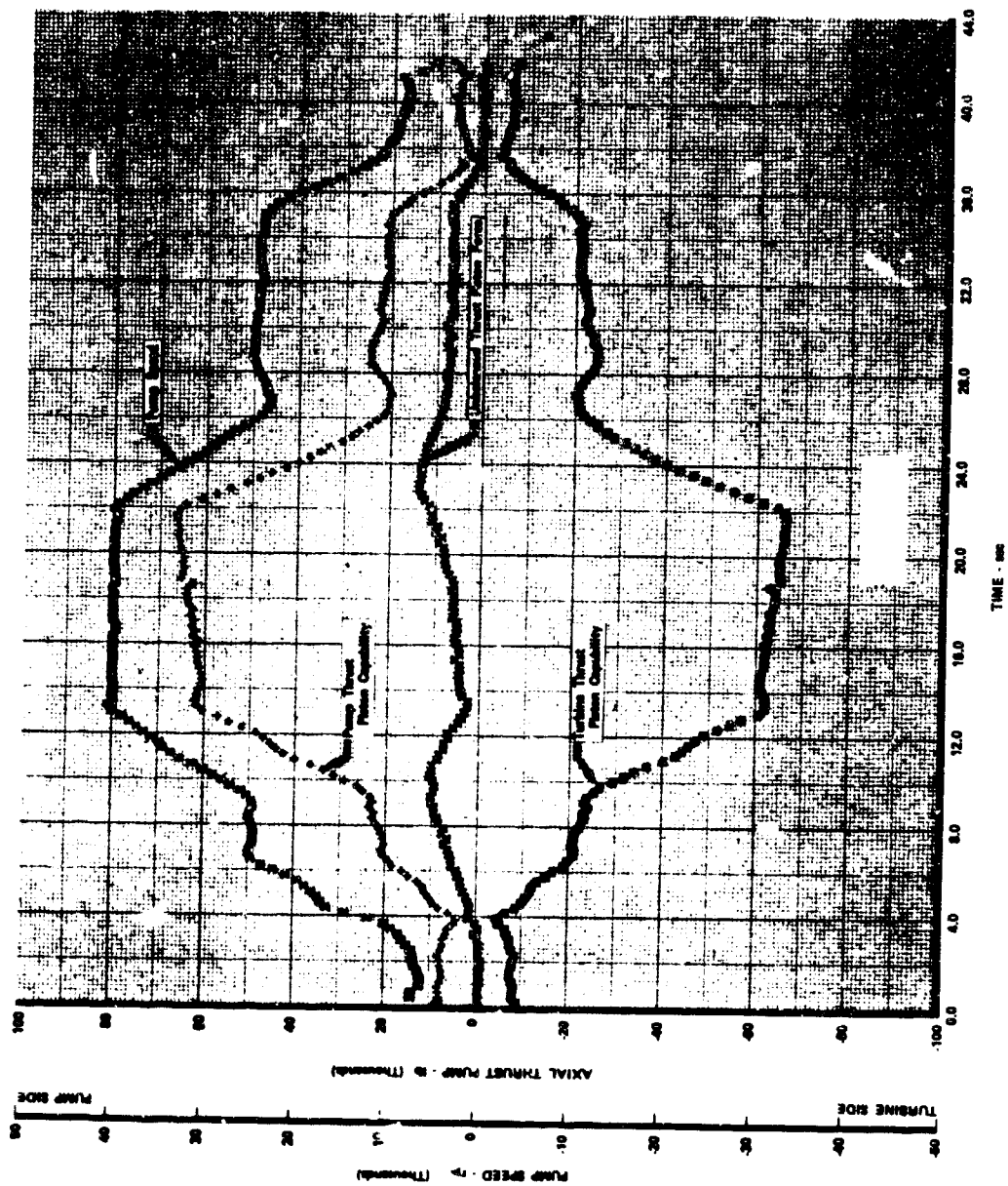


Figure 679. Axial Thrust and Speed vs Time, Test 6.01

FD 38751

Test No. 7.01, conducted on 6 March 1970, was advanced to shutdown 20 sec after start by the ± 20 g vibration monitor system. The objectives of this test were flow excursions at the 96% (46,000 rpm) and 68% (32,500 rpm) speed levels. Before the test was terminated the pump had accelerated to and stabilized at the 46,000 rpm speed level. The vibration was a combination of 1E and another vibration component approximately 0.89E, similar to that experienced on test No. 5.01 of the previous build (F35138-1). However, the vibration on test No. 7.01 did not build up as rapidly, nor to as high a level as was experienced previously. Figures 680 through 682 show plots of the significant turbopump parameters vs time, and figure 683 shows axial thrust vs time for this test. Figure 684 is a comparison of the accelerometer traces of tests No. 5.01 and 7.01.

Test No. 8.01 was conducted on 13 March 1970, and was programed for flow excursions at the 89, 96, and 68% speed levels. Because the previous test (No. 7.01) was terminated by the vibration monitor system at the 96% speed level, it was the intent of this test to determine if the vibration was the result of the pump pressure, flow or speed level. The test was scheduled to complete a flow excursion at the 89% speed level from 9500 to 6600 gpm and then to accelerate the pump to 46,000 rpm along a constant Q/N line. This would allow the pump to obtain the 46,000 rpm speed level at a lower flow level (approximately 7100 gpm) and a higher pressure level than on the previous test. In addition, the axial thrust is more toward the pump at this lower Q/N and this should increase the 2nd-stage pumping clearance slightly in case the rubbing of the impeller that was detected by borescope inspection after test No. 7.01 was causing the high vibration. The test was terminated after 18.0 sec of testing by the ± 30 g vibration abort system at the 96% speed level. Before the test was terminated a flow excursion from 9500 to 6600 gpm was completed at 89% speed and then the pump was accelerated along a constant Q/N line to approximately 44,000 rpm. At this speed level the facility power limit was reached and the pump did not accelerate until the flow control valve started to open. This allowed the pump speed to accelerate to 46,000 rpm, but at a flow value higher than planned. A flow excursion was completed from 9300 to 10,100 gpm at 46,000 rpm before the run was terminated by the ± 30 g vibration abort.

During this test the pump was operated at the engine 100% thrust level, mixture ratio of 5, 6, and 7 conditions and at a maximum discharge pressure of 6398 psia. The pump discharge pressure versus flow map recorded for test No. 7.01 and 8.01 by the x-y plotter used to monitor the tests is shown in figure 685.

The post-test inspection of the test rig revealed a slight rub on the 2nd-stage impeller blade tips, but otherwise no discrepancy was detected. Figure 686 shows the vibration trace for this test. Data analysis showed that the shutdown was caused by a combination of 1E and another vibration component that was approximately 0.89E as on test No. 7.01. Figures 687 through 689 show plots of significant turbopump parameters vs time, and figure 690 shows axial thrust vs time for this test.

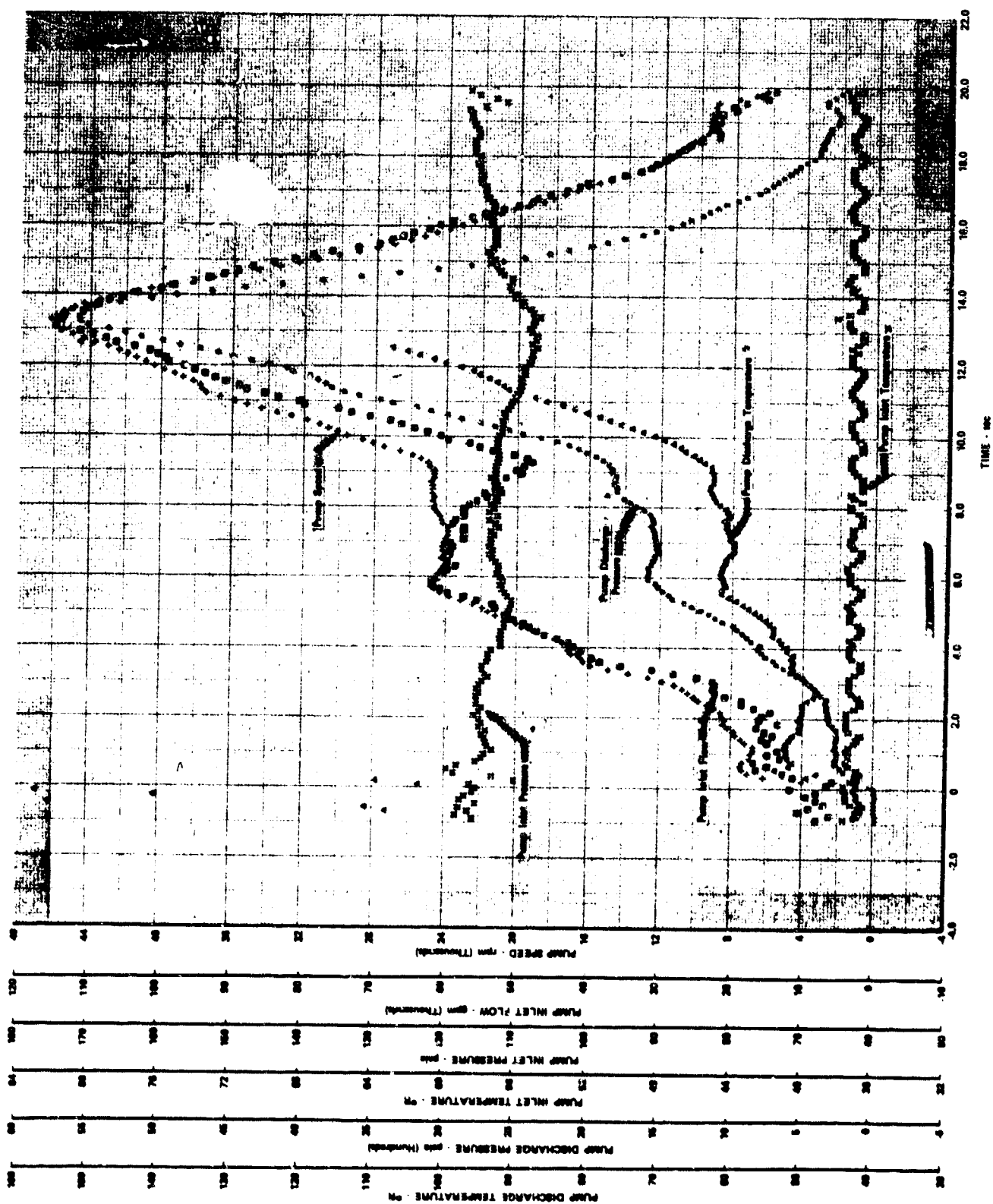


Figure 680. Significant Turbopump Parameters vs Time, Test 7.01, Sheet 1 of 3

FD 38799

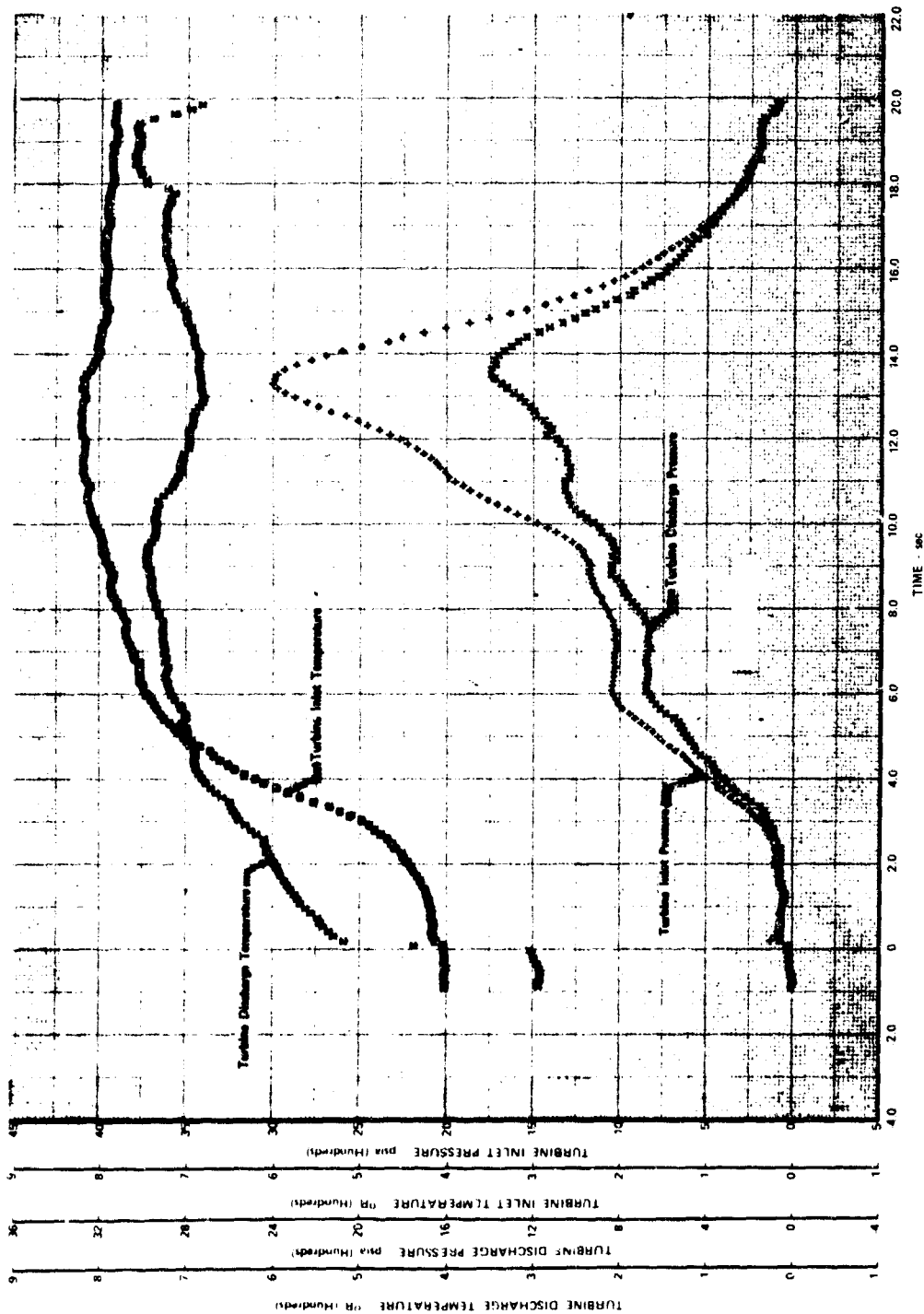


Figure 681. Significant Turbopump Parameters vs Time, Test 7.01, Sheet 2 of 3

FD 38800

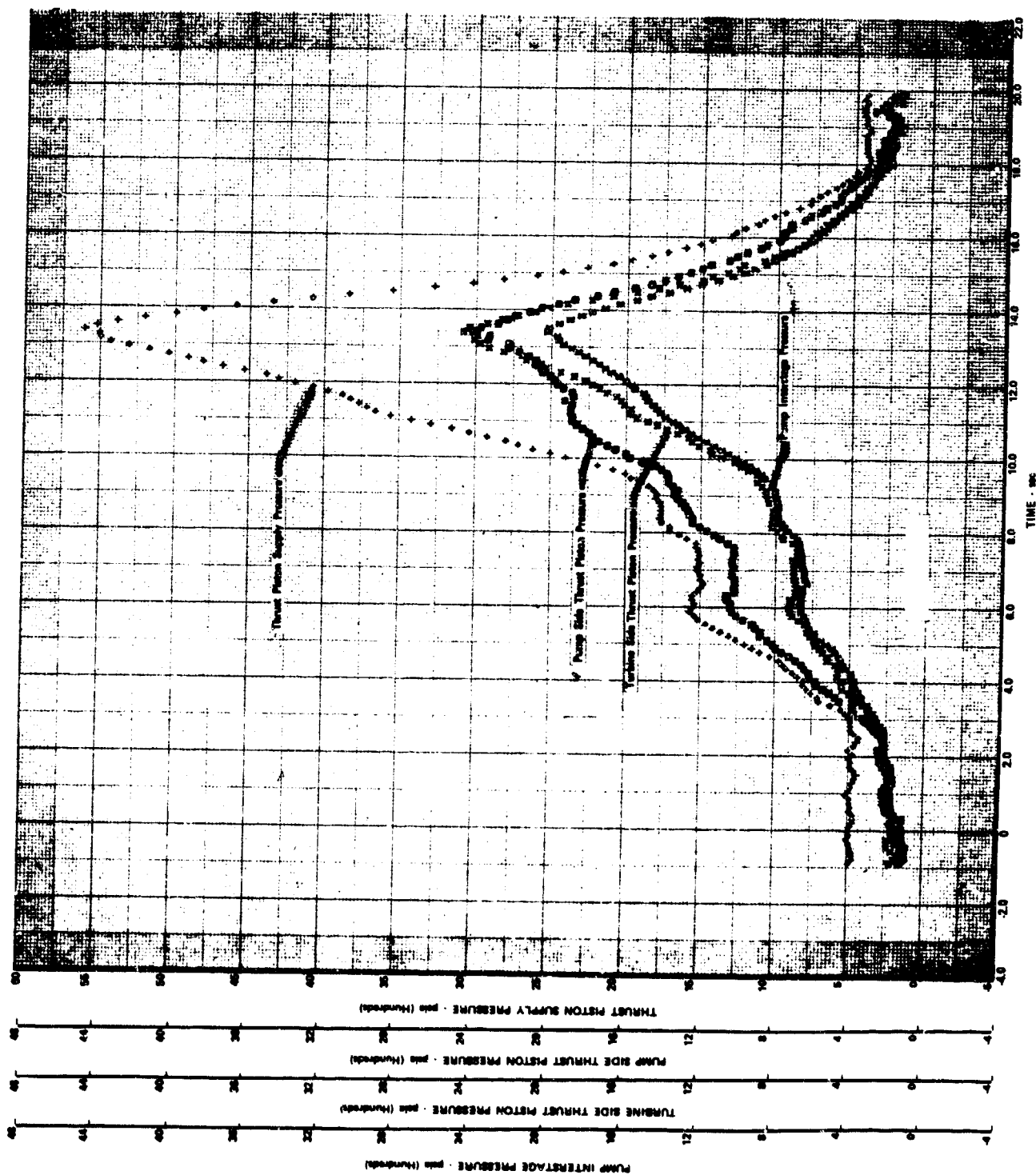


Figure 682. Significant Turbopump Parameters vs Time, Test 7.01, Sheet 3 of 3

FD 37143

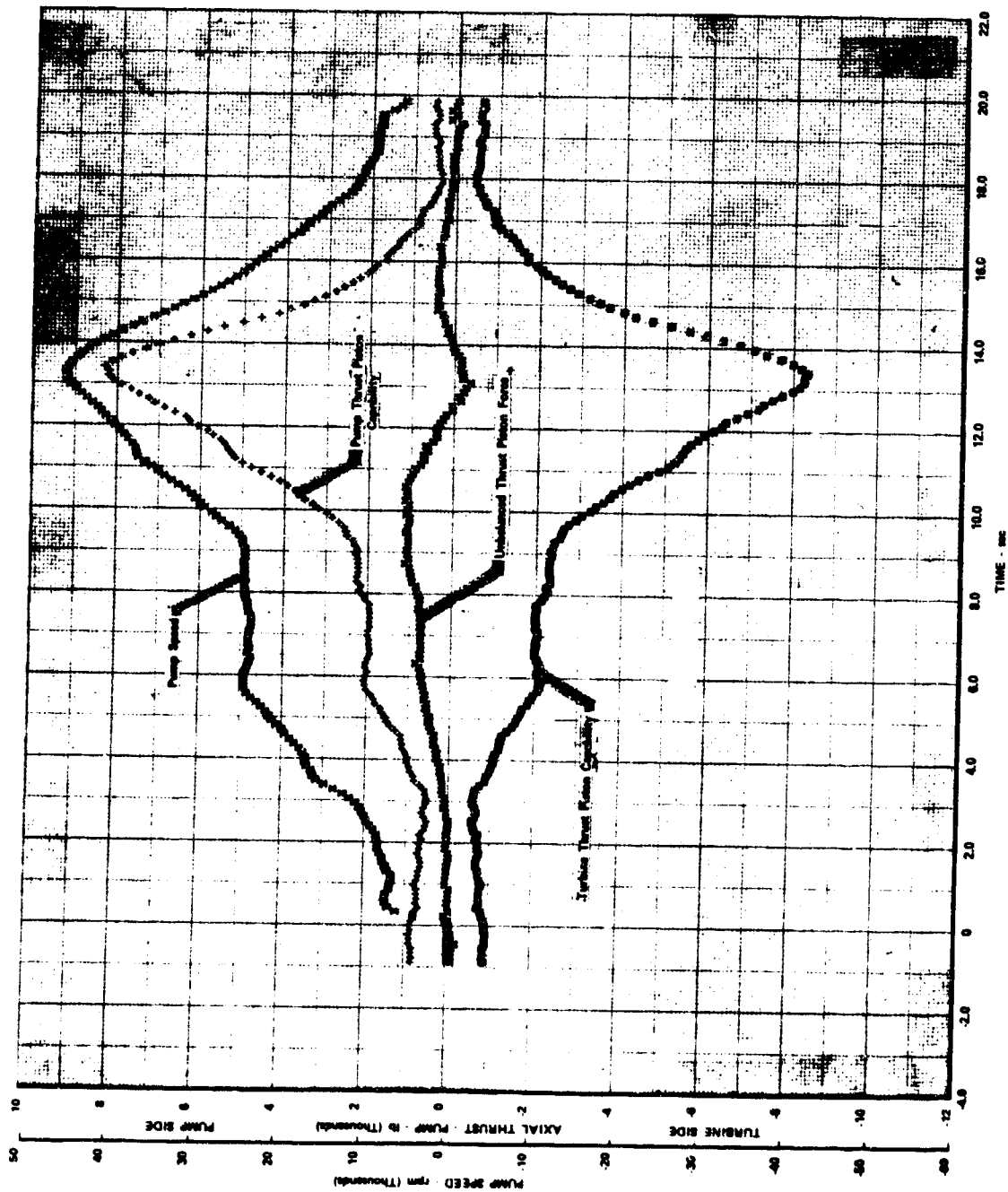


Figure 683. Axial Thrust and Speed vs Time, Test 7.01

FD 37176

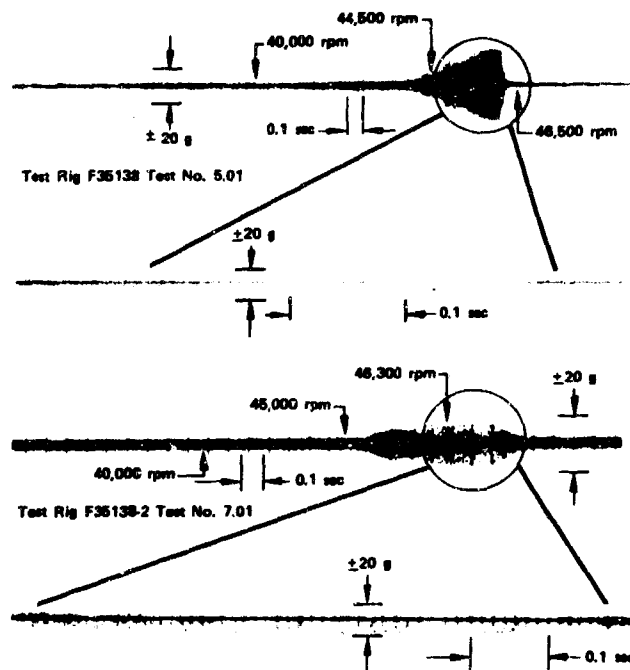


Figure 684. Comparative Acceleration Vibration Traces, Test 5.01 FD 37643A

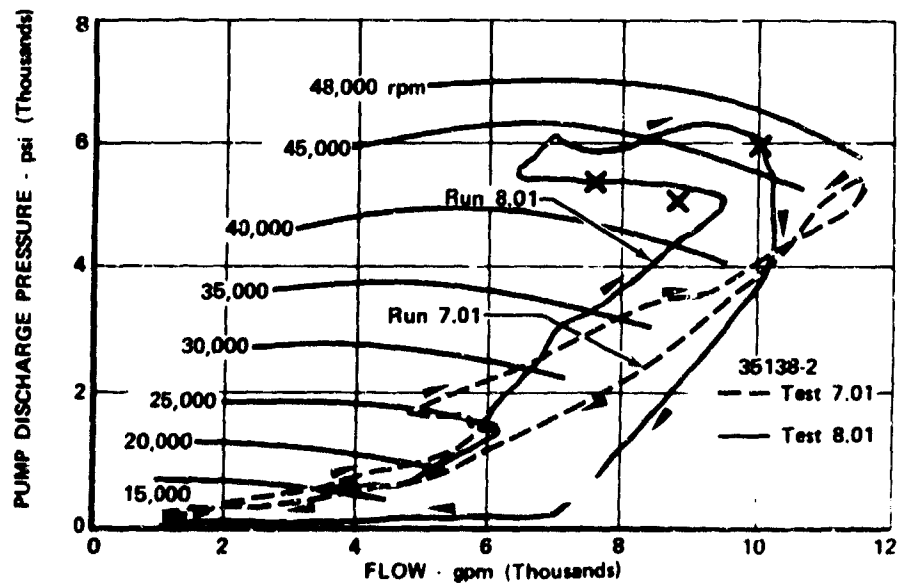


Figure 685. Pump Discharge Pressure vs Flow, Tests 7.01 and 8.01 FD 38750

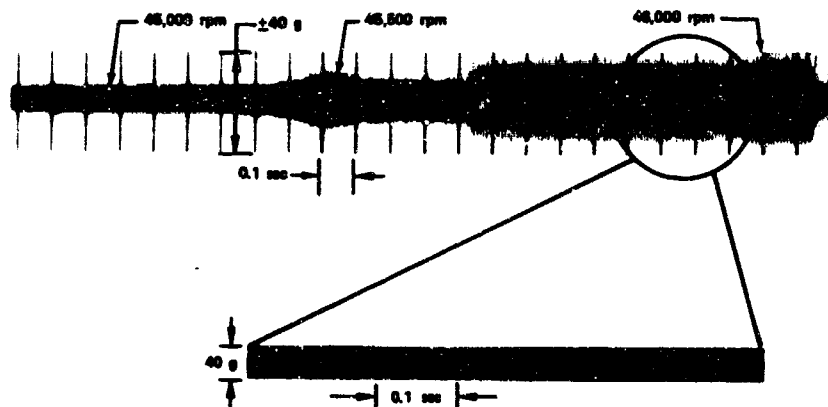


Figure 686. Vibration Trace, Test 8.01

FD 45314

Test No. 9.01 conducted on 24 March 1970, was the initial NPSH test. The objectives of this test were to conduct flow excursions at the 68% (32,500 rpm) speed level and to perform an NPSH test at the engine 20% thrust, mixture ratio of 7 point ($Q/N = 0.073$) at 46% (22,000 rpm) speed level. During this test a helium shuttle valve was coupled to the test rig to accumulate data for use in evaluating this component for possible use with the liftoff seal on subsequent test rigs. All objectives were accomplished during the 83 sec test duration. The flow excursion was completed at 32,500 rpm and the pump speed and flow were trimmed to 22,000 rpm and 1600 gpm for the cavitation test. Pump inlet pressure was reduced slowly to obtain a falloff in pump head for use in determination of the suction performance of the pump. This head falloff was not obtained before pressure and flow oscillations became excessive and the test was terminated. During the shutdown sequence the pump cavitated and the rotor accelerated to 36,200 rpm before the turbine power was depleted by the overspeed abort system. During this overspeed condition insufficient pump discharge pressure was available to the thrust balance system to provide the required axial thrust balance capability. The thrust balance piston momentarily contacted the rub faces. As the rotor decelerated the pump recovered from cavitation and the pressurization of the thrust balance system was restored and the thrust piston operated normally for the remainder of the shutdown transient. Significant turbopump parameters vs time are shown in figures 691 through 693, and axial thrust vs time for this test is shown in figure 694.

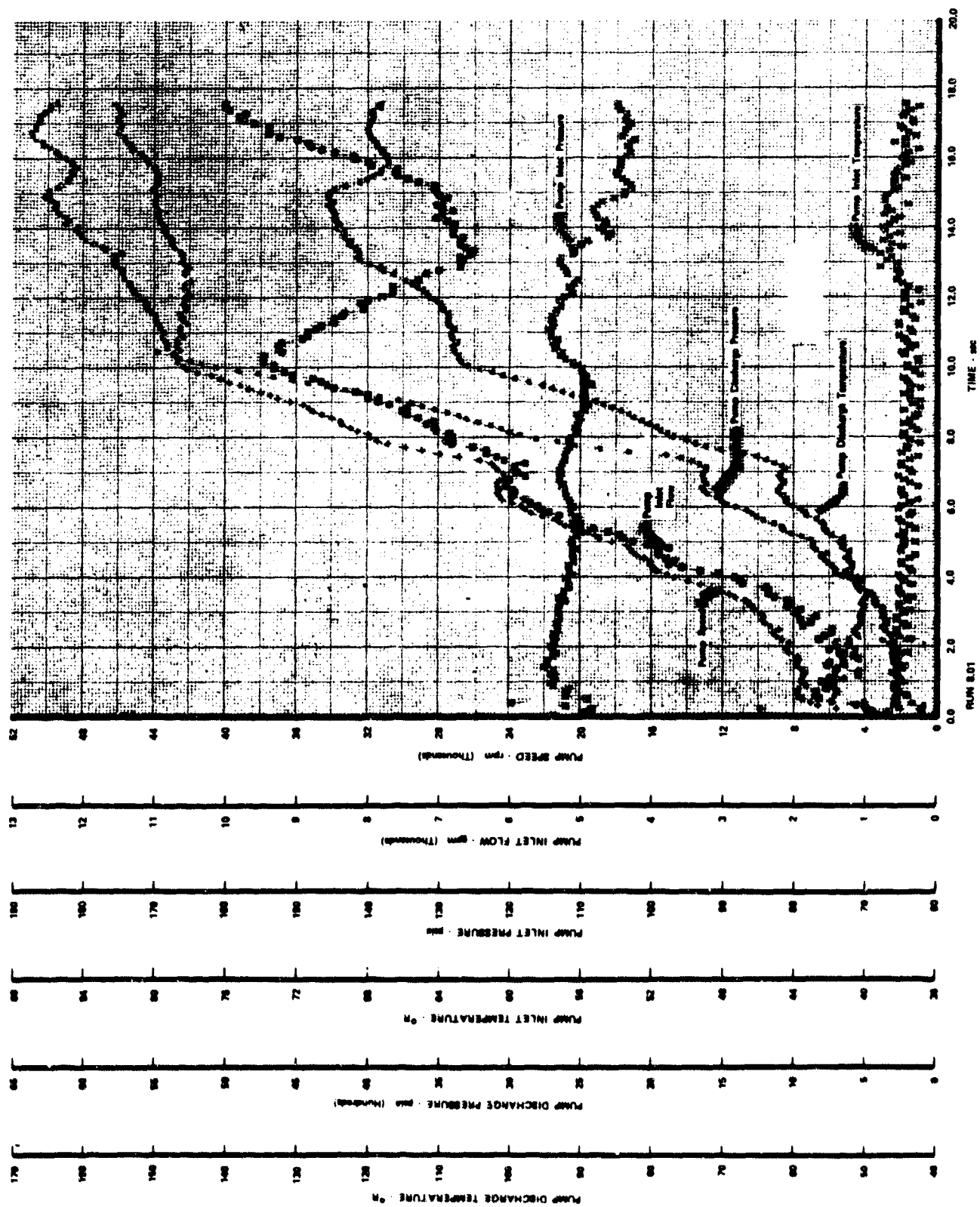


Figure 687. Significant Turbopump Parameters vs Time, Test 8.01, Sheet 1 of 3

FD 37865

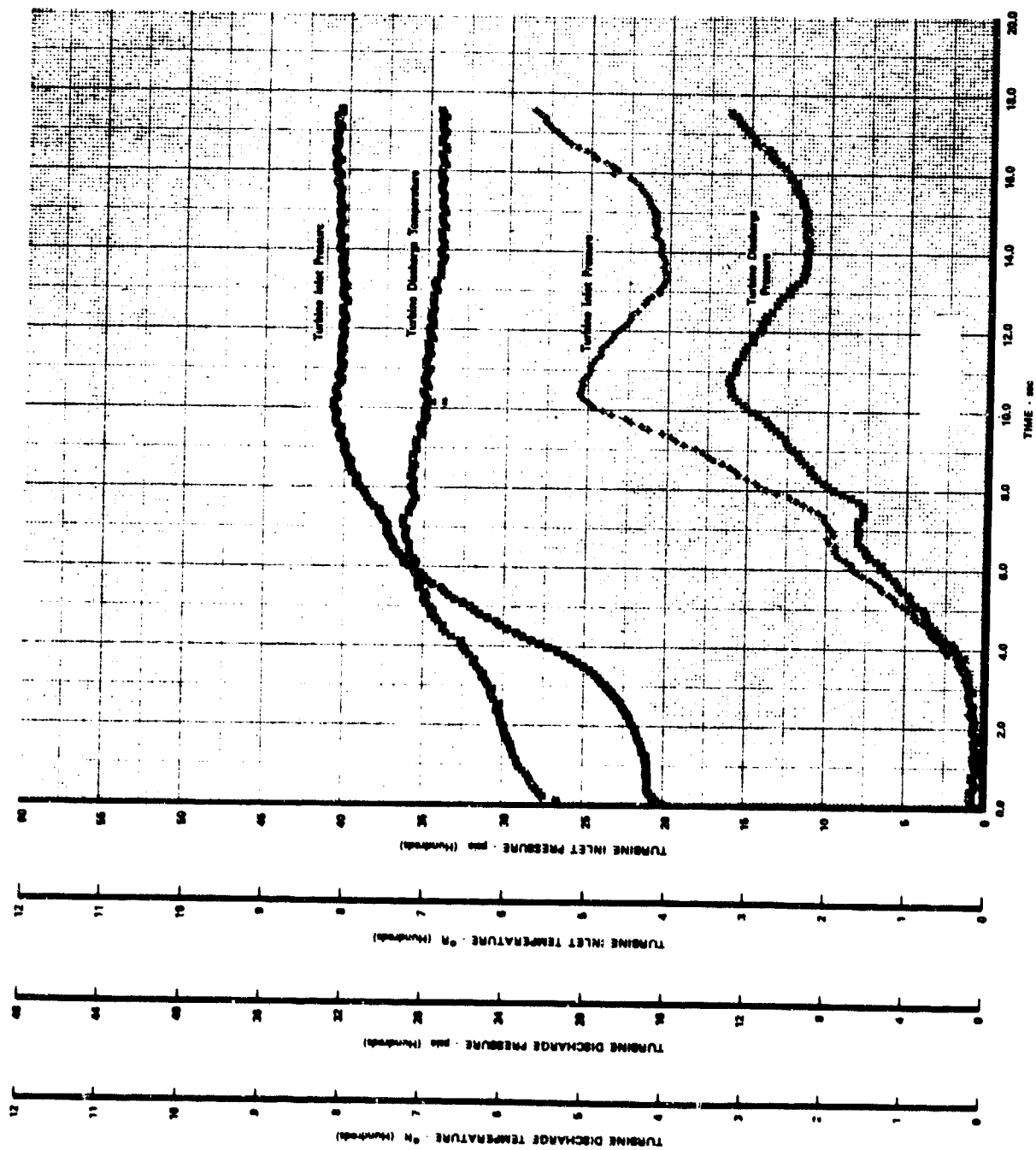


Figure 688. Significant Turbopump Parameters vs Time, Test 8.01, Sheet 2 of 3

FD 37866

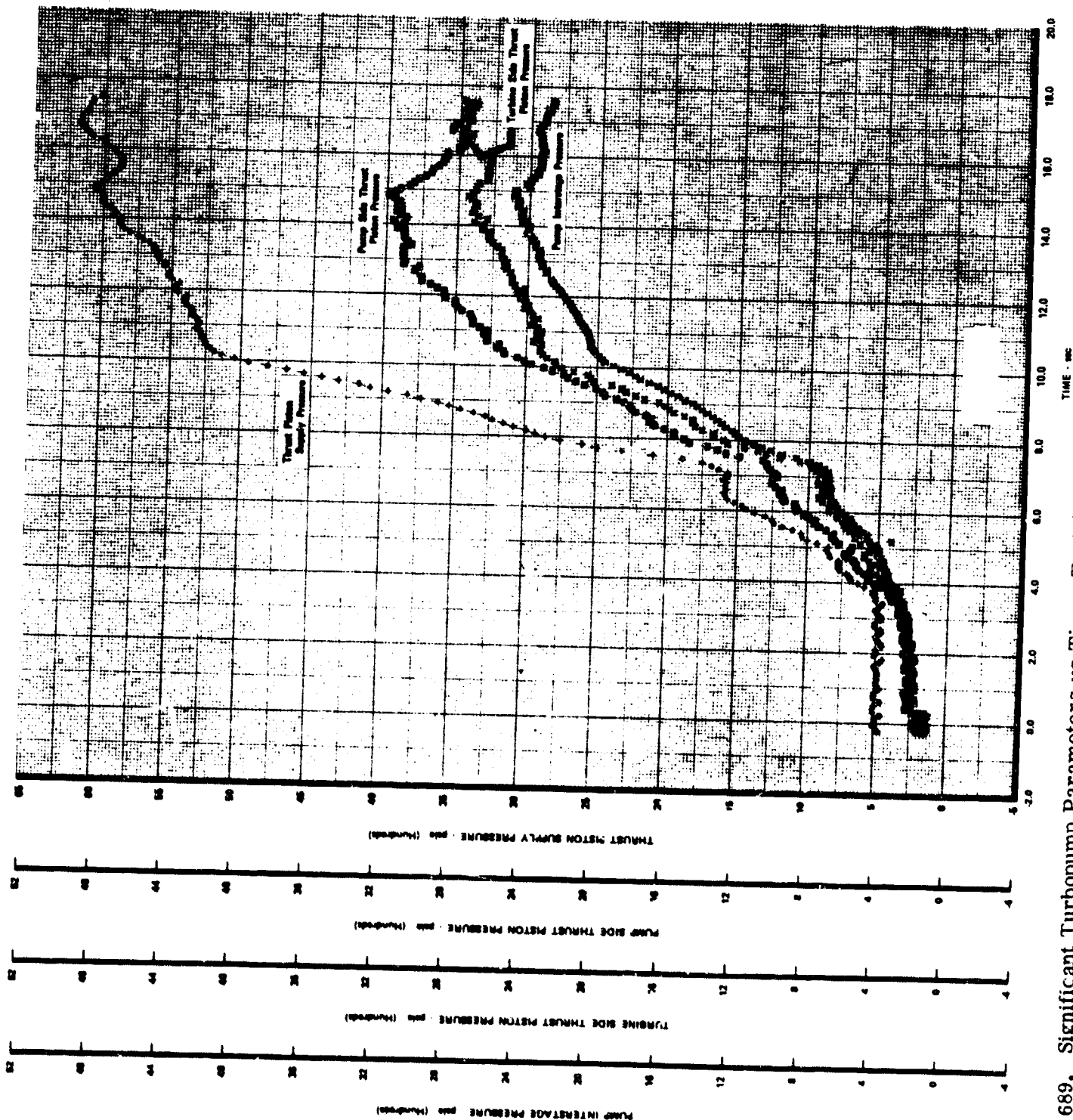


Figure 689. Significant Turbopump Parameters vs Time, Test 8.01, Sheet 3 of 3

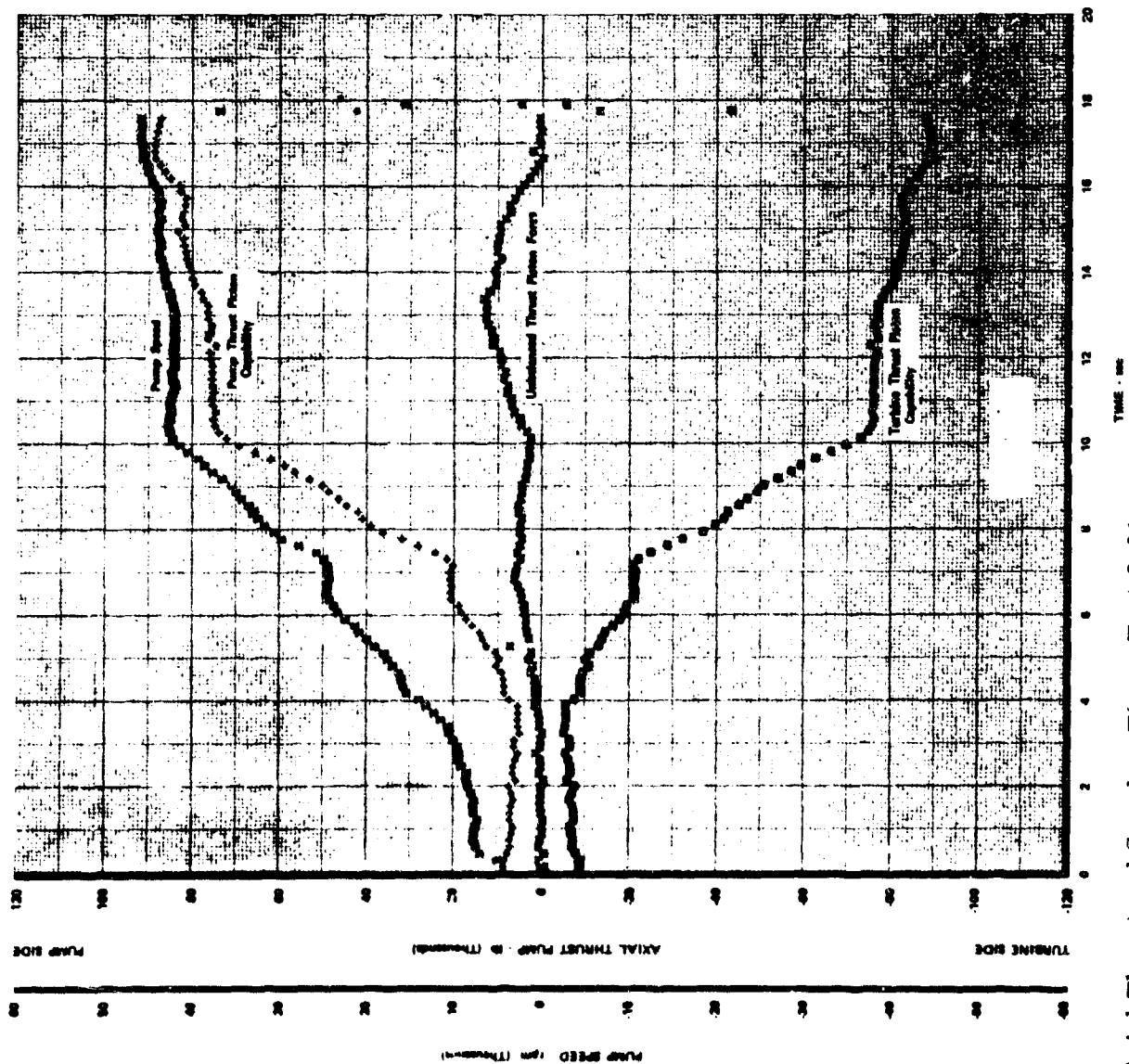


Figure 690. Axial Thrust and Speed vs Time, Test 8.01

FD 37868

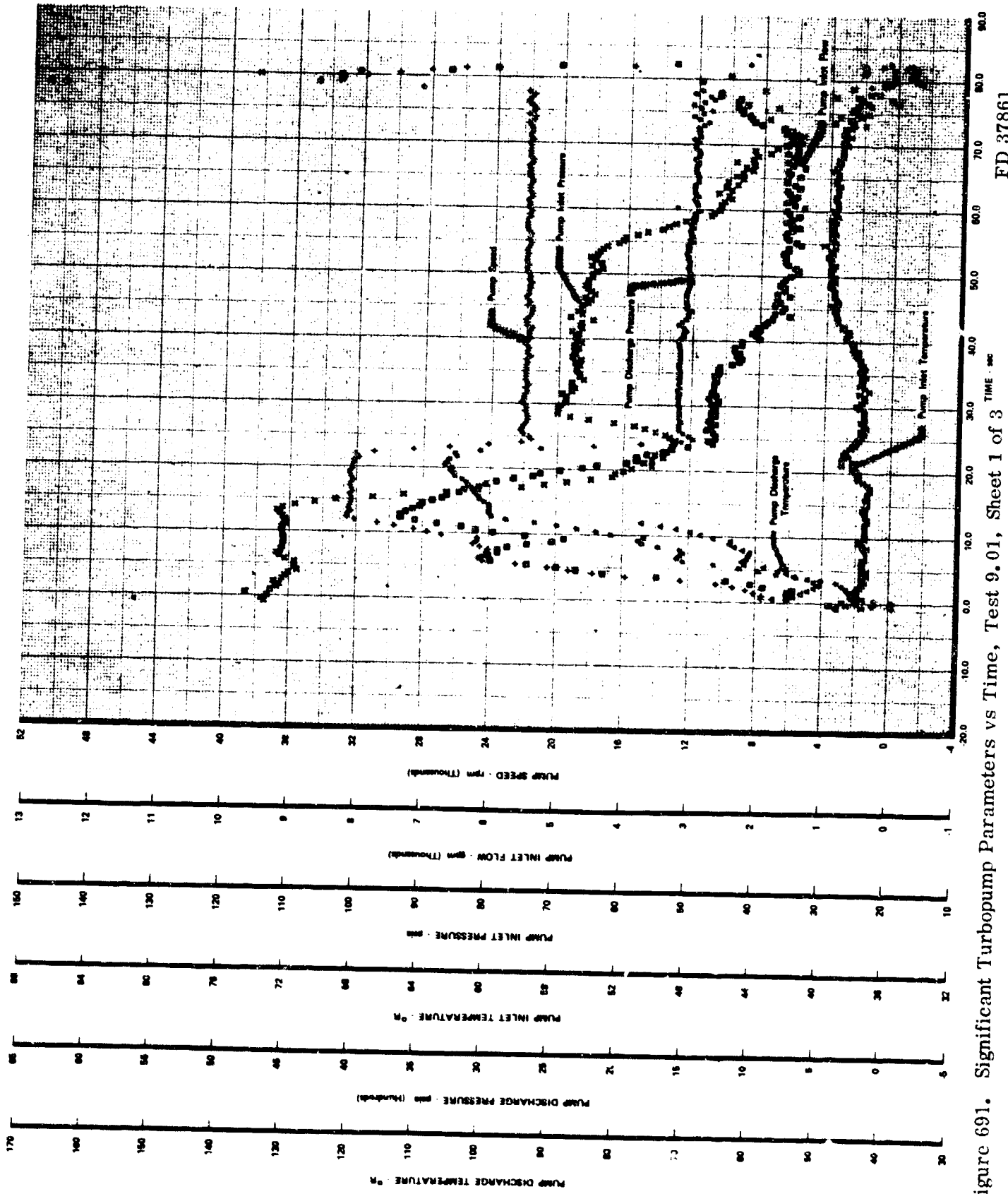


Figure 691. Significant Turbopump Parameters vs Time, Test 9.01, Sheet 1 of 3

FD 37861

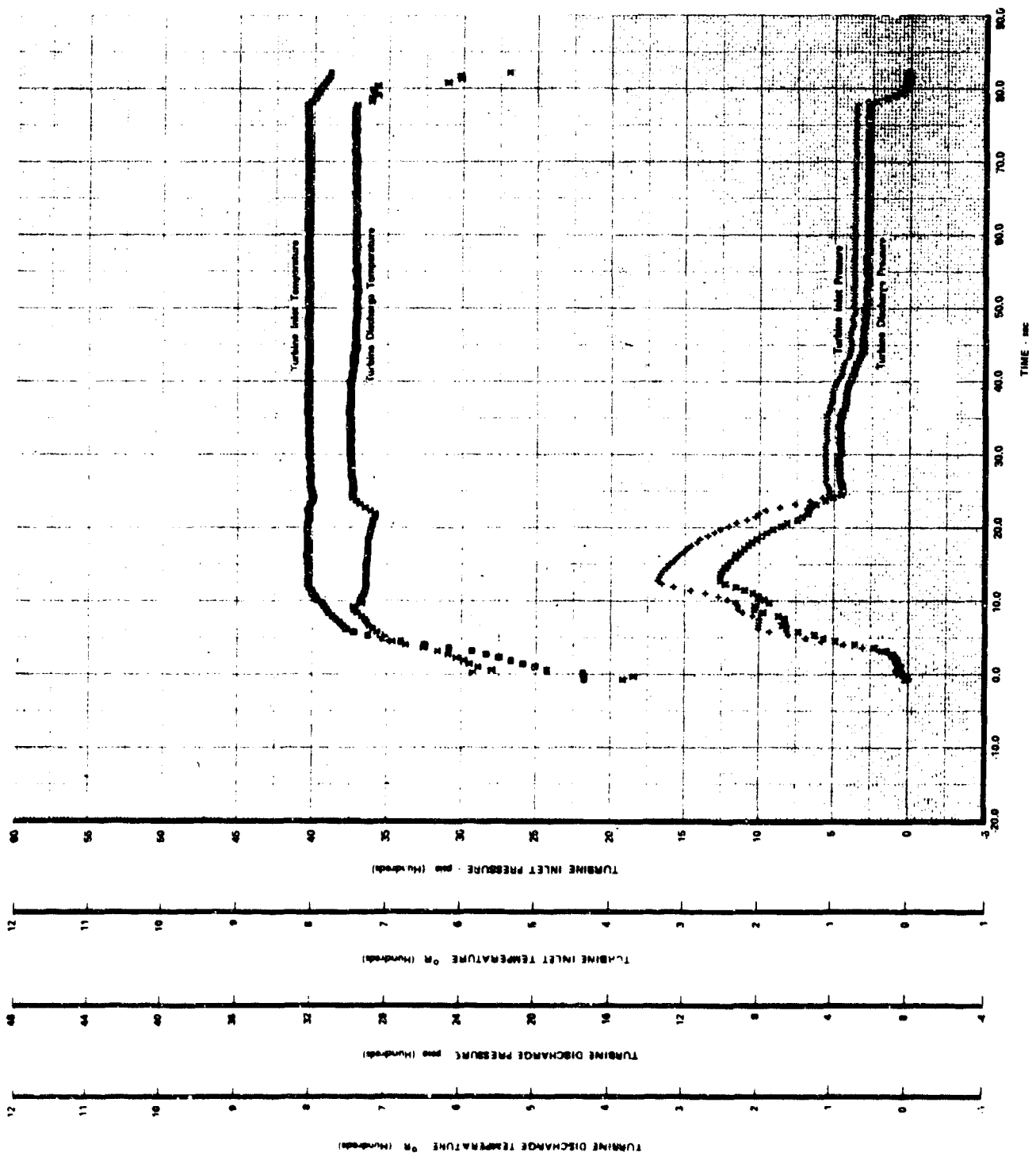
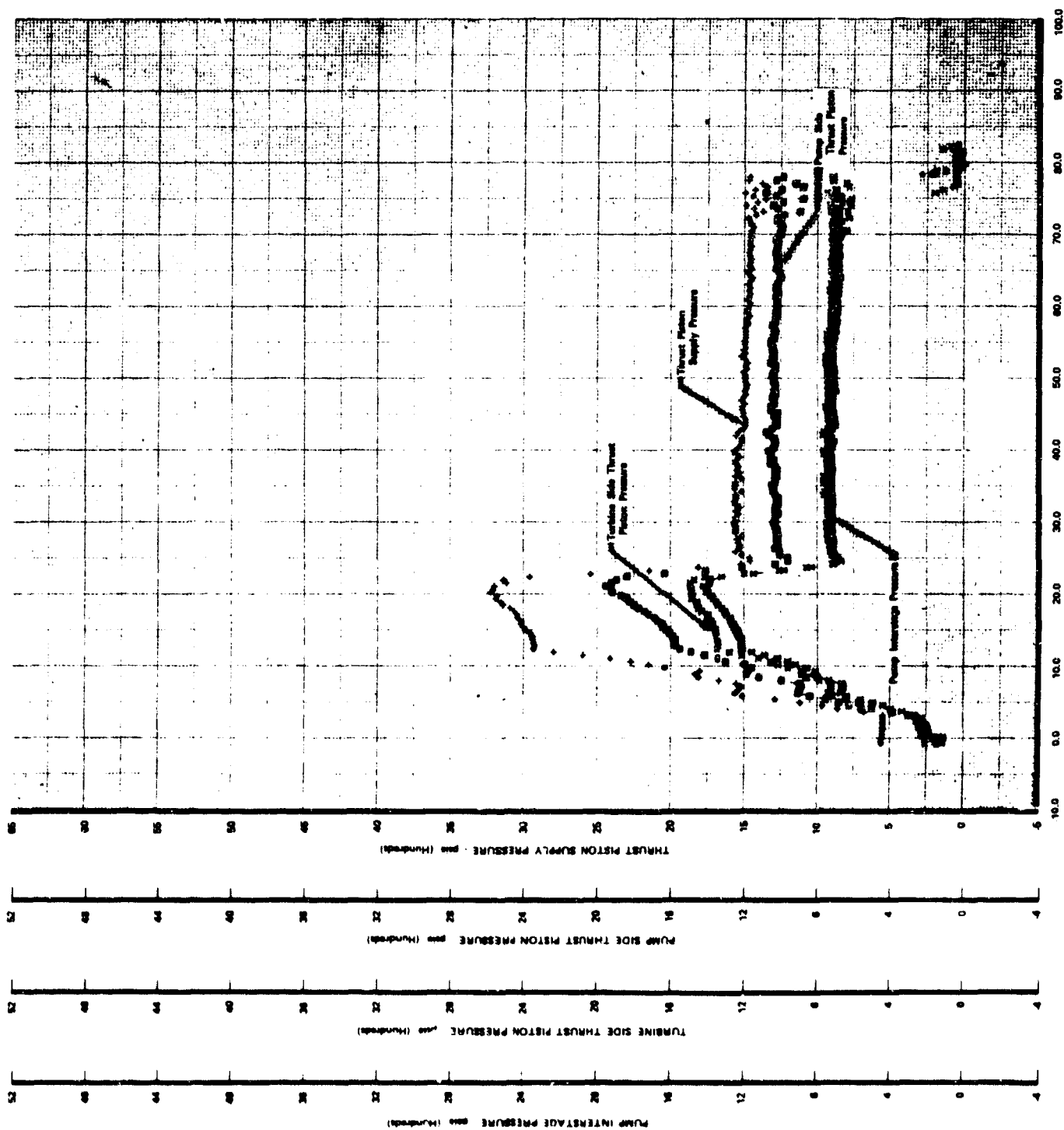


Figure 692. Significant Turbopump Parameters vs Time, Test 9.01, Sheet 2 of 3



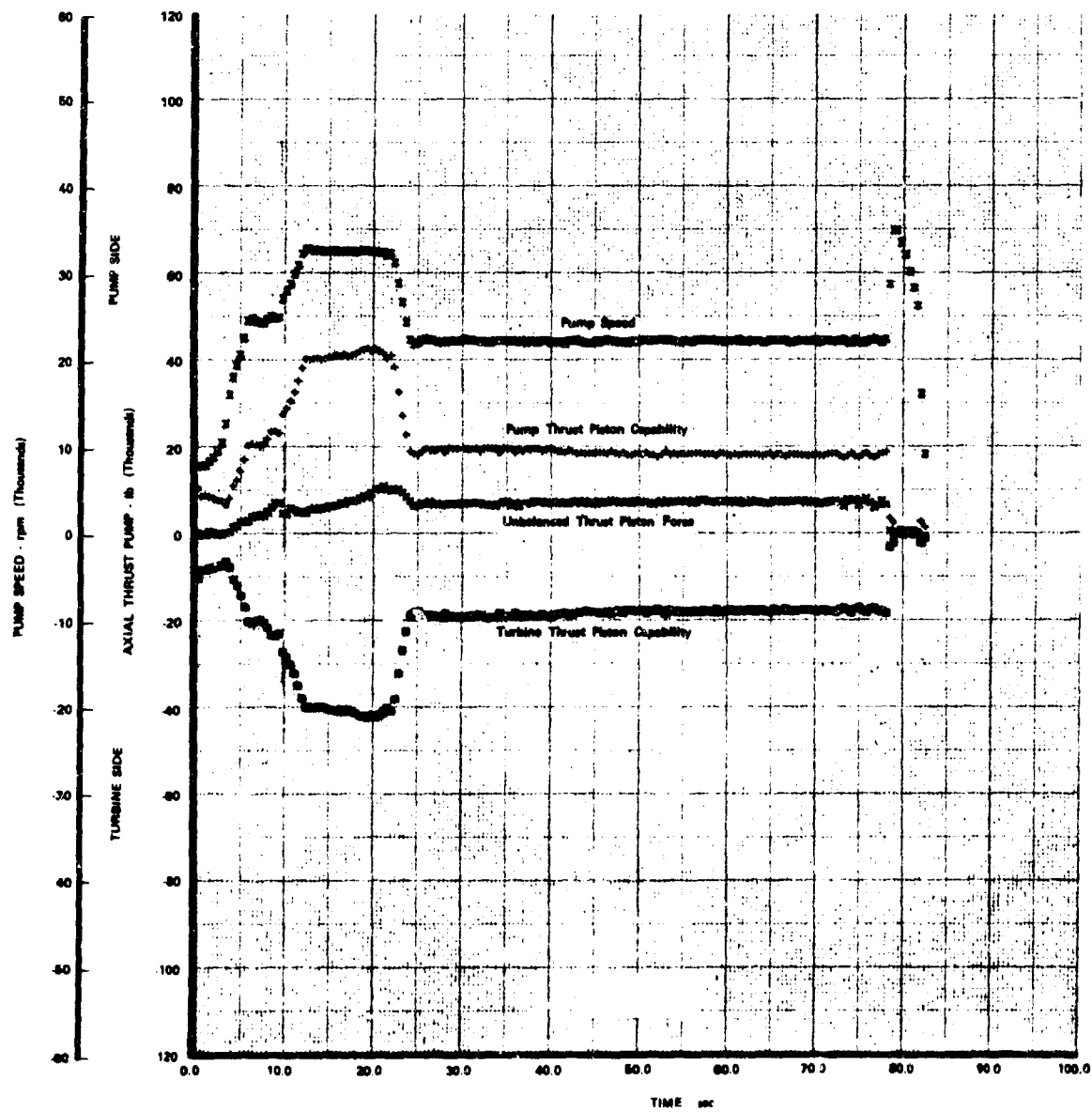


Figure 694. Axial Thrust and Speed vs Time,
Test 9.01

FD 37864

Test No. 10.01, conducted on 25 March 1970, was programed for NPSH testing at the engine 100% thrust, mixture ratio of 7 point ($Q/N = 0.183$) at 42,500 rpm and the engine 20% thrust, mixture ratio of 5 point ($Q/N = 0.098$) at 20,500 rpm. The pump was accelerated to the 42,500 rpm speed level, $Q/N = 0.183$ set point and inlet pressure was ramped from 90 psia to 35 psia without the pump cavitating. Because cavitation had been anticipated at 45 psia inlet pressure at approximately +19 sec run time, new (lower) overspeed advance and abort levels were sequenced in at +25 sec because the pump speed was to be reduced to 20,500 rpm when cavitation occurred at the 42,500 rpm speed level. Pump pressure rise at the 42,500 rpm speed level did not indicate the desired cavitation level was obtained before the sequencer triggered in the lower advance and abort levels and the run was aborted to shutdown. During the test the inlet pressure was reduced to 34 psia with no significant head falloff and a maximum suction specific speed of greater than 27,600* was demonstrated. The significant turbopump parameters vs time are shown in figures 695 through 697. Figure 698 shows axial thrust vs time for test No. 10.01.

The final test, test No. 11.01, was conducted on 26 March 1970 and was a full duration test 74.6 sec in duration. The objectives of this test were to conduct a NPSH test at the engine 100% thrust mixture ratio of 5 ($Q/N = 0.212$) point at 42,500 rpm and at an intermediate Q/N level of 0.127 at 20,500 rpm. All test objectives were accomplished during this test. The pump demonstrated a suction specific speed of 34,000* at the 42,500 rpm $Q/N = 0.212$ set point. The pump speed was reduced to 20,500 rpm and the flow was trimmed to the $Q/N = 0.127$ set point. The hydrogen supply tank pressure was reduced to ambient with no significant falloff in pump head. Significant turbopump parameters vs time are shown in figures 669 through 701, and figure 702 shows axial thrust vs time for this test.

The rig was removed from the test stand on 30 March 1970 and the tear-down inspection was completed with nondestructive testing showing no parts defects. The 2nd-stage impeller and 2nd-stage impeller housing showed a moderate rub indication near the blade tips, and a light rub indication near the eye of the impeller as shown in figures 703 and 704. Light fretting indications were also noted on the impeller face splines as shown in figure 705. The thrust piston revealed light contact on the front face outer seal land, and relatively heavy contact on both rear face seal lands, as shown in figures 706 and 707. The latter condition is attributed to the overspeed occurring on test No. 9.01 during the suction performance determination portion of the test. During this overspeed, there was insufficient thrust piston supply pressure available because of the deep cavitation of the pump, causing the thrust piston to rub.

$$* N_{ss} = \frac{(\text{rpm})(\text{gpm})^{1/2}}{(\text{ft})^{3/4}}$$

These suction specific speeds have been corrected to a waterbase by adding 83 ft of TSH to the hydrogen test data for the 36.9°R inlet temperature on this test.



Figure 695. Significant Turbopump Parameters vs Time, Test 10.01, Sheet 1 of 3

FD 37853

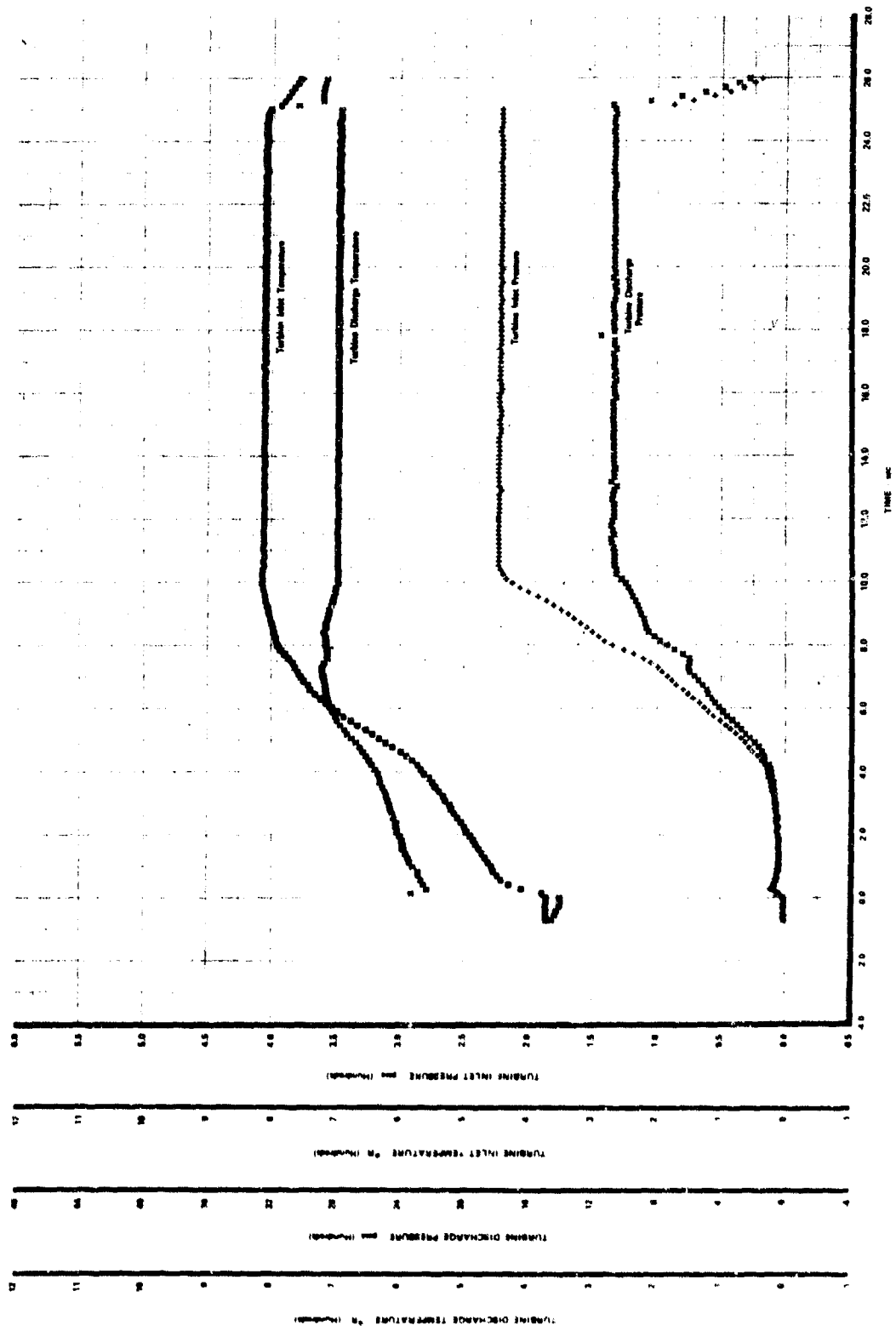


Figure 696. Significant Turbopump Parameters vs Time, Test 10.01, Sheet 2 of 3

FD 37854

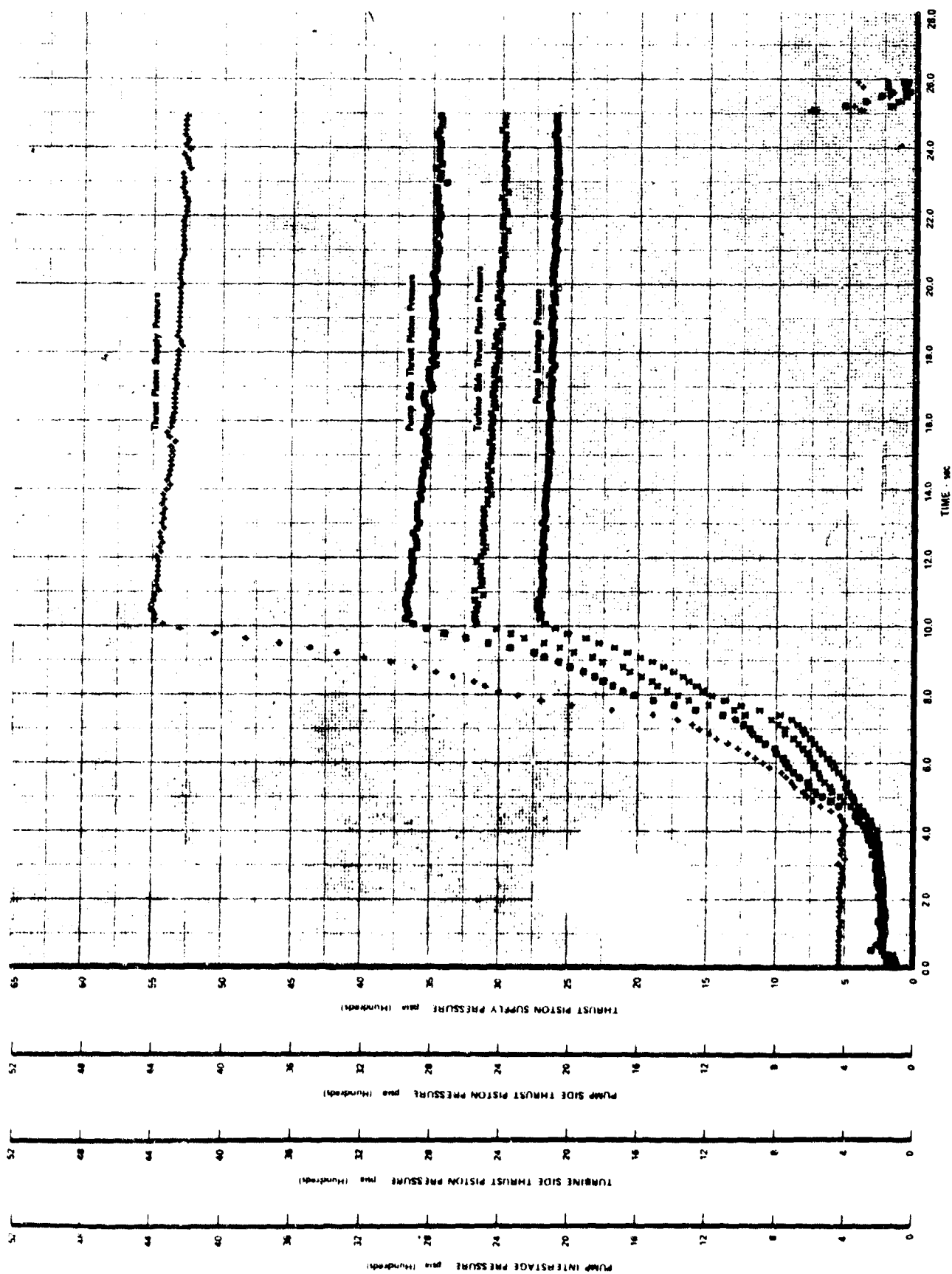


Figure 697. Significant Turbopump Parameters vs Time, Test 10.01, Sheet 3 of 3

FD 37855

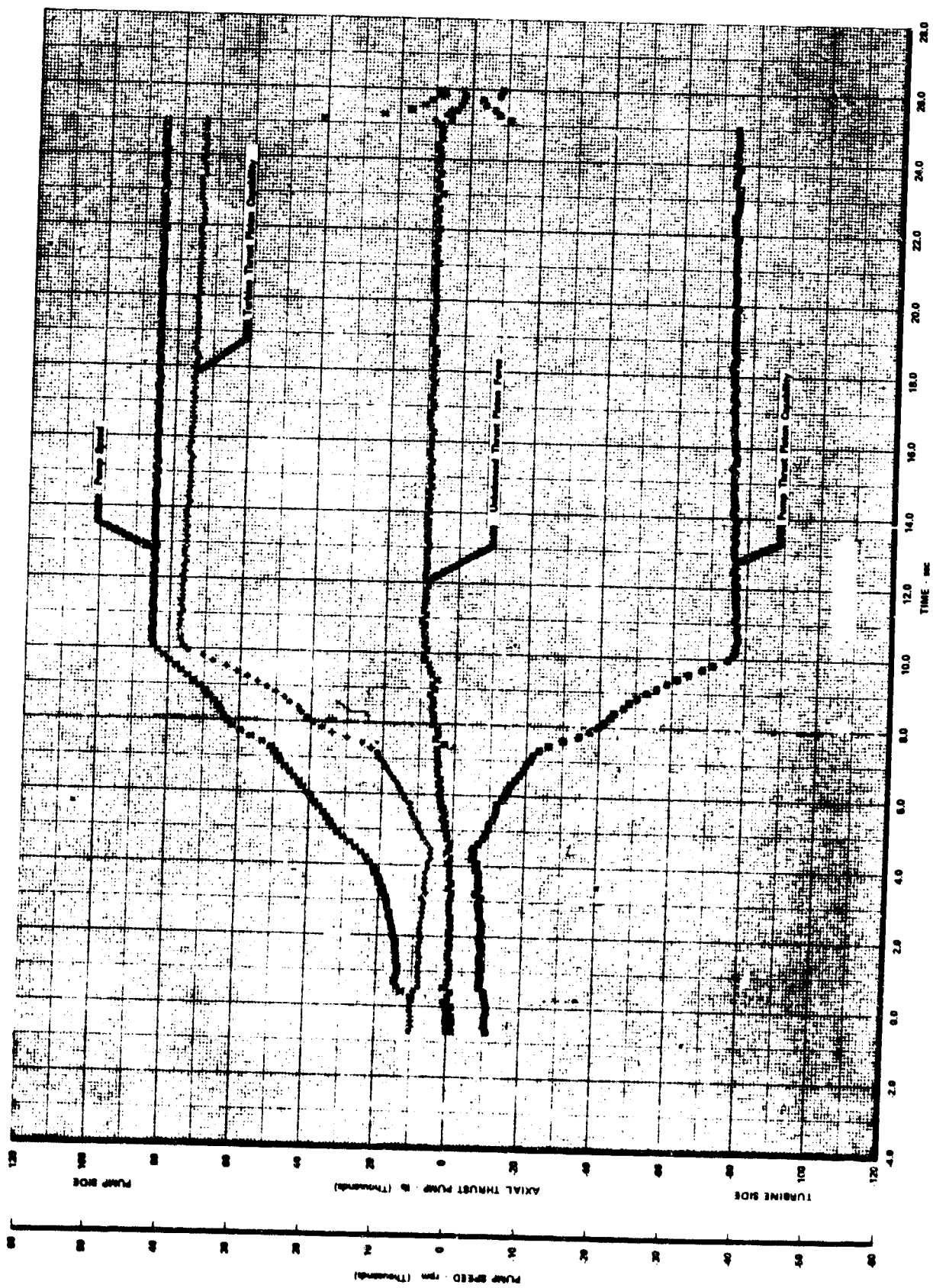


Figure 693. Axial Thrust and Speed vs Time, Test 10.01

FD 37856

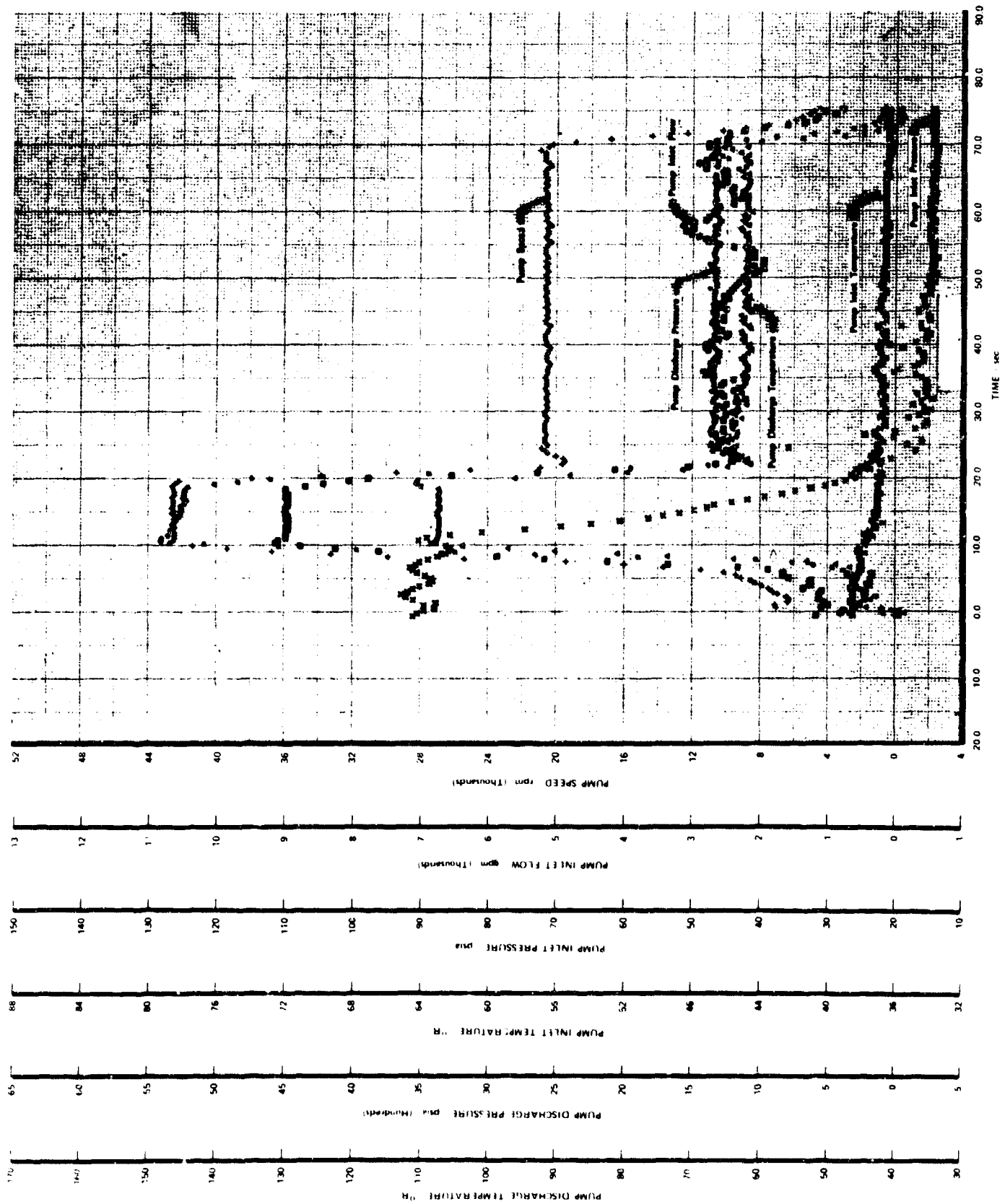


Figure 699. Significant Turbopump Parameters vs Time, Test 11.01, Sheet 1 of 3.

FD 37857

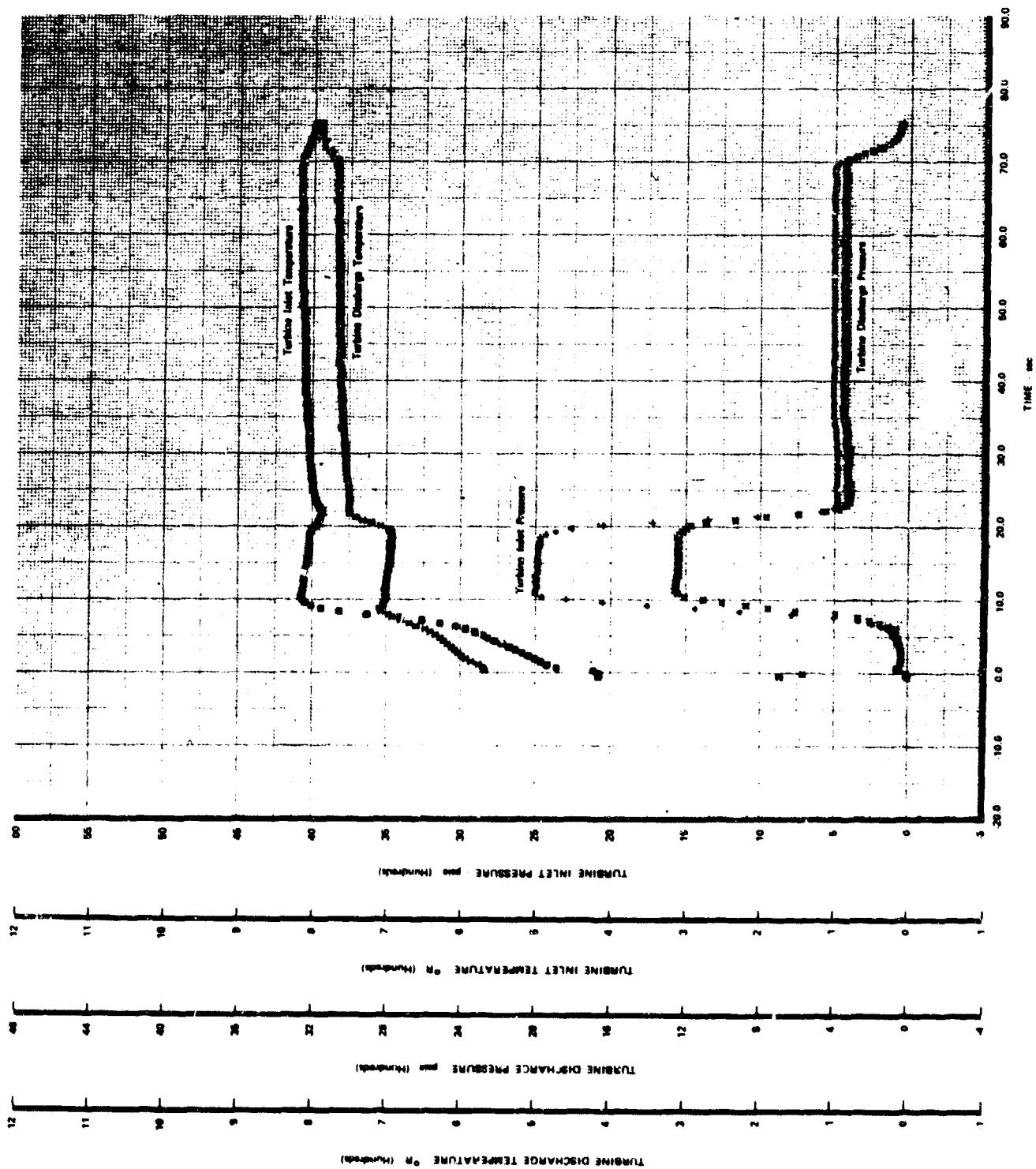


Figure 700. Significant Turbopump Parameters vs Time, Test 11.01, Sheet 2 of 3

FD 37858

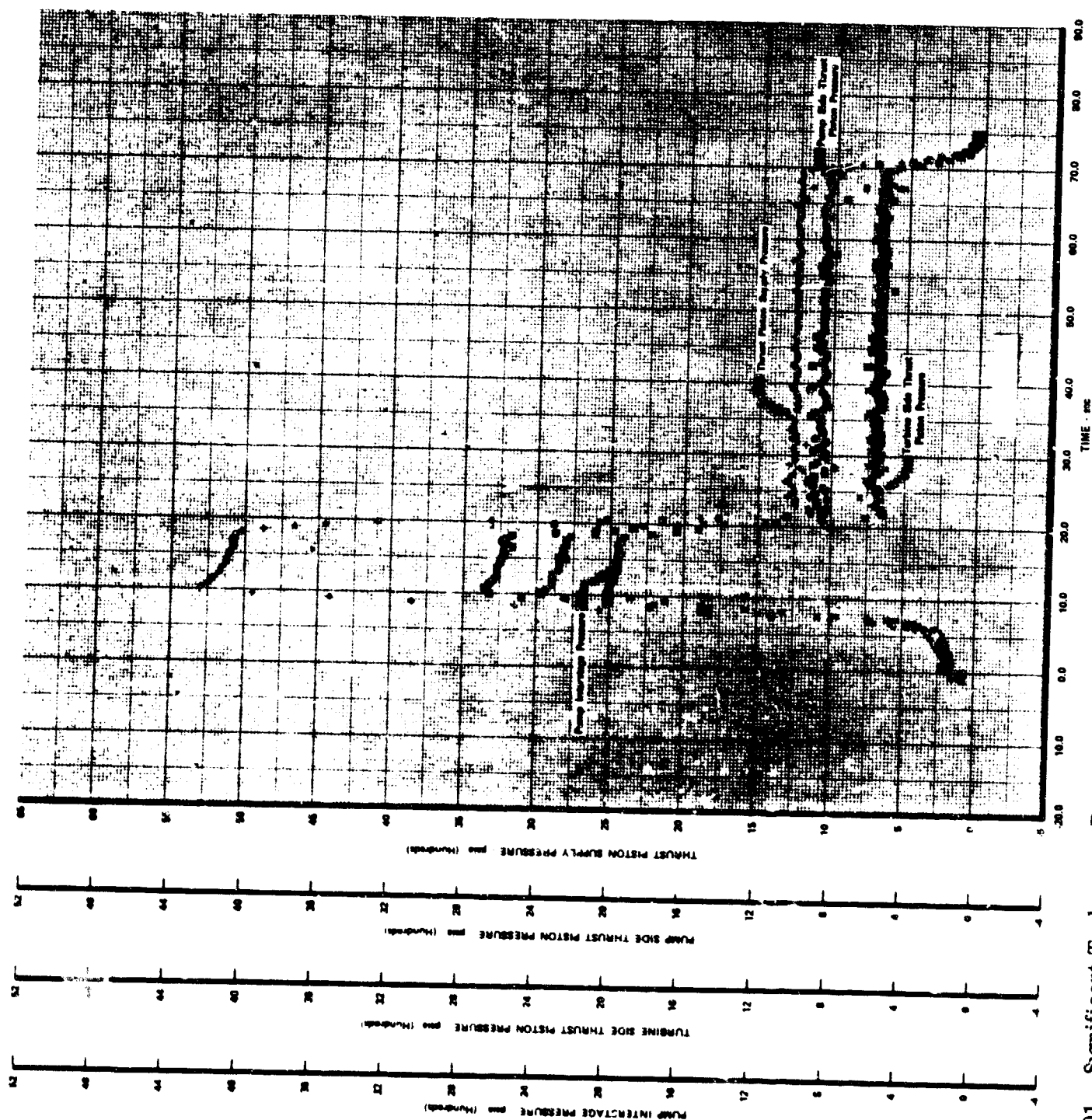


Figure 701. Significant Turbopump Parameters vs Time, Test 11.01, Sheet 3 of 3

FD 37859

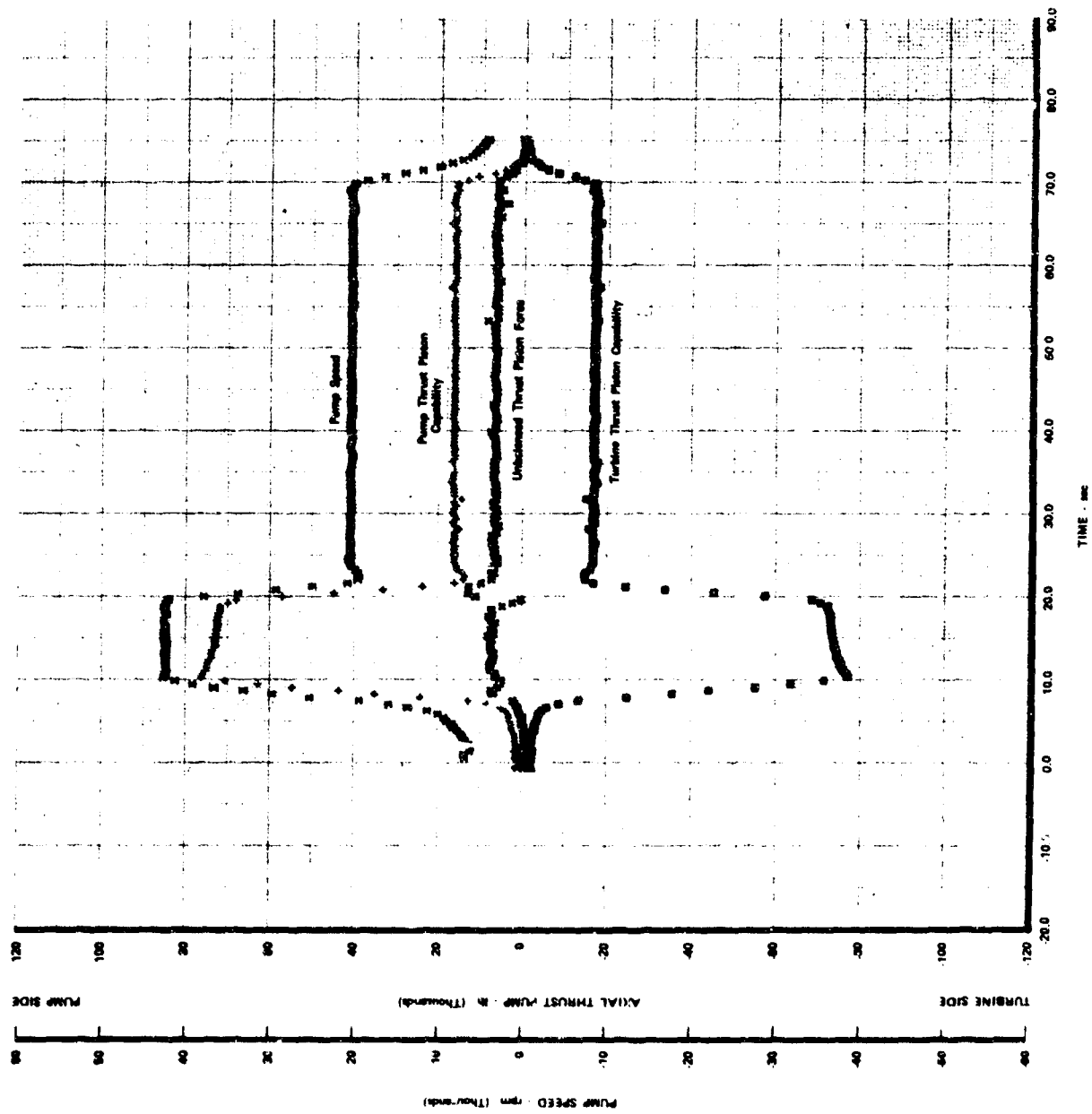


Figure 702. Axial Thrust and Speed vs Time, Test 11.01

FD 37860

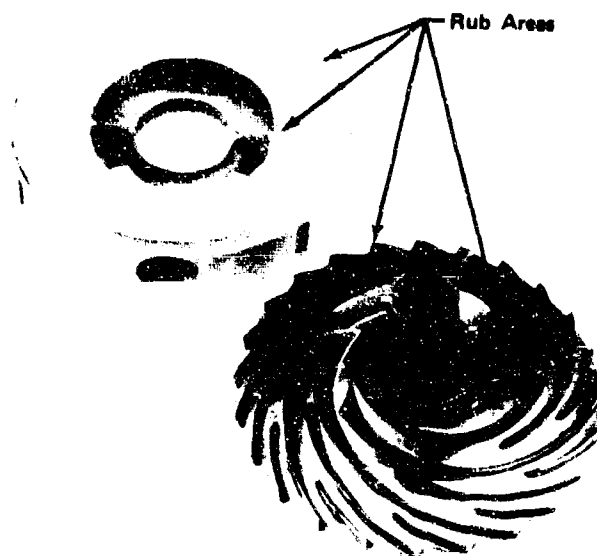


Figure 703. F35138-2 Post-Test View Showing Moderate Rub Indications on 2nd-Stage Impeller and Pumping Shroud

FD 39156

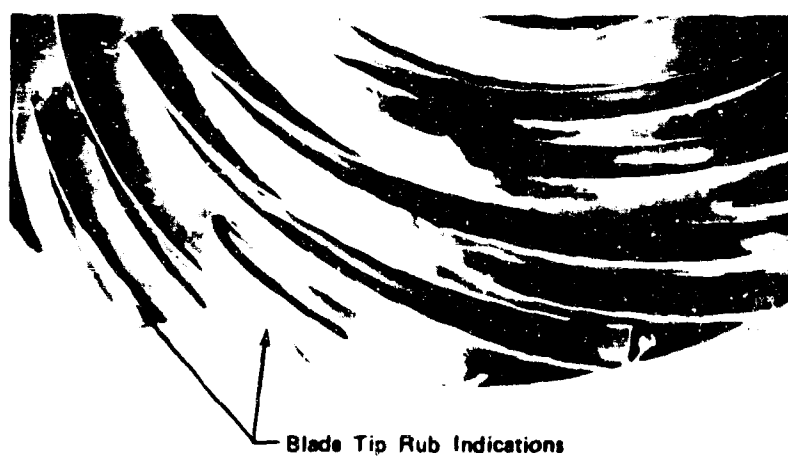


Figure 704. Post-Test View of 2nd-Stage Impeller Showing Blade Tip Rub

FD 39158

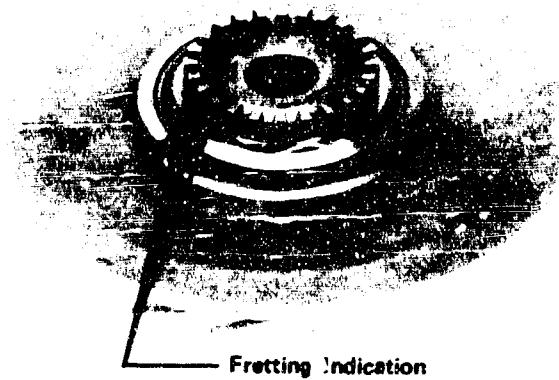


Figure 705. F35138-2 Post-Test View of 2nd-Stage Impeller Showing Fretting Indications on the Face Splines

FD 39159

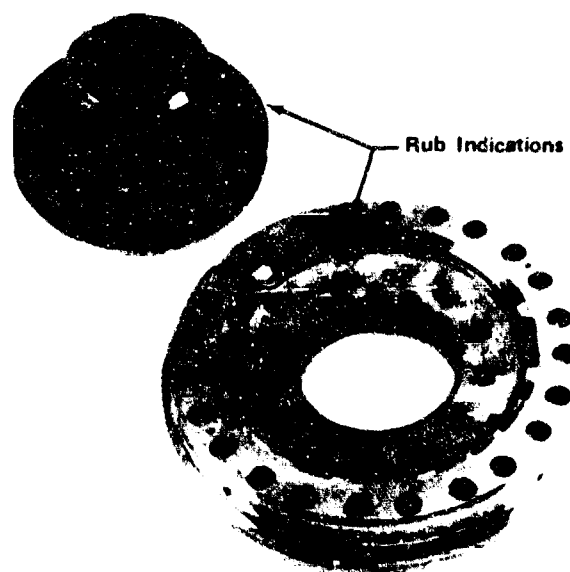


Figure 706. Post-Test View Showing Light Rub Indications on Thrust Piston Front Face Outer Seal

FD 40033

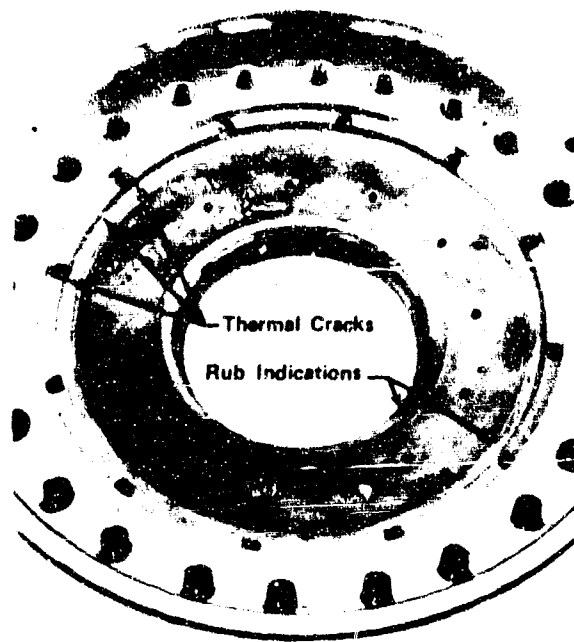


Figure 707. Build 2 Post-Test View Showing Thermal Cracks in the Rear Leaded Bronze Rub Face and Rub Indications from Both Rear Thrust Piston Seal Lands

FD 40034

When pump speed was reduced, after the overspeed abort, the pump recovered from cavitation and the thrust balance system operated normally for the remainder of the shutdown transient, and on the subsequent two tests. This recovery of the cold thrust piston hydrogen supply and its contact with the heated rub face resulted in the thermal cracks also shown in figure 707.

The labyrinth seals were all in good condition and only the impeller inter-stage seal showed any significant contact with the stationary element. There was no damage to the labyrinth because of the favorable rubbing characteristics of the leaded bronze stationary element. All turbine details were in excellent condition, except the internal turbine inlet conical flow duct, which was buckled in one quadrant, as shown in figure 708. This buckling appears to have been the result of excessive differential pressure across this flow duct that developed during the very rapid pressure transients experienced during the abort type shutdowns, which occurred during the test series. A stiffening modification was made for subsequent tests.

The bearings were in good condition. The only discrepancy detected on the front bearing was slight outer race rotation, and fretting on the rear face of the outer race and carrier. The rear bearing showed light front side rail scuffing and moderate rear side rail scoring, similar to the condition

observed on rollers from the bearing test rig, which were disassembled after dynamic balancing. The outer race showed slight outer race rotation similar to that found in the front bearing, and fretting with the bearing carrier. The post-test condition of the bearings is shown in figures 709 and 710. All other parts were in excellent condition and no abnormalities were noted.

Data analysis of the tests performed on fuel turbopump test rig F35138-2 show close agreement with the previous test results and that overall pump performance exceeds the design goals. Figure 711 shows the predicted pump pressure rise vs inlet flow at lines of constant speed and the test data from the six tests. Figure 712 shows a plot of overall efficiency vs inlet unit flow showing the design point and the predicted off-design characteristics with the test data from these tests. Figures 713 and 714 show the 1st- and 2nd-stage pump efficiencies vs flow coefficient data points and the predicted design points and the off-design characteristics. Figure 715 shows the overall unit head vs inlet flow, with the design point, engine cycle requirements and the test data from these tests. The 1st- and 2nd-stage head coefficient vs flow coefficient characteristics of the pump are presented in figures 716 and 717. Figure 718 is a plot of the turbine efficiency vs velocity ratio, and the cycle requirement curve and design point are also shown.

The axial thrust unbalance was primarily toward the pump inlet at all normal operating levels. The greatest unbalance was at the lowest speed and lowest flow condition and the thrust unbalance decreased with the increased speed and flow conditions, as was seen on the previous tests. However, the unbalance reversed during the overspeed that was experienced during the cavitation on test No. 9.01, and the thrust piston rubbed on the turbine side of the thrust piston housing. Suction specific speed demonstrated during these tests exceeds the cycle requirements and is better than predicted, as shown in figures 719 and 720.

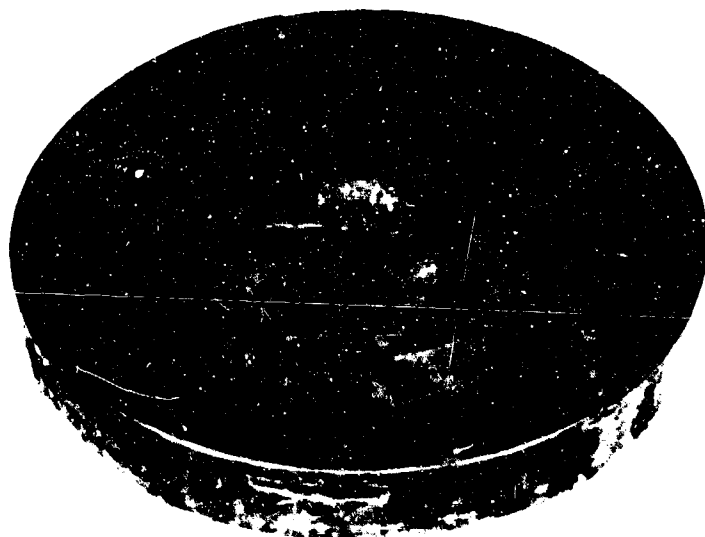


Figure 708. Turbine Inlet Conical Flow Duct
Buckled by Excessive Pressure
Transient

FE 97320

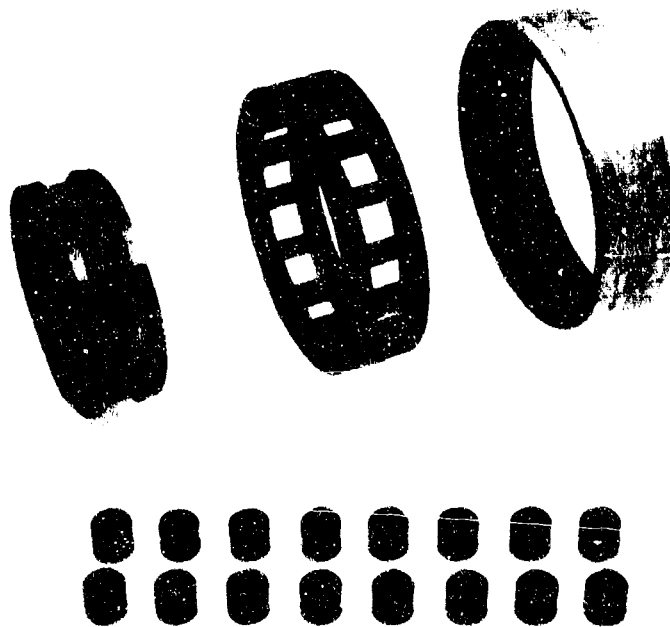


Figure 709. Rig F35138, Build 2 Post-Test View of Front Bearing Showing Good Condition of Detail Parts FF 97190

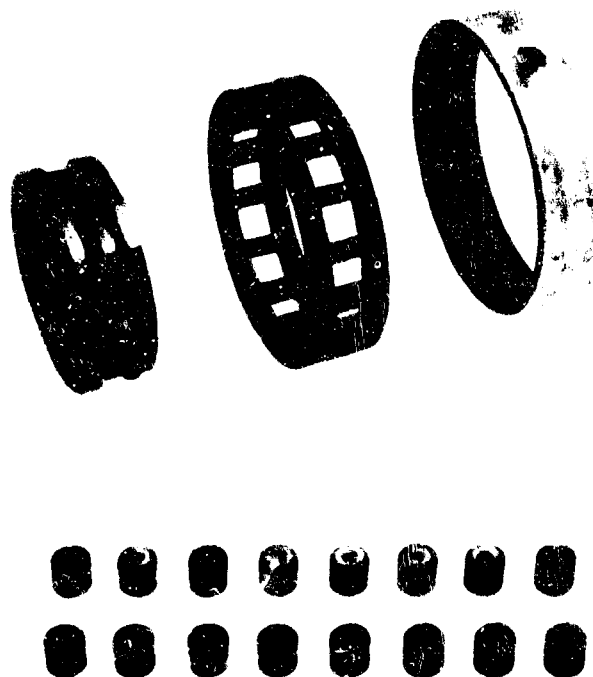


Figure 710. Rig F35138, Build 2 Post-Test View of Rear Bearing Showing Good Condition of Detail Parts FF 97192

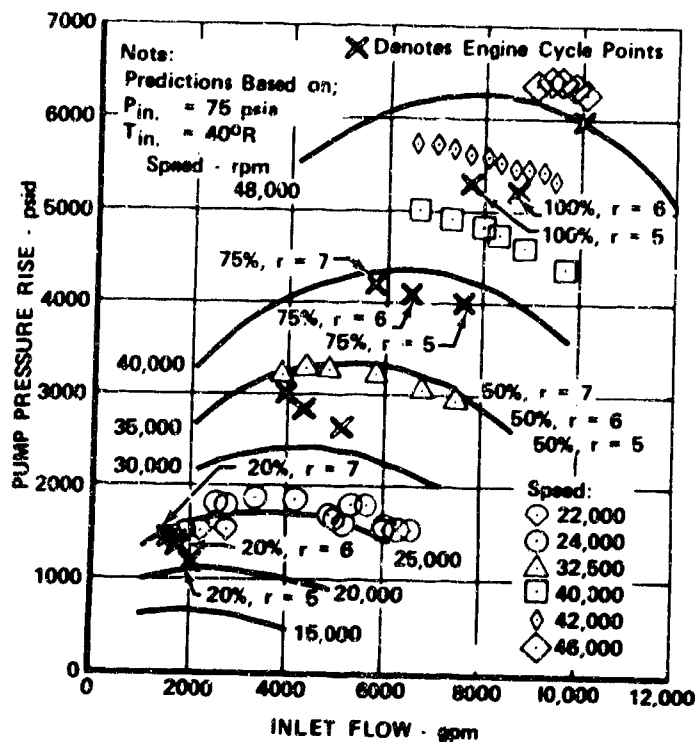


Figure 711. Pump Pressure Rise vs Inlet Flow, Rig 35138-2 FD 37644

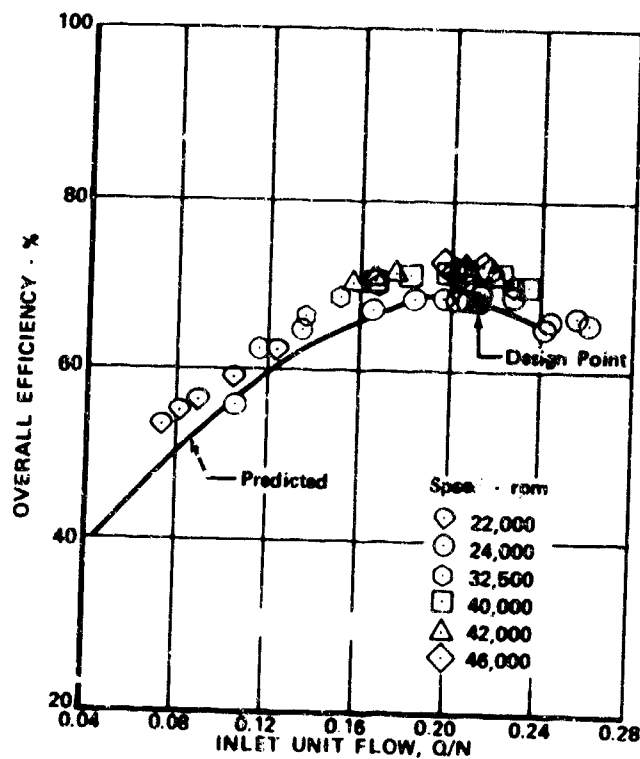


Figure 712. Overall Efficiency vs Inlet Unit Flow, Rig 35138-2 FD 37645

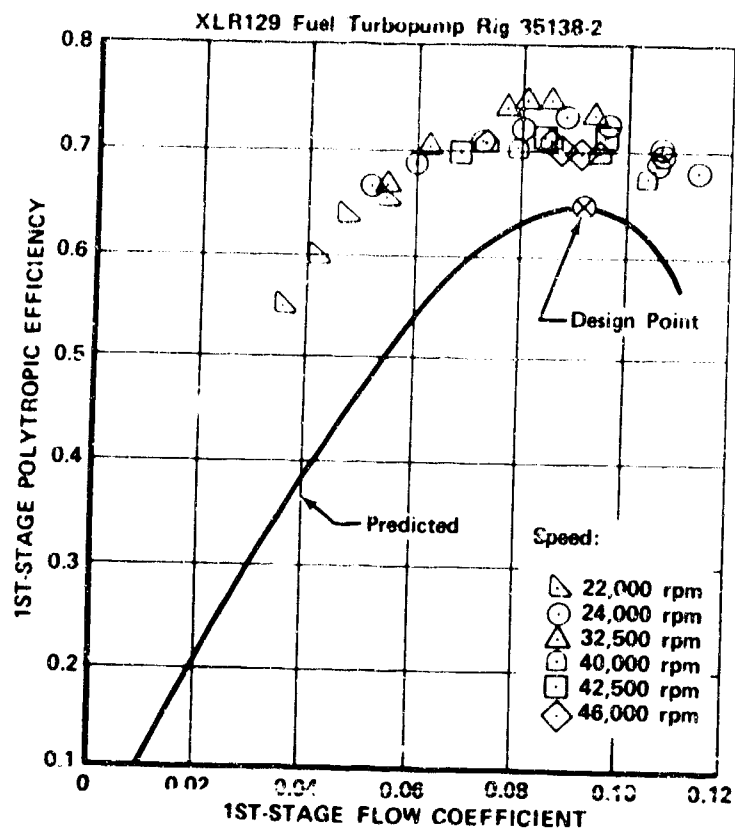


Figure 713. First Stage Efficiency Characteristic FD 44212

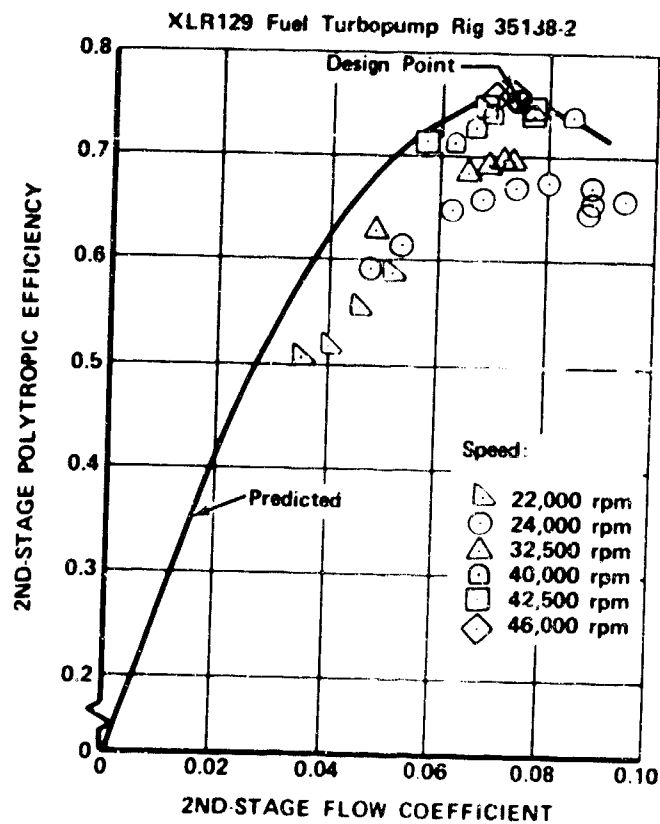


Figure 714. Second Stage Efficiency Characteristic FD 44213

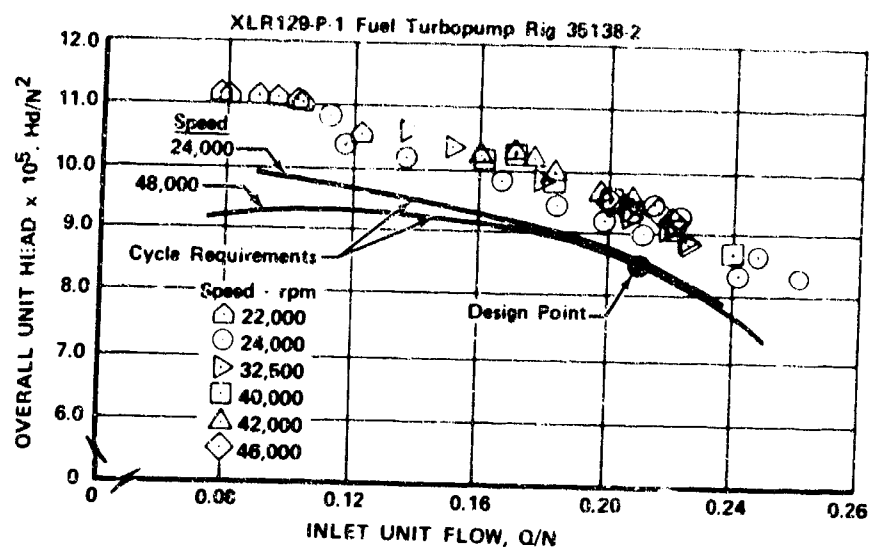


Figure 715. Overall Unit Head vs Inlet Unit Flow, FD 37646
Rig 35138-2

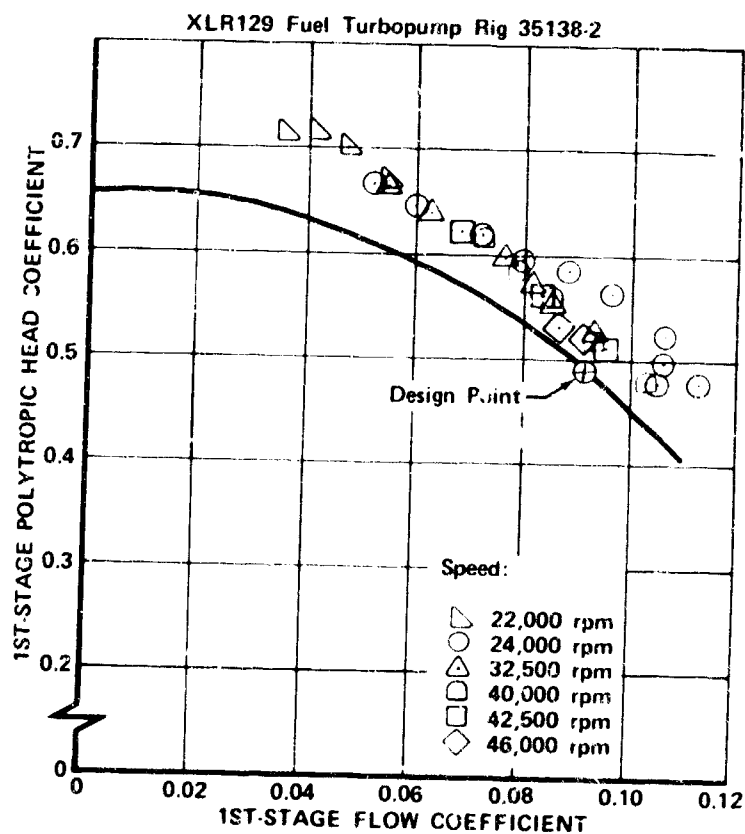


Figure 716. First Stage Head Coefficient FD 44214

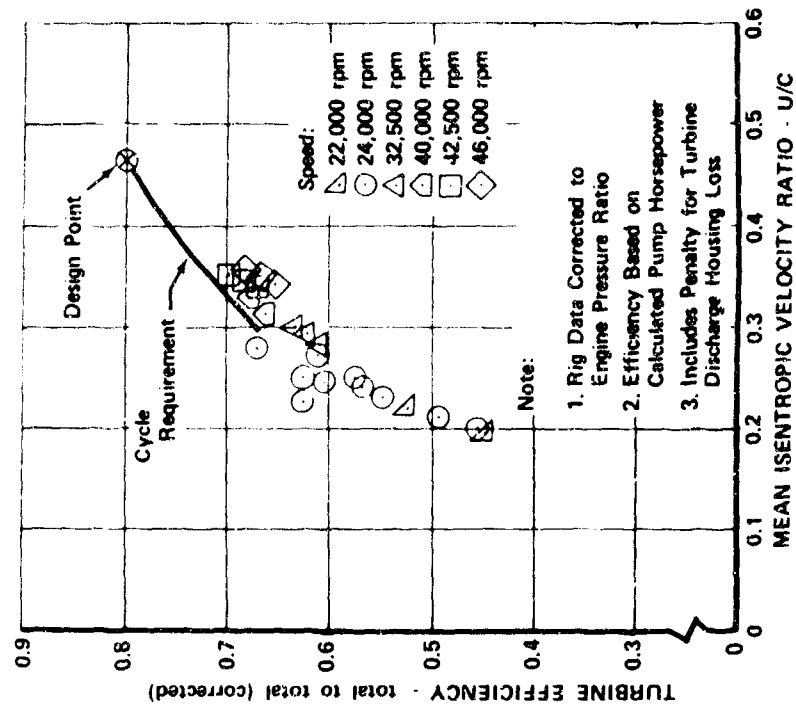
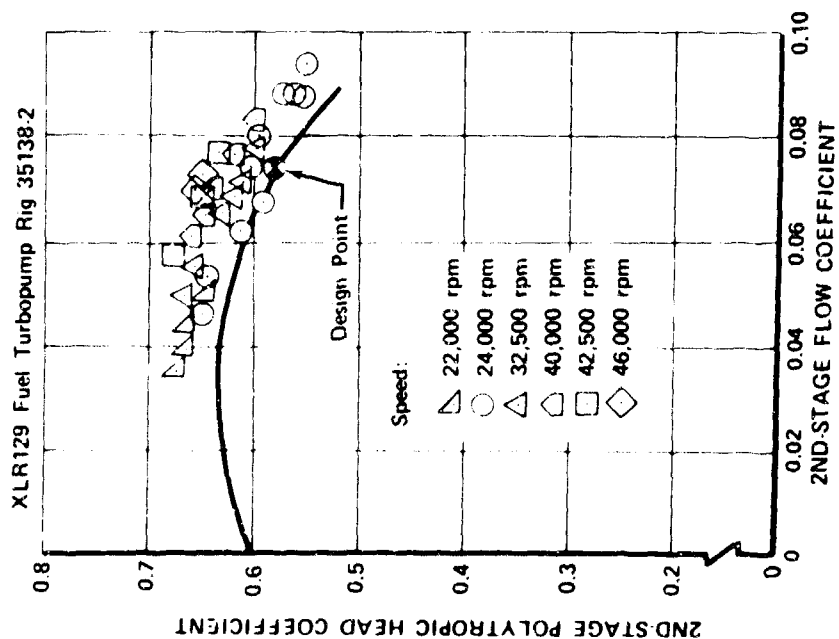


Figure 717. Second Stage Head Coefficient

Figure 718. Turbine Efficiency

FD 44216

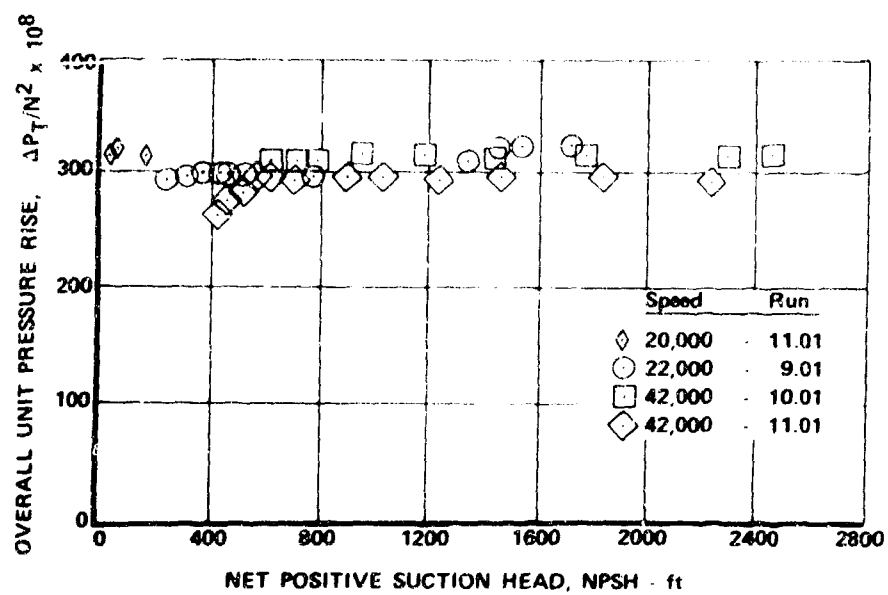


Figure 719. Overall Unit Pressure vs Net Positive Suction Head, Rig 35138-2 FD 37647

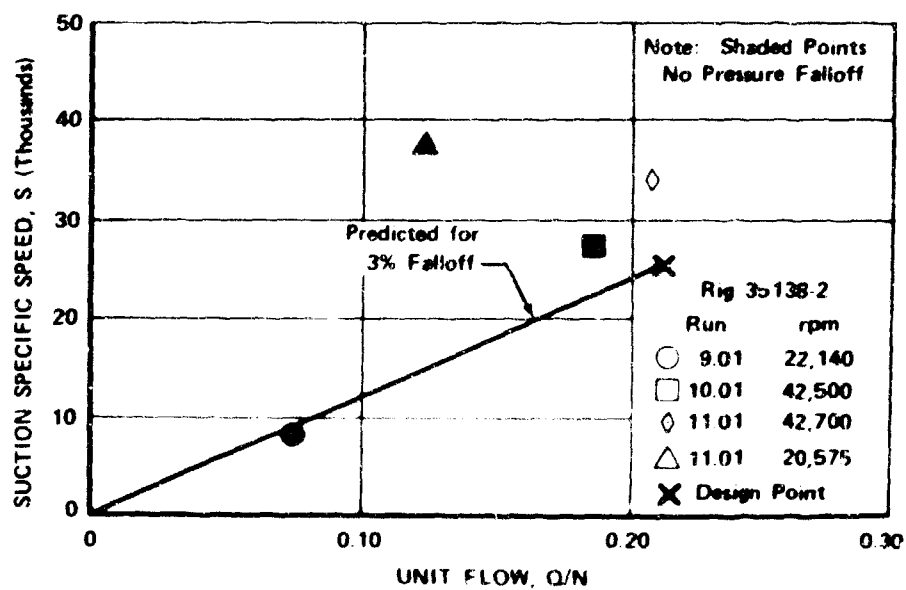


Figure 720. Suction Specific Speed vs Unit Flow, Rig 35138-2 FD 37648

As a result of the fuel turbopump tests associated with test rig F35138-2, it was concluded:

1. Pressure rise was approximately 12% above predicted values at design speed and flow.
2. Overall efficiency near design speed was 4 points higher than predicted and approximately one point higher than build 1.
3. Thrust balance over the operating range was satisfactory during normal operation.
4. The trend of increasing peak overall efficiency with increasing speed observed on build 1 also occurred on build 2.
5. 2nd-stage efficiency was 4 points higher and head rise was 7% higher than build 1, reflecting the reduced clearance on this stage.
6. Suction capability exceeds cycle requirements at conditions corresponding to engine operation at 20% and 100% thrust at mixture ratios $r = 5$ to 7.
7. Cavitation testing at 20% thrust, $r = 7$ (22,100 rpm) resulted in pressure oscillations at inlet pressures slightly below cycle requirements.
8. Cavitating operation at 42,000 rpm near the design Q/N ratio was stable.
9. No pressure decay was experienced at 20% thrust, $r = 5$, (20,575 rpm) with the supply tank vented to ambient pressure. Two phase flow was indicated at pump inlet.
10. Turbine performance was similar to build 1.
11. Turning losses in the turbine are estimated to equal predicted at design conditions.
12. Off-design cycle performance is in excellent agreement with the test data.
13. Higher-than-predicted pump efficiency permits maximum preburner combustion temperature to be reduced by an estimated 46° R.

(c) Rig F35147-1A

This test rig was built to the same configuration as the previous rig (F35138-2) with the following exceptions:

1. The 2nd-stage impeller housing was recontoured in the area of the tip rub to increase the impeller-to-housing clearance by 0.015 to 0.020 in. at this location. The area of contact near the impeller eye was also recontoured to provide additional clearance at the two flow splitter vanes.
2. The 1st-stage impeller was scalloped approximately 0.150 in. between blades to trim the axial thrust balance. This reoperation was to reduce unbalance toward the pump approximately 2500 lb at the low flow, low speed condition where the unbalance was maximum in terms of thrust balance capability (approximately 50%) on the previous tests.
3. The tie bolt stretch was increased 0.003 in. to provide approximately 10,000 lb additional loading because of fretting indications on the interstage splines.
4. A stiffener was incorporated in the internal turbine inlet conical flow duct because of the buckling experienced on this part during the previous testing.
5. A stamped bellows configuration liftoff seal was used instead of the dummy liftoff seal used on rig F35138-2.

During the third and final test series, two tests were completed on fuel turbopump rig F35147-1A for a total rotational time of 83.4 sec. The objectives of this series of test were pump calibration in preparation for hot turbine tests, evaluation of rotor thrust balance, and an operational check of the liftoff seal pressurization control system.

Test No. 1.01 was conducted on 28 May 1970 and was a full duration test at 41 sec. Flow excursions were performed at the 50% (24,000 rpm), 83% (40,000 rpm), and 68% (32,500 rpm) speed levels and a repeat calibration at the 50% (24,000 rpm) level. Data analysis revealed that overall pump performance again exceeded the design goals as was experienced on the first test rig, F35138, builds 1 and 2. Plots of significant turbopump parameters vs time are shown in figures 721 through 724.

Test 2.01 was also a full duration test lasting 36.1 sec and was conducted on 2 June 1970. The test included flow excursions at the 67%, 88%, and 100% speed levels. Analysis of test data indicated that the turbopump performance exceeded the predicted performance. Plots of significant turbopump parameters vs time are shown in figure 725 through 728. On 4 June 1970, following the data analysis of test 2.01, the rig was removed from B-6 test stand in preparation for hot turbine testing on E-8 test stand with the preburner injector and transition case.

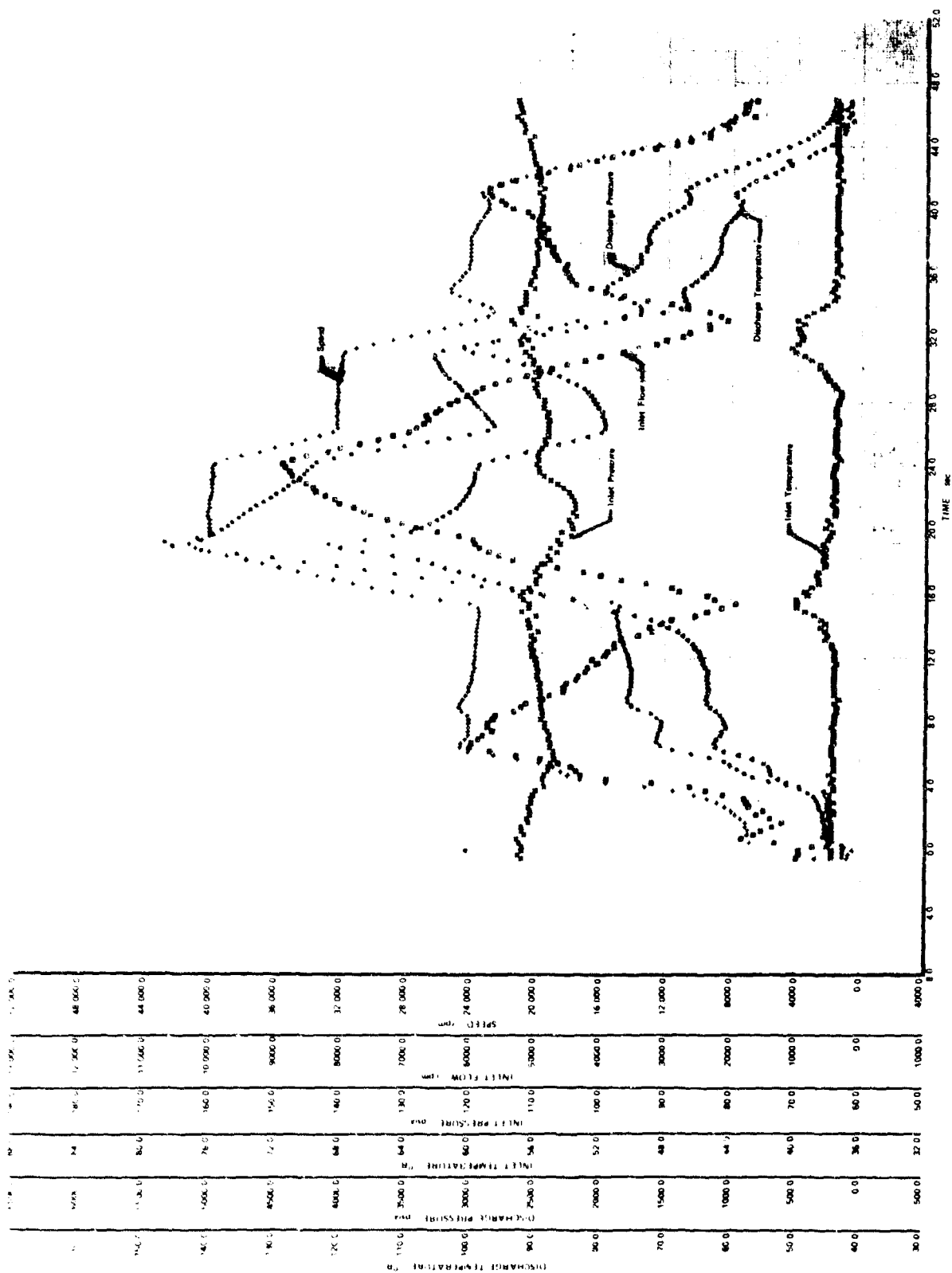


Figure 721. Significant Turbopump Parameters vs Time, Test 1.01, Sheet 1 of 3

FD 40666

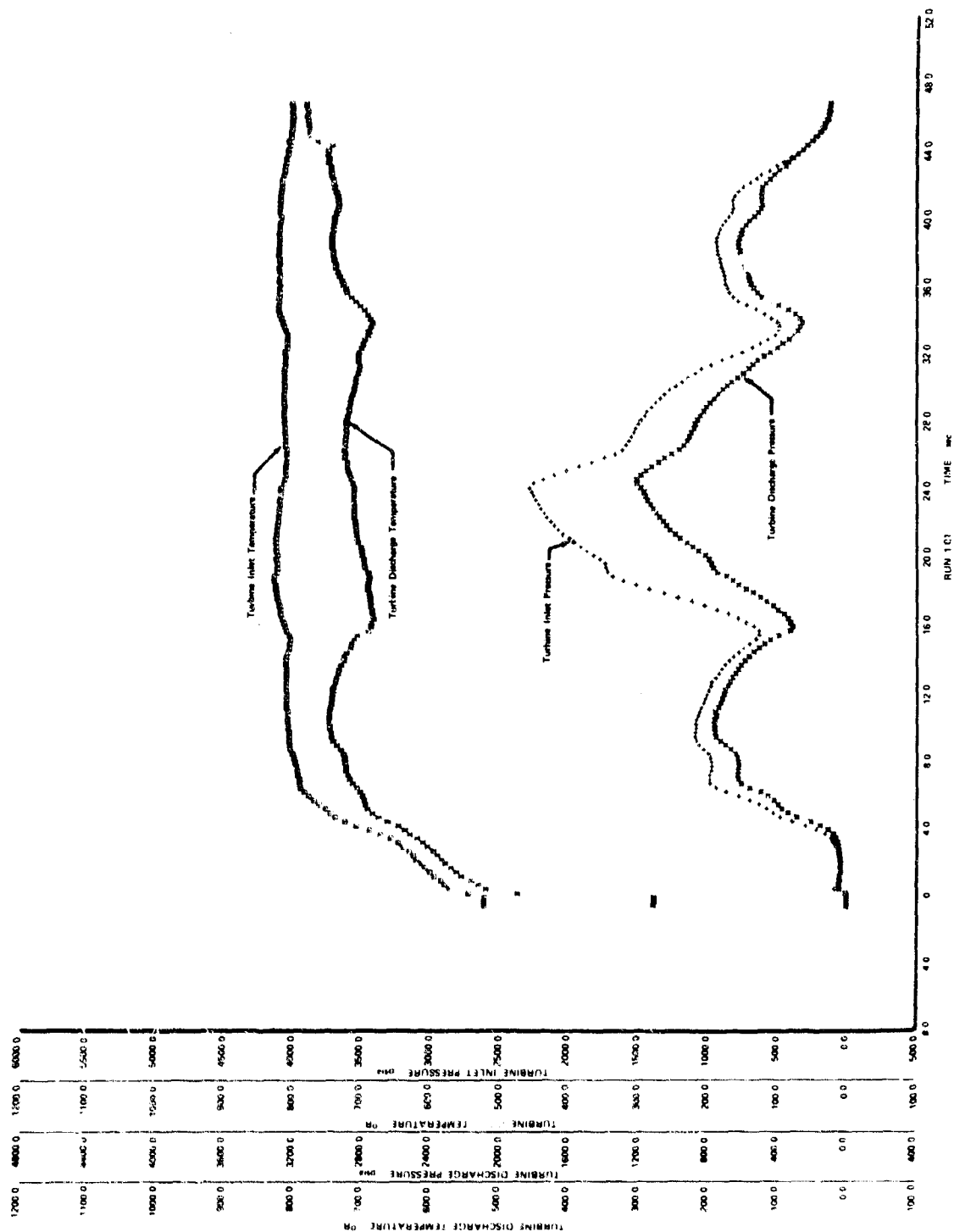


Figure 722. Significant Turbopump Parameters vs Time, Test 1.01, Sheet 2 of 3

FD 40667

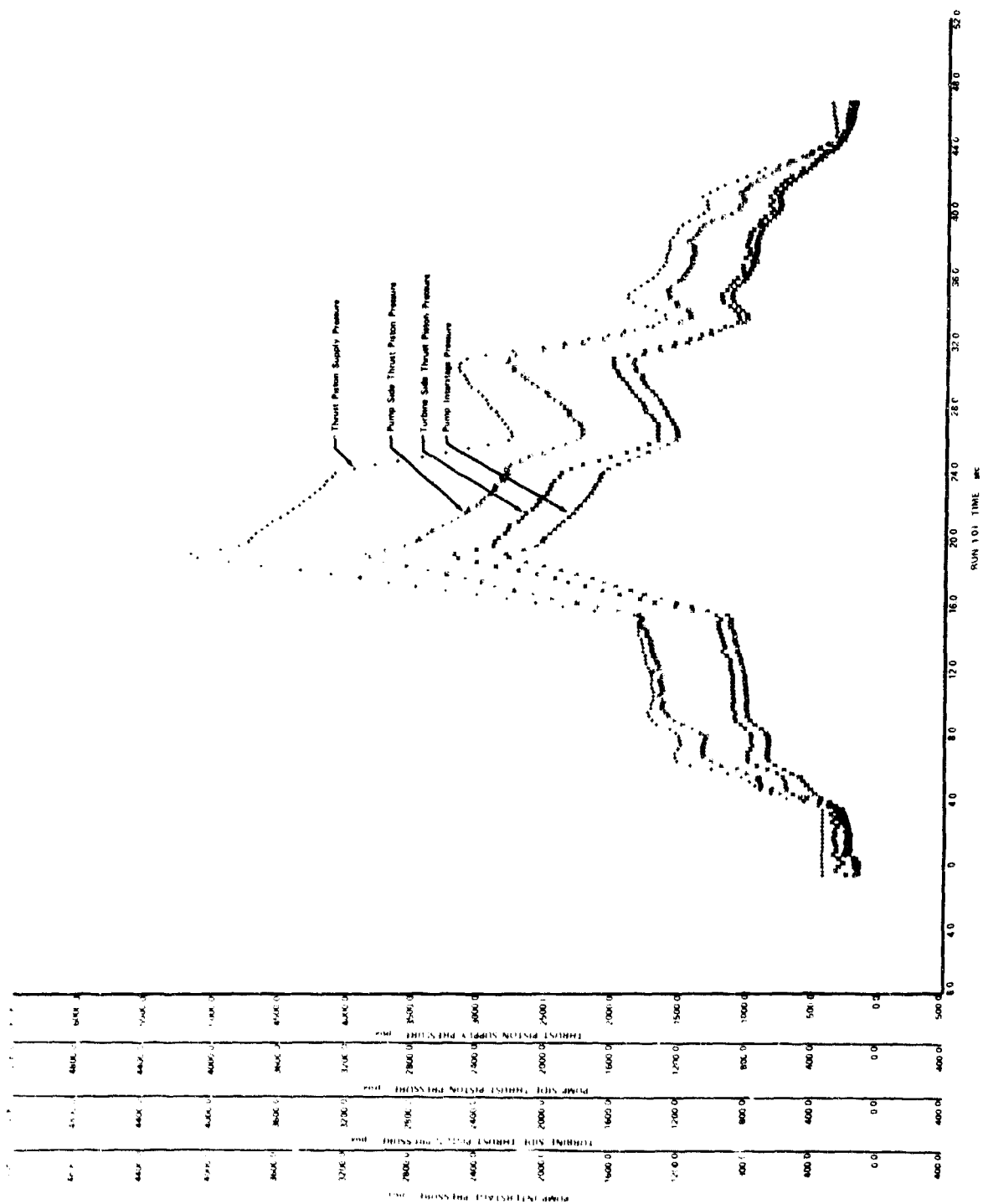


Figure 723. Significant Turbopump Parameters vs Time, Test 1.01, Sheet 3 of 3

FD 40668

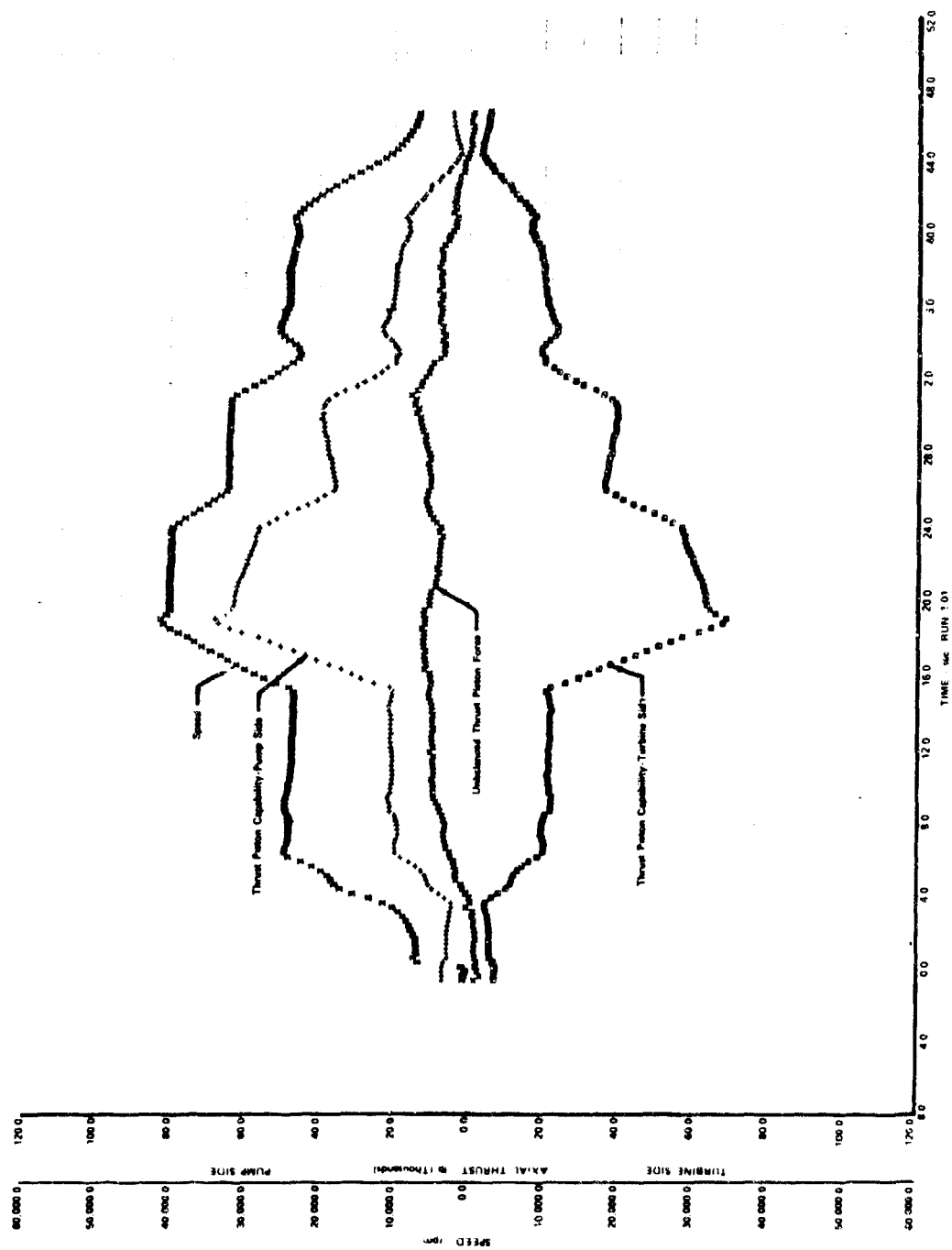


Figure 724. Axial Thrust and Speed vs Time, Test 1.01

FD 40669

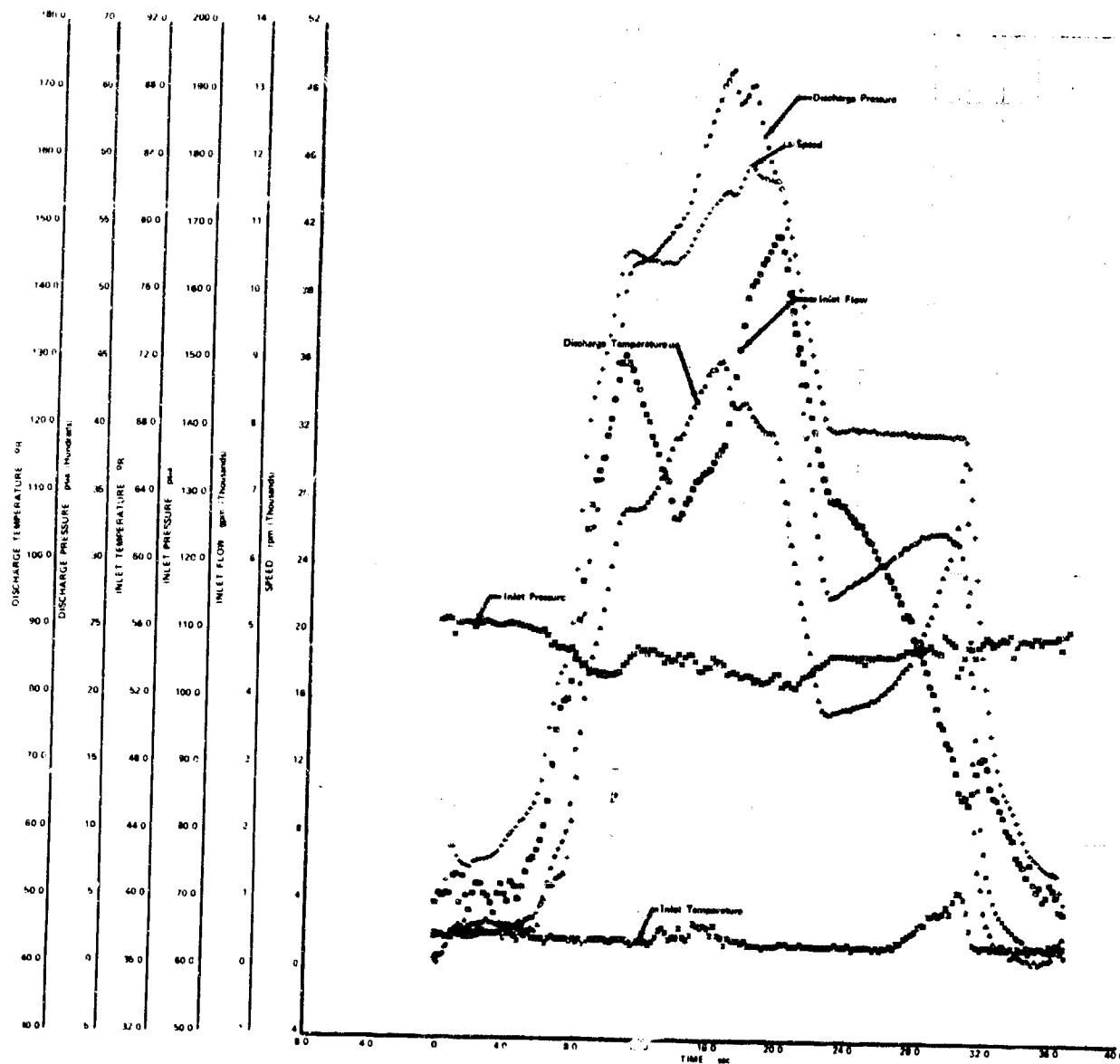


Figure 725. Significant Turbopump Parameters vs Time, Test 2.01, Sheet 1 of 3 FD 40897

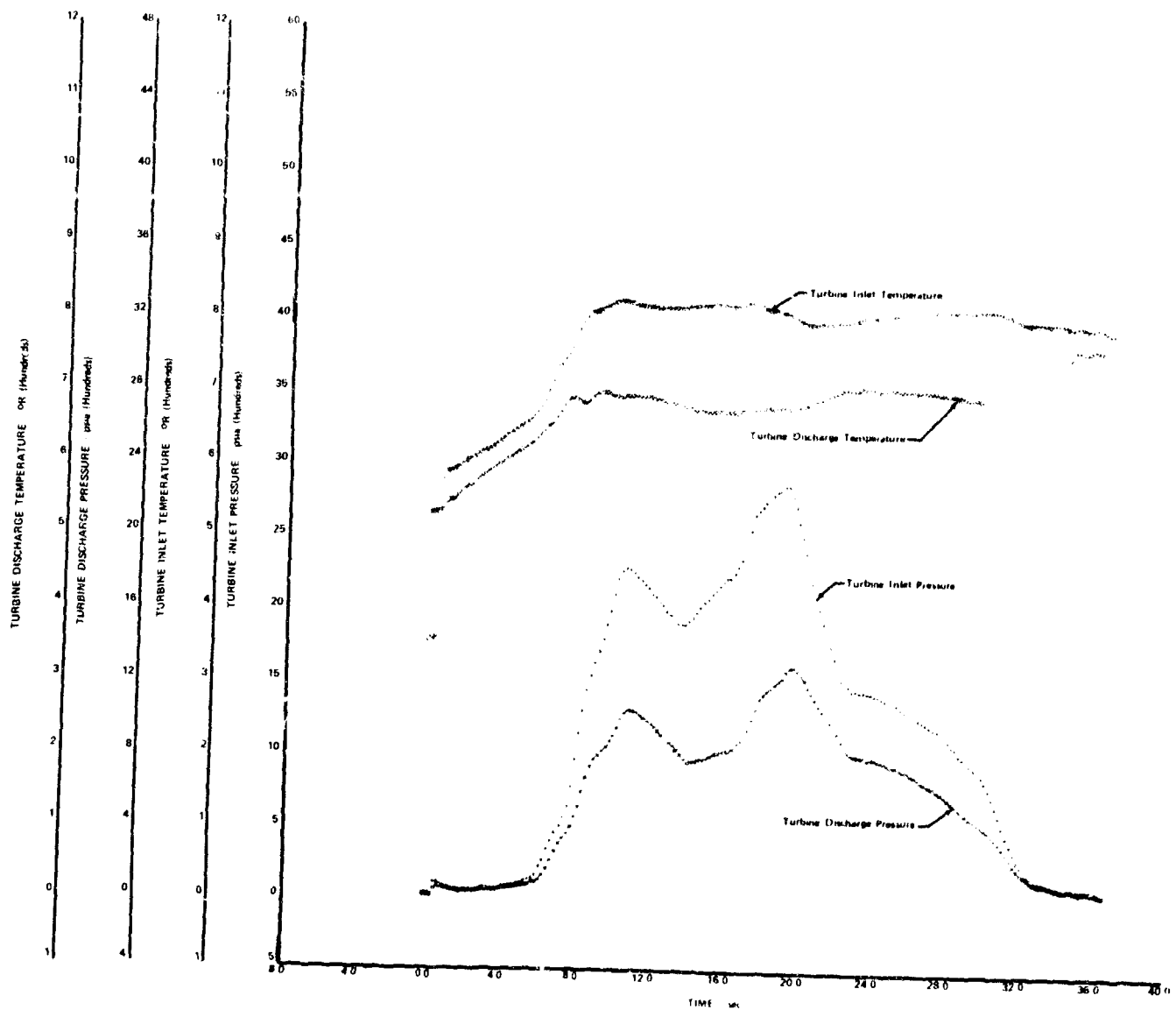


Figure 726. Significant Turbopump Parameters vs Time, Test 2.01, Sheet 2 of 3 FD 40896

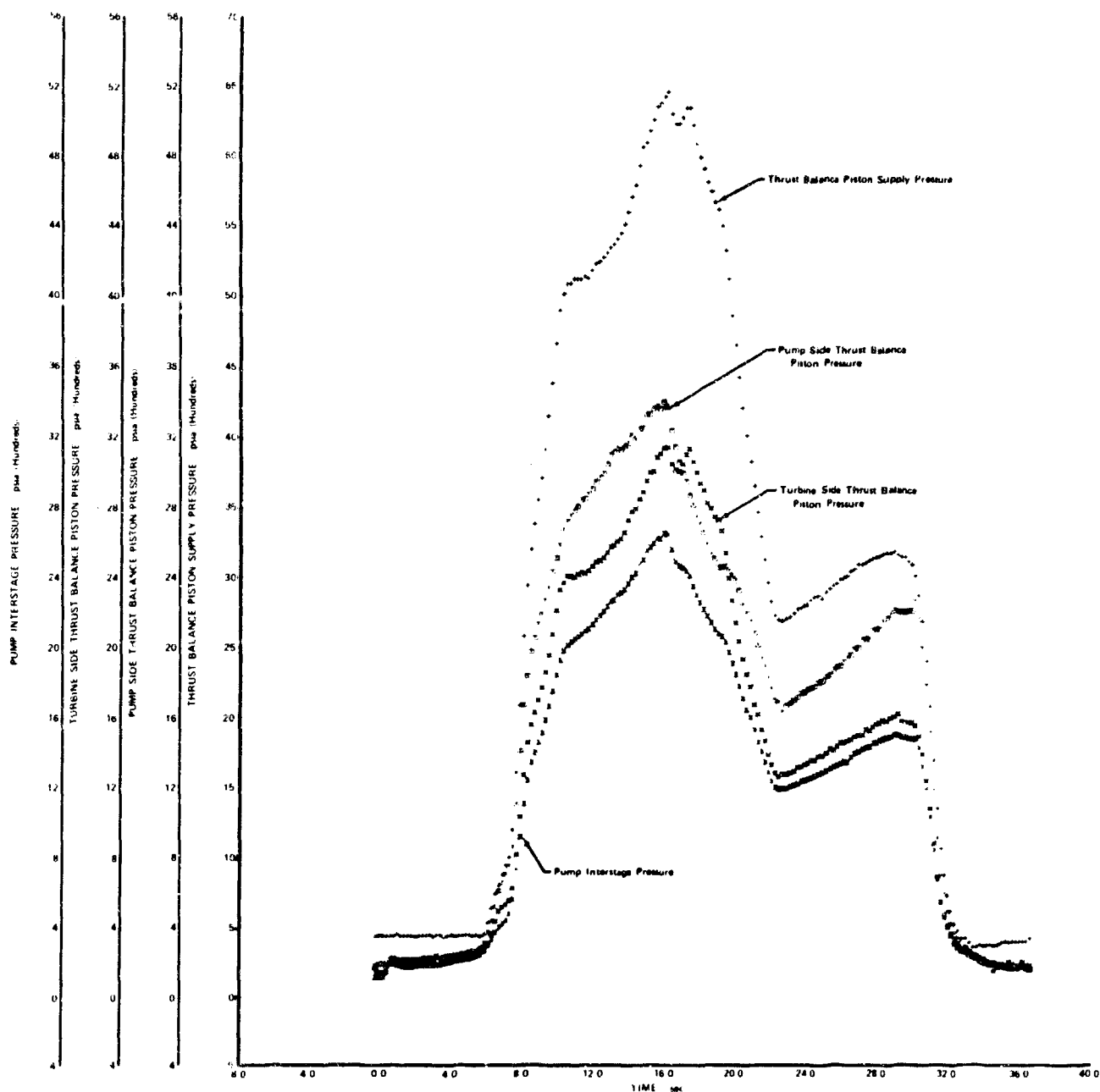


Figure 727. Significant Turbopump Parameters vs Time, Test 2.01, Sheet 3 of 3 FD 40899

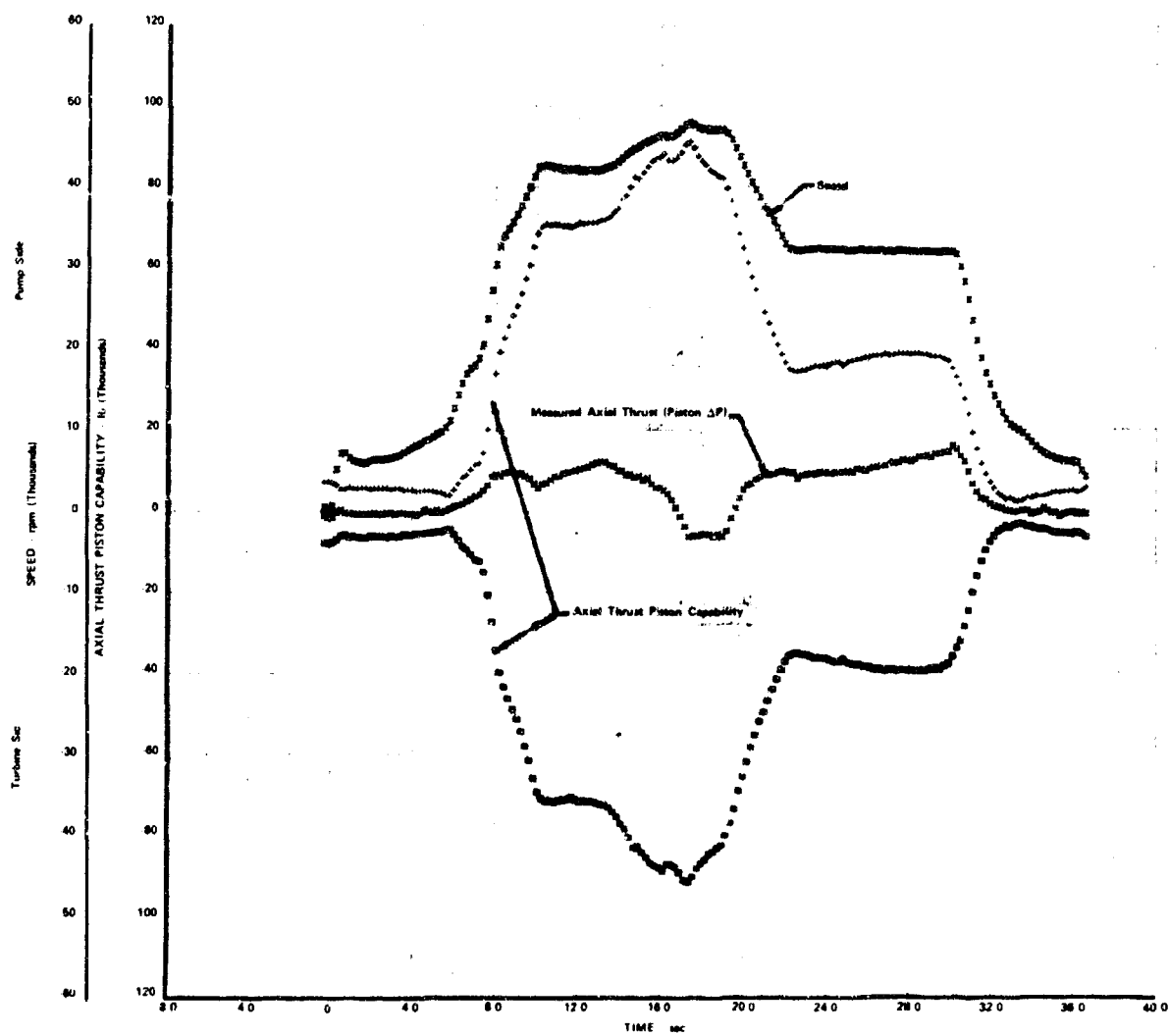


Figure 728. Axial Thrust and Speed vs Time,
Test 2.01

FD 40898

Analysis of test data from these tests indicates close agreement with previous test results obtained during test of rig F35138-2. A moderate decrease in overall performance and stage performance, relative to rig F35138-2 was observed during test 1.01 and 2.01. The overall decrease was attributed to scalloping the 1st-stage impeller and the increase in impeller blade tip-to-housing clearance. Figure 729 shows predicted pump pressure rise vs inlet flow at lines of constant speed with the test data points. Overall efficiency vs inlet unit flow are shown in figure 730, showing design point and off-design characteristics with data points for the tests. Figures 731 and 732 show the 1st- and 2nd-stage pump efficiencies vs flow coefficient data points and the predicted design points and off-design characteristics. Figure 733 shows overall unit head vs inlet unit flow with the design point and cycle requirements indicated. The 1st- and 2nd-stage head coefficient vs flow coefficient characteristics are presented in figures 734 and 735. Figure 736 is a plot of turbine efficiency vs velocity ratio, and the cycle requirement curve and design point are also shown. During tests 1.01 and 2.01, axial thrust balance was satisfactory at all speeds and flowrates, and vibration or impeller rubbing problems were not encountered. Vibration analysis of data obtained during these tests indicates the 1E vibrations measured on the front housing ranged from 3 to 5 g with a peak of 9 g at 48,000 rpm, as shown in figure 737.

As a result of the fuel turbopump tests associated with test rig F35147-1A, it is concluded:

1. At design speed and flow, all design goals were equaled or exceeded.
2. Pressure rise was approximately 7% above predicted values at design speed and flow. Overall efficiency at design speed and flow was 3 points higher than predicted.
3. Thrust balance was satisfactory at all speeds and flows. At design speed and flow, the thrust bearing was operating with 93% margin.
4. Overall efficiency and head rise were generally lower than rig F35138-2 because of 1st-stage impeller scalloping and 2nd-stage tip clearance. Scalloping of the 1st-stage impeller for thrust balance reduced stage efficiency approximately 2 points.
5. Turbine performance was similar to previous builds and is near predicted performance.
6. The excellent operational and performance characteristics of the rig during the two calibration tests demonstrated that this fuel turbopump could be assembled in the hot gas system test rig for continued testing. The hot turbine tests, performed on hot turbine test rig F35155, are described in Section VII.

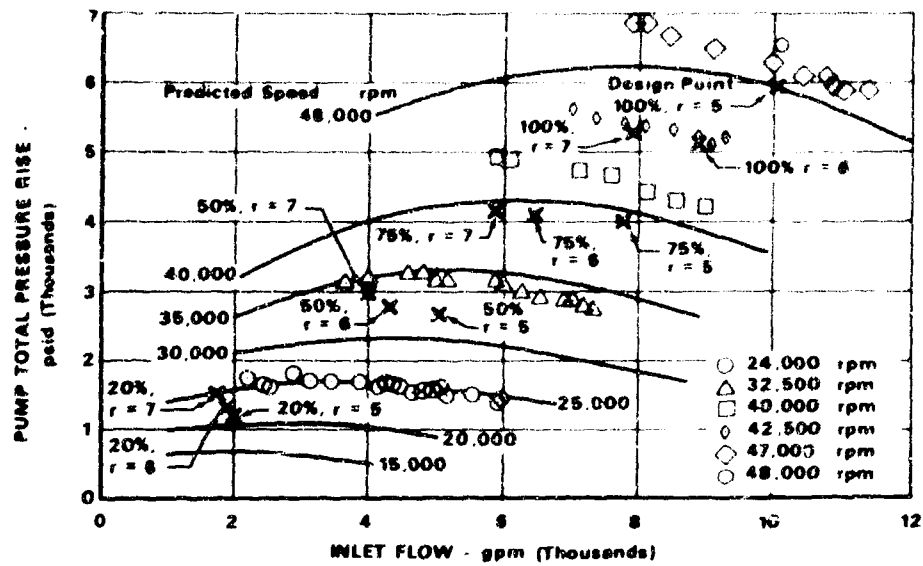


Figure 729. Pump Total Pressure Rise vs Inlet Flow, Rig 35147-1A

FD 41270

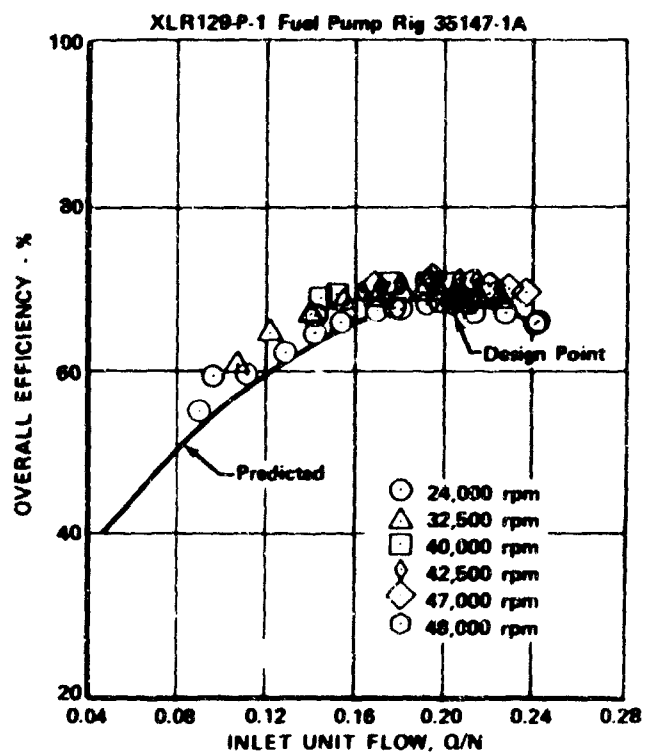


Figure 730. Overall Efficiency vs Inlet Unit Flow, Rig 35147-1A

FD 41271

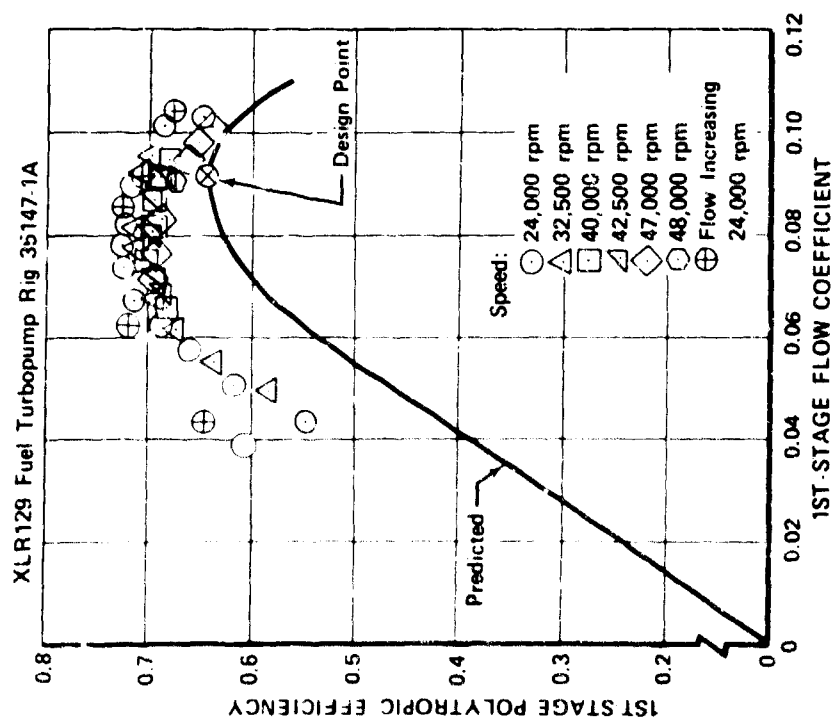


Figure 731. First Stage Efficiency Characteristics

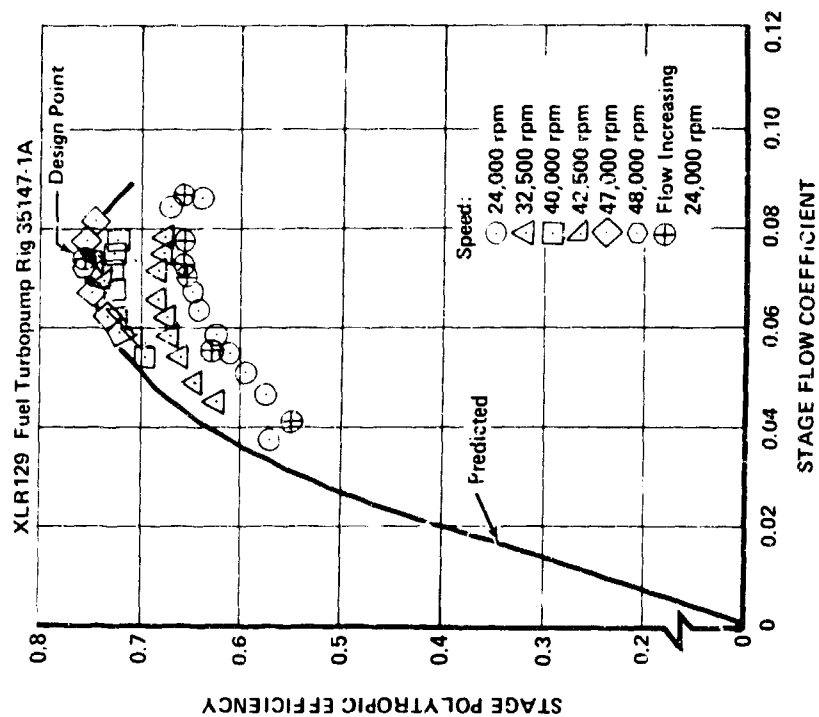


Figure 732. Second Stage Efficiency Characteristics

FD 44218

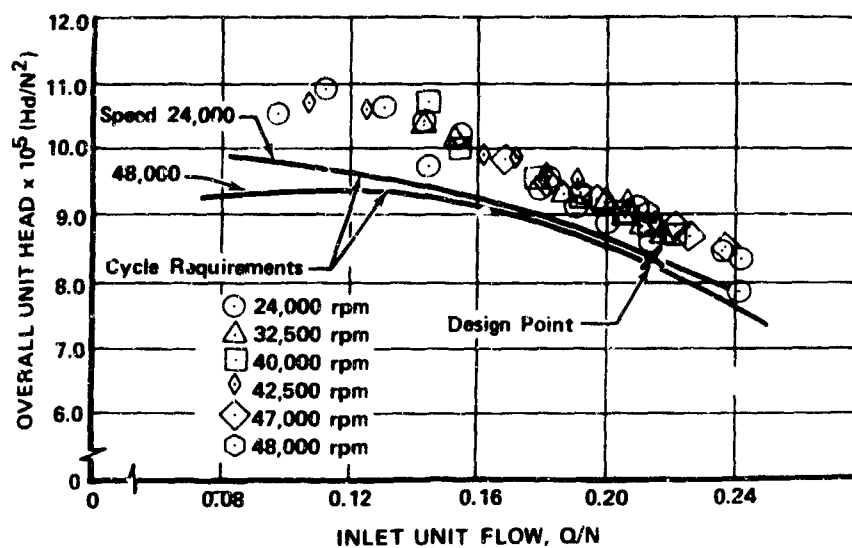


Figure 733. Overall Unit Head vs Inlet Unit Flow, FD 41283
Rig 35147-1A

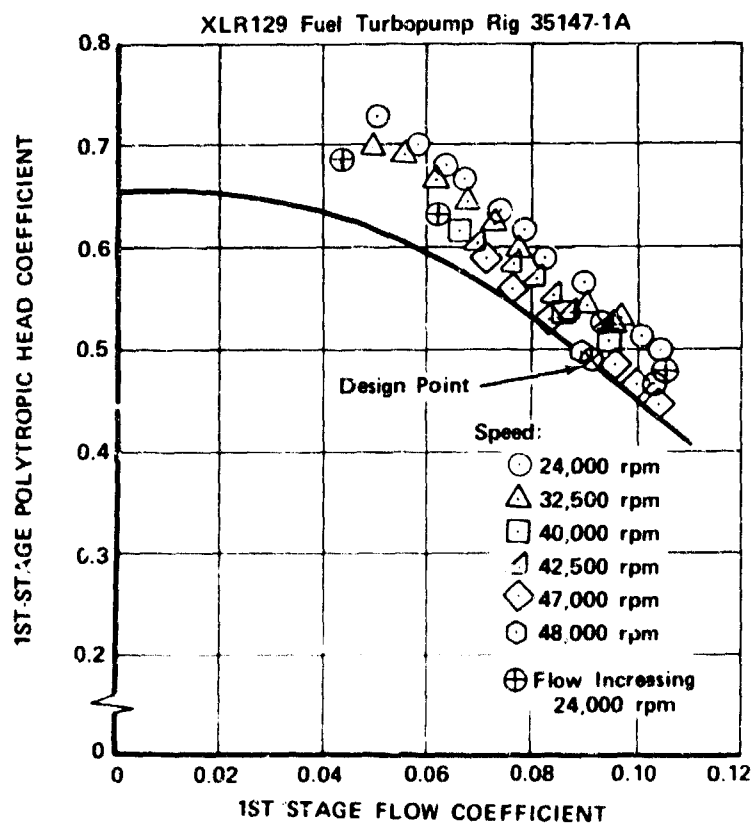


Figure 734. First Stage Head Coefficients FD 44219

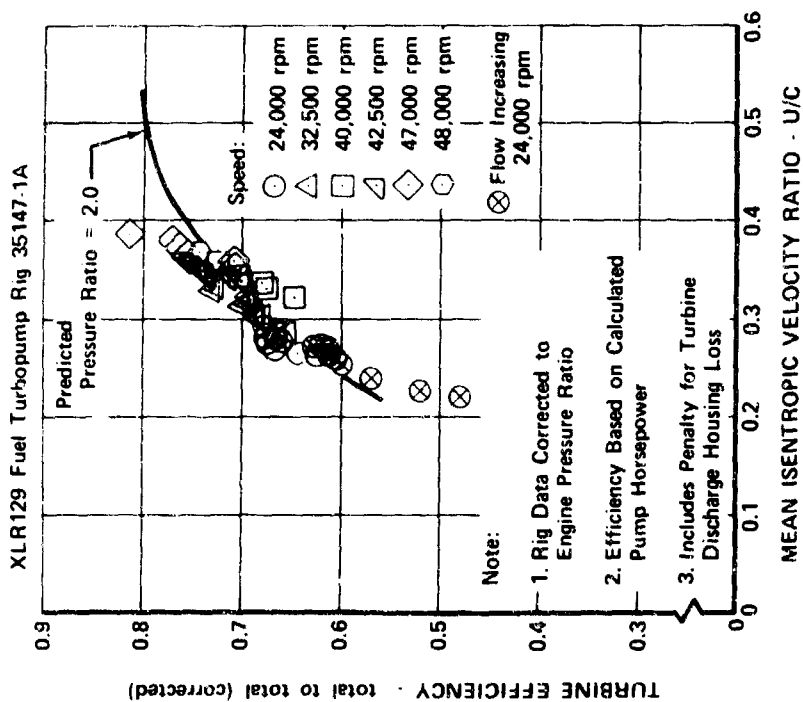
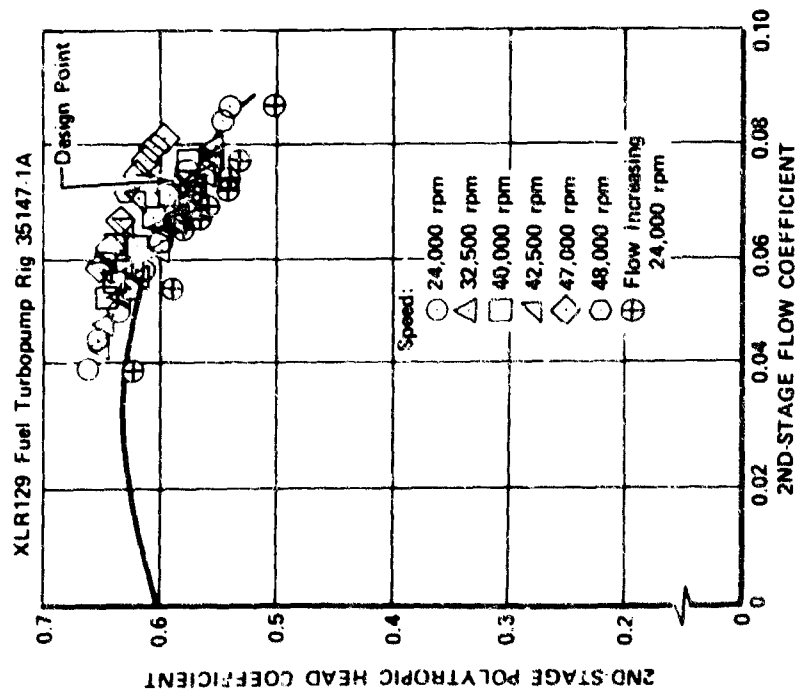


Figure 735. Second Stage Head Coefficients

Figure 736. Turbine Performance

FD 44221

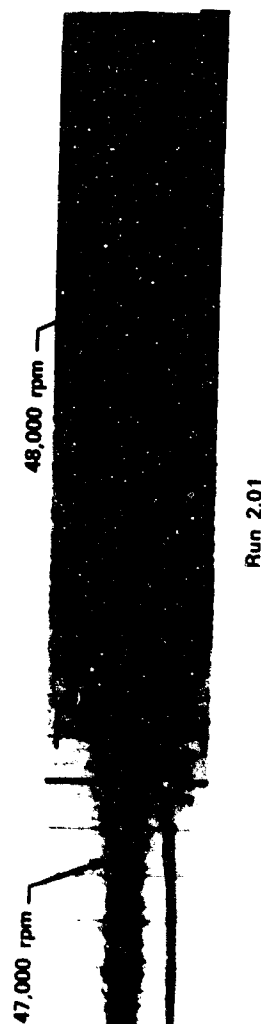
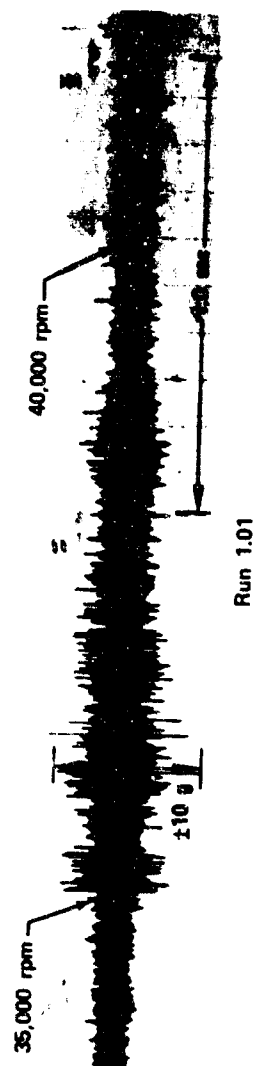


Figure 737. Vibration Trace, Rig 35147-1A, Tests 1.01 and 2.01

FD 45899

c. Data Presentation

Tables LXXXVI and LXXXVII are tabulations of test data obtained throughout the test series. Figure 738 illustrates the fuel pump rig instrumentation.

To establish blueprint flow requirements of the turbine stator castings and to provide turbine power adjustment capability, water flow calibration tests were performed on the "as received" castings as described in Subsection 5. A correlation of the water calibration tests was made with data from the B-6 pump rig tests. Instrumentation problems prevented analysis of the 1st-stage stator due to erratic downstream pressure readings. The 2nd-stage stator effective area vs pressure ratio and the effective area based on water flow test data is presented in figure 739. It was determined that effective area, calculated from the pump rig tests on B-6 with gaseous hydrogen as the turbine drive fluid, was slightly lower than that determined during the water flow testing. However, these data are in close enough agreement to substantiate the validity of both calibration methods. If turbine performance requires an increase or reduction of stator effective area, data from either method may be used to select stators which show the desired percentage change in area when evaluated on a comparative basis.

6. Facilities

Three builds of the fuel turbopump were conducted on turbopump rig F35138-1 on B-6 test stand. The test facility was designed and built for pump rig testing during the 350K fuel turbopump demonstration program. Figure 740 is a schematic of B-6 stand, which uses the fluid pumped as the driving fluid in the following manner. Liquid hydrogen is supplied to the pump inlet, and at the pump discharge approximately 50,000 hp has been added to this fluid. It then passes through the preheater where energy is added from the turbine discharge gas. The fluid proceeds through the second heat exchanger where additional energy is added from a pressurized hot water supply. The fluid then enters the fuel pump turbine at approximately 760°R. Turbine discharge fluid passes through the shell of the preheater and proceeds to a burnstack disposal area. Speed control is provided by a turbine bypass valve. Pump flow control is provided by pump discharge throttle and bleed valves.

Modifications to the test facility before fuel turbopump testing are as follows:

1. A 10,000 gal liquid hydrogen run tank with 195 psia operating pressure was installed to replace the 65 psia transportable liquid hydrogen dewar used during 350K fuel pump testing. This modification was required because the XLR129 fuel turbopump is designed with a lower suction specific speed than the 350K fuel turbopump.
2. The vacuum jacketed propellant inlet line was modified to adapt to the smaller inlet diameter of the XLR129 fuel turbopump.
3. Pump discharge-to-facility plumbing was fabricated to adapt the smaller XLR129 fuel turbopump to the facility.

Table LXXXVI. XLR 129 Fuel Turbopump F35147-1A,
Performance Data Summary.

Run No.	1.01				2.01			
BDR Time	12064.7	12073.2	12077.2	12084.6	3751.7	3756.6	3758.5	3764.4
PS2DP1	1,754	5,103	4,403	3,242	N/A	N/A	N/A	N/A
PS2DP2	1,758	5,080	4,413	3,245	5,257	6,550	6,546	2,852
PSPI21	111.0	116	107	115	108	111.7	106	113
PSPI11	109.0	107	106	110	105	106.1	104	107
PSIND1	162.0	348	180	277	202	371	204	160
PSIS11	399.0	1,042	806	747	919	1,237	1,053	586
PSIF11	246	672	337	493	389	688	414	266
PSIF21	386	987	722	700	816	1,139	924	523
PSIF31	566	1,430	1,188	996	1,344	1,710	1,566	836
PSIDP1	793	2,133	1,740	1,444	2,003	2,596	2,357	1,204
PDIDP2	806	2,149	1,756	1,459	2,019	2,616	2,376	1,215
PSIB11	504	1,305	1,096	906	1,238	1,555	1,452	761
PSIB12	533	1,352	1,121	940	1,270	1,605	1,460	787
PSIB13	527	1,309	1,149	912	1,293	1,571	1,538	803
PS2IP1	793	2,145	1,758	1,450	2,013	2,605	2,376	1,203
PS2IP2	801	2,142	1,759	1,454	2,016	2,604	2,373	1,206
PS2F11	1,008	2,979	2,510	1,985	2,885	3,696	N/A	1,685
PS2F21	1,198	3,412	2,970	2,259	3,472	4,284	4,227	1,979
PS2F31	1,404	3,938	3,490	2,587	4,117	5,087	5,064	2,310
PS2B11	1,131	3,258	2,867	2,095	3,336	4,198	4,230	1,857
PS2B21	1,289	3,598	3,216	2,351	3,705	4,605	4,642	2,117
PS2B31	1,416	3,946	3,520	2,599	4,178	5,108	5,090	2,285
FTPS11	1,702	4,943	4,290	3,148	5,090	6,303	6,285	2,733
PSTB11	1,301	2,990	2,372	2,148	2,725	3,363	2,839	1,686
PSTB12	1,235	2,923	2,322	2,111	2,651	3,353	2,775	1,636
PSTB21	880	2,439	2,027	1,564	N/A	N/A	N/A	N/A
PSTR22	847	2,371	1,959	1,538	2,394	3,050	3,093	1,287
PRBS11	848	1,902	1,718	1,310	1,895	2,407	2,274	1,162
PSTI11	1,107	1,645	2,219	1,275	2,280	2,148	2,656	1,439
PTTI11	N/A	N/A	N/A	N/A	N/A	N/A	N/A	N/A
PTTI12	N/A	N/A	N/A	N/A	N/A	N/A	N/A	N/A
PSTUB1	876	1,093	1,558	920	1,558	1,435	1,796	1,045
PSSU21	912	1,129	1,601	956	1,608	1,465	1,822	1,078
PSDP11	219	521	626	330	N/A	N/A	N/A	N/A
PSDP21	146	415	466	226	557	574	825	274
PSTD12	N/A	N/A	N/A	N/A	N/A	N/A	N/A	N/A
PTTD11	N/A	N/A	N/A	N/A	N/A	N/A	N/A	N/A
PSTD11	N/A	N/A	N/A	N/A	N/A	N/A	N/A	N/A
PTTD21	N/A	N/A	N/A	N/A	N/A	N/A	N/A	N/A
PSTD21	N/A	N/A	N/A	N/A	N/A	N/A	N/A	N/A
PSTD31	780	679	1,122	716	1,034	802	1,020	798
TPI-2R	37.5	38.2	37.7	38.5	37.9	38.7	37.9	37.6
TPI-3R	37.3	38.2	37.8	38.4	N/A	38.7	N/A	N/A
TID-1R	N/A	N/A	N/A	N/A	66.5	75.7	72.5	54.7
TID-2R	48.2	71.7	62.8	60.2	66.5	75.6	72.4	54.7
TIL-11	70.9	128	114	97.7	123	145.7	142	89.6
TMHD1	N/A	N/A	N/A	N/A	N/A	N/A	N/A	N/A
T2I-1R	48.9	72.3	63.9	60.8	67.2	76.7	73.4	55.3
T2I-2R	48.6	72.4	63.7	60.6	67.2	76.7	73.4	55.0
T2D-1R	63.4	117	100.3	89.6	108.9	129.9	124.6	79.2
T2D-2R	63.3	117	99.8	89.6	108.8	130.8	124.8	78.9
TTI-11	813	833	828	821	823	821	821	805
TTI-21	N/A	N/A	N/A	N/A	N/A	N/A	821	N/A
TTI-31	816	838	834	826	826	825	826	810
TTD-11	N/A	N/A	N/A	N/A	N/A	N/A	N/A	N/A
TTD-21	752	696	718	719	695	673	678	707
RPM-11	N/A	N/A	N/A	N/A	42,946	46,045	46,051	32,469
RPM-31	24,219	40,393	40,101	32,219	42,953	46,040	46,055	32,499
FLOW	4,610	5,781	8,525	4,875	9,110	7,630	10,133	7,006

Table LXXXVII. XLR129 Fuel Turbopump F35138-1 and -2.

R. No.	B-01										C-01										D-01										E-01										F-01										G-01										H-01										I-01										J-01										K-01										L-01										M-01										N-01										O-01										P-01										Q-01										R-01										S-01										T-01										U-01										V-01										W-01										X-01										Y-01										Z-01									
	1-01		2-01		3-01		4-01		5-01		6-01		7-01		8-01		9-01		10-01		11-01		12-01		13-01		14-01		15-01		16-01		17-01		18-01		19-01		20-01		21-01		22-01		23-01		24-01		25-01		26-01		27-01		28-01		29-01		30-01		31-01		32-01		33-01		34-01		35-01		36-01		37-01		38-01		39-01		40-01		41-01		42-01		43-01		44-01		45-01		46-01		47-01		48-01		49-01		50-01		51-01		52-01		53-01		54-01		55-01		56-01		57-01		58-01		59-01		60-01		61-01		62-01		63-01		64-01		65-01		66-01		67-01		68-01		69-01		70-01		71-01		72-01		73-01		74-01		75-01		76-01		77-01		78-01		79-01		80-01		81-01		82-01		83-01		84-01		85-01		86-01		87-01		88-01		89-01		90-01		91-01		92-01		93-01		94-01		95-01		96-01		97-01		98-01		99-01		100-01																																																			
	1001	1002	1003	1004	1005	1006	1007	1008	1009	1010	1011	1012	1013	1014	1015	1016	1017	1018	1019	1020	1021	1022	1023	1024	1025	1026	1027	1028	1029	1030	1031	1032	1033	1034	1035	1036	1037	1038	1039	1040	1041	1042	1043	1044	1045	1046	1047	1048	1049	1050	1051	1052	1053	1054	1055	1056	1057	1058	1059	1060	1061	1062	1063	1064	1065	1066	1067	1068	1069	1070	1071	1072	1073	1074	1075	1076	1077	1078	1079	1080	1081	1082	1083	1084	1085	1086	1087	1088	1089	1090	1091	1092	1093	1094	1095	1096	1097	1098	1099	1100	1101	1102	1103	1104	1105	1106	1107	1108	1109	1110	1111	1112	1113	1114	1115	1116	1117	1118	1119	1120	1121	1122	1123	1124	1125	1126	1127	1128	1129	1130	1131	1132	1133	1134	1135	1136	1137	1138	1139	1140	1141	1142	1143	1144	1145	1146	1147	1148	1149	1150	1151	1152	1153	1154	1155	1156	1157	1158	1159	1160	1161	1162	1163	1164	1165	1166	1167	1168	1169	1170	1171	1172	1173	1174	1175	1176	1177	1178	1179	1180	1181	1182	1183	1184	1185	1186	1187	1188	1189	1190	1191	1192	1193	1194	1195	1196	1197	1198	1199	1200																																																		
1001	1002	1003	1004	1005	1006	1007	1008	1009	1010	1011	1012	1013	1014	1015	1016	1017	1018	1019	1020	1021	1022	1023	1024	1025	1026	1027	1028	1029	1030	1031	1032	1033	1034	1035	1036	1037	1038	1039	1040	1041	1042	1043	1044	1045	1046	1047	1048	1049	1050	1051	1052	1053	1054	1055	1056	1057	1058	1059	1060	1061	1062	1063	1064	1065	1066	1067	1068	1069	1070	1071	1072	1073	1074	1075	1076	1077	1078	1079	1080	1081	1082	1083	1084	1085	1086	1087	1088	1089	1090	1091	1092	1093	1094	1095	1096	1097	1098	1099	1100	1101	1102	1103	1104	1105	1106	1107	1108	1109	1110	1111	1112	1113	1114	1115	1116	1117	1118	1119	1120	1121	1122	1123	1124	1125	1126	1127	1128	1129	1130	1131	1132	1133	1134	1135	1136	1137	1138	1139	1140	1141	1142	1143	1144	1145	1146	1147	1148	1149	1150	1151	1152	1153	1154	1155	1156	1157	1158	1159	1160	1161	1162	1163	1164	1165	1166	1167	1168	1169	1170	1171	1172	1173	1174	1175	1176	1177	1178	1179	1180	1181	1182	1183	1184	1185	1186	1187	1188	1189	1190	1191	1192	1193	1194	1195	1196	1197	1198	1199	1200																																																			

5138-1 and -2, Performance Data Summary

Table 2															
7.01				8.01				9.01				10.01			
1629.001	1634.210	1639.205	1644.200	1649.013	1654.200	1659.708	1664.000	1669.008	1674.008	1679.008	1684.008	1689.008	1694.008	1699.008	1704.008
1.842	5.011	5.298	5.775	6.092	6.195	6.015	1.275	1.601	1.742	5.610	5.491	5.471	5.409	5.096	1.212
1.862	5.711	5.712	5.814	6.115	6.217	6.011	1.219	1.395	1.517	5.610	5.481	5.470	5.316	5.114	1.204
114	198	112	115	111	101	110	62	71	70	88	46	35	72	31	25
111	109	112	110	108	105	109	56	55	56	88	46	36	73	31	23
161	116	184	171	171	191	151	211	163	180	259	190	178	163	42	98
117	977	951	1,210	1,091	642	763	408	436	436	1,041	996	974	940	785	298
211	215	322	351	351	219	307	286	329	329	498	448	439	328	152	197
116	871	867	1,111	1,108	375	711	389	410	395	985	928	916	867	686	285
579	1,451	1,361	1,301	1,047	1,062	981	529	551	551	1,415	1,385	1,368	1,119	1,182	394
812	1,984	1,919	2,121	2,110	2,251	1,209	1,188	715	715	2,141	2,091	2,076	1,965	1,902	546
821	2,005	1,990	2,141	2,129	2,291	1,211	1,190	716	716	2,171	2,114	2,100	2,009	1,931	552
311	1,396	1,297	1,315	1,361	1,511	821	928	498	521	1,484	1,328	1,316	1,288	1,116	169
572	1,106	N A	N A	N A	N A	N A	N A	N A	N A	N A	N A	N A	N A	N A	N A
555	1,520	1,161	1,125	1,177	1,165	861	910	498	525	1,416	1,158	1,145	1,140	1,114	151
809	2,008	1,977	2,149	2,126	2,281	1,212	1,199	726	726	2,136	2,094	2,081	1,995	1,925	547
812	2,002	1,975	2,137	2,124	2,279	1,211	1,194	727	719	2,138	2,100	2,087	1,994	1,922	550
1,101	2,995	2,869	3,192	3,143	3,191	1,726	1,659	988	978	3,110	3,051	3,031	2,901	2,744	781
1,268	3,609	3,197	3,132	3,092	3,027	2,005	2,184	1,108	1,077	4,199	4,136	4,151	4,128	4,261	888
1,163	4,146	4,172	4,301	4,128	4,250	2,115	1,298	1,218	1,218	4,173	4,123	4,109	4,008	3,911	1,001
1,140	4,619	4,117	4,029	4,028	4,030	2,067	1,012	983	1,011	4,101	4,109	4,101	4,115	4,140	770
1,129	4,018	3,715	4,051	4,062	4,108	2,207	1,163	1,125	1,125	4,095	4,041	4,026	4,127	4,157	915
1,302	4,144	4,116	4,109	4,018	4,018	2,212	1,292	1,211	1,211	4,109	4,108	4,101	4,117	4,141	1,011
1,905	5,190	5,190	5,111	5,025	5,014	2,318	1,163	1,197	1,197	5,171	5,116	5,126	5,207	5,261	1,261
1,125	2,109	2,109	3,110	3,110	2,101	1,109	1,109	1,091	1,091	2,919	2,757	2,759	2,844	2,901	856
1,112	2,101	2,100	3,099	3,112	2,108	1,101	1,011	1,011	1,011	2,866	2,755	2,755	2,759	2,771	851
851	2,102	2,291	2,552	2,671	2,726	1,118	1,118	711	711	2,144	2,147	2,147	2,198	2,162	540
816	2,115	2,110	2,171	2,171	2,171	1,111	1,111	711	711	1,944	1,895	1,874	1,892	1,881	584
860	2,011	1,911	2,116	2,122	2,141	1,111	1,111	611	611	1,944	1,895	1,874	1,892	1,881	584
1,188	3,007	2,709	2,008	2,011	2,011	1,011	1,011	611	611	2,115	2,115	2,115	2,115	2,115	511
1,236	3,111	2,619	2,111	2,111	2,111	1,109	1,109	499	499	2,115	2,115	2,111	2,111	2,111	511
1,210	3,111	N A	N A	N A	N A	N A	N A	N A	N A	N A	N A	N A	N A	N A	N A
912	1,900	1,187	1,111	1,111	1,111	1,111	1,111	411	411	1,111	1,111	1,111	1,111	1,111	411
956	2,002	1,716	1,100	1,111	1,111	1,111	1,111	411	411	1,111	1,111	1,111	1,111	1,111	411
102	N A	808	706	706	706	411	411	294	294	1,111	1,111	1,111	1,111	1,111	411
172	711	611	611	611	611	291	291	222	222	1,111	1,111	1,111	1,111	1,111	411
N A	N A	N A	N A	N A	N A	N A	N A	N A	N A	N A	N A	N A	N A	N A	N A
819	1,101	1,122	1,101	1,101	1,101	1,101	1,101	1,101	1,101	1,101	1,101	1,101	1,101	1,101	1,101
819	1,174	1,128	975	975	975	975	975	601	601	1,111	1,111	1,111	1,111	1,111	411
816	1,110	1,291	1,001	911	1,011	1,011	1,011	611	611	1,111	1,111	1,111	1,111	1,111	411
780	1,191	1,104	811	790	920	611	611	111	111	911	911	911	1,101	1,101	509
819	1,111	1,207	911	872	1,210	861	611	111	111	1,010	1,025	1,025	1,207	1,201	516
17.2	17.2	17.1	18.9	18.8	17.1	17.1	18.7	17.1	17.1	17.1	17.1	17.1	17.1	17.1	17.1
17.2	17.1	17.1	18.7	18.7	17.1	17.1	18.7	17.1	17.1	17.1	17.1	17.1	17.1	17.1	17.1
17.2	N A	61.8	72.1	71.1	68.2	71.1	71.1	30.1	30.1	66.0	N A	N A	N A	N A	N A
17.2	81.1	61.1	72.1	71.1	68.2	71.1	71.1	30.1	30.1	66.0	N A	N A	N A	N A	N A
69.1	111.1	112.1	116.2	116.2	116.2	116.2	116.2	116.2	116.2	116.2	116.2	116.2	116.2	116.2	116.2
70.1	101.8	92.0	117.8	117.8	117.8	N A	N A	N A	N A	N A	N A	N A	N A	N A	N A
48.1	69.6	61.1	72.1	71.1	70.1	71.1	71.1	30.1	30.1	67.1	67.1	67.1	67.1	67.1	67.1
48.7	69.8	61.1	72.1	71.1	70.1	71.1	71.1	30.1	30.1	67.1	67.1	67.1	67.1	67.1	67.1
61.1	N A	107.1	121.1	121.1	121.1	N A	N A	N A	N A	110	110	110	110	110	110
62.1	N A	109.9	121.1	121.1	121.1	N A	N A	N A	N A	110	110	110	110	110	110
607	811	811	811	811	811	811	811	811	811	811	811	811	811	811	811
701	811	811	811	811	811	811	811	811	811	811	811	811	811	811	811
N A	N A	N A	N A	N A	N A	N A	N A	N A	N A	N A	N A	N A	N A	N A	N A
736	N A	00	690	691	691	691	691	691	691	691	691	691	691	691	691
740	692	691	691	691	691	691	691	691	691	691	691	691	691	691	691
11,711	46,077	42,171	42,171	41,171	41,171	41,171	41,171	41,171	41,171	41,171	41,171	41,171	41,171	41,171	41,171
21,098	46,012	42,171	42,171	41,171	41,171	41,171	41,171	41,171	41,171	41,171	41,171	41,171	41,171	41,171	41,171
1,848	11,478	9,301	6,011	6,818	10,010	1,120	1,800	1,120	1,110	7,815	7,850	7,820	8,015	8,010	1,811



FD 44515

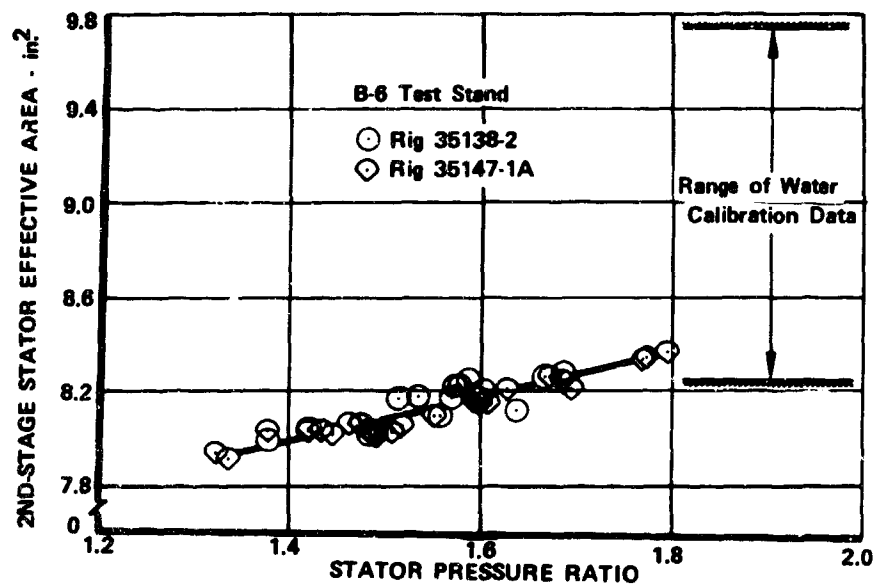


Figure 739. Fuel Pump 2nd-Stage Stator Calibration Data

FD 45329

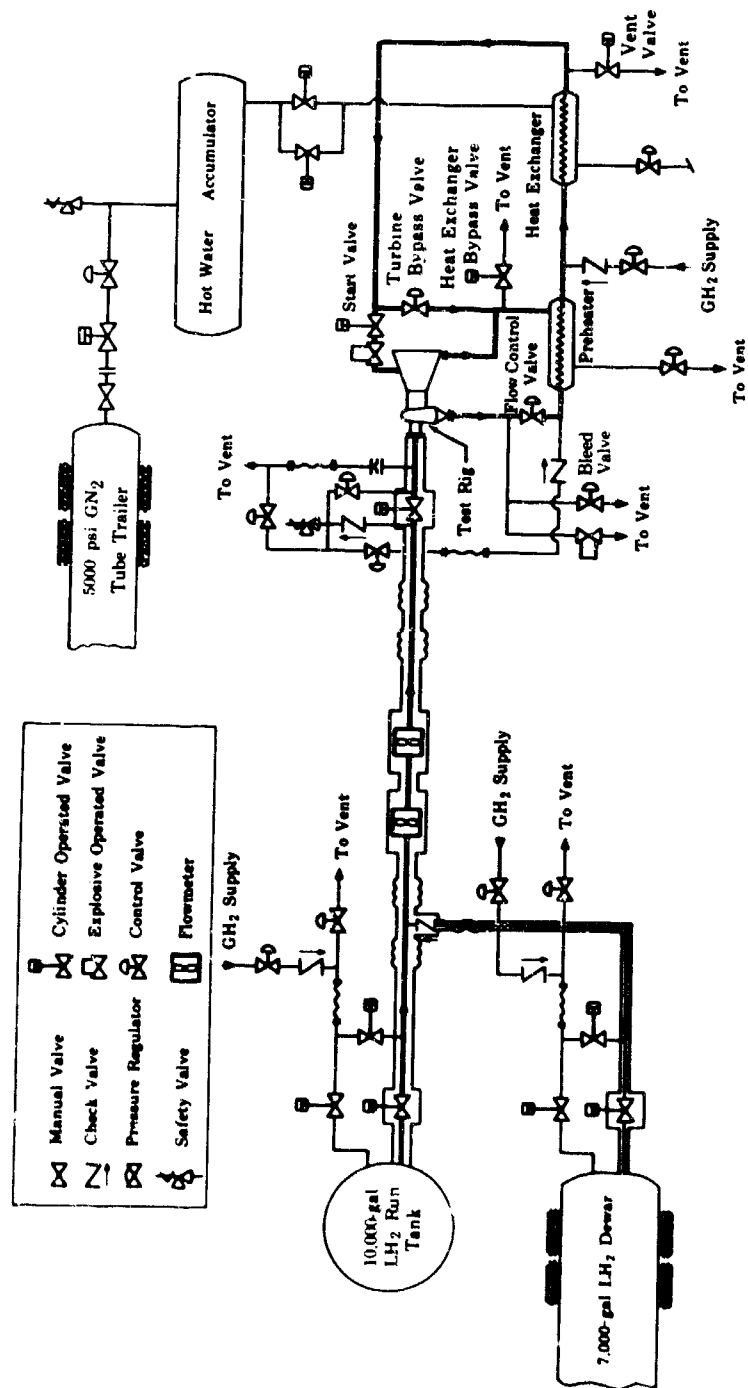


Figure 740. Test Facility Schematic

FD 13544D

An additional system was installed in the test facility to provide an external supply of ambient hydrogen or helium to the thrust balance piston for start and shutdown transients. This pressurizing system is actuated just before start and supplies 600 psia ambient gaseous hydrogen or helium to the thrust piston faces. The external system is shut off by a check valve when pump 2nd-stage discharge pressure exceeds the external supply pressure. Likewise during the shutdown transient, when the pump discharge pressure diminishes, the external supply again pressurizes the thrust balance piston. This system was used on the initial test series with gaseous hydrogen and successfully prevented the thrust balance piston from contacting rub faces during low speed pump operation. On subsequent tests, helium was used to evaluate the potential of this system in acting as a purge to prevent back flow of the hot preburner gases from the turbine during start transients occurring during the tests with the preburner, transition case, and fuel turbopump combined as a powerhead assembly. One test was also conducted with no external pressurization of the thrust piston, to demonstrate the capability of the thrust balance system to operate with only the pressure provided by the fuel turbopump. Thrust balance system operation was satisfactory in all three modes.

G. OXIDIZER TURBOPUMP

1. Introduction

The oxidizer turbopump, shown in figures 741 and 742, supplies liquid oxygen to the preburner injector and main burner injector at the prescribed pressures and flow rates for engine operation between 20 and 100% of maximum thrust within a mixture ratio range of 5 to 7. The oxidizer turbopump delivers liquid oxygen at a flow rate of 481 lb/sec and a pressure of 4800 psia at 100% thrust, and a mixture ratio of 7. The two-stage turbine delivers a maximum of 18,000 hp to the pump and operates at a maximum turbine inlet temperature of 2325°R.

The oxidizer turbopump is a single-shaft unit consisting of a single-stage, shrouded, centrifugal impeller driven by a full admission, axial flow, two-stage, pressure-compounded turbine having cooled disks and uncooled airfoils. The rotor shaft is supported by two antifriction ball bearings. The rear bearing is cooled by liquid hydrogen and the front bearing is cooled by liquid oxygen. The bearings are separated by a low leakage seal package that vents overboard.

2. Summary, Conclusions and Recommendations

The design layouts and detail parts prints were completed. Raw material and 95% of the detail parts were placed on order. Many of these were received. Some major parts such as bearings, turbine blade castings, the first impeller detail, partial orders of the stators and exit guide vane castings were also received.

The detail parts on order were placed on a hold status in January 1970 in an effort to limit program expenditures. These parts were reviewed to determine the cost of completion versus cancellation. Selected hardware for support of powerhead testing and parts nearing completion were allowed to continue working. All outstanding orders were cancelled in March 1970 because the program would not continue after August 1970. Fabrication of the oxidizer turbopump hardware was approximately 45% complete when terminated.



Figure 741. Oxidizer Turbopump Location

FD 35679

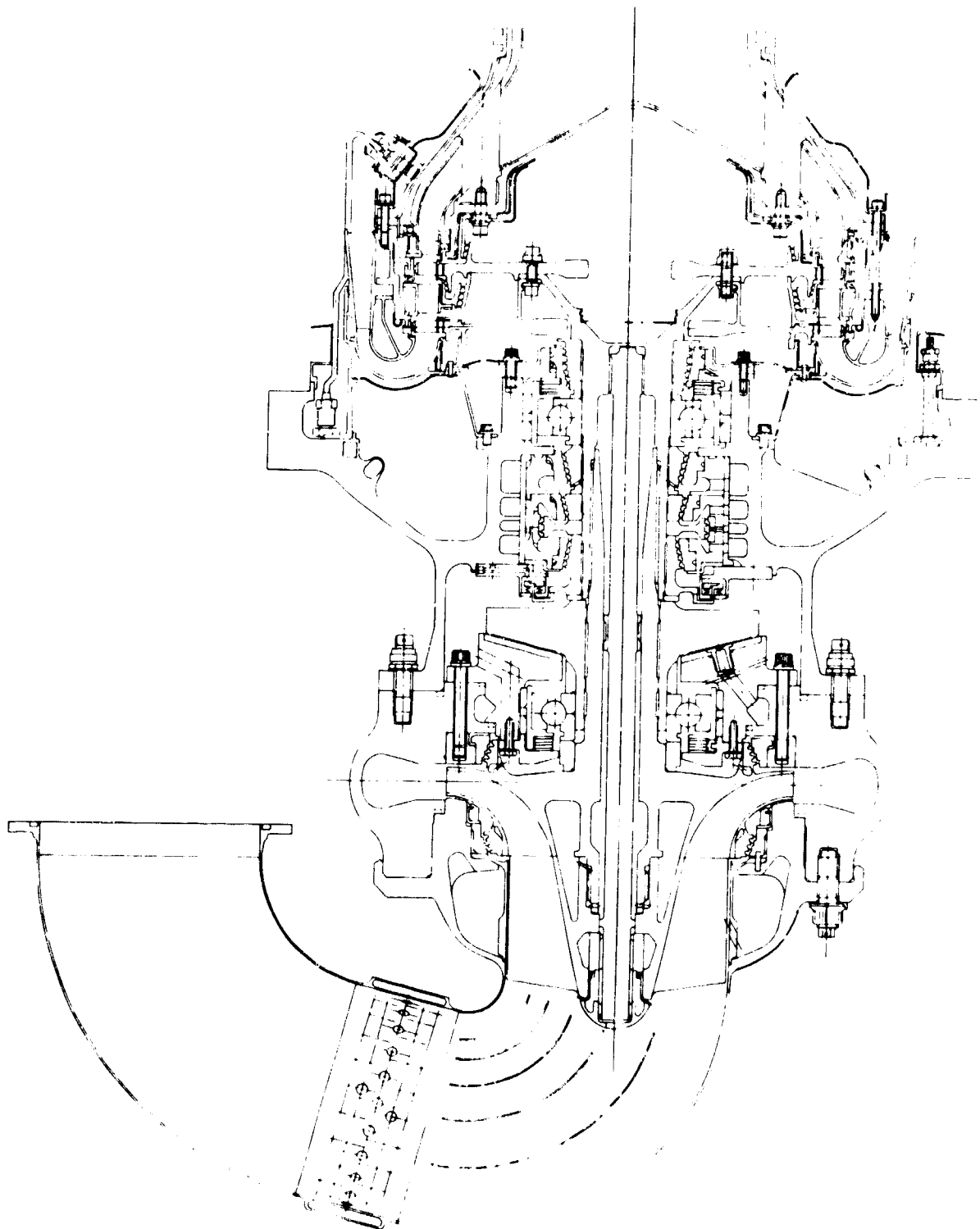


Figure 742. Oxidizer Turbopump Assembly

GS 12356.A

It is recommended that procurement be continued, and that a turbopump be assembled for testing to demonstrate the performance and design goals of the XLR129-P-1 oxidizer turbopump.

3. Hardware Description

The oxidizer turbopump consists of a pump, turbine, and housings. A description of each of these major components follows:

a. Pump

The pump section of the oxidizer turbopump includes the inducer, impeller, bearings and bearing supports, thrust balance system, and seal package.

(1) High-Speed Inducer

The high-speed inducer, shown in figure 743, consists of three unshrouded helical blades spaced 120 deg apart, with a constant tip diameter.

The inducer has an internal spline which engages mating splines on the oxidizer turbopump impeller, and absorbs inducer torque. A 50,000-lb load is applied during stackup by a hydraulic ram that pulls the tie bolt while compressing the rotor stackup. The spanner nut is then bottomed on the inducer hub and the ram load is released. The full tie bolt load is thus transferred through the spanner nut to the inducer hub. Maximum stresses in the high-speed inducer hub and blades at design point conditions are shown in figure 744. The inducer is fabricated of Inconel 718.

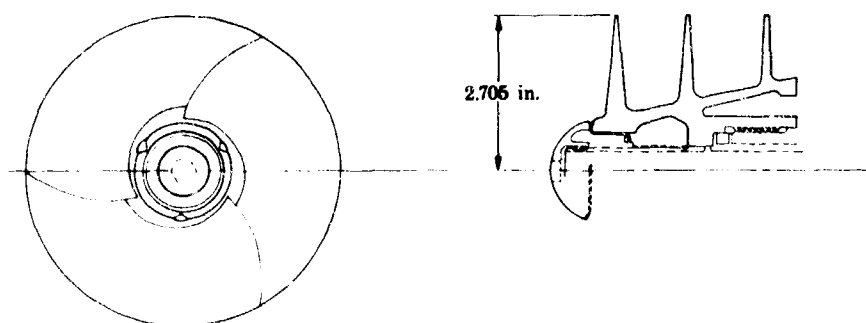


Figure 743. Oxidizer Turbopump High-Speed Inducer

FD 33092

(2) Impeller

The single-stage impeller shown in figure 745 has 12 equally spaced curved blades, consisting of three full blades, three long splitter blades, and six short splitter blades. The impeller is fully shrouded and is fabricated from Inconel 718 (AMS 5663). The impeller shroud is welded to the three full blades, and the remaining nine blades are gold-nickel brazed. The weld attachment has sufficient strength to retain the shroud, and the braze eliminates fretting and contamination of the area between the blade tips and shroud. The impeller is designed to have zero plastic deformation at 8% overspeed and maximum pressure. The average

tangential stress in the hub is 24,490 psia at 8% overspeed condition. The maximum local effective stress is 99,000 psia in the hub, and 89,000 psia in the shroud, while the allowable stress is 139,000 psia at cryogenic temperatures. Stresses existing in the impeller are shown in figure 746.

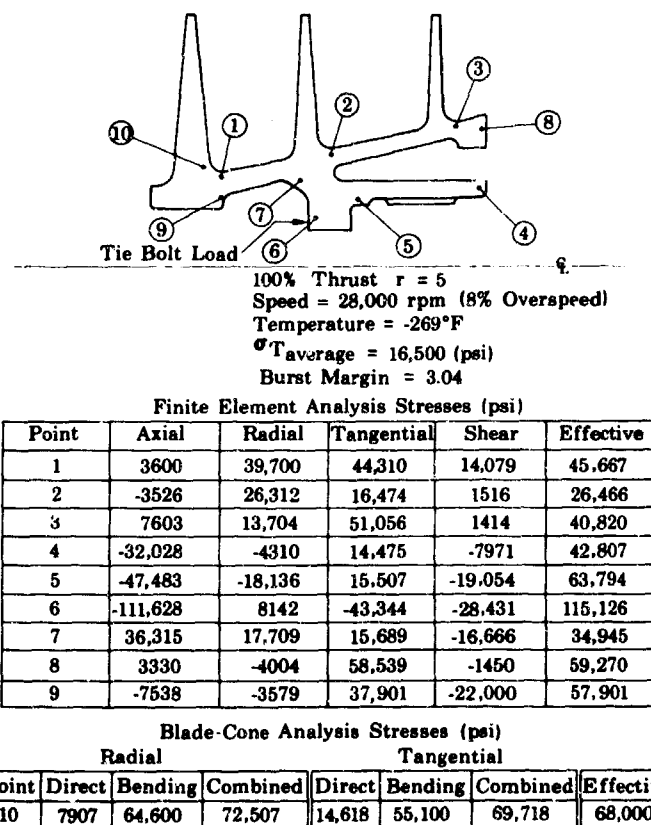


Figure 744. Oxidizer Turbopump High-Speed Inducer Stresses

FD 33093

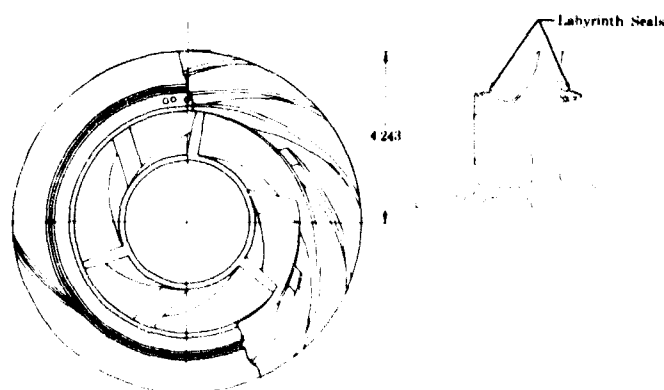


Figure 745. Oxidizer Turbopump Impeller

FD 33094

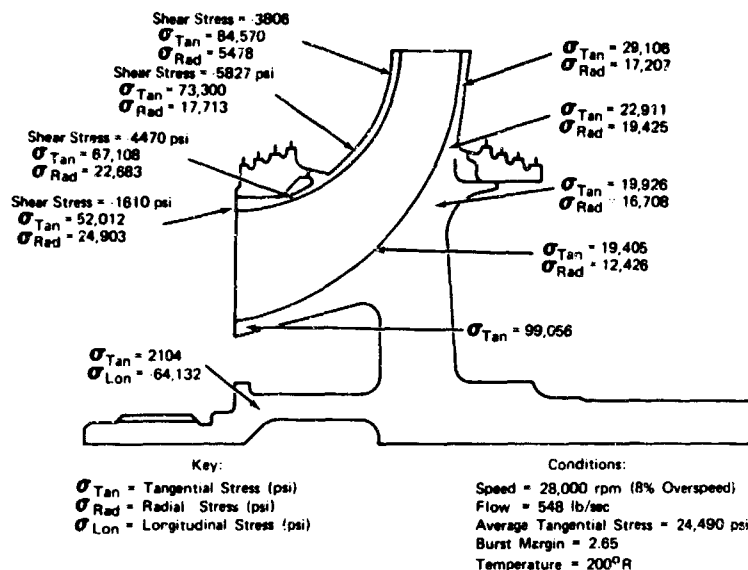


Figure 746. Oxidizer Turbopump Impeller Stresses FD 33095

The impeller has two radially staggered labyrinth seals that are tight fitting rings welded to the impeller shroud at the inlet and to the impeller hub at the discharge. The forward and aft lands are machined on equal diameters to minimize the axial thrust unbalance on the impeller. Leaded-bronze seal lands are installed in the housings to form the stationary portion of the seal. Leaded bronze was selected to prevent damage to the impeller labyrinth seal if rub is experienced. Because of great differences in coefficients of contraction for leaded bronze and Inconel 718 (AMS 5663), it is necessary to install the seals tightly at room temperature to ensure seal-to-housing contact while operating at cryogenic temperature. The impeller has provisions for assembly balance by adding balancing weights to the front of the shroud. Tapped holes in the shroud accommodate 36 balance weights, each with 0.113 oz-in. of balance correction.

(3) Bearings and Bearing Supports

The oxidizer turbopump is supported by two identical 55 x 110-mm ball bearings. As shown in figure 747, the forward bearing is located between the impeller and the thrust balance assembly. The rear bearing is located in front of the turbine and is separated from the turbine by a low-leakage labyrinth seal. Each bearing contains eleven 0.65625-in. diameter balls. The rings and balls are hardened to R_C 58 and R_C 62 with the rings and balls in each bearing within one point of hardness of each other. The inner and outer race curvatures are 57 and 51.5%, respectively. A 19-deg contact angle results in a spin-to-roll ratio of 0.40 under a peak radial load of 1430 lb with a fatigue life of 16.05 hr at 26,000 rpm. Table LXXXVIII summarizes the mounting effects on each bearing. The effects of thermals, centrifugals and pinch loads are tabulated with respect to changes in shaft-to-bearing fit and internal clearance. Each bearing has a recommended shaft fit that results in a running fit from 0.0002T to 0.0009T (diametral) at 26,000 rpm shaft speed.

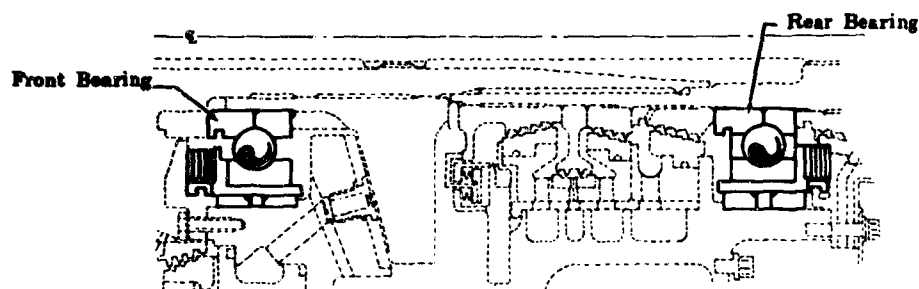


Figure 747. Oxidizer Turbopump Bearings and Bearing Mounts FD 33096

Table LXXXVIII. Mounting Effects on Oxidizer Turbopump Bearings

Bearing	Thermals	Change in Fit Due To:			Sum of Effects	Recommended Shaft and Bearing Diametral Fit
		Centrifugals	Pinch Load			
Front	+0.00077	+0.00037	+0.00031	+0.00145	0.00235T 0.00165T	
Rear	+0.00077	+0.00052	+0.00031	+0.00160	0.0025T 0.0018T	

Bearing	Thermals	Change in Internal Clearance (Diametral), ΔP_D , Due To:			Shaft Fit	Total Change in Internal Clearance
		Centrifugals	Pinch Load			
Front	-0.00013	-0.00066	-0.0004	-0.000141 -0.000635	-0.00133 -0.00183	
Rear	-0.00013	-0.00066	-0.0004	-0.00012 -0.00053	-0.00131 -0.00172	

A critical speed analysis of the oxidizer pump rotor indicated an effective spring rate of approximately 750,000 lb/in. is required at both supports. Because the bearings have a spring rate of 1.48×10^6 lb/in., the bearing supports must provide at least 1.53×10^6 lb/in. The calculated stiff bearing critical speed is 1.27 times the maximum operating speed. The calculated soft bearing critical speeds, assuming an effective spring rate of 1.5×10^6 lb/in. respectively, for the front and rear bearing systems are:

Mode	Speed
Pitch	20,480 rpm
Bounce	28,928 rpm
First Bending	59,904 rpm

Axial loading springs maintain an axial load approximately the same as the maximum expected radial load. These springs are incorporated between the bearing carrier and spring retainer. The spring retainer also acts as a stop to limit shaft axial travel. The bearing carrier engages an antirotation tab with the spring retainer to prevent carrier and outer race rotation, but allows axial movement to follow the shaft travel.

The front bearing is cooled by liquid oxygen from the thrust piston cavity. As shown in figure 748, a portion of the liquid oxygen used by the thrust balance piston is allowed to pass to the bearing. The majority of this flow returns through six 0.153-in. diameter passages in the bearing support to the thrust piston discharge cavity and then to the pump inlet. The remainder of the flow passes through the bearing and is returned to the thrust piston discharge cavity, and then to the pump inlet with the oxygen leakage past the impeller rear seal. The bearing coolant flow is regulated by setting the areas of an annular gap between the shaft and spring retainer and the bypass holes. The calculated flow through the front bearing is shown in table LXXXIX.

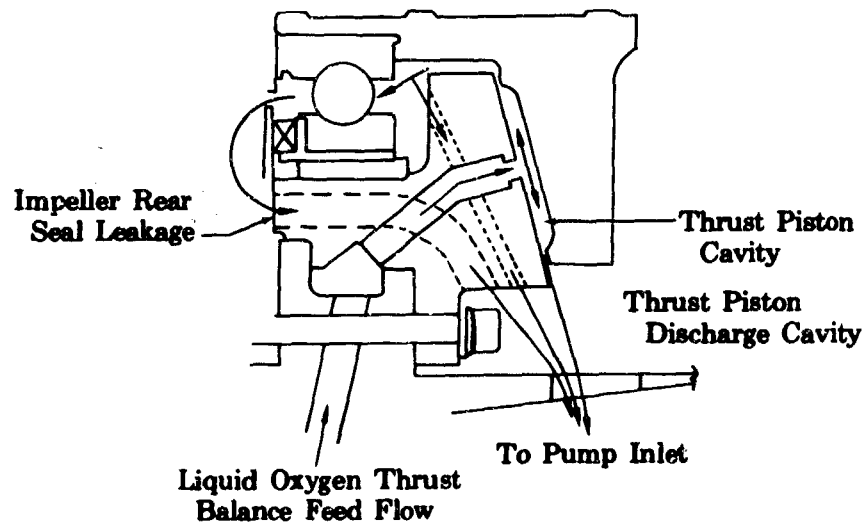


Figure 748. Oxidizer Turbopump Front Bearing Coolant FD 33097

Table LXXXIX. Front Bearing Coolant Flow

Thrust (%)	Mixture Ratio (r)	Coolant Flow (lb/sec)
100	5	1.745
100	7	1.594
20	5	0.8577
20	7	0.862

The rear bearing is cooled by liquid hydrogen tapped off at the preburner fuel valve. As shown in figure 749, hydrogen from the preburner fuel valve flows through the bearing and a labyrinth seal, and is routed back to the fuel pump 1st-stage impeller inlet. A second labyrinth seal limits overboard leakage from the seal package. The calculated flow through the rear bearing is shown in table XC.

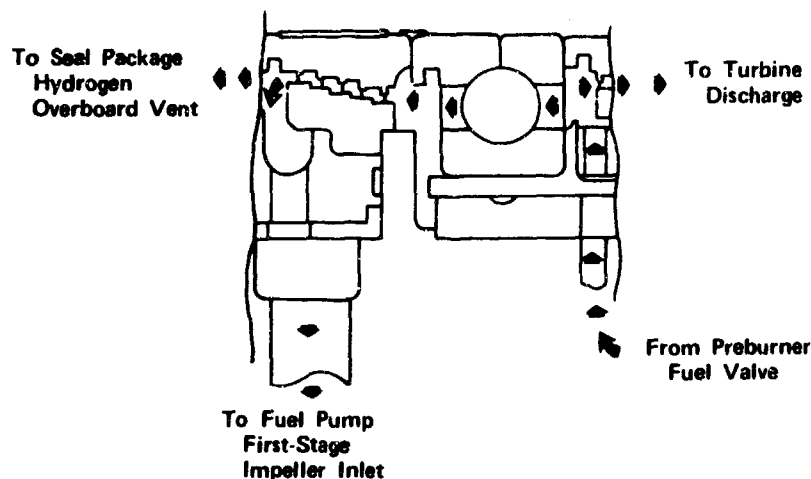


Figure 749. Oxidizer Turbopump Rear Bearing Coolant Flow

FD 33098A

Table XC. Rear Bearing Coolant Flow

Thrust (%)	Mixture Ratio (r)	Coolant Flow (lb/sec)
100	5	0.52
100	7	0.50
20	5	0.26
20	7	0.212

(4) Thrust Balance System

The oxidizer turbopump thrust balance system consists of a thrust piston that rotates with the turbopump shaft and a stationary thrust plate. As shown in figure 750, liquid oxygen from the pump discharge diffuser enters the thrust piston cavity through sixteen 0.091-in. -diameter metering orifices in the thrust plate. This high-pressure oxygen forces the piston away from the plate until the increased clearance at the piston OD and ID decreases the differential pressure across the thrust piston. In this way, the shaft is held within a few thousandths of an inch of the nominal axial position during steady-state operation. Bearing carrier stops limit total axial travel to approximately 0.032 in. during transients.

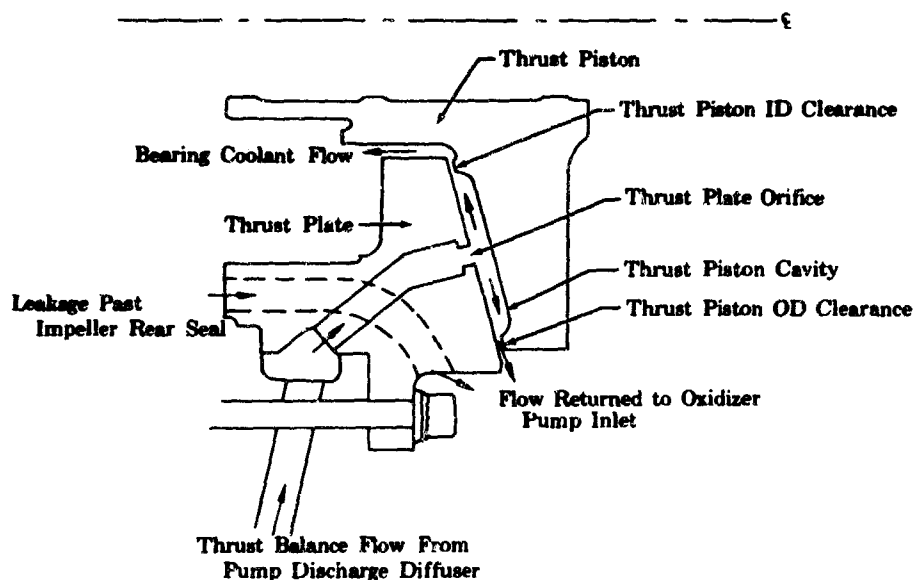


Figure 750. Oxidizer Turbopump Thrust Balance System FD 33099

The thrust piston seal lands are at 6.5 in. on the OD and 3.1 in. on the ID. This results in a working area of 25.6 in. and a thrust balance capability of 45,800 lb at 100% thrust and a mixture ratio of 5. The most critical operating point for the thrust piston occurs at 100% thrust and a mixture ratio of 5. At this point, the gap between the piston and plate is 0.0063 in., and the shaft bearings are unloaded except for axial spring loads. The gap can decrease to 0.0045 in. (0.0057 in. at room temperature) before the bearing receives any load from the shaft. At this condition, the thrust piston has a load capability of 1.5 times the load at nominal gap. The piston can carry much higher loads than this by running at smaller gaps. This will provide for start transient overloads when the thrust piston capability is increasing. During this transient, the bearings are capable of withstanding loads to 4000 lb for short durations. Figure 751 shows the thrust piston clearance and flowrate over the thrust range at minimum and maximum mixture ratios.

Both the thrust piston and piston plate are fabricated of Inconel 718. Loaded bronze is used to face the piston plate to withstand rubbing that may occur in a liquid oxygen environment.

The piston is designed with a conical face using centrifugal force to limit deflection. The 0.002-in. deflection shown in figure 752 is the difference between a deflection of 0.0035 in. caused by cavity pressure acting to bend the piston, and a deflection of 0.0015 in. caused by centrifugal force acting to straighten the piston. Deflections shown in figure 752 do not include thermal deflections because all parts in this area are held at nearly the same temperature by thrust balance and leakage flows.

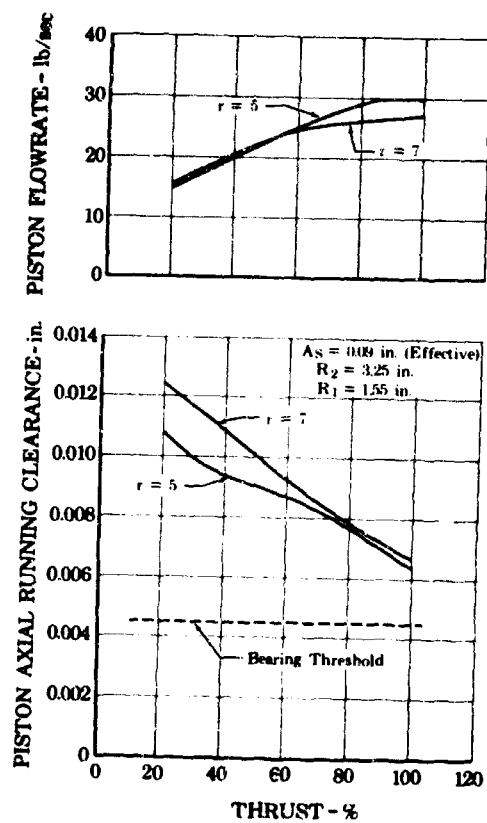


Figure 751. Thrust Piston Clearance and Flowrate FD 33310

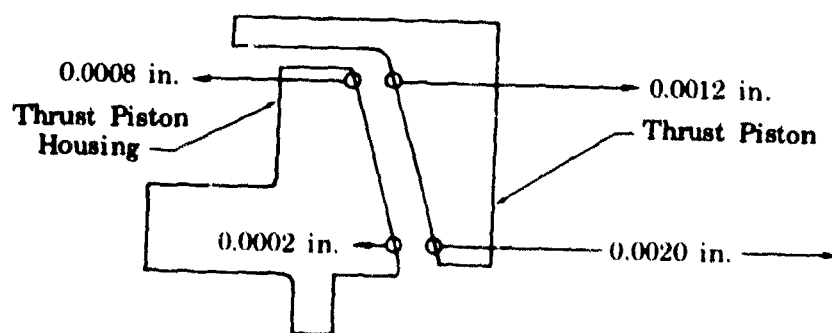


Figure 752. Oxidizer Turbopump Thrust Piston Deflection FD 33311B

The maximum effective stress in the piston is 63,000 psia, occurring at the bore. The maximum effective stress in the plate is 31,000 psia, occurring at the bolt flange. However, the crisscrossing network of holes in this piece make calculation of exact stress, rather than the average stress, difficult. The material yield strength at room temperature is 150,000 psia, and is slightly higher at operating temperature.

(5) Seal Package

The oxidizer turbopump seal package shown in figure 753 consists of one lift-off seal and five labyrinth seals. The following discussion of the seal package is keyed to figure 753.

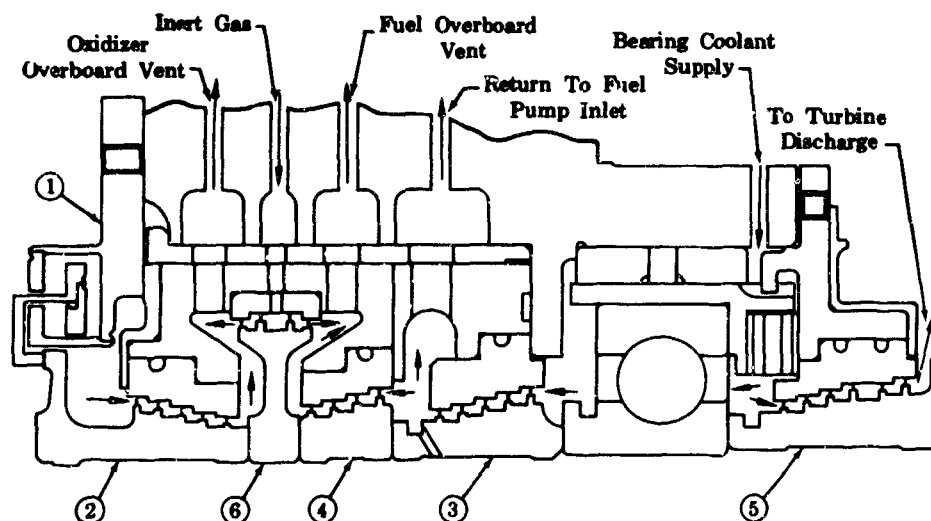


Figure 753. Oxidizer Turbopump Seal Package

FD 33067A

The bellows-actuated liftoff seal (1), shown in detail in figure 754, provides a positive seal from the thrust balance discharge cavity when the pump is not rotating. This prevents oxygen from flowing overboard when the pump is not operating.

The bellows assembly consists of two concentric, annular bellows. The lift-off seal housing provides axial support for pressure loads, preloads, and thermal loads relating to the labyrinth seal land supports. The bellows assembly and lift-off seal housing are fabricated of Inconel 718.

The minimum sealing force resulting from the bellows spring rate in the unactuated position is 100 lb. A Teflon coating 0.003 to 0.005 in. is bonded to the sealing face to conform to minor imperfections in the mating surface and limit maximum leakage below 10 sccs. Minimum bellows life is 10,000 cycles and the minimum natural frequency of the bellows is 1040 Hz. The maximum pressure on the bellows at actuation is 1500 psia. Maximum differential pressures across the inner and outer bellows, respectively, are 1500 and 1460 psid.

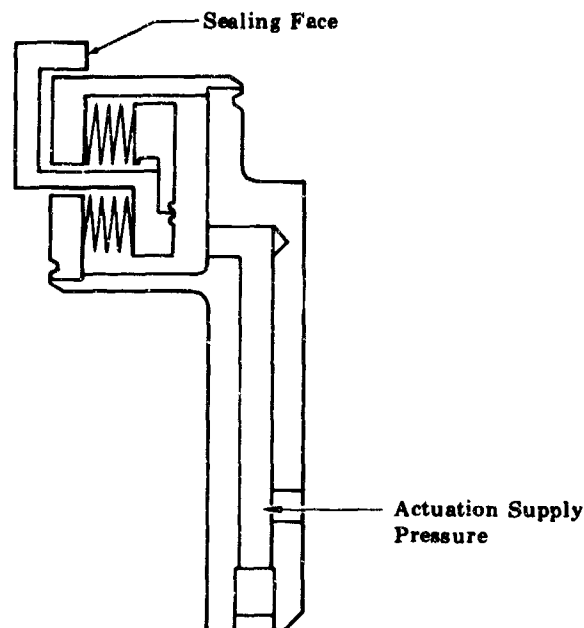


Figure 754. Oxidizer Turbopump Bellows Actuated Liftoff Seal FD 33313

When the lift-off seal is opened, oxygen leakage from the thrust balance discharge cavity leaks through a five-step labyrinth seal (2) and is vented overboard. Maximum flow across this seal is 1.01 lb/sec, occurring at 100% thrust and a mixture ratio of 5.

At the rear of the seal package, hydrogen from the preburner fuel valve enters the seal package at the maximum flow rate of 0.73 lb/sec occurring at 100% thrust and mixture ratio of 5. This flow is divided and a portion is used for the rear bearing coolant.

Hydrogen coolant flow across the rear bearing is controlled by a five-step labyrinth seal (3). Maximum flow across this seal is 0.52 lb/sec at 100% thrust and a mixture ratio of 5. Most of this flow is returned to the hydrogen pump first-stage impeller inlet. An additional four-step labyrinth seal (4) limits leakage to ambient. Maximum flow across this seal is 0.045 lb/sec at 100% thrust and a mixture ratio of 7.

Hydrogen not used for rear bearing cooling passes through the six-step labyrinth seal (5) at the rear of the seal package. Most of the hydrogen flowing through the first four steps of this seal is vented to the turbine discharge and the turbine duct area. The remainder of the flow passes through the last two steps of the seal and is vented to the pump side of the second turbine disk. Discharge from this seal is deflected away from the disk. Maximum flowrates across the first four and last two steps of this seal are, respectively, 0.205 and 0.086 lb/sec. These flowrates occur at 100% thrust and a mixture ratio of 7.

A helium dam seal (6) provides a dam between the oxygen leakage from the thrust balance discharge cavity and hydrogen leakage from the rear bearing coolant flow. A two step labyrinth seal is used between both the helium and oxygen and the helium and hydrogen.

All labyrinth seals are designed with the diameter of the seal decreasing in the direction of flow. This allows the minimum leakage from a labyrinth seal of specific diameters and steps. Lead bronze is used for the stationary lands for each labyrinth seal to withstand any rubbing occurring in an oxygen environment. Radial seal clearances are 0.005 in. for oxygen, 0.004 in. for helium, and 0.003 in. for hydrogen.

b. Turbine

The two-stage turbine, illustrated in figure 755, consists of the turbine inlet duct, the two turbine stages, turnaround manifold and exit diffuser, and turbine coolant system. The two stage, axial-flow turbine is cantilevered from the rear bearing assembly.

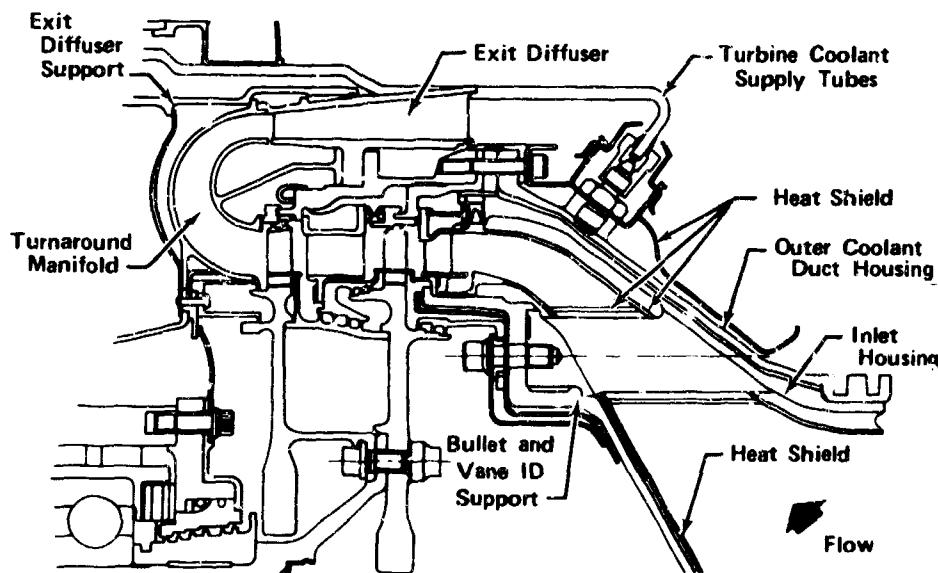


Figure 755. Oxidizer Turbopump Turbine

FD 33314A

(1) Inlet Duct

The oxidizer turbopump turbine inlet duct, shown in figure 756, is the structure that directs the flow from the transition case hot-gas discharge to the oxidizer turbopump turbine. The duct consists of the inlet housing, the outer coolant duct housing, the bullet and vane ID support, the mixing chamber seals, and the inlet duct coolant system. The inlet duct coolant system is discussed in paragraph (5), Turbine Cooling System.

The inlet housing is a single-piece, machined housing of Inconel 718 consisting of three sections; the duct, struts, and bullet mounting ring. The duct begins as a cylinder at the flow entrance, transitions to a cone increasing in

diameter in the direction of flow, and ends in a flange for mounting on the turbine stationary hardware. Six struts, parallel to the duct centerline, extend from the duct cone to the bullet mounting ring. The inlet housing and the struts are protected from hot gas scrubbing by a heat shield fabricated of Haynes 188. The inlet housing is the primary load carrying structure for the inlet. The struts carry the combined bullet blowoff and vane ID axial loads as a tension load, and the inlet housing carries the strut load plus a pressure load. The inlet housing and the outer coolant-duct distributor form a 0.050-in. passage for coolant flow.

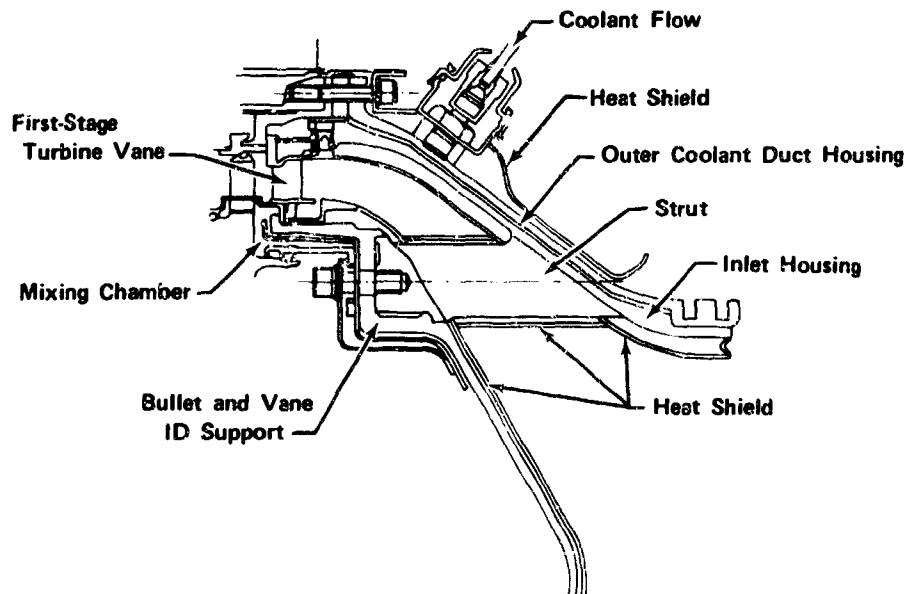


Figure 756. Oxidizer Turbopump Turbine Inlet Duct

FD 33316A

Cold hydrogen from the outer duct coolant is routed through eighteen 0.050-in. -diameter holes in the duct housing. Flowpath gas is then brought in and mixed. The vane-to-housing seal is a K-seal whose use prevents uncontrolled hot gas leakage passing into the OD mixing chamber.

The bullet and vane ID support is a one-piece removable structure that bolts to the inlet housing at the bullet mounting ring. The bullet and vane ID support is fabricated of Inconel 718.

Two seals form the inner diameter mixing chamber. The outer seal provides a seal between the flowpath and the mixing chamber, acts as a shim to adjust the axial load distribution of the vane, and serves as an axial seal having forty-five 0.050-in. -diameter orifices to admit hot gases to the mixing chamber. The inner seal is a three-step labyrinth seal with 830 psid differential pressure across the seal assembly. The inner seal is designed to grow in diameter with temperature, thus maintaining a constant clearance relative to the sealing surface on the disk.

(2) Stators

Figure 757 illustrates the turbine stators, blades, disks, and the turnaround manifold and exit diffuser. The turbine stators for both turbine stages are fabricated on IN100. This material was selected because of its superior 10-hour stress rupture properties of 26,000 psia and ductility of 25%, at the maximum turbine operating temperature of 2325°R.

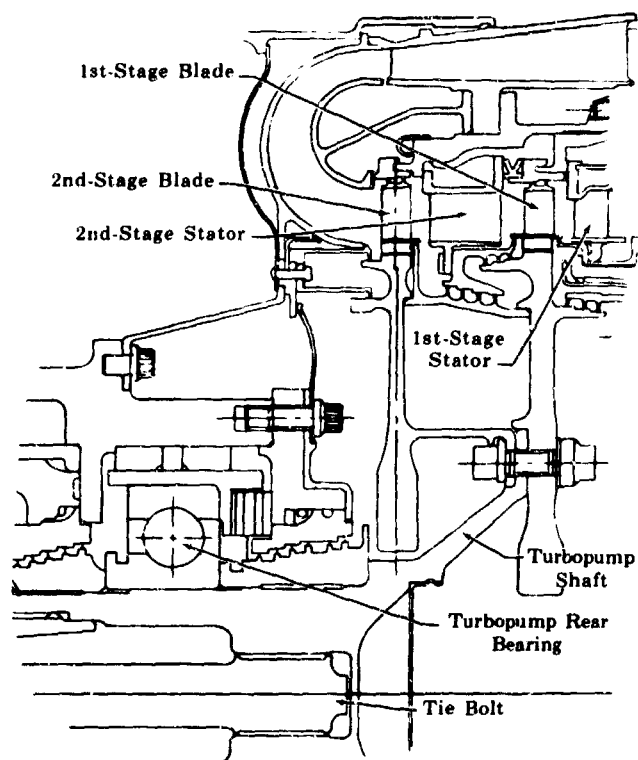


Figure 757. Oxidizer Turbopump Turbine Stages and Exhaust System

FD 33317B

The 1st-stage stator ring consists of integrally cast vanes and continuous cast inner and outer shroud platforms. The 53 vanes are supported both axially and tangentially at the outside platform. The inner platform is only axially supported. Tangential support of the inner platform is not required because the tangential load is only 50 lb per vane. Axial support of both platforms is required because the axial load is 190 lb per vane. The inner platform supports 79 lb axial load per vane and the outer platform supports the remainder.

Problems associated with thermal differences between inner and outer platform rings are avoided by adding a heat shield to the outer platform. Because hot gas is diverted from the flowpath at both the inner and outer platform rings, their temperatures should be approximately the same under all engine operating conditions. Both vane stages can withstand a 400-degree temperature differential between the ID and OD rings and remain within design stress limits.

The 2nd-stage stator also consists of integrally cast vanes and inner and outer platform rings. The 56 vanes are cantilevered from the outer platform, which has a square spline that allows the vanes to expand with respect to the

vane support ring. A seal ring secured to the inner platform reduces leakage across the vane stage. This seal ring is riveted to the vanes, but an oblong hole arrangement allows it to have thermal freedom of expansion.

Vane classification controls the flow area through the vane ring. Flow area is reduced by partially blocking the 1st-stage stator. To obtain vane classes above nominal, the vane airfoil trailing edge is cut back a maximum of 0.080 in. on the 1st-stage vanes and 0.145 in. on the 2nd-stage vanes.

(3) Blades and Disks

Turbine blades consist of uncooled, solid airfoils with integral tip shrouds, preloaded to contact adjacent shrouds and damp blade vibrations. A rectangular platform at the base of the airfoil isolates the attachment and disk from the main hot gas path. The ends of the platforms are closely machined surfaces, which act with knife edges on adjacent nonrotating parts to form an effective labyrinth seal. There are 136 1st-stage blades and 134 2nd-stage blades.

A single-tooth dovetail attachment transfers the centrifugal load of the blades to the disk by an axial slot cut through the disk rim. This slot is sized to allow controlled cooling gas flow around the attachments. Axial restraint of the blades is provided by a lug that bears on the side of the disk rim. The interstage labyrinth seal locks the 2nd-stage blades in place, and a small bent wire retains the 1st-stage blades.

Turbine blades are precision cast from IN100. The relatively low wheel speed of the turbine permits use of this material.

The 1st-stage disk has integral, stepped seal lands on each side, which act with mating stationary knife-edge seals to control coolant flow around the disk. This disk, in conjunction with the shaft, acts as a positive pressure dam to control cooling gas flow around the inside of the turbine. This flow is regulated by fifteen 0.130-in.-diameter orifices in the shaft. The cooling system is further defined in paragraph (5), Turbine Cooling System.

The 2nd-stage disk is supported by an integral arm, attached to the shaft and 1st-stage disk by a series of tie bolts. Holes are machined through the center of the tie bolts to maintain a minimum temperature gradient between the bolts and the disks during start and shutdown.

The thermal gradient is small and a low wheel speed results in a small Poisson's effect, obviating the necessity to preload the tie bolts with more than the recommended standard torque of 100 in./lb. These bolts also hold an inter-stage rim spacer between the disks. This spacer has an integral coverplate that meters cooling gas through sixteen 0.040-in.-diameter holes to the 2nd-stage rim and features knife edge seals which control leakage of cooling gas across the 2nd-stage vanes.

Torque generated by the blades of both stages is transferred from the disks to the shaft by close fitting torque pins, equally spaced between the tie bolts. The shaft transfers the torque to the pump through an internal spline. The shaft is also supported by the rear shaft bearing from which the turbine rotor is cantilevered.

The turbine rotor assembly is balanced by adding weights to the forward side of the 2nd-stage disk and by adding variable weight nuts to the tie bolts. Torque pins are threaded on one end to accept nuts of different weights for balancing the pump assembly. The disks, shaft, and rim spacer are fabricated of Waspaloy because of its high strength and ductility.

Calculated and allowable attachment stresses for the blade and disk are presented in table XCI. The calculated stresses shown are for the 2nd-stage blades. The 1st-stage blade attachment stresses are 6.1% less than 2nd-stage stresses.

Because the shaft and the 1st-stage disk act as a positive pressure dam, a differential pressure exists across the disk. This pressure load and the axial component of the aerodynamic blade load are relatively high. As a result of this high bending load, the disk size and shape are based on deflection limits, rather than the usual burst or yield limits.

Table XCI. Calculated and Allowable 2nd-Stage Turbine Blade and Disk Stresses

	Blade		Disk	
	Calculated Stress (psia)	Allowable Stress (psia)	Calculated Stress (psia)	Allowable Stress (psia)
Neck Tension	26,200	28,500	37,000	50,000
Combined Tension	54,200	76,000	62,000	126,000
Tooth Bending	28,000	38,000	25,000	50,000
Tooth Bearing	74,500	85,500	74,500	126,000
Tooth Shear	19,000	23,700	19,600	44,000

The resulting disk has a burst margin of 1.4, assuming a burst factor of 0.8. The average tangential stresses are 70,200 psia for the 1st-stage disk and 67,433 psia for the 2nd-stage disk.

Three design features reduce disk rim deflections: (1) the rim spacer was pinched between the disks to force the 2nd-stage disk to deflect at the same rate as the 1st-stage disk, transferring some bending load to the 2nd-stage disk; (2) the blades on both stages were axially offset to induce a restoring moment at the disk rim; (3) design of the attachment between the 1st-stage and the shaft places high axial load on the turbine, causing the conical end of the shaft to deflect outwardly. This outward deflection is resisted by the disk snap, inducing a restoring moment into the disk.

The turbine disks are hot during steady-state operation while the forward end of the shaft operates at cryogenic temperatures. The resulting temperature gradient is isolated in the rear of the cylindrical portion of the shaft. A small heat shield has been added to the rear portion of the shaft to keep the shaft threads

near the same temperature as the mating tie bolt threads. Temperature distribution for this section of the assembly is shown in figure 758.

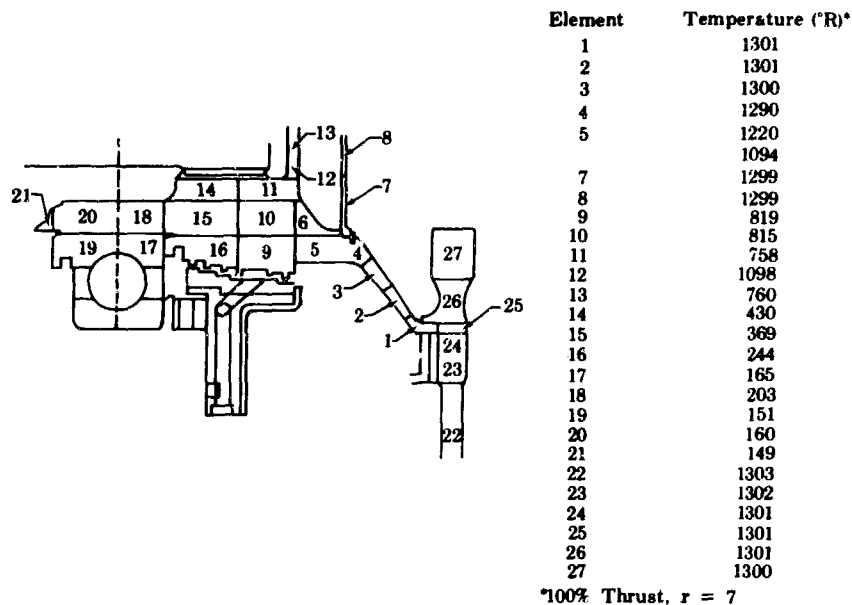


Figure 758. Oxidizer Turbopump Turbine Hub and Tie Bolt Temperature Profile FD 33327

(4) Exit Manifolds

The turnaround manifold and exit diffuser ducts the discharge flow from the 2nd-stage turbine blades to the transition case. Because the turbine inlet flow is toward the pump inlet, it is necessary to turn the turbine discharge flow 180-deg to exhaust into the transition case. Turbine exhaust also flows through a diffuser to convert velocity head to static head and minimize duct discharge losses. The diffuser section has exit guide vane struts to transfer axial and vane torque loads to the turbine housing.

An Inconel 625 forging is used for the turnaround manifold. This unit is lightly loaded below a yield stress of 30,000 psia at operating temperature.

Figure 759 shows the calculated temperatures in the turnaround manifold and exit diffuser that will exist during 100% thrust and a mixture ratio of 7. The outer duct of the turnaround manifold is matched to the inner duct providing a steadily decreasing flowpath area to achieve the given turbine area/diffuser area ratios. The ratio of turbine exit area to diffuser entrance area is 0.807, and the diffuser has a 7-deg included angle with an area ratio of 1.886. Because the internal turnaround duct is uncooled, hot turbine discharge gases are allowed to enter the static cavity behind the contoured surface. This results in a nearly uniform temperature throughout the duct with a small differential pressure across the walls. This method minimizes thermal stress and low cycle fatigue problems.

IN100 is used for the diffuser. This part is cast because of the complexity of the exit guide vane design. This material has a 0.2% yield strength of 70,000 psi at the steady-state temperature of 2184°R of the turbine exhaust gases, at

mixture ratio of 7. The maximum effective stress is lower than the 10-hour stress rupture for this temperature. The exit diffuser incorporates 24 struts to transmit loads from the inlet ducts and stators to the pump housings. The struts serve no aerodynamic function and are aligned with the direction of gas flow to minimize pressure losses.

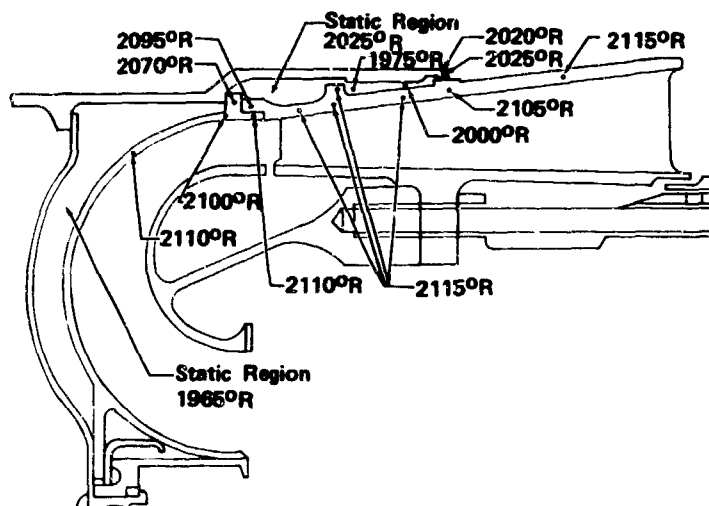


Figure 759. Oxidizer Turbopump Turnaround Manifold and Exit Diffuser Temperatures

FD 33318

The highest stress occurs at the load ring on the diffuser ID ring where the maximum effective stress is 40,000 psia. The diffuser tends to rotate because of unequal thermal effects, and a heat shield was added to isolate the cooling flow from the ID ring. Rotation from turbine loads is approximately 0.006 in. and pivots about the contact points between the diffuser and the attachment arm. Bending of the arm, by other than thermal effects, is limited to the friction load caused by diffuser rotation under load.

(5) Turbine Cooling System

Design of the oxidizer turbopump turbine includes a cooled inlet duct, struts, and bullet. The outer support structure is moderately cooled, while the turbine vanes and platforms are uncooled integral castings. Table XCII provides coolant system flowrates, maximum pressures, and orifice numbers and sizes. The table is keyed to figure 760 which identifies the locations.

The oxidizer turbine inlet duct structure is a one-piece, machined forging consisting of the inlet duct, bullet supporting struts, and bullet mounting ring. The turbine bullet distributes preburner gases around the turbine inlet and is subjected to a pressure load that is transmitted to the inlet duct by the six struts. The structure is cooled with hydrogen supplied from the fuel pump discharge through six 0.125-in. OD tubes which are equally spaced around the outer duct. Coolant is distributed between the inlet duct outer wall and the outer coolant duct inner wall and then is routed through the struts to the turbine bullet. Coolant distributors inside the turbine bullet form heat exchanger passages to promote cooling the bullet.

Table XCII. Oxidizer Turbopump Turbine Coolant Flow System Flow Rates, Pressures, Temperatures, and Orifice Sizes

Location*	Design Point Flowrate (lbm/sec)	Location*	Maximum Pressure (psia)	Location*	No. of Orifices	Orifice Diameter (in.)
1	1.09	1	4100	1	18	0.050
2	0.29	2	3950	2	57	0.064
3	0.80	3	3880	3	23	0.064
4	0.71	4	3300	4	35	0.064
5	1.59	5	2980	5	36	0.050
6	1.0			6	56	0.030
				7	24	0.10

* Locations are keyed to figure 760.

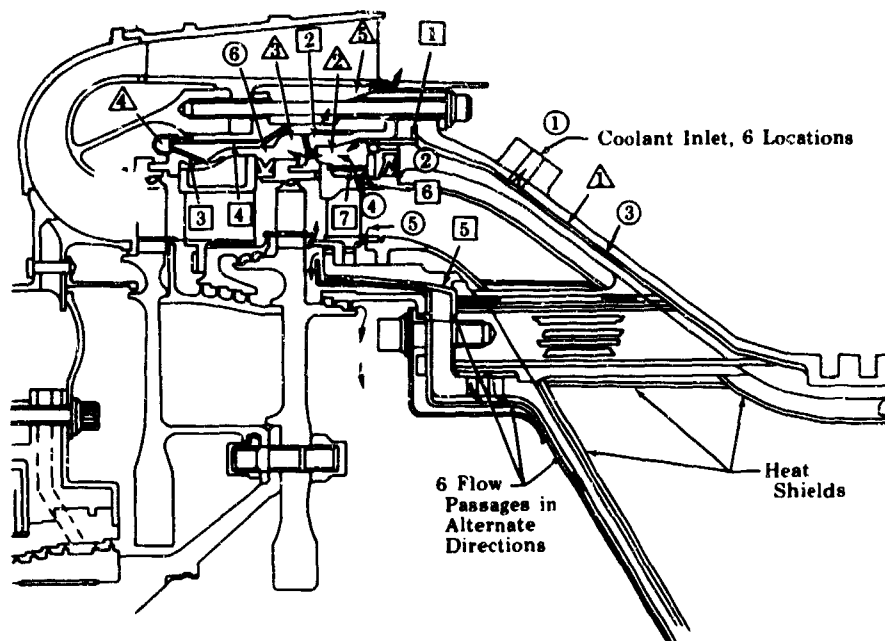


Figure 760. Oxidizer Turbopump Cooling System FD 33319

Coolant passes through slots in the strut mounting ring, and finally into a chamber, inboard of the first vane support, where it is mixed with high-temperature, mainstream gases from the turbine for turbine disk cooling. Figure 761 illustrates the turbine disk coolant flowpath. The strut mounting ring is coated with 0.020 in. of magnesium zirconate to reduce the temperature gradient through the thick section of the ring between the coolant slots. Surfaces exposed to the transition duct flow are further protected by shielding of Haynes 188 to reduce the heat transfer rate so structural and cycle life requirements can be met.

To maintain proper blade tip-to-shroud clearances and reduce thermal gradients in the turbine supporting members, cooling passages were provided to maintain essentially constant temperatures of these parts, as shown in figure 762. Cold fuel flow is introduced into the mixing cavity between the 1st-stage vane OD ring and the 1st-stage vane support. Hot turbine inlet gas is also introduced into the mixing cavity through controlled passages in the 1st-stage vane shroud. These gases are mixed in the cavity to produce coolant flow of the proper temperature to obtain an optimum blade tip-to-shroud clearance over the entire engine operating range, providing cooling for the vane supporting members. Coolant then flows through orifices in the 1st-stage vane support to the cavity formed by the 2nd-stage vane support and the 2nd-stage vane ring. From there coolant passes through the 2nd-stage vane support into a small turnaround manifold and again through the 2nd-stage vane support where it is dumped into the cavity between the 2nd-stage support and the turbine exit diffuser case.

Coolant is bled into the diffuser discharge gas stream by a slot immediately behind the diffuser case struts. The series of orifices in this system provides a controlled pressure drop along the coolant flow routing to keep pressure losses

at minimum between the cooling flow and mainstream gas pressure. This prevents excessive coolant leakage and reduces the buckling pressure load on various components.

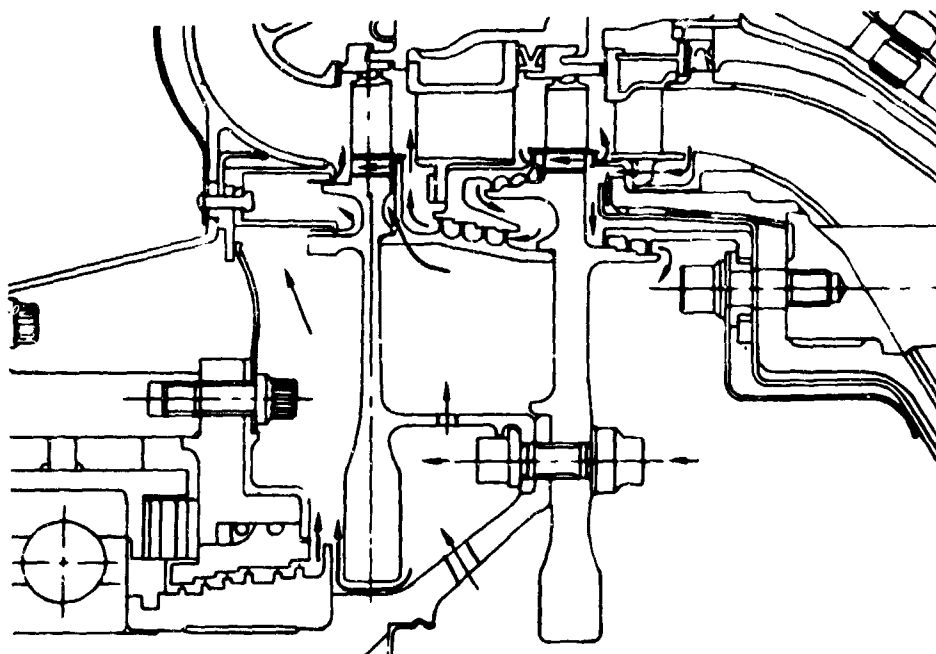


Figure 761. Oxidizer Turbopump Turbine Disk
Coolant Flow

FD 33325

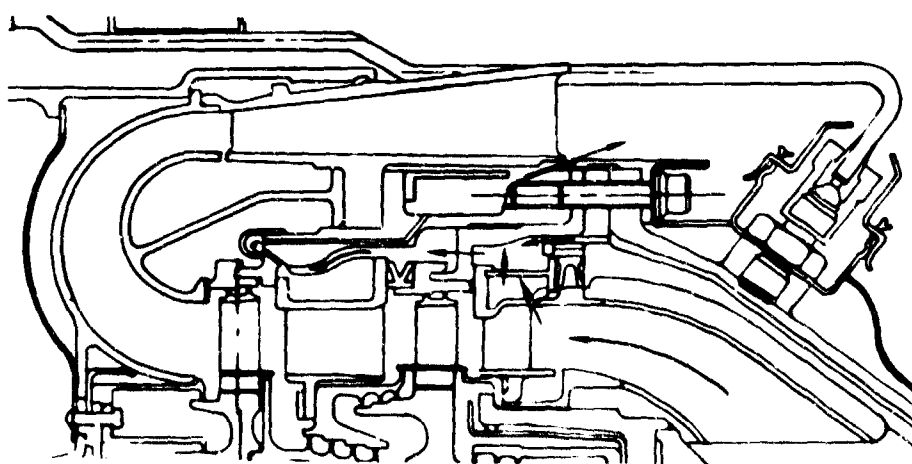


Figure 762. Oxidizer Turbopump Turbine Support
Coolant Flow

FD 33326

Based upon the experience gained in design of turbine vanes on the fuel pump turbine, the oxidizer turbine 1st-stage vane platforms are heated on both sides to reduce thermal gradients which are detrimental to engine cycle life. The outer platform on the 1st-stage vane is shielded from the outer supporting structure coolant to reduce the temperature differential between the inner and outer platforms. Because of lower mainstream gas temperatures at the 2nd-stage, it was not necessary to heat both sides of each platform to maintain a compatible temperature differential between the inner and outer shrouds. The

temperature of the interstage seal coolant was chosen to obtain the correct seal diameter clearance.

Coolant for the transition case is supplied from the transpiration cooling supply heat exchanger and discharges into a cavity through six fixed metering jets located approximately 60 deg apart. The metering jets are positioned to discharge tangentially outboard to increase circulation within the cavity and prevent direct impingement of coolant on the structural walls. Coolant flows from this cavity into the space between the transition case wall and the cooling liner.

c. Housings

The oxidizer turbopump housings consists of three major sections; the inlet housing, impeller housing, and rear housing.

(1) Inlet Housing

The inlet housing illustrated in figure 763 consists of an Inconel 625 forging welded to an inlet pipe fabricated from welded Inconel 625 sheet. The inlet pipe is a welded assembly having provisions for receiving thrust balance and impeller backface leakage. Guide vanes used for the short radius bend into the turbopump provide an acceptable pressure profile to the high-speed inducer.

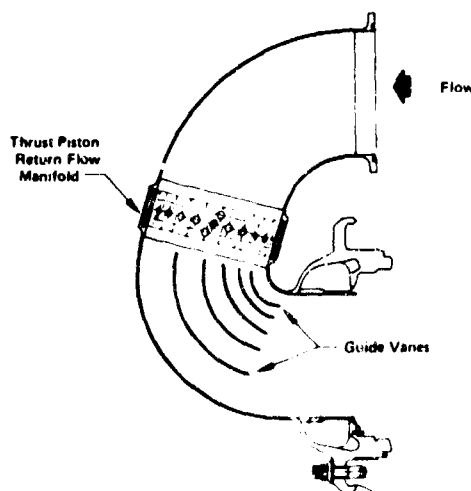


Figure 763. Oxidizer Turbopump Inlet Housing

FD 33320A

Studs for attaching the inlet housing are fitted in the impeller housing with the same loose fit as a bolt. The stud material is Inconel 718, and the nuts are silver plated, iron-base alloy. The stud is held stationary while the nut is torqued, thereby eliminating the shear stress on the stud and allowing higher loads.

The most critical structural point is at the weld joint where the inlet pipe joins the high-speed inducer housing. Because of space limitations of the design, this weld is located in a concentrated bending stress area. Inconel 625 was selected because it can withstand this stress.

(2) Impeller Housing

The impeller housing, shown in figure 764, is a twin-volute type made from an Inconel 718 forging. Twin volutes reduce radial unbalance on the impeller. The volutes guide the oxidizer from the impeller tip to the diffuser section at constant velocity. The diffuser section is connected to the volute passages by a short, constant-area passage.

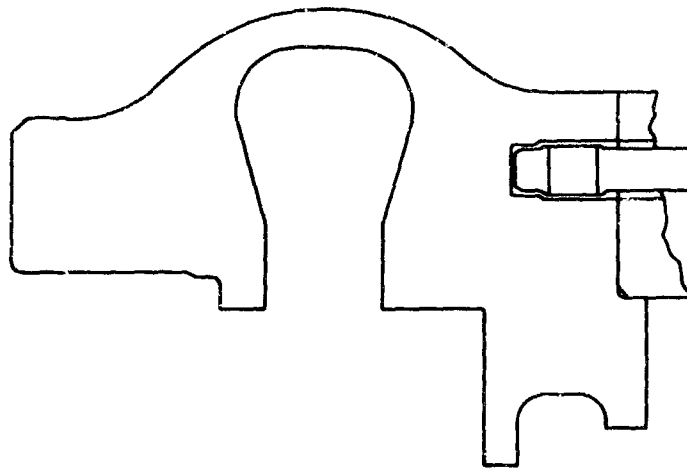


Figure 764. Oxidizer Turbopump Impeller Housing FD 33321

Bolts for attaching the impeller housing to the rear housing are also Inconel 718. Headless bolts with nuts are used because of space limitations, and because they can be held stationary while the nuts are being torqued. This eliminates shear stress in the bolts, allowing them to carry higher loads. The nuts are locked in place with tab washers. The bolts are sized to carry the sum of the following loads.

1. Load caused by tightening the bolts at assembly (includes 350 lb/in. to compress the seal)
2. Load caused by pump operating pressures
3. Loads caused by differences in thermal growth of housings
4. Maneuver loads
5. Plumbing loads caused by tolerances at assembly and thermal deflections in the complete engine.

(3) Rear Housing

The rear housing encases the seal package, thrust piston discharge cavity, and forward turbine area.

The rear housing is machined from an Inconel 718 forging. Selection of this material ensured thermal compatibility with adjacent housings. Thermal compatibility is necessary to limit deflections at sealing points and to minimize the attaching bolt loads.

Two tangential 1.40-in. diameter ports are provided to discharge the thrust piston discharge flow to the pump inlet. Tangential ports are incorporated to minimize pressure losses and to reduce the thrust piston discharge cavity pressure. The lowest possible discharge cavity pressure is desirable to provide maximum thrust piston capability and reduce the driving pressure, thereby forcing propellant overboard through the seal package.

The rear housing also provides ports for venting propellants from the seal package, supplying inert gas to the seal package, and supplying coolant to the rear bearing.

Figure 765 shows the rear housing mated to the center and inlet housings. Maximum stresses of the three housings and critical deflections are also shown in this figure.

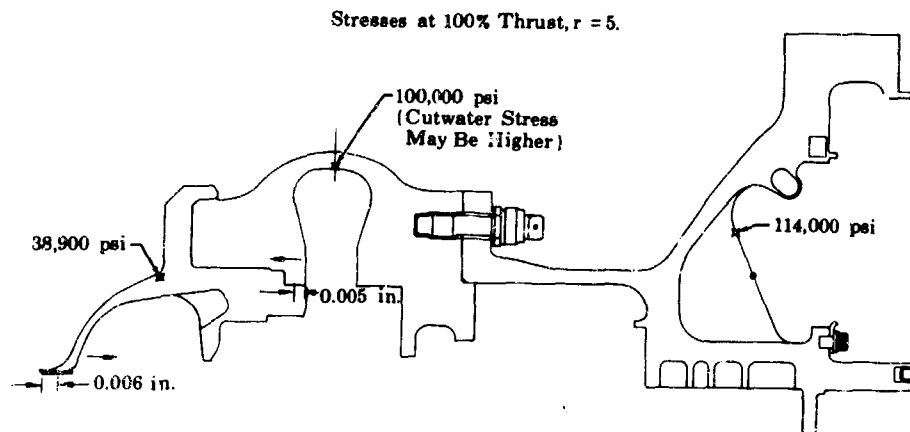


Figure 765. Oxidizer Turbopump Housing Stresses FD 33329

d. Weight

The calculated weight of the oxidizer turbopump is 393 lb including the manifolds for the transition case liner cooling and the test rig instrumentation bosses.

4. Operating Characteristics

The calculated pressure rise versus flow map for the oxidizer turbopump is presented in figure 766.

5. Fabrication

a. Pump

The inducer, impeller, thrust piston and tie bolt are fabricated from Inconel 718. Blading of the inducer and impeller are machined by manufacturing a master template and contour milling the forgings with a tracing machine. Other operations on these two details and the thrust piston and tie bolt are conventional milling, boring and turning operations.

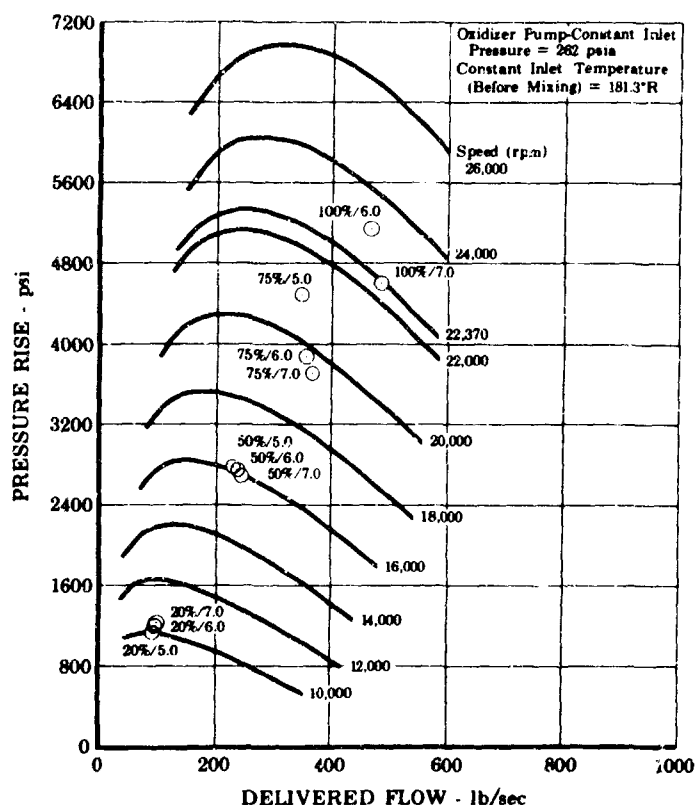


Figure 766. Oxidizer Turbopump Flow vs Pressure Rise FD 33328

After detail machining the impeller, a shroud is attached by electron-beam welding to the three long blades of the impeller. The remaining nine blades are gold-nickel brazed to the shroud to eliminate fretting and contamination of the area between the shroud and blade tips. Tight-fitting rings are installed at the front of the shroud and the rear of the impeller hub. These rings are electron-beam welded to the impeller and machined to form labyrinth seals.

The bearing races and balls are manufactured from vacuum melt AISI 440C, melted by consumable-electrode process, cold treated to 160°R and double tempered to 1060°R. Surface waviness of each race is maintained to less than 60 μ -in. per 30 deg of circumference. The cage is one piece construction, bronze-impregnated, fluorocarbon plastic with an aluminum alloy armor attached with stainless steel rivets.

The seal package rotating parts are machined from Inconel 718 forgings. These parts are manufactured by conventional turning and grinding operations. The stationary parts of the seal package are fabricated from corrosion and heat resistant martensitic iron base alloy with leaded bronze inserts. The leaded bronze inserts are installed in the supports with a 0.006 in.-tight fit prior to machining. This ensures a tight fit at cryogenic temperatures during turbopump operation. Machining of the leaded bronze in the support maintains a close tolerance inner diameter with the existing effects of the tight fit.

b. Turbine

(1) Inlet Duct

The inlet duct hardware is machined from Inconel 718 forgings. Conventional machining methods are employed for the majority of the work, but slots and holes are installed by EDM processes. The heat shields are installed by welding the heat shield segments into the support structure.

(2) Stators

Both stators are cast from IN100 and the inner and outer rings are machined to final dimensions. Casting techniques developed by the vendor for the fuel turbopump stators were applied to castings manufactured by the same vendor. The application of experience gained on similar parts greatly reduced the development time of suitable casting techniques.

(3) Blades and Disks

Turbine blades are cast from IN100. The entire order was cast by the vendor in the first attempt using multiple molds having 24 blades per mold. The root attachment and tip shroud seals are machined to produce the required closed tolerance. Six blades are shuttled and machined simultaneously using standard blade attachment machining, EDM, and grinding equipment.

The turbine disks are forged from Waspaloy and semimachined for sonic inspection. These parts are further machined to spin test configuration, spun, and final machined. The slots are machined for blade attachment by broaching.

(4) Exit Manifolds

Turnaround manifolds are machine from Inconel 625 forgings. No unusual processes or machines are required to produce these parts.

The exit guide vane is cast from IN100. The vendor produced an acceptable part on the first attempt because of the experience gained with a similar part supplied for the fuel turbopump. Critical exterior dimensions for heat shield attachment and installation fit are machined using standard techniques.

Astroloy, heat treated to Udimet 700 specifications, was selected as the material for the exit guide vane support. This piece is highly loaded because of thermal gradients, requiring the exceptional qualities of both Astroloy and Udimet 700. This is accomplished with the combination of Astroloy chemistry and Udimet 700 heat treatment. These forgings are machined using conventional methods.

c. Housings

The inlet housing is a machined and welded assembly. Conventional machining and welding techniques are used to manufacture this housing assembly. The same techniques are used to manufacture the impeller and rear housing assemblies.

H. LOW-SPEED INDUCERS

(A) Fuel Low-Speed Inducer

1. Introduction

The fuel low-speed inducer provides fuel to the main turbopump at a pressure sufficient to prevent fuel turbopump cavitation. This permits main pump operation at high speed, saving pump weight. Without the low-speed inducer, high engine inlet pressures are required. The three-bladed, low-speed inducer is driven by a single-stage, partial-admission turbine. The low-speed inducer operates independently of the main turbopump and at a lower speed than the main turbopump. This permits the low-speed inducer to operate at a low inlet pressure.

The fuel low-speed inducer assembly, with the location and major features indicated, is shown in figure 767 and figure 768.



Figure 767. Fuel Low Speed Inducer Location

FD 35193

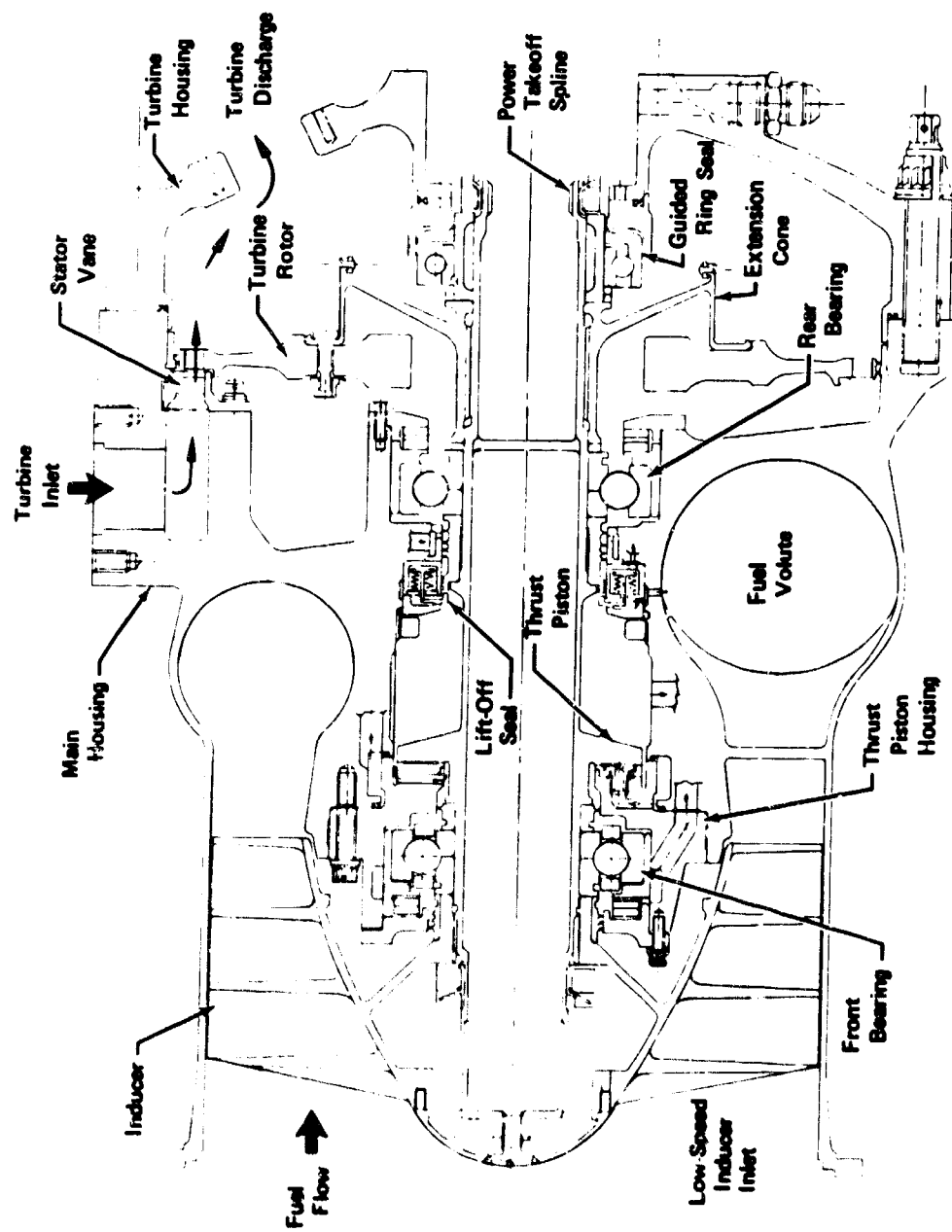


Figure 768. Fuel Low-Speed Inducer

The fuel low-speed inducer was designed to satisfy the requirements of the demonstrator engine and to demonstrate the following:

1. Overall inducer and turbine efficiency: 41.5%
2. Pressure rise: 88 psid
3. Suction specific speed: 46,800
4. Low-speed inducer weight: 90 lb
5. Propellant inlet conditions: 60 ft NPSH from 1 atmosphere boiling temperature to 45°R
6. Stable operation over the required engine operating range

2. Summary, Conclusions and Recommendations

The design layouts for the fuel low-speed inducer were completed. Preparation of the detail drawings and fabrication was deferred because of program redirection.

The fuel low-speed inducer is designed to satisfy the requirements of the demonstrator engine and the design goals established by contract. A review has been conducted on the available test results for components that have demonstrated performance similar to that required for this unit. Results of the review indicate the three principal requirements of this unit, suction performance, pressure rise and efficiency have been demonstrated to the levels required by design; however, these requirements have not been simultaneously demonstrated on a single component. It is recommended that components be fabricated and tested to demonstrate the attainment of suction specific speed of 46,800 rpm, moderate pressure rise of 90 psid, and 41.5% overall inducer and turbine efficiency on a single lightweight component.

3. Hardware

A mechanical description of the fuel low-speed inducer is provided by describing the major functional areas such as pump, turbine and housings.

a. Pump

The pump section consists of the inducer, bearings and supports, and the thrust balance system.

(1) Inducer

The inducer, shown in figure 769, is a helical design having three blades and is fabricated from A-110 titanium. It is attached to the drive shaft by means of an internal spline and is secured to the rotor assembly by a load nut. The inducer tip diameter is 10.5 in.

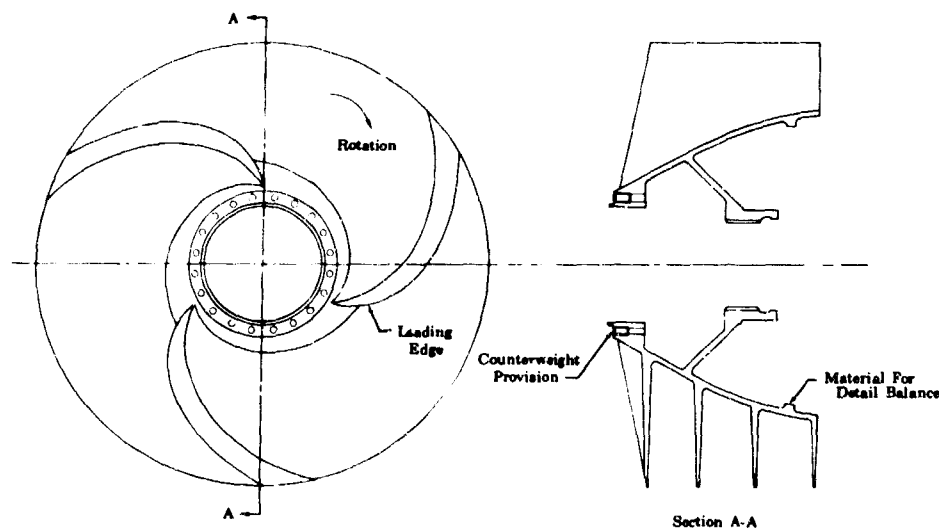


Figure 769. Fuel Low Speed Inducer

FD 33345

The inducer hub provides a ring at the rear for detail balancing and provides a maximum balance correction capability of 1.0 oz-in. per 120-deg segment. Provisions for counterweights in the front of the inducer may be used for assembly balance. The use of six counterweights in one continuous arc provides 0.5 oz-in. of correction.

(2) Bearing and Bearing Supports

The fuel low-speed inducer operates at a speed of 19,777 rpm at its design point condition of 100% thrust, and ratio of 5.0. The rotor assembly of the fuel inducer is supported on two 55 x 110-mm ball bearings, common to the bearings designed for the oxidizer turbopump. The rotor assembly is radially positioned by the ball bearings, but because a thrust balance piston is required, the bearing arrangement is designed to permit axial travel and is preloaded axially by springs on the outer race. The spring preload is adjustable by means of shims ground at assembly to fit between the front bearing spring retainer and thrust piston housing. The bearing preload is required to prevent ball skidding that would cause excessive heat generation and premature bearing failure. The DN value for the bearings in this application is 1.1×10^6 mm-rpm, which is within the limits of the bearing design. Bearing radial loads are calculated to be less than 50% of those for the oxidizer turbopump.

The bearings are made from AISI 440C stainless steel and the spring retainers are machined from A-110 titanium. The front and rear bearing carriers are a common design and are fabricated from AISI 410 stainless steel. Figure 770 shows the front bearing arrangement.

Bearing coolant is liquid hydrogen supplied from the fuel pump discharge and the flowrates are controlled by a labyrinth seal arrangement as shown in figure 771.

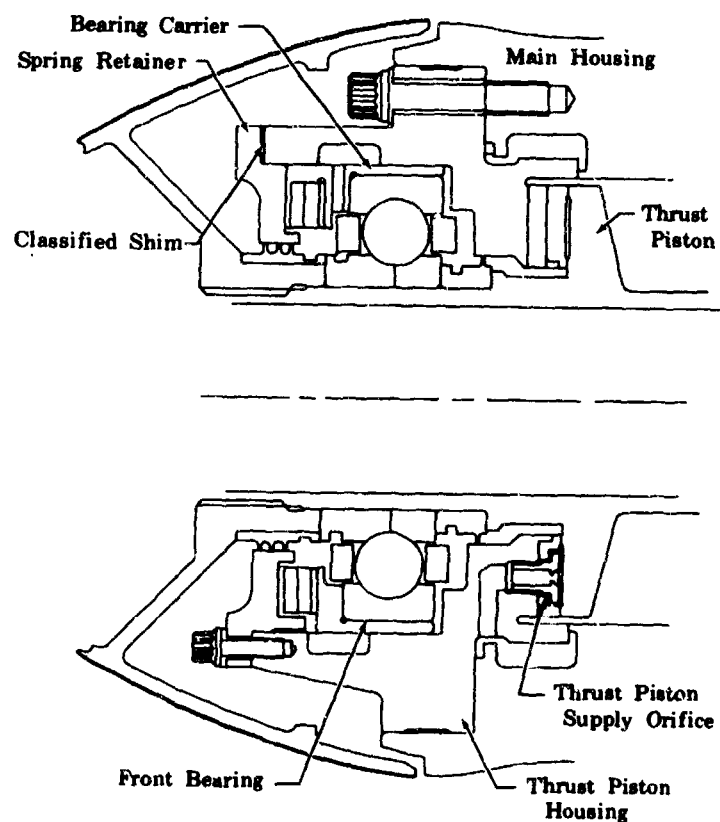


Figure 770. Fuel Low-Speed Inducer Thrust Piston FD 33413 and Front Bearing Arrangement

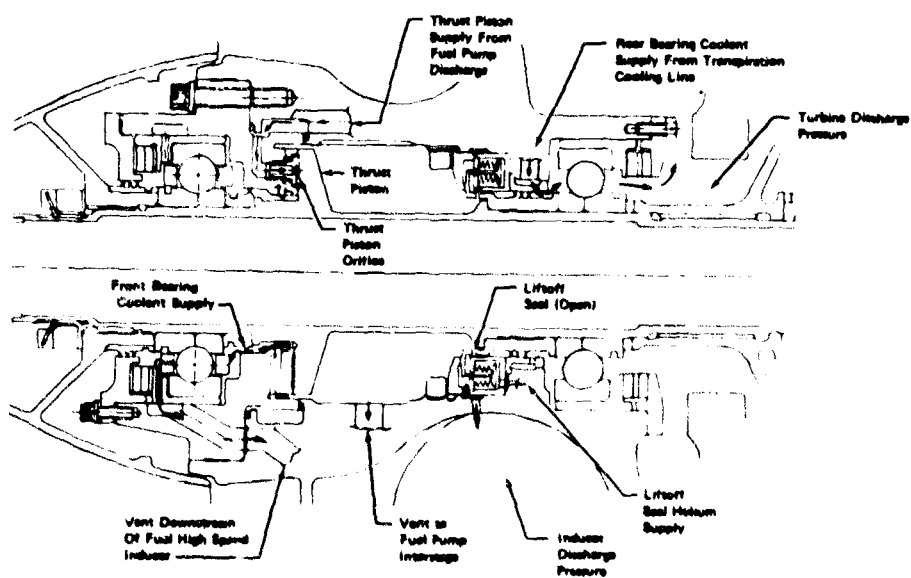


Figure 771. Fuel Low Speed Inducer Internal Flow Systems FD 33346

(3) Thrust Balance System

The fuel low-speed inducer incorporates an integral shaft and thrust piston arrangement. The axial thrust unbalance of the rotor acts toward the inlet of the inducer and is counteracted by the thrust piston. The shaft thrust piston unit is machined from an Inconel X-750 forging. The thrust piston is supplied high-pressure hydrogen from the fuel pump discharge through twelve 0.068-in.-diameter metering orifices. A portion of the thrust piston discharge flow is used for the front bearing coolant supply. Figure 771 also shows the thrust piston arrangement and the hydrogen flowpath.

The shaft is designed as a load bolt on both the pumping and turbine ends. Splines on each end of the shaft transmit turbine torque to the inducer. Load nuts on each end of the shaft secure the pump details and the turbine to the shaft independently. An internal spline on the turbine end of the shaft is provided for power takeoff.

In addition to use in the thrust piston system, the thrust piston housing was designed to serve as the front bearing support. It is fabricated of titanium to maintain thermal compatibility with the main housing and to minimize weight. Passages in the housing supply the high-pressure hydrogen for the thrust piston. The 12 metering orifices for the thrust piston fluid also serve as flow-through bolts to attach the Bearium B-10 thrust piston rub face. The housing and related flow passages are also shown in figure 771. The housing is also used as the stationary member in the front bearing coolant supply labyrinth seal, and an integral passage directs bearing coolant discharge flow to the main housing.

b. Turbine

The turbine section consists of the turbine rotor and the turbine stator.

(1) Turbine Rotor

Inducer drive power is provided by a single-stage, 7% partial-admission, axial-flow, impulse turbine, shown in figure 772. Turbine blades are designed to be integral with the disk. The turbine disk is fabricated from an aluminum alloy, with a mean flow diameter of 11.5 in., a blade height of 0.038, an axial chord of 0.35, a bore diameter of 4 in., and 182 blades with a brazed on, full ring shroud.

Turbine rotor design provides for detail disk balance, disk-cone assembly balance and final rotor balance.

(2) Turbine Stator

The turbine stator, also shown in figure 772, provides a maximum of 9.8% admission through the seven vane passages, with provisions for plugging two passages for turbine power adjustment. The turbine is designed with power takeoff capability up to 220 hp at 100% thrust, $r = 5$.

The stator assembly is fabricated from Inconel 718 and consists of a frame or window contoured at the inlet and end walls, with six straight section vanes fabricated from Inconel 718 and brazed into the frame. The vanes have a 0.3 axial chord, a 0.010-in. trailing edge diameter, and an approximate 13-deg exit

angle. The stator assembly is bolted to a shoulder in the main housing, positioned accurately by two dowel pins, and designed to provide for axial and radial sealing with the turbine motor. Aluminum plugs provide for the flow area variation. Differential pressure restrains the plugs against the vanes to minimize leakage and to relieve the aluminum pin, whose function is to retain the plug from any pressure load.

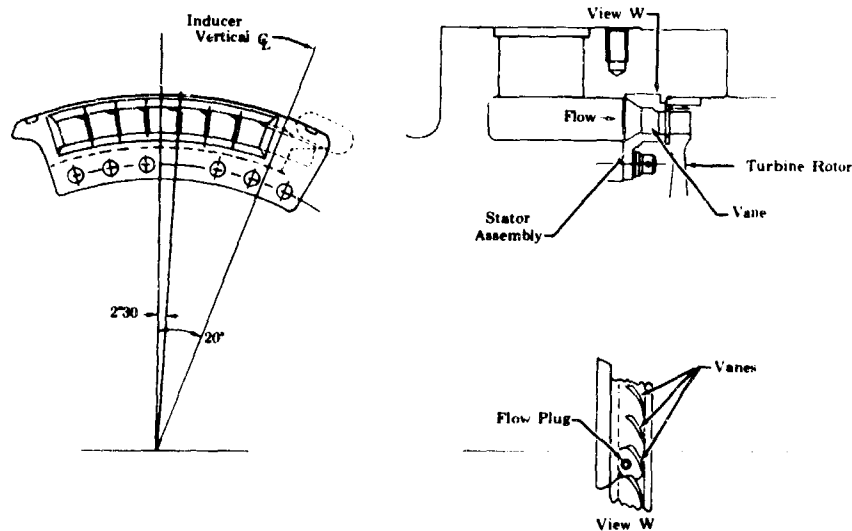


Figure 772. Fuel Low-Speed Inducer Turbine Stator Assy

FD 33412

c. Housings

The fuel low-speed inducer incorporates two housings; the main housing and the turbine housing.

(1) Main Housing

The fuel inducer main housing is machined from a titanium alloy forging in two sections; an inlet flange section and a volute diffuser section. The volute housing assembly, in addition to collecting and diffusing inducer flow, provides capabilities for:

1. Front and rear bearing mounting
2. Supply passages for bearing coolant and thrust piston flow
3. Drain passages for bearing coolant and thrust piston flow
4. A passage to admit helium flow to actuate the shaft liftoff seal
5. A turbine inlet flange and a flow annulus to direct hydrogen flow to the partial-admission turbine.

(2) Turbine Housing

The turbine housing attaches to the main housing aft of the turbine station and serves as a pressure vessel to collect the turbine discharge flow and provides an attachment for the turbine discharge line and accessory drive pad. It supports the guided ring seal on the turbine shaft which minimizes overboard leakage of the turbine discharge flow. Design provides a coverplate on the accessory drive mount pad when not being used. During operation of the low-speed inducer with the coverplate installed, guided ring seal leakage is vented through a boss in the mount pad. The vent is designed to allow a maximum pressure buildup of 180 psia at maximum seal leakage.

d. Liftoff Seal

A liftoff seal is incorporated between the thrust piston and the rear bearing to prevent liquid hydrogen from leaking into the turbine during engine operating intervals. The liftoff seal package is similar to the unit described for the main fuel and oxidizer pumps.

e. Weight

The calculated weight of the fuel low-speed inducer is 156 lb.

4. Operating Characteristics

The predicted pressure rise versus flow map for the fuel low-speed inducer is shown in figure 773.

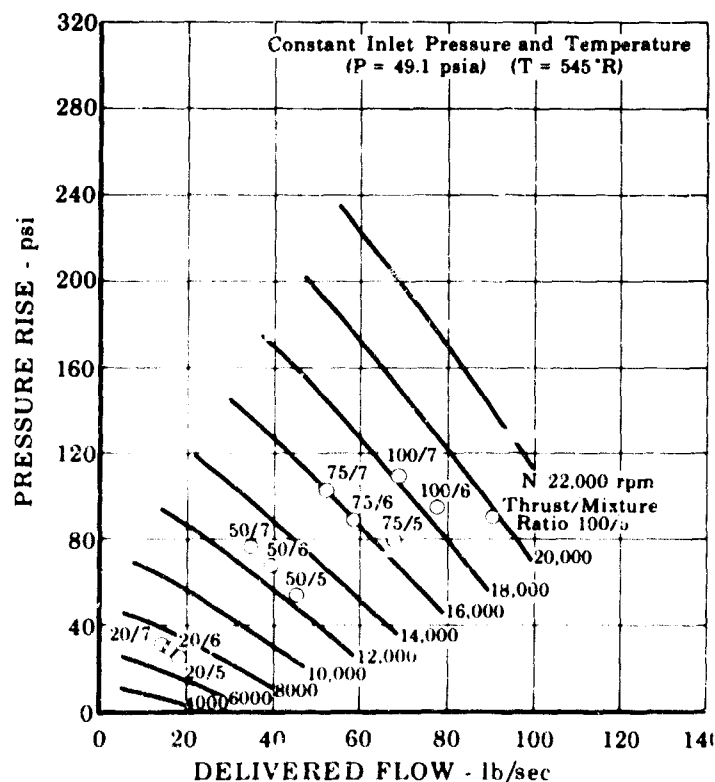


Figure 773. Fuel Low Speed Inducer Pressure Rise FD 33371

(B) Oxidizer Low-Speed Inducer

1. Introduction

The oxidizer low-speed inducer provides liquid oxygen to the oxidizer turbopump at a pressure sufficient to prevent turbopump cavitation. This permits oxidizer turbopump operation at high speed, thus saving turbopump weight. Without the low-speed inducer, high engine inlet pressures are required. The oxidizer low-speed inducer, shown in figure 774 and 775 is an axial flow unit with a high suction specific speed. It is driven by a variable admission single-stage, radial-inflow, hydraulic turbine. The turbine is driven by liquid oxygen discharged from the main oxidizer turbopump. The inducer is helical, has three blades, and is attached to the drive shaft and turbine assembly. The single-stage, radial-inflow turbine is a partial reaction device with a large rotor differential pressure affording minimal axial thrust unbalance. This unbalance is absorbed by a single-acting thrust balance piston.

The oxidizer low-speed inducer was designed to satisfy the requirements of the demonstrator engine and to demonstrate the following:

1. Overall inducer and turbine efficiency: 39.6%
2. Pressure rise: 252 psid
3. Suction specific speed: 40,000
4. Weight: 125 lb
5. Propellant inlet conditions: 16 feet NPSH from 1 atmosphere boiling temperature to 180°R
6. Stable operation: throughout the required engine operating range.

2. Summary, Conclusions and Recommendations

The design layouts for the oxidizer low-speed inducer were completed. Preparation of detail drawings and fabrication was deferred because of program redirection.

The oxidizer low-speed inducer was designed to satisfy the requirements of the demonstrator engine and the design goals. During the design period, a review was conducted of all available test results for components having a demonstrated performance similar to this unit. This review indicated that suction performance, pressure rise, and efficiency have each been demonstrated to the levels required by design. However, all of these requirements have not been simultaneously demonstrated on a single component.

It is recommended that an oxidizer low-speed inducer be fabricated and tested to demonstrate the attainment suction specific speed of 40,000, pressure rise of 252 psid, and 39.6% overall inducer and turbine efficiency on a single lightweight component.

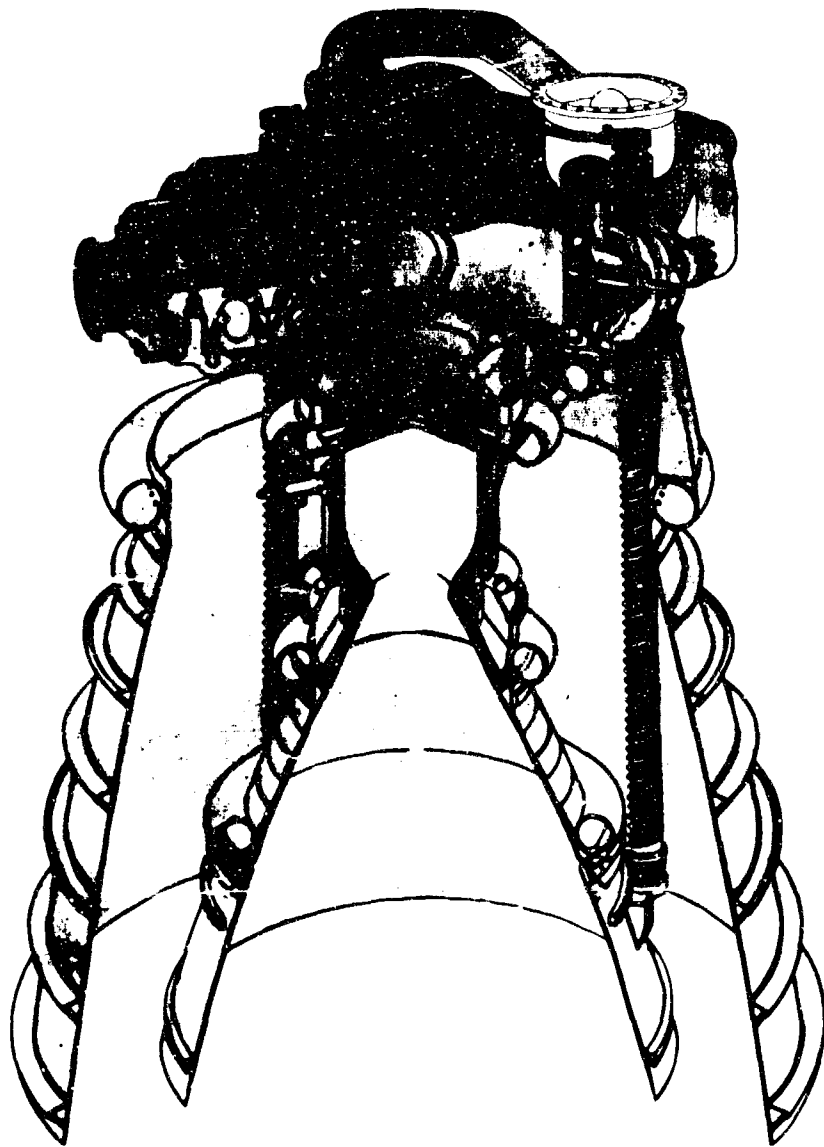


Figure 774. Oxidizer Low Speed Inducer

FD 35260

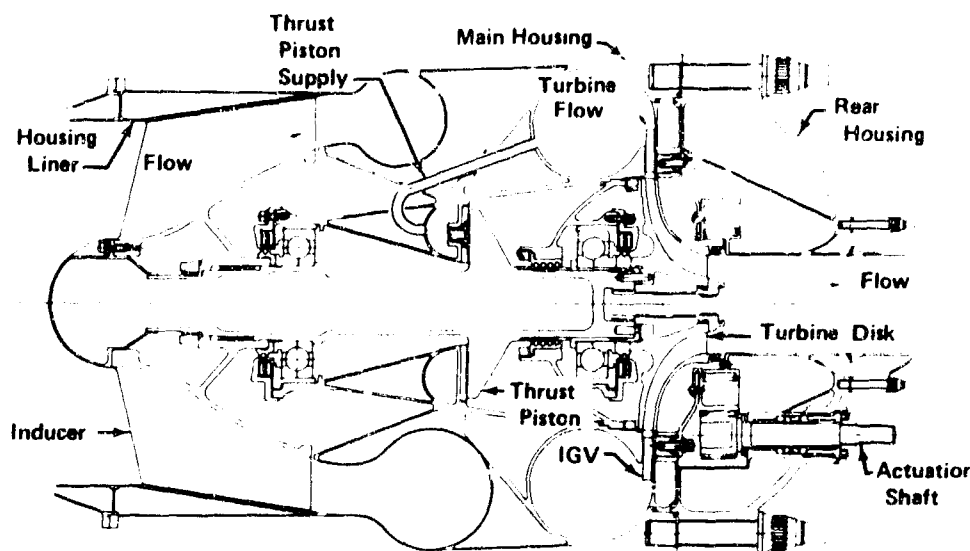


Figure 775. Oxidizer Low-Speed Inducer

FD 33343A

3. Hardware Description

The mechanical description of the oxidizer low-speed inducer is divided into three sections; pump, turbine, and housings.

a. Pump

(1) Inducer

The inducer is fabricated from AISI-A286. A cross section is shown in figure 776. The inducer is a three-bladed, helical design with an overall solidity of three. The helical section of the inducer extends for a solidity of one to meet high suction specific speed requirements. The aft section is cambered 3.6 deg at the tip for a solidity of two. The camber of the aft section ensures sufficient head rise for moving propellant to the oxidizer turbopump at flow conditions not detrimental to main pump operation. The inlet and exit tip diameters are 10.52 and 12.04 in., respectively. Provisions for detail balance are included by removing material from a ring inside the hub at the exit. Balance weights are threaded into tapped holes in the front of the hub to balance the low-speed inducer assembly.

An internal spline transmits torque from the shaft to the inducer. The spline was designed to transmit a maximum torque of 834 lb-in.

(2) Bearings and Bearing Supports

The oxidizer low-speed inducer operates at a speed of 5165 rpm at its design point engine 100% thrust, $r = 7$. The shaft assembly is radially located by two 55 x 110 mm ball bearings preloaded axially on the outer races to prevent ball skidding. The inducer bearings will operate well below the limiting bearing DN levels. The DN value for this design is 0.28×10^6 mm-rpm. Bearings used for the oxidizer low-speed inducer are identical to those used for the main oxidizer turbopump.

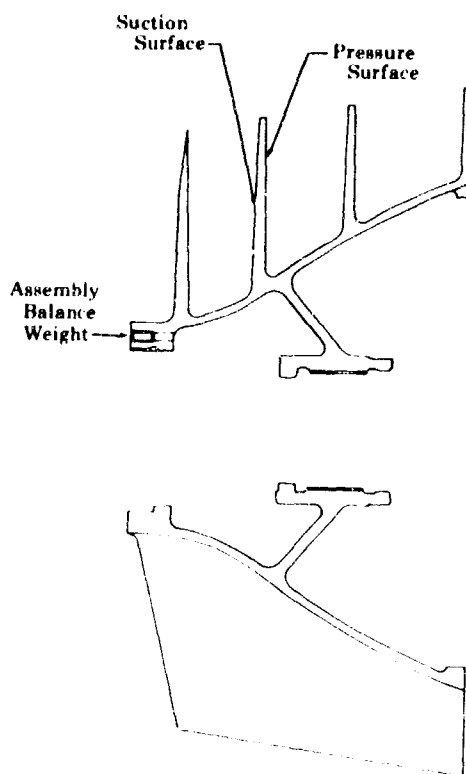


Figure 776. Oxidizer Inducer

FD 33336

Bearing support is provided by the low-speed inducer housings. Figure 777 shows the bearings mounted on the shaft assembly. Bearing outer race carriers allow axial travel of the shaft, but are slotted to prevent rotation of the outer race and carrier. Axial travel is limited by bearing carrier stops, which also act as spring retainers. Axial loading springs are trapped between the bearing carriers and spring retainers to provide axial loads approximately equal to the maximum radial load. This load combination minimizes ball skidding, and heat generation, thus providing the maximum predicted life for the bearing. Shims are used between the spring retainers and the main housings for adjustment of the spring cavity for proper bearing axial loads. Spring retainers also form the stationary portion of labyrinth seals that control bearing coolant flow. The ID of these retainers is coated with 0.005-in. flame sprayed nickel aluminum followed by 0.003 in. of flame sprayed pure aluminum. This coating provides dissimilar materials, desirable where unexpected rubs may be experienced. Spring retainers are machined from AISI-A286 forgings and the carriers are made from Inconel X-750 bar stock.

(3) Thrust Balance System

The oxidizer low-speed inducer has a single shaft with an integrally machined thrust-balance piston. The radial inflow turbine, being a partial reaction device, results in an axial thrust unbalance toward the inlet of the inducer. A thrust piston counteracts this axial load. The shaft thrust piston unit is machined from a forging of AISI-A286. The thrust piston is deflection limited rather than stress limited. The thrust piston has a capability of 34,100 lb

at 100% engine thrust and mixture ratio of 7. At this condition, the thrust piston clearance is 0.0043 in. and the flowrate is 18 lb/sec. The thrust piston cavity is supplied with high-pressure oxidizer from the hydraulic turbine inlet through ten metering orifices of 0.090 in. diameter. A leaded bronze faceplate is provided on the adjacent housing to withstand unexpected heavy rubs in liquid oxygen without material destruction.

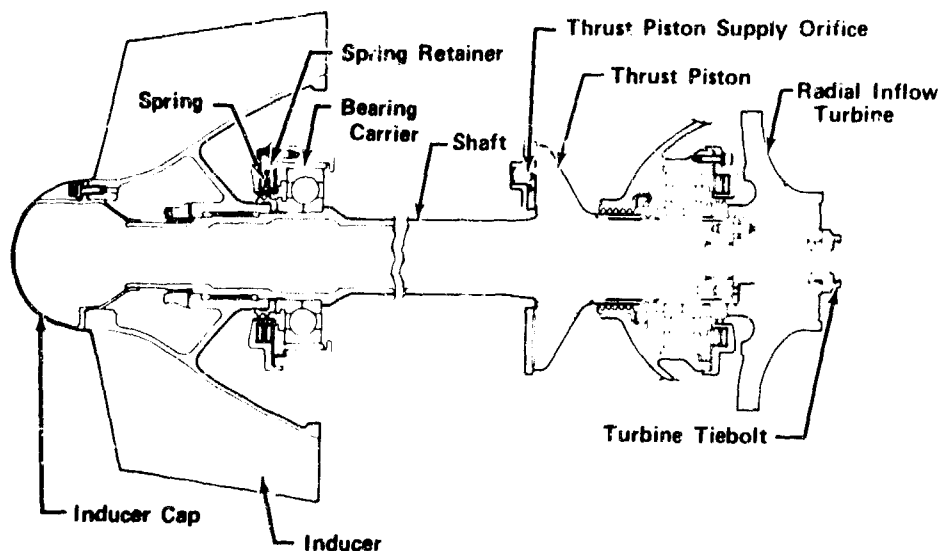


Figure 777. Oxidizer Low-Speed Inducer Rotor Assembly

FD 33335A

Pins at the rear of the shaft transmit torque from the radial-inflow turbine to the shaft. An internal thread accepts a tiebolt for securing the turbine to the shaft. A spline at the front of the shaft transmits torque from the shaft to the inducer. An external thread at the front of the shaft accepts the nut for securing the inducer, labyrinth seal, and bearing to the shaft. The nut is torqued to 3500 lb-in. and locked in place with a tab washer keyed to the shaft.

b. Turbine

(1) Inlet Guide Vanes

The turbine inlet guide vanes and actuation mechanism are shown in figure 778. The inlet of the radial-inflow turbine is formed by two circular flat plate surfaces axially spaced 0.3 in. apart. The surface toward the inducer is part of the inducer housing. The surface toward the turbine is a 0.750-in. thick, flat plate with provisions for mounting 31 equally spaced vanes on a 4.15 in. radius. To obtain light weight, this plate is a three piece weldment of Inconel 718 with a minimum wall thickness of 0.050 in.

The vanes, approximately 0.3 in. high, operate in the 0.3 in. axial gap between the two plate surfaces. Each vane and its trunnion are machined from one piece of Inconel 718. The trunnion axial and radial bearing surfaces are coated with molybdenum disulfide to reduce friction.

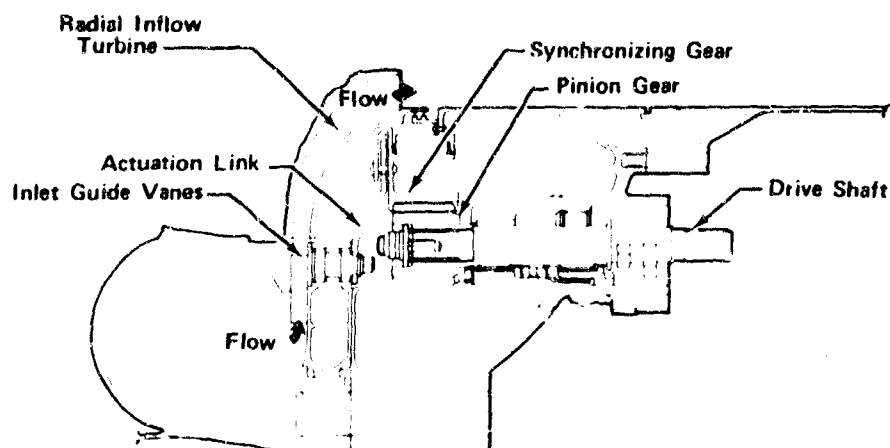


Figure 778. Oxidizer Low-Speed Inducer Turbine
and Variable Guide Vanes

FD 33337B

The trunnion extends through a hole in the flat plate, and is bolted and keyed to an actuation link. The links from all vanes extend radially inward to the synchronizing ring where they are riveted in position. As the ring rotates, the rivet rides in a slot at the end of each link which adjusts for the varying vane-to-rivet distance.

The synchronizing ring has a U-shaped cross section, with the vane links attached to the bottom of the U and the sides of the U extending axially in the direction of turbine discharge. The inside diameter of the U-shaped ring forms the outer race of a caged roller bearing. The inner race for this bearing is integral with the pump housing and is concentric with the low-speed inducer centerline. The ring, supported and located by its bearing, is driven through a segment of gear teeth on the outside diameter of the U.

The ring is driven from an external actuator through a shaft and meshed with a pinion with the synchronizing ring gear segment. The pinion is internally splined to the drive shaft and is axially held against a shoulder on the shaft by a washer, stud and nut arrangement. The differential pressure across the housing causes an axial load on the shaft and pinion. This load is absorbed by a thrust bearing beneath the pinion which rests on the pump housing. A washer against the pinion permits ease of manufacture of the gear teeth.

The pinion shaft is supported by two drawn-cup needle bearings. The first bearing is mounted in the pump housing and is held in place by the upper spacer of the lip seal package. Two axial lip seals, identical to those used on the preburner fuel valve, seal the shaft against leakage. The spacer between the two seals is vented. The seal package receives the specified assembly compressive load from a spanner nut that threads into the pump housing and contains the second needle bearing internally.

Two axially separated shaft lugs provide the stops for mechanically limiting movement of the vane. An adjustable screw in the housing provides the other half of the stop mechanism. A spline and a pad with four tapped holes are provided for attachment of the actuation mechanism.

(2) Turbine Disk

The turbine disk, consisting of a disk, blades, and shroud, is very similar to a shrouded pump impeller in shape and construction. The front (inducer side) of the turbine disk has an extended hub that guides the disk onto the shaft and also drives the turbine disk through 4-1/4-in. diameter pins pressed into the shaft. A tie bolt protrudes through the center of the turbine disk and fastens the turbine disk securely to the shaft. There are 36 radial blades spaced around the circumference. These blades are divided into 18 equally spaced long blades and 18 shorter blades alternately positioned between the long blades. All blades are slightly curved at their trailing edge toward the exit of the disk. The turbine disk also has an integral shroud at the tips of the blades and disk. The blades and shroud are of one-piece construction. The turbine disk shown in figure 779 is made of cast AISI 347 stainless steel.

c. Housings

The low-speed inducer housings are fabricated from Inconel 718. Thin wall construction using spheres and cones provide the lightest possible weight. The thrust piston is near the turbine because these sections operate at the highest pressures in the low-speed inducer. The thickness of the housing wall is minimized by this grouping, and it allows for thinner wall construction in the remaining lower pressure regions. The volute for the inducer discharge and the inlet for the turbine form rings at each end of the main housing and are connected by conical sections of thin wall material. The use of thin cross sections and careful selection of intersection points makes it possible to accurately predict stresses.

The inlet housing uses a removable liner coated with a Kel F rub-compatible material. This liner is removable to allow installation of the inducer during assembly.

The housing assembly also provides the structure for the bearing supports.

d. Weight

The calculated weight of the oxidizer low-speed inducer is 192 lb.

4. Operating Characteristics

The predicted pressure rise versus flow map for the oxidizer low-speed inducer is shown in figure 780.

5. Subcomponent Testing - Turbine Inlet Guide Vane Model Water Flow Tests

A test was conducted using the Pratt & Whitney Aircraft water table facility and a simulation of a portion of the inlet vanes of the hydraulic radial inflow turbine. This test determined the ability of the vanes to adequately direct the flow entering the rotor at minimum thrust and minimum mixture ratio. When vane incidence is high, the amount of flow turning is large, and the flow channel is short. It was concluded that an approximation is possible, although the configurations and performance of the vane simulation preclude an exact determination of vane exit deviation. Longer vanes were found to create less apparent deviation than shorter vanes. The average deviation for 1.5 in. chord vanes was approximately 5.5 to 6.0 deg, while the deviation for 1.0 in. chord vanes was 11 to 12 deg.

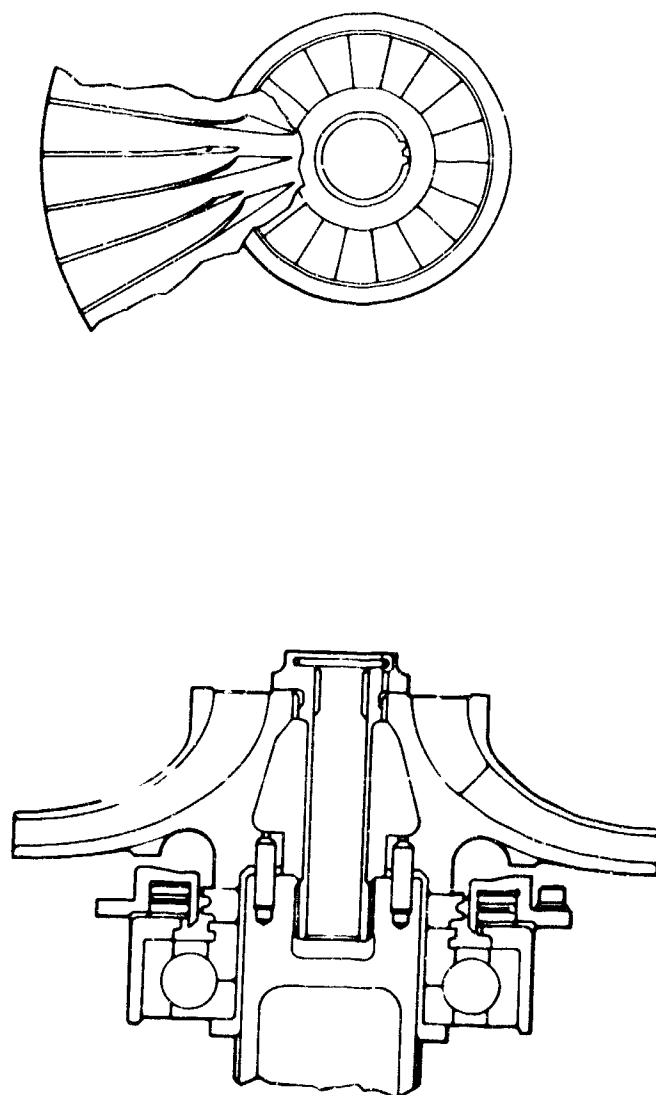


Figure 779. Oxidizer Low-Speed Inducer Turbine Disk

FD 33338

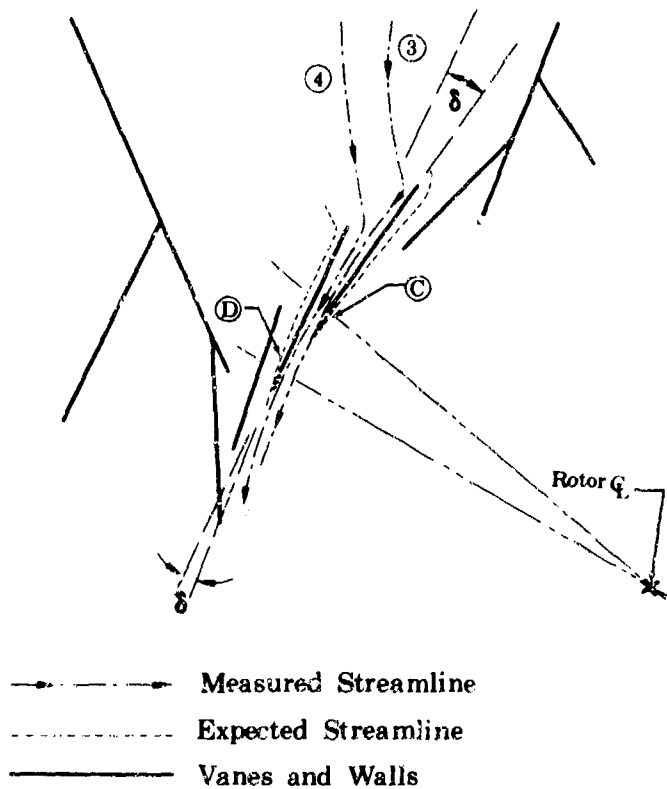


Figure 780. Oxidizer Low Speed Inducer Pressure Rise

FD 33344

Performance of the inlet guide vanes for the radial-inflow turbine was simulated by positioning five sheetmetal vanes on the water table, passing water through them and photographing the flow streamlines by using dye injections. The vanes were positioned in the same position as they would be for the minimum thrust condition, approximately 80 deg from a radial line through the rotor centerline. Inlet guide channels were created to simulate the expected vane flow incidence angle. Two different lengths of vanes were studied, 1.5 and 1.0 in. The water table slope was adjusted to cause flow of the largest depth possible at the vanes (0.5 in.), and the tests were made just below the water surface.

Table XCIII presents the approximate deviation estimated from photographs, for the four streamlines from the vane exit angle at the point where they cross the circumferential vane exit plane. Figures 781 and 782 graphically present table XCIII data.

These levels of deviation were used as guides, rather than absolute design levels, because the test setup is not an exact simulation of the actual case.

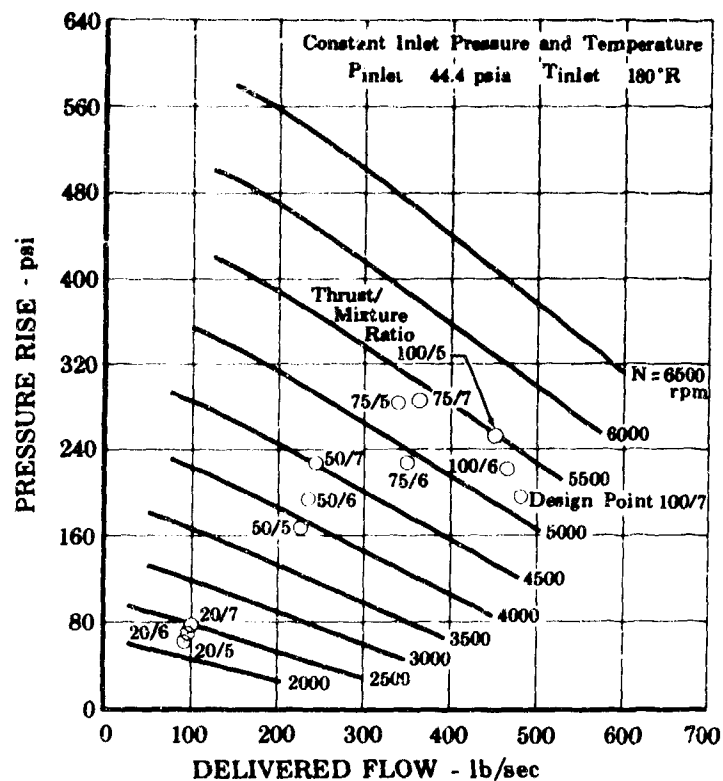


Figure 781. 1.5-Inch Chord Vane Flow Pattern Schematic FD 33414A

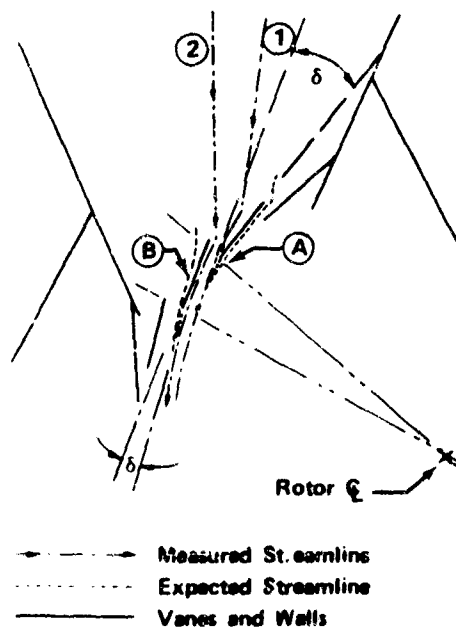


Figure 782. 1.0 In. Chord Vane Flow Pattern Schematic FD 36218

Table XCIII. Vane Streamline Deviation*

Streamline (1) from Vane (A)	18 deg
Streamline (2) from Vane (B)	6 deg
Average for 1.0 inch vane	12 deg
Streamline (3) from Vane (C)	8 deg
Streamline (4) from Vane (D)	3 deg
Average for 1.5 inch vane	5.5 deg

*Approximations only. Refer to figures 781 and 782 for test point locations.